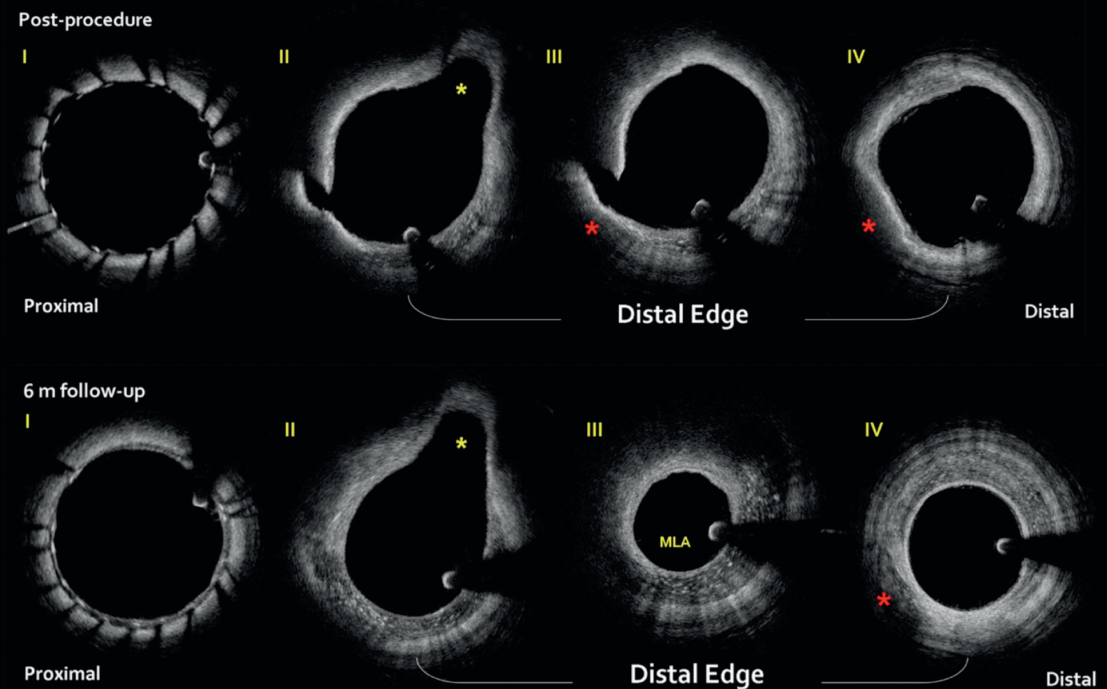
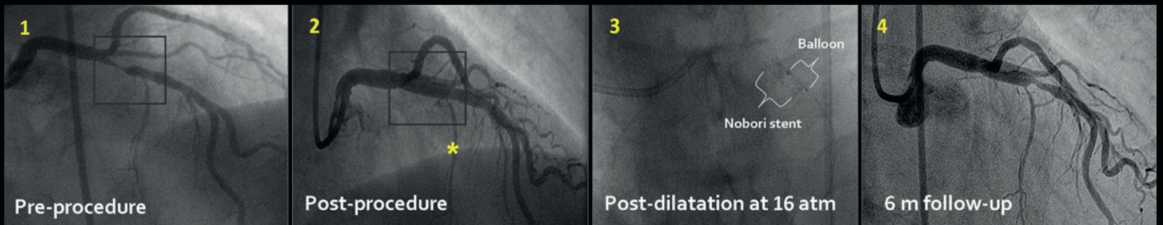


Multimodality Imaging of the Long-term Vascular Responses Following Implantation of Metallic and Bioresorbable Devices



Vasileios D.Gkogkas
(a.k.a. Bill D. Gogas)

Multimodality Imaging of the Long-term Vascular Responses Following Implantation of Metallic and Bioresorbable Devices

**Vasileios D. Gkogkas
(a.k.a. Bill D. Gogas)**

ISBN: 978-94-6169-527-7

Printed by Optima Grafische Communicatie, Rotterdam, The Netherlands

© Vasileios Gkogkas (a.k.a. Bill D. Gogas) 2014

Multimodality Imaging of the Long-term Vascular Responses Following Implantation of Metallic and Bioresorbable Devices

Multimodale beeldvorming van de vasculaire respons op de lange termijn
na implantatie van metaalhoudende en bioresorbabele hulpmiddelen

Thesis

to obtain the degree of Doctor from the
Erasmus University Rotterdam
by command of the
rector magnificus

Prof. dr. H.A.P.Pols

and in accordance with the decision of the Doctorate Board

The public defense shall be held on
Tuesday the 3d of June, 2014 at 15:30 hours

by

Vasileios Dimitrios Gkogkas
(a.k.a. Bill D. Gogas)

born in Athens, Greece

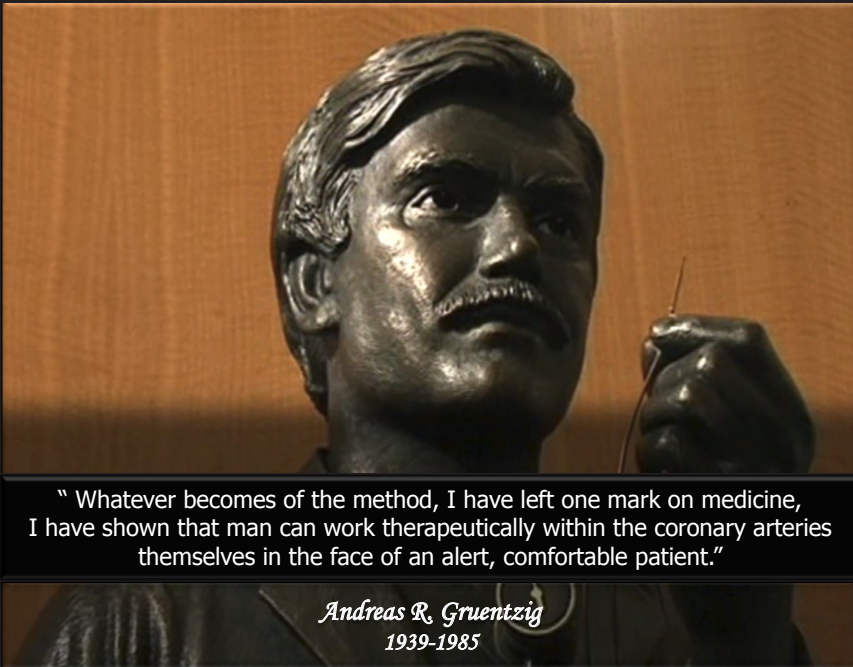


Promotor: Prof. P.W. Serruys

Inner Committee: Prof. E.W. Steyerberg
Prof. P.J.de Feyter
Prof. J.G.P. Tijssen

Co-Promotor: Dr. H.M. Garcia-Garcia

Multimodality Imaging of the Long-term Vascular Responses Following Implantation of Metallic and Bioresorbable Devices



Vasileios D. Gkogkas
(a.k.a. Bill D. Gogas)

*For,
Dimitrios,
& Maria- Angelliki,
Thanks for your principles, You are both wonderful parents.*

*For,
Dimitrios,
Georgios,
Angelliki,
Wishing them to learn from those who know.*

TABLE OF CONTENTS

Introduction and overview

Part 1:

Vascular Responses in the era of Metallic and Bioresorbable Devices

Part 2:

In Vivo Assessment of Vascular Responses Utilizing Intravascular Ultrasound (IVUS) and IVUS-based Imaging Modalities

Part 3:

In Vivo Assessment of Vascular Responses Utilizing Optical Coherence Tomography

Part 4:

Stent Implantation Assessment Utilizing Three-Dimensional Optical Coherence Tomography

Part 5:

In Vivo Assessment of the Absorb Bioresorbable Vascular Scaffold Utilizing Intracoronary Ultrasound and Optical Coherence Tomography

Part 6:

Summary and Conclusions

TABLE OF CONTENTS

Chapter 1:	Introduction and overview Bill D. Gogas	27
Part 1:	Vascular Responses in the era of Metallic and Bioresorbable Devices	
Chapter 2:	In-stent restenosis. Vasim Farooq, Lorenz Räber, Bill D. Gogas , Patrick W. Serruys In: "Percutaneous Interventional Cardiovascular Medicine", Editors: Eric Eeckhout, Patrick W. Serruys, William Wijns, Alec Vahanian, Marc van Sambeek, Rodney de Palma. PCR Publishing, Europa Organization.	35
Chapter 3:	Restenosis: Delineating the Numerous Causes of Drug-Eluting Stent Restenosis. Vasim Farooq, Bill D. Gogas , Patrick W. Serruys Circulation Cardiovascular Interventions. 2011. Apr 1; 4(2): 195-205 [IF: 6.06]	81
Chapter 4:	Edge Vascular Response after Percutaneous Coronary Intervention: An Intracoronary Ultrasound and Optical Coherence Tomography Appraisal: From Radioactive Platforms to First and Second-Generation Drug-eluting Stents and Bioresorbable Scaffolds. Bill D. Gogas , Hector M. Garcia-Garcia, , Yoshinobu Onuma, Vasim Farooq, Christos V. Bourantas, Patrick W. Serruys JACC Cardiovasc Interv. 2013 Mar; 6(3): 211-21 [IF: 6.83]	95

Part 2:	<i>In Vivo</i> Assessment of Vascular Responses Utilizing Intravascular Ultrasound (IVUS) and IVUS-based Imaging Modalities.	
Chapter 5:	Assessment of Coronary Atherosclerosis by IVUS and IVUS-based Imaging Modalities: Progression and Regression Studies, Tissue Composition and Beyond. Bill D. Gogas , Vasim Farooq, Patrick W. Serruys, Hector M. Garcia-Garcia International Journal of Cardiovascular Imaging. 2011. Feb; 27(2): 225-37 [IF: 2.53]	111
Chapter 6:	IVUS-based Imaging Modalities for Tissue Characterization: Similarities and Differences. Hector M. Garcia-Garcia, Bill D. Gogas , Patrick W. Serruys, Nico Bruining International Journal of Cardiovascular Imaging. 2011. Feb; 27(2): 215-24 [IF: 2.54]	127
Chapter 7:	Vascular Response of the Segments Adjacent to the Proximal and Distal Edges of the ABSORB Everolimus-Eluting Bioresorbable Vascular Scaffold: 6-month and 1-year Follow-up Assessment: A Virtual Histology Intravascular Ultrasound study from the First-In-Man ABSORB cohort B trial. Bill D. Gogas , Patrick W. Serruys, Roberto Diletti, Vasim Farooq, Salvatore Brugaletta, Maria D. Radu, Jung Ho Heo, Yoshinobu Onuma, Robert-Jan M. van Geuns, Evelyn Regar, Bernard De Bruyne, Bernard Chevalier, Leif Thuesen, Pieter C. Smits, Dariusz Dudek, Jacques Koolen, Stefan Windecker, Robert Whitbourn, Karine Miquel-Hebert, Cecile Dorange, Richard Rapoza, Hector M. Garcia-Garcia, Dougal McClean, John A. Ormiston JACC Cardiovascular Interventions. 2012. Jun; 5(6): 656-65 [IF: 6.83]	141

- Chapter 8:** **The Edge Vascular Response Following Implantation of the Absorb Everolimus Eluting Bioresorbable Vascular Scaffold and the Xience V Metallic Everolimus Eluting Stent. First Serial Follow-Up Assessment at 6-Months and 2-Years. Insights from the First in Man ABSORB Cohort B and SPIRIT II trials.** **155**
- Bill D. Gogas**, Christos V. Bourantas, Hector M. Garcia-Garcia, Yoshinobu Onuma, Takashi Muramatsu, Vasim Farooq, Roberto Diletti, Robert-Jan M. van Geuns, Bernard De Bruyne, Bernard Chevalier, Leif Thuesen, Pieter C. Smits, Dariusz Dudek, Jacques Koolen, Stefan Windecker, Robert Whitbourn, Dougal Mc Clean, Cecile Dorange, Karine Miquel-Hebert, Susan Veldhof, Richard Rapoza, John A. Ormiston, Patrick W. Serruys
EuroIntervention. 2013 Apr 30. Doi: 20120911-04 [Epub ahead of print] [IF: 3.17]
- Chapter 9:** **Vascular Compliance Changes of the Coronary Vessel wall After Bioresorbable Vascular Scaffold Implantation in the Treated and Adjacent Segments.** **177**
- Salvatore Brugaletta, **Bill D. Gogas**, Hector M. Garcia-Garcia, Vasim Farooq, Chrysafios Giris, Jung Ho Heo, Robert Jan van Geuns, Bernard de Bruyne, Dariusz Dudek, Jacques Koolen, Pieter Smits, Susan Veldhof, Richard Rapoza, Yoshinobu Onuma, John Ormiston, Patrick W. Serruys
Circulation Journal. 2012. Jun 25; 76(7): 1616-23 [IF: 3.58]
- Chapter 10:** **Computational Fluid Dynamics Applied to Virtually Deployed Drug-Eluting Coronary Bioresorbable Scaffolds. Clinical Translations Derived from a Proof-of-Concept.** **189**
- Bill D. Gogas**, Boyi Yang, Tiziano Passerini, Alessandro Veneziani, Girum Mekonnen, Emad Rasoul-Arzrumly, Michel T. Corban, Beth Holloway, Lucas Timmins, David S. Molony, Sungho Kim, Don P. Giddens, Spencer B. King III, Habib Samady
International Journal of Cardiology. 2013. Submitted

Part 3:	<i>In-Vivo Assessment of Vascular Responses Utilizing Optical Coherence Tomography</i>	
Chapter 11:	Evaluation with In Vivo Optical Coherence Tomography and Histology of the Vascular Effects of the Everolimus-Eluting Bioresorbable Vascular Scaffold at Two Years Following Implantation in a Healthy Porcine Coronary Artery Model: Implications of pilot Results for Future Pre-Clinical Studies.	215
	Bill D. Gogas , Maria Radu, Yoshinobu Onuma, Laura Perkins, Jennifer Powers, Josep Gomez-Lara, Vasim Farooq, Hector M.Garcia-Garcia, Roberto Diletti, Richard Rapoza, Renu Virmani, Patrick W. Serruys International Journal of Cardiovascular Imaging.2011. Mar; 28(3): 499-511 [IF: 2.53]	
Chapter 12:	Intracoronary Optical Coherence Tomography and Histology of Overlapping Everolimus-Eluting Bioresorbable Vascular Scaffolds in a Porcine Coronary Artery Model: The Potential Implications for Clinical Practice.	231
	Vasim Farooq, Patrick W Serruys, Jung Ho Heo, Bill D Gogas , Laura E Perkins, Yoshinobu Onuma, Roberto Diletti, Maria D. Radu, Lorenz Raber, Christos V Bourantas, Eric van Remortel, Ravindra Pawar, Richard J Rapoza, Jennifer C Powers, Heleen van Beusekom, Hector M. Garcia-Garcia, and Renu Virmani JACC Cardiovasc Interv. 2013 May; 6(5): 523-32 [IF: 6.83]	
Chapter 13:	In Vivo Three Dimensional Optical Coherence Tomography. A Novel Imaging Modality to Visualize the Edge Vascular Response.	245
	Bill D. Gogas , Takashi Muramatsu, Hector M. Garcia-Garcia, Christos V. Bourantas, Niels R. Holm, Leif Thuesen, Yoshinobu Onuma, Patrick W. Serruys International Journal of Cardiology. 2013 Apr 15; 164(3): e35-7 [IF: 4.12]	

- Chapter 14: Natural history of optical coherence tomography-detected edge dissections following drug-eluting stent implantation.** 251
Maria D. Radu, Lorenz Räber, Jung Ho Heo, **Bill D. Gogas**, Erik Jørgensen, Henning Kelbæk, Takashi Muramatsu, Steffen Helqvist, Vasim Farooq, Hector M. Garcia-Garcia, Stephan Windecker, Kari Saunamäki, Patrick W. Serruys
EuroIntervention 2013; 9-online publish-ahead-of-print August 2013 [IF: 3.17]
- Chapter 15: Biomechanical Assessment of Fully Bioresorbable Devices.** 265
Bill D. Gogas, Spencer B. King III, Lucas H. Timmins, Tiziano Passerini, Marina Piccinelli, Alessandro Veneziani, Sungho Kim, David S. Molony, Don P. Giddens, Patrick W. Serruys, Habib Samady
JACC Cardiovasc Interv. 2013 July; 6(7): 760-1 [IF: 6.83]

Part 4:	Stent Implantation Assessment Utilizing Three-Dimensional Optical Coherence Tomography	
Chapter 16:	Three-Dimensional Coronary Topographic Reconstructions Using <i>In Vivo</i> Intracoronary Optical Frequency Domain Imaging in the Setting of Acute Myocardial Infarction: The Clinical Perspective. Bill D. Gogas , Vasim Farooq, Patrick W. Serruys Hellenic Journal Cardiology. 2012. Mar; 53(2): 148-51 [IF: 1.23]	273
Chapter 17:	New Insights into the Coronary Artery Bifurcation. Hypothesis-Generating Concepts Utilizing 3-Dimensional Optical Frequency Domain Imaging. Vasim Farooq, Patrick W. Serruys, Jung Ho Heo, Bill D. Gogas , Takayuki Okamura, Josep Gomez-Lara, Salvatore Brugaletta, Hector M. Garcia-Garcia, Robert Jan van Geuns JACC Cardiovascular Interventions. 2011. Aug; 4(8): 921-31 [IF: 6.83]	281
Chapter 18:	Three-Dimensional Reconstruction of the Post-Dilated ABSORB Everolimus-Eluting Bioresorbable Vascular Scaffold in a True Bifurcation Lesion for Flow Restoration. Bill D. Gogas , Robert Jan van Geuns, Vasim Farooq, Evelyn Regar, Jung Ho-Heo, Jurgen Ligthart, Patrick W. Serruys JACC Cardiovascular Interventions. 2011. Oct; 4(10):1149-50 [IF: 6.83]	295
Chapter 19:	Three-Dimensional Optical Frequency Domain Imaging in Conventional Percutaneous Coronary Intervention: The Potential for Clinical Application. Vasim Farooq, Bill D. Gogas , Takayuki Okamura, Jung Ho-Heo, Michael Magro, Josep Gomez-Lara, Yoshinobu Onuma, Maria Radu, Salvatore Brugaletta, Glenda van Bochove, RJ vanGeuns, Hector M. Garcia-Garcia, Patrick W. Serruys European Heart Journal. 2011. [Epub ahead of print] [IF: 14.1]	299

Part 5:	<i>In Vivo</i> Assessment of the Absorb Bioresorbable Vascular Scaffold Utilizing Intracoronary Ultrasound and Optical Coherence Tomography	
Chapter 20:	The ABSORB Bioresorbable Vascular Scaffold: An Evolution or Revolution in Interventional Cardiology? Bill D. Gogas , Vasim Farooq, Yoshinobu Onuma, Patrick W Serruys Hellenic Journal Cardiology. 2012. Jul;53(4):301-9 [IF: 1.23]	315
Chapter 21:	Agreement and Reproducibility of Gray-Scale Intravascular Ultrasound and Optical Coherence Tomography for the Analysis of the Bioresorbable Vascular Scaffold. Josep Gómez-Lara, Salvatore Brugaletta, Roberto Diletti, Bill D. Gogas , Vasim Farooq, Yoshinobu Onuma, Pierre Gobbens, Gerrit Anne Van Es, Hector M. García-García, Patrick W. Serruys Catheter Cardiovascular Interventions. 2012. May 1;79(6):890-902 [IF: 2.51]	327
Chapter 22:	Proximal and Distal Maximal Luminal Diameters as a Guide to Appropriate Deployment of the ABSORB Everolimus-Eluting Bioresorbable Vascular Scaffold: A sub-study of the ABSORB Cohort B and the Ongoing ABSORB EXTEND Single Arm Study. Vasim Farooq, Josep Gomez-Lara, Salvatore Brugaletta, Bill D. Gogas , Hector M. Garcia-García, Yoshinobu Onuma, Robert Jan van Geuns, Antonio Bartorelli, Robert Whitbourn, Alexander Abizaid, Patrick W. Serruys Catheter Cardiovascular Interventions. 2012. May 1; 79(6): 880-8 [IF: 2.51]	343
Chapter 23:	A Comparative Assessment by Optical coherence Tomography of the Performance of the First and Second Generation of the Everolimus-Eluting Bioresorbable Vascular Scaffolds. Josep Gomez-Lara, Salvatore Brugaletta, Roberto Diletti, Scot Garg , Yoshinobu Onuma, Bill D. Gogas , Robert Jan van Geuns, Cecile Dorange, Susan Veldhof, Richard Rapoza, Robert Whitbourn, StephanWindecker, Hector M. Garcia-García, Evelyn Regar, Patrick W. Serruys European Heart Journal. 2011. Jul; 53(4): 301-9 [IF: 14.1]	355

Part 6:	Summary and Conclusions	
Chapter 24:	Summary and Conclusions	371
	Samenvatting en Conclusies	381
	Acknowledgements	391
	Curriculum Vitae	399
	List of Publications	401

Chapter 1

Introduction and overview

Bill D. Gogas

Interventional Cardiovascular Medicine has witnessed tremendous progress since September 16, 1977 when Andreas Roland Gruentzig performed the first balloon angioplasty. Although this mode of treatment was undoubtedly a significant breakthrough it was plagued by several drawbacks including intimal and media dissections, acute vessel recoil or subacute closure, late constrictive remodeling, and a diffuse proliferative neointimal response implicated for increased rates of in-segment restenosis. Since then, further technological advances such as the utilization of metallic and bioresorbable devices proved to be a successful strategy in the field, replacing balloon angioplasty as the preferred method for percutaneous coronary interventions. Meanwhile, the unfavourable vascular responses presenting as in-segment restenosis or stent thrombosis (ST) remain the cautionary tale of these technologies.^{1,2}

The pattern of vascular responses following device implantation manifests as in-stent vascular response (focal or diffuse), or edge vascular response (EVR) at the transition zones (focal) and each of these patterns have been previously associated with important prognostic implications. Pathologic reports since the era of endovascular brachytherapy have demonstrated that the predominating tissue at the transition zones in the case of an abnormal EVR consists of smooth muscle cells in disarray and abundant extracellular matrix.³ In the drug-eluting stent (DES) era, the pattern of vascular responses appeared to have focal distribution, aggregating at the proximal stent edge.⁴

Intravascular imaging either sound- or light-based has become pivotal at delineating the in-segment vascular responses following coronary interventions with metallic and bioresorbable devices. These, have been longitudinally assessed with sound-and light-based imaging such as intravascular ultrasound (IVUS), virtual histology IVUS (VH-IVUS) and optical coherence tomography (OCT) following implantation of metallic devices: bare-metal stents, radioactive platforms, 1st and 2nd generation DES.⁵ The majority of these studies demonstrated clinically significant proximal edge lumen loss implicated for restenotic rates of ~6% in real world practise. Distal edge was primarily associated with tissue composition changes of fibro-fatty and dense calcium tissue components.

The aim of this thesis was to assess *in vivo* the long-term (~ 2-years) vascular responses following implantation of newer generation devices such as DES and bioresorbable scaffolds with the aforementioned imaging modalities. The global overview of the in-segment vascular responses utilizing bare-metal stents, radioactive platforms, 1st and 2nd generation DES, and bioresorbable scaffolds are discussed in Part 1.

In Part 2, we focus on the sound-based assessment of the device / tissue interaction. Chapters 5 & 6 embrace the principles of this imaging modality and give an insight into where IVUS is placed compared to other sound-based imaging techniques. Chapter 7 is

a landmark piece of work and draws upon our first observations of the tissue responses at the transition zones utilizing commercially approved bioresorbable devices.

Chapter 8 compares the induced vascular responses of a metallic stent vs. a polymeric device at the proximal and distal edges at short-, mid-, and long-term follow-up utilizing in-vivo IVUS and VH-IVUS imaging. It is important to note that implantation of either a metallic or polymeric device affects vascular compliance at the stented/scaffolded segments inducing compliance mismatch with subsequent alterations of flow dynamics adjacent to the implanted device. Chapters 9 & 10 demonstrate the transient nature of compliance mismatch and altered flow patterns over the scaffolded segments and the scaffold edges utilizing IVUS-palpography and virtual numerical modelling.

The use of OCT in evaluating vascular responses following implantation of metallic and bioresorbable devices is an important angle of this thesis which is explored in Part 3. OCT is a relatively novel imaging modality with ultra high spatial resolution used for the *in vivo* quantification of vascular anatomy and qualitative tissue characterization.^{6,7} In Chapter 11, we describe the feasibility of this imaging technique to quantitatively assess the vascular reactions following implantation of bioresorbable scaffolds at long-term, applying further comparisons with pathology for reproducibility evaluation. Chapter 12 explores the use of OCT in overlapping bioresorbable scaffolds compared with overlapping newer generation metallic stents, identifying the influence of cell design on strut coverage. Chapters 13 & 14 focus on the significant advantages of this modality in precisely evaluating stent edges providing additional clinical implications. Although sound-based imaging was until recently the sole intravascular imaging modality for edge assessment, this technique compared to OCT appears to have technical limitations. Despite the low penetration depth of OCT which limits the precise assessment of vessel remodeling, the sharply defined stent edges makes this imaging tool a more accurate modality to evaluate the vessel responses at the transition zones. Chapter 15 describes for the first time the use of 3-Dimensional (3D) OCT for biomechanical analysis of bioresorbable devices which may yield important insights into potential advantages of bioresorbable technologies over metal stents by these methods.

Part 4 evaluated the potential applications of post-processed three-dimensional OCT in conventional interventional procedures for various clinical settings following implantation of metallic and bioresorbable vascular scaffolds. The final section of this thesis (Part 5) deals with the newly developed Absorb bioresorbable vascular scaffold and its evaluation with intravascular imaging. In conclusion the aim of this thesis was therefore: 1. To assess in-vivo with sound-based imaging the long-term vascular responses following implantation of metallic stents and bioresorbable scaffolds, used for the treatment of coronary atherosclerosis; 2. To validate and explore the importance of intracoronary

light-based imaging in the assessment of the device/tissue interaction; 3. To explore the potential importance of three-dimensional post-processed light-based imaging in the clinical setting.

REFERENCES:

1. Mehran R, Dangas G, Abizaid AS, et al. Angiographic patterns of in-stent restenosis: classification and implications for long-term outcome. *Circulation*. Nov 2 1999;100(18):1872-1878.
2. Finn AV, Joner M, Nakazawa G, et al. Pathological correlates of late drug-eluting stent thrombosis: strut coverage as a marker of endothelialization. *Circulation*. May 8 2007;115(18):2435-2441. **3.** Kim HS, Waksman R, Kollum M, et al. Edge stenosis after intracoronary radiotherapy: angiographic, intravascular, and histological findings. *Circulation*. May 1 2001;103(17):2219-2220.
4. Corbett SJ, Cosgrave J, Melzi G, et al. Patterns of restenosis after drug-eluting stent implantation: Insights from a contemporary and comparative analysis of sirolimus- and paclitaxel-eluting stents. *European heart journal*. Oct 2006;27(19):2330-2337.
5. Wakabayashi K, Waksman R, Weissman NJ. Edge effect from drug-eluting stents as assessed with serial intravascular ultrasound: a systematic review. *Circulation. Cardiovascular interventions*. Apr 2012;5(2):305-311.
6. Tearney GJ, Regar E, Akasaka T, et al. Consensus standards for acquisition, measurement, and reporting of intravascular optical coherence tomography studies: a report from the International Working Group for Intravascular Optical Coherence Tomography Standardization and Validation. *J Am Coll Cardiol*. Mar 20 2012;59(12):1058-1072.
7. Mintz GS, Garcia-Garcia HM, Nicholls SJ, et al. Clinical expert consensus document on standards for acquisition, measurement and reporting of intravascular ultrasound regression/progression studies. *EuroIntervention*. Apr 2011;6(9):1123-1130, 1129.

Part 1

Vascular Responses in the era of Metallic and Bioresorbable Devices

Chapter 2

In-stent restenosis.

Vasim Farooq, Lorenz Räber, **Bill D. Gogas**, Patrick W. Serruys

In: "Percutaneous Interventional Cardiovascular Medicine", Editors: Eric Eeckhout, Patrick W. Serruys, William Wijns, Alec Vahanian, Marc van Sambeek, Rodney de Palma. PCR Publishing, Europa Organization.

In-stent restenosis

VASIM FAROOQ, LORENZ RÄBER, BILL D. GOGAS, PATRICK W. SERRUYS

SECTION TITLE

Introduction

Classification system of in-stent restenosis
 Risk factors associated with in-stent restenosis
 Histopathological basis of in-stent restenosis
 In-stent restenosis: a benign entity?

Overview

Biological factors

Resistance to antiproliferative drugs
 Potentially overcoming drug resistance
 Hypersensitivity reactions (the polymer)
 The inflammatory and hypersensitivity response
 Hypersensitivity reactions (the metallic platform)
 Inflammatory biomarkers and genetics
 Inflammatory biomarkers
 Genetics
 Potential clinical application

Arterial factors

Wall shear stress
 Thromborestenosis phenomenon
 Vessel remodelling
 Crew resource management
 Small vessels
 Late restenosis

Decreasing drug dose

Chronic inflammation

Neoatherosclerosis

Angiographic and imaging data

Angiographic data
 Newer-generation drug-eluting stents
 Clinical significance of late catch-up

Stent factors

Polymer release kinetics
 Type of DES? Type of drug?
 Stent gap, non-uniform strut and drug distribution
 Small vessels and strut thickness
 "On" and "off" label use of DES
 Polymer disruption and cracking
 Stent fractures

Implantation factors

Incomplete stent expansion
 Geographical miss/barotrauma to unstented segments
 Deployment of DES in a clot-laden arterial segment

Personal perspective

References

SUMMARY

Despite the enormous progress made in reducing the incidence of restenosis with first and second-generation drug-eluting stents (DES), the incidence of in-stent restenosis (ISR) requiring target vessel revascularisation (TVR), so-called "DES failure", is approximately 5-10%, with one estimate suggesting approximately 200,000 repeat revascularisations performed in the US alone. Emerging evidence is now challenging the traditionally held view that ISR is a benign phenomenon with between 30-60% of cases presenting with acute coronary syndrome. The underlying mechanisms of DES restenosis are complex and can be broadly divided into 4 main causes, namely biological, arterial, stent and implantation factors. Evolving concepts concerning mechanisms relating to late restenosis and "neo-atherosclerosis" are also discussed. The treatment of ISR and the determinant factors involved in the development of late stent thrombosis are well described elsewhere and are outside the scope of this review. In this review the numerous causes of DES restenosis are delineated to help identify the potentially controllable and non-controllable factors from the perspective of the interventional cardiologist intending to implant a DES.

KEYWORDS

- Drug-eluting stents
- In-stent restenosis
- Mechanisms
- Percutaneous coronary intervention



This chapter also includes supplementary data which can be found in the online version of this Textbook at www.pcronline.com

INTRODUCTION

In the last decade, tremendous progress has been made in reducing the incidence of restenosis with the advent of the drug-eluting stent (DES). With “plain old balloon angioplasty” (POBA), rates of acute and chronic vessel restenosis were unacceptably high at approximately 30-60%, secondary to acute and chronic recoil and constrictive remodelling [1-3]. The advent of bare metal stents (BMS) appeared to eliminate the issue of acute and chronic recoil but introduced a new entity – neointimal hyperplasia (NIH) with classical manuscripts unequivocally demonstrating a strong and linear relationship between NIH formation and late lumen loss (LLL) [4]. The restenosis rates with BMS were reported to be between 16-44% with higher rates of stenosis attributable to several risk factors, in particular long lesion length and small vessel calibre [3,5-7].

Consequently, attempts were made to limit the neointimal response after stent implantation with vascular brachyther-

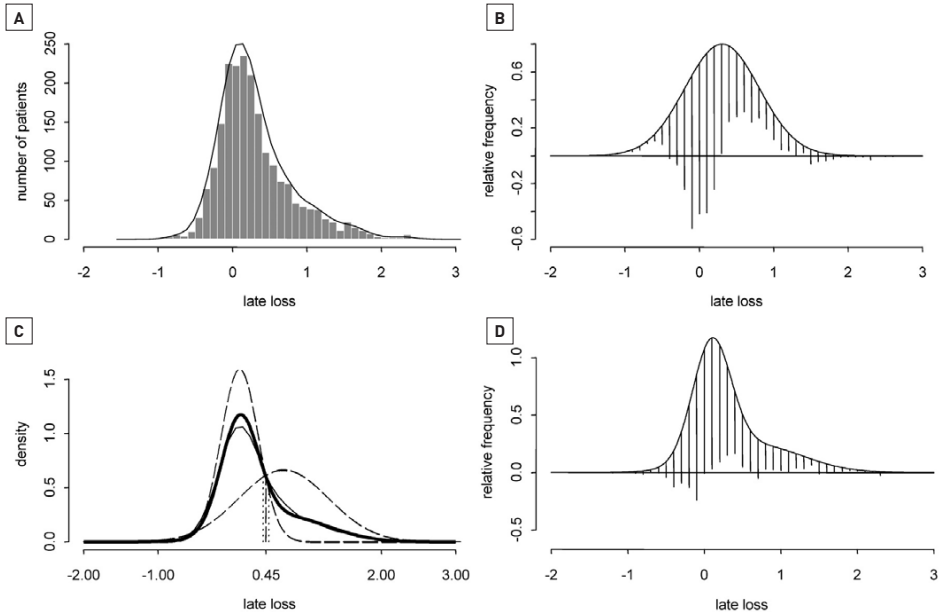
apy. This involved the use of radioactive stents and initially appeared feasible in partially eliminating the NIH response. However, this technology resulted in a significant “edge effect” or “candy-wrapper” phenomenon at the stent edges - secondary to the radioactive dose fall-off at the stent edges and low-level vessel injury - thus precluding its widespread clinical use [8-10].

DES were thus conceived as the next step in tackling this iatrogenic entity of NIH, with large-scale reductions in restenosis rates reported at 0% in highly selective lesions and up to 16% in a broader range of patients and lesions with first-generation DES [3,6,11].

In contrast to POBA [12] and BMS [13], where an almost classical Gaussian (normal) distribution of late loss is broadly seen post-procedurally, the distribution of LLL after DES implantation has been shown to follow a bimodal pattern of distribution with both paclitaxel- (PES) and sirolimus- (SES) eluting stents (➤ Figure 1) [14].

FIGURE 1

The bimodal distribution of late lumen loss (LLL) [A, B] and percentage diameter stenosis [C, D] after Cypher (left) and Taxus (right) implantation. LLL indicates late lumen loss. Reproduced with permission from Byrne et al. [14]. In each panel the observed frequency distribution curve (thin solid line), two subpopulations' normal distribution curves (dashed lines) and the composite distribution curve (thick solid line) are displayed; the vertical dashed line denotes the intersection point between the two subpopulation distribution curves.



Despite the significant advances in the technology to reduce restenosis, conservative estimates would, however, still suggest the incidence of ISR requiring repeat revascularisation, so-called “DES failure,” to be approximately 5-10%, with one estimate suggesting approximately 200,000 repeat revascularisations in the United States alone [15].

CLASSIFICATION SYSTEM OF IN-STENT RESTENOSIS

In 1999, Mehran et al [16] first described a classification system for the patterns of restenosis seen with coronary stents. Two broad categories were described, namely focal and diffuse restenosis, with multiple subtypes within each group. The pattern of restenosis seen with DES is usually focal, in contrast to BMS which is primarily diffuse. In one series, over 60% of in-stent restenosis (ISR) cases with both PES and SES were focal, with the most common location for focal restenosis appearing to be at the proximal DES edge [17]. Despite this, over one fifth of cases of ISR remains diffuse and approximately 10-20% of cases are even occlusive (➤ Figure 2).

RISK FACTORS ASSOCIATED WITH IN-STENT RESTENOSIS

In 2004, there was the first reported description of the risk factors associated with DES restenosis in patients with the

unrestricted use of SES since approval of its CE mark [18,19]. Despite the apparent differences in the distribution of LLL between BMS and DES as previously described, the main message of these and subsequent findings was that the usual patient characteristics, lesion types and procedural factors incriminated with restenosis in BMS were equally responsible with DES, with diabetes mellitus being implicated as one of the strongest risk factors for the development of restenosis [17-21]. It should, however, be emphasised that the distribution of restenosis with DES appears more attenuated compared with BMS, especially in long lesions and small vessels, highlighting the importance of drug elution in potentially diminishing the NIH response.

HISTOPATHOLOGICAL BASIS OF IN-STENT RESTENOSIS

The inflammatory reaction which occurs after arterial injury is a critical factor that influences the extent of neointimal response, with the persistence of this inflammatory response beyond 90 days being strongly associated with an increased level of neointimal thickness and consequent restenosis [3,22,23]. In keeping with these findings, it has been demonstrated that restenotic lesions have a higher number of chronic inflammatory cells compared to non-restenotic lesions [22]. Histopathological analyses of ISR, involving samples taken by directional atherectomy at the time of reintervention, have been shown to be remarkably similar between BMS and DES. This is almost exclusively composed of proteoglycan-rich smooth muscle cells (SMC) and fibrolipidic areas rich in collagen and reticular fibres. A more “immature” restenotic process, as evidenced by differences in SMC phenotypes, however, has been shown potentially to exist with certain types of DES compared with BMS [24,25]. Fibrinoid tissue, indicative of a persistent inflammatory and incomplete healing response, has also been reported with DES [26-30] and implicated in the subsequent risk of late stent thrombosis (LST) [28].

IN-STENT RESTENOSIS: A BENIGN ENTITY?

ISR has traditionally been suggested as being potentially less benign with the recurrence of anginal symptoms alone. Emerging evidence now suggests that between 30-60% of ISR cases perhaps present with an acute coronary syndrome (ACS), with unstable angina being the most common presentation (➤ Figure 3) [31-41], and up to 5% of patients even being reported as presenting with an ST-elevation myocardial infarction (STEMI) [36,38-41].

Furthermore, as to whether a total vessel occlusion presenting with acute ischaemia is related to a stent thrombosis or a subtotal restenosis is often difficult to differentiate

FIGURE 2

The patterns of restenosis in SES and PES

The predominant pattern of restenosis is a focal pattern of restenosis, although diffuse and proliferative restenosis are still seen with DES. *P-value calculated for the overall observed difference in the pattern of restenosis in PES and SES groups. SES indicates sirolimus-eluting stent; PES: paclitaxel-eluting stent; DES: drug-eluting stent. Reproduced with permission from Corbett et al [17].

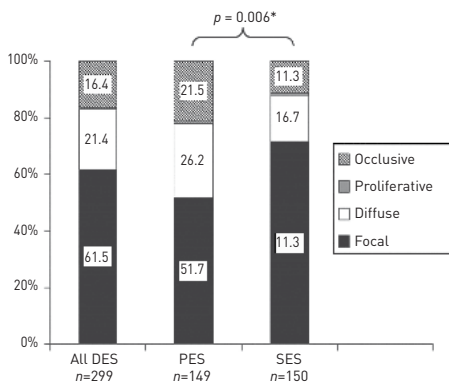
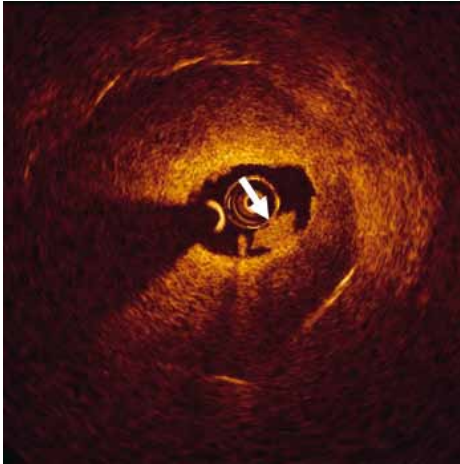


FIGURE 3

The presence of intraluminal material (white arrow), most probably thrombus, visualised in a restenotic segment. The OCT images were obtained from a patient referred for coronary angiography for unstable angina. Reproduced with permission from Gonzalo et al [229].



solely based on the clinical presentation and the angiographic findings. The consideration of the angiographic appearances, the behaviour of the lesion during balloon inflation and the patient history (such as the type of stent previously implanted) can potentially aid in identifying the aetiology of the ischaemic event. Intravascular imaging can serve as an additional supportive diagnostic tool, although the differentiation between thrombus and neointimal tissue is not always readily possible with currently available intravascular imaging techniques (intravascular ultrasound [IVUS] and optical coherence tomography [OCT]). This rapidly evolving concept is discussed in the *Late restenosis* section of *Arterial factors*.

OVERVIEW OF CHAPTER

The treatment of ISR and the determinant factors involved in the development of late stent thrombosis (LST) are well described elsewhere and are outside the scope of this chapter [42-44]. The underlying mechanisms of restenosis with DES can broadly be divided into 4 main causes (➤ Table 1), namely biological, arterial, stent and implantation factors, accepting that this classification is somewhat arbitrary with mechanisms of restenosis being attributable to more than one factor. In this chapter we explore these 4 main mechanisms and identify the potentially controllable and non-controllable

factors from the perspective of the interventional cardiologist intending to implant a DES.

BIOLOGICAL FACTORS

Resistance to antiproliferative drugs

The underlying mechanisms of action and causes of resistance to paclitaxel or sirolimus are well documented in the cancer literature and can either be present in genetically predetermined individuals or be acquired, following cytotoxic exposure to the drug [45,46].

The so-called “drug resistance gene expression programme,” described for paclitaxel resistance from the cancer literature, best exemplifies the complex pathways involved in the aetiology of drug resistance [45]. Essentially, the cellular context determines the genes that are expressed which contribute to drug resistance either in genetically predetermined cells or primed for expression following the cytotoxic insult after exposure to the drug. These genes may operate in conventional pathways that are well known (drug delivery and metabolism, apoptosis regulation, DNA repair), but the temporal (i.e., pro- and anti-apoptotic gene activity) and spatial regulation (i.e., cell survival signalling pathways) of these gene products after exposure to the drug also appear to be important.

As examples, polymorphisms in the genes that encode mTOR or proteins involved in paclitaxel or sirolimus metabolism have been shown to confer drug resistance both *in vitro* and *in vivo* [10,11]: decreased binding of sirolimus to

FOCUS BOX 1

- Drug-eluting stents (DES) were conceived as the next step - after balloon angioplasty and bare metal stents (BMS) - in tackling the iatrogenic entity of neointimal hyperplasia
- The distribution of late lumen loss (LLL) after drug-eluting stent implantation has been shown to follow a bimodal pattern of distribution with both paclitaxel (PES) and sirolimus (SES) eluting stents
- “DES failure” equates to approximately 5-10% of cases, with one estimate suggesting approximately 200,000 repeat revascularisations in the US alone [15]
- The pattern of restenosis seen with DES is usually focal. By contrast, the pattern of restenosis with BMS is primarily diffuse
- Persistence of the inflammatory response beyond 90 days after arterial injury is strongly associated with an increased level of neointimal thickness and consequent restenosis
- In-stent restenosis (ISR) may not be as “benign” as once originally thought with 30-60% of ISR cases presenting with an acute coronary syndrome (ACS)

TABLE 1
The underlying mechanisms of restenosis with DES

BIOLOGICAL FACTORS	ARTERIAL FACTORS	STENT FACTORS	IMPLANTATION FACTORS
Resistance to Antiproliferative drugs Hypersensitivity reaction (polymer) Hypersensitivity reaction (metallic stent platform) Inflammatory biomarkers Genetics	Wall shear stress "Thromborestenosis" Vessel remodeling Small vessels Late restenosis - Decreasing drug dose - Chronic inflammatory reactions - and persistent fibrin deposition - Neointerostenosis	Polymer drug release kinetics Type of DES? Type of drug? Stent gap, Non-uniform strut distribution and drug deposition Stent strut thickness "On" and "off" label use of DES Polymer disruption, peeling and cracking Stent fractures	Incomplete stent expansion Geographical miss Edge effect Barotrauma to Unstented Segments Incomplete lesion coverage Deployment of DES in a clot-laden arterial segment

mTOR due to mutations in FK-B12 and mTOR and mutations of downstream effector molecules of mTOR may all cause resistance to sirolimus [11].

Potentially overcoming drug resistance through the delivery of higher doses of antiproliferative agent to the implantation site

Given the possibility that drug resistance is one potential mechanism of restenosis, attempts have been made to give much higher doses of oral sirolimus to patients with refractory ISR in the theoretical attempt of overcoming drug resistance and delivering increased amounts of drug to the implantation site. The OSIRIS study [47] investigated the administration of higher doses of oral sirolimus to patients with refractory ISR and demonstrated a significant correlation between the level of sirolimus concentration in the bloodstream and rates of further late lumen loss (↻ Figure 4). Given that the patients received a short

duration of oral sirolimus (7 days), it was unclear if these findings would be maintained at longer-term follow-up. It has been anecdotally reported that courses of sirolimus given for 30 days after POBA to the restenotic lesion, in the theoretical attempt to cover the injury period following POBA, can reduce restenosis in refractory restenosis cases [48]. Larger-scale studies are required to establish if this is feasible or practical.

Furthermore, evidence has suggested that the concomitant administration of steroids to patients implanted with BMS, particularly in patients with a persistent inflammatory state, as indicated by elevated C-reactive protein, may reduce the incidence of ISR [49-53]. Further trials are needed, however, to assess the clinical utility of steroid therapy for the treatment of ISR after prior DES implantation.

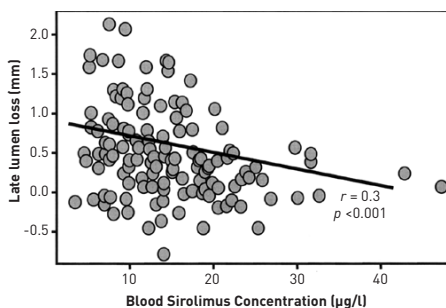
Hypersensitivity reactions (the polymer)

Polymer layers in DES are used as both drug reservoirs and non-drug-coated external films to allow optimal drug release kinetics, as described in Stent Factors. As examples with the first-generation DES, the Cypher® (SES) stent (Cordis Corporation, Johnson & Johnson, Warren, NJ, USA) consists of a stainless steel platform covered with a basecoat formulation (67%) consisting of the polymers PEVA (polyethylene vinyl acetate) and PBMA (poly n-butyl methacrylate) mixed with sirolimus (33%); a drug-free PBMA topcoat is also applied over the polymer drug mixture to control drug release kinetics. The Taxus® (PES) stent (Boston Scientific, Natick, MA, USA) consists of a stainless steel platform with Translute™ (poly [styrene-b-isobutylene-b-styrene]) polymer combined with paclitaxel without a primer or topcoat layer.

The inflammatory reaction that occurs after arterial injury is a critical factor which influences the extent of neointimal response, with the persistence of this inflammatory response beyond 90 days being strongly associated with delayed healing and implicated in an increased risk of LST and restenosis long term [13,14].

FIGURE 4
The patterns of restenosis in SES and PES

The association of sirolimus blood concentrations at the time of repeat intervention and the angiographic late lumen loss at 6-month angiographic follow-up from the OSIRIS study. Higher serum levels of sirolimus were found to correlate with the degree of 6-month angiographic late lumen loss. Reproduced with permission from Hausteiter et al [47].



The inflammatory and potential hypersensitivity response

Both PES and SES have been demonstrated to provoke distinctive inflammatory responses in animal models beyond 90 days, with SES triggering giant cell infiltrations and PES causing eosinophilic reactions around stent struts [26-30]. The inflammatory responses associated with SES have been shown to persist beyond 180 days and up to 2 years (Figure 5). This phenomenon has also been shown to be potentially further exacerbated at sites of overlapping DES [28]. This is in contrast to BMS and the second-generation everolimus-eluting stent (EES; Xience V; Abbott Vascular, Santa Clara, CA, USA)

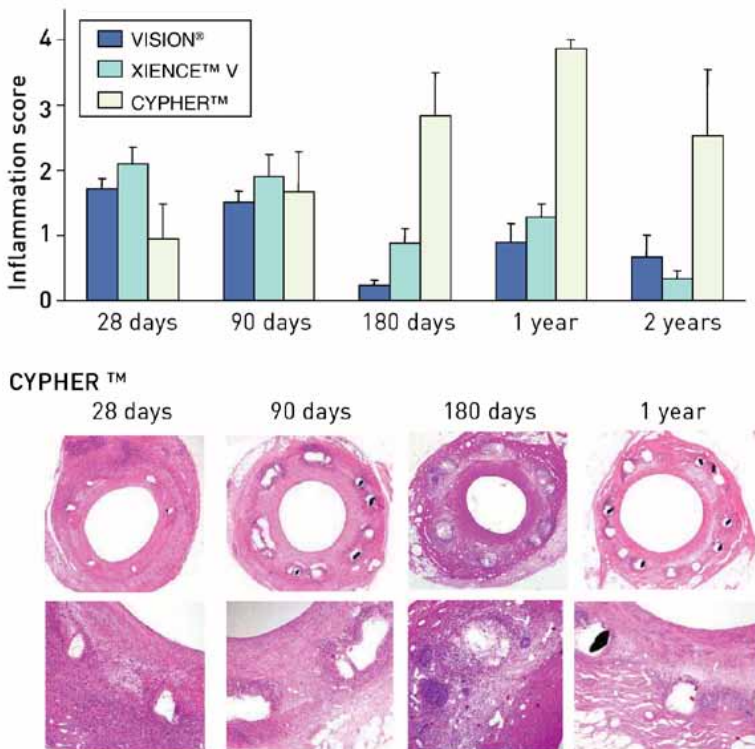
with a more biocompatible polymer, where the inflammatory responses have been demonstrated to be limited to a period of 90 days and 12 months, respectively (Figure 5) [54].

Evidence of persistent inflammatory responses in humans have also been reported both in autopsy cases, with one case reported to involve up to one third of struts in first-generation DES at 3 months, and demonstrating signs of persistent inflammation characterised by granuloma formation and extensive eosinophilic infiltration as seen in the animal models. Furthermore, evidence of persistent inflammation has been demonstrated from thrombus aspirates taken at the time of emergency PCI in patients presenting with very LST [55].

FIGURE 5

The persistent inflammatory response to Cypher stents for a period of up to 2 years

The panels below show the persistent granulomatous inflammatory response to Cypher stents in sections at low and high power at various time points. Reproduced with permission from Nakazawa et al [54].



Further details related to this “late restenosis” phenomenon are described in *Arterial factors*.

Hypersensitivity reactions (metallic stent platform)

Koster et al [56] first reported an apparent association between the risk of restenosis and metal allergy, namely nickel and molybdenum, with BMS. This study has been controversial, however, and the research methodology subjected to criticism, in particular the methodology of identifying nickel allergy [57-59]. Small-scale, predominantly retrospective studies have failed to show an association between metal allergy in BMS and restenosis [60,61]. Saito et al [62] did, however, report nickel allergy as being an independent predictor for refractory ISR in BMS (odds ratio 5.1, $p=0.0033$), with almost one fifth of patients with refractory ISR having a documented true allergy to nickel (24 of 128 patients). Of note is the fact that the nickel allergy assessment was performed by an independent dermatologist blinded to the study results. Conversely, Lijima et al [63] suggested an association between nickel allergy by patch test and the recurrence of ISR, in patients treated with POBA for ISR after BMS implantation. Within their study no association was found with BMS implantation and first presentation of ISR.

The issue of ISR has also been linked to gold-coated stents, where several studies have associated these with contact allergy and a considerable increase in the risk of ISR [64-68]. Consequently, the use of gold in coronary stents has been abandoned.

Whether the issue of nickel hypersensitivity is a potential issue with DES is both speculative and theoretical. To date, only one small study (Nakazawa et al [69]) has examined this issue and found no association between the risk of ISR and SES implantation.

Inflammatory biomarkers and genetics

Inflammatory biomarkers

The inflammatory status, as assessed by C-reactive protein levels, has consistently failed to demonstrate any association with ISR after DES implantation, despite being associated with ISR after BMS implantation; C-reactive protein levels have, however, been implicated in the risk of stent thrombosis [70,71].

Circulating matrix metalloproteinases (MMP) have been shown to be potentially useful in identifying patients at a greater risk of developing ISR following DES implantation [72]. It is well established that both MMP-2 and MMP-9 play fundamental roles in the migration of vascular SMCs and matrix remodelling during wound healing and are produced

by vascular SMCs, endothelial cells, macrophages, lymphocytes and mast cells in response to mechanical injury [73-75]. Significant elevations in MMP-9 levels at baseline and 24 hours post PCI, and MMP-2 levels 24 hours post PCI, have all proven to be strongly associated with the development of ISR following DES implantation [72]. Conversely, in the same study, low and near-normal MMP-2 and MMP-9 levels were strongly associated with a lack of a significant restenotic response.

Furthermore, other inflammatory biomarkers such as serum levels of PAI-1 [76] and complement components (C3a and C5a) [77] have also been implicated with ISR after DES implantation.

Genetics

It would also appear that the effects of ISR are perhaps not immune from genetics. As to whether this is due to the resistance (predetermined or acquired) to the drug as previously described, or due to biological mechanisms, in particular the inflammatory response of the restenosis process itself, is presently unclear. Inflammatory gene polymorphisms in 4 differing genes have been previously demonstrated to be associated with ISR [78]. For example, homozygosity of the 16/glycine variant in the beta2-adrenergic receptor (ADRB2), a mediator of nitrous oxide synthetase, has been associated with ADRB2 receptor down-regulation and an increased risk of restenosis [78]. Vogiatzi et al [79] have previously described a powerful association, by a factor of over 15-fold, between two functional polymorphisms of interleukin-8 (a strong mediator of inflammation) and the subsequent risk of restenosis. These latter gene polymorphisms were relatively rare, which subsequently limited any clinical application. Other gene mutations have also previously been described as being associated with restenosis [80,81]. Conversely, genetic markers such as angiotensin-converting enzyme (ACE), despite showing initial promise, have failed to demonstrate a clinical role – perhaps due to the multifactorial nature of ISR [82].

Potential clinical application

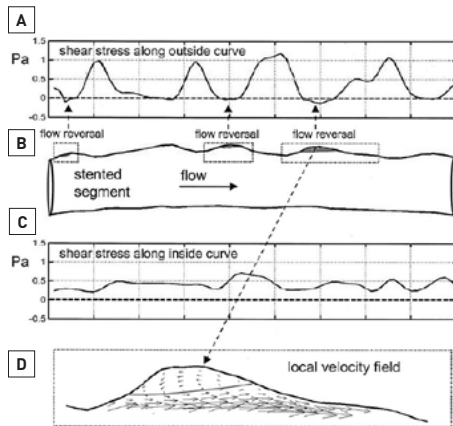
The prospect of potentially being able to identify patients with a greater propensity to develop ISR after DES implantation may perhaps allow a more “personalised revascularisation” with, for example, DES which deliver higher drug concentrations to the vessel or even the prospect of considering surgical revascularisation in this cohort of patients. This individualised approach to revascularisation based on individual genetic risk factor profiling is still in its infancy and extensive preclinical and clinical investigations are required before this can even be considered to enter conventional clinical practice.

FOCUS BOX 2

- Biological factors related to in-stent restenosis (ISR) can be secondary to resistance to antiproliferative drugs, hypersensitivity reactions to the polymer or metallic stent platform, and inflammatory biomarkers and genetics
- ISR secondary to antiproliferative drugs can either be present in genetically predetermined individuals or be acquired following cytotoxic exposure to the drug. Limited evidence exists for using oral sirolimus to overcome drug resistance – further trials are required to establish if this is feasible or practical
- Hypersensitivity to the polymer is well documented and has been associated with late restenosis (see *Arterial factors*) and stent thrombosis
- Hypersensitivity to the metallic platform of drug-eluting stents remains hypothetical and unproven with nickel. Gold-coated stents have a proven association with contact allergy and have been linked to restenosis: consequently, coronary stents are no longer manufactured from gold
- The identification of biomarkers (e.g., MMP) and genes associated with ISR is in its infancy – at the time of writing the clinical application is awaiting to be defined

FIGURE 6

Two-dimensional axial cross-section of a slightly curved stented coronary segment (B). The results of a computation of velocity and shear stress distribution in this segment at follow-up show regions with low shear stress (A) that coincide with the shallow pits in (B). Along the inner curve, the region with lower shear stress, the pits are virtually absent and shear stress distribution is much more homogeneous (C). In some of the pits along the outside curve, flow reversal can be observed (inset and D). The areas containing negative axial velocity are indicated by the shaded boxed regions in (B). Reproduced (Figure and Figure legend) with permission from Gijzen et al [89].



ARTERIAL FACTORS

Wall shear stress

Wall shear stress refers to the principle that fluid dynamics and vessel geometry may play a potential role in the cause of focal plaque or neointimal formation [83]. The concept of wall shear stress is that fluid (i.e., blood) does not move at the same velocity at every point within the vessel, with blood flowing fastest in the vessel centre (i.e., a high shear stress area) and slowest when closest to the vessel wall (i.e., a low shear stress area) due to frictional forces exerted by the vessel endothelium. For example, in coronary bifurcations this phenomenon becomes more notable with a lower shear stress occurring at the ostium of a side branch [83-85]. This may subsequently lead to the accumulation of growth factors, mitogenic cytokines and platelets, which may promote either atherosclerosis or neointimal formation if the side branch undergoes "vessel injury," such as after angioplasty or stenting [83,85-89]. Conversely, the carina of the side branch is a high shear stress area and atherosclerosis or restenosis rarely occurs here: indeed, animal models have shown that high shear stress areas can potentially directly inhibit SMC proliferation [90]. Other examples include differences in the shear stress in the inner and outer curvatures of a stented vessel (Figure 6) [89].

Clinical implications of wall shear stress

In a novel experiment in an animal model, Carlier et al [91] demonstrated that, through the implantation of a "flow divider" into the centre of a stent implanted in the iliac arteries, they were able to modulate the local wall shear stress and the subsequent growth of NIH. The flow divider significantly increased the local wall shear stress and was consequently found to lead to a local reduction in inflammation and injury, with reduced NIH growth and subsequent late lumen loss. The closest human model of this example has been the use of the principle of simultaneous V-stenting (so-called "shotgun stenting") with the formation of a metallic neo-carina in the left main stem or other suitably sized vessels [92,93]. Kim et al [92] demonstrated that in 36 consecutive patients (29 with left main stem interventions) using this technique with SES implantation, a 14% (5 patients) restenosis rate occurred over an average follow-up period of over 2 years. Interestingly, a "membranous diaphragm" at the carina was identified in 14 patients (47%) with restenosis occurring in just one of these patients. Conversely, Stinis et al [94] showed that, in 74 consecutive patients with predominantly left anterior descending-diagonal lesions, the target lesion revascularisation rate was more than twice as high in the simultaneous V-stenting group (14 patients, 40%), compared with the crush group (5 patients, 12.8%) at

a follow-up of >3 years. Whether lesion location played a role in the disparity of these results remains unclear. Robust, randomised controlled trials are therefore required to evaluate the feasibility of this technique.

The issue as to whether the actual presence of the stent in the vessel wall negatively alters the wall shear stress sufficiently to promote restenosis has proven to be controversial, with conflicting evidence existing in the literature. In a more recent, larger, well-designed trial, Papafaklis et al [95] demonstrated the presence of significant numbers of “pockets” of low shear stress within stented segments, secondary to local geometric factors such as angulation or curvature, and showed that these pockets were significantly associated with NIH formation at 6-month follow-up with BMS and PES. Interestingly, this was not seen with SES, suggesting that sirolimus significantly attenuated the neointimal response to low shear stress. Paclitaxel was unable to do this, perhaps because of its differing pharmacological mode of action or even its shorter drug-release kinetics as discussed in Stent factors [3].

“Thromborestenosis” phenomenon

“Thromborestenosis” is a term first described by Oikawa et al [96] to describe a novel theory in which chronic thrombus formation may play an integral part in the development of ISR following DES implantation. The uniqueness of this study was the combined use of intravascular ultrasound (IVUS), coronary angiography and histopathological analyses (taken by direct coronary atherectomy) in all patients who had presented with ISR following SES implantation. The major findings of this study were that, in patients presenting with ISR, the incidence of thrombus and fibrin deposition were substantially more frequently observed within ISR lesions associated with SES implantation (12 of 13 cases), as compared to BMS (2 of 8 cases), and that the thrombus seen was not only located at uncovered stent strut sites (if present) but also, more importantly, on covered stent strut sites (▶▶ Figure 7). A theory to explain the presence of neointimal thrombus put forward by the authors was that the neointima covering a SES strut site was potentially more thrombogenic.

Joner et al [26] have previously described evidence to support the concept of “thromborestenosis.” In 2 of 14 autopsy cases of patients who died of LST, evidence of ISR with superimposed thrombus was seen [26]. Further support comes from, Cook et al [55] who demonstrated evidence of the widespread presence of chronic thrombi, as evidenced by the presence of a chronic inflammatory response, within all thrombus aspirates taken at the time of emergency percutaneous coronary intervention (PCI) in patients presenting with very LST. This was in addition to the acute thrombus seen in all samples and “hypereosinophilia” (likely to be secondary to polymeric

hypersensitivity) observed in a proportion of aspirates [55].

Conversely, Rittersma et al [97] also showed evidence of chronic thrombi which was days to weeks old in at least 50% of 211 consecutive STEMI patients who had thrombus aspirates taken within 6 hours of onset of symptoms. Only 4 patients (2%) within the study group had prior PCI to the infarct-related artery, with the theory for the presence of older thrombi being speculated to be related to “clinically silent non-occlusive atherothrombotic events” in the preceding days to weeks prior to the clinical presentation of occlusive thrombosis.

As to whether “clinically silent non-occlusive atherothrombotic events” is also an explanation for the presence of chronic thrombi seen with ISR, or if this is related to “thromborestenosis”, is presently unclear.

Vessel remodelling

Implantation of DES in vessels that have previously undergone positive remodelling (the “Glagov” phenomenon [98]) secondary to a large plaque burden have been shown to be a significant predictor of restenosis (▶▶ Figure 8) [98-100]. Theoretically, the level of NIH formation would be the same between a non-remodelled and a remodelled vessel following stent implantation; however, the phenomenon of where the NIH would potentially grow post stent implantation would be significantly different between the two vessels. In vessels without positive remodelling, the NIH can be partially accommodated between the stent and the external elastic membrane (EEM), thereby limiting neointimal growth within the vessel lumen. Conversely, in a fully remodelled vessel, this process cannot occur to the same extent, and the bulk of the NIH growth would therefore preferentially occur within the stented lumen with a subsequent greater likelihood of restenosis.

Small vessels

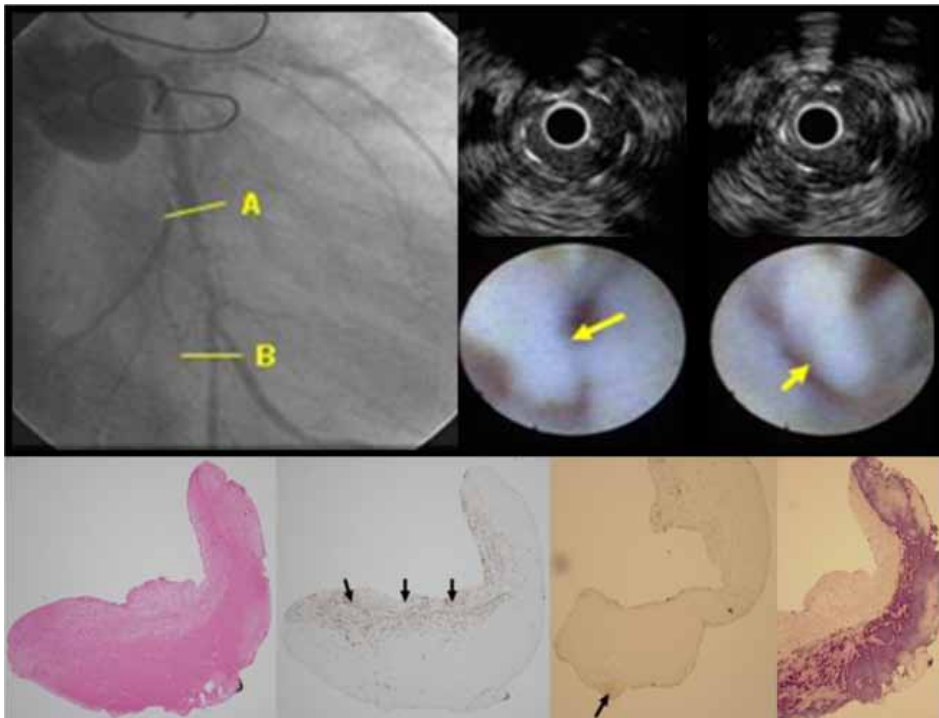
This is discussed in *Stent factors* with strut thickness.

FOCUS BOX 3

- Wall shear stress refers to the principle that blood flow is fastest (high shear stress) in the vessel centre and slowest (low shear stress) when closest to the vessel wall due to frictional forces exerted by the vessel endothelium. Low shear stress areas lead to the local accumulation of growth factors, mitogenic cytokines and platelets which may promote either atherosclerosis or neointimal formation after vessel injury
- SES, but not PES, are able to effectively inhibit the neointimal response in low shear stress areas
- “Thromborestenosis” describes the theory in which chronic thrombus formation may play an integral part in the development of ISR

FIGURE 7**Evidence of the "Thromborestenosis" theory?**

Upper image: in a patient with a diffuse long ISR in the mid circumflex (A-B), IVUS shows homogeneous isoechoic restenotic lesions (upper right images) and coronary angiography reveals flapping white thrombus attached to the restenotic segment (middle right images: yellow arrows). Lower image: histopathology of restenotic tissue taken by direct atherectomy from the restenotic site reveals (from left to right), homogeneous tissue and collagen matrix (seen on haematoxylin and eosin stain), smooth muscle cells in collagen matrix (black arrows) (α -SMA stain), few proteoglycans (versican and decorin stain) and rich fibrin corresponding to the homogeneous tissue. Reproduced with permission from Oikawa et al [96].

**Late restenosis**

Whereas parallel neointimal proliferation and healing with BMS have been shown to be complete after 3 to 6 months [101], potentially followed by a late lumen enlargement beyond one year, a different pattern of healing has emerged with early-generation DES. This has been characterised by delayed healing with an ongoing neointimal growth beyond 30 days in experimental studies [102] as previously described (Figure 5), and beyond 6 months in clinical studies [103]. Different mechanisms have been identified in the mechanisms of delayed neointimal growth and these are elaborated in the following paragraphs.

Decreasing drug dose

The antiproliferative drug concentration diminishes over time according to the individual elution profile of the different DES (see *Stent factors*): with decreasing drug dose, the antiproliferative inhibitive effect progressively declines. If the arterial healing is not terminated at the point in time when the drug elution has ceased, neointimal growth may continue to accrue (Figure 9).

Chronic inflammation

Chronic inflammation is a trigger for late neointimal growth. Animal studies have suggested that the inflammatory response among different DES is clearly distinct in terms of the pro-

FIGURE 8

The phenomenon of the increased likelihood of restenosis occurring in positively remodelled vessels. Red arrow indicates position where NIH can potentially grow since the NIH cannot be accommodated between the stent and the external elastic membrane (EEM). Adapted and reproduced with permission from Spanos et al. [230].

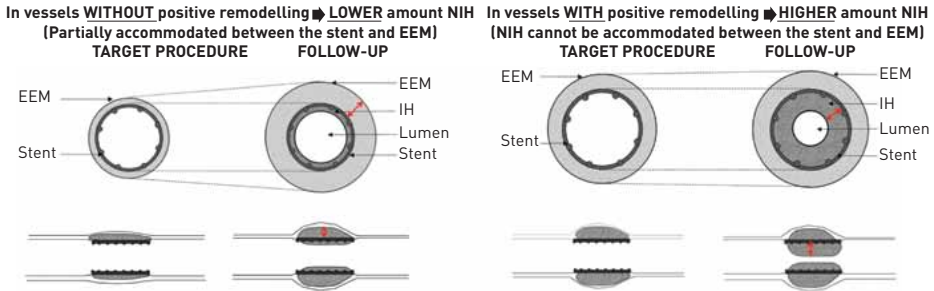
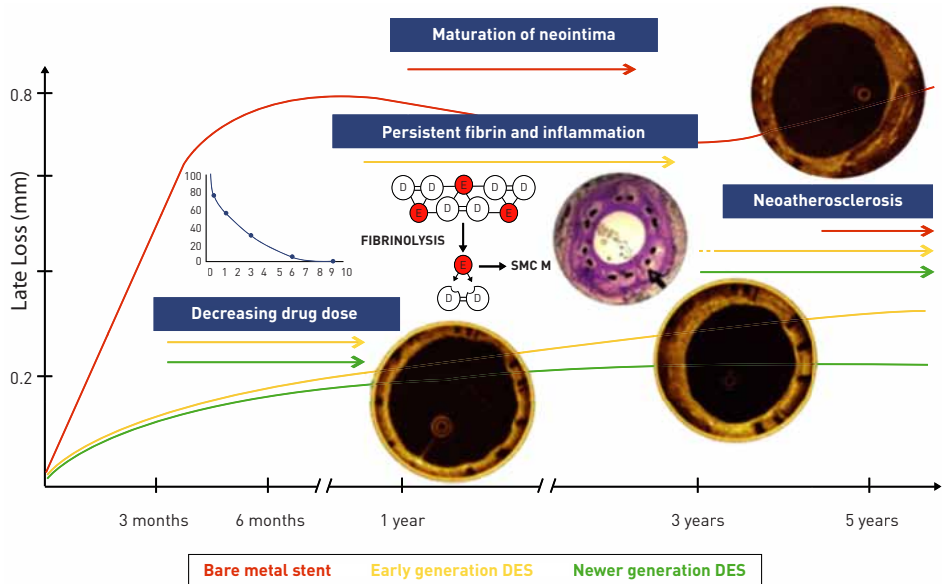


FIGURE 9

The different time courses of the neointimal growth (indicated by late lumen loss) for BMS, early and newer-generation DES are shown over a five-year period. Different mechanisms contributing to the late neointimal growth in DES are presented. In addition, a case example of a sirolimus-eluting stent showing delayed neointimal growth is depicted. SMC M: smooth muscle cell migration into neointima. D and E: D and E domains of fibrinogen. Arrow in histological cross-section depicts peri-strut inflammatory cell infiltrates. Reproduced [Figure and Figure legend] with permission from Räber et al [231].



portion of giant cells, granulomas, eosinophils, lymphocytes and fibrin deposition as previously described [26-30]. Carter et al compared SES and BMS in a porcine coronary artery model and found late neointimal formation between 30 and 90 days, which resulted in a similar amount of neointimal area at 90 days between SES and BMS, thus mitigating the initial suppression achieved with SES at 30 days [102]. Histological data documented a progressive increase in injury and inflammation scores between 30 and 180 days, probably representative of a chronic inflammatory response with a predominantly lymphocytic reaction with giant cells.

The presence of inflammatory reactions during the long-term time course following SES implantation was further corroborated by Virmani et al [104]. Histological evaluation of stented porcine coronary arteries demonstrated an intense circumferential granulomatous, eosinophil-rich inflammatory response during long-term follow-up (90 and 180 days) in SES, and to a lesser extent PES; conversely, inflammation was absent with BMS. PES as opposed to SES was further characterised by an increase in fibrin deposition. The presence of fibrin - which has been described in the vicinity of stent struts in experimental [104] and autopsy studies [105] is an initiator of smooth muscle cell migration and proliferation [106]. Porcine coronary models have demonstrated an increasing amount of fibrin in the long-term course (90 days), [104] which is analogous to delayed wound healing and excessive scarring. Delayed fibrinolysis is a stimulus to smooth muscle cell proliferation and excessive collagenous matrix deposition, leading to late restenosis.

The most likely culprits for the prolonged inflammatory reactions of the vessel wall are hypersensitivity reactions to the durable polymer. Durable polymers serve as a standard component of early-generation DES and are of importance as they facilitate drug delivery over a certain time (see *Stent factors*) [107]. Animal data have demonstrated that a peak in hypersensitivity reactions occurs only after the complete release of the drug (>60 days), supporting the notion that the durable polymer may be the more important cause [28].

Taken together, early-generation SES and PES showed distinct long-term vessel responses, which have not been described in BMS. Whereas SES may cause a granulomatous and eosinophilic reaction, PES is mainly characterised by fibrin deposition. Both of these inflammatory reactions may trigger a continued neointimal proliferation and thereby potentially cause late restenosis (Figure 9). Inflammatory reactions are most likely caused by the durable polymers which have made them the consequent targets for improving stent designs. Whether the strategy of more biocompatible polymers or biodegradable polymers will result in a lower inflammatory response and consequent lower late neointimal proliferation has yet to be demonstrated.

Neoatherosclerosis

Neoatherosclerosis is defined as the presence of atherosclerotic disease within the neointima of a stented segment, ranging from pathological intimal thickening with presence of intercellular lipid accumulations to ruptured/unruptured thin-cap fibroatheroma. It has been speculated that the presence of neoatherosclerosis, namely ruptured thin-cap fibroatheromas, may be responsible for the acute clinical presentation of patients suffering from late restenosis.

Nakazawa et al described in a pathology registry the incidence of neoatherosclerosis within 142 BMS, 81 SES and 76 PES post-mortem specimens [108]. The incidence of neoatherosclerosis was higher in DES (31%) as compared to BMS (16%, $p < 0.001$), whereas no meaningful differences were observed between the two early-generation DES. An important difference between BMS and early-generation DES was that the first occurrence of neoatherosclerosis occurred earlier with first-generation DES compared to BMS. Vulnerable plaques, namely thin-cap fibroatheroma (TCFA), were found in 1-4% of lesions without differences among stent types, but with a delayed occurrence in BMS as compared to early-generation DES.

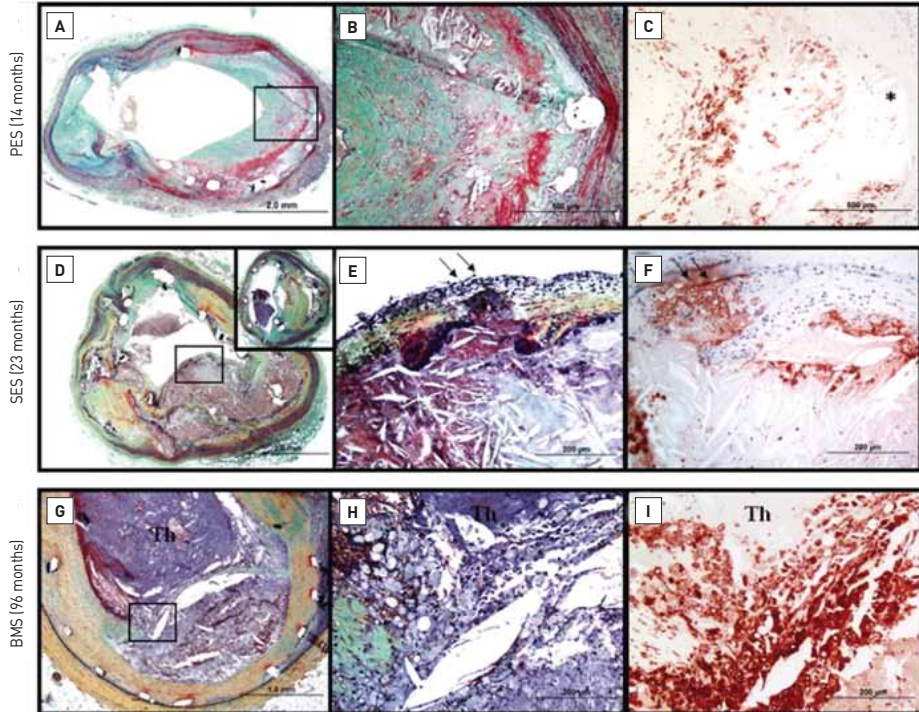
The underlying reason for the difference in the occurrence of neoatherosclerosis is currently speculative. The mechanisms of neoatherosclerosis in DES are likely to be different from the ones observed in BMS. DES have been associated with impaired re-endothelialisation and with a disturbed functionality of the neoendothelium. This potentially leads to the initialisation of the atherosclerotic cascade commencing with monocyte adhesion and migration into the neointima and an increased permeability of the endothelium for circulatory lipid migrating into the subendothelial matrix. Conversely, re-endothelialisation is faster and the endothelium exhibits a preserved functionality in BMS-treated segments, suggesting different mechanisms involved in the genesis of neoatherosclerosis. Nakazawa et al [108] speculated whether shear stress may be a major contributing explanatory factor, as evidenced by some differences in the longitudinal distribution of neoatherosclerosis, in particular an increased occurrence in the proximal part of BMS-treated segments.

Illustrative examples of histological cross-sections depicting neoatherosclerosis are provided in Figure 10 and two examples of OCT cross-sections displaying neoatherosclerotic lesions are shown in Figure 11.

To date, two *in vivo* studies have corroborated the aforementioned histopathological findings. Takano et al compared the appearances of neointimal tissue in BMS-treated lesions at 6 months and separate BMS-treated lesions more than 5 years previously [109]. Whereas neoatherosclerosis was absent in the early group, a transformation of the neointima during long-term follow-up was noted with lipid-rich intima (68%),

FIGURE 10

(A) Foamy macrophage clusters in the peri-strut region of sirolimus-eluting stents (SES) implanted for 13 months ante mortem are seen. **(B)** Fibroatheroma with foamy macrophage-rich lesion and early necrotic core formation in SES of 13 months' duration. **(C)** Fibroatheroma with peri-strut early necrotic core, cholesterol clefts, surface foamy macrophages, and early calcification [arrows] in SES at 13 months. **(D)** Peri-strut late necrotic core in the neointima characterised by large aggregates of cholesterol cleft in SES at 17 months. **(E)** Fibroatheroma with calcification in the necrotic core in SES of 10 months' duration. **(F)** A peri-strut calcification [arrows] with fibrin in SES of 7 months' duration. **(G and H)** A low-power magnification image **(H)** of a severely narrowed bare metal stent (BMS) implanted 61 months with a thin-cap fibroatheroma. Note macrophage infiltration and a discontinuous thin fibrous cap in a high-power magnification image **(G)**. **(I)** A low-power magnification image shows a plaque rupture with an acute thrombus that has totally occluded the lumen in BMS implanted for 61 months ante mortem. **(J)** A high-power magnification image shows a discontinuous thin-cap with occlusive luminal thrombus. Reproduced [Figure and Figure legend] with permission from Nakazawa et al [232].



calcifications (10%), intimal disruptions (38%), thrombi, and neovascularisation (52%). These results were confirmed in another OCT study by Habara et al who evaluated the neointimal composition in BMS-treated patients presenting with early (<1 year) versus late (>1 year) clinical restenosis [110]. Whilst the neointima appeared to be relatively normal in the early restenosis group, a significant proportion of late restenosis lesions presented with atherosclerotic changes, thrombi or neointimal tears. An extension of these findings to DES was obtained by Kang et al [111] in 50 patients presenting with clinical restenosis who underwent optical coher-

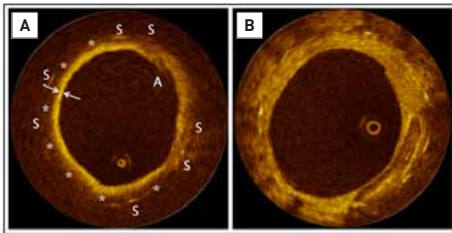
ence tomography (OCT), intravascular ultrasound (IVUS) and IVUS-VH (IVUS-virtual histology) after a mean duration of 32 months post DES implantation. The main finding was that 90% of all patients exhibited a lipid-rich intima, indicating that atherosclerotic transformation was indeed highly predominant in delayed restenotic lesions. Whilst a majority of patients with stable angina presented with a structurally intact intima, more than 50% of patients presenting with unstable clinical symptoms showed evidence of a ruptured and thrombosed thin-cap fibroatheroma.

FIGURE 11

This figure depicts 2 OCT cross-sections obtained 5 years following implantation of a sirolimus-eluting stent (Panel A) and a paclitaxel-eluting stent (Panel B). In Panel A, a signal-poor region between 4 and 1 o'clock is noted, suggestive of a lipid pool/necrotic core that is covered by a thick fibrous cap with a high signal intensity [100 microns at the location indicated by arrows). Due to the high attenuation of the lipid pool/necrotic core (*), the underlying stent struts are displaying an unusual low signal without shadowing (S). Taken together, the image suggests the presence of a thick-cap fibroatheroma within neointimal tissue. Note the artefact (A) at 2 o'clock.

In Panel B, the stent struts are displaying a much more intense signal with a typical shadowing. Between three and 6 o'clock, a sharply delineated region with low backscattering and low attenuation is noted, suggesting a calcific pool within the neointimal tissue.

Note that, in both images, there is no significant narrowing of the lumen, which refers to the fact that neoatherosclerosis does not necessarily lead to late restenosis. Image courtesy of Dr Lorenz Raber and Professor S. Windecker, Bern, Switzerland.



Taken together, the evidence derived from histology and *in vivo* imaging studies suggests that neoatherosclerosis occurs during the long-term time course after both BMS and DES implantation and can contribute to late restenosis.

Furthermore, neoatherosclerosis seems to be more prevalent in lesions causing symptomatic restenosis. The neoatherosclerotic transformation of the neointima potentially leads to the formation of (neo) thin-cap fibroatheromas, which can rupture and trigger an unstable clinical presentation. Therefore, in-stent neoatherosclerosis should also be considered as a differential diagnosis in patients presenting with stent thrombosis.

Angiographic and intravascular imaging data on late neointimal growth and restenosis in humans

Longitudinal angiographic and angioscopic follow-up series in patients implanted with BMS have observed late improvements in lumen diameter and an increased transparency (defined according to the visibility of the majority of the stent) respectively at three years of follow-up, suggesting late lumen remodelling on the basis of fibrotic maturation and regression of the neointima. Kimura et al reported a significant improvement in MLD from 1.94 ± 0.48 mm at 6 months to 2.09 ± 0.48 ($p \leq 0.001$) at 3 years [112]. A longitudinal angioscopic evaluation in 12 patients following BMS implantation exhibited a change in neointimal appearance from 6 months to 3 years characterised by an increase in transparency [113]. A prolongation of the angiographic follow-up of the above-mentioned study by Kimura et al demonstrated late re-narrowing beyond 4 years, [114] suggesting a triphasic pattern following BMS implantation: 1) pronounced neointimal proliferation within the first 6 months, followed by 2) a lumen enlargement with maturation of the neointima, and finally 3) leading to a re-narrowing, probably paralleled by an atherosclerotic transformation as previously described (Figure 9).

In contrast to BMS, angiographic and IVUS studies of early-generation DES documented a continued increase in neointimal formation beyond the time point at which neointimal proliferation is halted in BMS. Table 2 provides an overview of IVUS studies that assessed serial changes in neointimal volumes among different stent types. Whereas in BMS no increase in neointimal volume was observed, early-generation DES have been associated with an on-going growth up to 4 years. Notably, all of these studies have only provided a snapshot within the first year after implantation, and at a single time point beyond one year (e.g., at 2, 3, or 4 years). In view of this methodological limitation, there is no definite answer in respect to the exact dynamics of late neointimal growth, and presently it remains unclear whether

TABLE 2

Serial intravascular ultrasound (IVUS) assessment of neointimal volume in patients treated with BMS or DES during long-term follow-up

TRIAL OR FIRST AUTHOR	STENT TYPE	PATIENT NUMBER	4-6 MONTHS (MM ³)	1 YEAR (MM ³)	2 YEARS (MM ³)	4 YEARS (MM ³)	P-VALUE
TAXUS II [216]	BMS	77	28.7±33.2	na	23.9±25.1	na	0.02
Aoki et al [217]	SES	23	2.1±1.7	3.8±3.3	7.0±6.7	8.4±5.8	<0.0001
TAXUS II [216]	PES-SR	43	9.4±12.1	na	13.6±11.3	na	0.018
TAXUS II [216]	PES-MR	41	10.7±15.8	na	16.9±17.3	na	0.013
Collet et al [218]	SES	12	na	2.5±3.7	na	7.7±6.7	na
Collet et al [218]	BES	13	1.2±2.0	na	na	1.2±4.9	na

BMS: bare metal stent; SES: sirolimus-eluting stent; PES-SR: paclitaxel-eluting stent slow release; PES-MR: paclitaxel-eluting stent moderate release; BES: biolimus-eluting stent using biodegradable polymer; na=not applicable.

the continued growth is halted at 2, 3, or 4 years, or whether it continues beyond 4 years. Furthermore, serial IVUS data on newer-generation DES are, to date, scarce.

Angiographic data

Table 3 provides an overview of angiographic long-term studies investigating delayed late loss, namely the difference in late loss between 6-12 months and at long-term follow-up beyond one year.

In SIRTAX LATE, 293 patients underwent serial angiography at baseline, 8 months and 5 years (SES=142, PES=151) [103]. Overall, an ongoing reduction of the minimal lumen diameter was noted between 8 months and 5 years, resulting in a late loss of 0.33 ± 0.66 mm. Whilst SES was superior in terms of late loss at 8 months, differences between PES and SES were balanced at five years. This was explained by a late catch-up observed with SES, namely a numerically higher delayed late loss with SES (SES 0.37 ± 0.73 mm, PES 0.29 ± 0.59 mm, $p=ns$). In keeping with the findings from SIRTAX LATE, Byrne et al demonstrated

in a large, unpaired angiographic patient cohort that the late loss at 6-8 months further accrued with first-generation DES (PES and SES) [115]. A numerically higher increase of late loss was consistently shown with SES (0.17 ± 0.50 mm) compared to PES (0.13 ± 0.50 mm). As the absolute increase in late loss from 8 months to 2 years observed by Byrne et al was numerically lower than the increase from 8 months to 5 years in SIRTAX LATE, one may speculate that neointimal growth continued beyond 2 years. Interestingly, a third group in the study of Byrne et al, composed of polymer-free DES, exhibited only a minimal delayed late loss of 0.01 ± 0.42 mm, suggesting that polymer-free stents may be less affected.

Newer-generation drug-eluting stents

Histological data comparing the long-term inflammatory responses of newer-generation DES using durable polymer are to date scarce. As they relate to devices using biodegradable polymer technology for drug delivery, it will be of interest to investigate how the bio-absorption process, which is

TABLE 3 Serial angiographic assessment of late loss following BMS or DES implantation during long-term follow-up

FIRST AUTHOR	STENT TYPE	NUMBER OF LESIONS	LATE LOSS SHORT TERM (BL-FUP1) (MM)	LATE LOSS LONG TERM (BL-FUP 2) (MM)	DELAYED LATE LOSS/GAIN (MM)
Asakura et al [113]	BMS	12	6 mo 0.74 ± 0.32	3 yrs 0.51 ± 0.26	gain : 0.23
Kimura et al [112]	BMS	72	6 mo 0.61	3 yrs 0.46	gain : 0.15
Byrne et al [115]	PF- RES SES PES	375 704 501	6-8 mo 0.46 ± 0.57 0.25 ± 0.50 0.46 ± 0.59	2 yrs 0.47 ± 0.59 0.37 ± 0.60 0.55 ± 0.66	loss : 0.01 ± 0.42 loss : 0.17 ± 0.50 loss : 0.13 ± 0.50
Räber et al [219]	SES PES	179 203	8 mo 0.09 ± 0.18 0.13 ± 0.22	5 yrs 0.45 ± 0.73 0.42 ± 0.62	loss : 0.37 ± 0.73 loss : 0.29 ± 0.59
Kyung Woo Park et al [220]	SES PES	24 23	6-9 mo* 0.24 0.55	2 yrs* 0.50 0.65	loss : 0.26 loss : 0.10
Duk-Woo Park et al [221]	BMS LD-PES HD-PES	17 18 20	6 mo* 0.80 0.50 0.30	2 yrs* 0.70 0.90	gain : 0.40 loss : 0.20 loss : 0.60
Sousa et al [222]	FR-SES SR-SES	13 13	1 yr 0.08 ± 0.31 0.08 ± 0.23	4 yrs 0.41 ± 0.49 0.09 ± 0.23	loss : 0.33 loss : 0.01

PF: polymer free; SES: sirolimus-eluting stent; PES: paclitaxel-eluting stent; BMS: bare metal stent; LD: low dose; HD: high dose; FR: fast release; SR: slow release; mo: months; yrs: years ; where SD is missing, values have been calculated using MLD.

a known trigger for at least a transient inflammation, may enhance neointimal proliferation during the long-term follow-up [116]. With polymer-free DES, few animal studies have reported a decrease in both inflammatory reactions and fibrin deposition up to 180 days, with a subsequent lower extent of angiographically defined delayed late loss [115].

Clinical significance of late catch-up

The most relevant question emerging from the angiographic and intravascular imaging data is whether delayed neointimal proliferation translates into a clinically meaningful need for target lesion revascularisation (TLR) during long-term follow-up, reducing the early efficacy benefit of DES. Long-term results from randomised controlled trials of early and newer-genera-

tion DES consistently show a yearly TLR rate of less than 2% beyond one year, without meaningful differences compared to BMS (➤ Table 4). After subtraction of stent-thrombosis-related TLR - which are at least in part not related to restenosis - the annual TLR rate is as low as 1–1.5%. This relatively low frequency of late TLR is explainable by the magnitude of the delayed late loss (between 1 and 5 years = 0.30–0.40 mm), which is below the threshold that usually causes clinically significant restenosis. Against this backdrop it is reasonable to conclude that early-generation DES delay neointimal formation and healing during the long-term course, but without significantly compromising the early benefit in efficacy. Prolonged neointimal proliferation, however, may be a useful marker to assess the delay in healing. The presence of delayed healing

TABLE 4 Target lesion and stent thrombosis rates beyond one year in BMS, early and newer-generation DES

TRIAL ACRONYM	STENT TYPE AND NUMBER OF PATIENTS	CLINICAL SETTING	FOLLOW-UP PERIOD (YEARS)	INCIDENCE OF TLR UP TO LATEST FOLLOW-UP (%)	INCIDENCE OF TLR BETWEEN 1-5 YEARS (%)	ANNUAL TLR RATE BETWEEN 1 YEAR AND MAXIMUM FOLLOW-UP (%)	ARC DEFINITION VLST UP TO MAXIMUM FOLLOW-UP (%)	ANNUAL VLST INCIDENCE (%)
EARLY-GENERATION DES (RCTS WITH 5-YEAR FOLLOW-UP)								
RAVEL [223]	SES (n=120) vs. BMS (n=118)	Stable CAD	5		10.3 vs. 1.7*†	2.6 vs. 0.4*	0.8 vs. 0.8 p=1.0	0.2 vs. 0.2*
SIRIUS [224]	SES (n=533) vs. BMS (n=525)	Stable CAD	5	9.4 vs. 24.2 p<0.001	4.5 vs. 4.0 p=0.76	1.1 vs. 1.0*	0.8 vs. 0.4 p=0.56	0.2 vs. 0.1*
TAXUS IV-SR [225]	PES (n=651) vs. BMS (n=643)	Stable and unstable CAD	5	16.4 vs. 4.3 p<0.001	6.0 vs. 8.0*	1.5 vs. 2.0 p=0.26	0.8 vs. 0.4*	0.2 vs. 0.1 p=0.49
SIRTAX LATE [103]	SES (n=503) vs. PES (n=509)	Allcomers	5	13.1 vs. 15.1 p=0.29	7.4 vs. 4.9 p=0.16	2.0 vs. 1.4 p=0.17	2.6 vs. 2.4 p=0.83	0.7 vs. 0.6 p=0.85
NEWER-GENERATION DES (RCTS WITH AT LEAST 3 YEARS OF FOLLOW-UP)								
LEADERS (Wykrzyzkowska, 2011 #30)	BES (n=857) vs. SES (n=850)	Allcomers	3	7.6 vs. 8.8 p=0.38	2.7 vs. 3.4 p=0.41	1.3 vs. 1.7 p=0.56	0.3 vs. 0.9 p=0.09	0.1 vs. 0.4 p=0.12
ENDEAVOR pooled [226]	ZES (n=2,132)	Stable and unstable CAD	3	6.7	1.3	0.65*	0.8‡	0.4‡
SPIRIT II, III pooled [227]	EES (n=892) vs. PES (n=410)	Stable CAD	3	5.4 vs. 9.1	2.5 vs. 3.7 p=0.27	1.3 vs. 1.9*	0.2 vs. 0.5 p=0.59	0.1 vs. 0.3*

TLR is ischaemia-driven if available. *Unpublished data that was calculated using outcomes at 1 year and at the time point of the maximal follow-up, therefore no p-values † TLR between 9 months and 5 years. ‡ARC definite or probable stent thrombosis. BMS: bare metal stent; SES: sirolimus-eluting stent; PES: paclitaxel-eluting stent; ZES: zotarolimus-eluting stent; na: not applicable; VLST: very late stent thrombosis; TLR: target lesion revascularisation; ENDEAVOR: randomised controlled trials of the Medtronic Endeavor drug-eluting coronary stent system. LEADERS: limus eluted from a durable versus erodible stent coating. RAVEL: a randomised comparison of a sirolimus-eluting stent with a standard stent for coronary revascularisation. SIRIUS: sirolimus-eluting stent in de novo native coronary lesions. TAXUS II-SR: treatment of de novo coronary disease using a single paclitaxel-eluting slow release stent. SPIRIT: a clinical evaluation of the XIENCE V everolimus-eluting coronary stent system in the treatment of patients with de novo native coronary artery lesions. SIRTAX LATE: sirolimus versus paclitaxel-eluting stent for coronary revascularisation LATE trial.

may contribute to a mechanistic explanation of the ongoing risk of very late stent thrombosis as it has been identified as the principal pathological finding in an autopsy study distinguishing late thrombosed from patent early-generation DES [117].

Newer-generation DES, such as an everolimus-eluting stent, have shown superior clinical safety and efficacy outcomes when compared to PES up to 2 years [118,119]. The annual incidence of late (>1 year) TLR in patients included in SPIRIT IV amounted to 2.1% in EES and 2.9% in PES. Patients included in the allcomers study COMPARE showed 0.9% late TLR in the EES and 1.5% in the PES-treated patient group, respectively. Although there was no significant statistical difference in late TLR in both studies, it is important to note the continued separation of the TLR curves beyond 1 year. This continued separation suggests a potential decrease in late TLR with the use of newer-generation DES as compared to the early-generation PES, potentially due to a less extensive inflammatory reaction.

Functional stent coverage by endothelium and vasomotor response

As a consequence of stent implantation, there is a substantial reduction in the integrity of the vessel endothelium within the treated vessel segment. Furthermore, histological studies have confirmed that recovery of the endothelial cellular layer is significantly delayed following DES compared to BMS implantation [120]. It is commonly accepted that the delay in the recovery of the endothelial cellular layer following DES implantation is a consequence of the applied antiproliferative drug, which non-selectively inhibits mitosis of smooth muscle cells, fibroblasts and endothelial cells. The endothelial cell layer of the vessel wall has, however, a vital role in mediating vasomotion of the vessel wall by the excretion of nitric oxide (NO).

Notably, several studies have associated a lower vasoreactivity in the vessel segments adjacent to implanted early-generation DES compared to BMS [121-123]. Within these studies different methodologies have been used to induce vasomotion of the vessel segment edges, namely physical stress (e.g., bicycle stress test), rapid atrial pacing, and high dose acetylcholine infusion. Newer-generation DES, integrating features such as reduced strut thickness, lower drug dose and a more biocompatible polymer, have allowed for less traumatic delivery and improved biocompatibility of the stent. These features may be the reasons why further studies have shown an improvement in the vasoreactivity of the adjacent vessel segments in implanted newer-generation DES, compared to earlier-generation DES [124,125].

To date, the magnitude of the correlation between endothelial restoration within the stented segment of DES and the vasomotor response in the adjacent vessel segment remains unclear.

The introduction of intravascular optical coherence tomography (OCT) technology has permitted the assessment of vessel stent strut coverage, as an indicator of endothelial integrity. Fuji et al [126] assessed strut coverage 3 months after zotarolimus-eluting stent implantation and demonstrated a correlation between the degree of stent coverage and the vasomotor response assessed by acetylcholine infusion. Furthermore, an inverse correlation of the rate of uncovered struts with the vasomotor capacity of the vessel wall was shown, thus supporting the hypothesis of a relationship between restoration of the stent vessel endothelialisation and vasomotor response following DES implantation.

FOCUS BOX 4

- Three principal factors may be responsible for the formation of late restenosis: 1) decreasing drug dose; 2) chronic inflammatory reactions and persistent fibrin deposition; 3) neoatherosclerosis
- Early-generation SES and PES, but not BMS, have been associated with chronic inflammation and fibrin deposition during the long-term time course
- Neoatherosclerosis occurs earlier and more frequently in DES compared to BMS
- Incomplete re-endothelialisation and impaired functionality of the endothelium may be the source of neoatherosclerosis in DES, whereas shear stress has been suggested to be a relevant contributor in BMS
- Lipidic transformation of the neointima can lead to the formation of thin-cap fibroatheroma, which can be responsible for unstable presentations of restenosis
- Early-generation SES and PES have been associated with a delayed late loss of 0.3-0.4 mm between 1-5 years in angiographic long-term studies without significant differences between the two devices. Data on newer-generation DES are scarce
- The small magnitude of delayed late loss observed with early-generation DES does not translate into clinically significant late TLR rates (incidence <1.5% per annum) and does not compromise the early benefit in efficacy achieved with the introduction of DES
- Angiographic and clinical data suggest that some of the newer-generation DES (e.g., polymer-free DES) may be less vulnerable to late restenosis

STENT FACTORS

Polymer release kinetics

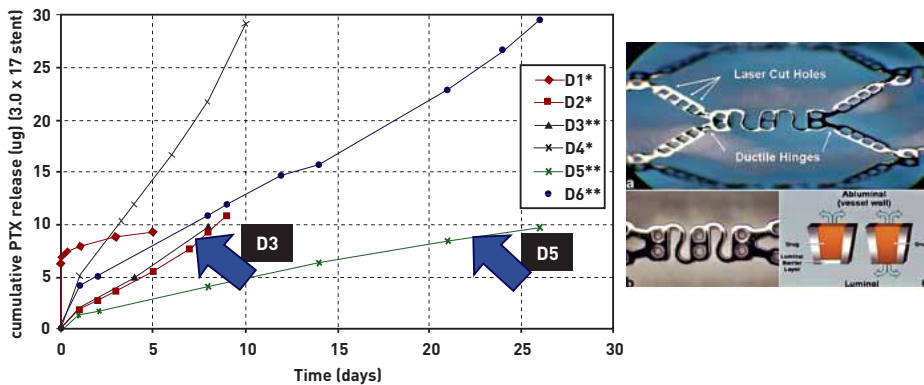
Polymer release kinetics play a key and fundamental role in the prevention of restenosis with the suggestion that it is not necessarily the total dosage of the antiproliferative drug delivered to the vessel wall that is important but more the kinetics

FIGURE 12

The PISCES trial involving the use of the Conor stent and six different polymer-drug-release formulations in humans

In this example, 10 mcg of paclitaxel released over 10 days (D3) following DES implantation appeared to have little effect on NIH production, whereas the same dosage of the drug released over a 30-day (D5) period led to a profound reduction in NIH, with a more than halving (57% reduction) of the rate of LLL. Interestingly, 30 mcg of the same drug released over a 10-day period (D4) was also less effective. Corresponding tables and graphs of the drug release kinetics are shown. The design of the Conor stent is also illustrated (lower right image). Adapted and reproduced with permission from Serruys et al [127].

	D1	D2	D3	D4	D5	D6
Dose (µg/17-mm stent)	10	10	10	30	10	30
Duration of elution (days)	5	10	10	10	30	30
Direction of elution	Abluminal and luminal (bidirectional)	Abluminal and luminal (bidirectional)	Abluminal (mural)	Abluminal and luminal (bidirectional)	Abluminal (mural)	Abluminal (mural)
Key	10/5b	10/10b	10/10/m	30/10b	10/30/m	30/30/m



of the release of the drug. The PISCES trial [127] was the first human study to demonstrate this principle involving the use of the Conor stent and six different polymer-drug release formulations. The main finding of the trial was that the duration of the drug release had a far greater impact on the inhibition of NIH than the dose of the drug delivered (➤ Figure 12).

The polymer-free biolimus A9-eluting stent, with 2 differing doses of biolimus, has been investigated in animal models [128] and the first-in-human BIOFREEDOM study [129]. Initial studies in animals indicated that the lower (112 µg/per 14 mm of stent length) and higher dose (225 µg/per 14 mm of stent length) biolimus A9-eluting stents have equivalent effects on the NIH response and both have a superior late reduction in NIH as compared to SES at 180 days [128]. In the subsequent BIOFREEDOM study [129] in humans, powered to test for non-inferiority, statistical equivalency was achieved in all 3 groups with an in-stent late lumen loss reported as 0.17 mm (“standard-dose biolimus” group - 15.6 µg/per mm of stent length), 0.22 mm (“low-dose biolimus” group - 7.8 µg/per mm of stent length) and 0.35 mm for the

Taxus stent with no differences in MACE or reported cases of stent thrombosis in all 3 groups.

It would therefore appear that a certain threshold of drug needs to be delivered to the vessel wall over a sustained, prolonged period of time, during the process of endothelialisation of the DES, in order to “dampen” down the inflammatory response and limit NIH formation. This is supported by molecular biology studies which have suggested that genes responsible for the proliferative response potentially remain active for a period of up to 21 days after vessel injury [130]. Achieving the fine balance between the drug type, dosage and delivery over the appropriate time are therefore crucial factors in DES design.

In addition, an early peak in drug release may theoretically be of importance to inhibit the early inflammatory reaction of the vessel wall caused by the traumatic vessel wall injury following stent implantation. The early suppression of injury-induced inflammation may result in an antithrombotic effect, which may explain the decreased risk of acute stent thrombosis observed in a recent study comparing the newer-

generation everolimus-eluting stent with a bare metal stent for primary PCI [131].

Type of DES? Type of drug?

Differences relating to first-generation DES are discussed in the Late restenosis section of *Arterial factors*. Data from the SCAAR registry, involving >35,000 patients implanted with four different types of DES (ZES, SES, Taxus® Express® [Boston Scientific] and Liberté® [Boston Scientific]) in real-world practice at 2-year follow-up, showed that the rates of restenosis with DES implantation were significantly higher in diabetics and that important differences existed in the efficacy of differing brands of DES to reduce restenosis [21]. In particular, the restenosis rates with Endeavor® (Medtronic, Inc., Minneapolis, MN, USA) were twice as high in diabetics as compared to other DES types. Higher restenosis rates were also evident in diabetics with Endeavor (RR: 1.77, 95% CI: 1.29 to 2.43) and SES (RR: 1.25, 95% CI: 1.04 to 1.51) when compared to non-diabetics. Five-year unpublished follow-up data from the SCAAR registry continued to demonstrate differences in the efficacy of the first and second-generation DES in reducing rates of stenosis, with a trend for better outcomes seen after nearly 2 years' use of the everolimus-eluting stent.

The EES releases 80% of the drug within 30 days and nearly all the drug within 4 months. In the Spirit I, II, and III trials, a LLL of 0.10, 0.16, and 0.33 mm and TVR rates of 3.8%, 3.4%, and 4.6% were observed at 6, 12, and 24 months, respectively [43]. Conversely, the Endeavor reported a LLL of 0.60 mm and 0.67 mm and TVR of 6.3% and 4.5%, respectively, in the Endeavor III and IV trials at 12 months. The Endeavor, however, elutes 95% of its drug very rapidly (within 14 days): this is highly likely to be the main reason for the poorer results seen.

The next-generation Endeavor® Resolute stent (Medtronic, Inc.), consisting of the same cobalt chromium metallic platform (Driver BMS; Medtronic, Inc.) and the same drug (zotarolimus) as the Endeavor stent, but incorporating the BioLinX™ polymer - an enhanced triple polymer combining a hydrophobic coating covering the stent, a hydrophilic, more biocompatible polymer on the abluminal surface with a third polymer binding the previous two polymers - allowed for substantially longer polymer drug release kinetics (180 days), compared to 14 days with the Endeavor stent. The Endeavor Resolute stent reported an in-stent LLL of 0.12, 0.22, and 0.27 mm at 4, 9, and 13 months, respectively, with angiographic equivalency (LLL 0.19 mm) in terms of meeting the criteria for non-inferiority being met when compared with EES. Equivalency in the 12-month primary endpoint of target lesion failure (a composite of cardiac death, target vessel

MI, and clinically driven target lesion revascularisation [8.2% versus 8.3%]) and a slight increase in the rate of definite stent thrombosis (1.2% versus 0.3%, $p=0.01$) were also seen [132].

Type of drug

Based on the vast experimental and clinical evidence associating inflammation with restenosis as previously discussed, multiple immunosuppressive and antiproliferative drugs - such as dexamethasone, actinomycin D, cytochalasin D, 17-beta-estradiol, mycophenolic acid, and angiopiptin - have been investigated for their effect in inhibiting the pathway of NIH [133,134]. As an example, methylprednisolone, although shown to be promising in a porcine model [135], demonstrated a restenosis (>50% diameter stenosis at follow-up) rate of 13.3% and a LLL of 0.45 mm at follow-up in the STRIDE (Study of anti-restenosis with BiodivYsio dexamethasone-eluting stent) European Study [136]. The very short release profile of the drug - almost completely eluted in the first 24 hours after deployment - no doubt had a strong influence on the clinical effect of the drug.

The drugs that have been demonstrated to have superior performance in a consistent and reproducible fashion both in preclinical investigations and in clinical trials are sirolimus (rapamycin) and paclitaxel in first-generation stents, and the limus family of drugs (which includes sirolimus) in second-generation DES [133,134]. Although polymer release kinetics are crucial to the antiproliferative effects of these drugs as previously described, because of the differing and potentially more potent mechanisms of action of the limus family of drugs compared to paclitaxel, the limus family of drugs are thought to deliver a more sustained antiproliferative NIH effect [133,134]. Furthermore, in the randomised PAINT trial, Lemos et al. [137] conducted a head-to-head comparison of 2 DES with the same metallic stent platform and biodegradable-polymer carrier but releasing either sirolimus or paclitaxel, and a BMS of the same metallic platform. Nine-month in-stent late loss was significantly more favourable towards sirolimus (paclitaxel: 0.54-0.44 mm, sirolimus: 0.32-0.43 mm, vs. BMS: 0.90-0.45 mm, respectively, $p<0.01$) in the 274 patients studied.

New-generation DES, such as the everolimus-eluting stent (XIENCE; Abbott Vascular) has shown superiority compared to the Taxus PES and shown itself to be a powerful independent predictor of 2-year freedom from ischaemia-driven target lesion revascularisation (hazard ratio: 0.59 [95% CI: 0.47-0.74], $p=0.0001$), ischaemia-driven target vessel revascularisation (0.70 [0.58,0.84]; $p=0.0002$), myocardial infarction (hazard ratio: 0.54 [95% CI: 0.41-0.71]; $p=0.0001$) and MACE (hazard ratio: 0.64 [0.54, 0.77]; $p<0.0001$) [138]. Furthermore, the biolimus-eluting stent with a biodegrad-

FIGURE 13

The modelling of the impact of different late losses on follow-up binary angiographic restenosis after PCI in coronary segments with small (<2.75 mm), medium (2.75–3.25 mm), and large (>3.25 mm) reference vessel diameter. Reproduced [Figure and Figure legend] with permission from Biondi-Zoccai et al [146].

RISK OF BINARY ANGIOGRAPHIC RESTENOSIS AFTER PERCUTANEOUS CORONARY INTERVENTION ACCORDING TO REFERENCE VESSEL DIAMETER OF THE TARGET SEGMENT			
	SMALL (<2.75 mm)	MEDIUM (2.75-3.25 mm)	LARGE (>3.25 mm)
Balloon-only PTCA	35-55%	25-40%	20-35%
Bare metal stents	25-50%	15-35%	15-20%
Drug-eluting stents with			
relatively high late loss (e.g. Endeavor™)	30-35%	20-30%	5-12.5%
medium late loss (e.g. Taxus™)	20-25%	10-20%	2.5-7.5%
low late loss (e.g. Cypher™ or Xience™)	10-15%	5-10%	0-5%

Data from Agostoni et al, C-SIRIUS, ENDEAVOR-2, ENDEAVOR-3, MICROSCOPE, SES-SMART, SIRIUS, SIRIUS, SPIRIT-2, SPIRIT-3, TAXUS-5, and TAXUS-6, or estimated from other unpublished sources

able polymer has demonstrated non-inferiority to the SES (Cypher) at up to 4 years follow-up [139,140]. It is likely that a combination of favourable polymer release kinetics and the limus-based drug are reasons for the more advantageous clinical effects seen. Conversely, the Endeavor DES, eluting the limus-based zotarolimus drug, led to unfavourable clinical outcomes due to the very short polymer release kinetics (14 days) as previously discussed.

Stent gap, non-uniform strut distribution and drug deposition

Takebayashi et al [141] classically described the number and distribution of DES struts, as identified by IVUS, as being independent significant risk factors (fewer struts and non-uniform stent strut distribution) for NIH formation and the subsequent risk of restenosis. Non-uniform DES strut distribution has been suggested as being attributable to features such as stent design (e.g., open versus closed cell), stent gap, vessel curvature, coronary bifurcations, ostial lesions, stent underexpansion or overexpansion, polymer peeling, and stent fracture.

Small vessels and strut thickness

Small coronary artery disease is a recognised challenging subset within the field of coronary artery intervention with significant and unacceptable risks of restenosis seen with both POBA and BMS [142-145]. A meta-analysis [146] of the use of DES in small vessel disease demonstrated that both late

loss and binary restenosis were largely dependent on the type of DES implanted (●) Figure 13).

Mechanisms suggested to explain the poorer outcomes associated with small vessels include: (1) a high degree of vessel stretch and injury, (2) a smaller post-procedural lumen area, and (3) a higher metal density [147]. The overstretch theory is, however, controversial, with evidence suggesting a possible adverse effect with increased NIH [119,120], no significant effect [148], or even potential benefit [142,148]. The latter beneficial effects have been proposed to be related to a higher balloon-to-artery ratio, the so-called bigger is better paradigm (see Implantation factors), leading to appropriate apposition of the stent to the vessel wall.

Thicker stent struts have been linked to an increased risk of restenosis with BMS [149] and small vessels [147,150,151]. The underlying rationale is that a thinner stent strut would have less of a “footprint” on the vessel wall with a consequential reduced inflammatory response. With DES, however, a complex relationship exists between the strut material and characteristics, stent design, polymer type, and drug release kinetics. Both Cypher and XIENCE appear to have the lowest risk of binary restenosis in small vessels, despite a large disparity in stent strut thicknesses (approximately 150 µm versus 90 µm); moreover, Endeavor had the worst outcomes despite its strut thickness being approximately 10 microns more than the XIENCE V® [146]. A fairer comparison perhaps would be between the Taxus Liberté and Express as both contain identical metallic platform materials, polymer coatings and drug concentrations (1 µg/mm² of paclitaxel), except that the Taxus Liberté contains thinner struts, more flexible cell geometry, and uniform cell distribution. In the SCAAR registry, the Taxus Express was shown to have a mild but significantly higher adjusted risk of restenosis compared to Taxus Liberté (RR: 1.32, 95% CI: 1.10-1.60).²¹

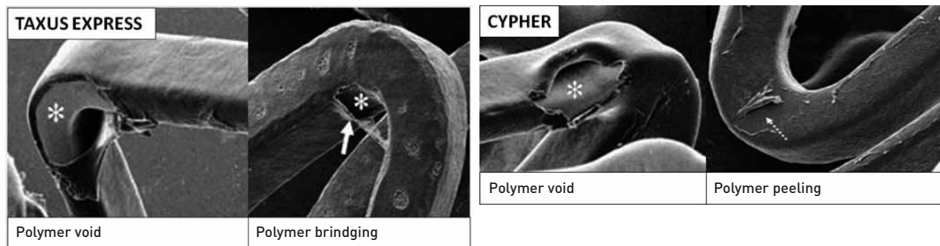
“On” and “off” label use of DES

The Strategic Transcatheter Evaluation of New Therapies (STENT) Group is the largest, multicentre, prospective registry involving >15,000 patients to have evaluated the late outcomes associated with DES implantation in the United States [152]. This compared on-label (short de novo lesions in coronary arteries measuring >2.5 mm and <3.5 mm for SES or <3.75 mm PES) and off-label (ostial, left main stem, chronic total occlusion, saphenous vein graft, small or large vessels/multivessel, STEMI, ISR lesions) indications for DES implantation. A near doubling in the TVR rate was seen in the off-label group at 9 months (5.7% versus 3.2%, p<0.0001) and 2 years (11.8% versus 6.5%, p<0.0001) [153].

Data from the Synergy between Percutaneous Coronary Intervention with TAXUS and Cardiac Surgery (SYNTAX)

FIGURE 14**Polymer defects in first-generation DES**

Polymer void and bridging on a Taxus Express stent and polymer void and peeling on a Cypher DES. Adapted and reproduced with permission from Otsuka et al [159].



study, reflecting a population of patients with highly complex off-label use of DES in 3-vessel or left main stem disease, have reported even higher rates of TVR at 1, 2, 3 and 4 years at 11.6%, 17.4%, 19.7% and 23%, respectively [154]. Furthermore, recent evidence has suggested that one of the main determinants of future clinical events, including revascularisation, is the clinical risk profile of the patient. High EuroSCORE patients from the SYNTAX trial - in particular in the 3VD population - have been associated with more adverse clinical outcomes [155,156]. Registries have also suggested these observations in patients with left main disease [157,158]. Further study is required to validate these findings.

Polymer disruption, peeling and cracking

Polymer disruption, peeling and cracking have been demonstrated to occur in bench studies involving both first [159] (Figure 14) and second (Figure 15) generation DES, [160,161] using light or scanning electron microscopy.

Although there is no direct evidence to suggest that the integrity of the polymer coating is a direct cause of restenosis, there are sufficient theoretical concerns to warrant concern through non-uniform local drug distribution or the disrupted polymer potentially acting as a nidus for an ongoing inflammatory response with the subsequent risk of restenosis [27-29,54].

Other concerns with regard to the potential for polymer disruption involve the percutaneous coronary intervention procedure itself. Wiemer et al. [162,163] demonstrated that, in DES that had failed to be delivered to the intended implantation site in tortuous calcified lesions, significant damage and cracking of the polymer had occurred to varying extents with multiple types of second-generation DES. Scanning electron microscopy revealed many cases of deep damage to the polymer with exposure of the bare metal: in particular, the Endeavor RX stents showed up to 20% damage to the

surface area (Figure 16). With polymer-free DES, a large proportion of the surface area was shown to be without any layer of drug (Figure 16).

Bifurcation stenting, especially if very complex, has been hypothesised as possibly leading to polymer disruption, peeling or even polymer void [159], with the consequent risk of non-uniform drug distribution and focal stenosis. In bench work utilising scanning electron microscopy of the polymer integrity of 5 different types of DES (Cypher, Cypher Select, Endeavor, Taxus Express, and Taxus Liberté) after undergoing kissing balloon post-dilatation, Guerin et al. [164] demonstrated significantly greater coating damage to the ostial struts, especially along the overstretched segments, with cracking of the polymer seen in all cases and even exposure of bare metal. Of note is that the Endeavor stent showed a subtotal destruction of its coating on the luminal surface in all segments, whereas the other DES demonstrated more focal localised abnormalities.

Stent fractures

Stent fracture related to DES implantation in coronary arteries was first reported in 2004 (Figure 17) [165]. Subsequent retrospective and prospective registries have quoted restenosis rates ranging from 15% to 100% in patients identified as having stent fractures [166]. In the only randomised controlled trial reporting the incidence of stent fracture and outcomes after DES implantation and subsequent mandatory angiographic follow-up (LONG-DES-II study), a 14% incidence of restenosis was observed [167].

The pattern of restenosis associated with DES fractures appears to be focal, reflecting the local trauma sustained by the vessel at the fracture site once this has occurred. Due to the underlying mechanism of DES fracture (as explained below), restenosis tends to occur fairly late, and invariably after most if not all of the antiproliferative drug has been eluted.

FIGURE 15

Polymer defects seen in second-generation DES
 Adapted and reproduced with permission from Basalus et al [160].

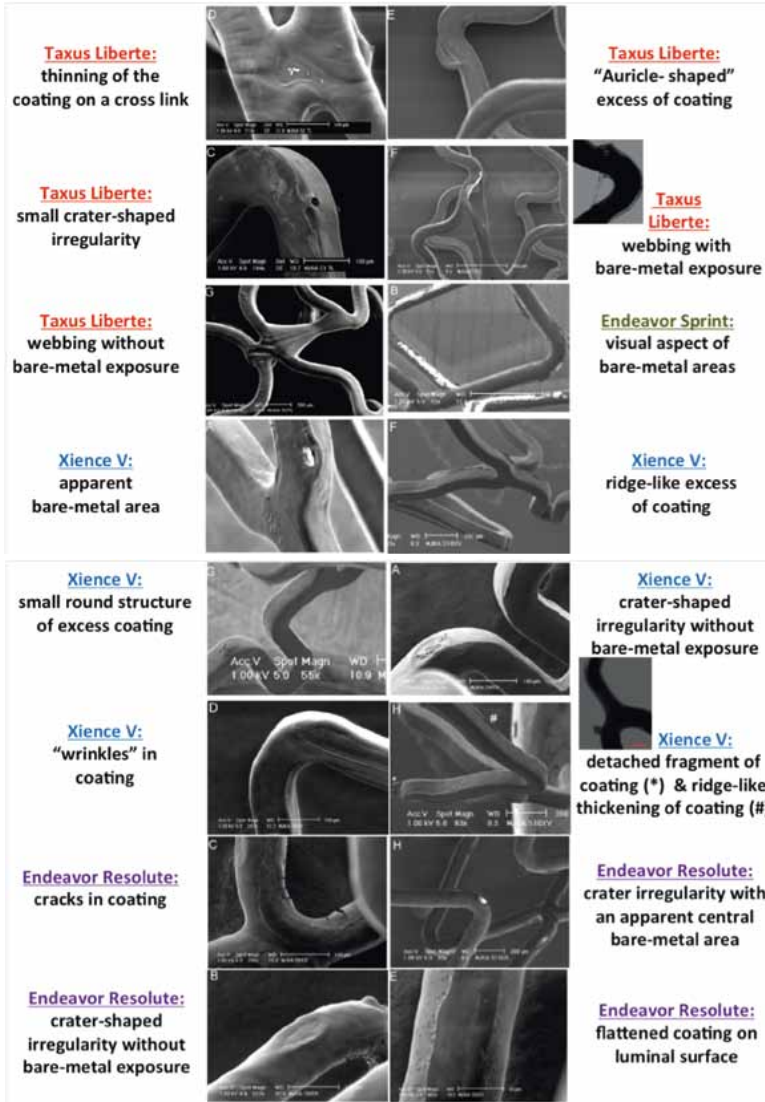
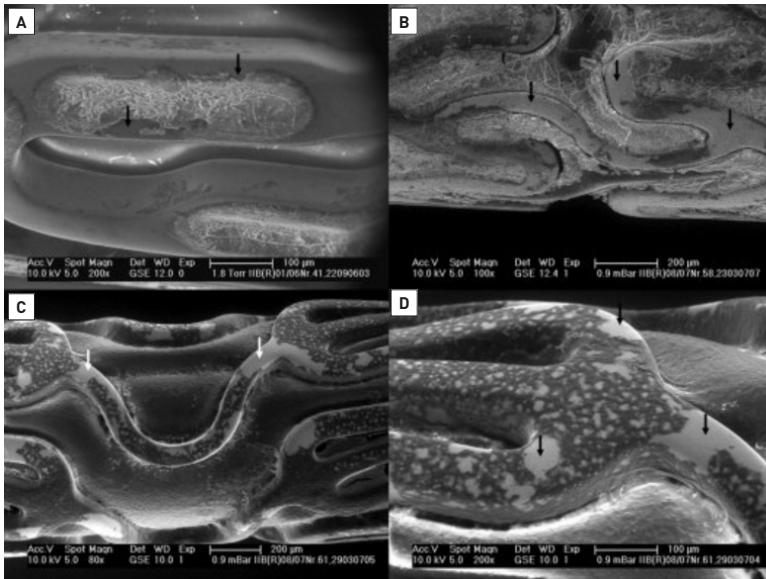


FIGURE 16

Polymer defects in second-generation DES that could not be delivered through calcified, tortuous vessels. Adapted and reproduced with permission from Wiemer et al [163].

- A:** unexpanded Janus Carbostent Flex (Sorin, Milan, Italy): small polymer irritations [black arrows] at the fringe [magnification x 200].
B: unexpanded Yukon Choice Stent (Translumina GmbH, Hechingen, Germany): very thin, irregular drug layer covering stent and balloon. A large area of the surface of the stent was found to be without drug coverage [black arrows] [magnification ? (x100)].
C: unexpanded Axion (Biosensors International, Singapore): large continuous areas and spots without any drug coverage [white arrows] [magnification x80].
D: unexpanded XIENCE V®: typical wrinkling and cracking of polymer with bare metal exposure at loop region [black arrows] after failed attempt to pass the DES through a calcified vessel [magnification x 150].



The subsequent healing response therefore occurs without any drug to suppress the NIH response, which in itself is exacerbated by further exposure of the vessel to the disrupted polymer. The aetiology of the DES fractures also appears to be relatively well understood and is related to two principal factors.

The first is the location of the implantation site of the DES. Mechanical fatigue of the metallic stent can occur due to excessive movement during cardiac contraction, especially at a “hinge point” where the potential for 2 opposing forces may occur at the same site [168]. In these situations, excessive movements can occur to the DES implanted in one part of a vessel during cardiac contraction, in particular in the right coronary artery or a saphenous vein graft, because of their greater propensity for angulation and tortuosity [166,168].

Secondly, the design of the DES itself has been strongly incriminated with causing DES fracture. A closed-cell design,

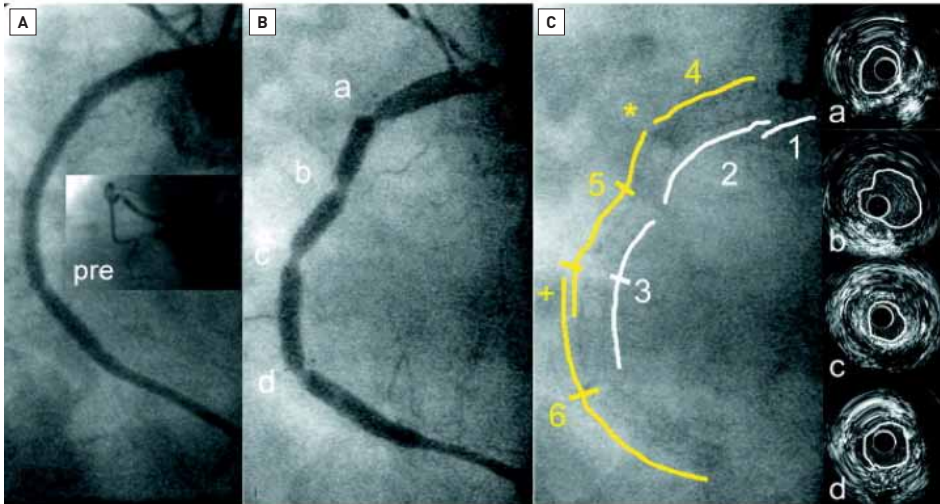
such as occurs with SES, is less likely to be able to withstand the pressures related to excessive movements compared with the open-cell design of a PES. In a recent meta-analysis, [166] the incidence of stent fracture was reported to be less than 0.1% with the open-cell PES and approximately 2.3% with the closed-cell SES.

Long stents, overlapping stents, tight lesions that have been “vigorously post-dilated and expanded,” [167] myocardial bridge sites, areas of significant curvature (due to the lack of conformability of certain DES, especially of closed-cell design) are all other factors which may predispose to DES fracture [165-173].

Newer-generation DES have consequently aimed to maintain the open-cell design and have thinner struts by using new metallic alloys. Although the radial strength has been preserved with next-generation DES - recent case reports have suggested that, with certain types of next-generation DES,

FIGURE 17**The first reported DES fracture in the literature made by our group in 2004**

The initial RCA result (A) following implantation of 3 overlapping 3 mm Cypher DES (post-dilated with a 3.5 mm balloon). 5 months later the patient re-presented with unstable angina – 4 very focal lesions, giving the vessel a beaded appearance, were demonstrated on both coronary angiography (B-C) and IVUS C), indicative of DES fracture. Reproduced with permission from Sianos et al [165].



the longitudinal strength of the device may potentially be affected, increasing the likelihood for stent deformation (longitudinal elongation or compression) requiring post-dilation or further stent placement - episodes of late stent thrombosis have also been reported [174-176]. Higher incidences of restenosis have, at the time of writing, not yet been reported.

IMPLANTATION FACTORS**Incomplete stent expansion**

A smaller post-procedural minimal lumen diameter (MLD) and a greater residual stenosis (➤ Figure 17) have been associated with long-term DES patency and clinical outcomes [177-187]. Evidence of stent underexpansion has been reported in 20-40% of cases when assessed by quantitative coronary angiography (QCA) and 38-70% of cases when assessed by IVUS [182-184]. However, what proportion of these cases with stent underexpansion are clinically relevant in causing restenosis remains unclear. Serial IVUS analyses from the SIRIUS trial [185] and other studies [186,187] investigating SES use, have demonstrated a cut-off of a post-

procedural MSA of between 5.0-5.5 mm² as being the optimal area to reduce the likelihood of restenosis.

In an important meta-analysis, Casella et al [188] compared IVUS against angiographic-guided BMS implantation (n=2,972 patients) and demonstrated that, at 6 months follow-up, there was reduced TVR (OR 0.62; 95% CI: 0.49-0.78; p=0.00003), binary restenosis (OR 0.75; 95% CI: 0.60-0.94; p=0.01) and MACE (OR 0.79; 95% CI: 0.64-0.98; p=0.03) when an IVUS approach to BMS implantation was used. Since then, the only new published randomised controlled trials of IVUS versus angiographic-guided stent implantation were the AVID trial [189] for BMS and a small trial (Jakabcin et al [190]) for DES.

The AVID trial was published 10 years after the data collection and had mixed results, with no benefit in the incidence of 12-month TLR, a larger minimum stent area post BMS implantation and, on subgroup analysis, a lower 12-month TLR rate for vessels ≥ 2.5 mm or vessels with a high-grade pre-stent stenosis. With DES, Jakabcin et al failed to show any differences in the clinical endpoints of MACE (death, myocardial infarction and reintervention) at 18 months.

FOCUS BOX 5

- Polymer release kinetics – namely antiproliferative drug dose and time course of delivery – play a crucial role in the prevention of restenosis
- The genes responsible for the proliferative response potentially remain active for a period of up to 21 days after vessel injury – a critical time period for antiproliferative drug delivery from DES
- DES with shorter drug release kinetics, such as Endeavor [14 days], lead to greater restenosis compared to DES with longer drug release kinetics
- Newer-generation DES with thinner struts, longer drug release kinetics, more biocompatible polymers have led to more effective neointima inhibition
- Off-label use of DES, such as in ostial, left main stem, chronic total occlusion, saphenous vein graft, small or large vessels/multivessel, STEMI, ISR lesions, are associated with higher restenosis and revascularisation rates
- Polymer disruption, peeling and cracking, either on the DES at baseline or induced by delivery or by interventional procedure, have been demonstrated with first and second-generation DES. As to whether this is implicated in restenosis is theoretical
- Stent fractures are more likely to occur with the closed-cell design of first-generation DES and in sites where there is greater angulation or tortuosity (i.e., hinge points). They tend to occur late, when there is little or no antiproliferative drug to cover the vessel injury

Furthermore, the initial results of the AVIO (Angiographic Versus IVUS Optimisation) randomised, multicentre trial assessing IVUS-guided DES implantation were presented in 2010 [191,192]. In 142 patients with complex lesions implanted with IVUS-guided DES, no clinical benefit was demonstrated compared to controls, with comparable clinical outcomes in the combined endpoint of MI, target lesion revascularisation (TLR), TVR or cardiac death at 30 days and 9 months (85.9% vs. 83.1%, $p=0.47$). The primary endpoint of a higher MLD was seen in the IVUS-guided DES implantation group (2.70 mm vs. 2.51 mm, $p=0.0002$). As only 39% of patients had QCA at 9 months, no comments could be made as to whether this approach would potentially lead to a reduction in restenosis rates. Until large-scale trials unequivocally demonstrate the clinical efficacy of an IVUS-guided DES implantation approach, IVUS will remain to be used at the operator's discretion.

The most plausible and the strongest theory to explain the underlying mechanism relating stent underexpansion to restenosis is the so-called “bigger-is-better” paradigm [193]. Effectively, if the minimum stent area (MSA) is smaller at baseline, then the expected NIH formation post DES implan-

tation would be more likely to be of significance in leading to a flow-limiting lesion. Conversely, if the MSA was larger, then the growth of the same amount of NIH would be clinically less relevant in causing binary restenosis [193]. Other suggestions of DES underexpansion as a cause of ISR have been related to possible asymmetrical stent expansion, which may affect the pattern of neointimal growth through possible uneven drug delivery [194,195]. Numerous factors, includ-

TABLE 5

Factors associated with an increased risk of suboptimal stent deployment [228]

LIST OF CONDITIONS ASSOCIATED WITH AN INCREASED RISK OF SUBOPTIMAL STENT DEPLOYMENT

Low-pressure stent deployment (<12 atm)
Lesions with heavy calcification
Lesions with large plaque burden (severe stenosis)
Lesions with a mismatch of proximal and distal reference size
Ostial lesions
Bifurcation lesions treated with stenting of side branch
Long lesions requiring multiple stents
Small vessel treatment
Treatment of diffuse in-stent restenosis

ously described, are involved in increasing the risk of suboptimal stent deployment (➤ Table 5).

Geographical miss/barotrauma to unstented segments

Geographical miss (➤ Figure 18), as the name suggests, is essentially a failure to cover appropriately an injured vessel or atherosclerotic plaque. This may be a consequence of lesion predilatation, balloon-associated vessel barotrauma and the subsequent failure to cover the entire injured site with a DES, incomplete coverage of the diseased segment of the vessel with significant plaque remaining at the stent margins, or failure adequately to overlap DES in long segments of disease.

Geographical miss has more accurately been described as longitudinal geographical miss (LGM: injured or diseased stenotic segment not fully covered by DES) or axial geographical miss (AGM: balloon-artery size ratio <0.9 or >1.3 mismatch) (➤ Figure 19) [196]. Geographical miss, associated with the implantation of SES, was investigated in the STLLR study [196]. As a whole, geographical miss was observed in nearly two thirds of the study group (66.5%), with almost half the patients experiencing LGM (47.6%), over one third AGM (35.2%), and 16.5% a combination of the two. At 1-year follow-up, there was more than a 2-fold increase in TVR (5.1% vs. 2.5%; $p=0.025$) and a 3-fold increase in MI (2.4% vs. 0.8%; $p=0.04$) in patients with geographical miss. Subgroup analyses indicated that these findings were almost exclusively related to LGM (6.1% vs. 2.6%; $p=0.001$), with two thirds of cases being second-

FIGURE 18

The potential benefit of IVUS-guided stent implantation

Comparison of angiographic and IVUS findings before and after high-pressure stent post-dilatation. Reproduced with permission from Romagnoli et al. [228]

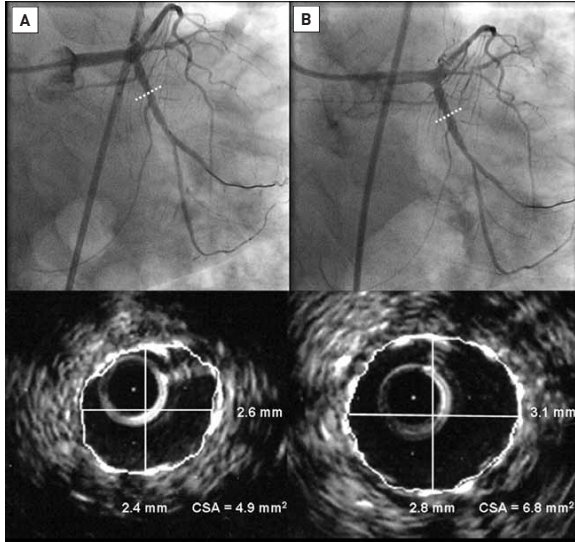
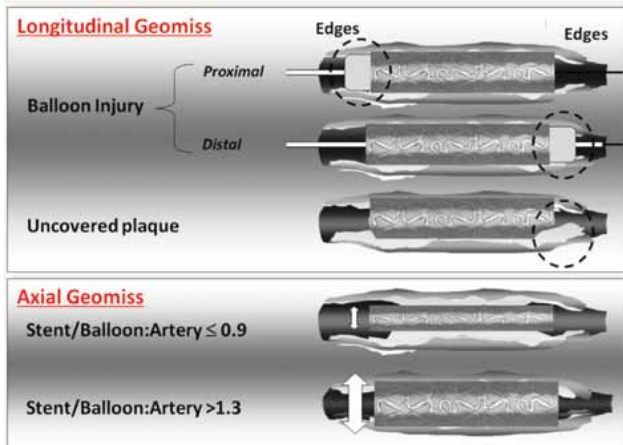


FIGURE 19

Geographical miss

Illustration of the mechanism of longitudinal (LGM) and axial geographical miss (AGM). Reproduced and adapted with permission from Costa et al [196].



ary to balloon injury outside the stent margins, and AGM not seeming to be an important factor (4.2% vs. 4.3%; *p* non-significant). This latter finding has been corroborated, where it was shown that the balloon-to-artery ratio [148] or the occurrence of edge dissections (potentially associated with AGM) [197] did not have a significant impact on the risk of restenosis: this does perhaps argue against the practice of IVUS-guided DES implantation. The occurrence of edge dissections has, however, been linked to an increased periprocedural and 1-month MACE rate, driven primarily by an elevated risk of stent thrombosis and subsequent TVR [198].

More recently, a substudy of the STLLR study demonstrated that the clinical effects of balloon injury secondary to LGM were more pronounced in diabetics [199]. More than a four-fold increase (8%) in the need for target lesion revas-

cularisation in diabetics, and almost a two-fold increase in non-diabetics (3.8%), in the presence of LGM were reported compared to no LGM being present.

The vascular response at the stent edges has been evaluated with first-generation DES. It appears to be dependent on the implanted device and the periprocedural-induced vascular trauma, as a consequence of the geographical miss phenomenon, as described. [196] Within the IVUS substudies of the E-SIRIUS and SIRIUS trials, both AGM and LGM were shown to be potentially reduced when periprocedural implantation parameters such as conservative pre-dilatation, less forceful stent implantation (~16 atm) and selective post-dilatation with balloons shorter than the stent were undertaken [200].

The landing zone of the implanted device may be a potential mechanism for restenosis. Failure to cover fully a stenotic lipid-core lesion due to LGM as described has potentially been shown to increase the likelihood of DES failure due to plaque progression at the DES edge and subsequent edge restenosis (➤ Figure 20) [17,170,196,201,202]. Further studies are required to assess if the use of intracoronary imaging to ensure full lesion/plaque coverage is undertaken and to assess whether this leads to improved clinical outcomes.

Deployment of a DES in a clot-laden arterial segment

Deployment of a DES in a clot-laden arterial segment has been shown in an *ex vivo* model to lead to significant variability in arterial drug distribution [203] which may potentially affect clinical outcomes (➤ Figure 21). Essentially in this study it was shown that thrombus between the stent strut and vessel wall lead to a reduction in drug penetration into the vessel wall by a factor of up to 10-fold. Despite these theoretical concerns, multiple studies [204-212] and a meta-analysis of 13 trials (*n*=7,244) [213] have shown the significant short-term benefits of DES over BMS. Specifically in the meta-analysis by Piscione et al, [213] a reduction of TVR (5.11% versus 11.19%, *p*<0.00001) and recurrent MI (3.03% versus 3.70%, *p*=0.02) in patients with STEMI were demonstrated up to 1 year. The widespread use of glycoprotein-IIb/IIIa inhibitors and aspiration thrombectomy may be the reasons why these concerns have not materialised in clinical trials in the short term.

Concerns over the long-term safety of DES in STEMI do persist, however, because of the potential risk of late-acquired stent malapposition and consequent LST [214,215]. The concerns about reduced absorption of the drug from DES should be borne in mind in a thrombus-laden vessel, especially when there has been inadequate resolution of thrombus and DES implantation is to be considered.

FIGURE 20

Late drug-eluting stent (DES) failure

This report illustrates a case of incomplete stent coverage of a necrotic-core plaque mass, despite adequate coverage of the angiographic stenosis. Incomplete coverage of the lipid-core lesion with the DES at the index procedure [A, C] appeared to be associated with plaque progression leading to stent failure due to angiographic edge restenosis at 15 months [B, D]. Corresponding 2D OCT images (not illustrated) demonstrated the mechanism of restenosis to be progression of the necrotic core rather than neointimal hyperplasia. Red colour indicates artery wall; green, macrophages; yellow, lipid core; blue, stent; white, calcium; purple, thrombus; grey, guidewire. White arrow denotes side branch in [C] and [D]. *Guidewire shadow. Reproduced with permission from Waxman et al [201].

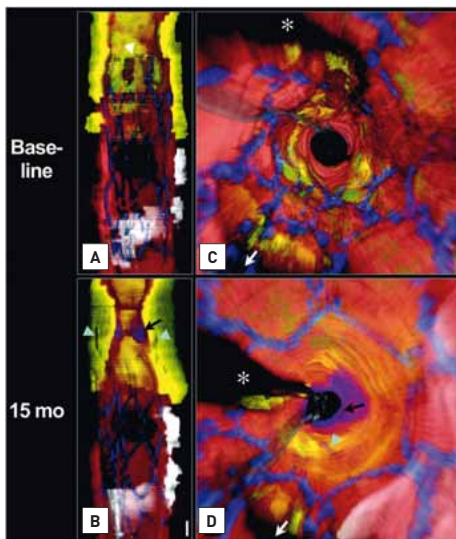
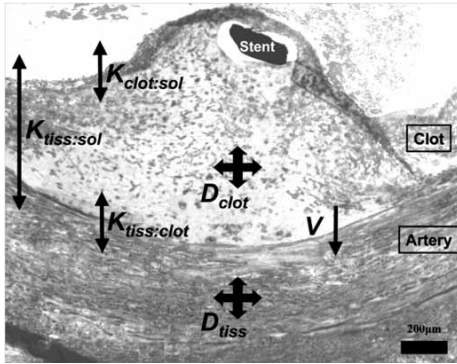


FIGURE 21**Deployment of a DES in a clot-laden arterial segment**

This can potentially lead to variability in arterial drug distribution in *ex vivo* models, potentially affecting clinical outcomes. The concepts of drug diffusivities in clot (D_{clot}) and tissue (D_{tiss}), drug capacity of clot relative to solution ($K_{clot:sol}$), drug capacity of arterial tissue relative to clot ($K_{tiss:clot}$), drug capacity of arterial tissue relative to solution ($K_{tiss:sol}$) and drug convective velocities (V), as illustrated, demonstrate the complexity of stenting in acute myocardial infarction. Reproduced with permission from Hwang et al [203].

**FOCUS BOX 6**

- Implantation factors are the most controllable factors for potentially reducing restenosis
- A smaller post-procedural minimal lumen diameter (MLD) and a greater residual stenosis have been strongly associated with long-term DES patency and clinical outcomes
- IVUS-guided BMS implantation has been associated with a reduced TVR and binary restenosis in classical meta-analyses
- To date, no randomised controlled trial has demonstrated the clinical superiority of IVUS-guided DES implantation despite being associated with a post-procedural higher MLD
- Longitudinal geographical miss has been associated with greater TVR and MI, an effect that may be pronounced in diabetics
- Reductions in TVR and MI have been associated with DES implanted after STEMI at up to 1 year, despite theoretical concerns that thrombus may interfere with local drug absorption. Concerns over the long-term safety of DES in STEMI do persist

PERSONAL PERSPECTIVE – PATRICK W. SERRUYS

Despite the low incidence of DES restenosis, the burden of ISR in absolute numbers will probably continue to grow with the increasing uptake of second-generation DES in conventional percutaneous coronary intervention practice. Moreover, it is probable that these cases will select themselves as more resistant cases which may make treatment subsequently more challenging. Large-scale clinical trials and registries are required to translate these restenotic mechanisms best into either enhanced DES design or further effective treatment options. For example, the pooled data of the randomised controlled trials investigating EES comprise almost 15,000 patients and, apart from mortality, would potentially be of sufficient power to detect rare events such as stent thrombosis.

Although the treatment of ISR is beyond the scope of this review, an understanding of the mechanisms involved in DES restenosis and the controllable and non-controllable factors can give the practising interventional cardiologist further useful clinical information to reduce DES restenosis in his/her own practice. Apart from biological factors, there are potentially controllable factors within arterial and *stent factors*. However, it should be acknowledged that in the treatment of ISR the evidence for using a DES with a different drug remains unproven [44]. Ultimately, the implantation factors are the most important controllable factors from the perspective of the interventional cardiologist.

REFERENCES

1. Thornton MA, Gruentzig AR, Hollman J, King SB, 3rd, Douglas JS. Coumadin and aspirin in prevention of recurrence after transluminal coronary angioplasty: a randomized study. *Circulation*. 1984;69:721-7.
2. Holmes DR, Jr, Vlietstra RE, Smith HC, Vetrovec GW, Kent KM, Cowley MJ, Faxon DP, Gruentzig AR, Kelsey SF, Detre KM, et al. Restenosis after percutaneous transluminal coronary angioplasty (PTCA): a report from the PTCA Registry of the National Heart, Lung, and Blood Institute. *Am J Cardiol*. 1984;53:77C-81C.
3. Henricus J Duckers EGN, Patrick W Serruys. Essentials of Restenosis For the Interventional Cardiologist: Humana Press; 2007.
4. Hoffmann R, Mintz GS, Dussaillant GR, Popma JJ, Pichard AD, Satler LF, Kent KM, Griffin J, Leon MB. Patterns and Mechanisms of In-Stent Restenosis: A Serial Intravascular Ultrasound Study. *Circulation*. 1996;94:1247-1254.
5. Ruygrok PN, Webster MW, Ardill JJ, Chan CC, Mak KH, Meredith IT, Stewart JT, Ormiston JA, Price S. Vessel caliber and restenosis: a prospective clinical and angiographic study of NIR stent deployment in small and large coronary arteries in the same patient. *Catheter Cardiovasc Interv*. 2003;59:165-71.
6. Moses JW, Leon MB, Popma JJ, Fitzgerald PJ, Holmes DR, O'Shaughnessy C, Caputo RP, Kereiakes DJ, Williams DO, Teirstein PS, Jaeger JL, Kuntz RE. Sirolimus-eluting stents versus standard stents in patients with stenosis in a native coronary artery. *N Engl J Med*. 2003;349:1315-23.
7. Cutlip DE, Chauhan MS, Baim DS, Ho KK, Popma JJ, Carrozza JP, Cohen DJ, Kuntz RE. Clinical restenosis after coronary stenting: perspectives from multicenter clinical trials. *J Am Coll Cardiol*. 2002;40(12):2082-9.
8. Serruys PW, Kay IP. I like the candy, I hate the wrapper: the (32)P radioactive stent. *Circulation*. 2000;101:3-7.
9. Albiero R, Nishida T, Adamian M, Amato A, Vaghetti M, Corvaja N, Di Mario C, Colombo A. Edge restenosis after implantation of high activity (32)P radioactive beta-emitting stents. *Circulation*. 2000;101:2454-7.
10. van Der Giessen WJ, Regar E, Hartevelde MS, Coen VL, Bhagwandien R, Au A, Levendag PC, Ligthart J, Serruys PW, den Boer A, Verdouw PD, Boersma E, Hu T, van Beusekom HM. "Edge Effect" of (32)p radioactive stents is caused by the combination of chronic stent injury and radioactive dose falloff. *Circulation*. 2001;104:2236-41.
11. Thom T, Haase N, Rosamond W, Howard VJ, Rumsfeld J, Manolio T, Zheng ZJ, Flegal K, O'Donnell C, Kittner S, Lloyd-Jones D, Goff DC, Jr, Hong Y, Adams R, Friday G, Furie K, Gorelick P, Kissela B, Marler J, Meigs J, Roger V, Sidney S, Sorlie P, Steinberger J, Wasserthiel-Smoller S, Wilson M, Wolf P. Heart disease and stroke statistics--2006 update: a report from the American Heart Association Statistics Committee and Stroke Statistics Subcommittee. *Circulation*. 2006;113:e85-151.
12. Rensing BJ, Hermans WR, Deckers JW, de Feyter PJ, Tijssen JG, Serruys PW. Lumen narrowing after percutaneous transluminal coronary balloon angioplasty follows a near gaussian distribution: a quantitative angiographic study in 1,445 successfully dilated lesions. *J Am Coll Cardiol*. 1992;19:939-45.
13. Mauri L, Orav EJ, Kuntz RE. Late loss in lumen diameter and binary restenosis for drug-eluting stent comparison. *Circulation*. 2005;111:3435-42.
14. Byrne RA, Eberle S, Kastrati A, Dibra A, Ndrepepa G, Iijima R, Mehilli J, Schomig A. Distribution of angiographic measures of restenosis after drug-eluting stent implantation. *Heart*. 2009;95:1572-8.
15. Lloyd-Jones D, Adams R, Carnethon M, De Simone G, Ferguson TB, Flegal K, Ford E, Furie K, Go A, Greenlund K, Haase N, Hailpern S, Ho M, Howard V, Kissela B, Kittner S, Lackland D, Lisabeth L, Marelli A, McDermott M, Meigs J, Mozaffarian D, Nichol G, O'Donnell C, Roger V, Rosamond W, Sacco R, Sorlie P, Stafford R, Steinberger J, Thom T, Wasserthiel-Smoller S, Wong N, Wylie-Rosett J, Hong Y. Heart disease and stroke statistics--2009 update: a report from the American Heart Association Statistics Committee and Stroke Statistics Subcommittee. *Circulation*. 2009;119:480-6.
16. Mehran R, Dangas G, Abizaid AS, Mintz GS, Lansky AJ, Satler LF, Pichard AD, Kent KM, Stone GW, Leon MB. Angiographic patterns of in-stent restenosis: classification and implications for long-term outcome. *Circulation*. 1999;100:1872-8.
17. Corbett SJ, Cosgrave J, Melzi G, Babic R, Biondi-Zoccai GG, Godino C, Morici N, Airoldi F, Michev I, Montorfano M, Sangiorgi GM, Bonizzoni E, Colombo A. Patterns of restenosis after drug-eluting stent implantation: Insights from a contemporary and

- comparative analysis of sirolimus- and paclitaxel-eluting stents. *Eur Heart J*. 2006;27:2330-7.
18. Lemos PA, Hoye A, Goedhart D, Arampatzis CA, Saia F, van der Giessen WJ, McFadden E, Sianos G, Smits PC, Hofma SH, de Feyter PJ, van Domburg RT, Serruys PW. Clinical, angiographic, and procedural predictors of angiographic restenosis after sirolimus-eluting stent implantation in complex patients: an evaluation from the Rapamycin-Eluting Stent Evaluated At Rotterdam Cardiology Hospital (RESEARCH) study. *Circulation*. 2004;109:1366-70.
 19. Lemos PA, Serruys PW, van Domburg RT, Saia F, Arampatzis CA, Hoye A, Degertekin M, Tanabe K, Daemen J, Liu TKK, McFadden E, Sianos G, Hofma SH, Smits PC, van der Giessen WJ, de Feyter PJ. Unrestricted Utilization of Sirolimus-Eluting Stents Compared With Conventional Bare Stent Implantation in the "Real World": The Rapamycin-Eluting Stent Evaluated At Rotterdam Cardiology Hospital (RESEARCH) Registry. *Circulation*. 2004;109:190-195.
 20. Kastrati A, Dibra A, Mehilli J, Mayer S, Pinieck S, Pache J, Dirschinger J, Schomig A. Predictive factors of restenosis after coronary implantation of sirolimus- or paclitaxel-eluting stents. *Circulation*. 2006;113:2293-300.
 21. Frobert O, Lagerqvist B, Carlsson J, Lindback J, Stenstrand U, James SK. Differences in restenosis rate with different drug-eluting stents in patients with and without diabetes mellitus: a report from the SCAAR (Swedish Angiography and Angioplasty Registry). *J Am Coll Cardiol*. 2009;53:1660-7.
 22. Farb A, Kolodgie FD, Hwang JY, Burke AP, Tefera K, Weber DK, Wight TN, Virmani R. Extracellular matrix changes in stented human coronary arteries. *Circulation*. 2004;110:940-7.
 23. Welt FG, Rogers C. Inflammation and restenosis in the stent era. *Arterioscler Thromb Vasc Biol*. 2002;22:1769-76.
 24. van Beusekom HM, Saia F, Zindler JD, Lemos PA, Swager-Ten Hoor SL, van Leeuwen MA, de Feijter PJ, Serruys PW, van der Giessen WJ. Drug-eluting stents show delayed healing: paclitaxel more pronounced than sirolimus. *Eur Heart J*. 2007;28:974-9.
 25. Chieffo A, Foglieni C, Nodari RL, Briguori C, Sangiorgi G, Latib A, Montorfano M, Airolidi F, Michev I, Carlino M, Colombo A, Maseri A. Histopathology of clinical coronary restenosis in drug-eluting versus bare metal stents. *Am J Cardiol*. 2009;104:1660-7.
 26. Joner M, Finn AV, Farb A, Mont EK, Kolodgie FD, Ladich E, Kutys R, Skoriya K, Gold HK, Virmani R. Pathology of drug-eluting stents in humans: delayed healing and late thrombotic risk. *J Am Coll Cardiol*. 2006;48:193-202.
 27. Finn AV, Kolodgie FD, Harnek J, Guerrero LJ, Acampado E, Tefera K, Skoriya K, Weber DK, Gold HK, Virmani R. Differential response of delayed healing and persistent inflammation at sites of overlapping sirolimus- or paclitaxel-eluting stents. *Circulation*. 2005;112:270-8.
 28. Finn AV, Nakazawa G, Joner M, Kolodgie FD, Mont EK, Gold HK, Virmani R. Vascular responses to drug eluting stents: importance of delayed healing. *Arterioscler Thromb Vasc Biol*. 2007;27:1500-10.
 29. Finn AV, Nakazawa G, Kolodgie FD, Virmani R. Temporal course of neointimal formation after drug-eluting stent placement: is our understanding of restenosis changing? *JACC Cardiovasc Interv*. 2009;2(4):300-2.
 30. Farb A, Burke AP, Kolodgie FD, Virmani R. Pathological mechanisms of fatal late coronary stent thrombosis in humans. *Circulation*. 2003;108:1701-6.
 31. Steinberg DH, Gaglia MA, Jr, Pinto Slottow TL, Roy P, Bonello L, De Labriolle A, Lemesle G, Torguson R, Kineshige K, Xue Z, Suddath WO, Kent KM, Satler LF, Pichard AD, Lindsay J, Waksman R. Outcome differences with the use of drug-eluting stents for the treatment of in-stent restenosis of bare-metal stents versus drug-eluting stents. *Am J Cardiol*. 2009;103:491-5.
 32. Baaney KR, Norris CM, Graham MM, Ghali WA, Knudtson ML, Welsh RC. Clinical in-stent restenosis with bare metal stents: is it truly a benign phenomenon? *Int J Cardiol*. 2008;128(3):378-82.
 33. Walters DL, Harding SA, Walsh CR, Wong P, Pomerantsev E, Jang IK. Acute coronary syndrome is a common clinical presentation of in-stent restenosis. *Am J Cardiol*. 2002;89:491-4.
 34. Park CB, Hong MK, Kim YH, Park DW, Han KH, Lee CW, Kang DH, Song JK, Kim JJ, Park SW, Park SJ. Comparison of angiographic patterns of in-stent restenosis between sirolimus- and paclitaxel-eluting stent. *Int J Cardiol*. 2007;120:387-90.
 35. Drozd J, Wojcik J, Malek R, Korona B, Zapolski T, Wysokinski A. Acute coronary syndrome - a frequent clinical manifestation of bare metal in-stent restenosis. *Kardiol Pol*. 2010;68:637-45.
 36. Rathore S, Kinoshita Y, Terashima M, Katoh O, Matsuo H, Tanaka N, Kimura M, Tsuchikane E, Nasu K, Ehara M, Asakura K, Asakura Y, Suzuki T. A

- comparison of clinical presentations, angiographic patterns and outcomes of in-stent restenosis between bare metal stents and drug eluting stents. *EuroIntervention*. 2010;5:841-6.
37. Bonello L, De Labriolle A, Lemesle G, Roy P, Steinberg DH, Slottow TL, Xue Z, Torguson R, Kaneshige K, Suddath WO, Satler LF, Kent KM, Lindsay J, Pichard AD, Waksman R. Comparison of outcomes of drug-eluting stents versus bare-metal stents in nonostial proximal left anterior descending coronary arteries. *Am J Cardiol*. 2009;103:496-500.
 38. Steinberg DH, Pinto Slottow TL, Buch AN, Javadi A, Roy PK, Garg S, Okabe T, Torguson R, Smith KA, Xue Z, Suddath WO, Kent KM, Satler LF, Pichard AD, Lindsay J, Waksman R. Impact of in-stent restenosis on death and myocardial infarction. *Am J Cardiol*. 2007;100:1109-13.
 39. Bossi I, Klersy C, Black AJ, Cortina R, Choussat R, Cassagneau B, Jordan C, Laborde JC, Laurent JP, Bernies M, Fajadet J, Marco J. In-stent restenosis: long-term outcome and predictors of subsequent target lesion revascularization after repeat balloon angioplasty. *J Am Coll Cardiol*. 2000;35:1569-76.
 40. Chen MS, John JM, Chew DP, Lee DS, Ellis SG, Bhatt DL. Bare metal stent restenosis is not a benign clinical entity. *Am Heart J*. 2006;151:1260-4.
 41. Nayak AK, Kawamura A, Nesto RW, Davis G, Jarbeau J, Pyne CT, Gossman DE, Piemonte TC, Riskalla N, Chauhan MS. Myocardial infarction as a presentation of clinical in-stent restenosis. *Circ J* 2006;70:1026-9.
 42. Garg S, Serruys PW. Coronary stents: looking forward. *J Am Coll Cardiol*. 2010;56:S43-78.
 43. Garg S, Serruys PW. Coronary stents: current status. *J Am Coll Cardiol* 2010;56:S1-42.
 44. Alfonso F. Treatment of drug-eluting stent restenosis the new pilgrimage: quo vadis? *J Am Coll Cardiol*. 2010;55:2717-20.
 45. Richardson A, Kaye SB. Drug resistance in ovarian cancer: the emerging importance of gene transcription and spatio-temporal regulation of resistance. *Drug Resist Updat*. 2005;8:311-21.
 46. Huang S, Houghton PJ. Mechanisms of resistance to rapamycins. *Drug Resist Updat*. 2001;4:378-91.
 47. Hausleiter J, Kastrati A, Mehilli J, Vogeser M, Zohnhofer D, Schuhen H, Goos C, Pache J, Dotzer F, Pogatsa-Murray G, Dirschinger J, Heemann U, Schomig A. Randomized, double-blind, placebo-controlled trial of oral sirolimus for restenosis prevention in patients with in-stent restenosis: the Oral Sirolimus to Inhibit Recurrent In-stent Stenosis (OSIRIS) trial. *Circulation*. 2004;110:790-5.
 48. Teirstein PS. Drug-eluting stent restenosis: an uncommon yet pervasive problem. *Circulation*. 2010;122:5-7.
 49. Ribichini F, Tomai F, De Luca G, Bocuzzi G, Presbitero P, Pesarini G, Ferrero V, Ghini AS, Abukareh R, Aurigemma C, De Luca L, Zavalloni D, Soregaroli D, Marino P, Garbo R, Zanolta L, Vassanelli C. Immunosuppressive therapy with oral prednisone to prevent restenosis after PCI. A multicenter randomized trial. *The American journal of medicine*. 2011;124:434-43.
 50. Ribichini F, Tomai F, Ferrero V, Versaci F, Bocuzzi G, Proietti I, Prati F, Crea F, Vassanelli C. Immunosuppressive oral prednisone after percutaneous interventions in patients with multi-vessel coronary artery disease. The IMPRESS-2/MVD study. *EuroIntervention : journal of EuroPCR in collaboration with the Working Group on Interventional Cardiology of the European Society of Cardiology*. 2005;1:173-80.
 51. Ribichini F, Ferrero V, Rognoni A, Marino P, Brunelleschi S, Vassanelli C. Percutaneous treatment of coronary bifurcations: lesion preparation before provisional bare metal stenting and subsequent immunosuppression with oral prednisone. The IMPRESS-Y study. *Journal of interventional cardiology*. 2007;20:114-21.
 52. Versaci F, Gaspardone A, Tomai F, Ribichini F, Russo P, Proietti I, Ghini AS, Ferrero V, Chiariello L, Gioffre PA, Romeo F, Crea F. Immunosuppressive Therapy for the Prevention of Restenosis after Coronary Artery Stent Implantation (IMPRESS Study). *JACC*. 2002;40:1935-42.
 53. Ferrero V, Tomai F, Versaci F, Feola M, Proietti I, Rognoni A, Ghini AS, Gaspardone A, Vacca G, De Luca L, Vassanelli C, Ribichini F. Long-term results of immunosuppressive oral prednisone after coronary angioplasty in non-diabetic patients with elevated C-reactive protein levels. *EuroIntervention : journal of EuroPCR in collaboration with the Working Group on Interventional Cardiology of the European Society of Cardiology*. 2009;5:250-4.
 54. Nakazawa G, Finn AV, Ladich E, Ribichini F, Coleman L, Kolodgie FD, Virmani R. Drug-eluting stent safety: findings from preclinical studies. *Expert Rev Cardiovasc Ther*. 2008;6:1379-91.
 55. Cook S, Ladich E, Nakazawa G, Eshtehardi P, Neidhart M, Vogel R, Togni M, Wenaweser P, Billinger M, Seiler C, Gay S, Meier B, Pichler WJ, Juni P,

- Virmani R, Windecker S. Correlation of intravascular ultrasound findings with histopathological analysis of thrombus aspirates in patients with very late drug-eluting stent thrombosis. *Circulation*. 2009;120:391-9.
56. Koster R, Vieluf D, Kiehn M, Sommerauer M, Kahler J, Baldus S, Meinertz T, Hamm CW. Nickel and molybdenum contact allergies in patients with coronary in-stent restenosis. *Lancet*. 2000;356:1895-7.
 57. Keane FM, Morris SD, Smith HR, Rycroft RJ. Allergy in coronary in-stent restenosis. *Lancet*. 2001;357:1205-6; author reply 1206-7.
 58. Ha T, Lalla S. Allergy in coronary in-stent restenosis. *Lancet* 2001;357(9263):1206; author reply 1206-7.
 59. Mimouni D, Trattner A, David M. Allergy in coronary in-stent restenosis. *Lancet*. 2001;357:1206-7; author reply 1206-7.
 60. Norgaz T, Hobikoglu G, Serdar ZA, Aksu H, Alper AT, Ozer O, Narin A. Is there a link between nickel allergy and coronary stent restenosis? *Tohoku J Exp Med*. 2005;206:243-6.
 61. Hillen U, Haude M, Erbel R, Goos M. Evaluation of metal allergies in patients with coronary stents. *Contact Dermatitis*. 2002;47:353-6.
 62. Saito T, Hokimoto S, Oshima S, Noda K, Kojiyo Y, Matsunaga K. Metal allergic reaction in chronic refractory in-stent restenosis. *Cardiovasc Revasc Med*. 2009;10:17-22.
 63. Iijima R, Ikari Y, Amiya E, Tanimoto S, Nakazawa G, Kyono H, Hatori M, Miyazawa A, Nakayama T, Aoki J, Nakajima H, Hara K. The impact of metallic allergy on stent implantation: metal allergy and recurrence of in-stent restenosis. *Int J Cardiol*. 2005;104:319-25.
 64. Pache J, Dibra A, Schaut C, Schuhlen H, Dirschinger J, Mehilli J, Kastrati A, Schomig A. Sustained increased risk of adverse cardiac events over 5 years after implantation of gold-coated coronary stents. *Catheterization and cardiovascular interventions*. 2006;68:690-5.
 65. Ekqvist S, Svedman C, Moller H, Kehler M, Pripp CM, Bjork J, Gruvberger B, Holmstrom E, Gustavsson CG, Bruze M. High frequency of contact allergy to gold in patients with endovascular coronary stents. *The British journal of dermatology*. 2007;157:730-8.
 66. Kastrati A, Schomig A, Dirschinger J, Mehilli J, von Welsch N, Pache J, Schuhlen H, Schilling T, Schmitt C, Neumann FJ. Increased risk of restenosis after placement of gold-coated stents: results of a randomized trial comparing gold-coated with uncoated steel stents in patients with coronary artery disease. *Circulation*. 2000;101:2478-83.
 67. Svedman C, Moller H, Gustavsson CG, Bruze M. Coronary restenosis and contact allergy to stent material. *The Journal of invasive cardiology*. 2011;23:3 p following E94.
 68. Svedman C, Ekqvist S, Moller H, Bjork J, Pripp CM, Gruvberger B, Holmstrom E, Gustavsson CG, Bruze M. A correlation found between contact allergy to stent material and restenosis of the coronary arteries. *Contact Dermatitis*. 2009;60:158-64.
 69. Nakazawa G, Tanabe K, Aoki J, Onuma Y, Higashikuni Y, Yamamoto H, Ohtsuki S, Yachi S, Yagishita A, Nakajima H, Hara K. Sirolimus-eluting stents suppress neointimal formation irrespective of metallic allergy. *Circ J*. 2008;72:893-6.
 70. Niccoli G, Montone RA, Ferrante G, Crea F. The evolving role of inflammatory biomarkers in risk assessment after stent implantation. *JACC*. 2010;56:1783-93.
 71. Park DW, Lee CW, Yun SC, Kim YH, Hong MK, Kim JJ, Park SW, Park SJ. Prognostic impact of pre-procedural C reactive protein levels on 6-month angiographic and 1-year clinical outcomes after drug-eluting stent implantation. *Heart*. 2007;93:1087-92.
 72. Katsaros KM, Kastl SP, Zorn G, Maurer G, Wojta J, Huber K, Christ G, Speidl WS. Increased restenosis rate after implantation of drug-eluting stents in patients with elevated serum activity of matrix metalloproteinase-2 and -9. *JACC Cardiovasc Interv*. 2010;3:90-7.
 73. Bendeck MP, Zempo N, Clowes AW, Galardy RE, Reidy MA. Smooth muscle cell migration and matrix metalloproteinase expression after arterial injury in the rat. *Circ Res*. 1994;75:539-45.
 74. Galis ZS, Khatir JJ. Matrix metalloproteinases in vascular remodeling and atherogenesis: the good, the bad, and the ugly. *Circ Res*. 2002;90:251-62.
 75. Southgate KM, Fisher M, Banning AP, Thurston VJ, Baker AH, Fabunmi RP, Groves PH, Davies M, Newby AC. Upregulation of basement membrane-degrading metalloproteinase secretion after balloon injury of pig carotid arteries. *Circ Res*. 1996;79:1177-87.
 76. Katsaros KM, Speidl WS, Kastl SP, Zorn G, Huber K, Maurer G, Glogar D, Wojta J, Christ G. Plasminogen activator inhibitor-1 predicts coronary in-stent restenosis of drug-eluting stents. *Journal of thrombosis and haemostasis : JTH*. 2008;6:508-13.
 77. Speidl WS, Katsaros KM, Kastl SP, Zorn G, Huber K, Maurer G, Wojta J, Christ G. Coronary late lumen loss

- of drug eluting stents is associated with increased serum levels of the complement components C3a and C5a. *Atherosclerosis*. 2010;208:285-9.
78. Monraats PS, Pires NM, Agema WR, Zwinderman AH, Schepers A, de Maat MP, Doevendans PA, de Winter RJ, Tio RA, Waltenberger J, Frants RR, Quax PH, van Vlijmen BJ, Atsma DE, van der Laarse A, van der Wall EE, Jukema JW. Genetic inflammatory factors predict restenosis after percutaneous coronary interventions. *Circulation*. 2005;112:2417-25.
 79. Vogiatzi K, Apostolakis S, Voudris V, Thomopoulou S, Kochiadakis GE, Spandidos DA. Interleukin 8 gene polymorphisms and susceptibility to restenosis after percutaneous coronary intervention. *J Thromb Thrombolysis*. 2010;29:134-40.
 80. Kastrati A, Koch W, Berger PB, Mehilli J, Stephenson K, Neumann FJ, von Beckerath N, Bottiger C, Duff GW, Schomig A. Protective role against restenosis from an interleukin-1 receptor antagonist gene polymorphism in patients treated with coronary stenting. *J Am Coll Cardiol*. 2000;36:2168-73.
 81. de Maat MP, Jukema JW, Ye S, Zwinderman AH, Moghaddam PH, Beekman M, Kastelein JJ, van Boven AJ, Bruschke AV, Humphries SE, Klufft C, Henney AM. Effect of the stromelysin-1 promoter on efficacy of pravastatin in coronary atherosclerosis and restenosis. *Am J Cardiol*. 1999;83:852-6.
 82. Kitsios G, Zintzaras E. ACE (LD) polymorphism and response to treatment in coronary artery disease: a comprehensive database and meta-analysis involving study quality evaluation. *BMC medical genetics* 2009;10:50.
 83. Shaaban AM, Duerinckx AJ. Wall Shear Stress and Early Atherosclerosis: A Review. *Am. J. Roentgenol*. 2000;174:1657-1665.
 84. Wentzel JJ, Gijssen FJ, Schuurbijs JC, van der Steen AF, Serruys PW. The influence of shear stress on in-stent restenosis and thrombosis. *EuroIntervention*. 2008;4 Suppl C:C27-32.
 85. Wentzel JJ, Gijssen FJ, Stergiopoulos N, Serruys PW, Slager CJ, Krams R. Shear stress, vascular remodeling and neointimal formation. *J Biomech*. 2003;36:681-8.
 86. Suzuki N, Nanda H, Angiolillo DJ, Bezerra H, Sabate M, Jimenez-Quevedo P, Alfonso F, Macaya C, Bass TA, Ilegbusi OJ, Costa MA. Assessment of potential relationship between wall shear stress and arterial wall response after bare metal stent and sirolimus-eluting stent implantation in patients with diabetes mellitus. *Int J Cardiovasc Imaging*. 2008;24:357-64.
 87. Bassiouny HS, Song RH, Hong XF, Singh A, Kocharyan H, Glagov S. Flow regulation of 72-kD collagenase IV (MMP-2) after experimental arterial injury. *Circulation*. 1998;98:157-63.
 88. Bassiouny HS, Song RH, Kocharyan H, Kins E, Glagov S. Low flow enhances platelet activation after acute experimental arterial injury. *J Vasc Surg*. 1998;27:910-8.
 89. Gijssen FJ, Oortman RM, Wentzel JJ, Schuurbijs JC, Tanabe K, Degertekin M, Ligthart JM, Thury A, de Feyter PJ, Serruys PW, Slager CJ. Usefulness of shear stress pattern in predicting neointima distribution in sirolimus-eluting stents in coronary arteries. *JACC*. 2003;92:1325-8.
 90. Sterpetti AV, Cucina A, D'Angelo LS, Cardillo B, Cavallaro A. Shear stress modulates the proliferation rate, protein synthesis, and mitogenic activity of arterial smooth muscle cells. *Surgery*. 1993;113:691-9.
 91. Carlier SG, van Damme LCA, Blommerde CP, Wentzel JJ, van Langehove G, Verheye S, Kockx MM, Knaapen MWM, Cheng C, Gijssen F, Duncker DJ, Stergiopoulos N, Slager CJ, Serruys PW, Krams R. Augmentation of Wall Shear Stress Inhibits Neointimal Hyperplasia After Stent Implantation: Inhibition Through Reduction of Inflammation? *Circulation*. 2003;107:2741-2746.
 92. Kim YH, Park DW, Suh IW, Jang JS, Hwang ES, Jeong YH, Lee SW, Lee CW, Hong MK, Kim JJ, Park SW, Park SJ. Long-term outcome of simultaneous kissing stenting technique with sirolimus-eluting stent for large bifurcation coronary lesions. *Catheter Cardiovasc Interv* .2007;70:840-6.
 93. Morton AC, Siotia A, Arnold ND, Korgul P, Bowles J, Heppenstall J, Gunn J. Simultaneous kissing stent technique to treat left main stem bifurcation disease. *Catheter Cardiovasc Interv*. 2007;69:209-15.
 94. Stinis CT, Hu SP, Price MJ, Teirstein PS. Three-year outcome of drug-eluting stent implantation for coronary artery bifurcation lesions. *Catheter Cardiovasc Interv*. 2010;75:309-14.
 95. Papafaklis MI, Bourantas CV, Theodorakis PE, Katsouras CS, Naka KK, Fotiadis DI, Michalis LK. The Effect of Shear Stress on Neointimal Response Following Sirolimus- and Paclitaxel-Eluting Stent Implantation Compared With Bare-Metal Stents in Humans. *J Am Coll Cardiol Intv*. 2010;3:1181-1189.
 96. Oikawa Y YJ, Costa M, Matsuno S, Akabane M, Funada R, Inaba T, Nakagawa Y, Nakamura M, Nagashima K, Kirigaya H, Ogasawara K, Sawada H,

- Aizawa T. Intravascular ultrasound, angioscopic and histopathological characterisation of heterogeneous patterns of restenosis after sirolimus-eluting stent implantation: insights into potential “thromborestenosis” phenomenon. *EuroInterv*. 2010;6:380-387.
97. Rittersma SZH, van der Wal AC, Koch KT, Piek JJ, Henriques JPS, Mulder KJ, Ploegmakers JPHM, Meesterman M, de Winter RJ. Plaque Instability Frequently Occurs Days or Weeks Before Occlusive Coronary Thrombosis: A Pathological Thrombectomy Study in Primary Percutaneous Coronary Intervention. *Circulation*. 2005;111:1160-1165.
 98. Glagov S, Zarins C, Giddens DP, Ku DN. Hemodynamics and atherosclerosis. Insights and perspectives gained from studies of human arteries. *Arch Pathol Lab Med* .1988;112:1018-31.
 99. Okura H, Morino Y, Oshima A, Hayase M, Ward MR, Popma JJ, Kuntz RE, Bonneau HN, Yock PG, Fitzgerald PJ. Preintervention arterial remodeling affects clinical outcome following stenting: an intravascular ultrasound study. *J Am Coll Cardiol*. 2001;37:1031-5.
 100. Nakamura M, Yock PG, Bonneau HN, Kitamura K, Aizawa T, Tamai H, Fitzgerald PJ, Honda Y. Impact of peri-stent remodeling on restenosis: a volumetric intravascular ultrasound study. *Circulation*. 2001;103:2130-2.
 101. Farb A, Sangiorgi G, Carter AJ, Walley VM, Edwards WD, Schwartz RS, Virmani R. Pathology of acute and chronic coronary stenting in humans. *Circulation*. 1999;99:44-52.
 102. Carter AJ, Aggarwal M, Kopia GA, Tio F, Tsao PS, Kolata R, Yeung AC, Llanos G, Dooley J, Falotico R. Long-term effects of polymer-based, slow-release, sirolimus-eluting stents in a porcine coronary model. *Cardiovasc Res*. 2004;63:617-24.
 103. Raber L, Wohlwend L, Wigger M, Togni M, Wandel S, Wenaweser P, Cook S, Moschovitis A, Vogel R, Kalesan B, Seiler C, Eberli F, Luscher TF, Meier B, Juni P, Windecker S. Five-year clinical and angiographic outcomes of a randomized comparison of sirolimus-eluting and paclitaxel-eluting stents: results of the Sirolimus-Eluting Versus Paclitaxel-Eluting Stents for Coronary Revascularization LATE trial. *Circulation*. 2011;123:2819-28, 6 p following 2828.
 104. Wilson GJ, Nakazawa G, Schwartz RS, Huibregtse B, Poff B, Herbst TJ, Baim DS, Virmani R. Comparison of inflammatory response after implantation of sirolimus- and paclitaxel-eluting stents in porcine coronary arteries. *Circulation*. 2009;120:141-9, 1-2.
 105. Nakazawa G, Finn AV, Vorpahl M, Ladich ER, Kolodgie FD, Virmani R. Coronary responses and differential mechanisms of late stent thrombosis attributed to first-generation sirolimus- and paclitaxel-eluting stents. *J Am Coll Cardiol*. 2011;57:390-8.
 106. Naito M, Stirck CM, Smith EB, Thompson WD. Smooth muscle cell outgrowth stimulated by fibrin degradation products. The potential role of fibrin fragment E in restenosis and atherogenesis. *Thromb Res*. 2000;98:165-74.
 107. Liistro F, Stankovic G, Di Mario C, Takagi T, Chieffo A, Moshiri S, Montorfano M, Carlino M, Briguori C, Pagnotta P, Albiero R, Corvaja N, Colombo A. First clinical experience with a paclitaxel derivate-eluting polymer stent system implantation for in-stent restenosis: immediate and long-term clinical and angiographic outcome. *Circulation*. 2002;105:1883-6.
 108. Nakazawa G, Otsuka F, Nakano M, Vorpahl M, Yazdani SK, Ladich E, Kolodgie FD, Finn AV, Virmani R. The pathology of neoatherosclerosis in human coronary implants bare-metal and drug-eluting stents. *J Am Coll Cardiol*. 2011;57:1314-22.
 109. Takano M, Yamamoto M, Inami S, Murakami D, Ohba T, Seino Y, Mizuno K. Appearance of lipid-laden intima and neovascularization after implantation of bare-metal stents extended late-phase observation by intracoronary optical coherence tomography. *J Am Coll Cardiol*. 2009;55:26-32.
 110. Habara M, Terashima M, Nasu K, Kaneda H, Inoue K, Ito T, Kamikawa S, Kurita T, Tanaka N, Kimura M, Kinoshita Y, Tsuchikane E, Matsuo H, Ueno K, Katoh O, Suzuki T. Difference of tissue characteristics between early and very late restenosis lesions after bare-metal stent implantation: an optical coherence tomography study. *Circ Cardiovasc Interv*. 2010;4:232-8.
 111. Kang SJ, Mintz GS, Akasaka T, Park DW, Lee JY, Kim WJ, Lee SW, Kim YH, Whan Lee C, Park SW, Park SJ. Optical coherence tomographic analysis of in-stent neoatherosclerosis after drug-eluting stent implantation. *Circulation*. 2011;123:2954-63.
 112. Kimura T, Yokoi H, Nakagawa Y, Tamura T, Kaburagi S, Sawada Y, Sato Y, Hamasaki N, Nosaka H, et al. Three-year follow-up after implantation of metallic coronary-artery stents. *N Engl J Med*. 1996;334:561-6.
 113. Asakura M, Ueda Y, Nanto S, Hirayama A, Adachi T, Kitakaze M, Hori M, Kodama K. Remodeling of in-stent neointima, which became thinner and transpar-

- ent over 3 years: serial angiographic and angioscopic follow-up. *Circulation*. 1998;97:2003-6.
114. Kimura T, Abe K, Shizuta S, Odashiro K, Yoshida Y, Sakai K, Kaitani K, Inoue K, Nakagawa Y, Yokoi H, Iwabuchi M, Hamasaki N, Nosaka H, Nobuyoshi M. Long-term clinical and angiographic follow-up after coronary stent placement in native coronary arteries. *Circulation*. 2002;105:2986-91.
 115. Byrne RA, Iijima R, Mehilli J, Piniack S, Bruskina O, Schomig A, Kastrati A. Durability of antirestenotic efficacy in drug-eluting stents with and without permanent polymer. *JACC Cardiovasc Interv*. 2009;2:291-9.
 116. van der Giessen WJ, Lincoff AM, Schwartz RS, van Beusekom HM, Serruys PW, Holmes DR, Jr, Ellis SG, Topol EJ. Marked inflammatory sequelae to implantation of biodegradable and nonbiodegradable polymers in porcine coronary arteries. *Circulation*. 1996;94(7):1690-7.
 117. Finn AV, Joner M, Nakazawa G, Kolodgie F, Newell J, John MC, Gold HK, Virmani R. Pathological correlates of late drug-eluting stent thrombosis: strut coverage as a marker of endothelialization. *Circulation*. 2007;115:2435-41.
 118. Smits PC, Kedhi E, Roayaards KJ, Joesoef KS, Wassing J, Rademaker-Havinga TA, McFadden E. 2-year follow-up of a randomized controlled trial of everolimus- and paclitaxel-eluting stents for coronary revascularization in daily practice. COMPARE (Comparison of the everolimus eluting XIENCE-V stent with the paclitaxel eluting TAXUS LIBERTE stent in all-comers: a randomized open label trial). *JACC*. 2011;58:11-8.
 119. Stone GW, Rizvi A, Sudhir K, Newman W, Applegate RJ, Cannon LA, Maddux JT, Cutlip DE, Simonton CA, Sood P, Kereiakes DJ. Randomized comparison of everolimus- and paclitaxel-eluting stents. 2-year follow-up from the SPIRIT (Clinical Evaluation of the XIENCE V Everolimus Eluting Coronary Stent System) IV trial. *JACC*. 2011;58:19-25.
 120. Joner M, Nakazawa G, Finn AV, Quee SC, Coleman L, Acampado E, Wilson PS, Skorija K, Cheng Q, Xu X, Gold HK, Kolodgie FD, Virmani R. Endothelial cell recovery between comparator polymer-based drug-eluting stents. *J Am Coll Cardiol*. 2008;52:333-42.
 121. Togni M, Windecker S, Cocchia R, Wenaweser P, Cook S, Billinger M, Meier B, Hess OM. Sirolimus-eluting stents associated with paradoxical coronary vasoconstriction. *J Am Coll Cardiol*. 2005;46:231-6.
 122. Togni M, Raber L, Cocchia R, Wenaweser P, Cook S, Windecker S, Meier B, Hess OM. Local vascular dysfunction after coronary paclitaxel-eluting stent implantation. *Int J Cardiol*. 2007; 21;120:212-20.
 123. Hofma SH, van der Giessen WJ, van Dalen BM, Lemos PA, McFadden EP, Sianos G, Ligthart JM, van Essen D, de Feyter PJ, Serruys PW. Indication of long-term endothelial dysfunction after sirolimus-eluting stent implantation. *Eur Heart J*. 2006;27:166-70.
 124. Hamilos MI, Ostojic M, Beleslin B, Sagic D, Mangovski L, Stojkovic S, Nedeljkovic M, Orlic D, Milosavljevic B, Topic D, Karanovic N, Wijns W. Differential effects of drug-eluting stents on local endothelium-dependent coronary vasomotion. *J Am Coll Cardiol*. 2008;51:2123-9.
 125. Hamilos M, Sarma J, Ostojic M, Cuisset T, Sarno G, Melikian N, Ntalianis A, Muller O, Barbato E, Beleslin B, Sagic D, De Bruyne B, Bartunek J, Wijns W. Interference of drug-eluting stents with endothelium-dependent coronary vasomotion: evidence for device-specific responses. *Circ Cardiovasc Interv*. 2008;1:193-200.
 126. Fujii K, Kawasaki D, Oka K, Akahori H, Fukunaga M, Sawada H, Masutani M, Lee-Kawabata M, Tsujino T, Ohyanagi M, Masuyama T. Endothelium-dependent coronary vasomotor response and neointimal coverage of zotarolimus-eluting stents 3 months after implantation. *Heart*. 2011;97:977-82.
 127. Serruys PW, Sianos G, Abizaid A, Aoki J, den Heijer P, Bonnier H, Smits P, McClean D, Verheye S, Belardi J, Condado J, Pieper M, Gambone L, Bressers M, Symons J, Sousa E, Litvack F. The effect of variable dose and release kinetics on neointimal hyperplasia using a novel paclitaxel-eluting stent platform: the Paclitaxel In-Stent Controlled Elution Study (PISCES). *J Am Coll Cardiol*. 2005;46:253-60.
 128. Tada N, Virmani R, Grant G, Bartlett L, Black A, Clavijo C, Christians U, Betts R, Savage D, Su S-H, Shulze J, Kar S. Polymer-Free Biolimus A9-Coated Stent Demonstrates More Sustained Intimal Inhibition, Improved Healing, and Reduced Inflammation Compared With a Polymer-Coated Sirolimus-Eluting Cypher Stent in a Porcine Model. *Circ Cardiovasc Interv*. 2010;3:174-183.
 129. Grube E. 12-Month angiographic follow-up of the novel non-polymeric Biolimus A9-coated stent for the treatment of de novo coronary lesions: results from the prospective, multicenter, randomized BIOFREEDOM Clinical Trial. Paper presented at: Transcatheter

- Cardiovascular Therapeutics; September 21 to 25, 2010; Washington DC.
130. Tanner FC, Yang ZY, Duckers E, Gordon D, Nabel GJ, Nabel EG. Expression of cyclin-dependent kinase inhibitors in vascular disease. *Circ Res.* 1998;82:396-403.
 131. Sabate M. A randomised comparison between everolimus-eluting stents and cobalt-chromium bare-metal stents in ST-elevation myocardial infarction. Presented at European Society of Cardiology Congress, August 30, 2011; Paris, France 2011.
 132. Serruys PW, Silber S, Garg S, van Geuns RJ, Richardt G, Buszman PE, KelbÄk H, van Boven AJ, Hofma SH, Linke A, Klauss V, Wijns W, Macaya C, Garot P, DiMario C, Manoharan G, Kornowski R, Ischinger T, Bartorelli A, Ronden J, Bressers M, Gobbens P, Negoita M, van Leeuwen F, Windecker S. Comparison of Zotarolimus-Eluting and Everolimus-Eluting Coronary Stents. *New England Journal of Medicine.* 2010;363:136-146.
 133. Papafaklis MI, Chatzizisis YS, Naka KK, Giannoglou GD, Michalis LK. Drug-eluting stent restenosis: Effect of drug type, release kinetics, hemodynamics and coating strategy. *Pharmacol Ther.* 2011 Dec 22. 2012;134:43-53.
 134. Giordano A, Romano A. Inhibition of human in-stent restenosis: a molecular view. *Current opinion in pharmacology.* 2011;11:372-7.
 135. de Scheerder I, Wang K, Wilczek K, van Dorpe J, Verbeken E, Desmet W, Schacht E, Piessens J. Local methylprednisolone inhibition of foreign body response to coated intracoronary stents. *Coronary artery disease.* 1996;7:161-6.
 136. Costa MA, Simon DI. Molecular basis of restenosis and drug-eluting stents. *Circulation.* 2005;111:2257-73.
 137. Lemos PA, Moulin B, Perin MA, Oliveira LA, Arruda JA, Lima VC, Lima AA, Caramori PR, Medeiros CR, Barbosa MR, Brito FS, Jr, Ribeiro EE, Martinez EE. Randomized evaluation of two drug-eluting stents with identical metallic platform and biodegradable polymer but different agents (paclitaxel or sirolimus) compared against bare stents: 1-year results of the PAINT trial. *Catheterization and cardiovascular interventions.* 2009;74:665-73.
 138. Kereiakes DJ, Smits PC, Kedhi E, Parise H, Fahy M, Serruys PW, Stone GW. Predictors of death or myocardial infarction, ischaemic-driven revascularisation, and major adverse cardiovascular events following everolimus-eluting or paclitaxel-eluting stent deployment: pooled analysis from the SPIRIT II, III, IV and COMPARE trials. *EuroIntervention.* 2011;7:74-83.
 139. Windecker S, Serruys PW, Wandel S, Buszman P, Trznadel S, Linke A, Lenk K, Ischinger T, Klauss V, Eberli F, Corti R, Wijns W, Morice MC, di Mario C, Davies S, van Geuns RJ, Eerdmans P, van Es GA, Meier B, Juni P. Biolimus-eluting stent with biodegradable polymer versus sirolimus-eluting stent with durable polymer for coronary revascularisation (LEADERS): a randomised non-inferiority trial. *Lancet.* 2008;372:1163-73.
 140. Stefanini GG, Kalesan B, Serruys PW, Heg D, Buszman P, Linke A, Ischinger T, Klauss V, Eberli F, Wijns W, Morice MC, Di Mario C, Corti R, Antoni D, Sohn HY, Eerdmans P, van Es GA, Meier B, Windecker S, Juni P. Long-term clinical outcomes of biodegradable polymer biolimus-eluting stents versus durable polymer sirolimus-eluting stents in patients with coronary artery disease (LEADERS): 4 year follow-up of a randomised non-inferiority trial. *Lancet.* 2011;378:1940-8.
 141. Takebayashi H, Mintz GS, Carlier SG, Kobayashi Y, Fujii K, Yasuda T, Costa RA, Moussa I, Dangas GD, Mehran R, Lansky AJ, Kreps E, Collins MB, Colombo A, Stone GW, Leon MB, Moses JW. Nonuniform strut distribution correlates with more neointimal hyperplasia after sirolimus-eluting stent implantation. *Circulation.* 2004;110:3430-4.
 142. Elezi S, Kastrati A, Neumann FJ, Hadamitzky M, Dirschinger J, Schomig A. Vessel size and long-term outcome after coronary stent placement. *Circulation.* 1998;98:1875-80.
 143. Kasaoka S, Tobis JM, Akiyama T, Reimers B, Di Mario C, Wong ND, Colombo A. Angiographic and intravascular ultrasound predictors of in-stent restenosis. *J Am Coll Cardiol.* 1998;32:1630-5.
 144. Akiyama T, Moussa I, Reimers B, Ferraro M, Kobayashi Y, Blengino S, Di Francesco L, Finci L, Di Mario C, Colombo A. Angiographic and clinical outcome following coronary stenting of small vessels: a comparison with coronary stenting of large vessels. *J Am Coll Cardiol.* 1998;32:1610-8.
 145. Agostoni P, Biondi-Zoccai GG, Gasparini GL, Anselmi M, Morando G, Turri M, Abbate A, McFadden EP, Vassanelli C, Zardini P, Colombo A, Serruys PW. Is bare-metal stenting superior to balloon angioplasty for small vessel coronary artery disease? Evidence from a meta-analysis of randomized trials. *Eur Heart J.* 2005;26:881-9.

146. Biondi-Zoccai G, Moretti C, Abbate A, Sheiban I. Percutaneous coronary intervention for small vessel coronary artery disease. *Cardiovasc Revasc Med*. 2010;11:189-98.
147. Briguori C, Sarais C, Pagnotta P, Liistro F, Montorfano M, Chieffo A, Sgura F, Corvaja N, Albiero R, Stankovic G, Toutoutzas C, Bonizzoni E, Di Mario C, Colombo A. In-stent restenosis in small coronary arteries: impact of strut thickness. *J Am Coll Cardiol*. 2002;40:403-9.
148. Eshtehardi P, Cook S, Wandel S, Raber L, Wenaweser P, Togni M, Vogel R, Garachemani A, Eberli FR, Luscher TF, Juni P, Hess OM, Meier B, Windecker S. Impact of arterial injury on neointimal hyperplasia after implantation of drug-eluting stents in coronary arteries: an intravascular ultrasound study. *EuroIntervention*. 2010;6:467-74.
149. Kastrati A, Mehilli J, Dirschinger J, Dotzer F, Schuhlen H, Neumann FJ, Fleckenstein M, Pfafferott C, Seyfarth M, Schomig A. Intracoronary stenting and angiographic results: strut thickness effect on restenosis outcome (ISAR-STEREO) trial. *Circulation*. 2001;103:2816-21.
150. Raisuke I, Yuji I, Akiyoshi M, Hiroyoshi N, Kazuhiro H. Predictors of restenosis after implantation of 2.5 mm stents in small coronary arteries. *Circ J*. 2004;68:236-40.
151. Pache J, Kastrati A, Mehilli J, Schuhlen H, Dotzer F, Hausleiter J, Fleckenstein M, Neumann FJ, Sattelberger U, Schmitt C, Muller M, Dirschinger J, Schomig A. Intracoronary stenting and angiographic results: strut thickness effect on restenosis outcome (ISAR-STEREO-2) trial. *J Am Coll Cardiol*. 2003;41:1283-8.
152. Brodie BR, Stuckey T, Downey W, Humphrey A, Bradshaw B, Metzger C, Hermiller J, Krainin F, Juk S, Cheek B, Duffy P, Smith H, Edmunds J, Varanasi J, Simonton CA, STENT Group. Outcomes and Complications With Off-Label Use of Drug-Eluting Stents: Results From the STENT (Strategic Transcatheter Evaluation of New Therapies) Group. *J Am Coll Cardiol Intv*. 2008;1:405-414.
153. Brodie BR, Stuckey T, Downey W, Humphrey A, Bradshaw B, Metzger C, Hermiller J, Krainin F, Juk S, Cheek B, Duffy P, Smith H, Edmunds J, Varanasi J, Simonton CA. Outcomes and complications with off-label use of drug-eluting stents: results from the STENT (Strategic Transcatheter Evaluation of New Therapies) group. *JACC Cardiovasc Interv*. 2008;1:405-14.
154. Kappetein AP, Feldman TE, Mack MJ, Morice MC, Holmes DR, Stahle E, Dawkins KD, Mohr FW, Serruys PW, Colombo A. Comparison of coronary bypass surgery with drug-eluting stenting for the treatment of left main and/or three-vessel disease: 3-year follow-up of the SYNTAX trial. *European Heart Journal*. 2011;32:2125-34.
155. Serruys PW, Farooq V, Vranckx P, Brugaletta S, Holmes DR, Kappetein AP, Mack M, Feldman T, Morice MC, Stähle E, Colombo A, Pereda P, Huang J, Morel MA, Van Es GA, Dawkins KD, Mohr FW, Steyerberg EW. The SYNTAX Trial at 3 Years: a Global Risk approach to identify patients with 3-vessel and/or left main stem disease who could safely and efficaciously be treated with percutaneous coronary intervention. Part 1: the randomised population. Presented at: TCT, San Francisco, USA, 8 Nov 2011.
156. Farooq V, Serruys PW, Vranckx P, Brugaletta S, Holmes DR, Kappetein AP, Mack M, Feldman T, Morice MC, Stähle E, Colombo A, Pereda P, Huang J, Morel MA, Van Es GA, Dawkins KD, Mohr FW, Steyerberg EW. The SYNTAX trial at 3 years: a Global Risk approach to identify patients with 3-vessel and/or left main stem disease who could safely and efficaciously be treated with percutaneous coronary intervention. Part 2: The 'All-Comers' population. Presented at: TCT, San Francisco, USA, 8 Nov 2011.
157. Capodanno D, Caggegi A, Miano M, Cincotta G, Dipasqua F, Giacchi G, Capranzano P, Ussia G, Di Salvo ME, La Manna A, Tamburino C. Global Risk Classification and Clinical SYNTAX (Synergy between Percutaneous Coronary Intervention with TAXUS and Cardiac Surgery) Score in Patients Undergoing Percutaneous or Surgical Left Main Revascularization. *J Am Coll Cardiol Intv*. 2011;4:287-297.
158. Capodanno D, Miano M, Cincotta G, Caggegi A, Ruperto C, Bucalo R, Sanfilippo A, Capranzano P, Tamburino C. EuroSCORE refines the predictive ability of SYNTAX score in patients undergoing left main percutaneous coronary intervention. *American heart journal*. 2010;159:103-9.
159. Otsuka Y, Chronos NA, Apkarian RP, Robinson KA. Scanning electron microscopic analysis of defects in polymer coatings of three commercially available stents: comparison of BiodivYsio, Taxus and Cypher stents. *J Invasive Cardiol*. 2007;19:71-6.
160. Basalus MW, Ankone MJ, van Houwelingen GK, de Man FH, von Birgelen C. Coating irregularities of durable polymer-based drug-eluting stents as assessed

- by scanning electron microscopy. *EuroIntervention*. 2009;5:157-65.
161. Basalus MW, Tandjung K, van Westen T, Sen H, van der Jagt PK, Grijpma DW, van Apeldoorn AA, von Birgelen C. Scanning electron microscopic assessment of coating irregularities and their precursors in Unexpanded durable polymer-based drug-eluting stents. *Catheter Cardiovasc Interv*. 2011 Jul 29. 2012 1;79:644-53.
 162. Wiemer M, Butz T, Mahmood K, Horstkotte D. Major polymer damage of drug-eluting stents. *Circ Cardiovasc Interv*. 2008;1:154.
 163. Wiemer M, Butz T, Schmidt W, Schmitz KP, Horstkotte D, Langer C. Scanning electron microscopic analysis of different drug eluting stents after failed implantation: from nearly undamaged to major damaged polymers. *Catheter Cardiovasc Interv*. 2010;75:905-11.
 164. Guerin P, Pilet P, Finet G, Goueffic Y, N'Guyen JM, Crochet D, Tijou I, Pacaud P, Loirand G. Drug-eluting stents in bifurcations: bench study of strut deformation and coating lesions. *Circ Cardiovasc Interv*. 2010;3:120-6.
 165. Sianos G, Hofma S, Ligthart JM, Saia F, Hoye A, Lemos PA, Serruys PW. Stent fracture and restenosis in the drug-eluting stent era. *Catheter Cardiovasc Interv*. 2004;61:111-6.
 166. Canan T, Lee MS. Drug-eluting stent fracture: incidence, contributing factors, and clinical implications. *Catheter Cardiovasc Interv*. 2010;75:237-45.
 167. Kim HS, Kim YH, Lee SW, Park DW, Lee CW, Hong MK, Park SW, Ko JK, Park JH, Lee JH, Choi SW, Seong IW, Cho YH, Lee NH, Kim JH, Chun KJ, Park SJ. Incidence and predictors of drug-eluting stent fractures in long coronary disease. *Int J Cardiol*. 2009;133:354-8.
 168. Aoki J, Nakazawa G, Tanabe K, Hoye A, Yamamoto H, Nakayama T, Onuma Y, Higashikuni Y, Otsuki S, Yagishita A, Yachi S, Nakajima H, Hara K. Incidence and clinical impact of coronary stent fracture after sirolimus-eluting stent implantation. *Catheter Cardiovasc Interv*. 2007;69:380-6.
 169. Yamada KP, Koizumi T, Yamaguchi H, Kaneda H, Bonneau HN, Honda Y, Fitzgerald PJ. Serial angiographic and intravascular ultrasound analysis of late stent strut fracture of sirolimus-eluting stents in native coronary arteries. *Int J Cardiol*. 2008;130:255-9.
 170. Lemos PA, Saia F, Ligthart JMR, Arampatzis CA, Sianos G, Tanabe K, Hoye A, Degertekin M, Daemen J, McFadden E, Hofma S, Smits PC, de Feyter P, van der Giessen WJ, van Domburg RT, Serruys PW. Coronary Restenosis After Sirolimus-Eluting Stent Implantation: Morphological Description and Mechanistic Analysis From a Consecutive Series of Cases. *Circulation*. 2003;108:257-260.
 171. Umeda H, Gochi T, Iwase M, Izawa H, Shimizu T, Ishiki R, Inagaki H, Toyama J, Yokota M, Murohara T. Frequency, predictors and outcome of stent fracture after sirolimus-eluting stent implantation. *Int J Cardiol*. 2009;133:321-6.
 172. Okumura M, Ozaki Y, Ishii J, Kan S, Naruse H, Matsui S, Ishikawa M, Hattori K, Gochi T, Nakano T, Yamada A, Kato S, Motoyama S, Sarai M, Takagi Y, Ismail TF, Nomura M, Hishida H. Restenosis and stent fracture following sirolimus-eluting stent (SES) implantation. *Circ J*. 2007;71:1669-77.
 173. Lee SH, Park JS, Shin DG, Kim YJ, Hong GR, Kim W, Shim BS. Frequency of stent fracture as a cause of coronary restenosis after sirolimus-eluting stent implantation. *Am J Cardiol*. 2007;100:627-30.
 174. Hanratty CG, Walsh SJ. Longitudinal compression: a "new" complication with modern coronary stent platforms - time to think beyond deliverability? *EuroIntervention*. 2011;7:872-7.
 175. Mortier P, De Beule M. Stent design back in the picture: an engineering perspective on longitudinal stent compression. *EuroIntervention*. 2011;7:773, 775.
 176. Williams PD, Mamas MA, Morgan KP, El-Omar M, Clarke B, Bainbridge A, Fath-Ordoubadi F, Fraser DG. Longitudinal stent deformation: a retrospective analysis of frequency and mechanisms. *EuroIntervention*. 2011 Nov 4.
 177. Castagna MT, Mintz GS, Leiboff BO, Ahmed JM, Mehran R, Satler LF, Kent KM, Pichard AD, Weissman NJ. The contribution of "mechanical" problems to in-stent restenosis: An intravascular ultrasonographic analysis of 1090 consecutive in-stent restenosis lesions. *Am Heart J*. 2001;142:970-4.
 178. Bertrand OF, De Larochelliere R, Joyal M, Bonan R, Mongrain R, Tardif JC. Incidence of stent under-deployment as a cause of in-stent restenosis in long stents. *Int J Cardiovasc Imaging*. 2004;20:279-84.
 179. Fujii K, Mintz GS, Kobayashi Y, Carlier SG, Takebayashi H, Yasuda T, Moussa I, Dangas G, Mehran R, Lansky AJ, Reyes A, Kreps E, Collins M, Colombo A, Stone GW, Teirstein PS, Leon MB, Moses JW. Contribution of stent underexpansion to recurrence

- after sirolimus-eluting stent implantation for in-stent restenosis. *Circulation*. 2004;109:1085-8.
180. Escolar E, Mintz GS, Canos D, Cheneau E, Pichard AD, Satler LE, Kent KM, Waksman R, Weissman NJ. Serial intravascular ultrasound comparison of the extent and distribution of intimal hyperplasia six months after stent implantation for de novo versus in-stent restenosis lesions. *Am J Cardiol*. 2005;96:897-900.
 181. Doi H, Maehara A, Mintz GS, Yu A, Wang H, Mandinov L, Popma JJ, Ellis SG, Grube E, Dawkins KD, Weissman NJ, Turco MA, Ormiston JA, Stone GW. Impact of post-intervention minimal stent area on 9-month follow-up patency of paclitaxel-eluting stents: an integrated intravascular ultrasound analysis from the TAXUS IV, V, and VI and TAXUS ATLAS Workhorse, Long Lesion, and Direct Stent Trials. *JACC Cardiovasc Interv*. 2009;2:1269-75.
 182. de Ribamar Costa J, Jr, Mintz GS, Carlier SG, Fujii K, Sano K, Kimura M, Tanaka K, Costa RA, Lui J, Na Y, Castellanos C, Biro S, Moussa I, Stone GW, Moses JW, Leon MB. Intravascular ultrasound assessment of drug-eluting stent expansion. *Am Heart J*. 2007;153:297-303.
 183. Yoon SC, Laskey WK, Assadourian A, Kelly D, Gellman J, Herzog W, Stafford JL. Assessment of contemporary stent deployment using intravascular ultrasound. *Catheter Cardiovasc Interv*. 2002;57:150-4.
 184. Hanekamp CE, Koolen JJ, Pijls NH, Michels HR, Bonnier HJ. Comparison of quantitative coronary angiography, intravascular ultrasound, and coronary pressure measurement to assess optimum stent deployment. *Circulation*. 1999;99:1015-21.
 185. Sonoda S, Morino Y, Ako J, Terashima M, Hassan AH, Bonneau HN, Leon MB, Moses JW, Yock PG, Honda Y, Kuntz RE, Fitzgerald PJ. Impact of final stent dimensions on long-term results following sirolimus-eluting stent implantation: serial intravascular ultrasound analysis from the sirius trial. *J Am Coll Cardiol*. 2004;43:1959-63.
 186. Takebayashi H, Kobayashi Y, Mintz GS, Carlier SG, Fujii K, Yasuda T, Moussa I, Mehran R, Dangas GD, Collins MB, Kreps E, Lansky AJ, Stone GW, Leon MB, Moses JW. Intravascular ultrasound assessment of lesions with target vessel failure after sirolimus-eluting stent implantation. *Am J Cardiol*. 2005;95:498-502.
 187. Hong MK, Mintz GS, Lee CW, Park DW, Choi BR, Park KH, Kim YH, Cheong SS, Song JK, Kim JJ, Park SW, Park SJ. Intravascular ultrasound predictors of angiographic restenosis after sirolimus-eluting stent implantation. *Eur Heart J*. 2006;27:1305-10.
 188. Casella G, Klaus V, Ottani F, Siebert U, Sangiorgio P, Bracchetti D. Impact of intravascular ultrasound-guided stenting on long-term clinical outcome: a meta-analysis of available studies comparing intravascular ultrasound-guided and angiographically guided stenting. *Catheter Cardiovasc Interv*. 2003;59:314-21.
 189. Russo RJ, Silva PD, Teirstein PS, Attubato MJ, Davidson CJ, DeFranco AC, Fitzgerald PJ, Goldberg SL, Hermiller JB, Leon MB, Ling FS, Lucisano JE, Schatz RA, Wong SC, Weissman NJ, Zientek DM. A randomized controlled trial of angiography versus intravascular ultrasound-directed bare-metal coronary stent placement (the AVID Trial). *Circ Cardiovasc Interv*. 2009;2:113-23.
 190. Jakabcin J, Spacek R, Bystron M, Kvasnak M, Jager J, Veselka J, Kala P, Cervinka P. Long-term health outcome and mortality evaluation after invasive coronary treatment using drug eluting stents with or without the IVUS guidance. Randomized control trial. HOME DES IVUS. *Catheter Cardiovasc Interv*. 2010;75:578-83.
 191. Rogacka R, Latib A, Colombo A. IVUS-Guided Stent Implantation to Improve Outcome: A Promise Waiting to be Fulfilled. *Curr Cardiol Rev*. 2009;5:78-86.

192. Colombo A. AVIO: a prospective randomized trial of intravascular-ultrasound guided compared to angiography guided stent implantation in complex coronary lesions. Presented at: Transcatheter Cardiovascular Therapeutics; September 21 to 25, 2010; Washington, DC.
193. Honda Y, Fitzgerald PJ. Stent expansion as a mechanical parameter to predict late stent patency: back to the basics. *JACC Cardiovasc Interv.* 2009;2:1276-8.
194. Hwang C-W, Wu D, Edelman ER. Physiological Transport Forces Govern Drug Distribution for Stent-Based Delivery. *Circulation.* 2001;104:600-605.
195. Lambert T, Dev V, Rechavia E, Forrester J, Litvack F, Eigler N. Localized arterial wall drug delivery from a polymer-coated removable metallic stent. Kinetics, distribution, and bioactivity of forskolin. *Circulation.* 1994;90:1003-1011.
196. Costa MA, Angiolillo DJ, Tannenbaum M, Driesman M, Chu A, Patterson J, Kuehl W, Battaglia J, Dabbons S, Shamoon F, Flieshman B, Niederman A, Bass TA. Impact of stent deployment procedural factors on long-term effectiveness and safety of sirolimus-eluting stents (final results of the multicenter prospective STLLR trial). *Am J Cardiol.* 2008;101:1704-11.
197. Liu X, Tsujita K, Maehara A, Mintz GS, Weisz G, Dangas GD, Lansky AJ, Kreps EM, Rabbani LE, Collins M, Stone GW, Moses JW, Mehran R, Leon MB. Intravascular ultrasound assessment of the incidence and predictors of edge dissections after drug-eluting stent implantation. *JACC Cardiovasc Interv.* 2009;2:997-1004.
198. Biondi-Zoccai GG, Agostoni P, Sangiorgi GM, Airolidi F, Cosgrave J, Chieffo A, Barbagallo R, Tamburino C, Vittori G, Falchetti E, Margheri M, Briguori C, Remigi E, Iakovou I, Colombo A. Incidence, predictors, and outcomes of coronary dissections left untreated after drug-eluting stent implantation. *Eur Heart J.* 2006;27:540-6.
199. Tahara S, Bezerra HG, Kyono H, Carrigan T, Mehanna E, Wang W, Costa MA. Impact of acute gain on clinical outcomes of patients treated with sirolimus-eluting stent. - A sub-analysis study from the STLLR trial. *Circulation journal.* 2011;75:2113-9.
200. Hoffmann R, Guagliumi G, Musumeci G, Reimers B, Petronio AS, Disco C, Amoroso G, Moses JW, Fitzgerald PJ, Schofer J, Leon MB, Breithardt G. Vascular response to sirolimus-eluting stents delivered with a nonaggressive implantation technique: comparison of intravascular ultrasound results from the multicenter, randomized E-SIRIUS, and SIRIUS trials. *Catheter Cardiovasc Interv.* 2005;66:499-506.
201. Waxman S, Freilich MI, Suter MJ, Shishkov M, Bilazarian S, Virmani R, Bouma BE, Tearney GJ. A case of lipid core plaque progression and rupture at the edge of a coronary stent: elucidating the mechanisms of drug-eluting stent failure. *Circ Cardiovasc Interv.* 2010;3:193-6.
202. Sarno G, Garg S, Gomez-Lara J, Garcia Garcia HM, Ligthart J, Bruining N, Onuma Y, Witberg K, van Geuns RJ, de Boer S, Wykrzykowska J, Schultz C, Duckers HJ, Regar E, de Jaegere P, de Feyter P, van Es GA, Boersma E, van der Giessen W, Serruys PW. Intravascular ultrasound radiofrequency analysis after optimal coronary stenting with initial quantitative coronary angiography guidance: an ATHEROREMO sub-study. *EuroIntervention : journal of EuroPCR in collaboration with the Working Group on Interventional Cardiology of the European Society of Cardiology* 2011;6:977-84.
203. Hwang CW, Levin AD, Jonas M, Li PH, Edelman ER. Thrombosis modulates arterial drug distribution for drug-eluting stents. *Circulation.* 2005;111:1619-26.
204. Spaulding C, Henry P, Teiger E, Beatt K, Bramucci E, Carrie D, Slama MS, Merkely B, Erglis A, Margheri M, Varenne O, Cebrian A, Stoll HP, Sneed DB, Bode C. Sirolimus-eluting versus uncoated stents in acute myocardial infarction. *N Engl J Med.* 2006;355:1093-104.
205. Valgimigli M, Percoco G, Malagutti P, Campo G, Ferrari F, Barbieri D, Cicchitelli G, McFadden EP, Merlini F, Ansani L, Guardigli G, Bettini A, Parrinello G, Boersma E, Ferrari R. Tirofiban and sirolimus-eluting stent vs abciximab and bare-metal stent for acute myocardial infarction: a randomized trial. *JAMA.* 2005;293:2109-17.
206. Valgimigli M, Campo G, Percoco G, Bolognese L, Vassanelli C, Colangelo S, de Cesare N, Rodriguez AE, Ferrario M, Moreno R, Piva T, Sheiban I, Pasquetto G, Prati F, Nazzaro MS, Parrinello G, Ferrari R. Comparison of angioplasty with infusion of tirofiban or abciximab and with implantation of sirolimus-eluting or uncoated stents for acute myocardial infarction: the MULTISTRATEGY randomized trial. *JAMA.* 2008;299:1788-99.
207. Laarman GJ, Suttorp MJ, Dirksen MT, van Heerebeek L, Kiemeneij F, Slagboom T, van der Wieken LR, Tijssen JG, Rensing BJ, Patterson M. Paclitaxel-eluting

- versus uncoated stents in primary percutaneous coronary intervention. *N Engl J Med*. 2006;355:1105-13.
208. Stone GW, Lansky AJ, Pocock SJ, Gersh BJ, Dangas G, Wong SC, Witzenbichler B, Guagliumi G, Peruga JZ, Brodie BR, Dudek D, Mockel M, Ochala A, Kellock A, Parise H, Mehran R. Paclitaxel-eluting stents versus bare-metal stents in acute myocardial infarction. *N Engl J Med*. 2009;360:1946-59.
 209. Menichelli M, Parma A, Pucci E, Fiorilli R, De Felice F, Nazzaro M, Giulivi A, Alborino D, Azzellino A, Violini R. Randomized trial of Sirolimus-Eluting Stent Versus Bare-Metal Stent in Acute Myocardial Infarction (SESAMI). *J Am Coll Cardiol*. 2007;49:1924-30.
 210. Diaz de la Llera LS, Ballesteros S, Nevado J, Fernandez M, Villa M, Sanchez A, Retegui G, Garcia D, Martinez A. Sirolimus-eluting stents compared with standard stents in the treatment of patients with primary angioplasty. *Am Heart J*. 2007;154:164 e1-6.
 211. van der Hoeven BL, Liem SS, Jukema JW, Suraphakdee N, Putter H, Dijkstra J, Atsma DE, Bootsma M, Zeppenfeld K, Oemrawsingh PV, van der Wall EE, Schalij MJ. Sirolimus-eluting stents versus bare-metal stents in patients with ST-segment elevation myocardial infarction: 9-month angiographic and intravascular ultrasound results and 12-month clinical outcome results from the MISSION! Intervention Study. *J Am Coll Cardiol*. 2008;51:618-26.
 212. Kelbaek H, Thuesen L, Helqvist S, Clemmensen P, Klovgaard L, Kaltoft A, Andersen B, Thuesen H, Engstrom T, Botker HE, Saunamaki K, Krusell LR, Jorgensen E, Hansen HH, Christiansen EH, Ravkilde J, Kober L, Kofoed KF, Terkelsen CJ, Lassen JF. Drug-eluting versus bare metal stents in patients with st-segment-elevation myocardial infarction: eight-month follow-up in the Drug Elution and Distal Protection in Acute Myocardial Infarction (DEDICATION) trial. *Circulation*. 2008;118:1155-62.
 213. Piscione F, Piccolo R, Cassese S, Galasso G, De Rosa R, D'Andrea C, Chiariello M. Effect of drug-eluting stents in patients with acute ST-segment elevation myocardial infarction undergoing percutaneous coronary intervention: a meta-analysis of randomised trials and an adjusted indirect comparison. *EuroIntervention*. 2010;5:853-60.
 214. Hassan AK, Berghean SC, Stijnen T, van der Hoeven BL, Snoep JD, Plevier JW, Schalij MJ, Wouter Jukema J. Late stent malapposition risk is higher after drug-eluting stent compared with bare-metal stent implantation and associates with late stent thrombosis. *European Heart Journal*. 2010;31:1172-80.
 215. Alfonso F, Cruz A, Garcia J. Late stent malapposition: innocent phenomenon or major risk marker? *European Heart Journal* 2010;31:260; author reply 260-1.
 216. Aoki J, Colombo A, Dudek D, Banning AP, Drzewiecki J, Zmudka K, Schiele F, Russell ME, Koglin J, Serruys PW. Persistent remodeling and neointimal suppression 2 years after polymer-based, paclitaxel-eluting stent implantation: insights from serial intravascular ultrasound analysis in the TAXUS II study. *Circulation*. 2005;112:3876-83.
 217. Aoki J, Abizaid AC, Serruys PW, Ong AT, Boersma E, Sousa JE, Bruining N. Evaluation of four-year coronary artery response after sirolimus-eluting stent implantation using serial quantitative intravascular ultrasound and computer-assisted grayscale value analysis for plaque composition in event-free patients. *J Am Coll Cardiol*. 2005;46:1670-6.
 218. Collet CA, Costa JR, Abizaid A, Chamie D, Staico R, Costa R, Siquera D, Obregon J, Feres F, Sousa A, Sousa JE. Assessing the temporal course of neointimal hyperplasia formation after different generations of drug-eluting stents. *JACC Cardiovasc Interv*. 2011;4:1067-74.
 219. Raber L, Serruys PW. Late vascular response following drug-eluting stent implantation. *JACC Cardiovasc Interv*. 2011;4:1075-8.
 220. Park KW, Kim CH, Lee HY, Kang HJ, Koo BK, Oh BH, Park YB, Kim HS. Does "late catch-up" exist in drug-eluting stents: insights from a serial quantitative coronary angiography analysis of sirolimus versus paclitaxel-eluting stents. *Am Heart J*. 2010;159:446-453 e3.
 221. Park DW, Hong MK, Mintz GS, Lee CW, Song JM, Han KH, Kang DH, Cheong SS, Song JK, Kim JJ, Weissman NJ, Park SW, Park SJ. Two-year follow-up of the quantitative angiographic and volumetric intravascular ultrasound analysis after nonpolymeric paclitaxel-eluting stent implantation: late "catch-up" phenomenon from ASPECT Study. *J Am Coll Cardiol*. 2006;48:2432-9.
 222. Sousa JE, Costa MA, Abizaid A, Feres F, Seixas AC, Tanajura LF, Mattos LA, Falotico R, Jaeger J, Popma JJ, Serruys PW, Sousa AG. Four-year angiographic and intravascular ultrasound follow-up of patients treated with sirolimus-eluting stents. *Circulation*. 2005;111:2326-9.
 223. Morice MC, Serruys PW, Barragan P, Bode C, Van Es GA, Stoll HP, Snead D, Mauri L, Cutlip DE, Sousa E.

- Long-term clinical outcomes with sirolimus-eluting coronary stents: five-year results of the RAVEL trial. *J Am Coll Cardiol*. 2007;50:1299-304.
224. Weisz G, Leon MB, Holmes DR, Jr, Kereiakes DJ, Popma JJ, Teirstein PS, Cohen SA, Wang H, Cutlip DE, Moses JW. Five-year follow-up after sirolimus-eluting stent implantation results of the SIRIUS (Sirolimus-Eluting Stent in De-Novo Native Coronary Lesions) Trial. *J Am Coll Cardiol*. 2009;53:1488-97.
225. Silber S, Colombo A, Banning AP, Hauptmann K, Drzewiecki J, Grube E, Dudek D, Baim DS. Final 5-year results of the TAXUS II trial: a randomized study to assess the effectiveness of slow- and moderate-release polymer-based paclitaxel-eluting stents for de novo coronary artery lesions. *Circulation*. 2009;120:1498-504.
226. Mauri L, Massaro JM, Jiang S, Meredith I, Wijns W, Fajadet J, Kandzari DE, Leon MB, Cutlip DE, Thompson KP. Long-term clinical outcomes with zotarolimus-eluting versus bare-metal coronary stents. *JACC Cardiovasc Interv*. 2010;3:1240-9.
227. Caixeta A, Lansky AJ, Serruys PW, Hermiller JB, Ruygrok P, Onuma Y, Gordon P, Yaqub M, Miquel-Hebert K, Veldhof S, Sood P, Su X, Jonnavithula L, Sudhir K, Stone GW. Clinical follow-up 3 years after everolimus- and paclitaxel-eluting stents: a pooled analysis from the SPIRIT II (A Clinical Evaluation of the XIENCE V Everolimus Eluting Coronary Stent System in the Treatment of Patients With De Novo Native Coronary Artery Lesions) and SPIRIT III (A Clinical Evaluation of the Investigational Device XIENCE V Everolimus Eluting Coronary Stent System [EECSS] in the Treatment of Subjects With De Novo Native Coronary Artery Lesions) randomized trials. *JACC Cardiovasc Interv*. 2010;3:1220-8.
228. Romagnoli E, Sangiorgi GM, Cosgrave J, Guillet E, Colombo A. Drug-Eluting Stenting: The Case for Post-Dilation. *J Am Coll Cardiol Intv*. 2008;1:22-31.
229. Gonzalo N, Serruys PW, Okamura T, van Beusekom HM, Garcia-Garcia HM, van Soest G, van der Giessen W, Regar E. Optical coherence tomography patterns of stent restenosis. *Am Heart J*. 2009;158:284-93.
230. Spanos V, Stankovic G, Tobis J, Colombo A. The challenge of in-stent restenosis: insights from intravascular ultrasound. *Eur Heart J*. 2003;24:138-50.
231. Raber L, Serruys PW. Late vascular response following drug-eluting stent implantation. *JACC. Cardiovascular interventions*. 2011;4:1075-8.
232. Nakazawa G, Otsuka F, Nakano M, Vorpahl M, Yazdani SK, Ladich E, Kolodgie FD, Finn AV, Virmani R. The pathology of neoatherosclerosis in human coronary implants bare-metal and drug-eluting stents. *Journal of the American College of Cardiology*. 2011;57:1314-22.

UNIVERSAL PCR CLASSIFICATION

Theme	Coronary interventions
Clinical presentation	ACS
	STEMI
	stable
Specific technique treatment	bare metal stent
	drug-eluting stent
	drug-eluting balloon
Complication	miscellaneous

Chapter 3

Restenosis: Delineating the Numerous Causes of Drug-Eluting Stent Restenosis.

Vasim Farooq, **Bill D. Gogas**, Patrick W. Serruys

Circulation Cardiovascular Interventions. 2011. Apr 1; 4(2): 195-205 [IF: 6.06]

Restenosis

Delineating the Numerous Causes of Drug-Eluting Stent Restenosis

Vasim Farooq, MBChB, MRCP; Bill D. Gogas, MD; Patrick W. Serruys, MD, PhD

In the past decade, tremendous progress has been made in reducing the incidence of restenosis with the advent of the drug-eluting stent (DES). With “plain old balloon angioplasty,” rates of acute and chronic vessel occlusion were unacceptably high at $\approx 30\%$ to 60% , secondary to acute and chronic recoil and constrictive remodeling. The advent of bare-metal stents (BMS) appeared to eliminate the issue of acute and chronic recoil but introduced a new entity, neointimal hyperplasia (NIH), with classical papers unequivocally demonstrating a strong and linear relationship between NIH formation and late lumen loss (LLL). The restenosis rates with BMS were reported to be between 16% and 44% , with higher rates of stenosis attributable to several risk factors, in particular, long lesion length and small vessel caliber.¹

DES were thus conceived as the next step in tackling this iatrogenic entity of NIH, with large-scale reductions in restenosis rates reported at 0% in highly selective lesions and up to 16% in a broader range of patients and lesions with first-generation DES.¹ In contrast to plain old balloon angioplasty and BMS, in which an almost classical gaussian distribution of LLL is seen postprocedurally, the LLL after DES implantation appears to follow a bimodal pattern of distribution (Figure 1).²

Despite the significant advances in the technology to reduce DES restenosis, conservative estimates still suggest that the incidence of in-stent restenosis (ISR) requiring target vessel revascularization (TVR), so-called DES failure, to be $\approx 5\%$ to 10% , with one estimate suggesting $\approx 200\,000$ repeat revascularizations in the United States alone.³

Whereas the pattern of restenosis in BMS has been shown to be primarily diffuse, with DES it has been demonstrated to be usually focal (Figure 2) and most commonly located at the proximal DES edge, as demonstrated in $>60\%$ of ISR with either paclitaxel-eluting stent (PES) or sirolimus-eluting stent (SES) implantation. However, over one-fifth of ISR cases remain diffuse, and 10% to 20% are even occlusive.⁴

In 2004, the first report of risk factors associated with DES restenosis in patients with the unrestricted use of SES since approval of its CE mark was made by our group. Despite the apparent differences in the distribution of LLL between BMS and DES as previously described, the main message of these and subsequent findings was that the usual patient character-

istics, lesion types, and procedural factors incriminated with restenosis in BMS were equally responsible with DES, with diabetes mellitus implicated as one of the strongest risk factors. It should however be emphasized that the “slope” of the distribution of restenosis with DES appears to be much flatter compared with BMS, especially in long lesions and small vessels, highlighting the importance of drug elution in potentially attenuating the NIH response.³

Histopathologic analyses of in-stent neointima taken by directional atherectomy at the time of reintervention also have been shown to be remarkably similar between BMS and DES. This is almost exclusively composed of proteoglycan-rich smooth muscle cells (SMCs) and fibrolipidic areas rich in collagen and reticular fibers. A more “immature” restenotic process, as evidenced by differences in SMC phenotypes, however, has been shown to potentially exist with certain types of DES compared with BMS.^{5,6}

ISR traditionally has been suggested as being potentially less benign with the recurrence of anginal symptoms alone. However, emerging evidence now suggests that between 30% and 60% of ISR cases present with an acute coronary syndrome with unstable angina being the most common presentation and up to 5% of patients even reported to present with ST-elevation myocardial infarction (STEMI).^{7,8} However, one series has suggested no differences in the incidence of acute coronary syndrome associated with either BMS or DES restenosis.⁷

The treatment of ISR and the determinant factors involved in the development of late stent thrombosis (LST) are well described elsewhere and are outside the scope of this review.^{3,9} The underlying mechanisms of restenosis with DES can broadly be divided into 4 main causes (Table), namely, biological, arterial, stent, and implantation factors, accepting that this classification is somewhat arbitrary and that mechanisms of restenosis may be attributable to more than one factor. In this review we explore these 4 main mechanisms and identify the potentially controllable and uncontrollable factors from the perspective of the interventional cardiologist intending to implant a DES.

Biological Factors

Resistance to Antiproliferative Drugs

The underlying mechanisms of action and causes of resistance to paclitaxel or sirolimus are well documented in the

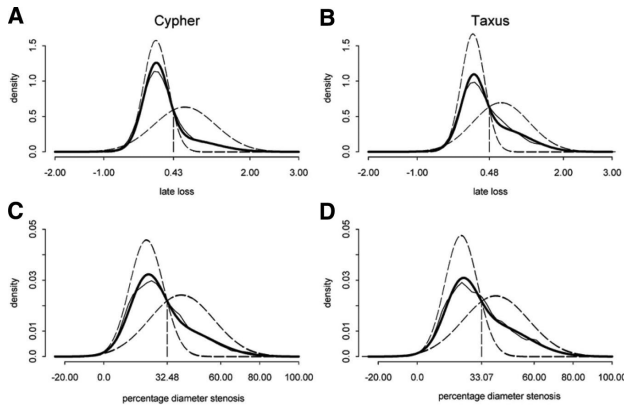


Figure 1. The bimodal distribution of LLL (A, B) and percentage diameter stenosis (C, D) after Cypher (left) and Taxus (right) implantation. LLL indicates late lumen loss. Reproduced with permission from Byrne et al.²

cancer literature and either can be present in genetically predetermined individuals or be acquired following cytotoxic exposure to the drug.^{10,11}

The so-called drug resistance gene expression program, described for paclitaxel resistance, best exemplifies the complex pathways involved in the etiology of drug resistance.¹⁰ Essentially, the cellular context determines the expression of the genes that contribute to drug resistance, either in genetically predetermined cells or primed for expression following the cytotoxic insult after drug exposure. These genes may operate in conventional pathways that are well known (drug delivery and metabolism, apoptosis regulation, DNA repair), but the temporal (ie, pro- and antiapoptotic gene activity) and spatial regulation (ie, cell survival signaling pathways) of these gene products after drug exposure also appears to be important.

As examples, polymorphisms in the genes that encode mTOR or proteins involved in paclitaxel or sirolimus metabolism have been shown to confer drug resistance both in vitro and in vivo^{10,11}; decreased binding of sirolimus to mTOR because of mutations in FK-B12 and mTOR and mutations of downstream effector molecules of mTOR may all cause resistance to sirolimus.¹¹

The OSIRIS study investigated the administration of higher doses of oral sirolimus to patients with refractory ISR in the theoretical attempt of overcoming drug resistance and delivering increased amounts of drug to the implantation site.¹² A significant correlation was demonstrated between the level of sirolimus concentration in the bloodstream and rates of further LLL (Figure 3). However, given that the patients received a short duration of oral sirolimus (7 days), it was unclear whether these findings would be maintained at longer-term follow-up.

Hypersensitivity Reactions (the Polymer)

The inflammatory reaction that occurs after arterial injury is a critical factor that influences the extent of neointimal response, with the persistence of this inflammatory response beyond 90 days being strongly associated with delayed healing and implicated in an increased risk of LST and restenosis long term.^{13,14}

PES and SES have each been demonstrated to provoke distinctive inflammatory responses in animal models beyond 90 days: SES triggering giant cell infiltrations and PES eosinophilic reactions around stent struts. The inflammatory responses associated with SES have been shown to persist beyond 180 days and up to 2 years (Figure 4); this phenomenon may also be further exacerbated at sites of overlapping DES. This is in contrast to BMS and the second-generation everolimus-eluting stent (EES-Xience V) with a more biocompatible polymer, in which the inflammatory responses have been demonstrated to be limited to a period of 90 days and 12 months, respectively (Figure 4).^{13,14}

Evidence of persistent inflammatory responses in humans also has been reported in both autopsy cases, with one case

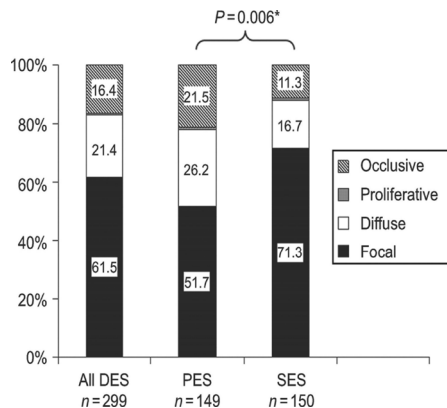


Figure 2. The patterns of restenosis in SES and PES. The predominant pattern of ISR is focal, although diffuse and proliferative restenosis is still seen with DES. SES indicates sirolimus-eluting stent; PES, paclitaxel-eluting stent; DES, drug-eluting stent. Reproduced with permission from Corbett et al.⁴

Table. The Underlying Mechanisms of Restenosis With Drug-Eluting Stent

Biological Factors	Arterial Factors	Stent Factors	Implantation Factors
Resistance to antiproliferative drugs	Wall shear stress	Polymer drug release kinetics	Incomplete stent expansion
Hypersensitivity reaction (polymer)	Progression of atherosclerosis within a stented segment	Type of DES? Type of drug?	Geographical miss
Hypersensitivity reaction (metallic stent platform)	"Thromborestenosis"	Stent gap, nonuniform strut distribution, and drug deposition	Barotrauma to unstented segments
Serum matrix metalloproteinases	Vessel remodeling	Stent strut thickness	Deployment of DES in a clot-laden arterial segment
Genetics	Small vessels	"On- and off-label" use of DES Polymer disruption, peeling, and cracking Stent fractures	

involving up to one third of struts in first-generation DES at 3 months,^{1,14} and from thrombus aspirates taken at the time of emergency percutaneous coronary intervention in patients presenting with very LST.¹⁵

The timing of restenosis associated with DES implantation, therefore, appears complex and may potentially be related to this persistent inflammatory response not usually associated with BMS, with some evidence to suggest a "catch-up" in LLL with SES as discussed in Stent Factors.

Hypersensitivity Reactions (Metallic Stent Platform)

Despite retrospective studies suggesting an association between nickel hypersensitivity and ISR, to date, no prospective studies have confirmed such an association. A few small prospective studies, however, have suggested a possible association between nickel hypersensitivity and recurrent ISR with BMS that previously had been treated with plain old balloon angioplasty; this, however, was found not to be associated with the initial BMS implantation.¹⁶ Whether the issue of nickel hypersensitivity is a potential issue with DES is both speculative and theoretical. Only one small study (Nakazawa et al¹⁷) has examined this issue and found no association with SES implantation.

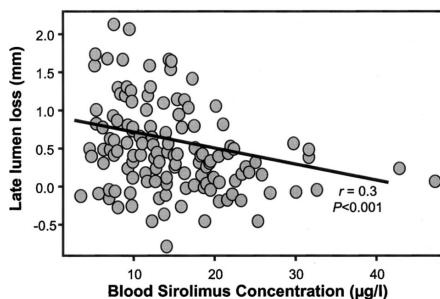


Figure 3. The association of sirolimus blood concentrations at the time of repeat intervention and LLL at 6-month angiographic follow-up from the OSIRIS study. LLL indicates late lumen loss. Reproduced with permission from Hausleiter et al.¹²

Serum Matrix Metalloproteinase (MMP) Activity and Genetics

Circulating MMPs recently have been demonstrated to be potentially useful in identifying patients at greater risk of developing ISR following DES implantation.¹⁸ MMP-2 and MMP-9 are well known to play fundamental roles in the migration of vascular SMCs and matrix remodeling during wound healing and are produced by vascular SMCs, endothelial cells, macrophages, lymphocytes, and mast cells in response to mechanical injury. Significant elevations in MMP-9 levels at baseline and MMP-2 and MMP-9 levels 24 hours post-percutaneous coronary intervention have proven to be strongly associated with the development of ISR following DES implantation. Conversely low and near-normal MMP-2 and MMP-9 levels were associated with a lack of a significant restenotic response.¹⁸

Gene polymorphisms linked with the inflammatory response have been found to be associated with ISR.¹⁹ As examples, homozygosity of the 16/glycine variant in the β_2 -adrenergic receptor (a mediator of nitrous oxide synthetase) has been associated with β_2 -adrenergic receptor down-regulation and an increased risk of restenosis¹⁹; Vogiatzi et al²⁰ described a 15-fold increase in the risk of restenosis associated with 2 functional polymorphisms of interleukin-8 (a strong mediator of inflammation). However, the reported gene polymorphisms are relatively rare, thus limiting any clinical applicability.

Arterial Factors

Wall Shear Stress

Wall shear stress refers to the principle that fluid dynamics and vessel geometry may play a potential role in the cause of focal plaque or neointimal formation. The concept of wall shear stress is that blood does not move at the same velocity at every point within the vessel, with blood flowing fastest in the vessel center or, for example, at the carina of a bifurcation (ie, a high-shear stress area) and slowest when closest to the vessel wall or, using the same example, at the ostium of a bifurcation (ie, a low-shear stress area), because of frictional forces exerted by the vessel endothelium. Low shear stress consequently may lead to the accumulation of growth factors, mitogenic cytokines, and platelets, which may promote atherosclerosis or neointimal formation after vessel injury.

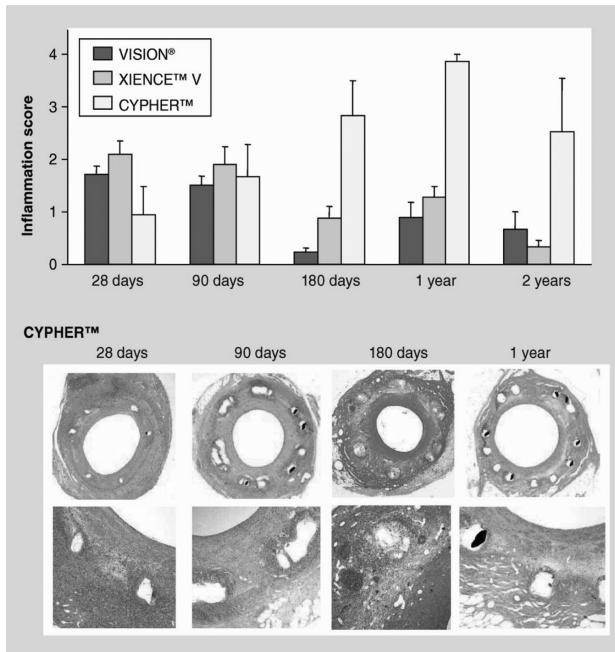


Figure 4. The persistent granulomatous inflammatory response to Cypher stents for a period of up to 2 years in a porcine model. Reproduced from *Expert Rev Cardiovasc Ther.* 2008;6:1379–1391, with permission of Expert Reviews Ltd.¹³

Conversely, high shear stress can potentially directly inhibit SMC proliferation and therefore limit atherosclerosis or restenosis unless it progresses from a low-shear stress area.^{1,21,22}

In a novel experiment in an animal model, Carlier et al²³ demonstrated that through the implantation of a “flow divider” into the center of a stent implanted in the iliac arteries, they were able to modulate and increase the local wall shear stress with a consequential reduction in local inflammation and neointima formation.

The most similar human model of this example has been with so-called “shotgun stenting,” in which simultaneous V-stenting is performed with the formation of a “new” carina in the left main stem or other suitably sized vessels.^{24–26} Kim et al²⁴ showed that in 36 consecutive patients (29 with left main stem interventions) using SES, a 14% (5 patients) restenosis rate occurred over an average follow-up period of >2 years. Interestingly, a “membranous diaphragm” at the carina was identified in nearly half the patients, with restenosis occurring in just one of these patients.

Conversely, Stinis et al²⁶ showed that in 74 consecutive patients with predominantly left anterior descending-diagonal lesions, that the target lesion revascularization rate was more than twice as high in the simultaneous V-stenting group (14 patients, 40%), compared with the crush group (5 patients, 12.8%) at a follow-up of >3 years. Whether lesion location played a role in the disparity of these results remains unclear.

Robust, well-designed trials are required to evaluate the feasibility of this technique further.

The issue as to whether the actual presence of the stent in the vessel wall negatively alters the wall shear stress sufficiently to promote restenosis has proven to be controversial, with conflicting evidence existing in the literature. In a recent, larger, well-designed trial, Papafaklis et al²⁷ demonstrated the presence of significant numbers of “pockets” of low shear stress within stented segments, secondary to local geometric factors such as angulation or curvature, and that these pockets were significantly associated with NIH formation at 6-month follow-up with BMS and PES. Interestingly, this was not seen with SES, suggesting that sirolimus significantly attenuated the neointimal response to low shear stress. Paclitaxel was unable to do this, perhaps because of its differing pharmacological mode of action or even its shorter drug-release kinetics, which will be discussed later.^{1,3,27}

Progression of Atherosclerosis Within a Stented Segment

Plaque progression and rupture leading to myocardial infarction (MI) have been reported in rare case reports involving BMS^{28,29} and more recently DES.³⁰ The underlying pathological mechanisms are one of necrotic core plaque progression and rupture either within the stent with BMS or at the stent edge in incompletely covered lipid-core plaque with DES (see Implantation Factors).³⁰

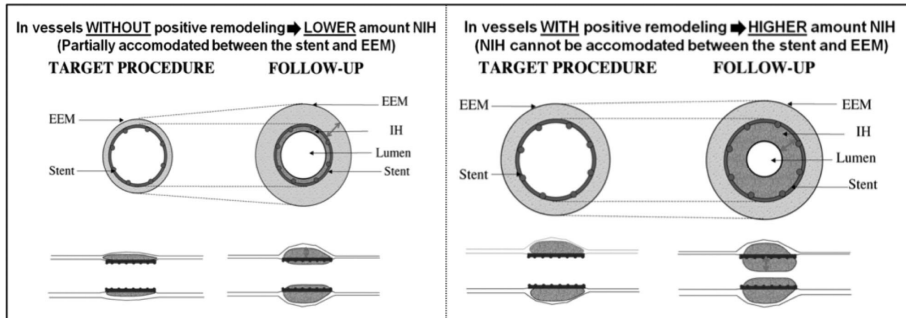


Figure 5. The phenomenon of the increased likelihood of restenosis occurring in positively remodeled vessels. Red arrow indicates position where NIH can potentially grow in nonremodeled (between the stent and EEM) (left image) and remodeled vessels (right image). Because the NIH cannot be accommodated between the stent and the EEM in remodeled vessels, this results in luminal compromise. NIH indicates neointimal hyperplasia; EEM, external elastic membrane. Adapted and reproduced with permission from Spanos et al.³⁷

In the Moderate Vein Graft Lesion Stenting With the Taxus Stent and Intravascular Ultrasound (VELETI) pilot trial,³¹ it was potentially shown that PES implantation to cover moderately diseased, flow-limiting lesions in old saphenous vein grafts lead to apparent “plaque sealing.” A reduced rate of saphenous vein graft disease progression, as evidenced by a lower 12-month minimum lumen area on intravascular ultrasound (IVUS) assessment and a trend toward a lower incidence of major adverse cardiovascular events at 1-year follow-up was found, compared with medical treatment alone. Conversely, Jensen et al³² showed in a serial IVUS study of 74 patients with diabetes post-DES implantation that, at 8-month follow-up, PES led to a significant, but mild, increase in the rate of plaque progression compared with SES.

“Thromborestenosis” Phenomenon

“Thromborestenosis” is a term first described by Oikawa et al³³ to describe an intriguing theory in which chronic thrombus formation may play an integral part in the development of ISR. Within their study, the incidences of thrombus and fibrin deposition were more frequently observed with ISR lesions associated with SES implantation (12 of 13 cases) compared with BMS (2 of 8 cases). In support of this theory is the fact that plaque rupture with nonocclusive thrombus is a well-recognized mechanism of progression of disease in de novo atherosclerotic lesions.³⁴ Furthermore in a study of patients who died of LST, 2 of 14 autopsy cases revealed evidence of ISR with superimposed thrombus.³⁵

Conversely, Rittersma et al³⁶ also showed evidence of chronic thrombi that were days to weeks old in at least 50% of 211 consecutive STEMI patients with de novo lesions who had thrombus aspirates taken within 6 hours of the onset of their symptoms. Hypothetically the presence of older thrombi was speculated to be related to clinically silent nonocclusive athero-thrombotic events in the preceding days to weeks before the clinical presentation of occlusive thrombosis. Whether this latter theory is also an explanation for the presence of thrombi seen with ISR is presently unclear.

Vessel Remodeling

The implantation of DES in vessels that previously have undergone positive remodeling secondary to a large plaque burden, the “Glagov” phenomenon, also has been shown to be a significant predictor of restenosis (Figure 5).³⁷

Small Vessels

This is discussed in Stent Factors with strut thickness.

Stent Factors

Polymer Release Kinetics

Polymer release kinetics plays a key and fundamental role in the prevention of restenosis. The Paclitaxel In-Stent Controlled Elution Study (PISCES) trial³⁸ was the first human study to demonstrate this principle involving the use of the Conor stent with 6 different polymer-drug release formulations. The main finding of this trial was that the duration of the drug release had a far greater impact on the inhibition of NIH than the dose of drug delivered. For example, 10 μg of paclitaxel released over 10 days following DES implantation appeared to have little effect on NIH formation, whereas the same dosage of drug released over a 30-day period led to a profound reduction in NIH, with a more than halving (57% reduction) of the LLL. Interestingly, 30 μg of the same drug released over a 10-day period also was less effective.

The polymer-free biolimus A9-eluting stent, with two different doses of biolimus, demonstrated noninferiority compared to PES in the first-in-human BIOFREEDOM study.³⁹ An in-stent LLL of 0.17 mm (standard-dose biolimus group: 15.6 $\mu\text{g}/\text{mm}$ stent length), 0.22 mm (low-dose biolimus group: 7.8 $\mu\text{g}/\text{mm}$ stent length) and 0.35 mm (PES) were reported, with no significant differences in major adverse cardiovascular events or cases of stent thrombosis observed.

Molecular biology studies have suggested that the genes responsible for the proliferative response potentially remain active for a period of up to 21 days after vessel injury.⁴⁰ These clinical findings therefore support the concept of a certain threshold of drug, delivered over a sustained prolonged

period of time, being required to “dampen” down the inflammatory and subsequent NIH response.

Type of DES? Type of Drug?

Schomig et al.⁴¹ in a meta-analysis of 16 trials comparing SES with PES, suggested the benefit of SES over PES over a median 2-year follow-up, with a significant reduction in TVR (hazard ratio 0.74, 95% [confidence interval] CI 0.63 to 0.87, $P < 0.001$) and stent thrombosis (hazard ratio 0.66, 95% CI 0.46 to 0.94, $P = 0.02$) without a mortality benefit. The reasons for this apparent benefit are complex but have been suggested to be related to the slower polymer release kinetics of SES compared with PES. However, data from the Sirolimus-Eluting Stent Compared with Paclitaxel-Eluting Stent for Coronary Revascularization (SIRTAX) trial have suggested a possible “catch-up” in LLL with SES over a 5-year follow-up, with no significant differences in LLL observed between the 2 groups.³

Data from the Swedish Coronary Angiography and Angioplasty Registry (SCAAR), registry involving >35 000 patients implanted with 4 different types of DES (Endeavor, SES, Taxus Express, and Liberté) in real-world practice at 2-year follow-up showed that the rates of restenosis with DES implantation were significantly higher in patients with diabetes mellitus and that important differences in the efficacy of differing types of DES existed.⁴² In particular, the restenosis rates with Endeavor were twice as high in diabetic patients compared with other DES types. Higher restenosis rates were also evident in diabetic patients with Endeavor (relative risk 1.77, 95% CI 1.29 to 2.43) and SES (relative risk 1.25, 95% CI 1.04 to 1.51) when compared with nondiabetic patients. Five-year unpublished follow-up data from the SCAAR registry⁴³ continued to demonstrate differences in the efficacy of the first- and second-generation DES in reducing the rates of restenosis, with a trend toward better outcomes seen after nearly 2 years of EES use.

The EES releases 80% of the drug within 30 days and nearly all the drug within 4 months. In the Spirit I, II, and III trials, a LLL of 0.10, 0.16, and 0.33 mm and TVR rates of 3.8%, 3.4%, and 4.6% were observed at 6, 12, and 24 months, respectively.³

Conversely, the Endeavor reported a LLL of 0.60 mm and 0.67 mm and TVR of 6.3% and 4.5%, respectively, in the Endeavor III and IV trials at 12 months. The Endeavor, however, elutes 95% of its drug very rapidly (within 14 days); this is highly likely to be the main reason for the poorer results seen. The next-generation Endeavor Resolute stent, consisting of the same cobalt chromium metallic platform (Driver BMS) and the drug (zotarolimus) as the Endeavor stent, but with substantially longer polymer drug release kinetics (180 days), reported an in-stent LLL of 0.12, 0.22, and 0.27 mm at 4, 9, and 13 months respectively, with angiographic equivalency (LLL 0.19 mm) in terms of meeting the criteria for noninferiority ($P = 0.08$), being met when compared with EES. Equivalency in the 12-month primary end point of target lesion failure (a composite of cardiac death, target vessel MI, and clinically driven target lesion revascularization (8.2% versus 8.3%) and a slight increase in

the rate of definite stent thrombosis (1.2% versus 0.3%, $P = 0.01$) were also seen.⁴⁴

Stent Gap, Nonuniform Strut Distribution and Drug Deposition

Takebayashi et al.⁴⁵ classically described the number and distribution of DES struts, as identified by IVUS, as being independent significant risk factors (fewer struts and nonuniform stent strut distribution) for NIH formation and the subsequent risk of restenosis. Nonuniform DES strut distribution has been suggested to be attributable to features such as stent design (eg, open versus closed cell), stent gap, vessel curvature, coronary bifurcations, ostial lesions, stent under or overexpansion, polymer peeling, and stent fracture.

Small Vessels and Strut Thickness

Small-vessel disease is a recognized challenging lesion subset with significant risks of restenosis seen with plain old balloon angioplasty and BMS.¹ A recent meta-analysis of the use of DES in small-vessel disease demonstrated that both LLL and binary restenosis were largely dependent on the type of DES implanted.⁴⁶ In particular, Xience and Cypher led to restenosis rates of 10% to 15% (5% to 10% and 0% to 5% in medium and large vessels, respectively), compared with 20% to 25% with Taxus (10% to 20% and 2.5% to 7.5% in medium and large vessels, respectively) and 30% to 35% with Endeavor (20% to 30% and 5 to 12.5% in medium and large vessels, respectively).

Mechanisms suggested to explain the poorer outcomes associated with small vessels include: (1) a high degree of vessel stretch and injury, (2) a smaller postprocedural lumen area, and (3) a higher metal density.⁴⁷ The overstretch theory, however, is controversial with evidence suggesting a possible adverse effect with increased NIH,⁴⁷ no significant effect,⁴⁸ or even potential benefit.⁴⁹ The latter beneficial effects have been proposed to be related to a higher balloon-to-artery ratio, the so-called bigger is better paradigm (see Implantation Factors) leading to appropriate apposition of the stent to the vessel wall.

Thicker stent struts have been linked to an increased risk of restenosis with BMS and small vessels.⁴⁷ The underlying rationale is that a thinner stent strut would have less of a “footprint” on the vessel wall with a consequential reduced inflammatory response. With DES, however, a complex relationship exists between the strut material and characteristics, stent design, polymer type, and drug release kinetics, with Cypher and Xience appearing to have the lowest risk of binary restenosis in small vessels, despite a large disparity in stent strut thicknesses ($\approx 150 \mu\text{m}$ versus $90 \mu\text{m}$). A fairer comparison perhaps would be between the Taxus Liberté and Express because both are identical except the Taxus Liberté contains thinner struts, more flexible cell geometry, and uniform cell distribution. In the SCAAR registry,⁴² the Taxus Express was shown to have a mild but significantly higher adjusted risk of restenosis compared to Taxus Liberté.

“On- and Off-Label” Use of DES

The Strategic Transcatheter Evaluation of New Therapies (STENT) Group, is the largest, multicenter, prospective

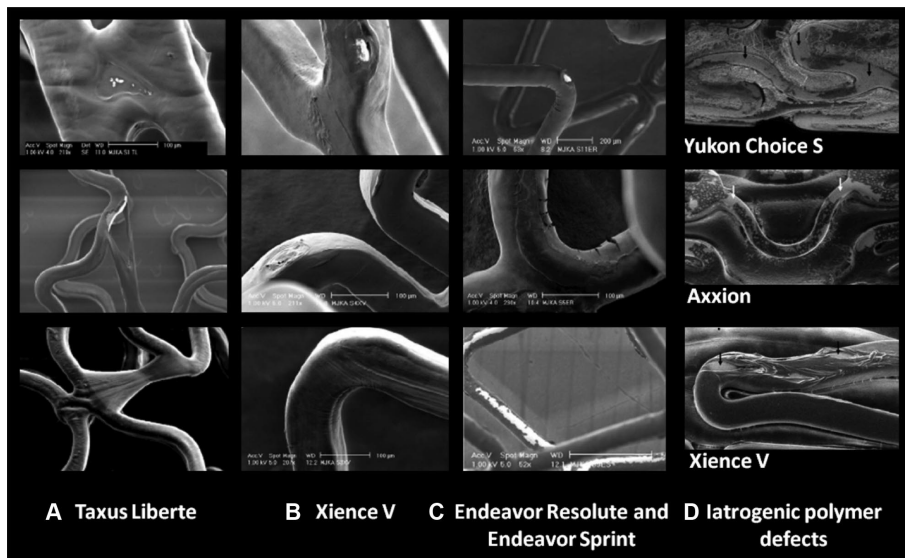


Figure 6. Polymer defects seen in second-generation DES. DES indicates drug-eluting stent. **A**, Taxus Liberté: thinning (top), webbing with (middle), and without (bottom) bare-metal exposure of the polymer coating. **B**, Xience V: apparent bare-metal area (top), crater-shaped irregularity without bare-metal exposure (middle), and “wrinkles” in the polymer coating (bottom). **C**, Endeavor Resolute: crater irregularity with an apparent central bare-metal area (top), cracks in the polymer coating (middle); Endeavor Sprint: polymer peeling with exposure of significant bare-metal areas (bottom). Iatrogenic polymer defects: **D**, No drug coverage was seen in up to 40% of the surface area of the unexpanded Yukon Choice S (black arrows) and Axxion (white arrows); **D**, Xience V: wrinkling and cracking of polymer with bare metal exposure (black arrows). **A–C**, Adapted and reproduced from Basalus et al, *EuroIntervention*. 2009;5:160, Copyright (2009), with permission from Europa Edition.⁵³ **D**, Adapted and reproduced with permission from Wiemer et al.⁵⁴

registry involving >15 000 patients, evaluated the late outcomes associated with DES implantation in the United States.⁵⁰ This compared on-label (short de novo lesions in coronary arteries measuring >2.5 mm and <3.5 mm for SES or <3.75 mm PES) and off-label (ostial, left main stem, chronic total occlusion, saphenous vein graft, small or large vessels/multivessel, STEMI, ISR lesions) indications for DES implantation. An almost doubling in the TVR rate was seen in the off-label group at 9 months (5.7% versus 3.2%, $P<0.0001$) and 2 years (11.8% versus 6.5%, $P<0.0001$).

Data from the Synergy between Percutaneous Coronary Intervention with TAXUS and Cardiac Surgery (SYNTAX) study, reflecting a population of patients with highly complex off-label use of DES in 3-vessel or left main stem disease, have reported even higher rates of TVR at 1, 2, and 3 years at 11.6%, 17.4%, and 19.7%, respectively.⁵¹

Polymer Disruption, Peeling, and Cracking

Polymer disruption, peeling, and cracking, and subsequent exposure of bare-metal areas have been demonstrated to occur in bench studies involving both first- and second-generation DES (Figure 6) using light or scanning electron microscopy.^{52,53} Although there is no direct evidence to suggest that the integrity of the polymer coating is a direct cause of restenosis, there are sufficient theoretical concerns to

warrant concern through nonuniform local drug distribution or the disrupted polymer potentially acting as a nidus for an ongoing inflammatory response.¹⁴

Other concerns with regard to the potential for polymer disruption involve the percutaneous coronary intervention procedure itself. Wiemer et al⁵⁴ demonstrated that in DES that had failed to be delivered to the intended implantation site in tortuous calcified lesions, significant damage and cracking of the polymer had occurred to varying extents with multiple types of second-generation DES. Scanning electron microscopy revealed many cases of deep damage to the polymer with exposure of the bare metal, in particular, the Endeavor RX stents showed up to 20% damage to the surface area. With polymer-free DES, a large proportion of the surface area was shown to be without any layer of drug (Figure 6).

In bench work utilizing scanning electron microscopy of the polymer integrity of 5 different types of DES (Cypher, Cypher Select, Endeavor, Taxus Express, and Taxus Liberté) after undergoing kissing balloon postdilatation, Guerin et al⁵⁵ demonstrated significantly greater coating damage to the ostial struts, especially along the overstretched segments, with cracking of the polymer seen in all cases and even exposure of bare metal. Of note is that the Endeavor stent showed a subtotal destruction of its coating on the luminal surface in all segments, whereas the other DES demonstrated more focal localized abnormalities.

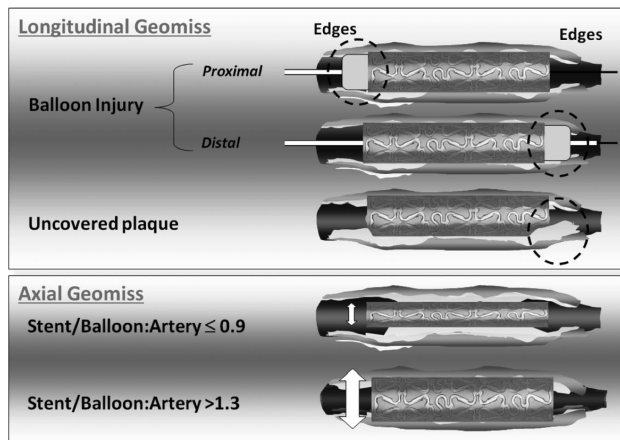


Figure 7. Illustration of the mechanisms of longitudinal (LGM) and axial geographical miss (AGM). Adapted and reproduced with permission from Costa et al.⁶⁴

Stent Fractures

Stent fracture related to DES implantation in coronary arteries was first reported by our group in 2004. Subsequent retrospective and prospective registries have quoted restenosis rates ranging from 15% to 100% in patients identified to have stent fractures.⁵⁶ In the only randomized controlled trial reporting the incidence of stent fracture and outcomes after DES implantation and subsequent mandatory angiographic follow-up (LONG-DES-II study), a 14% incidence of restenosis was observed.⁵⁷

The restenosis associated with DES fractures tends to occur fairly late and focally, reflecting the local trauma sustained by the vessel at the fracture site. Consequently, the subsequent healing response occurs without any drug to suppress the NIH response, which in itself may be further exacerbated by exposure of the vessel to the disrupted polymer.

The etiology of the DES fractures appears to be related to 2 principle factors. First, mechanical fatigue of the metallic stent can occur because of excessive movements during cardiac contraction, especially at a hinge-point where the potential for 2 opposing forces may occur at the same site. In particular, this may occur in the right coronary artery or a saphenous vein graft, because of their greater propensity for angulation and tortuosity. Second, a closed-cell design, such as occurs with SES, is less likely to be able to withstand the pressures related to excessive movements compared with the open-cell design of a PES. The incidence of stent fracture is reported as less than 0.1% with the PES and approximately 2.3% with SES.⁵⁶

Long stents, overlapping stents, tight lesions that have been vigorously postdilated and expanded, myocardial bridge sites, and areas of significant curvature are all factors that may predispose patients to DES fracture.⁵⁶

Implantation Factors

Incomplete Stent Expansion

A smaller postprocedural minimal lumen diameter and a greater residual stenosis have been shown to be significant

predictors of long-term patency and clinical outcomes. Evidence of stent underexpansion, as assessed by IVUS and despite apparently successful angiographic results, has been reported to be as high as 24% and 28% with SES and PES, respectively.^{58,59} However, what proportion of these cases is clinically relevant remains unclear.

In a classical meta-analysis (n=2972 patients) investigating IVUS versus angiographic-guided BMS implantation, Casella et al⁶⁰ demonstrated at 6-month follow-up a reduction in TVR (OR 0.62; 95% CI 0.49 to 0.78; $P=0.00003$), binary restenosis (OR 0.75; 95% CI 0.60 to 0.94; $P=0.01$), and major adverse cardiovascular events (OR 0.79; 95% CI 0.64 to 0.98; $P=0.03$). Of note is that only one small, single-center randomized controlled trial on IVUS-guided DES implantation has been published; this failed to show any differences in the clinical end points of major adverse cardiovascular events (death, MI, and reintervention) at 18 months.⁶¹

The initial results of the important Angiographic versus IVUS Optimization (AVIVO) randomized, multicenter trial, however, have recently been presented.⁶² IVUS versus angiographic-guided DES implantation in complex lesions was investigated, with 142 patients in each study arm. At 30 days and 9 months, no significant differences were seen in the combined end point of MI, target lesion revascularization, TVR, or cardiac death (85.9% versus 83.1%, $P=0.47$). The primary end point of a higher minimal lumen diameter, however, was seen in the IVUS-guided DES implantation group (2.70 mm versus 2.51 mm, $P=0.0002$). Because only 39% of patients had quantitative coronary angiography at 9 months, no comments could be made regarding whether this approach would potentially lead to a reduction in restenosis rates.

The most plausible and strongest theory to explain the underlying mechanism relating stent underexpansion to restenosis is the so-called bigger-is-better paradigm. Effectively, if the minimum stent area is smaller at baseline, then the expected NIH formation post-DES implantation would be

more likely to be of significance, whereas if the minimum stent area was larger, then the same amount of NIH would be clinically less relevant in causing binary restenosis.⁶³ Other theories postulated have included possible asymmetrical stent expansion affecting the subsequent pattern of neointimal growth through uneven drug delivery.¹

Geographical Miss/Barotrauma to Unstented Segments

Geographical miss (GM) is essentially a failure to appropriately cover an injured vessel, such as occurs after balloon-associated vessel barotrauma, or incomplete coverage of atherosclerotic plaque. GM associated with SES implantation was investigated in the prospective evaluation of the impact of Stent deployment Techniques on cLinicalL outcomes of patients treated with the cypheR stent (STLLR) study.⁶⁴ GM was observed in nearly two-thirds (66.5%) of the study group with almost half (47.6%) of the patients experiencing longitudinal GM, over one-third (35.2%) axial GM, and 16.5% a combination of the two. Longitudinal GM was defined as injured or diseased stenotic segment not fully covered by DES, and axial GM was defined as potentially undersizing or oversizing the balloon (Figure 7).

At 1-year follow-up, there was more than a 2-fold increase in TVR (5.1% versus 2.5%; $P=0.025$) and a 3-fold increase in MI (2.4% versus 0.8%; $P=0.04$) in patients with GM. These findings were almost exclusively related to longitudinal GM (6.1% versus 2.6%; $P=0.001$) with two-thirds of cases being secondary to balloon injury outside the stent margins. The lack of effect of axial GM (4.2% versus 4.3%; p non significant) recently has been corroborated, in which it was shown that the balloon-to-artery ratio or the occurrence of edge dissections (potentially associated with axial GM) did not have a significant impact on the risk of restenosis^{48,65} and does perhaps argue against the IVUS optimization of DES deployment.

Deployment of a DES in a Clot-Laden Arterial Segment

The deployment of a DES in a clot-laden arterial segment has been shown in an ex vivo model to lead to a 10-fold reduction in drug penetration into the vessel wall,⁶⁶ which may potentially affect clinical outcomes (Figure 8). Despite these theoretical concerns, a recent meta-analysis of 13 trials ($n=7244$) has shown the significant benefits of DES over BMS in primarily reducing TVR (5.11% versus 11.19%, $P<0.00001$) and recurrent MI (3.03% versus 3.70%, $P=0.02$) in patients with STEMI at up to 1 year.⁶⁷

The widespread use of glycoprotein-IIb/IIIa inhibitors and aspiration thrombectomy devices may be the reasons why these concerns may have not materialized in clinical trials in the short term. Concerns over the long-term safety of DES in STEMI do persist, however, because of the potential risk of late-acquired stent malapposition and consequent LST.³ The concerns about reduced absorption of the drug from DES should be borne in mind in a thrombus-laden vessel, especially when there has been inadequate resolution of thrombus and DES implantation is to be considered.

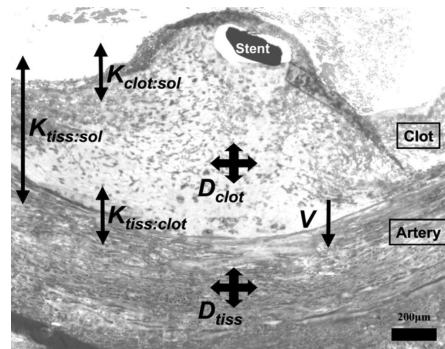


Figure 8. Deployment of a DES in a clot-laden arterial segment. The concepts of drug diffusivities in clot (D_{clot}) and tissue (D_{tiss}), drug capacity of clot relative to solution ($K_{clot:sol}$), drug capacity of arterial tissue relative to solution ($K_{tiss:clot}$), drug capacity of arterial tissue relative to solution ($K_{tiss:sol}$) and drug convective velocities (V) are illustrated and demonstrate the complexities of stenting in acute MI. DES indicates drug-eluting stent; MI, myocardial infarction. Reproduced with permission from Hwang et al.⁶⁶

Conclusion

Despite the low incidence of DES restenosis, the burden of ISR in absolute numbers probably will continue to grow with the increasing uptake of second-generation DES in conventional percutaneous coronary intervention practice. Large-scale clinical trials and registries, therefore, are required to best translate these restenotic mechanisms into either enhanced DES design or further effective treatment options. For example, the pooled data of the RCTs investigating EES comprises almost 15 000 patients and, apart from mortality, would potentially be of sufficient power to detect rare events such as stent thrombosis.⁶⁸

Apart from biological factors, there are potentially controllable factors within arterial and stent factors. However, it should be acknowledged that in the treatment of in-stent-restenosis, the evidence for using a DES with a different drug remains unproven.⁹ Ultimately, the implantation factors are the most important controllable factors from the perspective of the interventional cardiologist.

Acknowledgments

Dr Farooq wishes to acknowledge the support of The Dickinson Trust Traveling Scholarship Fund, Manchester Royal Infirmary, Manchester, England, United Kingdom. Dr Gogas has received grant support from the Hellenic Heart Foundation (ELIKAR), Athens, Greece.

Disclosures

None.

References

1. Duckers HJ, Nabel EG, Serruys PW, eds. *Essentials of Restenosis: For the Interventional Cardiologist*. Totowa, NJ: Humana Press; 2007.
2. Byrne RA, Eberle S, Kastrati A, Dibra A, Ndrepepa G, Iijima R, Mehilli J, Schomig A. Distribution of angiographic measures of restenosis after drug-eluting stent implantation. *Heart*. 2009;95:1572-1578.

3. Garg S, Serruys PW. Coronary stents: current status. *J Am Coll Cardiol*. 2010;56:S1–S42.
4. Corbett SJ, Cosgrave J, Melzi G, Babic R, Biondi-Zoccai GG, Godino C, Morici N, Airolidi F, Michev I, Montorfano M, Sangiorgi GM, Bonizzoni E, Colombo A. Patterns of restenosis after drug-eluting stent implantation: Insights from a contemporary and comparative analysis of sirolimus- and paclitaxel-eluting stents. *Eur Heart J*. 2006;27:2330–2337.
5. van Beusekom HM, Saia F, Zindler JD, Lemos PA, Swager-Ten Hoor SL, van Leeuwen MA, de Feijter PJ, Serruys PW, van der Giessen WJ. Drug-eluting stents show delayed healing: paclitaxel more pronounced than sirolimus. *Eur Heart J*. 2007;28:974–979.
6. Chieffo A, Foglieni C, Nodari RL, Briguori C, Sangiorgi G, Latib A, Montorfano M, Airolidi F, Michev I, Carlino M, Colombo A, Maseri A. Histopathology of clinical coronary restenosis in drug-eluting versus bare metal stents. *Am J Cardiol*. 2009;104:1660–1667.
7. Rathore S, Kinoshita Y, Terashima M, Katoh O, Matsuo H, Tanaka N, Kimura M, Tsuchikane E, Nasu K, Ehara M, Asakura K, Asakura Y, Suzuki T. A comparison of clinical presentations, angiographic patterns and outcomes of in-stent restenosis between bare metal stents and drug eluting stents. *EuroIntervention*. 2010;5:841–846.
8. Steinberg DH, Pinto Slotow TL, Buch AN, Javaid A, Roy PK, Garg S, Okabe T, Torgerson R, Smith KA, Xue Z, Suddath WO, Kent KM, Sattler LF, Pichard AD, Lindsay J, Waksman R. Impact of in-stent restenosis on death and myocardial infarction. *Am J Cardiol*. 2007;100:1109–1113.
9. Alfonso F. Treatment of drug-eluting stent restenosis the new pilgrimage: quo vadis? *J Am Coll Cardiol*. 2010;55:2717–2720.
10. Richardson A, Kaye SB. Drug resistance in ovarian cancer: the emerging importance of gene transcription and spatio-temporal regulation of resistance. *Drug Resist Updat*. 2005;8:311–321.
11. Huang S, Houghton PJ. Mechanisms of resistance to rapamycins. *Drug Resist Updat*. 2001;4:378–391.
12. Hausleiter J, Kastrati A, Mehilli J, Vogeser M, Zohnhofer D, Schuhlen H, Goos C, Pache J, Dotzer F, Pogatsis-Murray G, Dirschinger J, Heemann U, Schomig A. Randomized, double-blind, placebo-controlled trial of oral sirolimus for restenosis prevention in patients with in-stent restenosis: the Oral Sirolimus to Inhibit Recurrent In-stent Stenosis (OSIRIS) trial. *Circulation*. 2004;110:790–795.
13. Nakazawa G, Finn AV, Ladich E, Ribichini F, Coleman L, Kolodgie FD, Virmani R. Drug-eluting stent safety: findings from preclinical studies. *Expert Rev Cardiovasc Ther*. 2008;6:1379–1391.
14. Wilson GJ, Nakazawa G, Schwartz RS, Huijbregte B, Poff B, Herbst TJ, Baim DS, Virmani R. Comparison of inflammatory response after implantation of sirolimus- and paclitaxel-eluting stents in porcine coronary arteries. *Circulation*. 2009;120:141–149; 1–2.
15. Cook S, Ladich E, Nakazawa G, Eshetehardi P, Neidhart M, Vogel R, Togni M, Wenaweser P, Billinger M, Seiler C, Gay S, Meier B, Pichler WJ, Juni P, Virmani R, Windecker S. Correlation of intravascular ultrasound findings with histopathological analysis of thrombus aspirates in patients with very late drug-eluting stent thrombosis. *Circulation*. 2009;120:391–399.
16. Patil SU, Long A. Nickel hypersensitivity and coronary artery stents. In: Basow DS, ed., *UpToDate*. Waltham, MA: UpToDate; 2010.
17. Nakazawa G, Tanabe K, Aoki J, Onuma Y, Higashikuni Y, Yamamoto H, Ohtsuki S, Yachi S, Yagishita A, Nakajima H, Hara K. Sirolimus-eluting stents suppress neointimal formation irrespective of metallic allergy. *Circ J*. 2008;72:893–896.
18. Katsaros KM, Kastl SP, Zorn G, Maurer G, Wojta J, Huber K, Christ G, Speidl WS. Increased restenosis rate after implantation of drug-eluting stents in patients with elevated serum activity of matrix metalloproteinase-2 and -9. *J Am Coll Cardiol Cardiovasc Interv*. 2010; 3:90–97.
19. Monraats PS, Pires NM, Agema WR, Zwiderman AH, Schepers A, de Maat MP, Doevendans PA, de Winter RJ, Tio RA, Waltenberger J, Frants RR, Quax PH, van Vlijmen BJ, Atsma DE, van der Laarse A, van der Wall EE, Jukema JW. Genetic inflammatory factors predict restenosis after percutaneous coronary interventions. *Circulation*. 2005;112:2417–2425.
20. Voziatzi K, Apostolakis S, Voudris V, Thomopoulou S, Kochiadakis GE, Spandidos DA. Interleukin 8 gene polymorphisms and susceptibility to restenosis after percutaneous coronary intervention. *J Thromb Thrombolysis*. 2010;29:134–140.
21. Sterpetti AV, Cucina A, D'Angelo LS, Cardillo B, Cavallaro A. Shear stress modulates the proliferation rate, protein synthesis, and mitogenic activity of arterial smooth muscle cells. *Surgery*. 1993;113:691–699.
22. Wentzel JJ, Gijzen FJ, Schuurbiens JC, van der Steen AF, Serruys PW. The influence of shear stress on in-stent restenosis and thrombosis. *EuroIntervention*. 2008;4(suppl C):C27–C32.
23. Carlier SG, van Damme LCA, Blommerde CP, Wentzel JJ, van Langehove G, Verheye S, Kockx MM, Knaepen MWM, Cheng C, Gijzen F, Duncker DJ, Stergiopoulos N, Slager CJ, Serruys PW, Krams R. Augmentation of wall shear stress inhibits neointimal hyperplasia after stent implantation: inhibition through reduction of inflammation? *Circulation*. 2003;107:2741–2746.
24. Kim YH, Park DW, Suh IW, Kang JS, Hwang ES, Jeong YH, Lee SW, Lee CW, Hong MK, Kim JJ, Park SW, Park SJ. Long-term outcome of simultaneous kissing stenting technique with sirolimus-eluting stent for large bifurcation coronary lesions. *Catheter Cardiovasc Interv*. 2007;70:840–846.
25. Morton AC, Siotia A, Arnold ND, Korgul P, Bowles J, Heppenstall J, Gunn J. Simultaneous kissing stent technique to treat left main stem bifurcation disease. *Catheter Cardiovasc Interv*. 2007;69:209–215.
26. Stinis CT, Hu SP, Price MJ, Teirstein PJ. Three-year outcome of drug-eluting stent implantation for coronary artery bifurcation lesions. *Catheter Cardiovasc Interv*. 2010;75:309–314.
27. Papafaklis MI, Bourantas CV, Theodorakis PE, Katsouras CS, Naka KK, Fotiadis DI, Michalis LK. The effect of shear stress on neointimal response following sirolimus- and paclitaxel-eluting stent implantation compared with bare-metal stents in humans. *J Am Coll Cardiol Interv*. 2010;3:1181–1189.
28. Ramcharitar S, Garcia-Garcia HM, Nakazawa G, Kukreja N, Lighthart J, Virmani R, Serruys PW. Ultrasonic and pathological evidence of a neointimal plaque rupture in patients with bare metal stents. *EuroIntervention*. 2007;3:290–291.
29. Hoole SP, Starovoytov A, Hamburger JN. In-stent restenotic lesions can rupture - A case against plaque sealing [Epub ahead of print September 17, 2010]. *Catheter Cardiovasc Interv*. doi: 10.1002/ccd.22791.
30. Waxman S, Freilich MI, Suter MJ, Shishkov M, Bilazarian S, Virmani R, Bouma BE, Tearney GJ. A case of lipid core plaque progression and rupture at the edge of a coronary stent: elucidating the mechanisms of drug-eluting stent failure. *Circ Cardiovasc Interv*. 2010;3:193–196.
31. Rodes-Cabau J, Bertrand OF, Larose E, Dery J-P, Rinfret S, Bagur R, Proulx G, Nguyen CM, Cote M, Landcop M-C, Boudreault J-R, Rouleau J, Roy L, Gleeton O, Barbeau G, Noel B, Couris J, Dagenais GR, Despres J-P, DeLarochelliere R. Comparison of Plaque Sealing With Paclitaxel-Eluting Stents Versus Medical Therapy for the Treatment of Moderate Nonsignificant Saphenous Vein Graft Lesions: The Moderate VEIn Graft Lesion Stenting With the Taxus Stent and Intravascular Ultrasound (VELETT) Pilot Trial. *Circulation*. 2009;120:1978–1986.
32. Jensen LO, Maeng M, Mintz GS, Christiansen EH, Hansen KN, Galloe A, Kelback H, Lassen JF, Thuesen L, Thyssen P. Serial intravascular ultrasound analysis of peri-stent remodeling and proximal and distal edge effects after sirolimus-eluting or paclitaxel-eluting stent implantation in patients with diabetes mellitus. *Am J Cardiol*. 2009;103:1083–1088.
33. Oikawa Y, Yajima J, Costa MA, Matsuno S, Akabane M, Funada R, Inaba T, Nakagawa Y, Nakamura M, Nagashima K, Kirigaya H, Ogasawara K, Sawada H, Aizawa T. Intravascular ultrasound, angiographic and histopathological characterisation of heterogeneous patterns of restenosis after sirolimus-eluting stent implantation: insights into potential "thromborestenosis" phenomenon. *EuroIntervention*. 2010;6:380–387.
34. Goldstein JA. Angiographic plaque complexity: the tip of the unstable plaque iceberg. *J Am Coll Cardiol*. 2002;39:1464–1467.
35. Joner M, Finn AV, Farb A, Mont EK, Kolodgie FD, Ladich E, Kutys R, Skorjia K, Gold HK, Virmani R. Pathology of drug-eluting stents in humans: delayed healing and late thrombotic risk. *J Am Coll Cardiol*. 2006;48:193–202.
36. Rittersma SZH, van der Wal AC, Koch KT, Piek JJ, Henriques JPS, Mulder KJ, Ploegmakers JPH, Meesterma M, de Winter RJ. Plaque instability frequently occurs days or weeks before occlusive coronary thrombosis: a pathological thrombectomy study in primary percutaneous coronary intervention. *Circulation*. 2005;111:1160–1165.
37. Spanos V, Stankovic G, Tobis J, Colombo A. The challenge of in-stent restenosis: insights from intravascular ultrasound. *Eur Heart J*. 2003;24:138–150.
38. Serruys PW, Sianos G, Abizaid A, Aoki J, den Heijer P, Bonnier H, Smits P, McClean D, Verheye S, Belardi J, Condado J, Pieper M, Gambone L, Bressers M, Symons J, Sousa E, Litvack F. The effect of variable dose and release kinetics on neointimal hyperplasia using a novel paclitaxel-

- eluting stent platform: the Paclitaxel In-Stent Controlled Elution Study (PISCES). *J Am Coll Cardiol*. 2005;46:253–260.
39. Grube E. 12-Month angiographic follow-up of the novel non-polymeric Biolimus A9-coated stent for the treatment of de novo coronary lesions: results from the prospective, multicenter, randomized BIOFREEDOM Clinical Trial. Paper presented at: Transcatheter Cardiovascular Therapeutics; September 21 to 25, 2010; Washington DC.
 40. Tanner FC, Yang ZY, Duckers E, Gordon D, Nabel GJ, Nabel EG. Expression of cyclin-dependent kinase inhibitors in vascular disease. *Circ Res*. 1998;82:396–403.
 41. Schomig A, Dibra A, Windecker S, Mehilli J, Suarez de Lezo J, Kaiser C, Park SJ, Goy JJ, Lee JH, Di Lorenzo E, Wu J, Juni P, Pfisterer ME, Meier B, Kastrati A. A meta-analysis of 16 randomized trials of sirolimus-eluting stents versus paclitaxel-eluting stents in patients with coronary artery disease. *J Am Coll Cardiol*. 2007;50:1373–1380.
 42. Frobert O, Lagerqvist B, Carlsson J, Lindback J, Stenestrand U, James SK. Differences in restenosis rate with different drug-eluting stents in patients with and without diabetes mellitus: a report from the SCAAR (Swedish Angiography and Angioplasty Registry). *J Am Coll Cardiol*. 2009;53:1660–1667.
 43. James S. Safety and drug-eluting stents. Paper presented at: European Society of Cardiology Congress; August 28 to September 1, 2010; Stockholm, Sweden.
 44. Serruys PW, Silber S, Garg S, van Geuns RJ, Richardt G, Buszman PE, Kelbäck H, van Boven AJ, Hofma SH, Linke A, Klauss V, Wijns W, Macaya C, Garot P, DiMario C, Manoharan G, Kornowski R, Ischinger T, Bartorelli A, Ronden J, Bressers M, Gobbens P, Negota M, van Leeuwen F, Windecker S. Comparison of zotarolimus-eluting and everolimus-eluting coronary stents. *N Engl J Med*. 2010;363:136–146.
 45. Takebayashi H, Mintz GS, Carlier SG, Kobayashi Y, Fujii K, Yasuda T, Costa RA, Moussa I, Dangas GD, Mehran R, Lansky AJ, Kreps E, Collins MB, Colombo A, Stone GW, Leon MB, Moses JW. Nonuniform strut distribution correlates with more neointimal hyperplasia after sirolimus-eluting stent implantation. *Circulation*. 2004;110:3430–3434.
 46. Biondi-Zoccai G, Moretti C, Abbate A, Sheiban I. Percutaneous coronary intervention for small vessel coronary artery disease. *Cardiovasc Revasc Med*. 2010;11:189–198.
 47. Briguori C, Sarais C, Pagnotta P, Liistro F, Montorfano M, Chieffo A, Sgura F, Corvaja N, Albiro R, Stankovic G, Toutoutzas C, Bonizzoni E, Di Mario C, Colombo A. In-stent restenosis in small coronary arteries: impact of strut thickness. *J Am Coll Cardiol*. 2002;40:403–409.
 48. Eshtehardi P, Cook S, Wandel S, Raber L, Wenaweser P, Togni M, Vogel R, Garachemani A, Eberli FR, Luscher TF, Juni P, Hess OM, Meier B, Windecker S. Impact of arterial injury on neointimal hyperplasia after implantation of drug-eluting stents in coronary arteries: an intravascular ultrasound study. *EuroIntervention*. 2010;6:467–474.
 49. Elezi S, Kastrati A, Neumann FJ, Hadamitzky M, Dirschinger J, Schomig A. Vessel size and long-term outcome after coronary stent placement. *Circulation*. 1998;98:1875–1880.
 50. Brodie BR, Stuckey T, Downey W, Humphrey A, Bradshaw B, Metzger C, Hermiller J, Krainin F, Juk S, Cheek B, Duffy P, Smith H, Edmunds J, Varanasi J, Simonon CA, STENT Group. Outcomes and complications with off-label use of drug-eluting stents: results from the STENT (Strategic Transcatheter Evaluation of New Therapies) Group. *J Am Coll Cardiol Interv*. 2008;1:405–414.
 51. Pieter Kappetein. Optimal revascularization strategy in patients with three-vessel disease and/or left main disease. The 3-year Outcomes of the SYNTAX Trial. Paper presented at: 24th EACTS Annual Meeting; September 11 to 15, 2010; Geneva, Switzerland.
 52. Otsuka Y, Chronos NA, Apkarian RP, Robinson KA. Scanning electron microscopic analysis of defects in polymer coatings of three commercially available stents: comparison of BiodivYsio, Taxus and Cypher stents. *J Invasive Cardiol*. 2007;19:71–76.
 53. Basalus MW, Ankone MJ, van Houwelingen GK, de Man FH, von Birgelen C. Coating irregularities of durable polymer-based drug-eluting stents as assessed by scanning electron microscopy. *EuroIntervention*. 2009;5:157–165.
 54. Wiemer M, Butz T, Schmidt W, Schmitz KP, Horstkotte D, Langer C. Scanning electron microscopic analysis of different drug eluting stents after failed implantation: from nearly undamaged to major damaged polymers. *Catheter Cardiovasc Interv*. 2010;75:905–911.
 55. Guerin P, Pilet P, Finet G, Goueffic Y, N'Guyen JM, Crochet D, Tijou I, Pacaud P, Loirand G. Drug-eluting stents in bifurcations: bench study of strut deformation and coating lesions. *Circ Cardiovasc Interv*. 2010;3:120–126.
 56. Canan T, Lee MS. Drug-eluting stent fracture: incidence, contributing factors, and clinical implications. *Catheter Cardiovasc Interv*. 2010;75:237–245.
 57. Kim HS, Kim YH, Lee SW, Park DW, Lee CW, Hong MK, Park SW, Ko JK, Park JH, Lee JH, Choi SW, Seong IW, Cho YH, Lee NH, Kim JH, Chun KJ, Park SJ. Incidence and predictors of drug-eluting stent fractures in long coronary disease. *Int J Cardiol*. 2009;133:354–358.
 58. de Ribamar Costa J Jr, Mintz GS, Carlier SG, Fujii K, Sano K, Kimura M, Tanaka K, Costa RA, Lui J, Na Y, Castellanos C, Biro S, Moussa I, Stone GW, Moses JW, Leon MB. Intravascular ultrasound assessment of drug-eluting stent expansion. *Am Heart J*. 2007;153:297–303.
 59. Fujii K, Mintz GS, Kobayashi Y, Carlier SG, Takebayashi H, Yasuda T, Moussa I, Dangas G, Mehran R, Lansky AJ, Reyes A, Kreps E, Collins M, Colombo A, Stone GW, Teirstein PS, Leon MB, Moses JW. Contribution of stent underexpansion to recurrence after sirolimus-eluting stent implantation for in-stent restenosis. *Circulation*. 2004;109:1085–1088.
 60. Casella G, Klauss V, Ottani F, Siebert U, Sangiorgio P, Bracchetti D. Impact of intravascular ultrasound-guided stenting on long-term clinical outcome: a meta-analysis of available studies comparing intravascular ultrasound-guided and angiographically guided stenting. *Catheter Cardiovasc Interv*. 2003;59:314–321.
 61. Jakabcin J, Spacek R, Bystron M, Kvasnak M, Jager J, Veselka J, Kala P, Cervinka P. Long-term health outcome and mortality evaluation after invasive coronary treatment using drug eluting stents with or without the IVUS guidance. Randomized control trial. HOME DES IVUS. *Catheter Cardiovasc Interv*. 2010;75:578–583.
 62. Colombo A. AVIO: a prospective randomized trial of intravascular-ultrasound guided compared to angiography guided stent implantation in complex coronary lesions. Paper presented at: Transcatheter Cardiovascular Therapeutics; September 21 to 25, 2010; Washington, DC.
 63. Honda Y, Fitzgerald PJ. Stent expansion as a mechanical parameter to predict late stent patency: back to the basics. *J Am Coll Cardiol Cardiovasc Interv*. 2009;2:1276–1278.
 64. Costa MA, Angiolillo DJ, Tannenbaum M, Driesman M, Chu A, Patterson J, Kuehl W, Battaglia J, Dabbons S, Shamoon F, Flishman B, Niederman A, Bass TA. Impact of stent deployment procedural factors on long-term effectiveness and safety of sirolimus-eluting stents (final results of the multicenter prospective STLLR trial). *Am J Cardiol*. 2008;101:1704–1711.
 65. Liu X, Tsujita K, Maehara A, Mintz GS, Weisz G, Dangas GD, Lansky AJ, Kreps EM, Rabbani LE, Collins M, Stone GW, Moses JW, Mehran R, Leon MB. Intravascular ultrasound assessment of the incidence and predictors of edge dissections after drug-eluting stent implantation. *J Am Coll Cardiol Cardiovasc Interv*. 2009;2:997–1004.
 66. Hwang CW, Levin AD, Jonas M, Li PH, Edelman ER. Thrombosis modulates arterial drug distribution for drug-eluting stents. *Circulation*. 2005;111:1619–1626.
 67. Piscione F, Piccolo R, Cassese S, Galasso G, De Rosa R, D'Andrea C, Chiariello M. Effect of drug-eluting stents in patients with acute ST-segment elevation myocardial infarction undergoing percutaneous coronary intervention: a meta-analysis of randomised trials and an adjusted indirect comparison. *EuroIntervention*. 2010;5:853–860.
 68. Patrick W Serruys, Gregg W Stone. Comparison of everolimus vs paclitaxel stents: the SPIRIT program. Paper presented at: American Heart Association Scientific Sessions; November 13 to 17 2010; Chicago, IL.

KEY WORDS: percutaneous coronary intervention ■ coronary stents ■ drug-eluting stents ■ in stent restenosis ■ mechanisms

Chapter 4

Edge Vascular Response after Percutaneous Coronary Intervention: An Intracoronary Ultrasound and Optical Coherence Tomography Appraisal: From Radioactive Platforms to First and Second-Generation Drug-eluting Stents and Bioresorbable Scaffolds.

Bill D. Gogas, Hector M. Garcia-Garcia, , Yoshinobu Onuma, Vasim Farooq, Christos V. Bourantas, Patrick W. Serruys

JACC Cardiovasc Interv. 2013 Mar; 6(3): 211-21 [IF: 6.83]

Edge Vascular Response After Percutaneous Coronary Intervention

An Intracoronary Ultrasound and Optical Coherence Tomography Appraisal: From Radioactive Platforms to First- and Second-Generation Drug-Eluting Stents and Bioresorbable Scaffolds

Bill D. Gogas, MD,*† Hector M. Garcia-Garcia, MD, MSc, PhD,* Yoshinobu Onuma, MD,* Takashi Muramatsu, MD, PhD,* Vasim Farooq, MBChB,* Christos V. Bourantas, MD, PhD,* Patrick W. Serruys, MD, PhD*

Rotterdam, the Netherlands; and Atlanta, Georgia

The concept of edge vascular response (EVR) was first introduced with bare-metal stents and later with radioactive stents of various activity levels. Although radioactive stents reduced intra-stent neointimal hyperplasia and thereby the incidence of in-stent restenosis in a dose-dependent manner, tissue proliferation at the non-irradiated proximal and distal stent edges resulted in the failure of this invasive treatment. The advent of first- and second-generation drug-eluting stents (DES) reduced in-stent restenosis to approximately 5% to 10%, depending on the lesion subset and DES type. When in-segment restenosis (stent and 5-mm proximal and distal margins) occurred, it was most commonly focal and located at the proximal edge. In addition, stent thrombosis, the other main contributing factor for DES failure, seemed in part to be associated with residual plaque presence and underlying tissue composition at the landing zone of the implanted device, particularly if landed in a necrotic core rich milieu. More recently, the introduction of bioresorbable scaffolds for the treatment of coronary artery disease has prompted the re-evaluation of the EVR. This has recently been assessed up to 2-years after implantation of the Absorb bioresorbable vascular scaffold (Abbott Vascular, Santa Clara, California). In general, the EVR consists of a focal but significant proximal lumen loss that in a few instances necessitates target lesion revascularization of a flow-limiting edge stenosis. Herein, we provide an overview of the in vivo evaluation of the EVR with intravascular ultrasound, virtual histology intravascular ultrasound, and the more recently developed optical coherence tomography. Our objective is to highlight the clinical importance of the EVR as a predisposing and contributing factor to device failure with either bare-metal stents, DES, or bioresorbable scaffolds. (*J Am Coll Cardiol Intv* 2013;6:211–21) © 2013 by the American College of Cardiology Foundation

The use of metallic or bioresorbable devices for the treatment of significant coronary artery disease

(CAD) has been proven to be a successful strategy in the field of interventional cardiology; however, the exuberant vascular responses resulting in either in-segment restenosis or stent thrombosis (ST) remain the cautionary tale of these technologies, as previously reported by preclinical studies (1,2). The pattern of vascular response after device implantation manifests either as in-stent vascular response (focal or diffuse) or as edge vascular response (EVR) at the transition zones (focal)—each of which have impor-

From the *Thoraxcenter, Erasmus University Medical Centre, Rotterdam, the Netherlands; and the †Andreas Gruentzig Cardiovascular Center, Division of Cardiology, Department of Medicine, Emory University, School of Medicine, Atlanta, Georgia. The authors have reported that they have no relationships relevant to the contents of this paper to disclose.

Manuscript received September 25, 2012; revised manuscript received January 24, 2013, accepted January 30, 2013.

tant prognostic implications (3). A significant response at the proximal or distal edge can manifest as edge restenosis that requires repeat revascularization or even vessel occlusion.

Previous pathological reports from the era of radioactive stents have shown that the predominant tissue found at the edges in the setting of an abnormal EVR consists of smooth muscle cells in disarray and abundant extracellular matrix (4).

The EVR can be assessed clinically with quantitative coronary angiography, intravascular ultrasound, or optical coherence tomography (OCT). In this review, we focus on the in vivo assessment with sound-based imaging modalities after implantation of metallic or bioresorbable devices and

further explore the feasibility to assess the EVR with optical technology (Fig. 1). Furthermore, the clinical implications of the EVR are reported.

Abbreviations and Acronyms

BMS = bare-metal stent(s)

CAD = coronary artery disease

DES = drug-eluting stent(s)

EEM = external elastic membrane

EVR = edge vascular response

FU = follow-up

GM = geographic miss

IVUS = intravascular ultrasound

LL = lumen loss

OCT = optical coherence tomography

PES = paclitaxel-eluting stent(s)

SES = sirolimus-eluting stent(s)

ST = stent thrombosis

TLR = target lesion revascularization

VH-IVUS = virtual histology intravascular ultrasound

ZES = zotarolimus-eluting stent(s)

EVR in the Era of Bare-Metal Stents and Radioactive Platforms

Although balloon angioplasty was undoubtedly a significant breakthrough in the invasive treatment of CAD, this mode of treatment was plagued by several drawbacks, including intimal and media dissections, acute vessel recoil or subacute closure, late constrictive remodeling, and a diffuse proliferative neointimal response because of vascular barotrauma (5). The advent of bare-metal stents (BMS) and the landmark BENESTENT (BELgian-NEtherlands STENT Study) (6) and STRESS (STent REStenosis Study) (7) trials were a significant leap forward in CAD treatment, as permanent metallic cages eliminated the previously observed acute vessel recoil/closure and scaffolded

the post-procedural dissection flaps observed with angioplasty. The EVR after BMS implantation was mainly attributed to plaque and media increase becoming more evident at the region adjacent (1 to 2 mm) to the proximal and distal stent edges. At further distances (3 to 10 mm), lumen loss (LL) was primarily due to constrictive remodeling (reduction of external elastic membrane [EEM]) rather than to plaque and media increase (8). Furthermore, late malapposition at BMS edges was evident in 4% to 5%, because of expansive remodeling without increase in intimal hyperplasia (9). Although some degree of EVR was observed with BMS, isolated margin re-narrowing, particu-

larly involving only the proximal and distal stent edges, was an uncommon cause of stent failure in the BMS era (10).

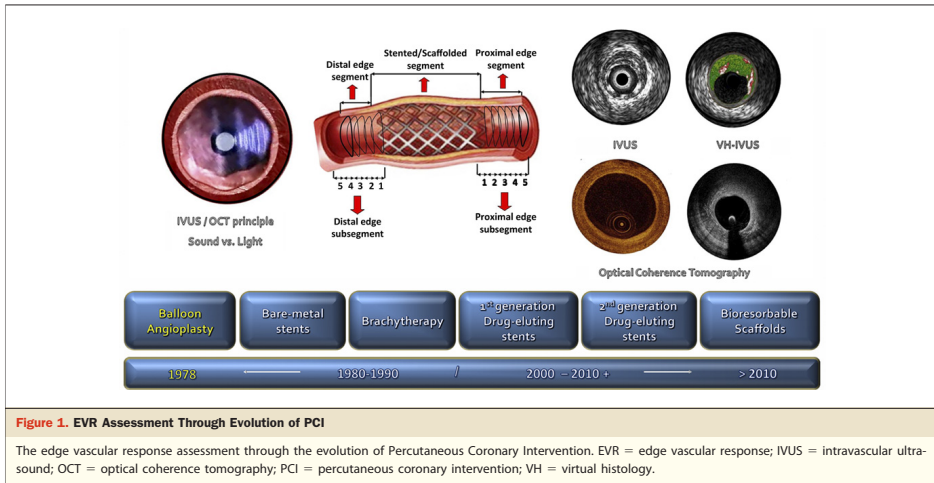
Experimental endovascular delivery—either catheter-based or through irradiation-emitting metallic stent platforms—of beta and gamma radiation initially proved to be a feasible and efficacious method to inhibit neointimal cell proliferation with significant reductions in restenosis rates in animal models (11–14).

The clinical validation of the catheter-based endovascular radiation delivery proved to be safe and feasible in the first-in-man studies (15–17).

Irradiation-emitting stent platforms (with various activity levels) were conceived as a more practical way to overcome the problem of neointimal hyperplasia associated with BMS. The Milan Dose-Response Study proved the feasibility of the ³²P radioactive beta-emitting stent (3.0 and 12 μ Ci) in completely inhibiting in-stent neointimal hyperplasia (>3 μ Ci). Despite these promising findings, the technology was offset by an increased late LL and restenosis adjacent to the proximal and distal edges of the implanted device, dubbed the edge effect or “candy-wrapper” phenomenon (18). The edge effect was defined angiographically at follow-up (FU) as a diameter stenosis at the proximal and distal stent edges of >50%. Bench studies investigating the pathogenesis of this effect incriminated the combination of radioactive dose fall-off at the transition zones (stent edges) in association with the peri-procedural geographic miss (GM) phenomenon (11). The GM (axial or longitudinal) is essentially the failure of the device to appropriately scaffold a balloon-injured vessel (e.g., under-expansion of stent/axial GM) or to completely cover the vessel wall (diseased or not) that had been previously baro-traumatized by balloon predilation, which can result from an overhanging balloon during stent deployment or by balloon post-dilation (longitudinal GM) (19,20). Although various modifications of the existing technologies were proposed to overcome the limitation of EVR (21)—such as the square-shouldered balloon, the hybrid radioactive stent, the self-expanding radioactive stent, the cold-end stent, the hot-end stent—radioactive platforms failed as an interventional technique and were replaced by the next endeavor in interventional cardiology, the DES.

EVR With Drug-Eluting Metallic Platforms

First-generation DES. SIROLIMUS-ELUTING METALLIC PLATFORM. The RAVEL trial (RANdomized study with the sirolimus-eluting Velocity balloon-expandable stent in the treatment of patients with de novo native coronary artery Lesions) was the first randomized double-blind study to establish the angiographic superiority of DES (sirolimus-eluting Bx Velocity balloon expandable stent [SES] [Cordis, Johnson and Johnson, Miami, Florida] over a BMS [Bx Velocity balloon expandable stent]). The EVR at 6 months revealed no significant LL at the proximal or distal SES



edges; however, a nonsignificant lumen gain at the distal edge of 0.09 ± 0.30 mm was present (22–24). Notably, the RAVEL trial was performed in noncomplex coronary lesions with an average stent length/lesion length ratio of approximately 2, and a nonaggressive implantation strategy was undertaken that involved pre-dilation of the stent landing zone located in angiographically normal segments. These favorable but artificial circumstances of implantation did not represent the real-world practice and might potentially explain the neutral EVR after SES implantation in this first pivotal trial.

Subsequently, the SIRIUS trials (multicenter, randomized, double-blind trial of the SIRIUS-coated Bx-Velocity stent in the treatment of patients with de novo coronary artery lesions) (SIRIUS-US and E-SIRIUS) compared SES versus BMS in more complex lesions (long lesions, small vessels).






The SIRIUS-US trial showed a rate of angiographic in-segment restenosis of 8.9%, which was a result of excessive neointimal tissue growth primarily at the proximal edge (approximately 5.8%), and the E-SIRIUS trial reported an in-segment restenosis rate of 5.9% with an almost equal contribution of both stent edges (approximately 2.5%). The IVUS substudy of the E-SIRIUS trial aimed to evaluate the EVR with a less-traumatizing implantation technique (direct stenting and only selective post-dilation) and demonstrated at 8 months no edge LL or vessel remodeling at either SES edge. The findings of this study highlighted the significant role of peri-procedural implantation factors of GM (axial or longitudinal) in the occurrence of the EVR (25–27).

The clinical importance of GM was further shown with the STLLR study (Impact of Stent deployment Techniques on cLinical outcomes of patients treated with the cypher stent), a multicenter prospective study that included patients with native CAD treated with an SES. Target vessel revascularization rates at 1 year were 59% higher in the GM group compared with the non-GM group, mostly due to longitudinal GM visible with a focal pattern of restenosis mainly located at the proximal and distal SES edges (20) (Table 1).

PACLITAXEL-ELUTING METALLIC PLATFORM. The ASPECT trial (ASian Paclitaxel-Eluting Stent Clinical Trial) randomized 81 patients to a BMS ($n = 25$), a low-dose polymer-free paclitaxel-eluting stent (PES) ($n = 28$), or a high-dose polymer-free PES ($n = 28$). Results indicated that there was no notable LL at 6 months at either stent edge; however, no formal report was disclosed (28).

In the first-in-man TAXUS I trial (Comparison Among a Paclitaxel Eluting Stent Versus an Uncoated Bare Metal Stent), no edge effect was demonstrated with the slow release polymer formulation of the PES. Conversely, in the TAXUS II trial the slow release and moderate release polymer formulations of the PES (Boston Scientific Corporation, Natick, Massachusetts) resulted in a proximal edge LL of 0.54 ± 2.1 mm² and 0.88 ± 1.9 mm², respectively, at 6-month FU, whereas the moderate release paclitaxel-eluting platform demonstrated an LL of only 0.19 ± 1.7 mm² at the distal edge (29,30). Although the plaque increased significantly at the edges of both devices, there were no compensative changes in the external elastic lamina.

Table 1. Edge Vascular Response With 1st- and 2nd-Generation Drug-Eluting Stents and Bioresorbable Vascular Scaffolds

Sirolimus-Eluting Platform	IVUS-Based Assessment			Proximal Edge		Distal Edge		Methodology to Assess the Stent, Scaffold Edge/TLR (%)	
	Trial	Follow-Up	First Author (Ref. #s)	Vessel Area (mm ²)	Lumen Area (mm ²)	Vessel Area	Lumen Area		
	RAVEL	Post to 6m	Morice/Serruys (22,23)	-	-	-	-	QCA/0% (22) IVUS: 5-mm adjacent, <360, SB/(-) (23)	
	SIRIUS	Post to 8m	Moses/Popma (10,25)	-	↓	-	-	QCA & IVUS: 5-mm adjacent/5.8%, proximal edge & 3.1%, distal edge	
	E-SIRIUS	Post to 8m	Hoffmann (27)	-	-	-	-	IVUS: 5-mm adjacent/<2.5% proximal & distal edges	
	DIABETES	Post to 9m	Jiménez-Quevedo (34)	↑	↑	↑	-	IVUS: 5-mm adjacent/(-)	
	TAXUS I	Post to 6m	Grube (29)	-	-	-	-	IVUS: 5-mm adjacent/0%	
	TAXUS II	Post to 6m	Serruys (30)	-	↓	-	↓	IVUS: five 1-mm adjacent, <360, SB/~ 3% proximal edge	
	TAXUS IV, V, VI	Post to 9m	Weissman (31)	↓	↓	-	↓	IVUS: five 1-mm adjacent/(-)	
	BETAX	Post to 6m	García-García (32)	↑	-	↑	-	IVUS: five 1-mm adjacent, <360, SB/(-)	
	EVEROLIMUS-ELUTING PLATFORM	SPiRiT II	Post to 6m/post to 2y	Gogas (54,55)	-/↓	-	↑/↓	-	IVUS: 5-mm adjacent, <360, SB/2% distal edge
	SPiRiT III JAPAN	Post to 8m	Shimohama (41)	↓	↓	↑	↓	IVUS: 5-mm adjacent/(-)	
	ENDEAVOR II	Post to 8m	Sakurai (44)	No edge effect		No edge effect		IVUS: 5 1-mm adjacent/(-)	
	ENDEAVOR III	Post to 8m	Miyazawa (44)	No edge effect		No edge effect		IVUS: 5-mm adjacent/(-)	
	ENDEAVOR IV	Post to 8m	Waseda (45)	↓	↓	↓	-	IVUS: 5-mm adjacent/(-)	
	ABSORB B ₁ /ABSORB B ₂	Post to 6m & post to 1y	Gogas (53)	↓/-	-/-	-/-	-/-	IVUS: 5-mm adjacent, <360, SB/3% proximal edge	
	ABSORB B ₁	Post to 2y	Gogas (54,55)	-	↓	-	-	IVUS: 5-mm adjacent, <360, SB/3% proximal edge	

The methodology to assess the stent/scaffold edge and the target lesion revascularization (TLR) rates are also demonstrated. The position of the arrows demonstrate either significant increase or decrease. The outgrowth of a side branch (SB) with an opening of >90° (1 quadrant)/cross-section was an exclusion criterion for the analysis of the stent edge.
 <360° = the stent edge was defined with this methodology; IVUS: intravascular ultrasound; m = month; post = post-procedure; QCA = quantitative coronary angiography.

The TAXUS IV, V, and VI trials were prospective randomized studies comparing the outcomes of PES (TAXUS Express) versus BMS (Express) over a 9-month imaging FU. In the TAXUS group, a decrease of the plaque area comparable to the BMS was documented at the proximal edge, whereas a combination of plaque progression with constrictive remodeling led to significant LL, notably in the 4- to 5-mm distal subsegments, at the distal edge (31). Finally, in the BETAX (Beside TAXUS) trial, which

used the Taxus Express DES, significant tissue compositional changes were observed—which was largely a result of an increase in the fibrofatty tissue component leading to expansive remodeling at both stent edges after plaque area increase (32) (Table 1).

In general, the TAXUS trials documented LL at the stent edges, but the mechanistic interpretation of the different investigators was not consistent. Additionally, the use of

platforms with different drug release kinetics potentially explains the diverse vascular response with PES.

EVR With First-Generation DES in Clinical Subsets

Diabetes mellitus. The initial report of risk factors associated with DES restenosis in patients treated during the first unrestricted use of SES since its CE mark approval was made by our group. In particular, diabetes mellitus was implicated as one of the strongest risk factors (33).

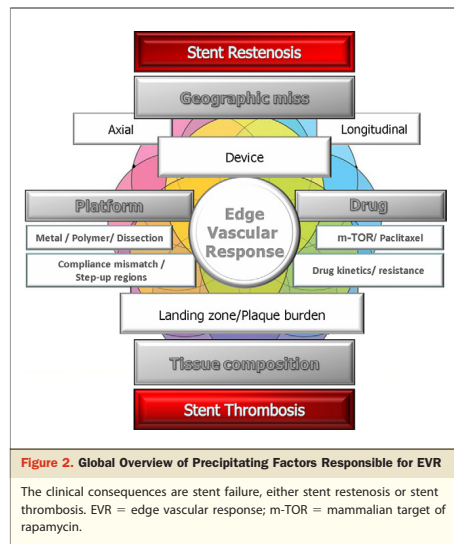
The DIABETES (Diabetes and Sirolimus Eluting Stent) trial was the first to investigate the EVR after implantation of an SES in diabetic patients at 9-month FU. At the proximal edge, significant expansive remodeling was seen (Δ EEM volume: $+8.6 \pm 19 \text{ mm}^3$, $p = 0.04$) to compensate for a mild degree of plaque volume increase with an increase of lumen volume. At the distal edge a similar response was observed, with plaque progression compensated by expansive remodeling: Δ EEM: $+5.1 \pm 12 \text{ mm}^3$, ($p = 0.04$) (34).

The DiabeDES trial (Diabetes and Drug-Eluting Stent intravascular ultrasound trial) randomized 74 diabetic patients to either an SES or PES. At 8 months, the SES arm demonstrated different tissue reactions compared with previous observations in the DIABETES trial. Notably, the EEM remained unchanged at both stent edges. A lumen area increase of $0.4 \pm 1.22 \text{ mm}^2$ ($p = 0.032$) was observed only at the distal edge, which was due to a trend toward significant decrease of the plaque area from 5.8 to 5.6 mm^2 (35).

Diabetic patients have an aggressive form of atherosclerosis compared with non-diabetic persons with a higher risk of target lesion revascularization (TLR) due to angiographic restenosis. Although the DIABETES and DiabeDES trials investigated the EVR after implantation of the same platform/drug at similar time points, the vascular response was not consistent, as plaque progression (DIABETES) or regression (DiabeDES) was documented.

This constitutes another example of discordance between investigations. Obviously, restenosis—in particular edge restenosis—is a multifactorial phenomenon, with multiple and overlapping precipitating factors (Fig. 2). However, in the present case, differences in platform, drug, and time point of investigation can reasonably be excluded as confounding factors. In the absence of a detailed methodological description, differences in assessment might be a suspected cause of discordance in the results (36–38).

Acute myocardial infarction. Two studies have previously investigated EVR in the setting of acute myocardial infarction. These studies were the Leiden MISSION and the HORIZONS AMI trials (Harmonizing Outcomes with Revascularization and Stents in Acute Myocardial Infarction). The Leiden MISSION trial compared the EVR in 40 patients undergoing implantation of either a Cypher stent ($n = 20$) or a BMS ($n = 20$) up to 8 months FU. The vessels treated with a Cypher DES demonstrated a signif-



icant reduction in lumen area at the proximal edge from 8.6 to 7.9 mm^2 , whereas at the distal edge a nonsignificant lumen gain from 6.5 to 6.7 mm^2 was evident (39).

In the IVUS substudy of the HORIZONS AMI trial, 464 patients were randomized in a 3:1 manner to either the TAXUS EXPRESS PES or the EXPRESS BMS. At 13-month FU, the proximal edge segment of the vessels treated with a PES demonstrated an LL of 0.7 mm^2 , because of plaque/media increase, whereas at the distal edge a lesser degree of LL of 0.2 mm^2 was observed after modest plaque/media increase (40). In the clinical setting of acute myocardial infarction a similar proximal EVR with some degree of LL was evident that was, however, not translated to a definite edge effect.

Second-Generation DES

Everolimus-eluting metallic platform. The EVR with the Xience V everolimus-eluting stent (Abbott Vascular, Santa Clara, California) was evaluated serially up to 8 months in the SPIRIT III JAPAN registry ($n = 73$) and the SPIRIT III US ($n = 110$) randomized trial (41). The SPIRIT III JAPAN registry demonstrated a significant increase in the EEM volume index (expansive remodeling) from 9.9 ± 4.2 to $10.3 \pm 4.5 \text{ mm}^3/\text{mm}$ ($p = 0.04$) at the distal edge without any significant changes in the lumen or plaque volumes. In the SPIRIT III US trial, at the same time point, a significant reduction of the lumen volume index from 7.3 ± 2.4

mm³/mm to 6.9 ± 2.4 mm³/mm at the proximal edge was evident (41).

The first serial assessment of the EVR after implantation of the Xience V everolimus-eluting stent at 6-month and 2-year FU has recently been reported in the IVUS substudy of the SPIRIT II trial (42). At the distal edge a significant increase of the EEM (expansive remodeling) area was evident (Δ EEM: $+0.62$ mm² [-0.22 to 1.27 mm²]) at 6 months, similar to the prior observation of the SPIRIT III JAPAN registry; however, from 6 months to 2 years, a different biological behavior became apparent as significant constrictive remodeling (Δ EEM: -0.50 [-1.19 to 0.14] mm²) was observed within this segment. From 6 months to 2 years, a significant reduction of the EEM area was also detected at the proximal edge, without significant lumen or plaque changes.

It has been speculated that this constrictive remodeling is potentially related to chronic alterations of the vascular compliance at the transition zones between the scaffolded and unscaffolded segments (43).

Zotarolimus-eluting metallic platform. The EVR with the Endeavor zotarolimus-eluting stent (ZES) (Medtronic Vascular, Santa Rosa, California) was reported in the ENDEAVOR II (Randomized Controlled Trial to Evaluate the Safety and Efficacy of the Medtronic AVE ABT-578 Eluting Driver Coronary Stent in De Novo Native Coronary Artery Lesions) and III trials (A Randomized Controlled Trial of the Medtronic Endeavor Drug (ABT-578) Eluting Coronary Stent System Versus the Cypher Sirolimus-Eluting Coronary Stent System in De Novo Native Coronary Artery Lesions). These studies compared serially up to 8-month FU the Endeavor ZES, the Driver BMS, and the first-generation Cypher SES. No edge effect was shown with the ZES either in the ENDEAVOR II or ENDEAVOR III trials (44).

In the ENDEAVOR IV trial (Randomized Comparison of Zotarolimus- and Paclitaxel-Eluting Stents in Patients with Coronary Artery Disease) the EVR was investigated serially up to 8 months with IVUS imaging. At the proximal edge, a significant decrease of the lumen volume index of $\Delta -0.4 \pm 1.0$ mm³/mm was evident, without signs of vessel remodeling. At the distal edge, the lumen volume index was reduced ($\Delta -0.5 \pm 1.1$ mm³/mm) after an almost significant increase of the plaque volume ($\Delta +0.2 \pm 0.6$ mm³/mm) (45) (Table 1).

Although the ENDEAVOR studies evaluated the same device platform with similar drug release kinetics at corresponding imaging FU time points, the EVR was not consistent. Excluding the device-related factors as precipitating components of the edge LL, we can only speculate that precipitating biological factors in association with methodological inconsistencies explain this finding, because the latter information was not provided.

Lessons Learned From an IVUS-Based Assessment of the EVR With First-Generation DES

The EVR, with first-generation DES in simple lesions, complex populations, and specific clinical subsets, demonstrated in most studies proximal edge LL that caused clinical restenosis (TLR) or edge effect (diameter stenosis >50%) in only a small percentage of cases. Proximal edge LL, however, was not shown with all studies. The explanations for this variance in the vascular responses at the edges are: 1) the mechanism of the EVR with its multifactorial etiology; and 2) potential methodological inconsistencies related to technical guidelines.

Three major implicated factors predispose to an abnormal EVR: 1) iatrogenic factors, related to the periprocedural GM, axial or longitudinal; 2) device factors, associated with the type of the implanted device (metallic or polymeric), device-induced edge dissections, type/release kinetics of the anti-proliferative drug (mammalian target of rapamycin inhibitor or paclitaxel or actinomycin), and phenomenon of drug resistance; and 3) biological factors mainly linked to the remaining plaque burden and necrotic core tissue at the edges when the “normal to normal” landing of the device has not been achieved.

Specific technical guidelines implemented by our group (Cardialysis BV, Rotterdam, the Netherlands) have been implemented by our group for the analysis of the EVR with first- and second-generation DES and bioresorbable devices (46). In particular, stent edge is defined as the first cross-section exhibiting visible struts in a circumference of <360°. The first and last cross-sections with visible struts in a circumference of 360° are defined as the stented segment (Fig. 3, Table 1). The rationale for this methodological approach is based on prior observations showing that the motorized IVUS pullback (0.5 mm/s) is highly affected by cardiac motion (systole/diastole) causing a longitudinal displacement of the IVUS transducer between systole and diastole of 1.5 ± 0.80 mm (range from 0.5 to 5.5 mm). This phenomenon known as the “scrambling effect” makes it difficult to sharply define the exact location of the stent edge (47). Although electrocardiogram-gated IVUS acquisition by selecting near-end diastolic frames can reduce motion-induced artefacts, this does not fully prevent the imaging of stent struts over the transition zones (48–50).

These technical limitations are potential confounding factors that alter the precise EVR assessment with IVUS-based imaging. Novel imaging modalities with higher spatial resolution and lesser motion-induced artefacts, such as OCT, have recently been investigated to assess the EVR.

OCT-Based Assessment of the EVR

Although sound-based imaging was until recently the sole intravascular imaging modality for the EVR assessment, this

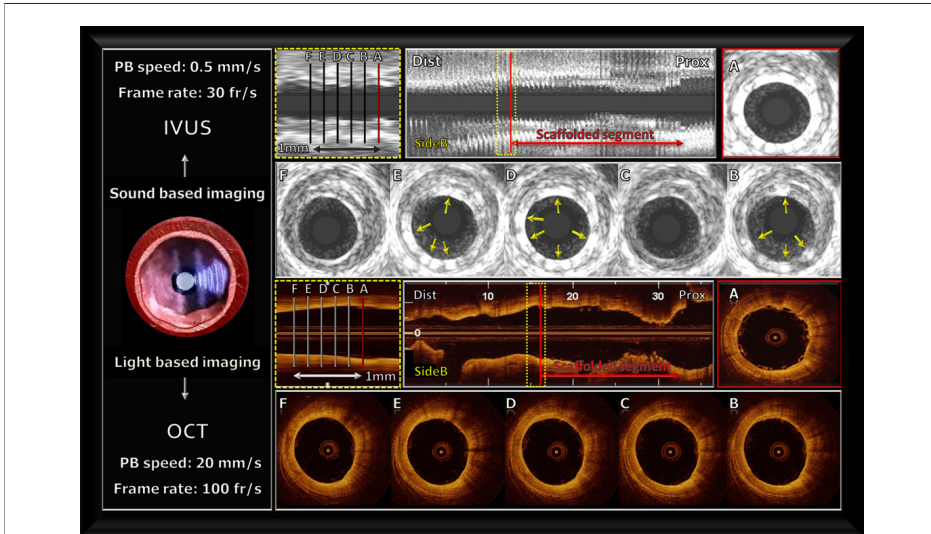


Figure 3. IVUS-Based and OCT-Based Assessment of EVR

(A) Demonstrates the last frame with visible struts in a circumference of 360° with both imaging modalities. (B to F) Demonstrate the difference between IVUS (presence of the scrambling effect) and OCT (absence of scrambling effect). In contrast to IVUS, OCT demarcates the edge sharply with the sudden disappearance of the struts in the cross-section defined as stent edge. Dist = distal; PB = pullback; Prox = proximal; other abbreviations as in Figure 1.

technique seems to have some limitations. Thus, our group has explored the EVR evaluation with light-based imaging, such as OCT. Despite the low penetration depth of this imaging technique—which limits the precise assessment of the EEM (vessel area) making it difficult to assess vessel remodeling—the sharply defined stent edges makes this imaging tool an alternative modality to evaluate the changes in lumen area and superficial plaque composition with a near-histological spatial resolution (51,52).

The methodology to assess the OCT-derived stent edge is similar to the previously IVUS-derived definition; however, the fast pullback speed of 20 to 40 mm/s compared with the 0.5 mm/s of IVUS detects the demarcation of the stent/scaffold edges more categorically.

The first OCT-based EVR assessment was performed in the ABSORB Cohort B [NCT00856856] trial ($n = 101$). The ABSORB Cohort B₁ ($n = 45$) underwent intracoronary multi-imaging assessment at post-procedure, 6 months, and 2 years, whereas the ABSORB Cohort B₂ ($n = 56$) underwent OCT assessment at post-procedure 1 year and is currently undergoing a 3-year imaging assessment. In Cohort B₁, 16 proximal and 18 distal edge segments were available for a serial analysis with OCT. There was no LL at either the proximal or distal scaffold edges. However, in Cohort B₂ where 20 proximal

and distal edge segments were serially assessed post-procedure and at 1 year, an LL of $0.50 \pm 1.79 \text{ mm}^2$ ($p = 0.012$) was observed at the proximal scaffold edge (Online Table 1).

The TROFI trial [NCT01271361] is the second OCT-based study in which the EVR was assessed in the setting of acute myocardial infarction after implantation of the Nobori (Terumo, Europe NV, Leuven, Belgium) metallic stent at 6-month FU.

Thirty-five proximal and 46 distal edge segments were analyzed serially, post-procedure, and at 6-month FU. At both edges a significant LL became evident. In particular, an LL of $0.52 \pm 1.19 \text{ mm}^2$ ($p = 0.001$) was measured at the proximal edge, whereas at the distal edge a lesser degree of LL was shown ($0.40 \pm 1.17 \text{ mm}^2$, $p = 0.015$) (Online Table 1). The OCT-based assessment of the EVR in these pilot studies shows proximal edge LL; however, larger cohorts are needed to validate these preliminary results.

EVR With Bioresorbable Scaffolds

EVR with the Absorb bioresorbable vascular scaffold. The Absorb bioresorbable vascular scaffold (Absorb BVS) (Abbott Vascular) has been evaluated within the ABSORB

Cohort A trial (A Clinical Evaluation of the Bioabsorbable Vascular Solutions Everolimus Eluting Coronary Stent System in the Treatment of Patients With Single de Novo Native Coronary Artery Lesions) up to 5 years and the ABSORB Cohort B trial up to 2 years. In total, 101 patients were enrolled, which were further divided to 2 subgroups—Cohort B₁ (n = 45), and Cohort B₂ (n = 56)—according to the predefined study design [NCT00300131]. The non-serial IVUS-based evaluation of the EVR at 6 months in Cohort B₁ demonstrated some degree of constrictive remodeling at the proximal edge: Δ EEM -1.80% [-3.18% to 1.30%], $p < 0.05$, which was similar to that previously seen with metallic stents at the same time point; however, this response was less evident in Cohort B₂ at 1 year: Δ EEM: 1.53% [-7.74% to 2.48%], $p = 0.06$ (53).

The serial evaluation of Cohort B₁ at 2 years (from post-procedure to 2 years) revealed a significant LL of 0.53 (-1.22 to 0.18) mm^2 with a trend toward plaque area increase of 0.48 (-0.25 to 1.03) mm^2 ($p = 0.06$) at the proximal edge. In addition, distal edge changes in tissue composition became evident with a significant increase of the fibrofatty tissue component from 0.09 (0.04 to 0.22) mm^2 to 0.22 (0.14 to 0.51) mm^2 and a percentile increase of $\Delta +68.37\%$ (17.82% to 171.17%) ($p = 0.013$) (54,55).

Although the ischemia-driven TLR rate in the ABSORB Cohort B trial at 1 year was as low as 4%, 2 of the TLR cases were attributed to a proximal edge effect related to iatrogenic factors and more in particular to longitudinal GM. At 2 years, the ischemia-driven TLR rate remained low (6%) without new episodes of exuberant EVR.

The 2-year imaging FU with the Absorb BVS for the assessment of the EVR is the longest available in the published data. Similar studies using the upcoming bioresorbable scaffold technologies at the same time point—such as the drug-eluting absorbable metal scaffold (DREAMS) (Biotronik, Bülach, Switzerland); the ReZolve Sirolimus-Eluting Bioresorbable Coronary Scaffold (REVA Medical, San Diego, California); and the Ideal Biostent (Xenogenics Corporation, Philadelphia, Pennsylvania) (the second-generation BTI stent [BTI, Menlo Park, California]), made of magnesium, tyrosine polycarbonate, and salicylic acid, respectively—are expected to establish the potential dynamic behavior of the transient scaffolds at the edges, compared with the permanent metallic stents.

The EVR up to 2 years with a fully bioresorbable device demonstrates LL at the proximal edge that results in clinical restenosis or edge effect in $<6\%$ of cases and tissue composition changes at the distal edge.

Clinical Implications of EVR

The EVR pathophysiology has been scrutinized and shown to be of multifactorial origin rather than a single etiology. It is the interplay among several factors: 1) peri-procedural; 2)

device-related; and 3) biological factors resulting in either device restenosis or ST (Fig. 2). The EVR in the current interventional practice with second-generation DES and in the future with bioresorbable devices will further reduce the incidence of edge effect and the subsequent need for TLR.

The implantation of metallic devices has been previously shown to cause alterations in 3-dimensional vessel geometry and induce compliance mismatch between the stented part of the artery and its upstream and downstream segments as assessed in preclinical models and human arteries (56,57). Additionally, diameter mismatch after stent implantation between the stented segment and the native artery (axial GM/over-dilation) might cause step-up regions at the transition zones with subsequent disturbance of the laminar flow and induction of flow separation and retrograde axial velocities (58). These effects induce local wall shear stress alterations at the stented segments and the transition zones, resulting in tissue growth and potentially restenosis. However, 2 fundamental technical aspects of deployment have been appreciated by the interventional community: 1) the optimal device deployment: avoidance of overstretching during the culprit lesion preparation, and the use of balloons shorter than the implanted device during pre- or post-dilation; and 2) the importance of the healthy “landing zone” (normal to normal) of the device during stenting.

Recent studies using VH-IVUS imaging have shown that the site of the plaque rupture is more likely to be located at the proximal edge of the plaque (43.7%) rather than the site of the minimum lumen area (25.6%), and the longitudinal distribution of the largest necrotic core is more often at the proximal edge of the plaque rather than at the minimum lumen area (59,60). In the European Collaborative Project on Inflammation and Vascular Wall Remodeling in Atherosclerosis - Intravascular Ultrasound Study (AtheroRemoIVUS) trial it was demonstrated that the landing of a device in a VH-IVUS-defined thin cap fibroatheroma (vulnerable plaque) reaches the rate of approximately 11% (61), whereas in the BETAX study necrotic core rich areas were left un-stented: proximal edge 17% (13.5%), and distal edge 18.5% (16.5%), with no reported episodes of ST during the 6-month FU (32).

It is important that these necrotic core rich lesions at the stent edges are covered with a small neointimal layer; the latter has been assessed in 80 patients where the long-term native artery vascular responses (median = 10 months) after 76 DES implantations compared with 32 BMS were evaluated by VH-IVUS. The incidence of necrotic core abutting the lumen within the adjacent reference segments decreased in the BMS-treated lesions (proximal 23% to 0%; distal 21% to 0%) but not in the DES-treated lesions (proximal 22% to 17%; distal 23% to 21%) (62). As a consequence, the normal to normal coverage of the culprit lesion is a mandatory approach for the interventionalist to avoid potential definite, probable, or possible ST (according to the Academic Research Consortium definition) (32,33,63,64).

Vasomotor dysfunction at the proximal and distal stent edges after implantation of first-generation DES has been reported to be associated with delayed vascular healing and impaired endothelialization, potentially caused by polymer-induced inflammation, drug toxicity, and hypersensitivity reactions with eosinophilic infiltrations. These pathological findings have been associated with increased risk of late and very late ST (1,65–69). Meanwhile, the advent of new devices with either bioresorbable polymers or bioresorbable platforms have shown restoration of vasomotor function at the device edges and might potentially eliminate the risk of ST arising from the transition zones (70,71).

Edge dissections after implantation of metallic devices have been previously associated with events of early ST. The incidence of OCT-detected edge dissections has been reported to be as high as 34%, compared with 19.3% of IVUS-detected dissections. Most dissection flaps heal with only a minority of patients experiencing clinical adverse events (72,73).

An exuberant EVR in the setting of a post-procedural dissection has been shown to be associated with the flap length. We have recently demonstrated the first OCT-based assessment of such an exuberant EVR implantation of a metallic device attributed to a large post-procedural dissection flap originating deep in the media, causing edge restenosis (74). The incidence of dissections at the transition zones of bioresorbable devices has not been investigated yet; meanwhile, this is expected to be rather low, because most of the treated lesions in the first-in-man studies were Type A.

Finally, the development of in-stent neoatherosclerosis with BMS and first-generation DES has been proposed as another rare contributing factor for episodes of ST (75). Lee et al. (76) demonstrated by IVUS that BMS implantation was associated with events of very late ST, because of disease progression and neoatherosclerotic plaque rupture, in contrast to DES where ST appeared earlier and was mainly associated with stent malapposition. More recently, similar findings were shown from thrombectomy specimens extracted from patients who presented with definite ST after BMS implantation. Disruption of de novo atherosclerotic plaques in stented segments and the proximal and distal edges were attributed as the main mechanism for the acute event (77,78).

Since the era of vascular brachytherapy, the ABSORB Cohort B and BETAX studies were the only studies that investigated tissue composition changes at the edges with VH-IVUS imaging. Although different drug-eluting platforms were used at various time points, both studies demonstrated an increase of the fibrofatty tissue component at 6-month FU. Adaptive expansive remodeling of the vessel treated with the TAXUS Express (from 6.2 to 7.7 mm²) was observed as well as nonsignificant adaptive expansion of the vessel treated with the Absorb BVS (3.45%). Fibrofatty tissue is a surrogate marker of extracellular matrix production, consisting of proteoglycans, hyalu-

ronan, and collagen (Type I and III) implicated for neointimal growth and remodeling (79).

Drug-eluting bioresorbable scaffolds with properties that allow for the repair of the treated vessel rather than permanent caging (vascular reparative therapy) have shown, both with IVUS and OCT, proximal edge LL at the transition zones up to 2 years. The upcoming 3-year imaging FU of the scaffold edges will help to unravel the ultimate state of EVR. At this time the polymer will have been replaced by connective tissue integrated with the vessel wall and will potentially help clarify the dynamic nature of the initially observed vascular response at the scaffold edges (80).

Conclusions

Edge vascular response has been observed with BMS, radioactive stenting, DES, and bioresorbable devices, demonstrating—in most studies—proximal edge LL that causes clinical restenosis or edge effect in a minority of cases. The advent of light-based imaging with its ultra-high spatial resolution is expected to improve the in vivo assessment of the EVR especially in those cases in which ST due to edge disease has devastating consequences.

Acknowledgments

Dr. Gogas thanks the American College of Cardiology Foundation for the International Society of Cardiovascular Translational Research Scholarship (ISCTR), the Hellenic Cardiological Society (HCS), and the Hellenic Heart Foundation (HHF).

The authors would like to thank Lucas Timmins, PhD, and Susan Veldhof, RN for their valuable comments.

Reprint requests and correspondence: Dr. Patrick W. Serruys, Erasmus University Medical Centre, Department of Interventional Cardiology, 's-Gravendijkwal 230, 3015 CE, Rotterdam, the Netherlands. E-mail: p.w.j.c.serruys@erasmusmc.nl.

REFERENCES

1. Finn AV, Nakazawa G, Joner M, et al. Vascular responses to drug eluting stents: importance of delayed healing. *Arterioscler Thromb Vasc Biol* 2007;27:1500–10.
2. Nakazawa G. Stent thrombosis of drug eluting stent: pathological perspective. *J Cardiol* 2011;58:84–91.
3. Mehran R, Dangas G, Abizaid AS, et al. Angiographic patterns of in-stent restenosis: classification and implications for long-term outcome. *Circulation* 1999;100:1872–8.
4. Cheneau E, Wolfram R, Leborgne L, Waksman R. Understanding and preventing the edge effect. *J Interv Cardiol* 2003;16:1–7.
5. Gruntzig A. Transluminal dilatation of coronary-artery stenosis. *Lancet* 1978;1:263.
6. Serruys PW, de Jaegere P, Kiemeneij F, et al. A comparison of balloon-expandable-stent implantation with balloon angioplasty in patients with coronary artery disease. Benestent Study Group. *N Engl J Med* 1994;331:489–495.
7. Fischman DL, Leon MB, Baim DS, et al. A randomized comparison of coronary-stent placement and balloon angioplasty in the treatment

- of coronary artery disease. Stent restenosis study investigators. *N Engl J Med* 1994;331:496–501.
8. Weissman NJ, Wilensky RL, Tanguay JF, et al. Extent and distribution of in-stent intimal hyperplasia and edge effect in a non-radiation stent population. *Am J Cardiol* 2001;88:248–52.
 9. Shah VM, Mintz GS, Apple S, Weissman NJ. Background incidence of late malapposition after bare-metal stent implantation. *Circulation* 2002;106:1753–5.
 10. Popma JJ, Leon MB, Moses JW, et al. Quantitative assessment of angiographic restenosis after sirolimus-eluting stent implantation in native coronary arteries. *Circulation* 2004;110:3773–80.
 11. Waksman R, Rodriguez JC, Robinson KA, et al. Effect of intravascular irradiation on cell proliferation, apoptosis, and vascular remodeling after balloon overstretch injury of porcine coronary arteries. *Circulation* 1997;96:1944–52.
 12. Waksman R, Robinson KA, Crocker IR, et al. Intracoronary low-dose beta-irradiation inhibits neointima formation after coronary artery balloon injury in the swine restenosis model. *Circulation* 1995;92:3025–31.
 13. Verin V, Popovskiy Y. Intraarterial beta irradiation to reduce restenosis after PTCA. Experimental and clinical experience. *Herz* 1998;23:347–55.
 14. Wiedermann JG, Marboe C, Amols H, Schwartz A, Weinberger J. Intracoronary irradiation markedly reduces restenosis after balloon angioplasty in a porcine model. *J Am Coll Cardiol* 1994;23:1491–8.
 15. Condao JA, Waksman R, Gurdziel O, et al. Long-term angiographic and clinical outcome after percutaneous transluminal coronary angioplasty and intracoronary radiation therapy in humans. *Circulation* 1997;96:727–32.
 16. Teirstein PS, Massullo V, Jani S, et al. Catheter-based radiotherapy to inhibit restenosis after coronary stenting. *N Engl J Med* 1997;336:1697–703.
 17. King SB III, Williams DO, Chougale P, et al. Endovascular beta-radiation to reduce restenosis after coronary balloon angioplasty: results of the beta energy restenosis trial (BERT). *Circulation* 1998;97:2025–30.
 18. Albiero R, Adamian M, Kobayashi N, et al. Short- and intermediate-term results of (32)P radioactive beta-emitting stent implantation in patients with coronary artery disease: the Milan dose-response study. *Circulation* 2000;101:18–26.
 19. van der Giessen WJ, Regar E, Harteveld MS, et al. “Edge Effect” of (32)P radioactive stents is caused by the combination of chronic stent injury and radioactive dose falloff. *Circulation* 2001;104:2236–41.
 20. Costa MA, Angiolillo DJ, Tannenbaum M, et al. Impact of stent deployment procedural factors on long-term effectiveness and safety of sirolimus-eluting stents (final results of the multicenter prospective STLLR trial). *Am J Cardiol* 2008;101:1704–11.
 21. Serruys PW, Kay IP. I like the candy, I hate the wrapper: the (32)P radioactive stent. *Circulation* 2000;101:3–7.
 22. Morice MC, Serruys PW, Sousa JE, et al. A randomized comparison of a sirolimus-eluting stent with a standard stent for coronary revascularization. *N Engl J Med* 2002;346:1773–80.
 23. Serruys PW, Degertekin M, Tanabe K, et al. Intravascular ultrasound findings in the multicenter, randomized, double-blind RAVEL (RAndomized study with the sirolimus-eluting VElocity balloon-expandable stent in the treatment of patients with de novo native coronary artery lesions) trial. *Circulation* 2002;106:798–803.
 24. Degertekin M, Lemos PA, Lee CH, et al. Intravascular ultrasound evaluation after sirolimus eluting stent implantation for de novo and in-stent restenosis lesions. *Eur Heart J* 2004;25:32–8.
 25. Moses JW, Leon MB, Popma JJ, et al. Sirolimus-eluting stents versus standard stents in patients with stenosis in a native coronary artery. *N Engl J Med* 2003;349:1315–23.
 26. Schofer J, Schlüter M, Gershlick AH, et al. Sirolimus-eluting stents for treatment of patients with long atherosclerotic lesions in small coronary arteries: double-blind, randomised controlled trial (E-SIRIUS). *Lancet* 2003;362:1093–9.
 27. Hoffmann R, Guagliumi G, Musumeci G, et al. Vascular response to sirolimus-eluting stents delivered with a nonaggressive implantation technique: comparison of intravascular ultrasound results from the multicenter, randomized E-SIRIUS, and SIRIUS trials. *Catheter Cardiovasc Interv* 2005;66:499–506.
 28. Hong MK, Mintz GS, Lee CW, et al. Paclitaxel coating reduces in-stent intimal hyperplasia in human coronary arteries: a serial volumetric intravascular ultrasound analysis from the Asian paclitaxel-eluting stent clinical trial (ASPECT). *Circulation* 2003;107:517–20.
 29. Grube E, Silber S, Hauptmann KE, et al. TAXUS I: six- and twelve-month results from a randomized, double-blind trial on a slow-release paclitaxel-eluting stent for de novo coronary lesions. *Circulation* 2003;107:38–42.
 30. Serruys PW, Degertekin M, Tanabe K, et al. Vascular responses at proximal and distal edges of paclitaxel-eluting stents: serial intravascular ultrasound analysis from the TAXUS II trial. *Circulation* 2004;109:627–33.
 31. Weissman NJ, Ellis SG, Grube E, et al. Effect of the polymer-based, paclitaxel-eluting TAXUS express stent on vascular tissue responses: a volumetric intravascular ultrasound integrated analysis from the TAXUS IV, V, and VI trials. *Eur Heart J* 2007;28:1574–82.
 32. García-García HM, Gonzalo N, Tanimoto S, Meliga E, de Jaegere P, Serruys PW. Characterization of edge effects with paclitaxel-eluting stents using serial intravascular ultrasound radiofrequency data analysis: the BETAX (BEside TAXus) study. *Rev Esp Cardiologia* 2008;61:1013–9.
 33. Lemos PA, Hoye A, Goedhart D, et al. Clinical, angiographic, and procedural predictors of angiographic restenosis after sirolimus-eluting stent implantation in complex patients: an evaluation from the rapamycin-eluting stent evaluated at Rotterdam Cardiology Hospital (RESEARCH) study. *Circulation* 2004;109:1366–70.
 34. Jiménez-Quevedo P, Sabaté M, Angiolillo DJ, et al. Vascular effects of sirolimus-eluting versus bare-metal stents in diabetic patients: three-dimensional ultrasound results of the diabetes and sirolimus-eluting Stent (DIABETES) trial. *J Am Coll Cardiol* 2006;47:2172–9.
 35. Jensen LO, Maeng M, Mintz GS, et al. Serial intravascular ultrasound analysis of peri-stent remodeling and proximal and distal edge effects after sirolimus-eluting or paclitaxel-eluting stent implantation in patients with diabetes mellitus. *Am J Cardiol* 2009;103:1083–8.
 36. Farooq V, Gogas BD, Serruys PW. Restenosis: delineating the numerous causes of drug-eluting stent restenosis. *Circ Cardiovasc Interventions* 2011;4:195–205.
 37. Huang S, Houghton PJ. Mechanisms of resistance to rapamycins. *Drug Resist Update* 2001;4:378–91.
 38. Kurmasheva RT, Huang S, Houghton PJ. Predicted mechanisms of resistance to mTOR inhibitors. *Br J Cancer* 2006;95:955–60.
 39. Atary JZ, Berghaneu SC, van der Hoeven BL, et al. Impact of sirolimus-eluting stent implantation compared with bare-metal stent implantation for acute myocardial infarction on coronary plaque composition at nine months follow-up: a virtual histology intravascular ultrasound analysis. Results from the Leiden MISSION! intervention study. *EuroIntervention* 2009;5:565–72.
 40. Machara A, Mintz GS, Lansky AJ, et al. Volumetric intravascular ultrasound analysis of paclitaxel-eluting and bare metal stents in acute myocardial infarction: the harmonizing outcomes with revascularization and stents in acute myocardial infarction intravascular ultrasound substudy. *Circulation* 2009;120:1875–82.
 41. Shimohama T, Ako J, Yamasaki M, et al. SPIRIT III JAPAN versus SPIRIT III USA: a comparative intravascular ultrasound analysis of the everolimus-eluting stent. *Am J Cardiol* 2010;106:13–7.
 42. Claessen BE, Beijk MA, Legrand V, et al. Two-year clinical, angiographic, and intravascular ultrasound follow-up of the XIENCE V everolimus-eluting stent in the treatment of patients with de novo native coronary artery lesions: the SPIRIT II trial. *Circ Cardiovasc Interventions* 2009;2:339–47.
 43. Brugaletta S, Gogas BD, Garcia-Garcia HM, et al. Vascular compliance changes of the coronary vessel wall after bioresorbable vascular scaffold implantation in the treated and adjacent segments. *Circ J* 2012;76:1616–23.
 44. Sakurai R, Bonneau HN, Honda Y, Fitzgerald PJ. Intravascular ultrasound findings in ENDEAVOR II and ENDEAVOR III. *Am J Cardiol* 2007;100:71M–6M.
 45. Waseda K, Miyazawa A, Ako J, et al. Intravascular ultrasound results from the ENDEAVOR IV trial: randomized comparison between zotarolimus- and paclitaxel-eluting stents in patients with coronary artery disease. *J Am Coll Cardiol Interv* 2009;2:779–84.

46. Okamura T, Gonzalo N, Gutiérrez-Chico JL, et al. Reproducibility of coronary Fourier domain optical coherence tomography: quantitative analysis of *in vivo* stented coronary arteries using three different software packages. *EuroIntervention* 2010;6:371–9.
47. Mintz GS, Garcia-Garcia HM, Nicholls SJ, et al. Clinical expert consensus document on standards for acquisition, measurement and reporting of intravascular ultrasound regression/progression studies. *EuroIntervention* 2011;6:1123–30, 1129.
48. Arbab-Zadeh A, DeMaria AN, Penny WF, Russo RJ, Kimura BJ, Bhargava V. Axial movement of the intravascular ultrasound probe during the cardiac cycle: implications for three-dimensional reconstruction and measurements of coronary dimensions. *Am Heart J* 1999;138: 865–72.
49. von Birgelen C, de Vrey EA, Mintz GS, et al. ECG-gated three-dimensional intravascular ultrasound: feasibility and reproducibility of the automated analysis of coronary lumen and atherosclerotic plaque dimensions in humans. *Circulation* 1997;96:2944–52.
50. Bruining N, von Birgelen C, de Feyter PJ, et al. ECG-gated versus nongated three-dimensional intracoronary ultrasound analysis: implications for volumetric measurements. *Cathet Cardiovasc Diagn* 1998; 43:254–60.
51. Tearney GJ, Regar E, Akasaka T, et al. Consensus standards for acquisition, measurement, and reporting of intravascular optical coherence tomography studies: a report from the international Working Group for Intravascular Optical Coherence Tomography Standardization and Validation. *J Am Coll Cardiol* 2012;59:1058–72.
52. Prati F, Guagliumi G, Mintz GS, et al. Expert review document part 2: methodology, terminology and clinical applications of optical coherence tomography for the assessment of interventional procedures. *Eur Heart J* 2012;33:2513–20.
53. Gogas BD, Serruys PW, Diletti R, et al. Vascular response of the segments adjacent to the proximal and distal edges of the ABSORB everolimus-eluting bioresorbable vascular scaffold: 6-month and 1-year follow-up assessment: a virtual histology intravascular ultrasound study from the first-in-man ABSORB cohort B trial. *J Am Coll Cardiol Intv* 2012;5:656–65.
54. Gogas BD, Bourantas CV, Garcia-Garcia HM. The edge vascular response following implantation of the Absorb everolimus eluting Bioresorbable Vascular Scaffold and the Xience V metallic everolimus eluting stent. First serial assessment at 6-months and 2-years follow-up. Insights from the first in man ABSORB cohort B and SPIRIT II trials. *EuroIntervention*. 2013 [in press].
55. Gogas BD, Serruys PW, Farooq V, et al. The dynamic vascular response at the proximal and distal edges following implantation of the ABSORB everolimus eluting bioresorbable vascular scaffold as assessed with virtual histology intravascular ultrasound: A2-year Follow-Up Assessment From the First in Man, ABSORB Cohort B Trial. Abstract presented at EuroPCR; May 15–18, 2012.
56. Vernhet H, Demaria R, Pérez-Martin A, et al. Wall mechanics of the stented rabbit aorta: long-term study and correlation with histological findings. *J Endovasc Ther* 2003;10:577–84.
57. Wentzel JJ, Whelan DM, van der Giessen WJ, et al. Coronary stent implantation changes 3-D vessel geometry and 3-D shear stress distribution. *J Biomech* 2000;33:1287–95.
58. Thury A, Wentzel JJ, Vinke RV, et al. Images in cardiovascular medicine. Focal in-stent restenosis near step-up: roles of low and oscillating shear stress? *Circulation* 2002;105:e185–7.
59. Maehara A, Mintz GS, Bui AB, et al. Morphologic and angiographic features of coronary plaque rupture detected by intravascular ultrasound. *J Am Coll Cardiol* 2002;40:904–10.
60. Kaple RK, Maehara A, Sano K, et al. The axial distribution of lesion-site atherosclerotic plaque components: an *in vivo* volumetric intravascular ultrasound radio-frequency analysis of lumen stenosis, necrotic core and vessel remodeling. *Ultrasound Med Biol* 2009;35: 550–7.
61. Sarno G, Garg S, Gomez-Lara J, et al. Intravascular ultrasound radiofrequency analysis after optimal coronary stenting with initial quantitative coronary angiography guidance: an ATHEROREMO sub-study. *EuroIntervention* 2011;6:977–84.
62. Kubo T, Maehara A, Mintz GS, et al. Analysis of the long-term effects of drug-eluting stents on coronary arterial wall morphology as assessed by virtual histology intravascular ultrasound. *Am Heart J* 2010; 159:271–7.
63. Holmes DR Jr., Kereiakes DJ, Garg S, et al. Stent thrombosis. *J Am Coll Cardiol* 2010;56:1357–65.
64. Farb A, Burke AP, Kolodgie FD, Virmani R. Pathological mechanisms of fatal late coronary stent thrombosis in humans. *Circulation* 2003; 108:1701–6.
65. Parry TJ, Brosius R, Thyagarajan R, et al. Drug-eluting stents: sirolimus and paclitaxel differentially affect cultured cells and injured arteries. *Eur J Pharmacol* 2005;524:19–29.
66. Fukuda D, Sata M, Tanaka K, Nagai R. Potent inhibitory effect of sirolimus on circulating vascular progenitor cells. *Circulation* 2005;111: 926–31.
67. Finn AV, Joner M, Nakazawa G, et al. Pathological correlates of late drug-eluting stent thrombosis: strut coverage as a marker of endothelialization. *Circulation* 2007;115:2435–41.
68. Virmani R, Guagliumi G, Farb A, et al. Localized hypersensitivity and late coronary thrombosis secondary to a sirolimus-eluting stent: should we be cautious? *Circulation* 2004;109:701–5.
69. Joner M, Finn AV, Farb A, et al. Pathology of drug-eluting stents in humans: delayed healing and late thrombotic risk. *J Am Coll Cardiol* 2006;48:193–202.
70. Hamilos MI, Ostojic M, Belesin B, et al. Differential effects of drug-eluting stents on local endothelium-dependent coronary vasomotion. *J Am Coll Cardiol* 2008;51:2123–9.
71. Brugaletta S, Heo JH, Garcia-Garcia HM, et al. Endothelial-dependent vasomotion in a coronary segment treated by ABSORB everolimus-eluting bioresorbable vascular scaffold system is related to plaque composition at the time of bioresorption of the polymer: indirect finding of vascular reparative therapy? *Eur Heart J* 2012;33: 1325–33.
72. Kume T, Okura H, Miyamoto Y, et al. Natural history of stent edge dissection, tissue protrusion and incomplete stent apposition detectable only on optical coherence tomography after stent implantation—preliminary observation. *Circ J* 2012;76:698–703.
73. Radu M, Raber L, Heo JH, et al. Natural history of optical coherence tomography detected edge dissections 12 months following drug-eluting stent implantation. (abstract). *TCT* 2011:659.
74. Gogas BD, Muramatsu T, Garcia-Garcia HM, et al. *In vivo* three dimensional optical coherence tomography. A novel imaging modality to visualize the edge vascular response. *Int J Cardiol* 2012, Oct. 15.
75. Nakazawa G, Otsuka F, Nakano M, et al. The pathology of neoatherosclerosis in human coronary implants bare-metal and drug-eluting stents. *J Am Coll Cardiol* 2011;57:1314–22.
76. Lee CW, Kang SJ, Park DW, et al. Intravascular ultrasound findings in patients with very late stent thrombosis after either drug-eluting or bare-metal stent implantation. *J Am Coll Cardiol* 2010;55:1936–42.
77. Yamaji K, Inoue K, Nakahashi T, et al. Bare metal stent thrombosis and in-stent neoatherosclerosis. *Circ Cardiovasc Interv* 2012;5:47–54.
78. Finn AV, Otsuka F. Neoatherosclerosis: a culprit in very late stent thrombosis. *Circ Cardiovasc Interv* 2012;5:6–9.
79. Farb A, Kolodgie FD, Hwang JY, et al. Extracellular matrix changes in stented human coronary arteries. *Circulation* 2004;110:940–7.
80. Onuma Y, Serruys PW, Perkins LE, et al. Intracoronary optical coherence tomography and histology at 1 month and 2, 3, and 4 years after implantation of everolimus-eluting bioresorbable vascular scaffolds in a porcine coronary artery model: an attempt to decipher the human optical coherence tomography images in the ABSORB trial. *Circulation* 2010;122:2288–300.

Key Words: edge vascular response ■ intracoronary ultrasound ■ optical coherence tomography ■ percutaneous coronary intervention.

▶ APPENDIX

For supplemental tables, please see the online version of this article.

Part 2

***In Vivo* Assessment of Vascular Responses
Utilizing Intravascular Ultrasound (IVUS)
and IVUS-based Imaging Modalities.**

Chapter 5

Assessment of Coronary Atherosclerosis by IVUS and IVUS-based Imaging Modalities: Progression and Regression Studies, Tissue Composition and Beyond.

Bill D. Gogas, Vasim Farooq, Patrick W. Serruys, Hector M. Garcia-Garcia
International Journal of Cardiovascular Imaging. 2011. Feb; 27(2): 225-37 [IF: 2.53]

Assessment of coronary atherosclerosis by IVUS and IVUS-based imaging modalities: progression and regression studies, tissue composition and beyond

Bill D. Gogas · Vasim Farooq ·
Patrick W. Serruys · Hector M. García-García

Received: 7 December 2010 / Accepted: 30 December 2010 / Published online: 4 March 2011
© The Author(s) 2011. This article is published with open access at Springerlink.com

Abstract Cardiovascular disease remains the leading cause of mortality, morbidity and disability in the developed world, predominantly affecting the adult population. In the early 1990s coronary heart disease (CHD) was established as affecting one in two men and one in three women by the age of forty. Despite the dramatic progress in the field of cardiovascular medicine in terms of diagnosis and treatment of heart disease, modest improvements have only been achieved when the reduction of cardiovascular mortality and morbidity indices are assessed. To better understand coronary atherosclerosis, new imaging modalities have been introduced. These novel imaging modalities have been used in two ways: (1) for the characterization of plaque types; (2) for the assessment of the progression and regression of tissue types. These two aspects will be discussed in this review.

Keywords Intravascular ultrasound · Tissue characterization · Atherosclerosis

Introduction

Atherogenesis is a chronic and evolving inflammatory process. Many theories have been proposed to explain the initiation and progression of the atheromatous plaque from the asymptomatic “raised fatty streak or intimal xanthoma” and proatheroma (types II and III lesions respectively_AHA classification) to the formation of the symptomatic and obstructive complicated fibroatheroma (type VI lesion_AHA classification). During the formation of these plaques, a critical primary step is the accumulation and oxidation of low-density lipoprotein (LDL) particles. Oxidized-LDL favours leukocyte recruitment and activation as well as cell death, which leads to the generation of complex atherosclerotic plaques [2]. These high-risk atherosclerotic plaques have a particular phenotype that is characterized by a high content of necrotic core, a thin inflamed fibrous cap (due to intense accumulation of macrophages) and the scarce presence of smooth muscle cells. Within the necrotic core, underlying the thin fibrous cap, hemorrhage, calcification and intraplaque vasa vasorum are frequently found [3, 4].

IVUS and IVUS-based imaging modalities have the potential to be able to provide useful insights into the different phases of the development of the plaque, as well as the different key players in this process (i.e. components of the plaque such as necrotic core). In this review, we will discuss the capabilities and limitations of IVUS-based tissue

B. D. Gogas · V. Farooq · P. W. Serruys ·
H. M. García-García (✉)
Department of Interventional Cardiology,
Thoraxcenter, Erasmus University Medical Center,
z120 Erasmus MC Dr Molerwaterplein 40,
3015 GD Rotterdam,
The Netherlands
e-mail: h.garciagarcia@erasmusmc.nl

characterization imaging modalities in providing this information.

Plaque type characterization

Detection of calcification

On IVUS, calcium appears as bright echoes with acoustic shadowing. Dense calcium obstructs the penetration of ultrasound Fig. 1. As a consequence, IVUS detects only the leading edge of calcium and therefore cannot determine its thickness. Calcification on IVUS is usually described by its circumferential angle (arc), longitudinal length and depth. Calcification can be located deeper in the arterial wall or at the surface of the plaque, in close contact with the lumen wall interface, and can produce reverberations or repeated reflections at reproducible distances. IVUS has shown a significantly higher sensitivity than fluoroscopy in the detection of coronary calcification. [5] As compared to histology, virtual histology has a predictive accuracy of 96.7% in the detection of dense calcium [6] (Fig. 1).

Arterial remodeling and plaque composition

Arterial remodeling refers to a continuous process involving changes in vessel size as measured by the EEM cross-sectional area; this is also known as the vessel cross-sectional area—CSA. “Positive remodeling” occurs when there is an outward increase in EEM and “negative remodeling” occurs when the EEM decreases in size (i.e. shrinkage of the vessel) [7]. The magnitude and direction of remodeling can be expressed by following index: EEM cross-sectional area at the plaque site divided by EEM CSA at the reference “non-diseased” vessel site. Positive remodeling demonstrates an index >1.05 whilst negative remodelling has an index <0.95 . Direct evidence of remodeling can only be demonstrated in serial studies showing changes in the EEM CSA over time, since remodeling may also occur at the “normal-appearing” reference coronary segment [7]. The limitations of coronary angiography in determining disease burden and stenosis severity are largely due to the effects of vessel remodeling. Pathological studies have also suggested a potential relationship between positive vessel remodeling and plaque vulnerability. Vessels

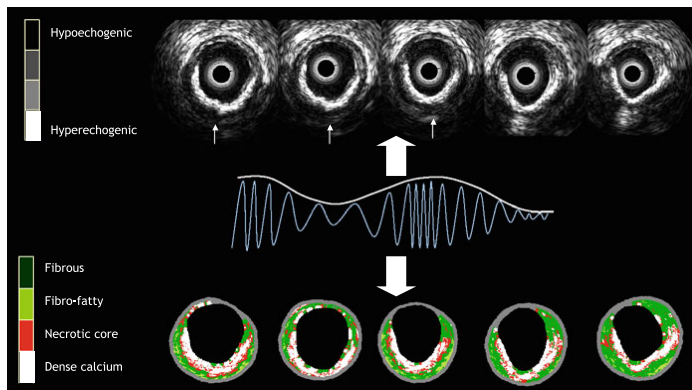


Fig. 1 Cross sections of IVUS and corresponding VH-IVUS frames characterizing a calcified plaque. Grey scale IVUS has both a high sensitivity and specificity in the detection of calcium. Calcium usually obstructs the penetration of ultrasound and consequently obscures the imaging of the underlying vascular wall; this phenomenon is known as acoustic shadowing (*thin white arrows* in the top panel). The

corresponding IVUS virtual histology frames are shown at the bottom of the figure with the dense calcium being shown in *white*. The greyscale image is reconstructed from the amplitude of the signal whereas with virtual histology, the underlying radiofrequency data is used for tissue characterization as illustrated

with positive remodeling have shown an increase in inflammatory marker concentrations, larger lipid cores, paucity of smooth muscle cells and medial thinning [8–10]. Several IVUS studies have linked positive vessel remodelling with culprit [11] and ruptured coronary plaques [12, 13]. Positive remodelling has also been observed more often in patients with acute coronary syndromes than in those with stable coronary artery disease [14, 15], and has been identified as an independent predictor of major adverse cardiac events in patients with unstable angina [16]. Plaques exhibiting positive remodelling also more often have evidence of thrombus and signs of rupture [17]. The patterns of remodelling have also been correlated with plaque composition; soft plaques are associated with positive remodelling whilst fibrocalcific plaques are more often associated with negative or constrictive remodelling [18]. Similar findings have been observed in studies utilizing IVUS virtual histology analyses, a technique developed specifically for tissue characterization; positive remodelling was found to directly correlate with the presence and size of necrotic core, and was inversely associated with the presence of fibrotic tissue [19].

Vulnerable plaque and thrombi

Acute coronary syndromes are often the first manifestation of coronary atherosclerosis, making the identification of plaques at high-risk of complications an important component of strategies to reduce casualties associated with atherosclerosis. Our current understanding of plaque biology suggests that ~60% of clinically evident plaque rupture originates within an inflamed thin-capped fibroatheroma [20, 21]. Pathological studies have demonstrated that ruptured plaques are mainly located in the proximal portions of the LAD and LCX and are more dispersed within the RCA [22]. This tendency of advanced plaques to preferentially develop in these locations has been explained by the low shear stress conditions generated in areas with tortuosity or many branches. Low shear stress may induce the migration of lipid and monocytes into the vessel wall, which may lead to further progression of the lesion towards a plaque with high risk of rupture [23].

The definition of an IVUS-derived TCFA is a lesion fulfilling the following criteria in at least 3

frames: (1) plaque burden $\geq 40\%$; (2) *confluent* necrotic core $\geq 10\%$ in direct contact with the lumen (i.e. no visible overlying tissue) [24]. By using this definition of IVUS-derived TCFA, in patients with ACS who underwent IVUS of all three epicardial coronaries, on average 2 IVUS-derived thin cap fibroatheromas were found per patient with half of these patients showing evidence of outward remodelling. [24].

Hong et al. [25] reported the frequency and distribution of TCFA identified by virtual histology intravascular ultrasound in acute coronary syndrome (ACS = 105 pts) and stable angina pectoris (SAP = 107 pts) in a 3-vessel IVUS-VH study. The findings showed that there were 2.5 ± 1.5 TCFAs per patient with ACS and 1.7 ± 1.1 TCFAs per patient with SAP, $P < 0.001$. The presentation of ACS was the only independent predictor for multiple ID-TCFA ($P = 0.011$). 83% of ID-TCFAs were located within 40 mm of the proximal coronary artery.

The potential value of these VH IVUS-derived plaque types to predict adverse coronary events was evaluated in an international multicentre prospective study, the Providing Regional Observations to Study Predictors of Events in the Coronary Tree study (PROSPECT study) [26].

The PROSPECT trial was a multi-center, natural history study of acute coronary syndrome patients. All patients underwent PCI to their culprit lesion at baseline, followed by an angiogram and IVUS virtual histology of all three major coronary arteries. One of the main findings was that a TCFA, with a minimum lumen area of $\leq 4 \text{ mm}^2$, and a large plaque burden ($\geq 70\%$), had a 17.2% likelihood of causing a future event within three years [26]. Interestingly, the anticipated higher frequency of acute thrombotic cardiovascular events did not occur, with only a 1% rate of myocardial infarction and no deaths directly attributable to non-culprit vessels over a period of 3 years follow-up. These results suggest that non-culprit obstructive coronary plaques were more likely to be associated with increasing anginal symptoms rather than thrombotic acute events, with 8.5% of patients presenting with worsening angina and 3.3% with unstable angina.

Plaque ruptures occur at sites of significant plaque accumulation, but are often not highly stenotic, as defined by coronary angiography due to positive vascular remodeling [12, 13, 27]. The transition to

plaque rupture has been characterized by the presence of active inflammation (monocyte and macrophage infiltration), thinning of the fibrous cap ($<65\ \mu\text{m}$), development of a large lipid necrotic core, endothelial denudation with superficial platelet aggregation and intraplaque hemorrhage [28]. The remaining plaques that can cause ACS contain calcium nodules ($\sim 10\%$) or have none of the pathological features described above ($\sim 20\%$). Superficial plaque erosion can explain at least a portion of the latter events, particularly in women and diabetics [29]. The lack of a cellular or anatomical signature of plaque erosion can make it difficult for existing imaging methods to have a high accuracy in predicting future ACS events. In addition, most plaque ruptures are frequently clinically silent; the occurrence of repetitive healed plaque ruptures may contribute to the progression of stable coronary disease into obstructive disease [30].

Ruptured plaques may have a variable appearance on IVUS. Most commonly, IVUS may reveal an “axial”, abrupt ulceration depicted as an echolucent “void” or cavity beginning at the luminal-intimal border. These features should be distinguished from a longitudinal tear of the intima and media associated with spontaneous or iatrogenic dissection. The tear of the rupture in the fibrous cap can be identified in approximately 60% of the cases and occurs more often at the shoulder of the plaque than in the centre [12, 31, 32]. Due to its relatively poor resolution, IVUS is unsuitable to detect a thin fibrous cap. However, IVUS often reveals other features of ruptured plaques which are large in volume, eccentric, have mixed or soft composition and irregular surface, and are associated with expansive remodeling [12, 13, 33, 34]. Ruptured plaques have been shown to have quantitatively less calcium, especially superficial calcium, but a larger number of small ($<90^\circ$ arc) calcium deposits, particularly deep calcium deposits [35]. IVUS can also reveal blood speckles passing through intra-plaque channels created by the rupture. These usually produce a typical hazy, complex with non stenotic angiographic appearances of the ruptured plaques.

Several IVUS studies have reported the frequency and distribution of plaque ruptures during investigation of the three coronary epicardial vessels. Rioufol et al. studied 24 patients (72 arteries) with ACS and found a mean prevalence of two ruptured plaques per patient. Interestingly, 12.5% of these patients had

ruptured plaques in the three major coronary arteries. Only 37.5% of the ruptured plaques were located at the culprit lesion, and 79% of the patients also had a ruptured plaque located somewhere other than at the culprit lesion [36]. In a similar study in 45 patients with acute myocardial infarction (AMI), plaque rupture was observed in 21 patients (47%) at the culprit site and 17 additional plaque ruptures were found at remote sites in 11 patients (24%) [37]. Hong et al., evaluated the incidence of plaque rupture depending on the clinical presentation. They performed 3-vessel IVUS examination in 235 patients (122 AMI and 113 stable angina pectoris—SAP). Plaque rupture of infarct-related or target lesions occurred in 66% of AMI patients and in 27% of SAP patients. Non-infarct-related or non-target artery plaque ruptures occurred in 17% of AMI patients and 5% of SAP patients. Multiple plaque ruptures were observed in 20% of AMI and 6% of SAP patients [38]. The same authors evaluated the distribution of plaque rupture in native coronary arteries in 392 patients (231 ACS and 161 SAP). Three-vessel IVUS imaging showed that plaque ruptures occurred mainly in the proximal segments of the LAD (83% of LAD ruptured plaques), the proximal and distal segments of the RCA (48 and 32% of RCA ruptured plaques, respectively), and the entire LCX [39]. These results are in line with another study that included 104 patients and studied 160 ruptured plaques in the LAD, the majority of plaque ruptures were located within the proximal 30 mm of the artery [40].

A study aimed at characterizing plaque ruptures in the left main coronary artery (LMCA) found 16 plaque ruptures in 17 patients (2 AMI, 13 unstable angina and 1 SAP). The ruptures were located in the distal portion and/or bifurcation of the LMCA, often did not compromise the lumen, and had an angiographic complex appearance. When ruptured plaques involved the bifurcation LAD-LCX, they often occurred opposite to the flow divider [41]. This is in line with findings made by our group; lesions involving the bifurcation LAD-LCX were predominantly located in the outer wall of the carina, and such locations were often associated with a larger necrotic core content [42].

Ruptured atherosclerotic plaques in native coronary arteries are well described with intravascular ultrasound; they are however, not well described in

saphenous vein grafts (SVGs). In 791 pre-intervention IVUS SVG studies, 95 ruptured plaques in 76 SVGs (73 patients) were identified (prevalence of 9.7%). These ruptured plaques were found to be associated with complex angiographic characteristics and expansive remodelling [43, 44]. Likewise, in an analysis of 300 ruptured plaques in SVGs in 254 patients, Maehara et al., demonstrated that ruptured plaques, as detected by IVUS, strongly correlated with a complex angiographic lesion morphology: ulceration in 81%, intimal flap in 40%, thrombus in 7%, and aneurysm in 7% [12].

IVUS has also been used to assess the natural evolution of ruptured plaques. IVUS studies have suggested that up to 50% of the ruptured plaques detected in a first ACS event heals with medical therapy, without a significant change in plaque size [45]. One study revealed complete healing of plaque rupture in 29% of patients treated with statins and incomplete healing in untreated patients [46].

The ruptured plaque profile in 40 patients referred for cardiac catheterization has previously been described [47]. In total, there were 13 patients with stable angina, 12 with unstable angina, and 15 with acute myocardial infarction. Ruptured plaque was identified in 26 patients and, as expected, was more frequent in patients with acute myocardial infarction and unstable angina. Patients with ruptured plaques were found to have a larger body mass index, were

more likely to be smokers and had more diffuse calcification and necrotic core areas when compared to those patients without plaque rupture. Of note, is that the location of plaque ruptures in this study mirrored the pathological findings [48]. In a study performed by our group, the proximal left anterior descending coronary artery was the most common site of plaque rupture. In a pathological series of 79 ruptures, Burke et al. [48] found 74% of the plaque ruptures occurred in the proximal left anterior descending artery.

Similarly, in a report by Hong et al., the frequency and distribution of ruptured plaques identified by IVUS-VH in acute coronary syndrome (ACS = 105 pts) and stable angina pectoris (SAP = 107 pts) in a 3-vessel IVUS-VH study were reported. [25] 76 ruptured plaques (55 in ACS and 21 in SAP) were described with the presentation of ACS being the only independent predictor for multiple plaque ruptures ($P = 0.013$).

Although plaque characteristics do not yet influence current therapeutic guidelines, the available clinical imaging modalities, IVUS and IVUS-based tissue characterization techniques such as virtual histology, integrated backscattered IVUS and iMap, have the ability to identify some of the pathological atheroma features described above (Fig. 2).

Thrombus represents the ultimate pathological feature leading to ACS. Thrombus is usually recognized as

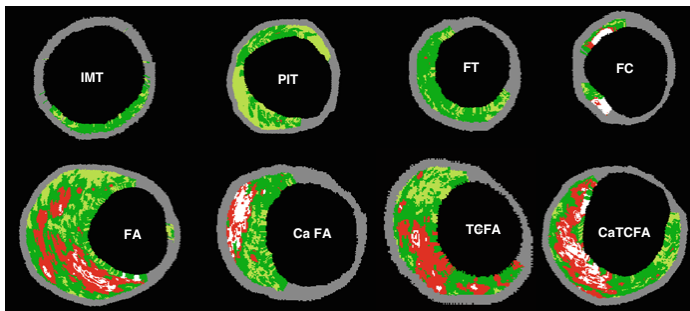


Fig. 2 Examples of VH-IVUS images classified by a two-dimensional lesion analysis. (IMT) intimal medial thickening; (PIT) pathological intimal thickening; (FT) fibrotic plaque; (FC) fibrocalcific plaque; (FA) fibroatheroma and (caFA) calcified fibroatheroma; (VH-TGFA) Virtual Histology-thin cap fibroatheroma and (VH-caTGFA) Virtual Histology-

calcified thin cap fibroatheroma. Reprinted from EuroIntervention Vol 5, number 2, Garcia-Garcia HM et al. Tissue characterisation using intravascular radiofrequency data analysis: recommendations for acquisition, analysis, interpretation and reporting. Pages 186. Copyright (2009), with permission from Europa Edition

an echolucent intraluminal mass, often with a layered or pedunculated appearance by IVUS [7]. Fresh or acute thrombus may appear as an echodense intraluminal tissue, which does not follow the circular appearance of the vessel wall, whilst older, more organized thrombus has a darker ultrasound appearance. However, none of these IVUS features are a hallmark for thrombus, and one should consider slow flow (fresh thrombus), air, stagnant contrast or black hole, an echolucent neointimal tissue observed after DES and radiation therapy, as differential diagnoses [7].

None of the IVUS-based imaging modalities available can reliably identify thrombus.

Assessment of progression/regression of coronary atherosclerosis

Quantification of atheroma or plaque area in cross-sectional IVUS images is performed by subtracting the lumen area from the EEL area. Hence, IVUS defined atheroma area is a combination of plaque plus media area. The atheroma area can be calculated in each frame (cross-sectional image), and total atheroma volume (TAV) can be calculated based on pullback speed during imaging acquisition. Atheroma volume can be reported as the percent of the volume of the external elastic membrane occupied by atheroma namely percent atheroma volume (PAV). Parameters commonly used to report the extent of the coronary atherosclerosis are shown in (Fig. 3).

Measurements are performed between the inner lumen border and the media, delineated by the IEL, which corresponds to the “true” histological area of

the atheroma. Intravascular imaging has played an important role in the understanding of atherosclerosis disease in humans and translation of novel therapies to the clinical arena.

Drug effects on atherosclerosis

The initial observations about a expansive continuous relationship between coronary heart disease risk and blood cholesterol levels led to the conduction of a number of IVUS-based studies to evaluate the effectiveness of differing lipid lowering drugs on atheroma size. Changes in plaque characteristics may be a more relevant endpoint to predict the risk of vascular thrombosis than plaque progression or regression of mild to moderate disease. Imaging tools to accurately evaluate plaque characteristics were not available until recently. Other limitations of using conventional grayscale IVUS to assess the natural history of atherosclerosis should be enumerated: (1) Catheterization, which is an invasive procedure, is required for serial imaging; (2) only a segment of the coronary tree can be studied; (3) plaque composition is not obtained; (4) there is no direct evidence linking changes in coronary plaques and clinical events.

The efficacy of lowering LDL-C with inhibitors of hydroxymethylglutaryl coenzyme A reductase (statins) is unequivocal; however the change in atheroma size by statins is not constant across all IVUS studies. There are many potential explanations for these discrepancies in IVUS studies, such as drug properties, dose, and duration of treatment. Other medications have been studied with IVUS greyscale and IVUS derived imaging modalities (Table 1).

Nevertheless, no single report has been described showing a clear and direct association between reduction in plaque size, composition and/or plaque type with the reduction in clinical events. This is in part due to the fact that clinical outcome studies are expensive, since they have to include a large population (that should be imaged in at least at 2 different time points) that have to be followed up for a prolonged period of time in order to ensure the required number of events have occurred (which are becoming scarce due to the improvements in standards of care) in order to best assess the treatment effect.

Volumetric quantification of the extent of atherosclerosis in coronary arteries	
$TAV = \sum (EEM_{CSA} - LUMEN_{CSA})$	
$TAV_{norm} = \sum$	$\frac{EEM_{CSA} - LUMEN_{CSA}}{\text{number of analyzed frames per patient}} \times \frac{\text{mean/median no. of analyzed frames in the population}}$
% change in TAV =	$\frac{TAV \text{ (follow-up)} - (baseline)}{TAV \text{ (baseline)}} \times 100$
$PAV =$	$\frac{\sum (EEM_{CSA} - LUMEN_{CSA})}{\sum EEM_{CSA}} \times 100$

Fig. 3 Parameters commonly used to report the extent of the coronary atherosclerosis are total atheroma volume (TAV) and percent atheroma volume (PAV). EEM, external elastic membrane; CSA, cross-sectional area

Table 1 Intravascular ultrasound progression/regression studies (published with permission of European Heart Journal)

Study	Design	Year	Treatment	n	FU	Primary endpoint	Results (mean ± SD)
Statin trials							
GAIN [49]	RCT	2001	Atorvastatin Control	48 51	12 months	Plaque volume	2.5 ± 24.9 mm ³ 11.8 ± 31 mm ³
ESTABLISH [50]	RCT	2004	Atorvastatin Control	24 24	6 months	% change in plaque volume	13.1 ± 12.8% 8.7 ± 14.9%
REVERSAL [51]	RCT	2004	Atorvastatin Pravastatin	253 249	18 months	% change in plaque volume	4.1 ± 29.6% 5.4 ± 20.1%
Jensen [52]	Observational	2004	Simvastatin	40	12 months	% change in plaque volume	6.30%
Petronio [53]	RCT	2005	Simvastatin Control	36 35	12 months	Plaque volume	-2.5 ± 3.0 mm ³ /mm 1.0 ± 3.0 mm ³ /mm
Nishioka [54]	Observational	2004	Pravastatin, atorvastatin, simvastatin and fluvastatin Control	22 26	6 months	Plaque Volume	30.9 ± 15.6 mm ³ 35.5 ± 12.7 mm ³
Tani [55]	RCT	2005	Pravastatin Control	52 23	6 months	% change in plaque volume	-14.4 ± 23% 1.1 ± 4.6%
ASTEROID [56]	Observational	2006	Rosuvastatin	349	24 months	Change in PAV	-0.98 ± 3.15%
Takashima [57]	Observational	2007	Pitavastatin Control	41 41	6 months	% change in plaque volume	-10.6 ± 9.4% 8.1 ± 14.0%
COSMOS [58]	Observational	2009	Rosuvastatin	126	18 months	Change in PAV	-5.1 ± 14.1%
JAPAN-ACS [59]	RCT	2009	Atorvastatin Pitavastatin	127 125	8–12 months	% change in plaque volume	-18.1 ± 14.2% -16.9 ± 13.9%
Hirayama	Observational	2009	Atorvastatin	28	28 weeks 80 weeks	% change in plaque volume	-9.4 ± 10.3% -18.9 ± 14.1%
ACAT (acyl coenzyme A: cholesterol acyltransferase) inhibitor trials							
A-PLUS [60]	RCT	2004	Avasimibe 50 mg Avasimibe 250 mg Avasimibe 750 mg Placebo	108 98 117 109	24 months	Change in PAV	0.7 ± 0.4% 0.8 ± 0.4% 1.0 ± 0.3% 0.4 ± 0.4%
ACTIVATE [61]	RCT	2006	Pactimibe Placebo	206 202	18 months	Change in PAV	0.69 ± 0.25% -0.59 ± 0.25%

Table 1 continued

Study	Design	Year	Treatment	n	FU	Primary endpoint	Results (mean ± SD)
Increasing high-density lipoprotein therapies							
ApoA-I Milano [62]	RCT	2003	ApoA-I Milano 15 mg/kg	21	5 weeks	Change in PAV	-1.29 ± 3.5%
			ApoA-I Milano 45 mg/kg	15			-0.73 ± 2.8%
			Placebo	11			0.14 ± 3.09%
ERASE [63]	RCT	2007	CSL-111 (reconstituted HDL infusion)	89	4 weeks	% change in plaque volume	-3.41 (IQR, -6.55-2.25)
			Placebo	47			-1.62 (IQR, -5.95-1.94)
CART-2 [64]	RCT	2008	Succinobucol (AGI-1067)	183	12 months	Absolute change in plaque volume	-3.4 ± 14.5 mm ³
			Placebo	49			-0.6 ± 13.4 mm ³
Others therapies							
CAMELOT [65]	RCT	2004	Amlodipine	91	24 months	Change in PAV	0.5 ± 3.9%
			Enalapril	88			0.8 ± 3.7%
			Placebo	95			1.3 ± 4.4%
Waseda	Observational	2006	Losartan	41	7 months	Change in plaque area	-9.9 ± 3.1 mm ²
			Non ARB	23	7 months		-9.1 ± 2.7 mm ²
ILLUSTRATE [66]	RCT	2007	Torcetrapib + atorvastatin	464	24 months	Change in PAV	0.12 ± 2.99%
			Atorvastatin	446			0.19 ± 2.83%
PERSPECTIVE [67]	RCT	2007	Perindopril	75	36 months	Change in plaque area	-0.2 ± 1.6mm ²
			Placebo	69			-0.1 ± 1.2 mm ²
PERISCOPE [68]	RCT	2008	Proglitazone,	179	18 months	Change in PAV	-0.16% (95% CI, -0.57-0.25%)
			Glimpiride	181			0.73% (95% CI, 0.33-1.12%)
STRADIVARIUS [69]	RCT	2008	Rimonabant	335	18 months	Change in PAV	0.25% (95% CI, -0.04-0.54%)
			Placebo	341			0.51% (95% CI, 0.22-0.80%)
ENCORE II [70]	RCT	2009	Nifedipine	97	18-24 months	% change in plaque volume	5.0 (95% CI, -1.3, 11.2)
			Placebo	96			3.2 (95% CI, -1.9, 8.3)
APPROACH [71]	RCT	2010	Rosiglitazone	233	18 months	Change in PAV	-0.21 (95% CI, -0.86, 0.44)
			Glipizide	229			0.43 (95% CI, -0.22, 1.08)

Table 1 continued

Study	Design	Year	Treatment	n	FU	Primary endpoint	Results (mean ± SD)
IVUS-based tissue characterization studies							
Yokoyama [72]	RCT	2005	Atorvastatin Control	25	6 months	Overall plaque size and tissue characterization by IB IVUS	Atorvastatin reduced plaque size and changed plaque composition
Kawasaki [73]	RCT	2005	Pravastatin, Atorvastatin Diet	25 18 17	6 months	Overall tissue characterization by IB IVUS	Statins reduced lipid without changes in plaque size
IBIS 2 [74]	RCT	2008	Darapladib	175	12 months	Necrotic core vol by IVUS VH	Darapladib reduced significantly necrotic core
Nasu [75]	Observational	2009	Placebo Fluvastatin	155 40	12 months	Overall tissue characterization by IVUS VH	Fluvastatin reduced plaque volume and fibro-fatty
Hong [76]	RCT	2009	Control Simvastatin	40 50	12 months	Overall tissue characterization by IVUS VH	Both reduced necrotic core and increased in fibro-fatty volume
Toi [77]	RCT	2009	Rosuvastatin Atorvastatin	50 80	2–3 weeks	Overall tissue characterization by IVUS VH	Pitavastatin reduced plaque volume and fibro-fatty
Miyagi [78]	Observational	2009	Pitavastatin Statin (pravastatin, pitavastatin, atorvastatin, fluvastatin, simvastatin) Non statin	80 44 56	6 months	Overall tissue characterization by IB IVUS	Statins reduced lipid and increased fibrous

IVUS intravascular ultrasound, IB integrated backscatter, VH virtual histology

Acknowledgments Bill D. Gogas has received grant support from the Hellenic Heart Foundation.

Open Access This article is distributed under the terms of the Creative Commons Attribution Noncommercial License which permits any noncommercial use, distribution, and reproduction in any medium, provided the original author(s) and source are credited.

Conflict of interest None.

References

- Lloyd-Jones DM, Larson MG, Beiser A, Levy D (1999) Lifetime risk of developing coronary heart disease. *Lancet* 353(9147):89–92
- Virmani R, Kolodgie FD, Burke AP, Farb A, Schwartz SM (2000) Lessons from sudden coronary death: a comprehensive morphological classification scheme for atherosclerotic lesions. *Arterioscler Thromb Vasc Biol* 20(5):1262–1275
- Burke AP, Farb A, Malcom GT, Liang Y, Smialek JE, Virmani R (1999) Plaque rupture and sudden death related to exertion in men with coronary artery disease. *JAMA* 281(10):921–926
- Burke AP, Farb A, Malcom GT, Liang YH, Smialek J, Virmani R (1997) Coronary risk factors and plaque morphology in men with coronary disease who died suddenly. *N Engl J Med* 336(18):1276–1282
- Mintz GS, Popma JJ, Pichard AD, Kent KM, Satler LF, Chuang YC, Ditrano CJ, Leon MB (1995) Patterns of calcification in coronary artery disease. A statistical analysis of intravascular ultrasound and coronary angiography in 1,155 lesions. *Circulation* 91(7):1959–1965
- MP Nair A, Kuban BD, Vince DG (2007) Automated coronary plaque characterization with intravascular ultrasound backscatter: ex vivo validation. *Eurointervention* 3:113–130
- Mintz GS, Nissen SE, Anderson WD, Bailey SR, Erbel R, Fitzgerald PJ, Pinto FJ, Rosenfield K, Siegel RJ, Tuzcu EM, Yock PG (2001) American college of cardiology clinical expert consensus document on standards for acquisition, measurement and reporting of intravascular ultrasound studies (IVUS). A report of the American college of cardiology task force on clinical expert consensus documents. *J Am Coll Cardiol* 37(5):1478–1492
- Pasterkamp G, Schoneveld AH, van der Wal AC, Haudenschild CC, Clarijs RJ, Becker AE, Hillen B, Borst C (1998) Relation of arterial geometry to luminal narrowing and histologic markers for plaque vulnerability: the remodeling paradox. *J Am Coll Cardiol* 32(3):655–662
- Varnava AM, Mills PG, Davies MJ (2002) Relationship between coronary artery remodeling and plaque vulnerability. *Circulation* 105(8):939–943
- Burke AP, Kolodgie FD, Farb A, Weber D, Virmani R (2002) Morphological predictors of arterial remodeling in coronary atherosclerosis. *Circulation* 105(3):297–303
- Kotani J, Mintz GS, Castagna MT, Pinnow E, Berzinger CO, Bui AB, Pichard AD, Satler LF, Suddath WO, Waksman R, Laird JR Jr, Kent KM, Weissman NJ (2003) Intravascular ultrasound analysis of infarct-related and non-infarct-related arteries in patients who presented with an acute myocardial infarction. *Circulation* 107(23):2889–2893
- Maehara A, Mintz GS, Bui AB, Walter OR, Castagna MT, Canos D, Pichard AD, Satler LF, Waksman R, Suddath WO, Laird JR Jr, Kent KM, Weissman NJ (2002) Morphologic and angiographic features of coronary plaque rupture detected by intravascular ultrasound. *J Am Coll Cardiol* 40(5):904–910
- von Birgelen C, Klinkhart W, Mintz GS, Papatheodorou A, Herrmann J, Baumgart D, Haude M, Wieneke H, Ge J, Erbel R (2001) Plaque distribution and vascular remodeling of ruptured and non ruptured coronary plaques in the same vessel: an intravascular ultrasound study in vivo. *J Am Coll Cardiol* 37(7):1864–1870
- Jeremias A, Spies C, Herity NA, Pomerantsev E, Yock PG, Fitzgerald PJ, Yeung AC (2000) Coronary artery compliance and adaptive vessel remodeling in patients with stable and unstable coronary artery disease. *Heart* 84(3):314–319
- Nakamura M, Nishikawa H, Mukai S, Setsuda M, Nakajima K, Tamada H, Suzuki H, Ohnishi T, Kakuta Y, Nakano T, Yeung AC (2001) Impact of coronary artery remodeling on clinical presentation of coronary artery disease: an intravascular ultrasound study. *J Am Coll Cardiol* 37(1):63–69
- Gyongyosi M, Yang P, Hassan A, Domanovits H, Laggner A, Weidinger F, Glogar D (2000) Intravascular ultrasound predictors of major adverse cardiac events in patients with unstable angina. *Clin Cardiol* 23(7):507–515
- Gyongyosi M, Yang P, Hassan A, Weidinger F, Domanovits H, Laggner A, Glogar D (1999) Arterial remodeling of native human coronary arteries in patients with unstable angina pectoris: a prospective intravascular ultrasound study. *Heart* 82(1):68–74
- Tauth J, Pinnow E, Sullebarger JT, Basta L, Gursoy S, Lindsay J Jr, Matar F (1997) Predictors of coronary arterial remodeling patterns in patients with myocardial ischemia. *Am J Cardiol* 80(10):1352–1355
- Rodríguez-Granillo GA, Serruys PW, Garcia-Garcia HM, Aoki J, Valgimigli M, van Mieghem CA, McFadden E, de Jaegere PP, de Feyter P (2006) Coronary artery remodeling is related to plaque composition. *Heart* 92(3):388–391
- Virmani R, Burke AP, Farb A, Kolodgie FD (2006) Pathology of the vulnerable plaque. *J Am Coll Cardiol* 47(8 Suppl):C13–C18
- Schaar JA, Muller JE, Falk E, Virmani R, Fuster V, Serruys PW, Colombo A, Stefanadis C, Ward Casscells S, Moreno PR, Maseri A, van der Steen AF (2004) Terminology for high-risk and vulnerable coronary artery plaques. Report of a meeting on the vulnerable plaque, June 17 and 18, 2003, Santorini, Greece. *Eur Heart J* 25(12):1077–1082
- Cheruvu PK, Finn AV, Gardner C, Caplan J, Goldstein J, Stone GW, Virmani R, Muller JE (2007) Frequency and distribution of thin-cap fibroatheroma and ruptured plaques in human coronary arteries: a pathologic study. *J Am Coll Cardiol* 50(10):940–949
- Cunningham KS, Gotlieb AI (2005) The role of shear stress in the pathogenesis of atherosclerosis. *Lab Invest* 85(1):9–23

24. Garcia-Garcia HM, Goedhart D, Schuurbiens JC, Kukreja N, Tanimoto S, Daemen J, Morel MA, Bressers M, van Es GA, Wentzel J, Gijzen F, van der Steen AF, Serruys PW (2006) Virtual histology and remodeling index allow in vivo identification of allegedly high risk coronary plaques in patients with acute coronary syndromes: a three vessel intravascular ultrasound radiofrequency data analysis. *Eurointervention* 2:338–344
25. Hong MK, Mintz GS, Lee CW, Lee JW, Park JH, Park DW, Lee SW, Kim YH, Cheong SS, Kim JJ, Park SW, Park SJ (2008) A three-vessel virtual histology intravascular ultrasound analysis of frequency and distribution of thin-cap fibroatheromas in patients with acute coronary syndrome or stable angina pectoris. *Am J Cardiol* 101(5): 568–572
26. Stone GW, Maehara A, Lansky AJ, de Bruyne B, Cristea E, Mintz GS, Mehran R, McPherson J, Farhat N, Marso SP, Parise H, Templin B, White R, Zhang Z, Serruys PW, PROSPECT Investigators (2011) A prospective natural-history study of coronary atherosclerosis. *N Engl J Med* 364(3):226–235
27. Fujii K, Mintz GS, Carlier SG, Costa JR Jr, Kimura M, Sano K, Tanaka K, Costa RA, Lui J, Stone GW, Moses JW, Leon MB (2006) Intravascular ultrasound profile analysis of ruptured coronary plaques. *Am J Cardiol* 98(4):429–435
28. Kologdie FD, Gold HK, Burke AP, Fowler DR, Kruth HS, Weber DK, Farb A, Guerrero LJ, Hayase M, Kutys R, Narula J, Finn AV, Virmani R (2003) Intraplaque hemorrhage and progression of coronary atherosclerosis. *N Engl J Med* 349(24):2316–2325
29. Kruk M, Pregowski J, Mintz GS, Maehara A, Tyczynski P, Witkowski A, Kalinczuk L, Hong YJ, Pichard AD, Satler LF, Kent KM, Suddath WO, Waksman R, Weissman NJ (2007) Intravascular ultrasonic study of gender differences in ruptured coronary plaque morphology and its associated clinical presentation. *Am J Cardiol* 100(2):185–189
30. Burke AP, Kologdie FD, Farb A, Weber DK, Malcom GT, Smialek J, Virmani R (2001) Healed plaque ruptures and sudden coronary death: evidence that subclinical rupture has a role in plaque progression. *Circulation* 103(7): 934–940
31. Jensen LO, Mintz GS, Carlier SG, Fujii K, Moussa I, Dangas G, Mehran R, Stone GW, Leon MB, Moses JW (2006) Intravascular ultrasound assessment of fibrous cap remnants after coronary plaque rupture. *Am Heart J* 152(2):327–332
32. Ge J, Chirillo F, Schwedtmann J, Gorge G, Haude M, Baumgart D, Shah V, von Birgelen C, Sack S, Boudoulas H, Erbel R (1999) Screening of ruptured plaques in patients with coronary artery disease by intravascular ultrasound. *Heart* 81(6):621–627
33. von Birgelen C, Klinkhart W, Mintz GS, Wieneke H, Baumgart D, Haude M, Bartel T, Sack S, Ge J, Erbel R (2000) Size of emptied plaque cavity following spontaneous rupture is related to coronary dimensions, not to the degree of lumen narrowing. A study with intravascular ultrasound in vivo. *Heart* 84(5):483–488
34. Fujii K, Kobayashi Y, Mintz GS, Takebayashi H, Dangas G, Moussa I, Mehran R, Lansky AJ, Kreps E, Collins M, Colombo A, Stone GW, Leon MB, Moses JW (2003) Intravascular ultrasound assessment of ulcerated ruptured plaques: a comparison of culprit and non culprit lesions of patients with acute coronary syndromes and lesions in patients without acute coronary syndromes. *Circulation* 108(20):2473–2478
35. Fujii K, Carlier SG, Mintz GS, Takebayashi H, Yasuda T, Costa RA, Moussa I, Dangas G, Mehran R, Lansky AJ, Kreps EM, Collins M, Stone GW, Moses JW, Leon MB (2005) Intravascular ultrasound study of patterns of calcium in ruptured coronary plaques. *Am J Cardiol* 96(3):352–357
36. Rioufol G, Finet G, Ginon I, Andre-Fouet X, Rossi R, Vialle E, Desjoyaux E, Convert G, Huret JF, Tabib A (2002) Multiple atherosclerotic plaque rupture in acute coronary syndrome: a three-vessel intravascular ultrasound study. *Circulation* 106(7):804–808
37. Tanaka A, Shimada K, Sano T, Namba M, Sakamoto T, Nishida Y, Kawarabayashi T, Fukuda D, Yoshikawa J (2005) Multiple plaque rupture and C-reactive protein in acute myocardial infarction. *J Am Coll Cardiol* 45(10): 1594–1599
38. Hong MK, Mintz GS, Lee CW, Kim YH, Lee SW, Song JM, Han KH, Kang DH, Song JK, Kim JJ, Park SW, Park SJ (2004) Comparison of coronary plaque rupture between stable angina and acute myocardial infarction: a three-vessel intravascular ultrasound study in 235 patients. *Circulation* 110(8):928–933
39. Hong MK, Mintz GS, Lee CW, Lee BK, Yang TH, Kim YH, Song JM, Han KH, Kang DH, Cheong SS, Song JK, Kim JJ, Park SW, Park SJ (2005) The site of plaque rupture in native coronary arteries: a three-vessel intravascular ultrasound analysis. *J Am Coll Cardiol* 46(2):261–265
40. Pregowski J, Tyczynski P, Mintz GS, Kim SW, Witkowski A, Satler L, Kruk M, Waksman R, Maehara A, Weissman NJ (2006) Intravascular ultrasound assessment of the spatial distribution of ruptured coronary plaques in the left anterior descending coronary artery. *Am Heart J* 151(4): 898–901
41. Tyczynski P, Pregowski J, Mintz GS, Witkowski A, Kim SW, Waksman R, Satler L, Pichard A, Kalinczuk L, Maehara A, Weissman NJ (2005) Intravascular ultrasound assessment of ruptured atherosclerotic plaques in left main coronary arteries. *Am J Cardiol* 96(6):794–798
42. Rodriguez-Granillo GA, Garcia-Garcia HM, Wentzel J, Valgimigli M, Tsuchida K, van der Giessen W, de Jaegere P, Regar E, de Feyter PJ, Serruys PW (2006) Plaque composition and its relationship with acknowledged shear stress patterns in coronary arteries. *J Am Coll Cardiol* 47(4):884–885
43. Pregowski J, Tyczynski P, Mintz GS, Kim SW, Witkowski A, Waksman R, Pichard A, Satler L, Kent K, Kruk M, Bieganski S, Ohlmann P, Weissman NJ (2005) Incidence and clinical correlates of ruptured plaques in saphenous vein grafts: an intravascular ultrasound study. *J Am Coll Cardiol* 45(12):1974–1979
44. Pregowski J, Tyczynski P, Mintz GS, Kim SW, Witkowski A, Waksman R, Pichard A, Satler L, Kent K, Kalinczuk L, Bieganski S, Ohlmann P, Maehara A, Weissman NJ (2006) Comparison of ruptured plaques in native coronary arteries and in saphenous vein grafts: an intravascular ultrasound study. *Am J Cardiol* 97(5):593–597
45. Rioufol G, Gilard M, Finet G, Ginon I, Boschat J, Andre-Fouet X (2004) Evolution of spontaneous atherosclerotic

- plaque rupture with medical therapy: long-term follow-up with intravascular ultrasound. *Circulation* 110(18):2875–2880
46. Hong MK, Mintz GS, Lee CW, Suh IW, Hwang ES, Jeong YH, Park DW, Kim YH, Han KH, Cheong SS, Kim JJ, Park SW, Park SJ (2007) Serial intravascular ultrasound evidence of both plaque stabilization and lesion progression in patients with ruptured coronary plaques: effects of statin therapy on ruptured coronary plaque. *Atherosclerosis* 191(1):107–114
 47. Rodriguez-Granillo GA, Garcia-Garcia HM, Valgimigli M, Vaina S, van Mieghem C, van Geuns RJ, van der Ent M, Regar E, de Jaegere P, van der Giessen W, de Feyter P, Serruys PW (2006) Global characterization of coronary plaque rupture phenotype using three-vessel intravascular ultrasound radiofrequency data analysis. *Eur Heart J*
 48. Burke AP, Joner M, Virmani R (2006) IVUS-VH: a predictor of plaque morphology? *Eur Heart J* 27(16):1889–1890
 49. Scharf M, Bocksch W, Koschyk DH, Voelker W, Karsch KR, Kreuzer J, Hausmann D, Beckmann S, Gross M (2001) Use of intravascular ultrasound to compare effects of different strategies of lipid-lowering therapy on plaque volume and composition in patients with coronary artery disease. *Circulation* 104(4):387–392
 50. Okazaki S, Yokoyama T, Miyachi K, Shimada K, Kurata T, Sato H, Daida H (2004) Early statin treatment in patients with acute coronary syndrome: demonstration of the beneficial effect on atherosclerotic lesions by serial volumetric intravascular ultrasound analysis during half a year after coronary event: the ESTABLISH Study. *Circulation* 110(9):1061–1068
 51. Nissen SE, Tuzcu EM, Schoenhagen P, Brown BG, Ganz P, Vogel RA, Crowe T, Howard G, Cooper CJ, Brodie B, Grines CL, DeMaria AN (2004) Effect of intensive compared with moderate lipid-lowering therapy on progression of coronary atherosclerosis: a randomized controlled trial. *JAMA* 291(9):1071–1080
 52. Jensen LO, Thayssen P, Pedersen KE, Stender S, Haghfelt T (2004) Regression of coronary atherosclerosis by simvastatin: a serial intravascular ultrasound study. *Circulation* 110(3):265–270
 53. Petronio AS, Amoroso G, Limbruno U, Papini B, De Carlo M, Micheli A, Ciabatti N, Mariani M (2005) Simvastatin does not inhibit intimal hyperplasia and restenosis but promotes plaque regression in normocholesterolemic patients undergoing coronary stenting: a randomized study with intravascular ultrasound. *Am Heart J* 149(3):520–526
 54. Nishioka H, Shimada K, Kataoka T, Hirose M, Asawa K, Hasegawa T, Yamashita H, Ehara S, Kamimori K, Sakamoto T, Kobayashi Y, Yoshimura T, Yoshiyama M, Takeuchi K, Yoshikawa J (2004) Impact of HMG-CoA reductase inhibitors for non-treated coronary segments. *Osaka City Med J* 50(2):61–68
 55. Tani S, Watanabe I, Anazawa T, Kawamata H, Tachibana E, Furukawa K, Sato Y, Nagao K, Kanmatsue K, Kushiro T (2005) Effect of pravastatin on malondialdehyde-modified low-density lipoprotein levels and coronary plaque regression as determined by three-dimensional intravascular ultrasound. *Am J Cardiol* 96(8):1089–1094
 56. Nissen SE, Nicholls SJ, Sipahi I, Libby P, Raichlen JS, Ballantyne CM, Davignon J, Erbel R, Fruchart JC, Tardif J-C, Schoenhagen P, Crowe T, Cain V, Wolski K, Gormastic M, Tuzcu EM (2006) For the ASTEROID Investigators. Effect of very high-intensity statin therapy on regression of coronary atherosclerosis: the ASTEROID trial. *JAMA* 295(13):1556–1565
 57. Takashima H, Ozaki Y, Yasukawa T, Waseda K, Asai K, Wakita Y, Kuroda Y, Kosaka T, Kuhara Y, Ito T (2007) Impact of lipid-lowering therapy with pitavastatin, a new HMG-CoA reductase inhibitor, on regression of coronary atherosclerotic plaque. *Circ J* 71(11):1678–1684
 58. Takayama T, Hiro T, Yamagishi M, Daida H, Hirayama A, Saito S, Yamaguchi T, Matsuzaki M (2009) Effect of rosuvastatin on coronary atheroma in stable coronary artery disease: multicenter coronary atherosclerosis study measuring effects of rosuvastatin using intravascular ultrasound in Japanese subjects (COSMOS). *Circ J* 73(11):2110–2117
 59. Hiro T, Kimura T, Morimoto T, Miyauchi K, Nakagawa Y, Yamagishi M, Ozaki Y, Kimura K, Saito S, Yamaguchi T, Daida H, Matsuzaki M (2009) Effect of intensive statin therapy on regression of coronary atherosclerosis in patients with acute coronary syndrome: a multicenter randomized trial evaluated by volumetric intravascular ultrasound using pitavastatin versus atorvastatin (JAPAN-ACS [Japan assessment of pitavastatin and atorvastatin in acute coronary syndrome] study). *J Am Coll Cardiol* 54(4):293–302
 60. Tardif JC, Gregoire J, L'Allier PL, Anderson TJ, Bertrand O, Reeves F, Title LM, Alfonso F, Schampaert E, Hassan A, McLain R, Pressler ML, Ibrahim R, Lesperance J, Blue J, Heinonen T, Rodes-Cabau J (2004) Effects of the acyl coenzyme A: cholesterol acyltransferase inhibitor avasimibe on human atherosclerotic lesions. *Circulation* 110(21):3372–3377
 61. Nissen SE, Tuzcu EM, Brewer HB, Sipahi I, Nicholls SJ, Ganz P, Schoenhagen P, Waters DD, Pepine CJ, Crowe TD, Davidson MH, Deanfield JE, Wisniewski LM, Hanyok JJ, Kassalow LM (2006) Effect of ACAT inhibition on the progression of coronary atherosclerosis. *N Engl J Med* 354(12):1253–1263
 62. Nissen SE, Tsunoda T, Tuzcu EM, Schoenhagen P, Cooper CJ, Yasin M, Eaton GM, Lauer MA, Sheldon WS, Grines CL, Halpern S, Crowe T, Blankenship JC, Kerensky R (2003) Effect of recombinant ApoA-I Milano on coronary atherosclerosis in patients with acute coronary syndromes: a randomized controlled trial. *JAMA* 290(17):2292–2300
 63. Tardif JC, Gregoire J, L'Allier PL, Ibrahim R, Lesperance J, Heinonen TM, Kouz S, Berry C, Basser R, Lavoie MA, Guertin MC, Rodes-Cabau J (2007) Effects of reconstituted high-density lipoprotein infusions on coronary atherosclerosis: a randomized controlled trial. *JAMA* 297(15):1675–1682
 64. Tardif JC, Gregoire J, L'Allier PL, Ibrahim R, Anderson TJ, Reeves F, Title LM, Schampaert E, LeMay M, Lesperance J, Scott R, Guertin MC, Brennan ML, Hazen SL, Bertrand OF (2008) Effects of the antioxidant succinobucol (AGI-1067) on human atherosclerosis in a randomized clinical trial. *Atherosclerosis* 197(1):480–486

65. Nissen SE, Tuzcu EM, Libby P, Thompson PD, Ghali M, Garza D, Berman L, Shi H, Buebendorf E, Topol EJ (2004) Effect of antihypertensive agents on cardiovascular events in patients with coronary disease and normal blood pressure: the CAMELOT study: a randomized controlled trial. *JAMA* 292(18):2217–2225
66. Nissen SE, Tardif JC, Nicholls SJ, Revkin JH, Shear CL, Duggan WT, Ruzyllo W, Bachinsky WB, Lasala GP, Tuzcu EM (2007) Effect of torcetrapib on the progression of coronary atherosclerosis. *N Engl J Med* 356(13):1304–1316
67. Rodriguez-Granillo GA, Vos J, Bruining N, Garcia-Garcia HM, de Winter S, Ligthart JM, Deckers JW, Bertrand M, Simoons ML, Ferrari R, Fox KM, Remme W, De Feyter PJ (2007) Long-term effect of perindopril on coronary atherosclerosis progression (from the perindopril's prospective effect on coronary atherosclerosis by angiography and intravascular ultrasound evaluation [PERSPECTIVE] study). *Am J Cardiol* 100(2):159–163
68. Nissen SE, Nicholls SJ, Wolski K, Nesto R, Kupfer S, Perez A, Jure H, De Larochehellere R, Staniloae CS, Mavromatis K, Saw J, Hu B, Lincoff AM, Tuzcu EM (2008) Comparison of pioglitazone vs glimepiride on progression of coronary atherosclerosis in patients with type 2 diabetes: the PERISCOPE randomized controlled trial. *JAMA* 299(13):1561–1573
69. Nissen SE, Nicholls SJ, Wolski K, Rodes-Cabau J, Cannon CP, Deanfield JE, Despres JP, Kastelein JJ, Steinhilb SR, Kapadia S, Yasin M, Ruzyllo W, Gaudin C, Job B, Hu B, Bhatt DL, Lincoff AM, Tuzcu EM (2008) Effect of rimonabant on progression of atherosclerosis in patients with abdominal obesity and coronary artery disease: the STRADIVARIUS randomized controlled trial. *JAMA* 299(13):1547–1560
70. Luscher TF, Pieper M, Tendera M, Vrolix M, Rutsch W, van den Branden F, Gil R, Bischoff KO, Haude M, Fischer D, Meinertz T, Munzel T (2009) A randomized placebo-controlled study on the effect of nifedipine on coronary endothelial function and plaque formation in patients with coronary artery disease: the ENCORE II study. *Eur Heart J* 30(13):1590–1597
71. Gerstein HC, Ratner RE, Cannon CP, Serruys PW, Garcia-Garcia HM, van Es GA, Kolatkar NS, Kravitz BG, Miller DM, Huang C, Fitzgerald PJ, Nesto RW. Effect of rosiglitazone on progression of coronary atherosclerosis in patients with type 2 diabetes mellitus and coronary artery disease. The assessment on the prevention of progression by rosiglitazone on atherosclerosis in diabetes patients with cardiovascular history trial. *Circulation*
72. Yokoyama M, Komiya N, Courtney BK, Nakayama T, Namikawa S, Kuriyama N, Koizumi T, Nameki M, Fitzgerald PJ, Komuro I (2005) Plasma low-density lipoprotein reduction and structural effects on coronary atherosclerotic plaques by atorvastatin as clinically assessed with intravascular ultrasound radio-frequency signal analysis: a randomized prospective study. *Am Heart J* 150(2):287
73. Kawasaki M, Sano K, Okubo M, Yokoyama H, Ito Y, Murata I, Tsuchiya K, Minatoguchi S, Zhou X, Fujita H, Fujiwara H (2005) Volumetric quantitative analysis of tissue characteristics of coronary plaques after statin therapy using three-dimensional integrated backscatter intravascular ultrasound. *J Am Coll Cardiol* 45(12):1946–1953
74. Serruys PW, Garcia-Garcia HM, Buszman P, Erne P, Verheye S, Aschermann M, Duckers H, Bleie O, Dudek D, Botker HE, von Birgelen C, D'Amico D, Hutchinson T, Zambanini A, Mastik F, van Es GA, van der Steen AF, Vince DG, Ganz P, Hamm CW, Wijns W, Zalewski A (2008) Effects of the direct lipoprotein-associated phospholipase A(2) inhibitor darapladib on human coronary atherosclerotic plaque. *Circulation* 118(11):1172–1182
75. Nasu K, Tsuchikane E, Katoh O, Tanaka N, Kimura M, Ehara M, Kinoshita Y, Matsubara T, Matsuo H, Asakura K, Asakura Y, Terashima M, Takayama T, Honye J, Hirayama A, Saito S, Suzuki T (2009) Effect of fluvastatin on progression of coronary atherosclerotic plaque evaluated by virtual histology intravascular ultrasound. *JACC Cardiovasc Interv* 2(7):689–696
76. Hong MK, Park DW, Lee CW, Kim YH, Kang DH, Song JK, Kim JJ, Park SW, Park SJ (2009) Effects of statin treatments on coronary plaques assessed by volumetric virtual histology intravascular ultrasound analysis. *JACC Cardiovasc Interv* 2(7):679–688
77. Toi T, Taguchi I, Yoneda S, Kageyama M, Kikuchi A, Tokura M, Kanaya T, Abe S, Matsuda R, Kaneko N (2009) Early effect of lipid-lowering therapy with pitavastatin on regression of coronary atherosclerotic plaque. Comparison with atorvastatin. *Circ J* 73(8):1466–1472
78. Miyagi M, Ishii H, Murakami R, Isobe S, Hayashi M, Amano T, Arai K, Ohashi T, Uetani T, Matsubara T, Murohara T (2009) Impact of long-term statin treatment on coronary plaque composition at angiographically severe lesions: a nonrandomized study of the history of long-term statin treatment before coronary angioplasty. *Clin Ther* 31(1):64–73

Chapter 6

IVUS-based Imaging Modalities for Tissue Characterization: Similarities and Differences.

Hector M. Garcia-Garcia, **Bill D. Gogas**, Patrick W. Serruys, Nico Bruining
International Journal of Cardiovascular Imaging. 2011. Feb; 27(2): 215-24 [IF: 2.54]

IVUS-based imaging modalities for tissue characterization: similarities and differences

Hector M. Garcia-Garcia · Bill D. Gogas ·
Patrick W. Serruys · Nico Bruining

Received: 8 December 2010 / Accepted: 30 December 2010 / Published online: 17 February 2011
© The Author(s) 2011. This article is published with open access at Springerlink.com

Abstract Gray-scale intravascular ultrasound (IVUS) is the modality that has been established as the golden standard for in vivo imaging of the vessel wall of the coronary arteries. The use of IVUS in clinical practice is an important diagnostic tool used for quantitative assessment of coronary artery disease. This has made IVUS the de-facto invasive imaging method to evaluate new interventional therapies such as new stent designs and for atherosclerosis progression-regression studies. However, the gray-scale representation of the coronary vessel wall and plaque morphology in combination with the limited resolution of the current IVUS catheters makes it difficult, if not impossible, to identify qualitatively (e.g. visually) the plaque morphology similar as that of histopathology, the golden standard to characterize and quantify coronary plaque tissue components. Meanwhile, this limitation has been partially overcome by new innovative IVUS-based post-processing methods such as: virtual histology IVUS (VH-IVUS, Volcano Therapeutics, Rancho Cordova, CA, USA), iMAP-IVUS (Bostoc Scientific, Santa Clara, CA, USA), Integrated Backscatter IVUS

(IB-IVUS) and Automated Differential Echogenicity (ADE).

Keywords Intravascular ultrasound · Radiofrequency data analysis · Atherosclerosis · Tissue characterization

Introduction

Atherogenesis is the leading cause of cardiovascular mortality and morbidity in the developed world. The imaging of coronary atherosclerosis and more in particular the high risk atheromatous plaque has made an explosive progress the last decade with the advent of innovative techniques that focus on the high-resolution visualization of the coronary vascular wall. Gray-scale intravascular ultrasound (IVUS) is the modality that has been established as the golden standard for in vivo imaging of the vessel wall of the coronary arteries [1, 2]. The use of IVUS is an important diagnostic tool used for quantitative assessment of coronary artery disease. This has made IVUS the de-facto invasive imaging method of choice to evaluate new interventional therapies such as new stent designs [3–5] and for atherosclerosis progression-regression studies [6–14]. However, the gray-scale representation of the coronary vessel wall and plaque morphology in combination with the limited

H. M. Garcia-Garcia · B. D. Gogas ·
P. W. Serruys · N. Bruining (✉)
Department of Interventional Cardiology, Thoraxcenter,
Erasmus University Medical Center, Room BA-571, Dr.
Molewaterplein 40, 3015, GD, Rotterdam, The
Netherlands
e-mail: n.bruining@erasmusmc.nl

resolution of the current IVUS catheters makes it difficult, if not impossible, to identify qualitatively (e.g. visually) the plaque morphology similar as that of histopathology, the golden standard to characterize and quantify coronary plaque tissue components. Meanwhile, this limitation has been partially overcome by new innovative IVUS-based post-processing methods such as: virtual histology IVUS [15, 16] (VH-IVUS, Volcano Therapeutics, Rancho Cordova, CA, USA), iMAP-IVUS [17] (Boston Scientific, Santa Clara, CA, USA), Integrated Backscatter IVUS [18] (IB-IVUS) and Automated Differential Echogenicity [19] (ADE).

Intravascular ultrasound (IVUS) principles

The size of current IVUS catheters are ranging from 2.6 to 3.5 French (0.87–1.17 mm) and are inserted into the coronary arteries through 6-French guiding catheters. The principle of IVUS imaging is based on the oscillatory movement (expansion and contraction) of a piezoelectric transducer (crystal) in order to produce sound waves when electrically excited. There are two major different transducer designs [2]: (1) the mechanical single element rotating device and (2) the electronic phased array. The mechanical rotating element device uses a single piezoelectric transducer that rotates with 1,800 rotations per minute, while the electronic phased array device uses multiple stationary placed piezoelectric transducers which are sequentially activated. The generated sound waves by the transducers propagates through the different tissues and is reflected according to the acoustic properties of the tissue it travels through [20].

Gray-scale IVUS based atheromatous plaque classification is limited due to its low spatial resolution and for the usual IVUS transducers (20 and 40 MHz) for which the axial resolution is 200 μm and the lateral 200–250 μm . Based on their visual appearance, not necessarily histological composition, atheromas have been classified in four categories by gray-scale IVUS: (1) soft plaque (lesion echogenicity less than the surrounding adventitia), (2) fibrous plaque (intermediate echogenicity between soft (echolucent) atheromas and highly echogenic calcified plaques), (3) calcified plaque (echogenicity higher than the adventitia with acoustic shadowing),

and (4) mixed plaques (no single acoustical subtype represents >80% of the plaques) [2].

IVUS based imaging modalities for tissue characterization

To overcome the limitations of qualitative visual interpretation of the IVUS images and to describe the coronary plaque morphology, several post-processing methods for computer-assisted quantification have been developed during the recent years. There are two basic different approaches: (1) Signal-based analysis (the so called raw radiofrequency analysis or RF-analysis) and (2) Image-based analysis. The different methods will be described below:

Tissue characterization using virtual histology IVUS (VH-IVUS)

The first commercial available RF-signal based tissue composition analysis tool was the so-called virtual histology (VH-IVUS, Volcano Therapeutics) software. It uses in-depth analysis of the backscattered RF-signal in order to provide a more detailed description of the atheromatous plaque composition and is performed with either a 20 MHz, 2.9F phased-array transducer catheter (Eagle EyeTM Gold, Volcano Therapeutics) or 45 MHz 3.2F rotational catheter (Revolution[®], Volcano Therapeutics) that acquires IVUS data electrocardiogram gated [21]. The main principle of this technique is that it uses not only the envelope amplitude of the reflected RF-signals (as gray-scale IVUS does), but uses also the underlying frequency content to analyze the tissue components present in coronary plaques. This combined information is processed using autoregressive models and thereafter in a classification tree that determines four basic plaque tissue components [15]: (1) Fibrous tissue (dark green), (2) Fibrofatty tissue (light green), (3) Necrotic core (red) and (4) dense calcium (white). The current software version assumes the presence of a media layer, which is artificially added, positioned just at the inside of the outer vessel contour. This technique has been compared in several studies against histology in humans and other species, see Table 1 for further details.

Table 1 Validation studies of IVUS and IVUS based imaging modalities

Author	Study settings	Year	Primary objective	Results
<i>Greyscale IVUS</i>				
Palmer [24]	In vitro	1999	IVUS for coronary atheromatous lesions compared to histology. Atheromatous plaque was classified as echodense, echolucent, heterogeneous or calcified by each observer and by one observer on separate occasions	Overall inter- and intra-observer reproducibility for plaque-type (Kappa 0.87[0.80–0.94] and 0.89[0.85–0.93 respectively]) and focal calcification (0.78[0.74–0.82] and 0.88[0.84–0.92]) was high Agreement for overall plaque type between intravascular ultrasound and histology occurred in 89% of sites (Kappa 0.73[0.69–0.77]). Specificity $\geq 90\%$ Lipid pools were observed by histology in 30 sections (25%). IVUS revealed the presence of lipid pools in 19 of these sections (16%; sensitivity 65%). Specificity $\geq 95\%$
Prati [25]	In vitro	2001	IVUS, high frequency transducer(40 MHz) for plaque composition compared to histomorphology Lipid/necrotic areas were defined by IVUS as large echolucent intraplaque areas surrounded by tissue with higher echodensity	
<i>VH IVUS</i>				
Nair [15]	Ex vivo	2002	Coronary plaque classification with intravascular ultrasound radiofrequency data analysis	Autoregressive classification schemes performed better than those from classic Fourier spectra with accuracies of 90.4% for fibrous, 92.8% for fibrolipidic, 90.9% for calcified, and 89.5% for calcified-necrotic regions in the training data set and 79.7, 81.2, 92.8, and 85.5% in the test data, respectively Predictive accuracy from all patients data: 87.1% for fibrous, 87.1% for fibro-fatty, 88.3% for necrotic core, and 96.5% for dense calcium regions, respectively Sensitivities: NC:67.3%, FT:86%, FF:79.3%, DC:50%. Specificities: NC:92.9%, FT:90.5%,FF:100%, DC:99%
Nasu [26]	In vivo	2006	Accuracy of in vivo coronary plaque morphology assessment: a validation study of in vivo virtual histology compared with in vitro histopathology	The overall predictive accuracies were 93.5% for FT, 94.1% for FF, 95.8% for NC, and 96.7% for DC Sensitivities: NC:91.7%, FT:95.7%, FF:72.3%, DC:86.5%. Specificities: NC:96.6%, FT:90.9%, FF:97.9%, DC:98.9%
Nair [16]	Ex vivo	2007	Automated coronary plaque characterisation with intravascular ultrasound backscatter: ex vivo validation	

Table 1 continued

Author	Study settings	Year	Primary objective	Results
Granada [27]	Ex vivo	2007	In vivo plaque characterization using intravascular ultrasound-virtual histology in a porcine model of complex coronary lesions	Compared with histology, IVUS-VH correctly identified the presence of fibrous, fibro-fatty, and necrotic tissue in 58.33, 38.33, and 38.33% of lesions, respectively Sensitivities: fibrous 76.1%, fibro-fatty 46%, and necrotic core 41.1%
Van Herk [28]	Ex vivo	2009	Validation of in vivo plaque characterisation by virtual histology in a rabbit model of atherosclerosis	VH-IVUS had a high sensitivity, specificity and positive predictive value for the detection of non-calcified thin cap fibroatheroma (88, 96, 87%, respectively) and calcified thin cap fibroatheroma (95, 99, 93%, respectively). These values were respectively 82, 94, 85% for non-calcified fibroatheroma and 78, 98, 84% for calcified fibroatheroma. The lowest values were obtained for pathological intimal thickening (74, 92, 70%, respectively). For all plaque types, VH-IVUS had a kappa-value of 0.79
Thim [29]	Ex vivo	2010	Unreliable assessment of necrotic core by VHTM IVUS in porcine coronary artery disease	No correlations were found between the size of the necrotic core determined by VH IVUS and histology. VH IVUS displayed necrotic cores in lesions lacking cores by histology
<i>IB IVUS</i> Kawasaki [22]	In vivo	2002	In vivo quantitative tissue characterization of human coronary arterial plaques by use of integrated backscatter intravascular ultrasound and comparison with angiographic findings	r:0.954 for each category, DC, FF, FT, NC
Kawasaki [23]	In vivo	2006	Diagnostic accuracy of optical coherence tomography and integrated backscatter intravascular ultrasound images for tissue characterization of human coronary plaques	Sensitivities: DC:100% FT:94% Lipid pool:84% Specificities: DC:99% FT:84% Lipid pool:97%
Okubo [18]	Ex vivo	2008	Development of integrated backscatter intravascular ultrasound for tissue characterization of coronary plaques	IB classified fibrous, lipid-rich and fibrocalcific plaque components with a high accuracy of 93, 90 and 96%, respectively
<i>iMAP</i> Sathyanarayana [17]	In vivo	2009	Characterisation of atherosclerotic plaque by spectral similarity of radiofrequency intravascular ultrasound signals	Ex vivo validation demonstrated accuracies at the highest level of confidence as: 97, 98, 95, and 98% for necrotic, lipidic, fibrotic and calcified regions respectively

Table 1 continued

Author	Study settings	Year	Primary objective	Results
<i>Echogenicity</i> Bruining [19]	Ex vivo	2007	Three-dimensional and quantitative analysis of atherosclerotic plaque composition by automated differential echogenicity	Areas of hypoechoogenicity correlated with the presence of smooth muscle cells. Areas of hyperchoogenicity correlated with presence of collagen, and areas of hyperchoogenicity with acoustic shadowing correlated with calcium

Tissue characterization using i-MAP-IVUS

Recently, another RF-based processing method has become commercially available for coronary plaque tissue characterization which is called iMAP-IVUS (Boston Scientific) [17]. In principle this software is comparable, from methodological point of view, in brief IVUS-RF parameters are processed using autoregressive models and matched to a database of known RF-signal profiles containing the characteristics of four tissue types. The colour-coded images contain the different colors overlaying the gray-scale IVUS images. However, there are differences, to start with the applied colour scheme: (1) Fibrous tissue (light green), (2) Lipid tissue (yellow), (3) Necrotic core (pink) and (4) Calcium (blue) [17]. Furthermore, the applied IVUS catheter is a 40 MHz rotating single element catheter. Ex vivo validation demonstrated accuracies at the highest level of confidence as: 97%, 98%, 95%, and 98% for necrotic, lipidic, fibrotic and calcified regions respectively (Table 2) [17].

Tissue characterization by integrated backscatter IVUS analysis (IB-IVUS)

IB-IVUS analysis is an alternative approach, as compared to the 2 previous ones, using the RF-signals of the IVUS catheters to characterize coronary plaque tissue components. IB-IVUS analyses the RF-signals generated by the 40 MHz mechanically rotating IVUS catheters by applying a fast Fourier transformation of the frequency components of the backscattered signals calculating the intensity of the signal measured in decibels (dB). Different tissue components reflect the RF-signals at different power levels, which, according to the developers, could be used to differentiate various tissue components. Analogue to the other methods it also applies a colour coded overlay onto the gray-scale IVUS images. It comprises the following different tissue components: (1) Calcification, (2) Fibrous tissue, and (3) Lipidic [18, 22, 23].

Tissue characterization using, automated differential echogenicity (ADE)

Automated differential echogenicity is a post-processing imaging analysis method that uses IVUS

Table 2 Similarities and differences of IVUS and IVUS-based imaging modalities

	Gray-scale IVUS	VH	i-MAP	Integrated backscatter	Echogenicity
Type of device	Mecanical and electrical	Mechanical and electrical	Mechanical	Mechanical	As IVUS
Transducer frequency	20–40 MHz	20–45 MHz	40 MHz	40 MHz	As IVUS
Colour code	Gray-scale	Fibrous: green Necrotic core: red Callcium: white Fibrofatty: light green	Fibrous: light green Necrotic core: pink Calcium: blue Fibrofatty: yellow	Fibrous: green Necrotic core: blue Calcium: red Fibrofatty: yellow	Gray-scale
Backscatter radiofrequency signal analysis	Amplitude (dB)	Autoregressive model	Fast Fourier transformation	Fast Fourier transformation	Computer analysis

images to characterize atheromatous coronary plaque components [19]. At variance with the previous described RF-signal analysis methods, it makes use of the differences in gray-value intensities within the gray-scale IVUS images which are caused by the different acoustic properties (e.g. echogenicity) of the different tissue components. It is known that adventitia tissue contains mostly fibrotic tissue components. Using the relative gray-value of the adventitia layer surrounding the external elastic membrane (EEM), which within quantitative IVUS analysis is detected and defined as the outer vessel wall, tissue components can be differentiated as hypo- (lower gray-values than the adventitia) or hyperechogenic (higher gray-values than the adventitia). Bright structures (very high gray-levels) combined with acoustic shadowing can be identified as calcium. The method classifies structures within these acoustic shadowed areas as unknown as the ultrasound signal is mostly completely reflected by thick layers of calcium and is not able to penetrate it (Figs. 1 and 2). The method has not been developed, such as the other methods, to generate colour-coded IVUS images that try to mimic as close as possible images as generated by histopathology, but to quantify differences over time to evaluate possible changes of the plaque components induced by new therapeutic treatments. It is of outmost importance, in order to better define the images, to follow a certain algorithm that includes: (1) accurate plaque identification (e.g. quantitative IVUS), (2) tunica adventitia definition and grey-level intensity determination (3) normal distribution of the gray-level intensity histogram of the adventitia tissue (image quality control), (4)

acoustic shadowing and calcification identification [19]. The advantages of this method are that it can be performed retrospectively on already acquired IVUS data and it is independent of the applied IVUS systems and/or catheters. However, it is recommended to apply within a longitudinal study the same console type and catheter during baseline and follow-up examinations not only within this method but also with respect to the other methods.

Discussion

As above described, IVUS has become over the past 20 years an important clinical intracoronary imaging tool. It not only facilitates clinical practice but it is also a reference method of which its quantitative parameters are often used as endpoints in first-in-man studies and larger clinical trials. However, the limited resolution, as compared to histology, and gray-scale (256 shades of gray are used when the image is optimal) representation, for which we humans have only limited capabilities with our eyes to make a distinction between them (on average we can only discriminate 8–12 different gray-levels) combined with the large amount of images acquired during a pullback examination (in an IVUS study of 4 cm there are 2,400 individual cross-sections acquired), requires another representation of the information we are looking for. Of course quantification is mandatory for research purposes and thus automated or semi-automated computer-assisted methods are necessary. In addition, humans can interpret colour-information much better than gray-scale information alone and

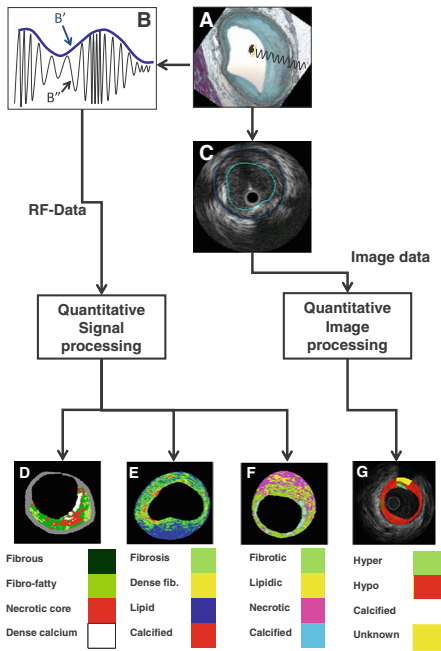


Fig. 1 A shows how an intravascular ultrasound signal is obtained from the vessel wall within a histology image. The *greyscale* IVUS image, as can be appreciated in C, is formed by the envelope (amplitude) (B') of the radiofrequency signal, which is illustrated in B. By *greyscale* atherosclerotic plaque can be classified into 3 categories: hypoechoogenic, hyperechoogenic and calcified. A 4th category is defined as unknown, which is tissue that is acoustically showed (G). C shows a cross-sectional view of a grayscale image. The *blue lines* limit the actual atheroma. The frequency and power of the signal commonly differ between tissues, regardless of similarities in the amplitude. From the backscatter radiofrequency data (identified by B'' in B) different types of tissue information can be retrieved: virtual histology (D), integrated backscattered (IB) IVUS (E) and iMAP (F). Virtual histology is able to detect four tissue types: necrotic core, fibrous, fibro-fatty and dense calcium. The tissues characterized by integrated backscattered (IB) IVUS are lipidic, fibrous and calcified; and iMAP detects fibrotic, lipidic, necrotic and calcified

therefore the plaque compositional tools as described in this overview are valuable additions to the use of standard IVUS gray-scale imaging alone. Until recently, there was only one tool (e.g. VH IVUS)

commercially and thus widely available. This has changed, now more methods are available which could potentially lead to different outcomes as they are using different mathematical methods and software algorithms. Certainly, in the near future the different methods will possibly be applied side-by-side in multi-center studies and it is yet unknown if this could result in possible different study outcomes, this needs to be explored in future research.

The name giving of virtual histology IVUS (VH-IVUS) could possibly lead to expectations that the results derived by this method are one-to-one comparable to histology, which is unfortunately not the case. The development of the RF-signal based methods have been performed empirically, in brief: explanted vessels are imaged by IVUS, the pathologist performs histology and the histology results are cross-correlated to the IVUS images. The derived and correlated RF-signal patterns have been used to build the signal pattern databases which are later used to identify the plaque tissue components *in vivo*. The crux in this development process is the cross-correlation between histology and IVUS, which due to the large differences in image resolution is difficult (by example the lateral resolution of IVUS is 200–250 μm while that for histology is 5 μm). Although histology is considered the golden standard it is also not free from possible artifacts, by example during the fixation and staining process. Interpretation of the images by different pathologists could also result in interobserver related-biases. It is therefore not realistic to expect similar results from the IVUS derived tissue compositional tools as from quantitative histology. However, if appropriately used, and with justified expectations, these quantitative plaque tissue compositional tools, with all of their limitations, can be of great additional value to investigate plaque compositional changes which cannot be performed with any other imaging method. Great care must thus be taken when trying to prove a hypothesis using these methods which could be out of range of the capabilities of the methods and the basic method, e.g. IVUS itself. An example of expectations which could lead to disappointing results when the RF-based methods are applied is within metallic stented segments. The RF-based methods do not have the signal profile of metallic stent struts in their tissue signal profile databases and this will thus result in an

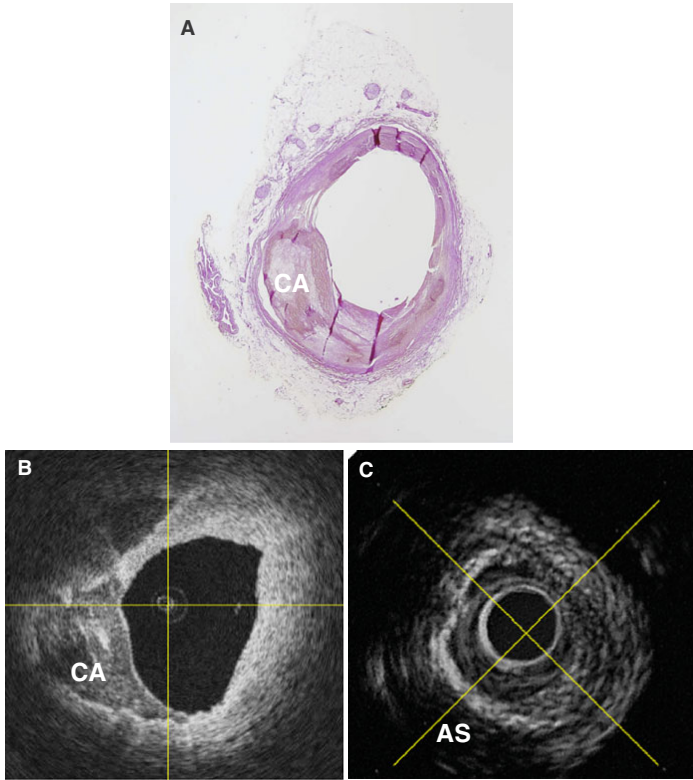


Fig. 2 One of the main limitations of processing the RAW radiofrequency data only, not taking into account other information available, such as visible acoustic shadowing, is that these signal processing methods identify tissue components in these acoustic *shadowed* regions while IVUS does not return any information about it. The ultrasound waves are reflected at the calcium interface as can be appreciated in this figure. **A** presents a histology sample of an explanted human coronary artery of which in **B** the OCT image is presented and in **C** the IVUS equivalent. It can be appreciated that OCT

presents the calcium very well between 6 and almost 12 o'clock. Also within the IVUS image it can be appreciated that between 6 and 12 o'clock there is a calcium layer present due to the *white* and bright interface but everything behind it is *shadowed* and thus IVUS does not contain any information deeper than this interface. When using IVUS as the only source to estimate the plaque composition tissue within these *shadowed* areas should therefore be classified as unknown tissue

artificial identification (in some research papers this is identified as misuse). This could later lead to unpredictable results and thus care must be taken applying these methods for research for which they are not designed.

However, encouraging results have been achieved applying the tissue composition methods to detect and to quantify as a surrogate the absorption of the

recently introduced bioabsorbable BVS stent (BVS, Abbott Vascular, Santa Clara, CA, USA). This information could help to explore into more detail the overall performance of this new stent platform.

A major limitation of the RF-based methods, as compared to the image-based echogenicity method, is that they do not take into account acoustic shadowed areas. They divide every individual RF-beam into

small regions of interest and compare the found signal profiles to their databases of known tissue profiles without taking into account what signal is found in front or behind that window (e.g. the larger picture is missing). This results in detection of tissue behind calcified areas, even if on the gray-scale IVUS image there is only shadow visible, thus the RF-signal will most likely contain noise (thick layers of calcium will reflect all acoustic energy back to the transducer causing the typical bright white appearance on gray-scale IVUS images) (Fig. 2). This could lead to two potential biases: (1) an observer related bias as the outer vessel boundaries are shadowed and thus the outer vessel contour must be interpolated by the observer and (2) a software related bias as the signal processing tools are not taking into account these shadowed areas and will assign the pixels in these regions to any of the tissue components within their database based on the “noise” of the ultrasound waves related to that area. In contrast, the image-based method of echogenicity at first examines every cross-sectional IVUS image if it contains acoustic shadowed areas and classifies tissue within these areas as unknown preventing possible software related deviations.

Although IVUS is proven to be safe and is a well-established method widely available, there are other promising imaging methods, such as optical coherence tomography, but for the time being they are not capable identifying quantitatively tissue components comparable to the described methods in this paper.

In-depth post-hoc analysis of IVUS data can be applied to quantify coronary plaque composition and possible changes of this composition over time which can be applied to evaluate new therapeutic treatment methods. However, there is still a large scientific debate how these different analysis methods exactly relate to each other and to that of the golden standard of histopathology. If these methods are also capable of identifying possible vulnerable segments is still under investigation.

Open Access This article is distributed under the terms of the Creative Commons Attribution Noncommercial License which permits any noncommercial use, distribution, and reproduction in any medium, provided the original author(s) and source are credited.

Conflict of interest None.

References

1. Roelandt JR, Serruys PW, Bom N, Gussenhoven WG, Lancee CT, ten Hoff H (1989) Intravascular real-time, two-dimensional echocardiography. *Int J Card Imaging* 4: 63–67
2. Mintz GS, Nissen, SE, Anderson, WD, Bailey, SR, Erbel R, Fitzgerald PJ, Pinto FJ, Rosenfield K, Siegel RJ, Tuzcu EM, Yock PG (2001) American College of Cardiology Clinical Expert Consensus Document on Standards for Acquisition, Measurement and Reporting of Intravascular Ultrasound Studies (IVUS). A report of the American College of Cardiology Task Force on Clinical Expert Consensus Documents. *J Am Coll Cardiol* 37:1478–1492
3. Nissen SE, Yock P (2001) Intravascular ultrasound: novel pathophysiological insights and current clinical applications. *Circulation* 103:604–616
4. Serruys PW, Ormiston JA, Onuma Y et al (2009) A bio-absorbable everolimus-eluting coronary stent system (ABSORB): 2-year outcomes and results from multiple imaging methods. *Lancet* 373:897–910
5. Serruys PW, Garcia-Garcia HM, Buszman P et al (2008) Effects of the direct lipoprotein-associated phospholipase A(2) inhibitor darapladib on human coronary atherosclerotic plaque. *Circulation* 118:1172–1182
6. Nissen SE, Nicholls SJ, Sipahi I et al (2006) Effect of very high-intensity statin therapy on regression of coronary atherosclerosis: the ASTEROID trial. *JAMA* 295: 1556–1565
7. Nissen SE, Nicholls SJ, Sipahi I et al (2006) Effect of very high-intensity statin therapy on regression of coronary atherosclerosis: the ASTEROID trial. *JAMA* 295: 1556–1565
8. Nissen SE, Nicholls SJ, Wolski K et al (2008) Comparison of pioglitazone vs glimepiride on progression of coronary atherosclerosis in patients with type 2 diabetes: the PERISCOPE randomized controlled trial. *JAMA* 299: 1561–1573
9. Nissen SE, Nicholls SJ, Wolski K et al (2008) Effect of rimonabant on progression of atherosclerosis in patients with abdominal obesity and coronary artery disease: the STRADIVARIUS randomized controlled trial. *JAMA* 299:1547–1560
10. Nissen SE, Tardif JC, Nicholls SJ et al (2007) Effect of torcetrapib on the progression of coronary atherosclerosis. *N Engl J Med* 356:1304–1316
11. Nissen SE, Tsunoda T, Tuzcu EM et al (2003) Effect of recombinant ApoA-I Milano on coronary atherosclerosis in patients with acute coronary syndromes: a randomized controlled trial. *JAMA* 290:2292–2300
12. Nissen SE, Tuzcu EM, Brewer HB et al (2006) Effect of ACAT inhibition on the progression of coronary atherosclerosis. *N Engl J Med* 354:1253–1263
13. Nissen SE, Tuzcu EM, Libby P et al (2004) Effect of antihypertensive agents on cardiovascular events in patients with coronary disease and normal blood pressure: the CAMELOT study: a randomized controlled trial. *JAMA* 292:2217–2225

14. Nissen SE, Tuzcu EM, Schoenhagen P et al (2004) Effect of intensive compared with moderate lipid-lowering therapy on progression of coronary atherosclerosis: a randomized controlled trial. *JAMA* 291:1071–1080
15. Nair A, Kuban BD, Tuzcu EM, Schoenhagen P, Nissen SE, Vince DG (2002) Coronary plaque classification with intravascular ultrasound radiofrequency data analysis. *Circulation* 106:2200–2206
16. Nair A, Margolis MP, Kuban BD, Vince DG (2007) Automated coronary plaque characterisation with intravascular ultrasound backscatter: ex vivo validation. *EuroIntervention* 3:113–120
17. Sathyanarayana S, Carlier S, Li W, Thomas L (2009) Characterisation of atherosclerotic plaque by spectral similarity of radiofrequency intravascular ultrasound signals. *EuroIntervention* 5:133–139
18. Okubo M, Kawasaki M, Ishihara Y et al (2008) Development of integrated backscatter intravascular ultrasound for tissue characterization of coronary plaques. *Ultrasound Med Biol* 34:655–663
19. Bruining N, Verheye S, Knaapen M et al (2007) Three-dimensional and quantitative analysis of atherosclerotic plaque composition by automated differential echogenicity. *Catheter Cardiovasc Interv* 70:968–978
20. Bartorelli AL, Potkin BN, Almagor Y, Keren G, Roberts WC, Leon MB (1990) Plaque characterization of atherosclerotic coronary arteries by intravascular ultrasound. *Echocardiography* 7:389–395
21. Garcia-Garcia HM, Mintz GS, Lerman A et al (2009) Tissue characterisation using intravascular radiofrequency data analysis: recommendations for acquisition, analysis, interpretation and reporting. *EuroIntervention* 5:177–189
22. Kawasaki M, Takatsu H, Noda T et al (2002) In vivo quantitative tissue characterization of human coronary arterial plaques by use of integrated backscatter intravascular ultrasound and comparison with angioscopic findings. *Circulation* 105:2487–2492
23. Kawasaki M, Bouma BE, Bressner J et al (2006) Diagnostic accuracy of optical coherence tomography and integrated backscatter intravascular ultrasound images for tissue characterization of human coronary plaques. *J Am Coll Cardiol* 48:81–88
24. Palmer ND, Northridge D, Lessells A, McDicken WN, Fox KA (1999) In vitro analysis of coronary atheromatous lesions by intravascular ultrasound; reproducibility and histological correlation of lesion morphology. *Eur Heart J* 20:1701–1706
25. Prati F, Arbustini E, Labellarte A et al (2001) Correlation between high frequency intravascular ultrasound and histomorphology in human coronary arteries. *Heart* 85:567–570
26. Nasu K, Tsuchikane E, Katoh O et al (2006) Accuracy of in vivo coronary plaque morphology assessment: a validation study of in vivo virtual histology compared with in vitro histopathology. *J Am Coll Cardiol* 47:2405–2412
27. Granada JF, Wallace-Bradley D, Win HK et al (2007) In vivo plaque characterization using intravascular ultrasound-virtual histology in a porcine model of complex coronary lesions. *Arterioscler Thromb Vasc Biol* 27:387–393
28. Van Herck J, De Meyer G, Ennekens G, Van Herck P, Herman A, Vrints C (2009) Validation of in vivo plaque characterisation by virtual histology in a rabbit model of atherosclerosis. *EuroIntervention* 5:149–156
29. Thim T, Hagensen MK, Wallace-Bradley D, Granada JF, Kaluza GL, Drouet L, Paaske WP, Bøtker HE, Falk E (2010) Unreliable assessment of necrotic core by VHTM IVUS in porcine coronary artery disease. *Circ Cardiovasc Imaging* 3(4):384–391

Chapter 7

Vascular Response of the Segments Adjacent to the Proximal and Distal Edges of the ABSORB Everolimus-Eluting Bioresorbable Vascular Scaffold: 6-month and 1-year Follow-up Assessment: A Virtual Histology Intravascular Ultrasound study from the First-In-Man ABSORB cohort B trial.

Bill D. Gogas, Patrick W. Serruys, Roberto Diletti, Vasim Farooq, Salvatore Brugaletta, Maria D. Radu, Jung Ho Heo, Yoshinobu Onuma, Robert-Jan M. van Geuns, Evelyn Regar, Bernard De Bruyne, Bernard Chevalier, Leif Thuesen, Pieter C. Smits, Dariusz Dudek, Jacques Koolen, Stefan Windecker, Robert Whitbourn, Karine Miquel-Hebert, Cecile Dorange, Richard Rapoza, Hector M. Garcia-Garcia, Dougal McClean, John A. Ormiston

JACC Cardiovascular Interventions. 2012. Jun; 5(6): 656-65 [IF: 6.83]

Vascular Response of the Segments Adjacent to the Proximal and Distal Edges of the ABSORB Everolimus-Eluting Bioresorbable Vascular Scaffold: 6-Month and 1-Year Follow-Up Assessment

A Virtual Histology Intravascular Ultrasound Study From the First-in-Man ABSORB Cohort B Trial

Bill D. Gogas, MD,* Patrick W. Serruys, MD, PhD,* Roberto Diletti, MD,* Vasim Farooq, MChB,* Salvatore Brugaletta, MD,* Maria D. Radu, MD,* Jung Ho Heo, MD,* Yoshinobu Onuma, MD,* Robert-Jan M. van Geuns, MD, PhD,* Evelyn Regar, MD, PhD,* Bernard De Bruyne, MD, PhD,† Bernard Chevalier, MD,‡ Leif Thuesen, MD,§ Pieter C. Smits, MD, PhD,|| Dariusz Dudek, MD,¶ Jacques Koolen, MD, PhD,# Stefan Windecker, MD,** Robert Whitbourn, MD,†† Karine Miquel-Hebert, PhD,‡‡ Cecile Dorange, MSc,‡‡ Richard Rapoza, PhD,§§ Hector M. Garcia-Garcia, MD, MSc, PhD,||| Dougal McClean, MD,¶¶ John A. Ormiston, MChB, PhD##

Rotterdam and Eindhoven, the Netherlands; Aalst and Diegem, Belgium; Massy, France; Aarhus, Denmark; Krakow, Poland; Bern, Switzerland; Fitzroy, Australia; Santa Clara, California; and Christchurch and Auckland, New Zealand

Objectives This study sought to investigate in vivo the vascular response at the proximal and distal edges of the second-generation ABSORB everolimus-eluting bioresorbable vascular scaffold (BVS).

Background The edge vascular response after implantation of the BVS has not been previously investigated.

Methods The ABSORB Cohort B trial enrolled 101 patients and was divided into B₁ (n = 45) and B₂ (n = 56) subgroups. The adjacent (5-mm) proximal and distal vessel segments to the implanted ABSORB BVS were investigated at either 6 months (B₁) or 1 year (B₂) with virtual histology intravascular ultrasound (VH-IVUS) imaging.

Results At the 5-mm proximal edge, the only significant change was modest constrictive remodeling at 6 months (Δ vessel cross-sectional area: -1.80% [$-3.18; 1.30$], $p < 0.05$), with a tendency to regress at 1 year (Δ vessel cross-sectional area: -1.53% [$-7.74; 2.48$], $p = 0.06$). The relative change of the fibrotic and fibrofatty (FF) tissue areas at this segment were not statistically significant at either time point. At the 5-mm distal edge, a significant increase in the FF tissue of 43.32% [$-19.90; 244.28$], ($p < 0.05$) 1-year post-implantation was evident. The changes in dense calcium need to be interpreted with caution since the polymeric struts are detected as “pseudo” dense calcium structures with the VH-IVUS imaging modality.

Conclusions The vascular response up to 1 year after implantation of the ABSORB BVS demonstrated some degree of proximal edge constrictive remodeling and distal edge increase in FF tissue resulting in nonsignificant plaque progression with adaptive expansive remodeling. This morphological and tissue composition behavior appears to not significantly differ from the behavior of metallic drug-eluting stents at the same observational time points. (J Am Coll Cardiol Intv 2012;5:656–65) © 2012 by the American College of Cardiology Foundation

The vascular response at the stent edges has been evaluated with first-generation drug-eluting stents and appears to be dependent on the implanted device and the periprocedural induced vascular trauma because of the geographic miss (GM) phenomenon (1). The initial trial with the sirolimus-eluting stent—RAVEL (RANdomized study with the sirolimus-eluting VELOCITY balloon-expandable stent in the treatment of patients with de novo native coronary artery Lesions)—demonstrated no significant edge effect, presumably due to the exceptional stent/lesion ratio of 2:1, due to the sole availability of stent length (18 mm). A significant proximal edge lumen loss was, however, observed in the SIRIUS (Sirolimus-Coated Bx VELOCITY Balloon-Expandable Stent in the Treatment of De Novo Native Coronary Artery Lesions) trial, which evaluated the same stent platform as in RAVEL, but with several stent lengths and diameters of the device in a more complex population. In the first-in-man TAXUS I trial, no edge effect was demonstrated with the use of the slow-release polymer formulation of the paclitaxel-eluting stent; conversely, in the TAXUS II trial, the slow-release and moderate-release polymer formulations of the paclitaxel-eluting stent resulted in an edge lumen area loss ($-0.54 \pm 2.1 \text{ mm}^2$ and $-0.88 \pm 1.9 \text{ mm}^2$, respectively) at both the proximal and distal stent edges (2,3). In the BETAX (BEside TAXus) trial, using the Taxus Express drug-eluting stent, significant tissue compositional changes were observed, mainly due to an increase in the fibrofatty (FF) tissue component causing expansive remodeling at both stent edges (4).

Pre-clinical research has demonstrated that the tissue response after stent implantation is exclusively composed of

proteoglycan-rich smooth muscle cells and fibrolipidic areas rich in collagen and reticular fibers (5). This iatrogenic entity of neointimal hyperplasia has been demonstrated to be usually focal and most commonly located at the proximal stent edge (6). The advent of scaffolds with bioresorbable properties and differing biological behavior compared with the currently used metallic devices, has prompted the re-evaluation of the edge vascular response using sound-based imaging modalities with tissue characterization properties. Such a modality is the virtual histology intravascular ultrasound (VH-IVUS), which allows for the evaluation of the vascular geometric changes and assessment of the atheromatous plaque progression/regression.

The purpose of this study is to investigate the edge effect after the implantation of the ABSORB bioresorbable vascular scaffold (BVS) in the assessment of the geometric and compositional changes of the segments adjacent to the 5-mm proximal and distal edges of the scaffolded vessel, in a population investigated at either 6 months or 1 year post scaffold implantation.

Methods

Study design and population.

The ABSORB Cohort B trial is a multicenter, ongoing, single-arm prospective, open-label trial assessing the safety and performance of the second-generation ABSORB BVS in the treatment of patients with a maximum of 2 de novo native coronary artery lesions. In total, 101 patients were enrolled and subdivided into 2 subgroups—Cohort B₁ (n = 45) and Cohort B₂ (n = 56)—according to the predefined study design. Both groups underwent invasive follow-up, Cohort B₁ at 6 months and Cohort B₂ at 1 year. Cohort B₁ is currently undergoing a second VH-IVUS imaging of the scaffold edges at 2-years and Cohort B₂ will undergo the final VH-IVUS imaging evaluation at 3 years (Fig. 1).

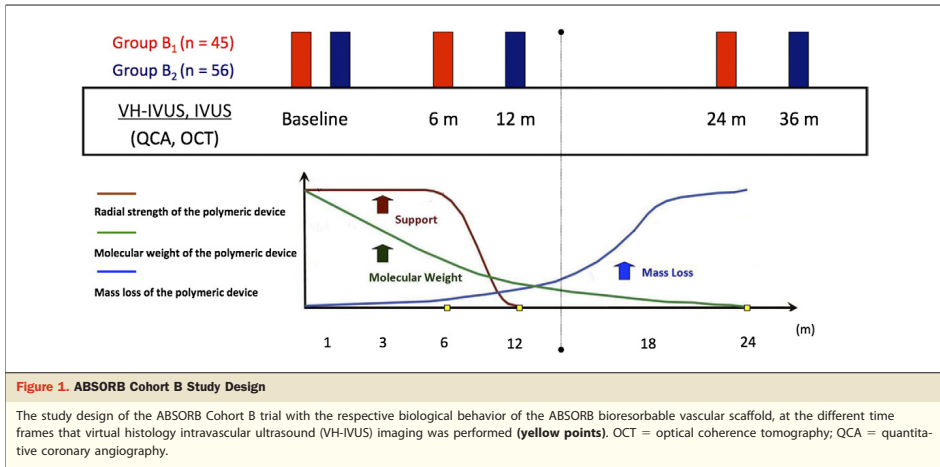
In the present study, patients over the age of 18 years, who had either stable or unstable angina pectoris or silent ischemia, were suitable for inclusion. All treated lesions were de novo lesions in a native coronary artery with a maximum diameter of 3.0 mm, a length of <14 mm, a percent diameter stenosis $\geq 50\%$ and <100%, and a Thrombolysis In Myocardial Infarction (TIMI) flow grade of ≥ 1 . Major exclusion criteria were patients presenting with an acute myocardial infarction or unstable arrhythmias, or patients who had a left ventricular ejection fraction <30%, restenotic lesions, lesions located in the left main coronary artery, lesions involving an epicardial side branch ≥ 2 mm in diameter by visual assessment, and the presence of thrombus or another clinically significant stenosis in the target vessel.

Abbreviations and Acronyms

CSA	= cross-sectional area
DC	= dense calcium
FF	= fibrofatty
GM	= geographic miss
NC	= necrotic core
VH-IVUS	= virtual histology intravascular ultrasound
WSS	= wall shear stress

From the *Thoraxcenter, Erasmus University Medical Center, Rotterdam, the Netherlands; †Cardiovascular Center, Aalst, Belgium; ‡Institut Jacques Cartier, Massy, France; §Skejby Sygehus, Aarhus University Hospital, Aarhus, Denmark; ||Maasstad Hospital, Rotterdam, the Netherlands; ¶Jagiellonian University, Krakow, Poland; #Catharina Hospital, Eindhoven, the Netherlands; **Bern University Hospital, Bern, Switzerland; ††St. Vincent's Hospital, Fitzroy, Australia; ‡‡Abbott Vascular, Diegem, Belgium; §§Abbott Vascular, Santa Clara, California; |||CardiAllysis, Rotterdam, the Netherlands; ¶¶Christchurch Hospital, Christchurch, New Zealand; and the ##Auckland City Hospital, Auckland, New Zealand. Dr. Gogas wishes to acknowledge the American College of Cardiology Foundation for the International Society of Cardiovascular Translational Research Award, and Hellenic Cardiological Society and Hellenic Heart Foundation for providing funding support. Dr. Chevalier is a consultant for Abbott Vascular. Prof. Dudek has received research grants or served as consultant/advisory board member for Abbott, Adamed, AstraZeneca, Biotronik, Balton, Bayer, BBraun, BioMatrix, Boston Scientific, Boehringer-Ingelheim, Bristol-Myers Squibb, Cordis, Cook, Eli Lilly & Co., EuroCor, GlaxoSmithKline, Inatec, Medtronic, The Medicines Company, MSD, Nycomed, Orbus-Neich, Pfizer, Possis, Promed, Sanofi-Aventis, Siemens, Solvay, Terumo, and Tyco. Dr. Windecker received research grants to the institution from Abbott, Biotronik, Biosensors, Boston Scientific, and Cordis. Dr. Ormiston was on the advisory board of and received minor honoraria from Abbott Vascular and Boston Scientific. Drs. Miquel-Hebert and Rapozo and Ms. Dorange are employees of Abbott Vascular. Michael Kutcher, MD, served as Guest Editor for this paper. All other authors have reported that they have no relationships relevant to the contents of this paper to disclose.

Manuscript received September 29, 2011; revised manuscript received January 9, 2012; accepted February 14, 2012.



The ethics committee at each participating institution approved the protocol, and each patient gave written informed consent before inclusion.

Treatment device. The ABSORB BVS (Abbott Vascular, Santa Clara, California) is a balloon-expandable device con-

sisting of a polymer backbone of poly-L-lactide coated with a thin layer of a 1:1 mixture of poly-D,L-lactide. The polymer controls the release of the antiproliferative drug everolimus, and forms an amorphous drug-eluting coating matrix that contains 100 μg of everolimus/ cm^2 of scaffold. According to

	6 Months		1 Year	
	Proximal Edge (n = 23)	Distal Edge (n = 18)	Proximal Edge (n = 24)	Distal Edge (n = 29)
Age, yrs	62.41 \pm 9.86	64.70 \pm 9.83	59.21 \pm 7.72	60.20 \pm 7.72
Male	14 (61%)	12 (67%)	15 (63%)	20 (69.0%)
Current smoking	3 (13.0%)	1 (6%)	5 (21%)	2 (7%)
Diabetes	5 (22%)	3 (17%)	7 (29%)	6 (21%)
Hypertension	16 (70%)	13 (72%)	17 (74%)	19 (68%)
Hypercholesterolemia	22 (96%)	18 (100%)	18 (75%)	22 (76%)
Prior myocardial infarction	8 (35%)	7 (39%)	5 (21%)	3 (11%)
Unstable angina	3 (13%)	3 (17%)	4 (17%)	6 (21%)
Stable angina	16 (70%)	14 (78%)	14 (58%)	17 (59%)
Treated vessel				
Right coronary artery	9 (39%)	7 (39%)	9 (36%)	8 (27%)
Left anterior descending artery	6 (26%)	6 (33%)	10 (40%)	16 (53%)
Left circumflex artery	7 (30%)	4 (22%)	6 (24%)	6 (20%)
ACC/AHA lesion class:				
Type A	1 (4%)	1 (5%)	0 (0%)	0 (0%)
Type B1	10 (44%)	9 (50%)	17 (71%)	22 (73%)
Type B2	11 (48%)	8 (44%)	6 (25%)	7 (23%)
Type C	1 (4%)	0 (0%)	1 (4%)	1 (3%)
RVD before intervention, mm	2.56 \pm 0.43	2.78 \pm 0.45	2.61 \pm 0.33	2.50 \pm 0.28

Values are mean \pm SD or n (%).
ACC/AHA = American College of Cardiology/American Heart Association; RVD = reference vessel diameter.

Table 2. Summary of the % Changes of the Entire 5-mm Segment, at the Proximal and Distal Edges, Regarding Geometric and Plaque Composition Parameters 6 Months and 1 Year Following Implantation of the ABSORB BVS

	Vessel CSA (mm ²)	Lumen CSA (mm ²)	Plaque CSA (mm ²)	
Proximal edge segment, (%) change				
6 months (n = 23)	-1.8 [-3.18; 1.30]	-4.1 [-11.61; 8.79]	-4.04 [-10.65; 11.05]	
p value	<0.05	NS	NS	
1 year (n = 25)	-1.53 [-7.74; 2.48]	-5.32 [-12.36; 4.24]	-2.03 [-8.39; 7.76]	
p value	NS	NS	NS	
Distal edge segment, (%) change				
6 months (n = 18)	-0.59 [-3.74; 7.09]	-0.32 [-7.71; 7.20]	7 [-11.97; 18.36]	
p value	NS	NS	NS	
1 year (n = 30)	3.45 [-2.08; 6.91]	0.95 [-7.56; 7.48]	5.73 [-6.49; 25.47]	
p value	NS	NS	NS	
	Dense Calcium (mm ²)	Fibrous (mm ²)	Fibrofatty (mm ²)	Necrotic Core (mm ²)
Proximal edge segment, (%) change				
6 months (n = 23)	12.02 [-31.62; 47.50]	4.44 [-16.83; 67.23]	10.3 [-46.38; 134.69]	24.14 [-22.32; 76.76]
p value	NS	NS	NS	NS
1 year (n = 25)	-7.91 [-42.19; 17.26]	-2.58 [-20.03; 11.86]	-9 [-36.77; 87.41]	-4.35 [-31.23; 30.40]
p value	NS	NS	NS	NS
Distal edge segment, (%) change				
6 months (n = 18)	44.09 [22.81; 159.23]	4.07 [-18.83; 107.39]	8.21 [-37.77; 91.48]	23.59 [-19.89; 74.33]
p value	<0.05	NS	NS	NS
1 year (n = 30)	-20.57 [-50.22; 54.11]	18.87 [-11.14; 108.93]	43.32 [-19.90; 244.28]	-6.25 [-44.20; 81.94]
p value	NS	NS	<0.05	NS

p values in **bold** are statistically significant.
 BVS = bioresorbable vascular scaffold; CSA = cross-sectional area; NS = not significant.

bench studies, the ABSORB BVS device has shown a dynamic biological behavior at 6 months, 1 year, and 2 years, at which time the complete bioresorption of the polymer backbone is expected (7).

At 6 months, a gradual and steep loss of the device radial strength in parallel to the continuous decrease of the device

molecular weight is observed because of the depolymerization and hydrolysis after implantation. The molecular weight of the polymeric platform continues to decrease until 1 year, when the radial strength is completely eliminated, and the device represents a passive structure without any supportive vascular properties. At 2 years, the ABSORB

Table 3. Summary of the Proximal and Distal Edge Changes at 6 Months and 1 Year After Implantation of the ABSORB BVS

	Time After the Imaging Procedure					
	Vessel CSA (mm ²)	Lumen CSA (mm ²)	Plaque CSA (mm ²)	Vessel CSA (mm ²)	Lumen CSA (mm ²)	Plaque CSA (mm ²)
	6 Months (n = 23)			1 Year (n = 25)		
Proximal Edge						
Baseline	13.2 [10.81; 15.90]	7.15 [5.80; 8.65]	5.88 [4.22; 7.08]	13.89 [12.55; 17.24]	7.25 [6.44; 8.40]	7.02 [5.52; 7.80]
Follow-up	13.38 [10.26; 15.39]	7.15 [5.60; 8.41]	5.49 [3.86; 7.25]	13.71 [12.22; 16.11]	7 [6.14; 8.30]	7.08 [5.36; 8.38]
Median absolute difference	-0.25 [-0.54; 0.18]	-0.27 [-0.78; 0.67]	-0.25 [-0.63; 0.60]	-0.19 [-1.06; 0.33]	-0.35 [-0.77; 0.25]	-0.15 [-0.59; 0.37]
p value	<0.05	NS	NS	NS	NS	NS
Distal Edge						
Baseline	12.79 [10.17; 16.38]	7.27 [5.62; 7.90]	7.02 [4.15; 7.89]	10.28 [9.13; 13.46]	6.7 [5.63; 7.80]	4.47 [2.29; 5.61]
Follow-up	13.87 [10.42; 16.15]	6.85 [6.11; 8.44]	6.07 [4.90; 8.40]	10.49 [9.88; 13.33]	6.76 [5.56; 7.78]	4.46 [3.20; 6.61]
Median absolute difference	-0.07 [-0.51; 1.00]	-0.03 [-0.55; 0.58]	0.35 [-0.82; 0.97]	0.4 [-0.26; 0.63]	0.09 [-0.49; 0.43]	0.27 [-0.27; 0.97]
p value	NS	NS	NS	NS	NS	NS

Values are medians (interquartile ranges). Analysis was performed at the lesion level.
 Abbreviations as in Table 2.

Table 4. Summary of the Tissue Composition Changes at the Proximal and Distal Edges, 1 Year After Implantation of the ABSORB BVS

	Dense Calcium (mm ²)	Dense Calcium (%)	Fibrous (mm ²)
Proximal edge segment (n = 25)			
Baseline	0.48 [0.24; 0.76]	12.55 [7.02; 20.20]	1.95 [1.01; 2.69]
1-year follow-up	0.33 [0.24; 0.54]	11.97 [8.31; 17.94]	2.02 [1.37; 2.41]
Median absolute difference	-0.02 [-0.20; 0.09]	-0.72 [-3.70; 4.65]	-0.04 [-0.33; 0.20]
p value	NS	NS	NS
Distal edge segment (n = 30)			
Baseline	0.18 [0.08; 0.57]	15.87 [10.17; 35.30]	0.91 [0.08; 1.61]
1-year follow-up	0.19 [0.08; 0.31]	10.5 [6.93; 17.07]	0.9 [0.28; 1.52]
Median absolute difference	-0.02 [-0.20; 0.07]	-4.22 [-12.18; 1.35]	0.09 [-0.07; 0.22]
p value	NS	<0.05	NS
p values in bold are statistically significant. Abbreviations as in Table 3.			

BVS is considered fully resorbed, having been metabolized into CO₂ and H₂O through the Krebs cycle (Fig. 1). This dynamic behavior of the polymeric device at the above-mentioned time points prompts the *in vivo* evaluation of the vascular response at the scaffold edges with VH-IVUS imaging in parallel to its evolving biological behavior (8).

Treatment procedure. Lesions were treated with routine interventional techniques that included mandatory predilation with a balloon shorter and 0.5 mm smaller in diameter than the study device. The ABSORB BVS was implanted at a pressure not exceeding the rated burst pressure (16 atm). Post-dilation with a balloon shorter than the implanted device was allowed at the discretion of the operator, as was bailout treatment.

Quantitative IVUS and VH-IVUS analysis. Geometric parameters in the complete 5-mm proximal and distal segments derived from the grayscale IVUS and VH-IVUS acquisition were analyzed in each separate frame—that is, vessel area, lumen area, plaque area, and tissue composition parameters—as absolute values. Furthermore, percentages were assessed for each cross section in the same region of interest. Both the proximal and distal vessel segments were further divided into 1-mm subsegments, numbered from 1 (adjacent to the scaffold) to 5, and underwent similar imaging evaluation as for the complete segment.

The tissue compositional analysis was obtained with a phased-array 20-MHz intravascular ultrasound catheter (Eagle Eye, Volcano Corporation, Rancho Cordova, California) after intracoronary administration of 100 to 200 μg of nitroglycerin, using automated pullback at 0.5 mm/second (30 frames/s). The raw radiofrequency data were capture gated to the R-wave. The main principle of the VH-IVUS imaging technique is that both the envelope amplitude of the reflected radiofrequency signals, as undertaken with standard grayscale IVUS analyses, and the underlying frequency content is used to analyze the tissue components present in coronary plaques. The combined information is subsequently processed using autoregressive

models and thereafter categorized into a classification tree that determines the 4 basic plaque tissue components: 1) fibrous tissue—dark green; 2) FF—light green; 3) necrotic core (NC)—red; and 4) dense calcium (DC)—white (9). All VH-IVUS analyses were performed offline using the pcVH 2.1 software (Volcano Corporation) by an independent clinical research organization (Cardialysis, Rotterdam, the Netherlands). At 6 months (Cohort B₁, n = 45), 23 proximal and 18 distal edge segments were suitable for analysis with grayscale IVUS and VH-IVUS imaging. At 1 year (Cohort B₂, n = 56), 25 proximal and 30 distal edge segments were analyzable. The reasons for the reduced number of our final tested samples were: 1) the dropout of patients at follow-up (the attrition rate of the ABSORB Cohort B trial was ~20%) and exclusion of the unpaired samples from our final data; and 2) exclusion of cases, according to the standard operational procedure of the independent core laboratory (Cardialysis), with side-branch outgrowth of >90° at the side of the scaffold edge that did not allow the analysis of the complete 5-mm segment and vessel wall out of the field of the view.

Statistical analysis. Discrete variables are presented as counts and percentages. Continuous variables are presented as medians and interquartile ranges. Comparison between baseline and follow-up was performed using the Wilcoxon signed rank test. Changes (differences) for each measurement were calculated as follow-up minus post-procedure values. Percent changes (differences) for each variable were calculated as follow-up post-procedure/post-procedure × 100%. A p value <0.05 was considered statistically significant. Data analyses were performed with SAS version 9.1 software (SAS Institute, Cary, North Carolina).

Results

The baseline clinical and lesion characteristics of the patients are demonstrated in Table 1. The percent (%) changes

Table 4. Continued				
Fibrous (%)	Fibrofatty (mm ²)	Fibrofatty (%)	Necrotic Core (mm ²)	Necrotic Core (%)
55.08 [46.10; 63.52]	0.26 [0.11; 0.45]	7.34 [4.99; 10.36]	0.85 [0.40; 1.28]	19.63 [17.16; 29.81]
53.62 [48.56; 59.95]	0.28 [0.09; 0.38]	8 [4.46; 11.39]	0.64 [0.42; 1.01]	20.49 [15.11; 29.02]
-0.1 [-4.67; 5.71]	-0.01 [-0.10; 0.19]	0.03 [-3.08; 3.42]	-0.06 [-0.32; 0.23]	-2.05 [-5.58; 5.65]
NS	NS	NS	NS	NS
54.72 [35.05; 62.19]	0.06 [0.01; 0.17]	4.7 [2.49; 7.87]	0.4 [0.04; 0.72]	21.96 [17.58; 28.00]
57.75 [51.27; 62.42]	0.1 [0.03; 0.28]	8.1 [4.23; 12.54]	0.3 [0.09; 0.64]	18.75 [14.65; 24.88]
1.83 [-4.36; 14.58]	0.02 [0.00; 0.09]	2.24 [0.48; 8.69]	-0.01 [-0.33; 0.09]	-2.82 [-7.26; 4.22]
NS	<0.05	<0.05	NS	NS

(median [interquartile range]) of the vessel cross-sectional area (CSA), lumen CSA, and plaque CSA at the 5-mm proximal edge segment were at 6 months: -1.80% $[-3.18; 1.30]$, ($p < 0.05$), -4.10% $[-11.61; 8.79]$, ($p = 0.22$), and -4.04% $[-10.65; 11.05]$ ($p = 0.55$); and at 1 year: -1.53% $[-7.74; 2.48]$, ($p = 0.06$), -5.32% $[-12.36; 4.24]$, ($p = 0.07$), and -2.03% $[-8.39; 7.76]$, ($p = 0.72$), respectively. The % changes of the vessel CSA, lumen CSA, and plaque CSA at the 5-mm distal edge segment were at 6 months: -0.59% $[-3.74; 7.09]$, ($p = 0.71$), -0.32% $[-7.71; 7.20]$,

($p = 0.97$), and 7.0% $[-11.97; 18.36]$, ($p = 0.50$); and at 1 year: 3.45% $[-2.08; 6.91]$, ($p = 0.07$), 0.95% $[-7.56; 7.48]$, ($p = 0.77$), and 5.73% $[-6.49; 25.47]$, ($p = 0.09$), respectively (Table 2). The absolute geometric and tissue composition changes and the subsegmental analysis at 1 year are tabulated in (Tables 3 and 4) and illustrated in Figs. 2, 3, and 4.

The absolute tissue compositional changes at 6 months at both edges and the subsegmental analysis at the same time point are tabulated and illustrated in the Online Appendix.

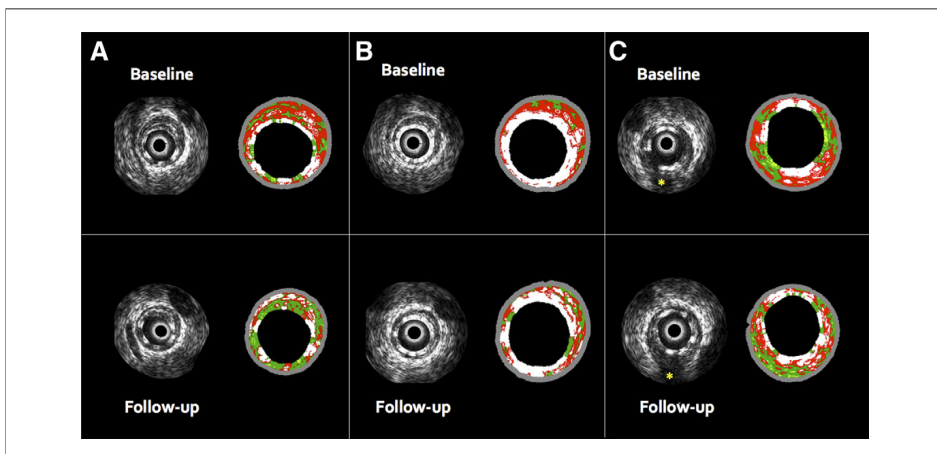
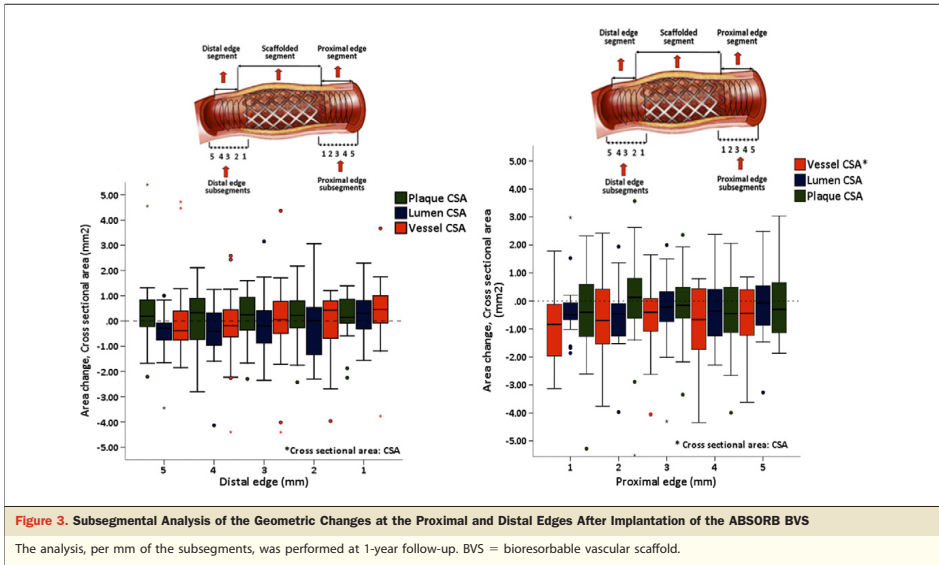


Figure 2. Grayscale IVUS and Corresponding VH-IVUS Still Frames at 1-Year After Implantation of the ABSORB BVS

(A) Distal edge segment. At this segment a significant increase of the fibrofatty (FF) tissue was observed. VH-IVUS demonstrates at this frame a change in FF tissue area from 0.07 to 0.14 mm². Dense calcium (DC) and necrotic core tissue components changed from 2.39 mm² and 3.7 mm² to 2.07 mm² and 1.8 mm², respectively, as a consequence of the bioresorption process. **(B)** Scaffolded segment. The polymeric struts of the ABSORB BVS are detected as “pseudo” DC surrounded by a red, halo. **(C)** Proximal edge segment. At this segment some degree of proximal edge constrictive vascular remodeling was observed. Grayscale IVUS shows for this frame a change in the lumen area from 9.4 mm² to 8.4 mm² (The external elastic membrane has been extrapolated at the side of the side branch, [yellow asterisk]).



Discussion

The main findings of this study at the time point of 1-year post-implantation of the ABSORB BVS are as follows. Constrictive vascular remodeling at the proximal edge was evident without significant changes in tissue composition parameters. At the distal edge, tissue composition changes were evident with a significant increase in the FF tissue resulting in nonsignificant plaque progression and adaptive expansive remodeling (Fig. 2).

The edge effects following the implantation of either a metallic or a polymeric device have common etiological mechanisms, namely: 1) periprocedural or iatrogenic technical issues affecting predominantly geometric parameters (1–11); 2) tissue composition characteristics of the lesion (12); and 3) local wall shear stress (WSS) conditions (13–15).

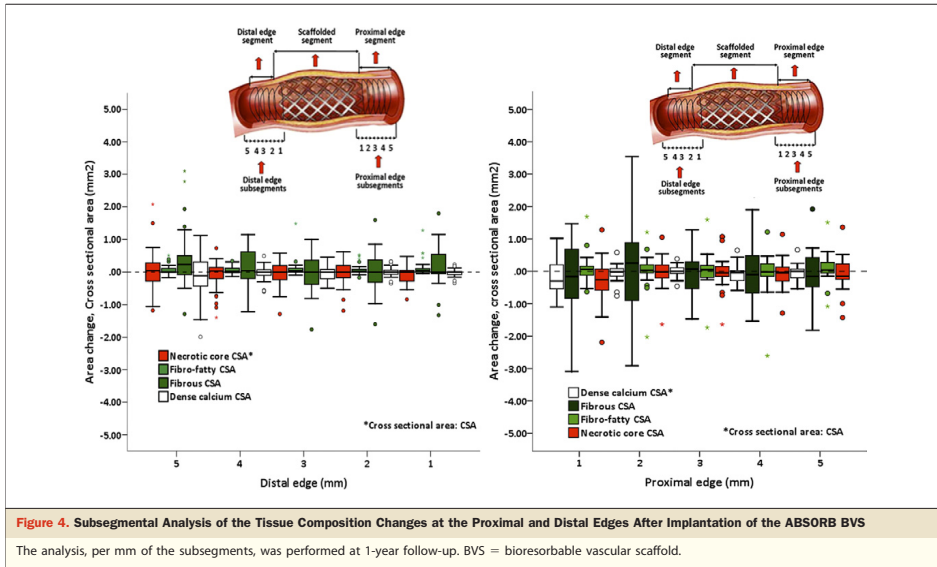
The GM phenomenon, associated with sirolimus-eluting stent implantation, was investigated in the STLLR (Stent Deployment Techniques on Clinical Outcomes of Patients Treated With the Cypher Stent) study and was reported to occur in nearly two-thirds (66.5%) of the study group; almost one-half of the patients (47.6%) experienced longitudinal GM, over one-third (35.2%) axial GM, and 16.5%, a combination of the 2 (1,10). Hoffmann et al. (10) demonstrated within the E-SIRIUS (European, multicenter, randomized, double blind trial of the SIRoImUS-coated Bx-Velocity stent in the treatment of patients with de novo coronary artery lesions)-IVUS

substudy versus the SIRIUS-US (US, multicenter, randomized, double blind trial of the SIRoImUS-coated Bx-Velocity stent in the treatment of patients with de novo coronary artery lesions) trial, that both axial and longitudinal GM were reduced (from 5.9% to 2.1%) when periprocedural implantation parameters were taken into account, such as conservative pre-dilation, less forceful stent implantation (~16 atm), and selective post-dilation with balloons shorter than the stent.

Despite multiple technical guidelines regarding the ABSORB BVS delivery system to minimize the axial (burst pressure: 16 atm) and longitudinal (balloon shorter and 0.5 mm smaller than the implanted device) GM phenomena, a significant proximal edge constrictive response was demonstrated at 6 months, whereas at 1 year, the constrictive remodeling was only observed in the following proximal subsegments, starting from the scaffold edge (subsegment 1: $\Delta -0.96 \text{ mm}^2$, $p < 0.05$); subsegment 2: $\Delta -0.71 \text{ mm}^2$, $p < 0.05$); and subsegment 4: $\Delta -0.57$ ($p < 0.05$) (Figs. 3 and 4).

The changes in WSS distribution adjacent to the stent edges post device implantation appear to follow alterations in vessel curvature and angulation, and have been reported to result in step-up regions of low shear stress, prone to neointimal growth (13–15).

Metallic devices have a more accentuated effect on vessel curvature and angulation compared to the ABSORB BVS; however, despite the clinical benefits associated with better



conformability (16) of the ABSORB BVS device, proximal constrictive remodeling was observed at 1-year after implantation, and further investigations are required to evaluate the changes of WSS at the scaffold edges or the in-scaffold area. Moreover, any of the initial flow–tissue interaction effects caused by the implantation of this bioresorbable device are expected to potentially subside after a 2-year period when the bioresorption process is expected to be complete and the polymeric platform is fully transformed to CO_2 and H_2O , with no consequent remaining compliance mismatch (8,16). Samady et al. (17) recently demonstrated, in a cohort of 20 patients, that coronary segments with low WSS (step-up regions) are segments that develop constrictive remodeling, in contrast to the high-WSS segments that present excessive expansive remodeling with tissue composition changes, mainly due to an increase in DC and NC tissue components. These reported observations are in parallel with the present findings in this study regarding vessel geometry and tissue composition.

The distal edge segment adjacent to the scaffold appeared to have major tissue composition changes with some degree of plaque progression, which caused a subsequent nonsignificant expansive remodeling. The VH-IVUS–derived tissue type that correlates with extracellular matrix is the FF tissue, which happens to be the one that increased the most (18). The DC tissue component appeared to have a biphasic response at this segment after the ABSORB BVS implan-

tation with a significant increase at 6 months and a trend toward a decrease at 1-year follow-up; conversely, the NC tissue changed nonsignificantly following sequential modifications of DC tissue.

The changes in DC and NC tissue components at follow-up should be interpreted with caution since the ABSORB BVS is made of bioresorbable polymeric material recognized as “pseudo” DC and NC, parameters that have previously been reported as surrogate markers of the bioresorption process (19,20). In addition, the edges of the polymeric scaffold are not sharply demarcated since the vessel surrounding the imaging device are affected by the “to and fro” motion of the cardiac contraction, causing a “pseudoaxial” displacement of the IVUS catheter related to the arterial wall.

Indeed, the cardiac cycle can cause a mean axial displacement of the IVUS transducer of 1.5 mm with a maximum distortion up to 6.5 mm; however, the use of electrocardiogram gating during IVUS data acquisition reduces the axial movement to a maximum of 0.8 mm (21–23) but does not fully prevent the imaging of the polymeric struts as “pseudo” DC in the adjacent edge of the implanted device. In keeping with the standard operational procedure of an independent core laboratory (Cardialysis), the quantification of the scaffold edges was initiated at the point where the visualization of the scaffold arc at each frame was $<360^\circ$, implying that the scaffold edge to some extent may include polymeric struts.

The apparent increase in DC at 6 months, followed by a trend toward a reduction at 1 year, accompanied by the parallel behavior of the NC, are attributed to the introduction of the bioresorbable device during the procedure and subsequent bioresorption process long term. Other possible factors that may have influenced the NC tissue component are the locally eluted drug everolimus and the systemic use of HMG-CoA inhibitors. Verheye et al. (24) recently demonstrated that everolimus—an inhibitor of the mammalian target of rapamycin (m-TOR)—has autophagic capabilities on macrophages, with a subsequent effect of diminishing NC formation, inflammation, and thrombosis. Hong et al. (25) reported a significant 13% relative reduction in plaque necrotic core volume, and a significant 27% relative increase in plaque FF content with the administration of HMG-CoA inhibitors, assessed with VH-IVUS at 1-year follow-up.

Coronary endothelial dysfunction has been previously associated with underlying plaque composition, in particular high content of DC and NC. Lavi et al. (26) have demonstrated impaired endothelial-dependent vasomotion in vessel segments with underlying NC-rich plaques. Our group has recently demonstrated that the restored normal vasodilatory response to acetylcholine in coronary segments that have previously undergone implantation with an ABSORB BVS, is associated with a reduction of NC (27), implying the potential restoration of the vasomotor function of the treated vessel with reductions of specific tissue components. Whether the present findings are due to the combined effects of locally eliminated m-TOR inhibitor everolimus, with the systemic use of the HMG-CoA inhibitors, or the natural history of the bioresorbable process of the implanted device, remains to be elucidated in future studies, where a potential restoration of the vasomotor function at the scaffold edges would be highly expected with the sustained tissue composition changes observed at 1-year follow-up. Furthermore, the combination of continuous polymer degradation and elaboration of the treated vessel from its foreign material beyond 1 year, with the restoration of vessel biological behavior (vasomotor function) and the interplay with pharmacological intervention may potentially eliminate the risk of late stent thrombosis.

The clinical outcome of the ABSORB Cohort B trial at 1-year post implantation of the ABSORB BVS revealed a hierarchical major adverse cardiac event rate of 6.9%, with no episodes of scaffold thrombosis (according to the protocol or Academic Research Consortium definitions). Pre-scaffolding VH-IVUS analysis can give an insight into the extent of plaque and NC within and beyond the intended scaffolded segment. This latter point is potentially important, since full coverage of the lesion by the implanted device is the desired goal of the interventionalist, as incomplete coronary plaque coverage has been reported to effect

long-term clinical events, especially in the presence of NC-containing plaques (11).

Study limitations. The main limitation of our study is the small number of the investigated scaffold edges. The complete cohort ($B_1 + B_2$) at the different time points without splitting the population would potentially have increased the sample size; this, however, was a predefined design of the study.

Conclusions

The edge vascular response, with the use of the ABSORB BVS device at 1-year post implantation, demonstrates a degree of proximal edge constrictive remodeling and distal edge plaque compositional changes, a biological behavior similar to that observed with the metallic devices. Full bioresorption of the device, expected to occur in approximately 2 years, will potentially allow for the evaluation and comparison of the exact biological composition of the treated vessel at the scaffold edges, utilizing the VH-IVUS imaging modality.

Reprint requests and correspondence: Prof. P. W. Serruys, Thoraxcenter, Bd583a, Dr. Molewaterplein 40, 3015-GD Rotterdam, the Netherlands. E-mail: p.w.j.c.serruys@erasmusmc.nl.

REFERENCES

- Costa MA, Angiolillo DJ, Tannenbaum M, et al. Impact of stent deployment procedural factors on long-term effectiveness and safety of sirolimus-eluting stents (final results of the multicenter prospective STLLR trial). *Am J Cardiol* 2008;101:1704–11.
- Grube E, Silber S, Hauptmann KE, et al. TAXUS I: six- and twelve-month results from a randomized, double-blind trial on a slow-release paclitaxel-eluting stent for de novo coronary lesions. *Circulation* 2003;107:38–42.
- Serruys PW, Degertekin M, Tanabe K, et al. Vascular responses at proximal and distal edges of paclitaxel-eluting stents: serial intravascular ultrasound analysis from the TAXUS II trial. *Circulation* 2004;109:627–33.
- García-García HM, Gonzalo N, Tanimoto S, Meliga E, de Jaegere P, Serruys PW. Characterization of edge effects with paclitaxel-eluting stents using serial intravascular ultrasound radiofrequency data analysis: the BETAX (BEside TAXus) study. *Rev Esp Cardiol* 2008;61:1013–9.
- Chieffo A, Foglieni C, Nodari RL, et al. Histopathology of clinical coronary restenosis in drug-eluting versus bare metal stents. *Am J Cardiol* 2009;104:1660–7.
- Byrne RA, Eberle S, Kastrati A, et al. Distribution of angiographic measures of restenosis after drug-eluting stent implantation. *Heart* 2009;95:1572–8.
- Onuma Y, Serruys PW, Perkins LE, et al. Intracoronary optical coherence tomography and histology at 1 month and 2, 3, and 4 years after implantation of everolimus-eluting bioresorbable vascular scaffolds in a porcine coronary artery model: an attempt to decipher the human optical coherence tomography images in the ABSORB trial. *Circulation* 2010;122:2288–300.
- Gogas BD, Radu M, Onuma Y, et al. Evaluation with in vivo optical coherence tomography and histology of the vascular effects of the everolimus-eluting bioresorbable vascular scaffold at two years following implantation in a healthy porcine coronary artery model: implications of pilot results for future pre-clinical studies. *Int J Cardiovasc Imaging* 2012;28:499–516.
- Gogas BD, Farooq V, Serruys PW, et al. Assessment of coronary atherosclerosis by IVUS and IVUS-based imaging modalities: progres-

- sion and regression studies, tissue composition and beyond. *Int J Cardiovasc Imaging* 2011;27:225–37.
10. Hoffmann R, Guagliumi G, Musumeci G, et al. Vascular response to sirolimus-eluting stents delivered with a nonaggressive implantation technique: comparison of intravascular ultrasound results from the multicenter, randomized e-Sirius, and Sirius trials. *Catheter Cardiovasc Interv* 2005;66:499–506.
 11. Farb A, Burke AP, Kolodgie FD, Virmani R. Pathological mechanisms of fatal late coronary stent thrombosis in humans. *Circulation* 2003;108:1701–6.
 12. Wentzel JJ, Gijzen FJ, Stergiopoulos N, Serruys PW, Slager CJ, Krams R. Shear stress, vascular remodeling and neointimal formation. *J Biomech* 2003;36:681–8.
 13. Wentzel JJ, Whelan DM, van der Giessen WJ, et al. Coronary stent implantation changes 3-d vessel geometry and 3-d shear stress distribution. *J Biomech* 2000;33:1287–95.
 14. Thury A, Wentzel JJ, Vinke RV, et al. Images in cardiovascular medicine. Focal in-stent restenosis near step-up: roles of low and oscillating shear stress? *Circulation* 2002;105:e185–7.
 15. Gomez-Lara J, Garcia-Garcia HM, Onuma Y, et al. A comparison of the conformability of everolimus-eluting bioresorbable vascular scaffolds to metal platform coronary stents. *J Am Coll Cardiol Intv* 2010;3:1190–8.
 16. Tortoriello A, Pedrizzetti G. Flow-tissue interaction with compliance mismatch in a model stented artery. *J Biomech* 2004;37:1–11.
 17. Samady H, Eshetehardi P, McDaniel MC, et al. Coronary artery wall shear stress is associated with progression and transformation of atherosclerotic plaque and arterial remodeling in patients with coronary artery disease. *Circulation* 2011;124:779–88.
 18. Farb A, Kolodgie FD, Hwang JY, et al. Extracellular matrix changes in stented human coronary arteries. *Circulation* 2004;110:940–7.
 19. Kim SW, Mintz GS, Hong YJ, et al. The virtual histology intravascular ultrasound appearance of newly placed drug-eluting stents. *Am J Cardiol* 2008;102:1182–6.
 20. Bruining N, de Winter S, Roelandt JR, et al. Monitoring in vivo absorption of a drug-eluting bioabsorbable stent with intravascular ultrasound-derived parameters a feasibility study. *J Am Coll Cardiol Intv* 2010;3:449–56.
 21. Arbab-Zadeh A, DeMaria AN, Penny WF, Russo RJ, Kimura BJ, Bhargava V. Axial movement of the intravascular ultrasound probe during the cardiac cycle: implications for three-dimensional reconstruction and measurements of coronary dimensions. *Am Heart J* 1999;138:865–72.
 22. von Birgelen C, de Vrey EA, Mintz GS, et al. ECG-gated three-dimensional intravascular ultrasound: feasibility and reproducibility of the automated analysis of coronary lumen and atherosclerotic plaque dimensions in humans. *Circulation* 1997;96:2944–52.
 23. Bruining N, von Birgelen C, de Feyter PJ, et al. ECG-gated versus nongated three-dimensional intracoronary ultrasound analysis: implications for volumetric measurements. *Cathet Cardiovasc Diagn* 1998;43:254–60.
 24. Verheye S, Martinet W, Kockx MM, et al. Selective clearance of macrophages in atherosclerotic plaques by autophagy. *J Am Coll Cardiol* 2007;49:706–15.
 25. Hong MK, Park DW, Lee CW, et al. Effects of statin treatments on coronary plaques assessed by volumetric virtual histology intravascular ultrasound analysis. *J Am Coll Cardiol Intv* 2009;2:679–88.
 26. Lavi S, Bae JH, Rihal CS, et al. Segmental coronary endothelial dysfunction in patients with minimal atherosclerosis is associated with necrotic core plaques. *Heart* 2009;95:1525–30.
 27. Brugaletta S, Heo HJ, Garcia-Garcia HM, et al. Endothelial-dependent vasomotion in coronary segment treated by ABSORB everolimus-eluting bioresorbable vascular scaffold system is related to plaque composition at the time of bioresorption of the polymer: indirect finding of vascular reparative therapy? *Eur Heart J* 2012 Apr 16 [E-pub ahead of print].

Key Words: ABSORB bioresorbable vascular scaffold ■ edge vascular response ■ virtual histology intravascular ultrasound assessment.

▶ APPENDIX

For supplemental material, please see the online version of this article.

Chapter 8

The Edge Vascular Response Following Implantation of the Absorb Everolimus Eluting Bioresorbable Vascular Scaffold and the Xience V Metallic Everolimus Eluting Stent. First Serial Follow-Up Assessment at 6-Months and 2–Years. Insights from the First in Man ABSORB Cohort B and SPIRIT II trials.

Bill D. Gogas, Christos V. Bourantas, Hector M. Garcia-Garcia, Yoshinobu Onuma, Takashi Muramatsu, Vasim Farooq, Roberto Diletti, Robert-Jan M. van Geuns, Bernard De Bruyne, Bernard Chevalier, Leif Thuesen, Pieter C. Smits, Dariusz Dudek, Jacques Koolen, Stefan Windecker, Robert Whitbourn, Dougal Mc Clean, Cecile Dorange, Karine Miquel-Hebert, Susan Veldhof, Richard Rapoza, John A. Ormiston, Patrick W. Serruys

EuroIntervention. 2013 Apr 30. Doi: 20120911-04 [Epub ahead of print] [IF: 3.17]

The edge vascular response following implantation of the Absorb everolimus-eluting bioresorbable vascular scaffold and the XIENCE V metallic everolimus-eluting stent. First serial follow-up assessment at six months and two years: insights from the first-in-man ABSORB Cohort B and SPIRIT II trials

Bill D. Gogas^{1,2}, MD; Christos V. Bourantas¹, MD, PhD; Hector M. Garcia-Garcia³, MD, MSc, PhD; Yoshinobu Onuma¹, MD; Takashi Muramatsu¹, MD, PhD; Vasim Farooq¹, MBChB; Roberto Diletti¹, MD; Robert-Jan M. van Geuns¹, MD, PhD; Bernard De Bruyne⁴, MD, PhD; Bernard Chevalier⁵, MD; Leif Thuesen⁶, MD; Pieter C. Smits⁷, MD, PhD; Dariusz Dudek⁸, MD; Jacques Koolen⁹, MD, PhD; Stefan Windecker¹⁰, MD; Robert Whitbourn¹¹, MD; Dougal McClean¹², MD; Cecile Dorange¹³, MSc; Karine Miquel-Hebert¹³, PhD; Susan Veldhof¹³, RN; Richard Rapoza¹⁴, PhD; John A. Ormiston¹⁵, MBChB, PhD; Patrick W. Serruys^{1*}, MD, PhD

B.D. Gogas and C.V. Bourantas contributed equally to this manuscript.

Guest Editor: Giulio Guagliumi, MD; Division of Cardiology; Cardiovascular Department, Ospedali Riuniti di Bergamo, Bergamo, Italy

Author affiliations can be found in the appendix following this article.

This paper also includes accompanying supplementary data published at the following website: www.eurointervention.org

KEYWORDS

- Absorb bioresorbable vascular scaffold
- edge vascular response
- XIENCE V metallic everolimus-eluting stent

Abstract

Aims: To assess serially the edge vascular response (EVR) of a bioresorbable vascular scaffold (BVS) compared to a metallic everolimus-eluting stent (EES).

Methods and results: Non-serial evaluations of the Absorb BVS at one year have previously demonstrated proximal edge constrictive remodelling and distal edge changes in plaque composition with increase of the percent fibrofatty (FF) tissue component. The 5 mm proximal and distal segments adjacent to the implanted devices were investigated serially with intravascular ultrasound (IVUS), post procedure, at six months and at two years, from the ABSORB Cohort B1 (n=45) and the SPIRIT II (n=113) trials. Twenty-two proximal and twenty-four distal edge segments were available for analysis in the ABSORB Cohort B1 trial. In the SPIRIT II trial, thirty-three proximal and forty-six distal edge segments were analysed. At the 5-mm proximal edge, the vessels treated with an Absorb BVS from post procedure to two years demonstrated a lumen loss (LL) of 6.68% (-17.33; 2.08) (p=0.027) with a trend toward plaque area increase of 7.55% (-4.68; 27.11) (p=0.06). At the 5-mm distal edge no major changes were evident at either time point. At the 5-mm proximal edge the vessels treated with a XIENCE V EES from post procedure to two years did not show any signs of LL, only plaque area decrease of 6.90% (-17.86; 4.23) (p=0.035). At the distal edge no major changes were evident with regard to either lumen area or vessel remodelling at the same time point.

Conclusions: The IVUS-based serial evaluation of the EVR up to two years following implantation of a bioresorbable everolimus-eluting scaffold shows a statistically significant proximal edge LL; however, this finding did not seem to have any clinical implications in the serial assessment. The upcoming imaging follow-up of the Absorb BVS at three years is anticipated to provide further information regarding the vessel wall behaviour at the edges.

*Corresponding author: Thoraxcenter, Erasmus University Medical Center, Bld583a, Dr. Molewaterplein 40, 3015 GD Rotterdam, The Netherlands. E-mail: p.w.j.c.serruys@erasmusmc.nl

Abbreviations

BVS	bioresorbable vascular scaffold
DES	drug-eluting stent
EEM	external elastic membrane
EES	everolimus-eluting stent
EVR	edge vascular response
FU	follow-up
GM	geographic miss
IVUS	intravascular ultrasound
LL	lumen loss
PCI	percutaneous coronary intervention
PES	paclitaxel-eluting stent
SES	sirolimus-eluting stent
VBT	vascular brachytherapy

Introduction

Although the initial use of radioactive devices in the era of vascular brachytherapy (VBT) and later the utilisation of first-generation drug-eluting stents (DES) partially eliminated the iatrogenic entity of neointimal hyperplasia^{1,2}, the vascular response at the stent-to-artery transitions, presenting as a late lumen loss (LL) at the margins of the treated segments, remains one of the pitfalls of percutaneous coronary intervention (PCI)³. The term “edge effect” – defining a flow-limiting lesion at the stent edges – is meant to describe one of the major drawbacks of VBT induced by a combination of factors: the radioactive dose fall-off at the transition zones in association with either the axial geographic miss (GM) (injured or diseased segment not covered by the device), or longitudinal GM phenomena (balloon-artery ratio <0.9 or >1.3)^{4,7}. DES failure as a consequence of LL has been shown to present with a focal pattern, affecting particularly the proximal stent edge, as was demonstrated in >60% of in-stent restenosis cases with either paclitaxel-eluting stents (PES) or sirolimus-eluting stents (SES)⁸.

In the SIRIUS trial (a multicentre study of the SIRoIlmUS-eluting Bx-Velocity stent in the treatment of patients with *de novo* coronary artery lesions) a significant proximal edge LL was observed and was attributed to the vascular “trauma” at the stent margins caused by pre/post balloon dilatation (100%/70%, respectively). Therefore, less traumatic stent implantation (e.g., direct stenting without high-pressure post-dilatation) was proposed which partially eliminated the procedure-related complication of proximal restenosis as shown in the intravascular ultrasound (IVUS) sub-study of the E-SIRIUS trial⁹.

In the TAXUS II trial, the slow release and moderate release polymer formulations of the PES resulted in proximal LL of $0.54 \pm 2.1 \text{ mm}^2$ and $0.88 \pm 1.9 \text{ mm}^2$, respectively, while in the BETAX trial, utilising the TaxusTM ExpressTM DES (Boston Scientific, Natick, MA, USA), significant plaque changes in tissue composition were observed, mainly due to an increase in the fibro-fatty (FF) tissue component causing adaptive expansive remodelling at both stent edges¹⁰.

In the ABSORB Cohort B trial the second-generation AbsorbTM BVS (Abbott Vascular, Santa Clara, CA, USA) has recently been evaluated non-serially at six-month and one-year follow-up (FU)

demonstrating some degree of proximal edge constrictive remodelling of: Δ vessel area: -1.80% ($-3.18; 1.30$) ($p < 0.05$), at six months that tended numerically to regress at one year and distal edge changes in plaque phenotype with an absolute increase of the FF tissue component from 0.06 mm^2 ($0.01; 0.17$) to 0.10 mm^2 ($0.03; 0.28$) translated to a relative increase of: $\Delta \text{FF} +43.32\%$ ($-19.90; 244.28$) ($p < 0.05$) that caused non-significant plaque progression with signs of adaptive expansion at this segment¹¹.

The advent of next-generation devices with either metallic or bioresorbable platforms has prompted the *in vivo* re-evaluation of the edge vascular response (EVR) with state-of-the-art sound-based imaging modalities like intravascular ultrasound (IVUS). The purpose of this study is to investigate the EVR following implantation of two different platforms which have the same everolimus drug elution: the second-generation bioresorbable Absorb BVS and the second-generation metallic XIENCE V[®] EES (Abbott Vascular, Santa Clara, CA, USA). We analysed greyscale IVUS data acquired serially post procedure, at six months and at two years, from patients who were included in the ABSORB Cohort B and the SPIRIT II trials to report for the first time the early and late vascular responses at the edges.

Methodology

ABSORB COHORT B TRIAL

STUDY DESIGN AND POPULATION

The ABSORB Cohort B trial (NCT00856856) is an ongoing multicentre single-arm prospective, open-label trial assessing the safety and performance of the second-generation Absorb BVS in the treatment of patients with a maximum of two *de novo* native coronary artery lesions. In total, 101 patients were enrolled, divided into two subgroups – Cohort B1 (n=45) and Cohort B2 (n=56) – according to the predefined study design. Both groups underwent invasive FU at different time points: Cohort B1 at six months and two years, and Cohort B2 at one year. Additionally, a three-year invasive imaging evaluation of Cohort B2 is expected.

TREATMENT DEVICE

The Absorb BVS (Abbott Vascular) is a balloon-expandable scaffold consisting of a polymer backbone of Poly-L-lactide (PLLA) coated with a thin layer of a 1:1 mixture of Poly-D, L-lactide (PDLLA). The polymer controls the release of the antiproliferative drug everolimus, and forms an amorphous drug-eluting coating matrix that contains 100 micrograms of everolimus/cm² of scaffold. According to non-human studies, the Absorb BVS has shown a dynamic biologic behaviour at six months, one year and two years, beyond which almost complete bioresorption of the polymeric backbone is expected^{12,13}.

TREATMENT PROCEDURE

Lesions were treated with routine interventional techniques that included mandatory predilatation with a balloon shorter, and 0.5 mm smaller in diameter, than the study device. The Absorb BVS was implanted at a pressure not exceeding the rated burst pressure (16 atm) (avoidance of axial GM). Post-dilatation with a balloon shorter than the implanted device (avoidance of longitudinal GM) was allowed at the discretion of the operator to optimise device expansion.

SPIRIT II TRIAL

STUDY DESIGN AND POPULATION

The SPIRIT II study (NCT00180310) was a prospective, two-arm trial that randomised 300 patients in a 3:1 ratio to either a XIENCE V EES (n=223) or a TAXUS PES (n=77) in the treatment of coronary artery disease. Serial intravascular imaging was performed in a subset of 152 patients (EES: n=113, and PES: n=39). Thirty-two patients were included in the serial evaluation of the proximal edge and 14 (42%) received at least one 3.0×18 mm device. At the distal edge 41 patients were included with 20 (43%) having undergone implantation of a 3.0×18 mm device.

TREATMENT DEVICE

The XIENCE V everolimus-eluting stent system (Abbott Vascular) is a balloon-expandable device which consists of serpentine rings connected by links fabricated from a single piece of medical grade L-605 cobalt-chromium alloy. Everolimus is blended in a non-erodable polymer coated over another non-erodable polymer primer layer. The coating consists of acrylic and fluoro polymers, both approved for use in blood-contacting applications. This layer of everolimus-polymer matrix with a thickness of 5-6 microns is applied to the surface of the stent and is loaded with 100 micrograms of everolimus/cm² of stent surface area with no topcoat polymer layer. The stent is designed to release approximately 80% of the drug within 30 days after implantation.

TREATMENT PROCEDURE

Lesions were treated using standard interventional techniques that included mandatory predilatation and stent implantation at a pressure not exceeding the burst pressure. Post-dilatation was left to the discretion of the physician; however, if performed, it was only to be done with balloons sized to fit within the boundaries of the stent.

QUANTITATIVE IVUS ANALYSIS

ABSORB COHORT B AND SPIRIT II TRIALS

Scaffold segments, including the 5-mm proximal and distal parts, underwent imaging evaluation post procedure, at six-month and two-year FU with a phased array 20 MHz IVUS catheter (Eagle Eye[®]; Volcano Corporation, Rancho Cordova, CA, USA, and Atlantis[™]; Boston Scientific, Natick, MA, USA) after intracoronary administration of 100-200 µg nitroglycerine, using automated pull-back at 0.5 mm/sec (30 frames/sec). Geometrical parameters in the 5-mm proximal and distal edge segments derived from the grey-scale IVUS acquisition^{14,15} were analysed in each separate frame, i.e., vessel area, lumen area, plaque area as absolute values and percentages by an independent clinical research organisation (Cardialysis BV, Rotterdam, The Netherlands).

STATISTICAL ANALYSIS

Continuous variables are presented as medians and interquartile ranges. Discrete variables are presented as counts and percentages. Paired comparisons between continuous variables within groups at different time points were estimated with the Wilcoxon signed-rank test, while the Mann-Whitney U test was used for independent two-sample comparisons. Changes (differences) for each measurement were calculated as: follow-up minus post procedure

values. Percent changes (differences) for each variable were calculated as: follow-up – post procedure/post procedure ×100%. A p-value <0.05 was considered statistically significant. Data analyses were performed with SAS version 9.1 software (SAS Institute Inc., Cary, NC, USA).

RESULTS

Twenty-two lesions from the ABSORB Cohort B1 and 33 from the SPIRIT II trial had IVUS imaging at the proximal edge in all time points and were included in the proximal edge analysis, while 24 from the ABSORB Cohort B1 and 46 from the SPIRIT II trial had serial IVUS assessment of the distal edge. None of the patients included in the serial analysis of the ABSORB Cohort B1 underwent TLR due to restenosis at the scaffold edges. However, two patients from the complete (non-serial) ABSORB Cohort B1 had a target lesion revascularisation (TLR), due to proximal edge restenosis¹⁶. The first patient returned on day 358 with progressive angina, and coronary angiography revealed proximal edge restenosis adjacent to the implanted Absorb BVS. The patient was revascularised with a XIENCE V EES. The second patient returned on day 168 with progressive angina, and repeat angiography also revealed proximal edge restenosis associated with operator-related mechanical trauma. These two patients were excluded from the final analysis as they did not have truly serial IVUS acquisitions at all time points. With regard to the SPIRIT II trial, two patients who had distal edge restenoses at days 175 and 731 were also excluded from the final analysis (similar to the ABSORB Cohort B) as they lacked truly serial IVUS imaging (Figure 1). However, the calculations including the IVUS results of the patients who underwent IVUS prior to the TLR were imputed at the two-year results stage (Table 2, Table 3, Table 4, and Online Appendix).

The baseline clinical, lesion and procedural characteristics of the studied populations are reported (Table 1A and Table 1B). There were no significant statistical differences between the patients treated with an Absorb BVS and a XIENCE V EES in the proximal edge analysis. At this segment, a higher lesion length and reference vessel diameter in the XIENCE V group was noted. The baseline characteristics between the two subgroups included in the distal edge analysis were similar; however, the Absorb BVS patients were more likely to suffer from hypercholesterolaemia and less likely to smoke. At this segment, a higher incidence of Type C lesions and a higher lesion length in the XIENCE V vs. the Absorb BVS treated vessels became evident (Table 1). With regard to the post procedure IVUS measurements there were no significant statistical differences of the lumen areas between the two groups; however, in the SPIRIT II population an increased plaque burden and vessel area were noted at the proximal edge.

ABSORB BVS

PROXIMAL EDGE

At the 5-mm segment, no major absolute or relative changes were shown in terms of vessel, lumen and plaque areas in the short term (post procedure to six months). In the long term (post procedure to two years), a LL of 6.68% (-17.33; 2.08) (p=0.027) was observed

Table 1. Baseline clinical, lesion and procedural characteristics of the ABSORB Cohort B1 and SPIRIT II trials.

Proximal edge	ABSORB B1 (n=22)	SPIRIT II (n=32)	p-value
Age, yrs	62.8±9.68	58.68±8.80	0.169
Male, n (%)	15 (68.0%)	27 (84%)	0.188
Current smoking, n (%)	4 (18%)	14 (44%)	0.082
Diabetes, n (%)	4 (18%)	6 (19%)	1.000
Hypertension, n (%)	13 (59%)	19 (59%)	1.000
Hypercholesterolaemia, n (%)	21 (95%)	24 (77%)	0.067
Prior myocardial infarction, n (%)	9 (40.9%)	14 (44%)	1.000
Unstable angina, n (%)	3 (14%)	12 (38%)	0.074
Stable angina, n (%)	16 (73%)	17 (53%)	0.258
Treated vessel			
Right coronary artery, n (%)	8 (36%)	14 (42%)	0.592
Left anterior descending artery, n (%)	7 (32%)	16 (48%)	0.282
Left circumflex artery, n (%)	6 (27%)	3 (9%)	0.133
ACC/AHA lesion class	ABSORB B1 (n=22)	SPIRIT II (n=33)	p-value
Type A, n (%)	1 (5%)	1 (3%)	1.000
Type B1, n (%)	11 (50%)	7 (24%)	0.076
Type B2, n (%)	9 (41%)	19 (66%)	0.092
Type C, n (%)	1 (5%)	1 (7%)	1.000
Pre-procedure QCA characteristics	ABSORB B1 (n=22)	SPIRIT II (n=33)	p-value
Lesion length (mm)	9.63 [7.77, 12.81]	13.90 [9.60, 16.70]	0.041
Reference vessel diameter (mm)	2.38 [2.19, 2.73]	2.90 [2.76, 3.14]	0.001
Minimum lumen diameter (mm)	0.92 [0.81, 1.30]	1.18 [0.74, 1.39]	0.680
Diameter stenosis (%)	61.42 [53.50, 66.00]	57.43 [53.11, 71.20]	0.542
Values are mean±SD or median [IQR] or n (%). ACC/AHA: American College of Cardiology/American Heart Association. *The balloon to artery ratio was derived from quantitative coronary angiography as the fraction of the largest balloon/reference vessel diameter. NS: non-significant			
Distal edge	ABSORB B1 (n=24)	SPIRIT II (n=41)	p-value
Age, yrs	63.36±9.24	59.98±10.11	0.222
Male, n (%)	18 (75%)	35 (85%)	0.329
Current smoking, n (%)	3 (12.5%)	18 (44%)	0.014
Diabetes, n (%)	4 (17%)	8 (19.5%)	1.000
Hypertension, n (%)	16 (67%)	26 (63%)	1.000
Hypercholesterolaemia, n (%)	24 (100%)	31 (77.5%)	0.009
Prior myocardial infarction, n (%)	9 (37.5%)	19 (46%)	0.611
Unstable angina, n (%)	5 (21%)	13 (32%)	0.566
Stable angina, n (%)	18 (75%)	21 (51%)	0.115
Treated vessel			
Right coronary artery, n (%)	8 (33%)	13 (28%)	0.791
Left anterior descending artery, n (%)	10 (42%)	23 (50%)	0.621
Left circumflex artery, n (%)	5 (21%)	10 (22%)	1.000

ACC/AHA lesion class	ABSORB B1 (n=24)	SPIRIT II (n=46)	p-value
Type A, n (%)	1 (4%)	1 (2.4%)	1.000
Type B1, n (%)	13 (54%)	7 (17%)	0.002
Type B2, n (%)	10 (42%)	26 (62%)	0.126
Type C, n (%)	0 (0.0%)	8 (19%)	0.043
Pre-procedure QCA characteristics	ABSORB B1 (n=24)	SPIRIT II (n=46)	p-value
Lesion length (mm)	10.13 [7.25, 13.43]	14.95 [9.60, 19.10]	0.007
Reference vessel diameter (mm)	2.60 [2.23, 3.00]	2.80 [2.50, 3.09]	0.244
Minimum lumen diameter (mm)	0.92 [0.75, 1.38]	1.06 [0.84, 1.30]	0.814
Diameter stenosis (%)	62.00 [48.50, 68.50]	57.81 [53.18, 68.50]	0.743
Values are mean±SD or median [IQR] or n (%). ACC/AHA: American College of Cardiology/American Heart Association. *The balloon to artery ratio was derived from quantitative coronary angiography as the fraction of the largest balloon/reference vessel diameter			
Proximal edge	ABSORB B1 (n=22)	SPIRIT II (n=33)	p-value
Post-procedure IVUS characteristics	ABSORB B1 (n=22)	SPIRIT II (n=33)	p-value
Vessel area (mm ²)	12.64 [10.81, 15.90]	16.27 [14.27, 18.46]	0.004
Lumen area (mm ²)	7.02 [5.80, 8.63]	7.97 [6.89, 9.77]	NS
Plaque area (mm ²)	5.51 [3.91, 7.51]	8.24 [6.62, 9.28]	0.002
Maximum balloon to artery ratio*	1.30 [1.24, 1.42]	1.21 [1.11, 1.26]	0.01
Distal edge	ABSORB B1 (n=24)	SPIRIT II (n=46)	p-value
Post-procedure IVUS characteristics	ABSORB B1 (n=24)	SPIRIT II (n=46)	p-value
Vessel area (mm ²)	11.91 [8.47, 15.45]	10.97 [9.39, 14.82]	NS
Lumen area (mm ²)	6.40 [5.65, 7.72]	6.91 [5.46, 7.81]	NS
Plaque area (mm ²)	5.03 [2.04, 7.38]	5.28 [3.20, 6.95]	NS
Maximum balloon to artery ratio*	1.25 [1.07, 1.36]	1.21 [1.11, 1.28]	NS

with a trend towards a plaque area increase of 7.55% (-4.68; 27.11) (p=0.06) (Figure 2, Figure 4 and Table 2).

DISTAL EDGE

At the distal edge no major changes were demonstrated either in the short or in the long term (Figure 3, Figure 4 and Table 2).

XIENCE V

PROXIMAL EDGE

At the 5-mm segment no major absolute or relative changes were shown in terms of vessel, lumen and plaque areas in the short term. In the long term the plaque area decreased by 6.90% (-17.86; 4.23) (p=0.035) while the lumen area remained unchanged indicating adaptive constrictive remodelling (Figure 2, Figure 5 and Table 3).

DISTAL EDGE

At the distal edge, a dynamic vascular response was evident: a compensative expansive remodelling of Δ vessel area: 5.12% (-2.64; 12.34)

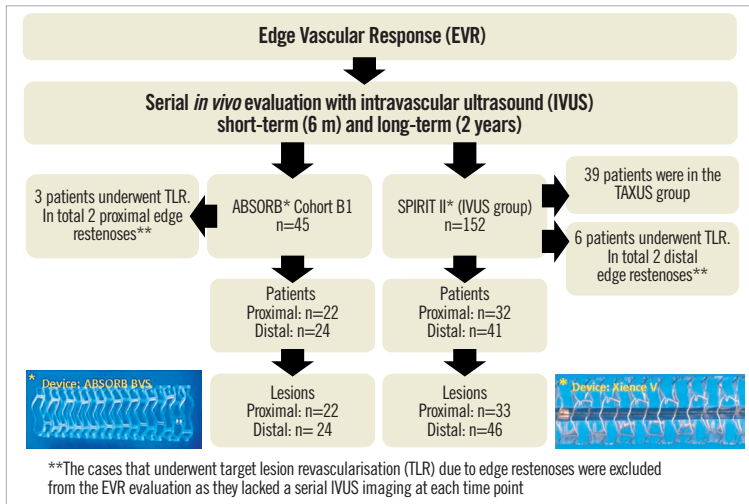


Figure 1. Flow chart of patient/lesion selection for the assessment of the edge vascular response after implantation of either an Absorb bioresorbable vascular scaffold or a metallic XIENCE V everolimus-eluting stent.

Table 2. Summary of the serial proximal and distal edge absolute/% changes following implantation of the Absorb BVS.

Proximal edge, Absorb BVS									
(n=22)	post-procedure	6 months (6 mo)	24 months (24 mo)	Absolute/% Δ post-6 mo	Absolute/% Δ 6 mo-24 mo	Absolute/% Δ post-24 mo	p-value, post-6 mo	p-value, 6 mo-24 mo	p-value, post-24 mo
Vessel area (mm ²)	12.64 [10.81, 15.90]	12.22 [10.26, 15.39]	13.66 [10.11, 15.91]	-0.19 [-0.51, 0.22]	0.17 [-0.63, 0.59]	-0.01 [-0.93, 0.76]	NS	NS	NS
				-1.35% [-3.18, 2.27]	1.05% [-3.33, 5.37]	-0.14% [-5.69, 6.58]			
Lumen area (mm ²)	7.02 [5.80, 8.63]	7.02 [5.60, 8.41]	6.11 [5.02, 8.83]	-0.25 [-0.78, 0.73]	-0.19 [-1.00, 0.36]	-0.53 [-1.22, 0.18]	NS	NS	0.027
				-3.44% [-12.56, 11.02]	-2.32% [-13.99, 4.99]	-6.68% [-17.33, 2.08]			
Plaque area (mm ²)	5.51 [3.91, 7.51]	5.07 [3.86, 7.25]	6.09 [3.97, 8.04]	-0.25 [-0.97, 0.55]	0.33 [-0.04, 1.15]	0.48 [-0.25, 1.03]	NS	NS	NS
				-4.16% [-12.76, 16.75]	6.02% [-0.67, 19.17]	7.55% [-4.68, 27.11]			
Distal edge, Absorb BVS									
(n=24)	post-procedure	6 months (6 mo)	24 months (24 mo)	Absolute/% Δ post-6 mo	Absolute/% Δ 6 mo-24 mo	Absolute/% Δ post-24 mo	p-value, post-6 mo	p-value, 6 mo-24 mo	p-value, post-24 mo
Vessel area (mm ²)	11.91 [8.47, 15.45]	11.74 [8.92, 15.71]	12.05 [8.79, 14.71]	0.08 [-0.51, 1.05]	-0.03 [-0.59, 0.71]	0.20 [-0.49, 0.91]	NS	NS	NS
				0.57% [-3.67, 9.92]	-0.34% [-4.39, 4.32]	1.83% [-4.02, 9.27]			
Lumen area (mm ²)	6.40 [5.65, 7.72]	6.42 [5.26, 7.64]	6.09 [5.34, 7.80]	-0.08 [-0.59, 0.64]	-0.13 [-0.89, 0.43]	-0.08 [-0.82, 0.69]	NS	NS	NS
				-0.85% [-9.46, 10.71]	-2.43% [-11.02, 6.72]	-1.23% [-10.58, 7.82]			
Plaque area (mm ²)	5.03 [2.04, 7.38]	4.90 [2.44, 7.63]	5.12 [2.59, 6.97]	0.22 [-0.59, 0.84]	0.02 [-0.34, 0.49]	0.24 [-0.45, 0.62]	NS	NS	NS
				7.58% [-9.54, 17.03]	0.45% [-8.13, 8.77]	3.00% [-6.47, 35.79]			

Data are expressed as medians [interquartile ranges]. Analysis was performed at lesion level. NS: non-significant; Δ: delta

Table 3. Summary of the serial proximal and distal edge absolute/% changes following implantation of a XIENCE V everolimus-eluting metallic stent (XIENCE V).

Proximal edge, XIENCE V									
(n=33)	post-procedure	6 months (6 mo)	24 months (24 mo)	Absolute/% Δ post-6 mo	Absolute/% Δ 6 mo-24 mo	Absolute/% Δ post-24 mo	p-value, post-6 mo	p-value, 6 mo-24 mo	p-value, post-24 mo
Vessel area (mm ²)	16.27 [14.27, 18.46]	16.30 [13.11, 18.92]	15.68 [12.57, 18.90]	-0.17 [-1.42, 0.67]	-0.73 [-1.19, 0.16]	-0.37 [-2.37, 0.68]	NS	0.022	NS
				-1.03% [-8.83, 4.87]	-4.71% [-8.78, 0.92]	-2.63% [-13.80, 3.75]			
Lumen area (mm ²)	7.97 [6.89, 9.77]	7.49 [6.59, 10.29]	7.40 [5.70, 10.87]	-0.16 [-0.68, 0.60]	-0.22 [-0.89, 0.55]	-0.25 [-1.26, 1.22]	NS	NS	NS
				-1.70% [-9.77, 6.90]	-2.98% [-11.91, 8.19]	-3.61% [-14.92, 14.43]			
Plaque area (mm ²)	8.24 [6.62, 9.28]	7.63 [6.49, 9.28]	7.05 [5.75, 8.64]	-0.07 [-0.96, 0.49]	-0.58 [-1.25, 0.35]	-0.61 [-1.48, 0.28]	NS	NS	0.035
				-1.06% [-9.90, 6.53]	-6.42% [-15.49, 6.92]	-6.90% [-17.86, 4.23]			
Distal edge, XIENCE V									
(n=46)	post-procedure	6 months (6 mo)	24 months (24 mo)	Absolute/% Δ post-6 mo	Absolute/% Δ 6 mo-24 mo	Absolute/% Δ post-24 mo	p-value, post-6 mo	p-value, 6 mo-24 mo	p-value, post-24 mo
Vessel area (mm ²)	10.97 [9.39, 14.82]	11.94 [9.85, 15.48]	11.95 [9.30, 14.29]	0.62 [-0.22, 1.27]	-0.50 [-1.19, 0.14]	-0.09 [-0.89, 0.91]	0.002	0.0046	NS
				5.12% [-2.64, 12.34]	-3.93% [-8.26, 1.39]	-1.00% [-7.15, 7.84]			
Lumen area (mm ²)	6.91 [5.46, 7.81]	7.08 [5.81, 8.22]	6.77 [5.96, 8.08]	0.31 [-0.64, 1.25]	-0.25 [-0.91, 0.28]	-0.06 [-0.66, 0.72]	NS	NS	NS
				4.31% [-8.32, 18.84]	-3.59% [-12.64, 3.61]	-1.12% [-11.19, 11.86]			
Plaque area (mm ²)	5.28 [3.20, 6.95]	5.10 [3.56, 7.23]	5.11 [3.18, 7.04]	0.17 [-0.15, 0.65]	-0.12 [-0.42, 0.32]	-0.04 [-0.56, 0.75]	NS	NS	NS
				5.77% [-3.59, 12.66]	-2.82% [-9.40, 6.26]	-1.02% [-9.44, 15.66]			

Data are expressed as medians [interquartile ranges]. Analysis was performed at lesion level. NS: non-significant; Δ: delta

Table 4. Comparison of the changes (deltas) between the groups treated with either a bioresorbable or a metallic platform at the proximal and distal edges (NS: non-significant).

Proximal edge				
p-value	Device type	post to 6 months	6 months to 2 years	post to 2 years
Δ Vessel area (mm ²)	BVS	NS	0.029	NS
	MP			
Δ Lumen area (mm ²)	BVS	NS	NS	NS
	MP			
Δ Plaque area (mm ²)	BVS	NS	0.002	0.006
Distal edge				
p-value	Device type	post to 6 months	6 months to 2 years	post to 2 years
Δ Vessel area (mm ²)	BVS	NS	NS	NS
	MP			
Δ Lumen area (mm ²)	BVS	NS	NS	NS
	MP			
Δ Plaque area (mm ²)	BVS	NS	NS	NS
	MP			

(p=0.002) at six months that tended to regress at two years losing its statistical significance (Figure 3, Figure 5 and Table 3).

Discussion

The main findings of this study are:

- Short term: i) the vessels treated with an Absorb BVS did not show any signs of remodelling or LL either at the proximal or at the distal edges; ii) the vessels treated with a XIENCE V did not show any signs of remodelling or LL at the proximal edge; however, compensative expansive remodelling at the distal edge was observed.
- Long term: i) the vessels treated with the Absorb BVS showed evidence of proximal edge LL (this finding is consistent with the previously reported reduction in the minimum lumen diameter assessed angiographically at the proximal edge - from post procedure: 2.39±0.50 mm, to two years: 2.31±0.42 [p=0.04])¹⁷; ii) the vessels treated with a XIENCE V did not show any signs of LL at either the proximal or the distal stent edges. At the proximal edge, a significant plaque decrease became evident with a trend towards adaptive constrictive remodelling.

The current analysis used serial IVUS data to evaluate for the first time the short-term and long-term EVR after Absorb BVS and

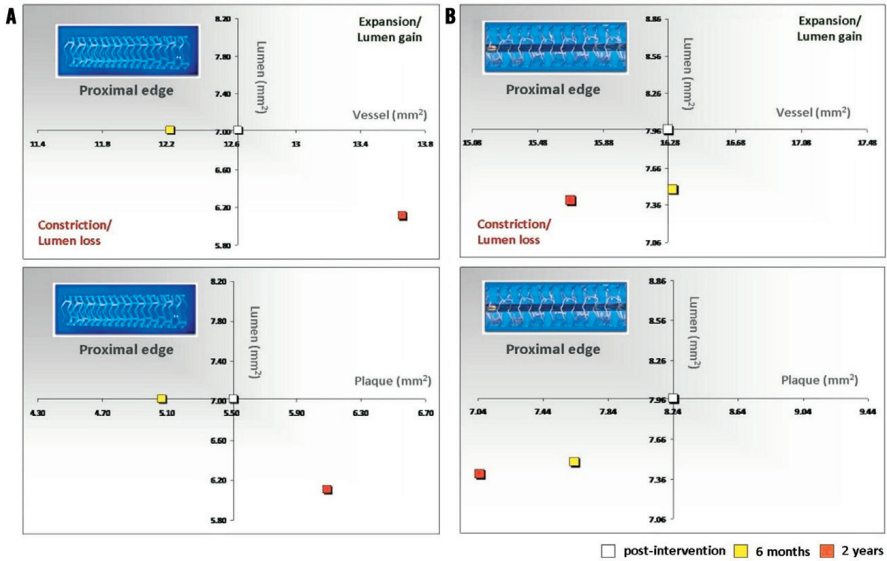


Figure 2. Absolute values of the vessel and plaque areas related to lumen area at the proximal edges of the Absorb BVS (A) and XIENCE V (B) devices.

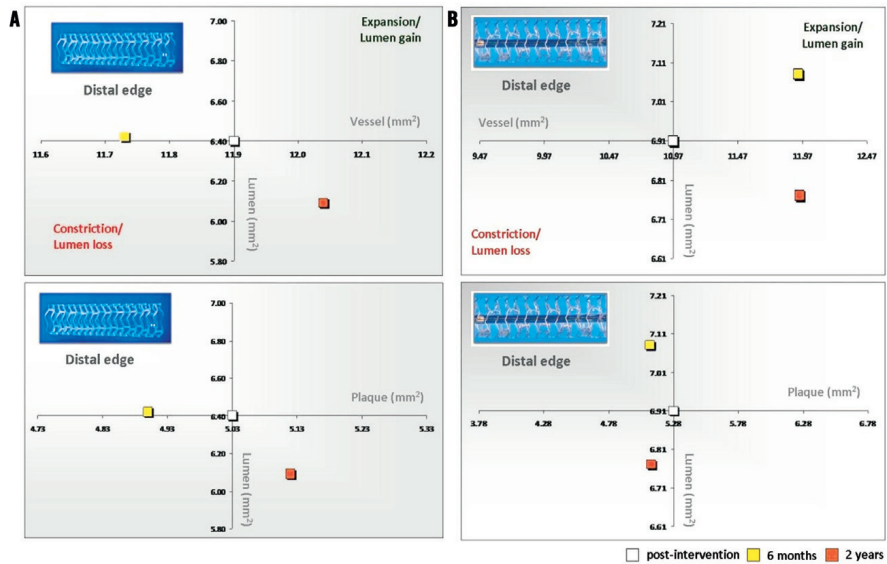


Figure 3. Absolute values of the vessel and plaque areas related to lumen area at the distal edges of the Absorb BVS (A) and XIENCE V (B) devices.

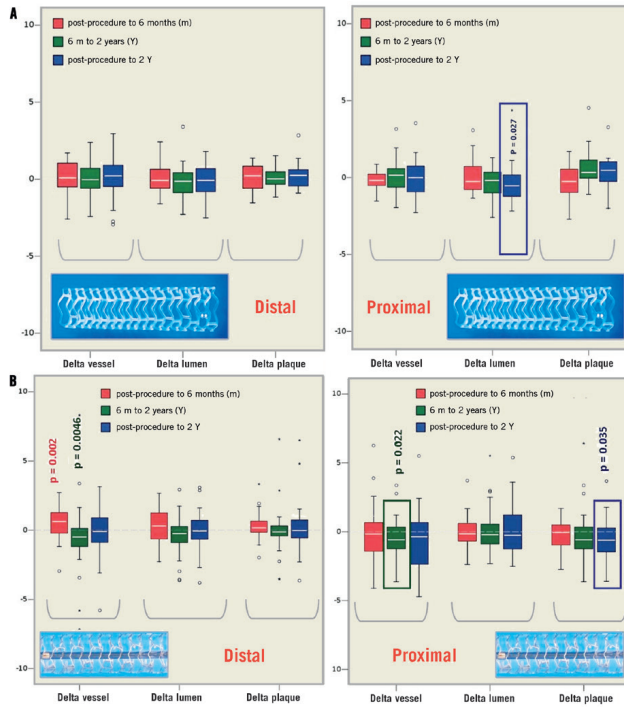


Figure 4. A) The changes (deltas) in vessel, lumen and plaque areas at the proximal and distal edges following implantation of the Absorb BVS post procedure, at 6 months and 2 years (significant changes are demonstrated with the p-value). B) The changes (deltas) in vessel, lumen and plaque areas at the proximal and distal edges following implantation of the XIENCE V EES, post procedure, at 6 months and 2 years (significant changes are demonstrated with the p-value).

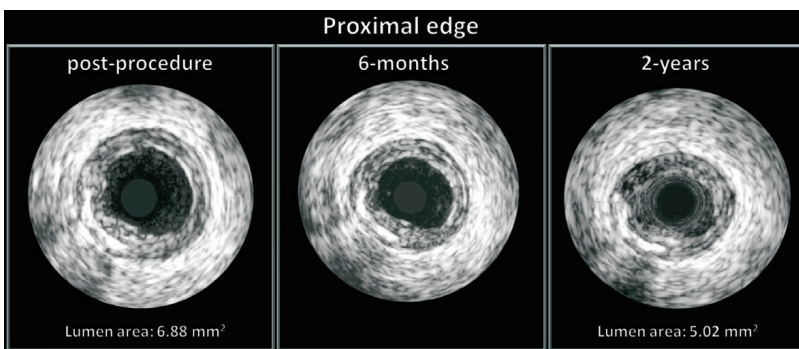


Figure 5. The vascular response at the proximal edge following implantation of a bioresorbable vascular scaffold. Greyscale IVUS cross-sections post procedure, at 6 months and 2 years demonstrating the gradual lumen loss. At the 5-mm proximal segment of this patient the mean lumen area decreased from 6.88 mm² (post procedure) to 5.02 mm² (2 years).

XIENCE V EES implantation. Although both devices share the same release kinetics and dose density of everolimus, we found a different vascular response at the proximal and distal edges, potentially attributed to the different mechanical properties of the investigated platforms.

The implantation of a device either metallic or polymeric induces local arterial stiffness of the stented/scaffolded segment, abrogating the physiologic cyclic strain and its vascular compliance and further creating compliance mismatch with the adjacent proximal and distal edges¹⁸. It has recently been confirmed that bioresorbable scaffolds can also transiently reduce the arterial compliance resulting in compliance mismatch between the scaffolded and the adjacent segments, an observation that tended to disappear at short and mid term (one year) following implantation of the Absorb BVS¹⁹. Additionally, the changes in three-dimensional vessel geometry and vessel curvature following implantation of either a polymeric or a metallic device alter the flow velocities at the transition zones (proximal and distal edges) creating regions of disturbed laminar flow, flow separation with retrograde axial velocities (low endothelial shear stress [ESS] regions) known to be proatherogenic and to alter cell mechanotransduction^{19,20,22}. These changes may potentially cause adaptive remodelling of the extracellular matrix through alterations of the physiological local mechanical loading conditions with various patterns of compensation (from poor to overcompensation)²³.

This concept became evident with the XIENCE V metallic EES in regard to vascular remodelling and matrix production that appeared to have a dynamic response at the distal edge. In particular, in the short term, a compensatory expansive remodelling of 5.12% (-2.64; 12.34) ($p=0.002$) was evident to counterbalance a trend towards plaque increase of 5.77% (-3.59; 12.66) ($p=0.083$) (low ESS region) that was further converted into constrictive remodelling between six months and two years resulting in a neutral net effect from post procedure to two years.

PROXIMAL EDGE

At this segment, the vessels treated with an Absorb BVS did not show any major changes at short-term FU; however, at long-term FU a slight but statistically significant LL was observed, attributed to plaque area increase. LL at the proximal edge has previously been reported with bare metal stents and DES; however, the reduction in lumen area with the Absorb BVS commenced at a later time point (after six months), suggesting that different mechanisms are involved in this process. The recently reported plaque/media and neointima increase from six months to two years in the scaffolded segment has been attributed to the vessel wall/scaffold interaction during the bioresorption process that affects the vessel wall physiology and alters the plaque's components^{18,24,25}. We surmise that the LL and plaque increase noted in the proximal edge are due to the potentially insufficient suppression of the EVR by the antiproliferative drug. On the contrary, the vessels treated with a XIENCE V stent did not show any signs of LL at both FU points. At late FU, a reduction in the plaque and vessel area became evident indicating an adaptive constrictive remodelling. This effect could be attributed

to the mechanical injury following stent implantation which triggers a pathophysiological process that leads to constrictive remodelling²⁶. This process appears to be initiated immediately after device implantation; however, the changes in plaque and vessel wall dimensions become significant at two years. In contrast to the bare metal stents and SES, the vessel response at the proximal edge of a XIENCE V EES did not affect the lumen area. This observation could be attributed to the smaller strut thickness of the XIENCE V (89 μm vs. 152 μm in the first-generation SES) and the presence of the antiproliferative drug everolimus that can potentially delay and attenuate the vascular tissue response^{27,28}.

DISTAL EDGE

In contrast to the proximal edge, at the distal edge the vessels treated with an Absorb BVS did not show any major changes either at short-term or at long-term FU. This difference in the EVR can potentially be explained by the sufficient concentration of the everolimus elution at the downstream vessel which can inhibit atherosclerosis and reduce local inflammation. Everolimus has been shown to inhibit strongly the development of progressive atherosclerotic lesions in animal models: 1) by delaying the transition from early macrophage-enriched lesions to advanced atherosclerotic plaques in LDL receptor $-/-$ (knockout) mice; and 2) by selective clearance of macrophages through autophagy in atherosclerotic plaques²⁹⁻³¹.

Our findings in the XIENCE V EES are in agreement with those previously reported, as there were no significant differences in the lumen and plaque area at short-term FU³²⁻³⁴. An increase in the vessel area was noted at six months which, however, appeared to be temporal as it decreased at two years. Of note, these observations were not accompanied by statistically significant changes in the lumen and plaque.

Expansive remodelling has previously been reported at the distal edge of other metallic DES and has been attributed to endothelial dysfunction. A dysfunctional endothelium can promote expansive remodelling and plaque progression especially in an unfavourable haemodynamic environment created by the modified vessel geometry and the compliance mismatch demonstrated in experimental setting at the distal edge³⁵⁻³⁷. Endothelial dysfunction at the edges of a DES can be present up to one year following device implantation^{38,39}. Unfortunately, long-term FU results which would allow us to estimate the duration of the endothelial dysfunction and the effect of a functional/dysfunctional endothelium on the progression/regression of atherosclerosis at the edges of these stents are not available.

Conclusion

The fully bioresorbable device (Absorb BVS) and the metallic platform (XIENCE V) demonstrated a different EVR at six months and two years which is likely to be associated with the distinct properties of each device. The serial assessment of the XIENCE V EES did not show any LL at both FU points, while the observed significant proximal edge LL induced by the Absorb BVS at two years did not have any clinical implications. The upcoming imaging FU of the ABSORB Cohort B2 trial at three years is anticipated to provide additional information about the EVR after Absorb BVS implantation.

Limitations

The major limitation of the present analysis is the small number of investigated proximal and distal edges (patient/lesion level). Thus the present study may be underpowered to evaluate the exact changes at the stent/scaffold edges during follow-up and the p-values should be considered exploratory and interpreted with caution. However, these cohorts of patients represent the only available data on the serial assessment of the edge vascular response utilising a metallic and a bioresorbable device at three different imaging time points. The approximate final tested samples of the Cohort B1 and SPIRIT II studies were <50%. The reasons for this were: 1) the dropout of patients at follow-up and exclusion of the unpaired samples from our final analysis; 2) the exclusion of cases according to the standard operational procedure of the independent core laboratory (Cardialysis, Rotterdam, The Netherlands) with: i) side-branch outgrowth of >90 degrees at the side of the scaffold edge that did not allow the analysis of the complete 5-mm segment; ii) vessel wall out of the field of the vessel; and 3) the exclusion of cases adjudicated as target lesion revascularisation – some of them attributed to edge restenosis – where serial assessment was not possible.

Although the SPIRIT II trial had more complex lesions compared to the ABSORB Cohort B, this was an exploratory study that investigated for the first time a second generation of devices with different platforms (metal vs. polymer) in a follow-up spanning two years. Future studies are expected to validate these preliminary results.

Funding

Abbott Vascular was the sponsor of the Absorb Cohort B trial.

Appendix

AUTHOR AFFILIATIONS

1. Thoraxcenter, Erasmus University Medical Center, Rotterdam, The Netherlands; 2. Andreas Gruentzig Cardiovascular Centre, Department of Interventional Cardiology, Emory University School of Medicine, Atlanta, GA, USA; 3. Cardialysis, Rotterdam, The Netherlands; 4. Cardiovascular Center, Aalst, Belgium; 5. Institut Jacques Cartier, Massy, France; 6. Skejby Sygehus, Aarhus University Hospital, Skejby, Denmark; 7. Maastad Hospital, Rotterdam, The Netherlands; 8. Jagiellonian University, Krakow, Poland; 9. Catharina Hospital, Eindhoven, The Netherlands; 10. Bern University Hospital, Bern, Switzerland; 11. St Vincent's Hospital, Fitzroy, Australia; 12. Christchurch Hospital, Christchurch, New Zealand; 13. Abbott Vascular, Diegem, Belgium; 14. Abbott Vascular, Santa Clara, CA, USA; 15. Auckland City Hospital, Auckland, New Zealand

Conflict of interest statement

K. Miquel-Hebert, C. Dorange, R. Rapoza and S. Veldhof are employees of Abbott Vascular. H.M. Garcia-Garcia is an employee of Cardialysis. The other authors have no conflicts of interest to declare. The Guest Editor, G. Guagliumi, is a consultant for Boston Scientific, St. Jude Medical, Volcano Corporation, and Cordis; and has received grant support from Abbott Vascular, Medtronic, Boston Scientific, and LightLab.

References

- Garg S, Serruys PW. Coronary stents: looking forward. *J Am Coll Cardiol*. 2010;56:S43-78.
- Garg S, Serruys PW. Coronary stents: current status. *J Am Coll Cardiol*. 2010;56:S1-42.
- Albiero R, Adamian M, Kobayashi N, Amato A, Vaghetti M, Di Mario C, Colombo A. Short- and intermediate-term results of (32)P radioactive beta-emitting stent implantation in patients with coronary artery disease: The Milan Dose-Response Study. *Circulation*. 2000;101:18-26.
- Serruys PW, Kay IP. I like the candy, I hate the wrapper: the (32)P radioactive stent. *Circulation*. 2000;101:3-7.
- Albiero R, Nishida T, Adamian M, Amato A, Vaghetti M, Corvaja N, Di Mario C, Colombo A. Edge restenosis after implantation of high activity (32)P radioactive beta-emitting stents. *Circulation*. 2000;101:2454-7.
- van Der Giessen WJ, Regar E, Hartevelde MS, Coen VL, Bhagwandien R, Au A, Levendag PC, Ligthart J, Serruys PW, den Boer A, Verdouw PD, Boersma E, Hu T, van Beusekom HM. "Edge Effect" of (32)P radioactive stents is caused by the combination of chronic stent injury and radioactive dose falloff. *Circulation*. 2001;104:2236-41.
- Costa MA, Angiolillo DJ, Tannenbaum M, Driesman M, Chu A, Patterson J, Kuehl W, Battaglia J, Dabbons S, Shamoon F, Flieshman B, Niederman A, Bass TA. Impact of stent deployment procedural factors on long-term effectiveness and safety of sirolimus-eluting stents (final results of the multicenter prospective STLLR trial). *Am J Cardiol*. 2008;101:1704-11.
- Farooq V, Gogas BD, Serruys PW. Restenosis: delineating the numerous causes of drug-eluting stent restenosis. *Circ Cardiovasc Interv*. 2011;4:195-205.
- Hoffmann R, Guagliumi G, Musumeci G, Reimers B, Petronio AS, Disco C, Amoroso G, Moses JW, Fitzgerald PJ, Schofer J, Leon MB, Breithardt G. Vascular response to sirolimus-eluting stents delivered with a nonaggressive implantation technique: comparison of intravascular ultrasound results from the multicenter, randomized E-SIRIUS, and SIRIUS trials. *Catheter Cardiovasc Interv*. 2005;66:499-506.
- Garcia-Garcia HM, Gonzalo N, Tanimoto S, Meliga E, de Jaegere P, Serruys PW. Characterization of edge effects with paclitaxel-eluting stents using serial intravascular ultrasound radiofrequency data analysis: the BETAX (BEside TAXus) Study. *Rev Esp Cardiol*. 2008;61:1013-9.
- Gogas BD, Serruys PW, Diletto R, Farooq V, Brugaletta S, Radu MD, Heo JH, Onuma Y, van Geuns RJ, Regar E, De Bruyne B, Chevalier B, Thuesen L, Smits PC, Dudek D, Koolen J, Windecker S, Whitbourn R, Miquel-Hebert K, Dorange C, Rapoza R, Garcia-Garcia HM, McClean D, Ormiston JA. Vascular response of the segments adjacent to the proximal and distal edges of the ABSORB everolimus-eluting bioresorbable vascular scaffold: 6-month and 1-year follow-up assessment: a virtual histology intravascular ultrasound study from the first-in-man ABSORB cohort B trial. *JACC Cardiovasc Interv*. 2012;5:656-65.

12. Onuma Y, Serruys PW, Perkins LE, Okamura T, Gonzalo N, Garcia-Garcia HM, Regar E, Kamberi M, Powers JC, Rapoza R, van Beusekom H, van der Giessen W, Virmani R. Intracoronary optical coherence tomography and histology at 1 month and 2, 3, and 4 years after implantation of everolimus-eluting bioresorbable vascular scaffolds in a porcine coronary artery model: an attempt to decipher the human optical coherence tomography images in the ABSORB trial. *Circulation*. 2010;122:2288-300.
13. Gogas BD, Radu M, Onuma Y, Perkins L, Powers JC, Gomez-Lara J, Farooq V, Garcia-Garcia HM, Diletti R, Rapoza R, Virmani R, Serruys PW. Evaluation with in vivo optical coherence tomography and histology of the vascular effects of the everolimus-eluting bioresorbable vascular scaffold at two years following implantation in a healthy porcine coronary artery model: implications of pilot results for future pre-clinical studies. *Int J Cardiovasc Imaging*. 2012;28:499-511.
14. Mintz GS, Garcia-Garcia HM, Nicholls SJ, Weissman NJ, Bruining N, Crowe T, Tardif JC, Serruys PW. Clinical expert consensus document on standards for acquisition, measurement and reporting of intravascular ultrasound regression/progression studies. *EuroIntervention*. 2011;6:1123-30, 9.
15. Mintz GS, Nissen SE, Anderson WD, Bailey SR, Erbel R, Fitzgerald PJ, Pinto FJ, Rosenfield K, Siegel RJ, Tuzcu EM, Yock PG. American College of Cardiology Clinical Expert Consensus Document on Standards for Acquisition, Measurement and Reporting of Intravascular Ultrasound Studies (IVUS): a report of the American College of Cardiology Task Force on Clinical Expert Consensus Documents. *J Am Coll Cardiol*. 2001;37:1478-92.
16. Gogas BD, Onuma Y, van Geuns RJ, Serruys PW. The edge vascular response following implantation of a fully bioresorbable device: 'A miss always counts'. *Int J Cardiol*. 2012;158:455-7.
17. Ormiston JA, Serruys PW, Onuma Y, van Geuns RJ, de Bruyne B, Dudek D, Thuesen L, Smits PC, Chevalier B, McClean D, Koolen J, Windecker S, Whitbourn R, Meredith I, Dorange C, Veldhof S, Hebert KM, Rapoza R, Garcia-Garcia HM. First serial assessment at 6 months and 2 years of the second generation of absorb everolimus-eluting bioresorbable vascular scaffold: a multi-imaging modality study. *Circ Cardiovasc Interv*. 2012;5:620-32.
18. Tortoriello A, Pedrizzetti G. Flow-tissue interaction with compliance mismatch in a model stented artery. *J Biomech*. 2004;37:1-11.
19. Brugaletta S, Gogas BD, Garcia-Garcia HM, Farooq V, Girasis C, Heo JH, van Geuns RJ, de Bruyne B, Dudek D, Koolen J, Smits P, Veldhof S, Rapoza R, Onuma Y, Ormiston J, Serruys PW. *Circ J*. 2012;76:1616-23.
20. Thury A, Wentzel JJ, Vinke RV, Gijsen FJ, Schuurbiens JC, Krams R, de Feyter PJ, Serruys PW, Slager CJ. Images in cardiovascular medicine. Focal in-stent restenosis near step-up: roles of low and oscillating shear stress? *Circulation*. 2002;105:e185-7.
21. Serruys PW, Garcia-Garcia HM, Onuma Y. From metallic cages to transient bioresorbable scaffolds: change in paradigm of coronary revascularization in the upcoming decade? *Eur Heart J*. 2012;33:16-25b.
22. Chatzizisis YS, Coskun AU, Jonas M, Edelman ER, Feldman CL, Stone PH. Role of endothelial shear stress in the natural history of coronary atherosclerosis and vascular remodeling: molecular, cellular, and vascular behavior. *J Am Coll Cardiol*. 2007;49:2379-93.
23. Gupta V, Grande-Allen KJ. Effects of static and cyclic loading in regulating extracellular matrix synthesis by cardiovascular cells. *Cardiovasc Res*. 2006;72:375-83.
24. Oberhauser JP, Hossainy S, Rapoza RJ. Design principles and performance of bioresorbable polymeric vascular scaffolds. *EuroIntervention*. 2009;5 Suppl F:F15-22.
25. Vorpahl M, Finn AV, Nakano M, Virmani R. The bioabsorption process: tissue and cellular mechanisms and outcomes. *EuroIntervention*. 2009;5 Suppl F:F28-35.
26. Newby AC. Dual role of matrix metalloproteinases (matrixins) in intimal thickening and atherosclerotic plaque rupture. *Physiol Rev*. 2005;85:1-31.
27. Pache J, Kastrati A, Mehilli J, Schühlen H, Dotzer F, Hausleiter J, Fleckenstein M, Neumann FJ, Sattlerberger U, Schmitt C, Müller M, Dirschinger J, Schomig A. Intracoronary stenting and angiographic results: strut thickness effect on restenosis outcome (ISAR-STERO-2) trial. *J Am Coll Cardiol*. 2003;41:1283-8.
28. Kastrati A, Mehilli J, Dirschinger J, Dotzer F, Schühlen H, Neumann FJ, Fleckenstein M, Pfaffert C, Seyfarth M, Schomig A. Intracoronary stenting and angiographic results: strut thickness effect on restenosis outcome (ISAR-STERO) trial. *Circulation*. 2001;103:2816-21.
29. Virmani R, Kolodgie FD, Burke AP, Farb A, Schwartz SM. Lessons from sudden coronary death: a comprehensive morphological classification scheme for atherosclerotic lesions. *Arterioscler Thromb Vasc Biol*. 2000;20:1262-75.
30. Mueller MA, Beutner F, Teupser D, Ceglarek U, Thiery J. Prevention of atherosclerosis by the mTOR inhibitor everolimus in LDLR^{-/-} mice despite severe hypercholesterolemia. *Atherosclerosis*. 2008;198:39-48.
31. Verheye S, Martinet W, Kockx MM, Knaapen MW, Salu K, Timmermans JP, Ellis JT, Kilpatrick DL, De Meyer GR. Selective clearance of macrophages in atherosclerotic plaques by autophagy. *J Am Coll Cardiol*. 2007;49:706-15.
32. Serruys PW, Degertekin M, Tanabe K, Russell ME, Guagliumi G, Webb J, Hamburger J, Rutsch W, Kaiser C, Whitbourn R, Camenzind E, Meredith I, Reeves F, Nienaber C, Benit E, Disco C, Koglin J, Colombo A. Vascular responses at proximal and distal edges of paclitaxel-eluting stents: serial intravascular ultrasound analysis from the TAXUS II trial. *Circulation*. 2004;109:627-33.
33. Wakabayashi K, Mintz GS, Weissman NJ, Stone GW, Ellis SG, Grube E, Ormiston JA, Turco MA, Pakala R, Xue Z, Desale S, Laynez-Camicero A, Romaguera R, Sardi G, Pichard AD, Waksman R. Impact of drug-eluting stents on distal vessels. *Circ Cardiovasc Interv*. 2012;5:211-9.
34. Weissman NJ, Ellis SG, Grube E, Dawkins KD, Greenberg JD, Mann T, Cannon LA, Cambier PA, Fernandez S, Mintz GS, Mandinov L, Koglin J, Stone GW. Effect of the polymer-based,

paclitaxel-eluting TAXUS Express stent on vascular tissue responses: a volumetric intravascular ultrasound integrated analysis from the TAXUS IV, V, and VI trials. *Eur Heart J.* 2007;28:1574-82.

35. Hofma SH, van der Giessen WJ, van Dalen BM, Lemos PA, McFadden EP, Sianos G, Ligthart JM, van Essen D, de Feyter PJ, Serruys PW. Indication of long-term endothelial dysfunction after sirolimus-eluting stent implantation. *Eur Heart J.* 2006;27:166-70.

36. Kim JW, Suh SY, Choi CU, Na JO, Kim EJ, Rha SW, Park CG, Seo HS, Oh DJ. Six-month comparison of coronary endothelial dysfunction associated with sirolimus-eluting stent versus Paclitaxel-eluting stent. *JACC Cardiovasc Interv.* 2008;1:65-71.

37. Jimenez-Quevedo P, Sabate M, Angiolillo DJ, Costa MA, Alfonso F, Gomez-Hospital JA, Hernandez-Antolin R, Banuelos C, Goicolea J, Fernandez-Aviles F, Bass T, Escaned J, Moreno R, Fernandez C, Macaya C. Vascular effects of sirolimus-eluting versus bare-metal stents in diabetic patients: three-dimensional ultrasound results of the Diabetes and Sirolimus-Eluting Stent (DIABETES) Trial. *J Am Coll Cardiol.* 2006;47:2172-9.

38. Traub O, Berk BC. Laminar shear stress: mechanisms by which endothelial cells transduce an atheroprotective force. *Arterioscler Thromb Vasc Biol.* 1998;18:677-85.

39. Hamilos M, Sarma J, Ostojic M, Cuisset T, Sarno G, Melikian N, Ntalianis A, Muller O, Barbato E, Beleslin B, Sagic D, De Bruyne B, Bartunek J, Wijns W. Interference of drug-eluting stents with endothelium-dependent coronary vasomotion: evidence for device-specific responses. *Circ Cardiovasc Interv.* 2008;1:193-200.

Online data supplement

Online Appendix. The edge vascular response following implantation of the Absorb everolimus-eluting bioresorbable vascular scaffold and the XIENCE V metallic everolimus-eluting stent. First serial follow-up assessment at six months and two years.

Online Table 1. QCA analysis of all available patients in the Absorb Cohort B1 trial.

Online Table 2. Summary of the proximal and distal edge absolute/% changes following implantation of the Absorb BVS including imputation of data from TLR patients.

Online Table 3. Summary of the proximal and distal edge absolute/% changes following implantation of a XIENCE V everolimus-eluting metallic stent (XIENCE V) including imputation of data from TLR patients.

Online Table 4. Comparison of the changes (deltas) between the groups treated with either a bioresorbable or a metallic platform at the proximal and distal edges including imputation of data from TLR patients.

Online Table 5. Summary of the serial proximal edge absolute/% changes regarding tissue area/percentage composition following implantation of the Absorb BVS.

Online Table 6. Summary of the serial distal edge absolute/% changes regarding tissue area/percentage composition following implantation of the Absorb BVS.

Online Figure 1. Serial proximal and distal edge per mm absolute changes regarding tissue composition from post intervention to 6 months following implantation of the Absorb BVS.

Online Figure 2. Serial proximal and distal edge per mm changes regarding tissue composition from 6 months to 2 years following implantation of the Absorb BVS.

Online Figure 3. Serial changes of the lumen (A), plaque (B) and vessel (C) areas at the proximal edge of the Absorb BVS on a per lesion basis.

Online Figure 4. Serial changes of the lumen (A), plaque (B) and vessel (C) areas on a per lesion basis at the proximal edge of the XIENCE V stent.

Online Figure 5. Serial changes of the lumen (A), plaque (B) and vessel (C) areas on a per lesion basis at the distal edge of the Absorb BVS.

Online Figure 6. Serial changes of the lumen (A), plaque (B) and vessel (C) areas on a per lesion basis at the distal edge of the XIENCE V stent.

Online data supplement

The edge vascular response following implantation of the Absorb everolimus-eluting bioresorbable vascular scaffold and the XIENCE V metallic everolimus-eluting stent. First serial follow-up assessment at 6 months and 2 years.

Online Table 1. QCA analysis of all available patients in the ABSORB Cohort B1 trial.

		Post-procedure (N=45) (L=45)	6-month (N=45) (L=45)	2-year (N=45) (L=45)
Proximal reference vessel diameter (mm)	Mean±SD (n) Median [Q1, Q3]	2.86±0.39 (45) 2.81 [2.61, 3.13]	2.72±0.36 (42) 2.73 [2.42, 2.99]	2.67±0.36 (38) 2.65 [2.42, 2.90]
Distal reference vessel diameter (mm)	Mean±SD (n) Median [Q1, Q3]	2.63±0.35 (44) 2.63 [2.38, 2.85]	2.55±0.37 (41) 2.55 [2.29, 2.77]	2.45±0.32 (37) 2.43 [2.27, 2.66]
Proximal minimal luminal diameter (mm)	Mean±SD (n) Median [Q1, Q3]	2.45±0.51 (45) 2.41 [2.12, 2.77]	2.39±0.49 (42) 2.39 [2.10, 2.65]	2.25±0.54 (38) 2.21 [2.04, 2.55]
Distal minimal luminal diameter (mm)	Mean±SD (n) Median [Q1, Q3]	2.23±0.43 (44) 2.12 [1.91, 2.54]	2.16±0.36 (41) 2.07 [1.93, 2.48]	2.11±0.35 (37) 2.01 [1.84, 2.37]
Proximal percent diameter stenosis (%)	Mean±SD (n) Median [Q1, Q3]	14.54±10.51 (45) 12.33 [6.00, 22.00]	12.52±11.48 (42) 11.00 [7.50, 16.50]	15.86±14.25 (38) 13.42 [6.33, 21.00]
Distal percent diameter stenosis (%)	Mean±SD (n) Median [Q1, Q3]	15.25±9.64 (44) 13.08 [8.50, 21.00]	14.86±9.50 (41) 14.50 [8.00, 21.00]	13.85±7.18 (37) 14.00 [8.00, 18.00]
Proximal late loss (mm)	Mean±SD (n) Median [Q1, Q3]		0.07±0.28 (42) 0.08 [-0.06, 0.20]	0.12±0.36 (38) 0.09 [-0.06, 0.29]
Distal late loss (mm)	Mean±SD (n) Median [Q1, Q3]		0.06±0.29 (41) 0.07 [-0.18, 0.23]	0.04±0.25 (37) 0.07 [-0.13, 0.24]
Proximal binary restenosis	[95% Confidence Interval]		2.4% (1/42) [0.06%, 12.57%]	5.3% (2/38) [0.64%, 17.75%]
Distal binary restenosis	[95% Confidence Interval]		0.0% (0/41) [0.00%, 8.60%]	0.0% (0/37) [0.00%, 9.49%]

Online table 2. Summary of the proximal and distal edge absolute/% changes following implantation of the Absorb BVS including imputation of data from TLR patients.

Proximal edge, Absorb BVS									
(n=23)	post-procedure	6 months (6 mo)	24 months (24 mo)	Absolute/% Δ post-6 mo	Absolute/% Δ 6 mo-24 mo	Absolute/% Δ post-24 mo	p-value, post-6 mo	p-value, 6 mo-24 mo	p-value, post-24 mo
Vessel area (mm ²)	12.88 [10.81, 16.87]	12.47 [10.26, 15.79]	13.77 [10.11, 17.36]	-0.16 [-0.51, 0.31]	0.12 [-0.63, 0.59]	0.01 [-0.93, 0.90]	NS	NS	NS
				-1.08% [-3.18, 2.70]	0.95% [-3.33, 5.37]	0.07% [-5.69, 6.74]			
Lumen area (mm ²)	7.15 [5.80, 8.65]	7.15 [5.60, 8.49]	6.15 [5.02, 8.86]	-0.24 [-0.78, 0.73]	-0.14 [-1.00, 0.36]	-0.50 [-1.22, 0.18]	NS	NS	0.020
				-2.77% [-12.56, 11.02]]	-2.26% [-13.99, 4.99]	-6.60% [-17.33, 2.08]			
Plaque area (mm ²)	5.13 [3.91, 7.51]	5.13 [3.86, 7.42]	6.09 [3.97, 8.04]	-0.25 [-0.97, 0.88]	0.22 [-0.04, 1.15]	0.56 [-0.25, 1.06]	NS	NS	0.032
				-4.04% [-12.76, 21.20]	4.93% [-0.67, 19.17]	8.29% [-4.68, 40.87]			
Distal edge, Absorb BVS									
(n=24)	post-procedure	6 months (6 mo)	24 months (24 mo)	Absolute/% Δ post-6 mo	Absolute/% Δ 6 mo-24 mo	Absolute/% Δ post-24 mo	p-value, post-6 mo	p-value, 6 mo-24 mo	p-value, post-24 mo
Vessel area (mm ²)	11.91 [8.47, 15.45]	11.74 [8.92, 15.71]	12.05 [8.79, 14.71]	0.08 [-0.51, 1.05]	-0.03 [-0.59, 0.71]	0.20 [-0.49, 0.91]	NS	NS	NS
				0.57% [-3.67, 9.92]	-0.34% [-4.39, 4.32]	1.83% [-4.02, 9.27]			
Lumen area (mm ²)	6.40 [5.65, 7.72]	6.42 [5.26, 7.64]	6.09 [5.34, 7.80]	-0.08 [-0.59, 0.64]	-0.13 [-0.89, 0.43]	-0.08 [-0.82, 0.69]	NS	NS	NS
				-0.85% [-9.46, 10.71]	-2.43% [-11.02, 6.72]	-1.23% [-10.58, 7.82]			
Plaque area (mm ²)	5.03 [2.04, 7.38]	4.90 [2.44, 7.63]	5.12 [2.59, 6.97]	0.22 [-0.59, 0.84]	0.02 [-0.34, 0.49]	0.24 [-0.45, 0.62]	NS	NS	NS
				7.58% [-9.54, 17.03]	0.45% [-8.13, 8.77]	3.00% [-6.47, 35.79]			

Data are expressed as medians (interquartile ranges).

Online table 3. Summary of the proximal and distal edge absolute/% changes following implantation of a XIENCE V everolimus-eluting metallic stent (XIENCE V) including imputation of data from TLR patients.

Proximal edge, XIENCE V									
(n=34)	post-procedure	6 months (6 mo)	24 months (24 mo)	Absolute/% Δ post-6 mo	Absolute/% Δ 6 mo-24 mo	Absolute/% Δ post-24 mo	p-value, post-6 mo	p-value, 6 mo-24 mo	p-value, post-24 mo
Vessel area (mm ²)	16.19 [14.27, 18.46]	15.96 [13.11, 18.92]	15.65 [12.57, 18.90]	-0.20 [-1.42, 0.67]	-0.71 [-1.19, 0.16]	-0.35 [-2.37, 0.68]	NS	0.022	NS
				-1.24% [-8.83, 4.87]	-4.68% [-8.78, 0.92]	-2.57% [-13.80, 3.75]			
Lumen area (mm ²)	7.91 [6.89, 9.77]	7.48 [6.59, 10.29]	7.29 [5.70, 10.87]	-0.17 [-0.76, 0.60]	-0.19 [-0.89, 0.55]	-0.28 [-1.26, 1.22]	NS	NS	NS
				-1.85% [-9.97, 6.90]	-2.88% [-11.91, 8.19]	-3.76% [-14.92, 14.43]			
Plaque area (mm ²)	8.22 [6.62, 9.28]	7.97 [6.49, 9.28]	7.13 [5.75, 8.76]	0.04 [-0.96, 0.59]	-0.50 [-1.25, 0.35]	-0.51 [-1.48, 0.29]	NS	0.057	0.047
				0.33% [-9.90, 6.67]	-5.21% [-15.49, 6.92]	-6.30% [-17.86, 4.45]			
Distal edge, XIENCE V									
(n=47)	post-procedure	6 months (6 mo)	24 months (24 mo)	Absolute/% Δ post-6 mo	Absolute/% Δ 6 mo-24 mo	Absolute/% Δ post-24 mo	p-value, post-6 mo	p-value, 6 mo-24 mo	p-value, post-24 mo
Vessel area (mm ²)	11.01 [9.39, 14.83]	12.14 [9.85, 15.48]	11.98 [9.30, 14.29]	0.62 [-0.47, 1.27]	-0.48 [-1.19, 0.14]	-0.13 [-0.95, 0.91]	0.006	0.0046	NS
				4.64% [-2.80, 12.34]	-3.84% [-8.26, 1.39]	-1.38% [-7.41, 7.84]			
Lumen area (mm ²)	6.93 [5.46, 7.83]	6.95 [5.71, 8.22]	6.74 [5.61, 8.08]	0.25 [-0.65, 1.25]	-0.25 [-0.91, 0.28]	-0.12 [-0.81, 0.72]	NS	NS	NS
				3.19% [-8.43, 18.84]	-3.17% [-12.64, 3.61]	-2.00% [-11.49, 11.86]			
Plaque area (mm ²)	5.38 [3.20, 7.02]	5.26 [3.56, 7.51]	5.12 [3.18, 7.18]	0.19 [-0.15, 0.74]	-0.11 [-0.42, 0.32]	-0.02 [-0.56, 0.75]	0.053	NS	NS
				5.90% [-3.59, 13.75]	-2.73% [-9.40, 6.26]	-1.01% [-9.44, 16.36]			

Data are expressed as medians [interquartile ranges]. NS: non-significant

Online table 4. Comparison of the changes (deltas) between the groups treated with either a bioresorbable or a metallic platform at the proximal and distal edges (NS: non-significant).

Proximal edge				
p-value	Device type	post to 6 months	6 months to 2 years	post to 2 years
Δ Vessel area (mm ²)	BVS	NS	0.029	NS
	MP			
Δ Lumen area (mm ²)	BVS	NS	NS	NS
	MP			
Δ Plaque area (mm ²)	BVS	NS	0.009	0.005
Distal edge				
p-value	Device type	post to 6 months	6 months to 2 years	post to 2 years
Δ Vessel area (mm ²)	BVS	NS	NS	NS
	MP			
Δ Lumen area (mm ²)	BVS	NS	NS	NS
	MP			
Δ Plaque area (mm ²)	BVS	NS	NS	NS
	MP			

Online table 5. Summary of the serial proximal edge absolute/% changes regarding tissue area/percentage composition following implantation of the Absorb BVS.

Proximal edge, Absorb BVS									
(n=16)	post-procedure	6 months (6 mo)	24 months (24 mo)	Absolute/% Δ post-6 mo	Absolute/% Δ 6 mo-24 mo	Absolute/% Δ post-24 mo	p-value, post-6 mo	p-value, 6 mo-24 mo	p-value, post-24 mo
Dense calcium (mm ²)	0.25 [0.09; 0.60]	0.23 [0.12; 0.76]	0.23 [0.14; 0.93]	0.05 [-0.09; 0.19]	0.01 [-0.11; 0.15]	0.06 [-0.15; 0.15]	NS	NS	NS
Dense calcium (%)	12.28 [7.22; 29.12]	16.82 [8.42; 30.54]	16.52 [12.86; 21.20]	5.43% [-25.32; 83.89]	3.43% [-28.30; 55.65]	2.28% [-14.30; 31.22]			
Fibrous (mm ²)	1.16 [0.57; 1.71]	1.14 [0.59; 1.65]	1.24 [0.58; 2.35]	-0.01 [-0.22; 0.13]	0.31 [-0.24; 0.65]	0.23 [-0.27; 0.61]	NS	NS	NS
Fibrous (%)	48.27 [36.41; 64.37]	52.82 [32.69; 63.00]	50.93 [43.33; 62.34]	-4.13% [-15.42; 15.24]	3.27% [-11.30; 30.30]	2.28% [-14.30; 31.22]			
Fibro-fatty (mm ²)	0.14 [0.04; 0.20]	0.09 [0.05; 0.32]	0.17 [0.06; 0.43]	-0.00 [-0.04; 0.10]	0.01 [-0.07; 0.24]	0.02 [-0.06; 0.22]	NS	NS	NS
Fibro-fatty (%)	4.25 [2.62; 9.36]	4.61 [2.17; 11.91]	8.06 [5.46; 10.05]	-6.20% [-39.13; 129.96]	94.81% [-45.74; 183.65]	40.80% [-62.63; 277.37]			
Necrotic core (mm ²)	0.40 [0.08; 1.33]	0.35 [0.20; 0.97]	0.51 [0.18; 1.23]	0.05 [-0.24; 0.26]	0.02 [-0.13; 0.29]	0.04 [-0.32; 0.31]	NS	NS	NS
Necrotic core (%)	23.08 [13.86; 33.67]	23.31 [14.41; 33.46]	22.23 [17.58; 28.18]	4.43% [14.42; 35.54]	-4.56% [-24.35; 54.20]	-5.25% [-26.98; 61.44]			

Online table 6. Summary of the serial distal edge absolute/% changes regarding tissue area/percentage composition following implantation of the Absorb BVS.

Distal edge, Absorb BVS									
(n=14)	post-procedure	6 months (6 mo)	24 months (24 mo)	Absolute/% Δ post-6 mo	Absolute/% Δ 6 mo-24 mo	Absolute/% Δ post-24 mo	p-value, post-6 mo	p-value, 6 mo-24 mo	p-value, post-24 mo
Dense calcium (mm ²)	0.30 [0.13; 0.96]	0.62 [0.24; 1.27]	0.46 [0.21; 1.00]	0.20 [0.06; 0.42]	-0.10 [-0.22; 0.02]	0.08 [-0.02; 0.22]	0.0024	NS	NS
Dense calcium (%)	15.19 [9.50; 20.87]	19.90 [14.98; 27.54]	19.02 [7.47; 23.11]	41.72% [9.77; 77.38]	-12.48% [-33.13; -0.40]	49.54% [-3.93; 59.71]	0.0012		
Fibrous (mm ²)	1.73 [0.93; 2.32]	1.64 [0.75; 2.30]	1.80 [0.56; 3.02]	0.02 [-0.29; 0.28]	0.12 [-0.35; 0.23]	0.16 [-0.26; 0.41]	NS	NS	NS
Fibrous (%)	49.99 [44.84; 63.27]	46.84 [42.29; 58.35]	50.31 [44.67; 60.59]	-9.82% [-20.51; -1.11]	7.48% [-4.14; 22.30]	1.11% [-14.96; 4.70]	0.017		
Fibro-fatty (mm ²)	0.12 [0.05; 0.35]	0.09 [0.04; 0.22]	0.22 [0.14; 0.51]	-0.01 [-0.07; 0.03]	0.07 [-0.00; 0.19]	0.09 [-0.01; 0.18]	NS	0.07	NS
Fibro-fatty (%)	5.37 [2.87; 11.14]	3.61 [2.21; 5.96]	6.40 [4.41; 10.17]	-31.10% [-48.25; -13.46]	68.37% [17.82; 171.17]	37.16% [-38.93; 99.10]	0.013	0.013	
Necrotic core (mm ²)	0.56 [0.16; 1.26]	0.93 [0.39; 1.10]	0.66 [0.32; 1.16]	0.23 [-0.15; 0.44]	-0.18 [-0.23; 0.07]	0.04 [-0.43; 0.35]	NS	NS	NS
Necrotic core (%)	21.60 [14.68; 29.29]	25.99 [19.19; 30.72]	23.93 [15.69; 26.88]	22.93% [3.34; 53.46]	-9.91% [-16.88; 2.38]	7.92% [-29.45; 57.14]			

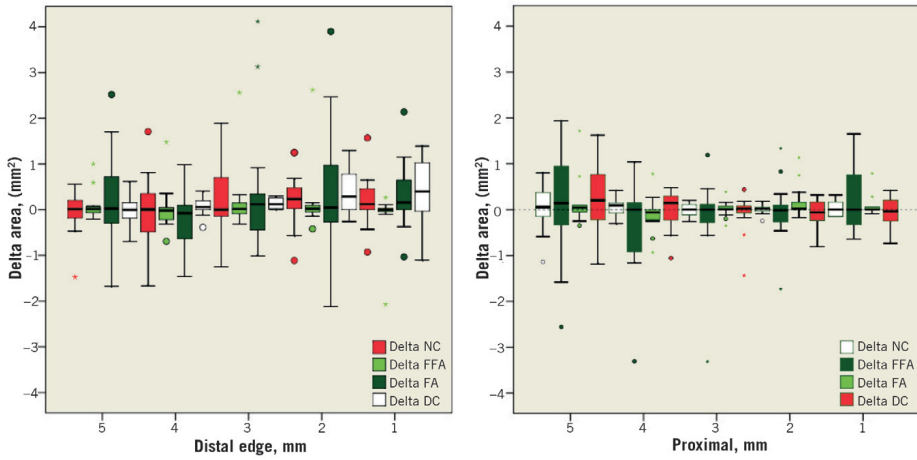


Figure 1. Serial proximal and distal edge per mm absolute changes regarding tissue composition from post intervention to 6 months following implantation of the Absorb BVS. The dense calcium (DC) tissue component increased significantly at the 2-mm distal subsegment $-\Delta DC: +0.29 \text{ mm}^2 [0.00, 0.78]$ ($p < 0.05$) and the 3-mm distal subsegment $-\Delta DC: +0.12 \text{ mm}^2 [0.02, 0.26]$ ($p < 0.001$).

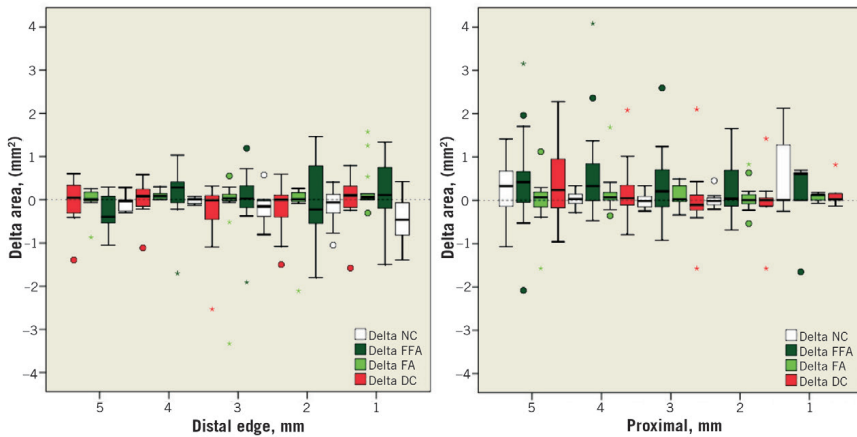


Figure 2. Serial proximal and distal edge per mm changes regarding tissue composition from 6 months to 2 years following implantation of the Absorb BVS. The dense calcium (DC) tissue component decreased significantly at the 1-mm distal subsegment $-\Delta DC: -0.47 \text{ mm}^2 [-0.81, -0.07]$ ($p < 0.01$) and the 3-mm distal subsegment $-\Delta DC: -0.16 \text{ mm}^2 [-0.39, -0.03]$ ($p = 0.02$).

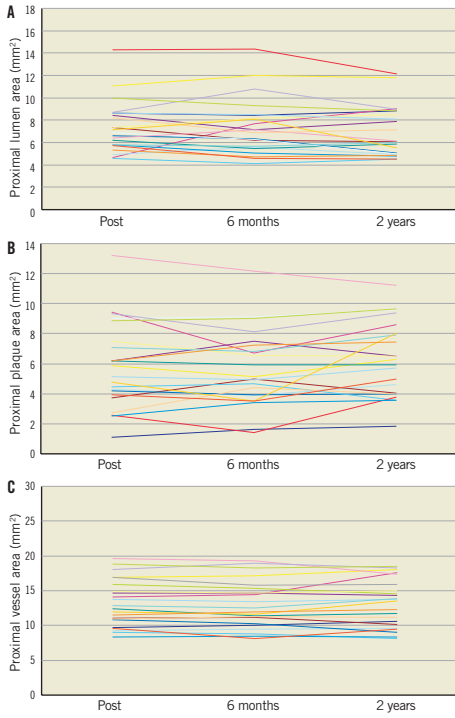


Figure 3. Serial changes of the lumen (A), plaque (B) and vessel (C) areas at the proximal edge of the Absorb BVS on a per lesion basis.

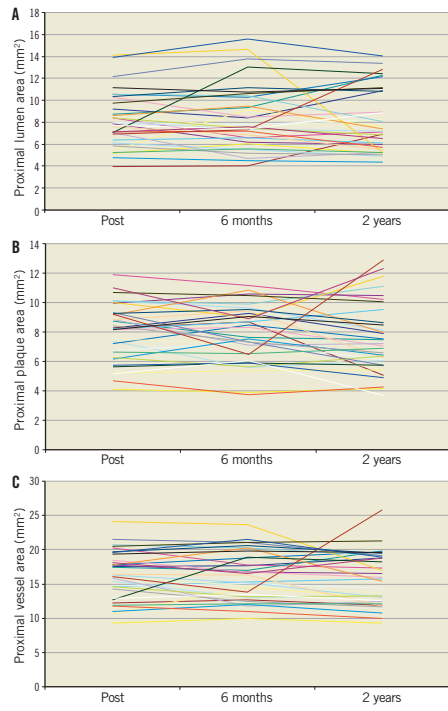


Figure 4. Serial changes of the lumen (A), plaque (B) and vessel (C) areas on a per lesion basis at the proximal edge of the XIENCE V stent.

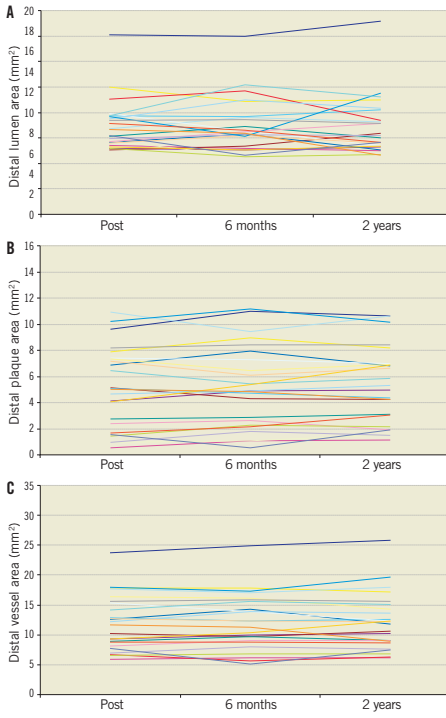


Figure 5. Serial changes of the lumen (A), plaque (B) and vessel (C) areas on a per lesion basis at the distal edge of the Absorb BVS.

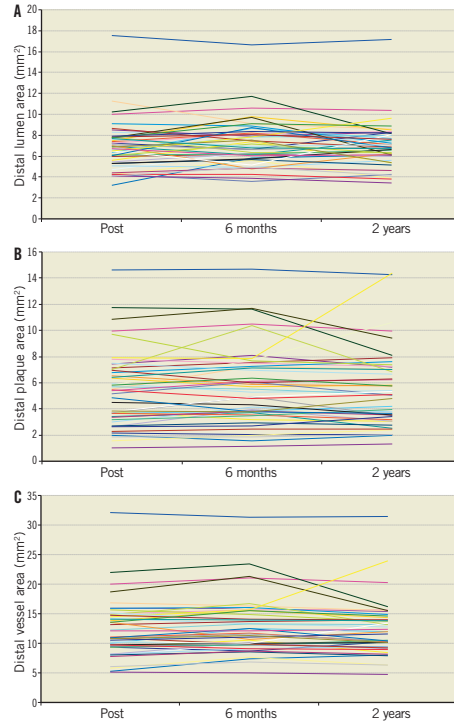


Figure 6. Serial changes of the lumen (A), plaque (B) and vessel (C) areas on a per lesion basis at the distal edge of the XIENCE V stent.

Chapter 9

Vascular Compliance Changes of the Coronary Vessel wall After Bioresorbable Vascular Scaffold Implantation in the Treated and Adjacent Segments.

Salvatore Brugaletta, **Bill D. Gogas**, Hector M. Garcia-Garcia, Vasim Farooq, Chrysafios Girasis, Jung Ho Heo, Robert Jan van Geuns, Bernard de Bruyne, Dariuz Dudek, Jacques Koolen, Pieter Smits, Susan Veldhof, Richard Rapoza, Yoshinobu Onuma, John Ormiston, Patrick W. Serruys

Circulation Journal. 2012. Jun 25; 76(7): 1616-23 [IF: 3.58]

Vascular Compliance Changes of the Coronary Vessel Wall After Bioresorbable Vascular Scaffold Implantation in the Treated and Adjacent Segments

Salvatore Brugaletta, MD, PhD; Bill D. Gogas, MD; Hector M. Garcia-Garcia, MD, PhD; Vasim Farooq, MD; Chrysafios Girasis, MD; Jung Ho Heo, MD; Robert Jan van Geuns, MD, PhD; Bernard de Bruyne, MD, PhD; Dariuz Dudek, MD; Jacques Koolen, MD, PhD; Pieter Smits, MD, PhD; Susan Veldhof, BSc; Richard Rapoza, PhD; Yoshinobu Onuma, MD; John Ormiston, MD; Patrick W. Serruys, MD, PhD

Background: Implantation of a metallic prosthesis creates local stiffness with a subsequent mismatch in the compliance of the vessel wall, disturbances in flow and heterogeneous distribution of wall shear stress. Polymeric bioresorbable ABSORB scaffolds have less stiffness than metallic platform stents. We sought to analyze the mismatch in vascular compliance after ABSORB implantation and its long-term resolution with bioresorption.

Methods and Results: A total of 83 patients from the ABSORB trials underwent palpography investigations (30 and 53 patients from ABSORB Cohorts A and B, respectively) to measure the compliance of the scaffolded and adjacent segments at various time points (from pre-implantation up to 24 months). The mean of the maximum strain values was calculated per segment by utilizing the Rotterdam Classification (ROC) score and expressed as ROC/mm. Scaffold implantation lead to a significant decrease in vascular compliance (median [IQR]) at the scaffolded segment (from 0.37 [0.24–0.45] to 0.14 [0.09–0.23], $P < 0.001$) with mismatch in compliance in a paired analysis between the scaffolded and adjacent segments (proximal: 0.23 [0.12–0.34], scaffold: 0.12 [0.07–0.19], distal: 0.15 [0.05–0.26], $P = 0.042$). This reported compliance mismatch disappears at short- and mid-term follow-up.

Conclusions: The ABSORB scaffold decreases vascular compliance at the site of scaffold implantation. A compliance mismatch is evident immediately post-implantation and in contrast to metallic stents disappears in the mid-term, likely leading to a normalization of the rheological behavior of the scaffolded segment. (*Circ J* 2012; **76**: 1616–1623)

Key Words: ABSORB; Poly-lactide; Vascular compliance

Over the past 20 years percutaneous implantation of metallic prostheses has increasingly been used to alleviate flow-limiting lesions by overstretching the plaque and underlying vessel wall.¹ From a mechanical perspective this treatment may locally stiffen the artery, reducing its compliance and creating a mismatch in compliance with respect to the segments contiguous to the implanted device.² This mismatch may eventually provoke flow disturbances and wall shear stress alterations with subsequent blood stasis³ (Figure 1). The wall shear stress distribution in a stented artery has been

reported as a determinant factor for cellular growth and the occurrence of thrombus formation.⁴

The ABSORB everolimus-eluting bioresorbable vascular scaffold system (ABSORB BVS) theoretically has many advantages over rigid metallic stents. In particular, because the scaffold is completely made of poly-lactide, it does not have the same stiffness as metal, thereby having the potential to overcome in part the problems related to local stiffening of the artery and compliance mismatch associated with metallic platform stents. In addition, the mismatch in compliance after

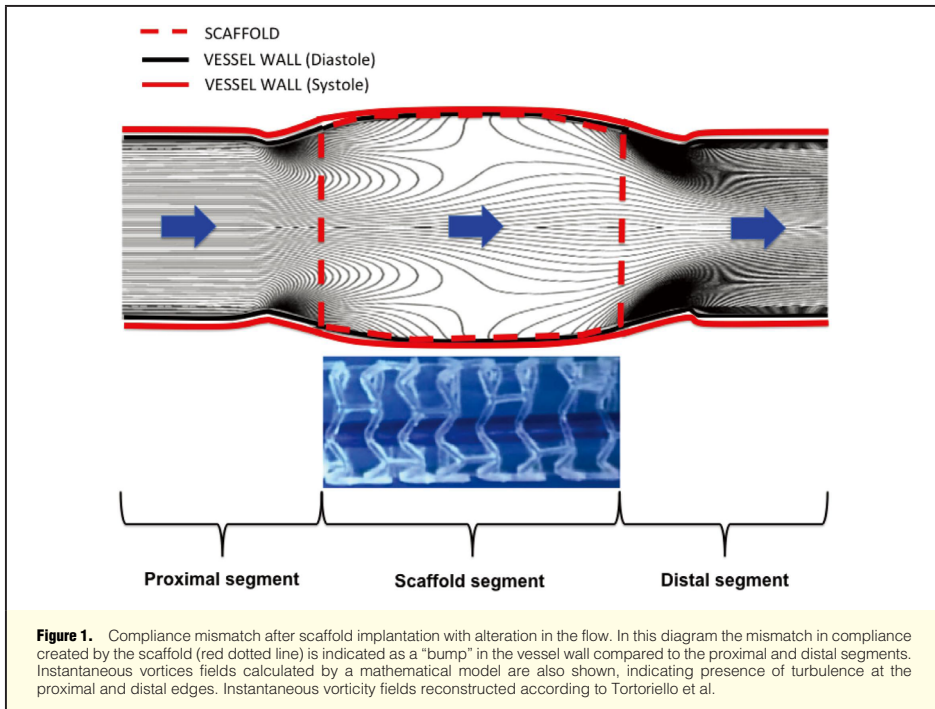
Received December 5, 2011; revised manuscript received February 25, 2012; accepted March 12, 2012; released online April 24, 2012
Time for primary review: 31 days

Thoraxcenter, Erasmus MC, Rotterdam (S.B., B.D.G., H.M.G.-G., V.F., C.G., J.H.H., R.J.v.G., Y.O., P.W.S.); Maastricht Hospital, Rotterdam (P.S.); Cardialysis B.V., Rotterdam (H.M.G.-G.); Catharina Hospital, Eindhoven (J.K.), The Netherlands; Department of Cardiology, Thorax Institute, University Hospital Clinic, Barcelona (S.B.), Spain; Cardiovascular Center, Aalst (B.D.B.), Belgium; Jagiellonian University, Krakow (D.D.), Poland; Abbott Vascular, Diegem (S.V.), Belgium; Abbott Vascular, Santa Clara, CA (R.R.), USA; Auckland City Hospital, Auckland (J.O.), New Zealand

Mailing address: Patrick W. Serruys, Professor, MD, PhD, Head of the Interventional Cardiology Department, Erasmus MC, Thoraxcenter, 's Gravenendijkwal 230, 3015 CE, Rotterdam, The Netherlands. E-mail: p.w.j.c.serruys@erasmusmc.nl

ISSN-1346-9843 doi:10.1253/circj.CJ-11-1416

All rights are reserved to the Japanese Circulation Society. For permissions, please e-mail: cj@j-circ.or.jp



scaffold implantation may potentially disappear in the long-term once the scaffold is completely bioresorbed.

The aim of the present analysis was to investigate the vascular compliance of the coronary segments treated with the bioresorbable scaffold and the adjacent proximal and distal edges, by measuring: (1) the changes in compliance immediately after ABSORB BVS implantation and at 6-, 12- and 24-month follow-up; and (2) the compliance mismatch between these 3 segments at the various time points.

Methods

Study Population

The ABSORB trial includes the ABSORB Cohorts A and B trials. In brief, the ABSORB Cohort A trial (NCT00300131) enrolled 30 patients with a diagnosis of stable or unstable angina or silent ischemia. All treated lesions were single and de novo in a native coronary artery of 3.0 mm diameter, shorter than 8 mm for the 12-mm scaffold and shorter than 14 mm for the 18-mm scaffold, with a diameter stenosis $\geq 50\%$ and $< 100\%$, and with a Thrombolysis in Myocardial Infarction flow grade ≥ 1 . Major exclusion criteria were acute myocardial infarction, unstable arrhythmias or left ventricular ejection fraction $< 30\%$, restenotic lesions, lesions located in the left main coronary artery, lesions involving an epicardial side branch ≥ 2 mm in diameter by visual assessment, and the presence of thrombus or other clinically significant stenosis in the target vessel. All

lesions were treated by implantation of ABSORB BVS first-generation scaffold (Generation 1.0) and invasively imaged at 6- and 24-month follow-up. The ABSORB Cohort B trial (NCT00856856) enrolled 101 patients with the same clinical profile and lesion type, divided into 2 groups according to the timeline of invasive follow-up: ABSORB Cohort B1 with invasive imaging at 6 and 24 months; ABSORB Cohort B2 with the same invasive imaging at 12 and 36 months. The 12-month follow-up has been reported.⁵ All lesions were treated by implantation of an ABSORB BVS second generation scaffold (Generation 1.1) (3.0 \times 18 mm).⁶ The ethics committee at each participating institution approved the protocol and each patient gave written informed consent before inclusion.

Study Device

The ABSORB BVS scaffold (Abbott Vascular, Santa Clara, CA, USA) consists of a polymer backbone of poly-L lactide (PLLA) coated with a thin layer of a 1:1 mixture of poly-D, L-lactide (PDLLA) polymer, and the antiproliferative drug, everolimus, to form an amorphous drug-eluting coating matrix containing 100 μg of everolimus/ cm^2 of scaffold. The details of the device have been previously described.⁷⁻¹¹ The ABSORB Cohort A and Cohort B trials evaluated the ABSORB BVS scaffold generations 1.0 and 1.1, respectively.^{12,13} The ABSORB BVS scaffold 1.1 has a smaller maximum circular unsupported surface area compared to 1.0, with the struts arranged as in-phase zigzag hoops linked together by 3 longitudi-

Table 1. Clinical Baseline Characteristics				
	All patients (n=83)	Cohort A (n=30)	Cohort B (n=53)	P value
Patient demographic and clinical data				
Age, years	61.71±8.59	62.46±8.98	61.28±8.41	0.605
Male, n (%)	56 (67.5)	18 (60.0)	38 (71.7)	0.332
Hypertension, n (%)	51 (62.2)	18 (60.0)	33 (63.5)	0.815
Hypercholesterolemia, n (%)	61 (74.4)	19 (65.5)	42 (79.2)	0.194
Diabetes, n (%)	10 (12.0)	1 (3.3)	9 (17.0)	0.085
Current smoking, n (%)	14 (17.0)	6 (20.0)	8 (15.1)	0.559
Prior PCI, n (%)	18 (21.7)	6 (20.0)	12 (22.6)	1.000
Prior MI, n (%)	13 (15.7)	3 (10.0)	10 (18.9)	0.359
Stable angina, n (%)	18 (21.7)	6 (20.0)	12 (22.6)	1.000
Unstable angina, n (%)	13 (15.7)	8 (26.7)	5 (9.4)	0.058
Silent ischemia, n (%)	2 (2.4)	1 (3.3)	1 (1.9)	1.000
Lesion and angiographic characteristics				
Treated vessel, n (%)				
Left anterior descending artery	39 (47.0)	14 (46.7)	25 (47.2)	1.000
Left circumflex artery	22 (26.5)	9 (30.0)	13 (24.5)	0.612
Right coronary artery	22 (26.5)	7 (23.3)	15 (28.3)	0.796
ACC/AHA lesion type, n (%)				
Type A	0 (0)	0 (0)	0 (0)	NA
Type B1	50 (61.0)	18 (60.0)	32 (61.5)	1.000
Type B2	31 (37.8)	12 (40.0)	19 (36.0)	0.815
Type C	1 (1.2)	0 (0)	1 (1.9)	1.000
QCA analysis pre-treatment				
RVD (mean±SD, mm)	2.64±0.39	2.69±0.47	2.61±0.34	0.628
MLD (mean±SD, mm)	1.04±0.26	1.05±0.26	1.04±0.27	0.837
Diameter stenosis, (mean±SD, %)	59.85±10.41	59.92±11.30	59.80±9.96	0.980
Medical treatment, n (%)				
β-blocker	62 (75)	21 (73)	41 (77)	0.646
ACEI	37 (45)	13 (44)	24 (45)	0.837
Statin	81 (98)	29 (98)	52 (98)	1.000

Continuous variables are expressed as mean±SD.

MI, myocardial infarction; NA, not applicable; RVD, reference vessel diameter; MLD, minimum lumen diameter; ACEI, angiotensin-converting enzyme inhibitor; SD, standard deviation.

dinal links, similar to the XIENCE V design.^{8,14} No differences in polymeric material, drug dose, drug release kinetics or strut thickness exist between the 2 generations. Of note is that changes implemented in the manufacture of ABSORB BVS 1.1 resulted in more prolonged luminal support post-implantation.^{6,15,16}

Study Procedure and Intravascular Ultrasound (IVUS) Acquisition/Analysis

Target lesions were treated using standard interventional techniques with mandatory pre-dilation. Post-dilation with a balloon that was shorter than the implanted scaffold was allowed at the operator's discretion up to the prescribed maximal post-dilation diameter.

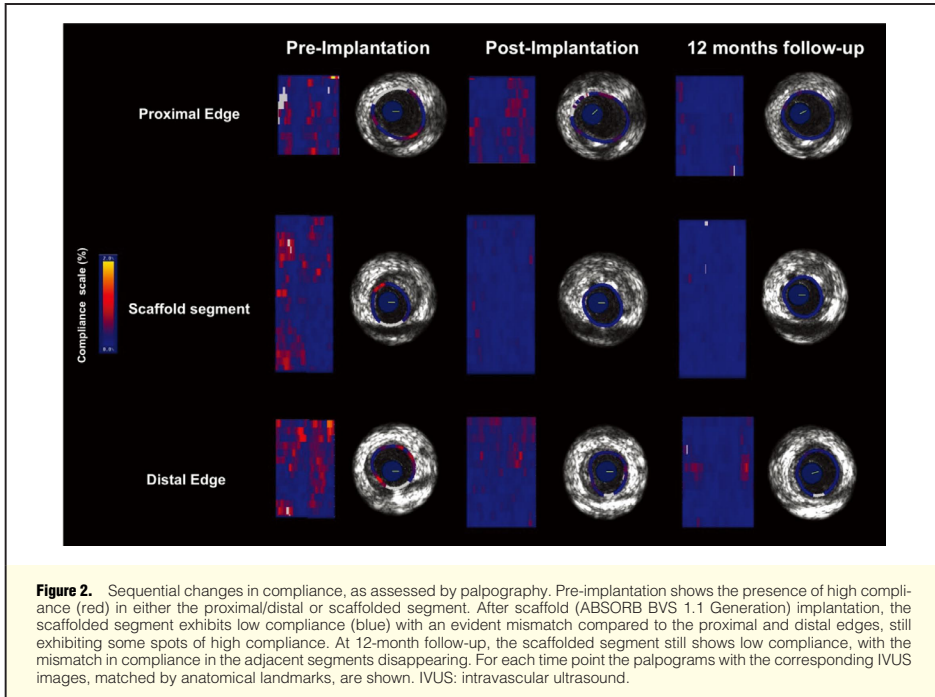
IVUS palpography analyses were performed using the Eagle Eye 20MHz catheter (Volcano Corp, Rancho Cordova, CA, USA) with an automated continuous pullback (0.5 mm/s, 30 frames/s) at the level of the scaffolded and adjacent segments, with simultaneous recordings of the electrocardiogram and aortic pressure, at various follow-up time points.

IVUS Palpography Acquisition and Analysis

IVUS palpography is a technique that allows for the assess-

ment of local mechanical tissue properties. The underlying principle is that at defined pressure differences soft tissue (eg, lipid-rich) components deform more than hard tissue components (eg, fibrous-calcified).¹⁷⁻¹⁹ In coronary arteries the tissue of interest is the vessel wall, whereas blood pressure, with its physiological changes during the heart cycle, is used as the excitation force. Radiofrequency data obtained at different pressure levels are compared to determine the local tissue deformation. The strain value is normalized to a pressure difference of 2.5 mmHg per frame: this allows the construction of a "strain" image in which hard (low strain/compliance) and soft (high strain/compliance) values range between 0% and 2%.¹⁷ In postmortem coronary arteries the sensitivity and specificity of palpography to detect high strain values have previously been reported as 88% and 89%, respectively.¹⁸

Digital radiofrequency data were acquired using a custom-designed workstation and subsequently stored on a DVD for sending to the imaging core laboratory for offline analyses (Cardialysis, Rotterdam, The Netherlands). Both the scaffolded and the 5-mm proximal and distal segments were analyzed.²⁰ Local strain was calculated from the gated radiofrequency traces using cross-correlation analyses, displayed and color-coded from blue (for 0% strain) to yellow (for 2% strain)



via red as previously described.¹⁹

Strain values were assigned a Rotterdam classification (ROC) score ranging from I to IV (ROC I, 0–0.5%; ROC II, 0.6–<0.9%; ROC III, 0.9–1.2%; ROC IV, >1.2%).²¹ A region was defined as high strain when it had ROC III–IV that spanned an arc of at least 12° at the surface of a plaque (identified on the IVUS recording), as previously reported. The highest value of strain in the cross-section was taken as the strain level of the site.²¹ The compliance of each segment was calculated per segment (proximal edge, scaffold segment and distal edge) and defined as the mean of the maximum strain values per cross-section in ROC I/II/III/IV sites, expressed as ROC/mm.^{22,23}

Ideally, the absence of a mismatch is the absence of difference in compliance along the vessel wall. For the purpose of the present analysis, mismatch was defined as statistically significant differences in compliance between the 3 segments analyzed on a paired basis, using a statistical test for trend (Figure 1).

Statistical Analysis

Categorical variables are presented using frequencies and percentages. Continuous variables are presented with mean and standard deviations or median and interquartile ranges, according to their distribution. Analyses of normality of the continuous variables were performed with the Kolmogorov-Smirnov test. Changes in compliance between various time points were evaluated by means of paired Wilcoxon signed rank test. Differences in compliance between the 3 segments analyzed

(scaffold, proximal and distal edges) at each time point were evaluated by the paired Friedman test. Comparison between 2 groups was performed with the Mann-Whitney test. A 2-sided P-value <0.05 indicated statistical significance. Statistical analyses were performed with SPSS 18.0 software (SPSS, Chicago, IL, USA).

Results

Baseline Clinical Characteristics (Table 1)

A total of 83 patients from the ABSORB Cohort A and B trials underwent palpography investigations (30 and 53 patients from ABSORB Cohort A and Cohort B, respectively). Specifically, palpography analyses were performed in 27 patients pre-scaffold implantation (13 and 14 from ABSORB Cohort A and Cohort B), 71 patients post-scaffold implantation (27 and 44 from ABSORB Cohort A and Cohort B), 42 patients at 6 months (27 and 15 from ABSORB Cohort A and Cohort B), 26 patients at 12 months and in 21 patients at 24 months.

Palpography analyses were completed for all 3 segments (scaffold, proximal and distal segments) in 14 patients at pre-scaffold implantation (5 and 9 from ABSORB Cohort A and Cohort B), 35 patients post-implantation (14 and 11 from ABSORB Cohort A and Cohort B), 27 patients at 6 months (16 and 11 from ABSORB Cohort A and ABSORB Cohort B), 11 patients at 12 months and 14 patients at 24 months.

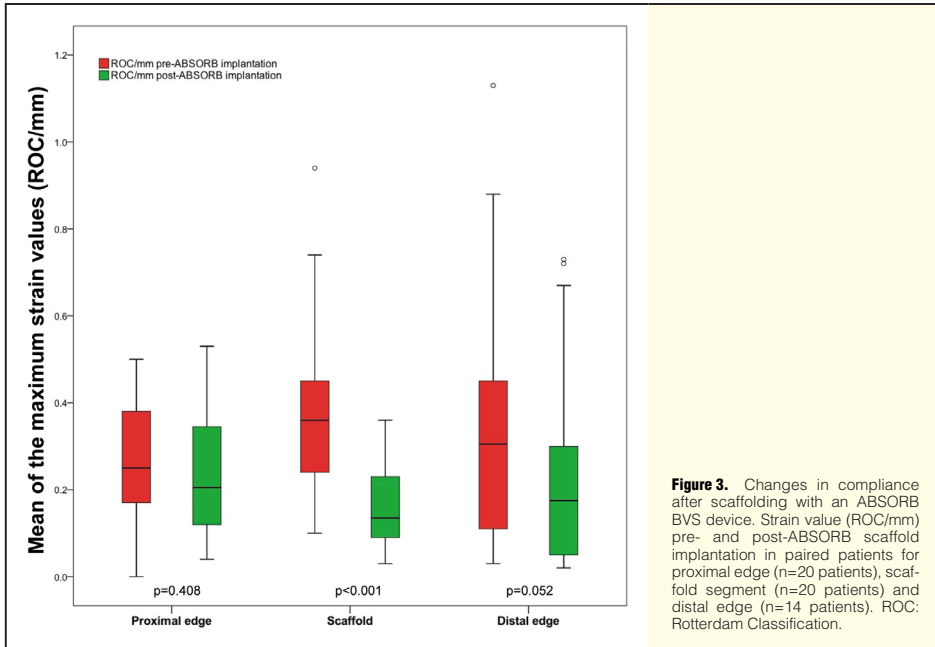


Figure 3. Changes in compliance after scaffolding with an ABSORB BVS device. Strain value (ROC/mm) pre- and post-ABSORB scaffold implantation in paired patients for proximal edge (n=20 patients), scaffold segment (n=20 patients) and distal edge (n=14 patients). ROC: Rotterdam Classification.

Modification in Vascular Compliance From Pre- to Post-Scaffold Implantation (Figure 2)

After scaffold implantation a significant decrease in compliance in the scaffolded segment was evident with no modification in the proximal/distal edges compliance. Of note, a trend towards a reduction in compliance was evident in the distal edge (Figure 3). The modifications in compliance after scaffold implantation did not significantly differ between ABSORB Cohort A and Cohort B in the 3 segments (scaffolded segment P=0.820; proximal edge P=0.310; distal edge P=0.606).

A mismatch in compliance tended to be present immediately after scaffold implantation (Figure 4).

Modification in Vascular Compliance During Follow-up (Tables 2.3)

In ABSORB Cohort A there was a significant increase in the compliance of the scaffolded segment at 6 and 24 months compared to post-implantation. Conversely, in ABSORB Cohort B no changes in compliance of the scaffolded segment were evident at either 6 (P<0.001 as compared to ABSORB Cohort A) or 12 months, compared to post-implantation. No other significant changes were found at the proximal/distal edges in either ABSORB Cohort A or B at the various time points.

At the various follow-up time points, no mismatch in compliance was found either in Cohort A (6 months=proximal edge 0.29 [0.18–0.35] vs. scaffold segment 0.10 [0.06–0.22] vs. distal edge 0.16 [0.05–0.24]; P=0.146; 24 months proximal edge 0.20 [0.09–0.30] vs. scaffold segment 0.24 [0.17–0.29] vs. distal edge 0.11 [0.05–0.24]; P=0.052) or Cohort B

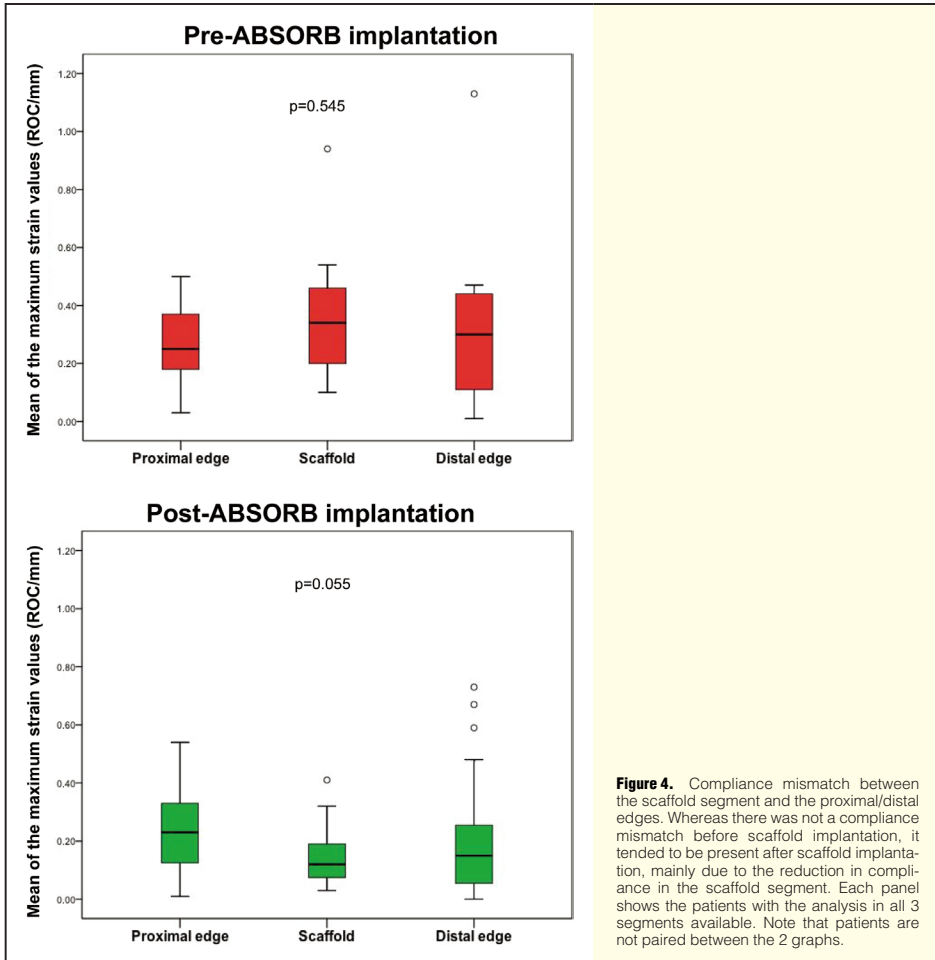
(6 months=proximal edge 0.28 [0.16–0.46] vs. scaffold segment 0.23 [0.14–0.29] vs. distal edge 0.11 [0.05–0.17]; P=0.449; 12 months=proximal edge 0.18 [0.10–0.36] vs. scaffold segment 0.16 [0.08–0.26] vs. distal edge 0.11 [0.02–0.20]; P=0.618).

Discussion

The major findings of the present analysis are: (1) scaffolding of a diseased vessel wall by an ABSORB BVS significantly reduces its compliance, with the compliance of the segment immediately distal to the device tending also to be reduced; (2) the mismatch in compliance that is present immediately after scaffold implantation disappears in the short- to mid-term; (3) the prolonged duration of mechanical support of the ABSORB BVS generation 1.1, compared to BVS 1.0, is responsible for the differing changes in vascular compliance in the scaffold segment between the 2 devices at 6 months.

Compliance and Pulsatility of the Scaffolded Segment

Palpography is a technique of assessing the elastic properties of the coronary vessel wall; in particular, it analyzes the ability of the artery to be distended, providing a measurement of its compliance.^{17,19,24} Deployment of a stiff metallic stent over coronary plaque may mechanically reduce the local compliance of the coronary vessel wall.²⁵ This reduction may be further explained by the fact that the foreign scaffold material may partially interfere with the palpography measurements due to the artifactual acoustic properties of the stent struts themselves.²⁵



Implantation of an ABSORB BVS, made of polymeric material, reduces the local compliance of the scaffolded segment and possibly the acute vulnerability of the treated coronary plaque.^{19,25} Nevertheless, with the first ABSORB Revision 1.0 at long term, an increase in compliance was observed in parallel with bioresorption of the scaffold.^{9,25} It is noteworthy that with the progressive disappearance of the polymeric scaffold, the vessel wall can recover a normal response to physiologic pulsatile cyclic strain and to shear stress; this positive interplay between cyclical strain and shear stress can be translated into chemical signals by cells with upregulation of the e-NOS gene, prostacyclin and metalloproteinases production, expression of anti-inflammatory genes, low permeability and low oxidative stress in the endothelial cells and in the smooth muscle cells.²⁶⁻²⁹ The presence of endothelial-dependent vaso-

motion in the vascular segment scaffolded by an ABSORB BVS device suggests that all these biological processes work appropriately.^{5,13} Conversely, cell signaling is altered in metallic scaffolded segments, where the vessel's distensibility is eliminated by metallic caging and it is exposed to static and non-pulsatile strain.³⁰⁻³²

It should be also noted that the vessel wall compliance over time may be modulated differently according to the type of polymeric device implanted. The 2 generations of ABSORB BVS were compared at post-implantation and at 6-month follow-up. No differences in their ability to reduce vascular compliance immediately after implantation were found, confirming the absence of differences in acute mechanical properties, such as acute recoil, between the 2 BVS generations.³³ Nevertheless, at 6 months the compliance of the scaffolded segment

Table 2. Modification in Strain Values After ABSORB Cohort A Scaffold Implantation (Generation 1.0)

	Post-scaffolding	6-month follow-up	24-month follow-up	P value*	P value**	P value***
Proximal edge	0.33 [0.18–0.40] (17)	0.25 [0.15–0.38] (18)	0.20 [0.09–0.36] (16)	0.679 (15)	0.275 (13)	0.391 (14)
Scaffolded segment	0.12 [0.07–0.25] (27)	0.25 [0.17–0.37] (27)	0.26 [0.17–0.32] (21)	<0.001 (25)	0.003 (19)	0.746 (20)
Distal edge	0.17 [0.05–0.30] (18)	0.16 [0.09–0.41] (18)	0.12 [0.07–0.28] (16)	0.715 (15)	0.127 (14)	0.391 (14)

All P-values are calculated by Wilcoxon paired test.

*Post vs. 6-month follow-up; **Post vs. 24-month follow-up; ***6- vs. 24-month follow-up. Values are reported as median [IQR] (n). IQR, interquartile range.

Table 3. Modification in Strain Values After ABSORB Cohort B Scaffold Implantation (Generation 1.1)

	Post-scaffolding	6-months follow-up	P value
Cohort B1			
Proximal edge	0.25 [0.11–0.41] (12)	0.17 [0.11–0.34] (11)	0.313 (7)
Scaffolded segment	0.22 [0.13–0.28] (16)	0.20 [0.12–0.28] (15)	0.053(11)
Distal edge	0.22 [0.11–0.31] (10)	0.19 [0.10–0.37] (14)	0.313 (7)
	Post-scaffolding	12-month follow-up	P value
Cohort B2			
Proximal edge	0.23 [0.10–0.35] (17)	0.17 [0.13–0.34] (17)	0.531 (14)
Scaffolded segment	0.17 [0.09–0.32] (28)	0.16 [0.11–0.21] (26)	0.226 (21)
Distal edge	0.15 [0.03–0.20] (18)	0.08 [0.04–0.23] (16)	0.747 (11)

All P-values are calculated by Wilcoxon paired test.

Values are reported as median [IQR] (n). IQR, interquartile range.

increased after ABSORB 1.0 implantation, whereas it tended to further decrease after ABSORB 1.1 implantation. These findings are in line with expectations: smaller maximum circular unsupported surface area and a slower rate of degradation of the generation 1.1 compared to 1.0 aim to improve and prolong the duration of lumen scaffolding and to avoid the “late recoil” phenomenon (scaffold area reduction over time), likely explaining the differing changes over time in compliance of the scaffolded segment between the 2 generations.^{5,6,14–16}

Compliance Mismatch Between the Scaffolded and Contiguous Segments

Local stiffness due to metallic stent implantation, in contrast to the compliance of the contiguous vascular segments, generates a compliance mismatch (Figures 1,2). Vernhet et al previously showed that metallic stent implantation within the normal rabbit abdominal aorta causes a persistent increase in upstream compliance, while simultaneously abolishing compliance in the stented segment, creating a compliance mismatch.³⁴ Similar findings have been demonstrated in human carotid arteries after stenting.³⁵ It has also been shown that ring vortices with in-flow stagnation points and rapid variations of wall shear stress can form at the edges of the prosthesis.^{3,26,36} All of these findings, in particular the increase in upstream compliance, have been related to the observation that late plaque rupture after stenting in human coronary arteries is more likely to occur at the stent inflow compared to elsewhere.²⁰

At variance with these metallic stent observations, ABSORB BVS implantation did not increase the compliance in the inflow segment, but conversely tended to decrease it in the outflow segment (Figure 3). Normally, there is propagation of pressure waves along the vessel wall (the so-called Windkessel effect) and at sites where this process is interrupted (eg, side branches, stent/scaffold) there is a reflection of pressure waves with prevention of their propagation.³⁷ This may eventually reduce wall motion and compliance distally, explaining the changes observed in the present analysis in the segment

distal to the scaffold.^{38,39}

Although a compliance mismatch between the scaffolded and adjacent segments was demonstrated immediately after polymeric scaffold implantation, it disappeared at 6 months in contrast to metallic stents (Figure 2). The abolition of a step-up compliance at the scaffold edges can theoretically lead to laminar flow, exposing the endothelial cells to a homogeneous shear stress, which can eventually result in atheroprotective and anti-restenosis effects.^{20,26,39,40} Long-term data from the ABSORB B trial up to 3 years are awaited to confirm these findings.

Study Limitations

The major limitation of the present analysis is the small group of patients with paired palpography analysis at the various time points. This cohort of patients does, however, currently represent the sole set of available data on polymeric scaffold and vascular compliance. The lack of a control group testing a metallic stent is another limitation to fully interpreting the present findings; other investigators have, however, previously studied the phenomenon of mismatch compliance in vessel scaffolded with metal.^{34,35}

Conclusions

Scaffold implantation with an ABSORB BVS device transiently reduces the vascular distensibility of a treated coronary segment. In contrast to metallic stents, the created mismatch in compliance with the proximal and distal segments disappeared at mid-term due to the bioresorption and disappearance of the scaffold. Potential clinical benefits of these findings, related to restoration of vessel wall pulsatility and absence of mismatch, will require longer term clinical follow-up in a larger population.

Acknowledgments

The ABSORB Trial is sponsored and funded by Abbott Vascular, Santa

Clara, California, USA. Susan Veldhof and Richard Rapoza are employees of Abbott Vascular.

References

- Garg S, Serruys PW. Coronary stents: Current status. *J Am Coll Cardiol* 2010; **56**(10 Suppl): S1–S42.
- Surovtsova I. Effects of compliance mismatch on blood flow in an artery with endovascular prosthesis. *J Biomech* 2005; **38**: 2078–2086.
- Tortoriello A, Pedrizzetti G. Flow-tissue interaction with compliance mismatch in a model stented artery. *J Biomech* 2004; **37**: 1–11.
- Wentzel JJ, Whelan DM, van der Giessen WJ, van Beusekom HM, Andharyswara I, Serruys PW, et al. Coronary stent implantation changes 3-D vessel geometry and 3-D shear stress distribution. *J Biomech* 2000; **33**: 1287–1295.
- Serruys PW, Onuma Y, Dudek D, Smits PC, Koolen J, Chevalier B, et al. Evaluation of the second generation of a bioresorbable everolimus-eluting vascular scaffold for the treatment of de novo coronary artery stenosis 12-month clinical and imaging outcomes. *J Am Coll Cardiol* 2011; **58**: 1578–1588.
- Serruys PW, Onuma Y, Ormiston JA, de Bruyne B, Regar E, Dudek D, et al. Evaluation of the second generation of a bioresorbable everolimus drug-eluting vascular scaffold for treatment of de novo coronary artery stenosis: Six-month clinical and imaging outcomes. *Circulation* 2010; **122**: 2301–2312.
- Ormiston JA, Webster MW, Armstrong G. First-in-human implantation of a fully bioresorbable drug-eluting stent: The BVS poly-L-lactic acid everolimus-eluting coronary stent. *Catheter Cardiovasc Interv* 2007; **69**: 128–131.
- Okamura T, Garg S, Gutierrez-Chico JL, Shin ES, Onuma Y, Garcia HM, et al. In-vivo evaluation of stent strut distribution patterns in the bioresorbable everolimus-eluting device: An OCT ad hoc analysis of the Revision 1.0 and Revision 1.1 stent design in the ABSORB clinical trial. *EuroIntervention* 2010; **5**: 932–938.
- Onuma Y, Serruys PW, Perkins LE, Okamura T, Gonzalo N, Garcia-Garcia HM, et al. Intracoronary optical coherence tomography and histology at 1 month and 2, 3, and 4 years after implantation of everolimus-eluting bioresorbable vascular scaffolds in a porcine coronary artery model: An attempt to decipher the human optical coherence tomography images in the ABSORB Trial. *Circulation* 2010; **122**: 2288–2300.
- Onuma Y, Ormiston J, Serruys PW. Bioresorbable scaffold technologies. *Circ J* 2011; **75**: 509–520.
- Gutierrez-Chico JL, Radu MD, Diletti R, Sheehy A, Kossuth MB, Oberhauser JP, et al. Spatial distribution and temporal evolution of scattering centers by optical coherence tomography in the poly(l-lactide) backbone of a bioresorbable vascular scaffold. *Circ J* 2012; **76**: 342–350.
- Ormiston JA, Serruys PW, Regar E, Dudek D, Thuesen L, Webster MW, et al. A bioresorbable everolimus-eluting coronary stent system for patients with single de-novo coronary artery lesions (ABSORB): A prospective open-label trial. *Lancet* 2008; **371**: 899–907.
- Serruys PW, Ormiston JA, Onuma Y, Regar E, Gonzalo N, Garcia-Garcia HM, et al. A bioresorbable everolimus-eluting coronary stent system (ABSORB): 2-year outcomes and results from multiple imaging methods. *Lancet* 2009; **373**: 897–910.
- Brugaletta S, Garcia-Garcia HM, Diletti R, Gomez-Lara J, Garg S, Onuma Y, et al. Comparison between the first and second generation bioresorbable vascular scaffolds: A six month virtual histology study. *EuroIntervention* 2011; **6**: 1110–1116.
- Brugaletta S, Gomez-Lara J, Serruys PW, Ferooq V, van Geuns RJ, Thuesen L, et al. Serial in vivo intravascular ultrasound-based echogenicity changes of everolimus-eluting bioresorbable vascular scaffold during the first 12 months after implantation insights from the ABSORB B Trial. *J Am Coll Cardiol Intv* 2011; **4**: 1281–1289.
- Gomez-Lara J, Brugaletta S, Diletti R, Garg S, Onuma Y, Gogas BD, et al. A comparative assessment by optical coherence tomography of the performance of the first and second generation of the everolimus-eluting bioresorbable vascular scaffolds. *Eur Heart J* 2011; **32**: 294–304.
- Schaar JA, De Korte CL, Mastik F, Strijder C, Pasterkamp G, Boersma E, et al. Characterizing vulnerable plaque features with intravascular elastography. *Circulation* 2003; **108**: 2636–2641.
- Schaar JA, Regar E, Mastik F, McFadden EP, Saia F, Disco C, et al. Incidence of high-strain patterns in human coronary arteries: Assessment with three-dimensional intravascular palpography and correlation with clinical presentation. *Circulation* 2004; **109**: 2716–2719.
- Schaar JA, van der Steen AF, Mastik F, Baldeuwings RA, Serruys PW. Intravascular palpography for vulnerable plaque assessment. *J Am Coll Cardiol* 2006; **47**(Suppl): C86–C91.
- Ward MR, Hibi K, Shaw JA, Furukawa E, Resnic FS, Kimura K. Effect of stent implantation on upstream coronary artery compliance—a cause of late plaque rupture? *Am J Cardiol* 2005; **96**: 673–675.
- Rodriguez-Granillo GA, Garcia-Garcia HM, Valgimigli M, Schaar JA, Pawar R, van der Giessen WJ, et al. In vivo relationship between compositional and mechanical imaging of coronary arteries: Insights from intravascular ultrasound radiofrequency data analysis. *Am Heart J* 2006; **151**: 1025 e1–e6.
- Serruys PW, Garcia-Garcia HM, Buszman P, Erne P, Verheye S, Aschermann M, et al. Effects of the direct lipoprotein-associated phospholipase A(2) inhibitor darapladib on human coronary atherosclerotic plaque. *Circulation* 2008; **118**: 1172–1182.
- Van Mieghem CA, McFadden EP, de Feyter PJ, Bruining N, Schaar JA, Mollet NR, et al. Noninvasive detection of subclinical coronary atherosclerosis coupled with assessment of changes in plaque characteristics using novel invasive imaging modalities: The Integrated Biomarker and Imaging Study (IBIS). *J Am Coll Cardiol* 2006; **47**: 1134–1142.
- Wada T, Fujishiro K, Fukumoto T, Yamazaki S. Relationship between ultrasound assessment of arterial wall properties and blood pressure. *Angiology* 1997; **48**: 893–900.
- Garcia-Garcia HM, Gonzalo N, Pawar R, Kukreja N, Dudek D, Thuesen L, et al. Assessment of the absorption process following bioresorbable everolimus-eluting stent implantation: Temporal changes in strain values and tissue composition using intravascular ultrasound radiofrequency data analysis: A substudy of the ABSORB clinical trial. *EuroIntervention* 2009; **4**: 443–448.
- Hahn C, Schwartz MA. Mechanotransduction in vascular physiology and atherogenesis. *Nat Rev Mol Cell Biol* 2009; **10**: 53–62.
- Gupta V, Grande-Allen KJ. Effects of static and cyclic loading in regulating extracellular matrix synthesis by cardiovascular cells. *Cardiovasc Res* 2006; **72**: 375–383.
- Slager CJ, Wentzel JJ, Gijzen FJ, Schuurbers JC, van der Wal AC, van der Steen AF, et al. The role of shear stress in the generation of rupture-prone vulnerable plaques. *Nat Clin Pract Cardiovasc Med* 2005; **2**: 401–407.
- Khattab A, Windecker S. Vascular restoration therapy: What should the clinical and angiographic measures for success be? *EuroIntervention* 2009; **5**(Suppl): F49–F57.
- Awolosi MA, Sessa WC, Sumpio BE. Cyclic strain upregulates nitric oxide synthase in cultured bovine aortic endothelial cells. *J Clin Invest* 1995; **96**: 1449–1454.
- Peng X, Halder S, Deshpande S, Irani K, Kass DA. Wall stiffness suppresses Akt/eNOS and cytoprotection in pulse-perfused endothelium. *Hypertension* 2003; **41**: 378–381.
- Balligand JL, Feron O, Dessy C. eNOS activation by physical forces: From short-term regulation of contraction to chronic remodeling of cardiovascular tissues. *Physiol Rev* 2009; **89**: 481–534.
- Onuma Y, Serruys PW, Gomez J, de Bruyne B, Dudek D, Thuesen L, et al. Comparison of in vivo acute stent recoil between the bioresorbable everolimus-eluting coronary scaffolds (revision 1.0 and 1.1) and the metallic everolimus-eluting stent. *Catheter Cardiovasc Interv* 2011; **78**: 3–12.
- Vernhet H, Juan JM, Demaria R, Oliva-Lauraire MC, Senac JP, Dauzat M. Acute changes in aortic wall mechanical properties after stent placement in rabbits. *J Vasc Interv Radiol* 2000; **11**: 634–638.
- Vernhet H, Jean B, Lust S, Laroche JP, Bonafe A, Senac JP, et al. Wall mechanics of the stented extracranial carotid artery. *Stroke* 2003; **34**: e222–e224.
- Yazdani SK, Moore JE Jr, Berry JL, Vlachos PP. DPIV measurements of flow disturbances in stented artery models: Adverse effects of compliance mismatch. *J Biomech Eng* 2004; **126**: 559–566.
- Van Den Bos GC, Westerhof N, Elzinga G, Sipkema P. Reflection in the systemic arterial system: Effects of aortic and carotid occlusion. *Cardiovasc Res* 1976; **10**: 565–573.
- Lyon RT, Runyon-Hass A, Davis HR, Glagov S, Zarins CK. Protection from atherosclerotic lesion formation by reduction of artery wall motion. *J Vasc Surg* 1987; **5**: 59–67.
- Schwarzacher SP, Tsao PS, Ward M, Hayase M, Niebauer J, Cooke JP, et al. Effects of stenting on adjacent vascular distensibility and neointima formation: Role of nitric oxide. *Vasc Med* 2001; **6**: 139–144.
- Benard N, Coisne D, Donal E, Perrault R. Experimental study of laminar blood flow through an artery treated by a stent implantation: Characterisation of intra-stent wall shear stress. *J Biomech* 2003; **36**: 991–998.

Chapter 10

Computational Fluid Dynamics Applied to Virtually Deployed Drug-Eluting Coronary Bioresorbable Scaffolds. Clinical Translations Derived from a Proof-of-Concept.

Bill D. Gogas, Boyi Yang, Tiziano Passerini, Alessandro Veneziani, Girum Mekonnen, Emad Rasoul-Arzrumly, Michel T. Corban, Beth Holloway, Lucas Timmins, David S. Molony, Sungho Kim, Don P. Giddens, Spencer B. King III, Habib Samady
International Journal of Cardiology. 2013. Submitted

Computational Fluid Dynamics Applied to Virtually Deployed Drug-Eluting Coronary Bioresorbable Scaffolds.

Clinical Translations Derived from a Proof-of-Concept

Bill D. Gogas, M.D., F.A.C.C.,^{1*} Boyi Yang, Ph.D.,^{2*} Tiziano Passerini, Ph.D.,² Alessandro Veneziani, Ph.D.,² Marina Piccinelli, Ph.D.,³ Girum Mekonnen, M.D., M.P.H.,¹ Olivia Y. Hung, M.D., Ph.D.,¹ Beth Holloway, R.N., B.S.N., C.C.R.C.,¹ Don P. Giddens, Ph.D.,⁴ Spencer B. King III, M.D., M.A.C.C.,^{1,4} Habib Samady, M.D., F.A.C.C.¹

¹ Andreas Gruentzig Cardiovascular Center, Division of Cardiology, Department of Medicine, Emory University School of Medicine, Atlanta, Georgia

² Department of Mathematics and Computer Science, Emory University, Atlanta, Georgia

³ Department of Radiology and Imaging Sciences, Emory University, Atlanta, Georgia

⁴ Wallace H. Coulter Department of Biomedical Engineering, Georgia Institute of Technology and Emory University, Atlanta, Georgia

⁴ Saint Joseph's Heart and Vascular Institute, Atlanta, Georgia

Brief Title: Modeling of Coronary Bioresorbable Scaffolds

Key Words: Bioresorbable scaffolds, Computational Fluid Dynamics, Virtual Modeling

Word Count: 2497

Address for correspondence:

Habib Samady, M.D.

Professor of Medicine,

Director, Interventional Cardiology,

Emory University School of Medicine

1364, Clifton Road, Suite F606

Atlanta, GA 30322

Tel: (404) 778 1237, Fax: (404) 712 5622

Email: hsamady@emory.edu

*Equally contributed authors

Abbreviations:

CAD= coronary artery disease

CFD= computational fluid dynamics

m= month

WSS= wall shear stress

Abstract

Background: Three-dimensional design simulations of coronary metallic stents utilizing mathematical and computational algorithms have emerged as an important tool for understanding biomechanical stent properties, predicting the interaction of the implanted platform with adjacent tissue, and informing stent design enhancements. Herein, we demonstrate the hemodynamic implications following virtual implantation of bioresorbable scaffolds using finite element methods and advanced computational fluid dynamics (CFD) simulations to visualize device-flow interaction immediately after implantation and following scaffold resorption over time.

Methods & Results: CFD simulations with time averaged wall shear stress (WSS) quantification following virtual bioresorbable scaffold deployment in idealized straight and curved geometries were performed. WSS was calculated at the inflow, endoluminal surface (top surface of the strut), and outflow of each strut surface post-procedure (stage I) and at a time point when 33% of scaffold resorption has occurred (stage II). The average WSS at stage I over the inflow and outflow surfaces were 3.2 and 3.1 dynes/cm² respectively and 87.5 dynes/cm² over endoluminal strut surface in the straight vessel. From stage I to stage II, WSS increased by 100% and 142% over the inflow and outflow surfaces, respectively, and decreased by 27% over the endoluminal strut surface. In a curved vessel, WSS change became more evident in the inner curvature with an increase of 63% over the inflow and 66% over the outflow strut surfaces. Similar analysis at the proximal and distal edges demonstrated a large increase of 486% at the lateral outflow surface of the proximal scaffold edge.

Conclusions: The implementation of CFD simulations over virtually deployed bioresorbable scaffolds demonstrates the transient nature of device/flow interactions as the bioresorption process progresses over time. Such hemodynamic device modeling is expected to guide future bioresorbable scaffold design.

Introduction:

Despite tremendous innovations in platform design such as strut thickness reductions, use of novel antiproliferative agents, coating with bioresorbable polymers or abluminal drug coating¹, the utilization of a permanent metallic prosthesis remains a precipitating factor for sustained vascular inflammation, neoatherosclerosis and impaired vasomotor function.² Therefore, the concept of a drug-eluting bioresorbable scaffold with properties that allow for short-term temporary scaffolding and long-term restoration of vascular physiology and anatomy when the device is fully resorbed is appealing. Several drug-eluting bioresorbable devices, such as the Absorb bioresorbable vascular scaffold (Abbott Vascular, SC, Calif.), the DESolve bioresorbable scaffold, (Elixir Medical, Sunnyvale, Calif.), and the Drug Eluting Absorbable Metal Scaffold (DREAMS) (Biotronik, Bülach, Switzerland) have been clinically tested in first-in-man studies utilizing multi modality imaging techniques showing encouraging clinical results up to 3-years. These endeavors have led the development of a novel concept in interventional cardiology, that of vascular restoration therapy.³

Recent data suggest that variations in the local hemodynamic environment post stenting result in wall shear stress (WSS) regional alterations that can invoke a differential vascular healing response around the stent struts.⁴ The vessel geometry after stenting is determined by several factors which influence vascular angulation and curvature including material properties of the implanted device, strut thickness and underlying plaque composition. By design, bioresorbable devices have thicker struts in order to retain the necessary scaffolding; meanwhile strut resorption associated with vascular healing over time balances the hemodynamic impairment observed during the post-implantation stage. Furthermore bioresorbable devices offer a more compliant platform that limits vascular straightening and thus reduces disturbed flow patterns at the proximal and distal edges.

Although, critical to understanding healing and long term performance of stents, these dynamic WSS alterations are difficult to measure in vivo as it would require detailed invasive measurements at different time points.

The utilization of computational modeling techniques to assess the performance of isolated or virtually deployed coronary stents has been proven to be an important tool to predict their mechanical behavior over time. These numerical simulations provide a preliminary “proof-of-concept” for new technologies to further qualify from bench to clinical application.⁵

Herein, we provide a series of three-dimensional simulations to test the hypothesis that local hemodynamic conditions derived from advanced CFD simulations change, as the virtually applied bioresorption process progresses over time. This translates in improved flow patterns over the scaffolded segments or the scaffold edges which potentially affect local tissue responses. **(Figures 1-3)**

Methodology

Computational Fluid Dynamics

Blood was approximated to behave as a Newtonian fluid with a density of 1 g/cm^3 and constant viscosity of 0.04 g/cm/sec for CFD simulations. Flow velocity and pressure in the coronary artery were computed by numerically solving the unsteady Navier-Stokes equations, which represent conservation of mass and balance of momentum. The spatial discretization of the Navier-Stokes equations was based on the Galerkin FEM. In particular, a piecewise linear approximation was adopted for pressure and piecewise quadratic for velocity. Time discretization was achieved with a semi-implicit backward Euler method with a time step of $5 \times 10^{-4} \text{ s}$. CFD simulations and post processing were carried out based on LifeV (EPFL, Switzerland; Politecnico di Milano, Italy; INRIA, France; and Emory University, USA), for numerical solution of partial differential equations. The CFD model consisted of the: 1. geometric construction of the scaffolded vessel; 2. meshing of geometry; 3. imposition of proper boundary conditions and quantities of interest. In brief the boundary conditions are applied at the inlet (proximal) and outlet (distal) surfaces of the CFD domain (the region where the blood is flowing). (**Fig 1: Panels A, B, C & Fig 2: Panels A, B, C**)

Geometric reconstruction of the scaffolded vessel

The geometry of the deployed scaffold was constructed based on the structure of an actual $3.0 \times 18 \text{ mm}$ Absorb BVS (Abbott Vascular, SC, Calif.) utilizing the validated software Rhino 5.0. (www.rhino3d.com) for solid modeling. We modeled 19 horizontal rings interconnected by 3 vertical bridges. We performed simulations in two idealized vessel geometries, a straight vessel and a curved vessel with a 90° angle. We examined 2 sequential stages in each vessel model Stage I: post-implantation, where the strut thickness is 0.015 cm ($150 \mu\text{m}$); the distance between each strut 0.1 cm , the degree of embedding in the vessel wall 50% simulating half-embedded struts, (the

distance between the endoluminal and abluminal strut surface: 0.0075cm) and the radius of the vessel lumen 0.15 cm and stage II: follow-up, where the strut thickness is reduced to 0.010cm (67%) reflecting a 33% strut bioresorption and the radius of the lumen reduced to 0.14975 cm simulating some degree of bioresorption and neointimal hyperplasia (NIH), respectively.

(electronic supplement)

Meshing of geometry

The geometry volume was discretized as an unstructured mesh of tetrahedral elements using Netgen (Linz, Australia) and Gmsh (<http://geuz.org/gmsh/>). Since the region of interest is close to the boundaries (wall and struts), we computed a mesh featuring more refined elements (resulting in a more accurate numerical solution) in these regions. In view of the complexity of the geometry induced by the stent the meshing process is split in two steps where the boundary layer with thickness 0.025cm and mesh size of 0.004cm are computed with NetGen and the lumen is filled by Gmsh. Both packages offer implementation of cutting-edge mesh optimization algorithms.

Imposition of Boundary Conditions and Quantities of Interest

We prescribed a constant and maximum inflow rate of 2.7 cm³/sec, under normal conditions. The vessel wall was assumed as rigid for the sake of computational time; however extension to the deformable case is feasible as well. The quantities of interest were the velocity (cm/sec), pressure (dynes) and wall shear stress (dynes/cm²) in the CFD domain. Flow rate was prescribed by means of a parabolic velocity profile properly adjusted to the desired boundary condition.

Statistical Analysis:

Variables are presented as average values. Change (difference) for each variable was estimated as: follow-up minus post-procedure (or stage II-stage I). Percent change was calculated as : follow-up-post-procedure/ post-procedure x 100% (or stage II- stage I/ stage I x 100%). Data analysis was performed with SPSS 19 for Mac (SPSS, Chicago, IL).

Results:**In-scaffold, straight vessel:**

The average WSS values following virtual scaffold deployment (stage I) over the inflow and outflow strut surfaces were 3.2 and 3.1 dynes/cm², respectively and 87.5 dynes/cm² at the endoluminal strut surface. The percent (%) WSS increased from stage I to stage II by 100% and 142% over the inflow and outflow surfaces respectively, and decreased by 27% over the endoluminal surface.

(Table 2)**In-scaffold, curved vessel:**

The average WSS of the inner curvature at stage I over the inflow and outflow strut surfaces were 4.3 and 2.9 dynes/cm², respectively, and at the endoluminal strut surface was 88.6 dynes/cm². Similar analysis of the outer curvature demonstrated WSS values of similar magnitude: 5.8, 3.9 and 118.1 dynes/cm² respectively. The WSS from stage I to stage II at the inner curvature increased by 63% in the inflow and by 66% in the outflow surface and decreased by 20% over the endoluminal surface. Similarly, at outer curvature the %WSS increased at the inflow and outflow surfaces by 29% and 56%, respectively, and decreased over the endoluminal surface by 28%. **(Table 1)**

Edge, straight vessel:

The average WSS following virtual scaffold implantation over the inflow surface of the proximal edge did not change significantly, however over the outflow surface of the proximal edge changed significantly: from 2.2 to 12.9 dynes/ cm², a percentile increase of 486%. At the distal edge percentile WSS increased by 59% at the inflow and by 79% over the outflow surface. **(Table 2)**

Edge, curved vessel:

In curved vessels, the average WSS change of the inflow and outflow strut surfaces of the proximal edge at the inner curvature increased by 79% and 66% respectively. At the distal edge similar analysis showed decrease by 67% and 3% respectively.

Discussion:

Computational fluid dynamic simulations performed in this study demonstrate that: 1) immediately post scaffold deployment WSS is high at the endoluminal strut surface and very low at the lateral inflow and lateral outflow region of each strut; 2) at a time point when 33% of the scaffold bioresorption occurs, the WSS reduces by approximately 30% at the endoluminal strut surface and increases by over 100% at the inflow and outflow regions of each strut resulting in a more uniform distribution of WSS across the endoluminal and strut surface; 3) these findings were more pronounced at the inner curvature than the outer curvature of curved vessels; and 4) WSS is very low at the scaffold edges immediately after scaffold deployment, variably changes at follow up but remains low enough to incite an edge neo-intimal response.

Dynamic endoluminal WSS and neointimal formation with bioresorbable scaffolds

It is known that low WSS such as created at the lateral inflow and outflow strut surfaces, promotes activation, migration, and phenotype shift of smooth muscle cells from a contractile to a more synthetic phenotype with production of extracellular matrix through up-regulation of the smooth muscle cell differentiation repressors: platelet-derived growth factor and KLF-4.^{4,6} These biologic responses initiate a neointima that fills in between the struts of the scaffold thereby reducing the effective thickness of the struts and increasing the value of WSS at the strut inflow and outflow. Simultaneously, bulk resorption of the strut results in a smaller and thinner effective strut thereby lowering the magnitude of the high WSS at the endoluminal strut surface. The net effect of this sequence of events is that the large variability of WSS around bioresorbable struts immediately after deployment (stage I) smoothens out when 33% of the struts are resorbed (stage II). Although no absolute WSS cutoff value after stent deployment has been definitively shown to predict an intense neointimal response, WSS values <0.5 Pa (5 dynes/cm²) maybe a ongoing stimulus for neointimal hyperplasia precipitating in-segment restenosis.⁷⁻⁹

In our models simulating a bioresorbable scaffold with strut thickness of 150 μ m and rectangular strut geometry, WSS was frequently noted to be <0.5 Pa in the lateral strut surfaces and always significantly ≥ 0.5 Pa at the endoluminal strut surface immediately after scaffold deployment. We found that following 33% bioresorption, WSS in lateral strut surfaces significantly increased and WSS at the endoluminal strut surface significantly decreased. These observations may reflect a biphasic tissue response with accelerated tissue proliferation in the low WSS segments in the lateral strut surfaces early post-implantation that subsequently plateaus when WSS rises above the threshold that promotes hyperplasia. Although we didn't model more advanced time points in the

resorption process, the peak and trough values of WSS in the endoluminal strut surface and the lateral strut surfaces with ongoing scaffold resorption continue to approximate one another until such time as the scaffold is fully degraded and the ongoing low WSS stimulus for neointimal hyperplasia between the struts is extinguished. This smooth surface and laminar hemodynamic environment is likely atheroprotective and conducive to a clinically stable vessel with appropriate medical therapy and risk factor modification. One can speculate that such a smooth surface created by a well healed bioresorbable scaffold can be applied towards plaque sealing and shielding. Clinical data supporting this notion are provided from a recent study of 58 patients who underwent Absorb BVS implantation for stable ischemic heart disease and acute coronary syndromes with optical coherence tomography imaging at 12 months demonstrating a robust neointimal layer that provides a thick fibrous cap overlying residual plaques.¹⁰

The feasibility of 3-D WSS reconstructions derived from two-dimensional OCT acquisitions following implantation of bioresorbable scaffolds has been recently described.¹¹ **(Figure 4)** The further association of local 3-D WSS alterations with underlying neointimal proliferation utilizing advanced light-based imaging remains to be elucidated in real-world randomized human data.

Clearly scaffold design, strut thickness, strut shape (rectangular, circular, elliptical or tear-drop shape) and the scaffold resorption rate will significantly impact the near wall-flow patterns (micro-environment), vascular hemodynamic milieu (macro-environment) and resulting time frame of vascular response. In contrast to this complex dynamic environment with transient scaffolds, the design of metallic stents has a sustained impact over the regional hemodynamic micro- and macro-environments. Indeed, rigid metallic stents have been shown to increase vascular angulation in the proximal stent edge by 121% and the distal edge by 100%, inducing regions of low WSS at these edges which were associated with a robust neo-intimal response.¹²⁻¹³ We have hypothesized that more compliant metallic stents and to a greater extent bioresorbable scaffolds deployed in curved

and angulated vessels will have less straightening effect at device edges and in the case of bioresorbable scaffolds will restore vessel geometry after the completion of bioresorption process.¹⁴⁻¹⁵

Edge WSS and neointimal formation

Edge restenosis accounts for approximately 6% of target lesion revascularization rates and manifests with both metallic and bioresorbable devices.¹⁶⁻¹⁷ The magnitude of proximal and distal edge vascular responses has been previously shown to be associated with the stent or scaffold design and strut thickness, axial and longitudinal geographical miss,¹⁸ underlying tissue composition at the landing zone¹⁹, and variable straightening of the stented segment at the edges.^{12,20} The magnitude of altered flow patterns which influence local WSS distributions and subsequently influence tissue proliferation have been numerically demonstrated in our model providing additional evidence for the association of flow-mediated tissue responses at the transition zones.

Conclusions:

The present study applied computational fluid dynamics to simulate the biologic behavior of virtually deployed bioresorbable scaffolds. This is the first proof-of-concept which potentially applies clinical translations for further development of bioresorbable platforms.

References:

1. Grube E, Schofer J, Hauptmann KE, et al. A novel paclitaxel-eluting stent with an ultrathin abluminal biodegradable polymer 9-month outcomes with the JACTAX HD stent. *JACC Cardiovasc Interv.* 2010 Apr;3(4):431-8.
2. Park SJ, Kang SJ, Virmani R, et al. In-stent neoatherosclerosis: a final common pathway of late stent failure. *J Am Coll Cardiol.* 2012 Jun 5;59(23):2051-7.
3. Wykrzykowska JJ, Onuma Y, Serruys PW. Vascular restoration therapy: the fourth revolution in interventional cardiology and the ultimate "rosy" prophecy. *EuroIntervention.* 2009 Dec 15;5 Suppl F:F7-8.
4. Koskinas KC, Chatzizisis YS, Antoniadis AP, et al. Role of endothelial shear stress in stent restenosis and thrombosis: pathophysiologic mechanisms and implications for clinical translation. *J Am Coll Cardiol.* 2012 Apr 10;59(15):1337-49.
5. Formaggia L, Quarteroni A, Veneziani A. *Cardiovascular Mathematics*, Springer, Milan, 2009
6. Chatzizisis YS, Coskun AU, Jonas M, et al. Role of endothelial shear stress in the natural history of coronary atherosclerosis and vascular remodeling: molecular, cellular, and vascular behavior. *J Am Coll Cardiol.* 2007 Jun 26;49(25):2379-93.
7. Liu SQ, Goldman J. Role of blood shear stress in the regulation of vascular smooth muscle cell migration. *IEEE Trans Biomed Eng.* 2001 Apr;48(4):474-83.
8. Nerem RM. Hemodynamics and the vascular endothelium. *J Biomech Eng.* 1993 Nov;115(4B):510-4.
9. Van der Heiden K, Gijssen FJ, Narracott A, et al. The effects of stenting on shear stress: relevance to endothelial injury and repair. *Cardiovasc Res.* 2013 Jul 15;99(2):269-75.
10. Brugaletta S, Radu MD, Garcia-Garcia HM, et al. Circumferential evaluation of the neointima by optical coherence tomography after ABSORB bioresorbable vascular scaffold implantation: can the scaffold cap the plaque? *Atherosclerosis.* 2012 Mar;221(1):106-12.
11. Gogas BD, King SB, 3rd, Timmins LH, et al. Biomechanical assessment of fully bioresorbable devices. *JACC Cardiovasc Interv.* 2013 Jul;6(7):760-1.
12. Wentzel JJ, Whelan DM, van der Giessen WJ, et al. Coronary stent implantation changes 3-D vessel geometry and 3-D shear stress distribution. *J Biomech.* 2000 Oct;33(10):1287-95.
13. Thury A, Wentzel JJ, Vinke RV, et al. Images in cardiovascular medicine. Focal in-stent restenosis near step-up: roles of low and oscillating shear stress? *Circulation.* 2002 Jun 11;105(23):e185-7.
14. Gomez-Lara J, Garcia-Garcia HM, Onuma Y, et al. A comparison of the conformability of everolimus-eluting bioresorbable vascular scaffolds to metal platform coronary stents. *JACC Cardiovasc Interv.* 2010 Nov;3(11):1190-8.
15. Serruys PW, Garcia-Garcia HM, Onuma Y. From metallic cages to transient bioresorbable scaffolds: change in paradigm of coronary revascularization in the upcoming decade? *Eur Heart J.* 2012 Jan;33(1):16-25b.
16. Gogas BD, Garcia-Garcia HM, Onuma Y, et al. Edge vascular response after percutaneous coronary intervention: an intracoronary ultrasound and optical coherence tomography appraisal: from radioactive platforms to first- and second-generation drug-eluting stents and bioresorbable scaffolds. *JACC Cardiovasc Interv.* 2013 Mar;6(3):211-21.
17. Gogas BD, Bourantas CV, Garcia-Garcia HM, et al. The edge vascular response following implantation of the Absorb everolimus-eluting bioresorbable vascular scaffold and the XIENCE V metallic everolimus-eluting stent. First serial follow-up assessment at six months and two years: insights from the first-in-man ABSORB Cohort B and SPIRIT II trials. *EuroIntervention.* 2013 Oct 22;9(6):709-20.
18. Costa MA, Angiolillo DJ, Tannenbaum M, et al. Impact of stent deployment procedural factors on long-term effectiveness and safety of sirolimus-eluting stents (final results of the multicenter prospective STLLR trial). *Am J Cardiol.* 2008 Jun 15;101(12):1704-11.
19. Waxman S, Freilich MI, Suter MJ, et al. A case of lipid core plaque progression and rupture at the edge of a coronary stent: elucidating the mechanisms of drug-eluting stent failure. *Circ Cardiovasc Interv.* 2010 Apr;3(2):193-6.
20. McDaniel MC, Samady H. The shear stress of straightening the curves: biomechanics of bioabsorbable stents. *JACC Cardiovasc Interv.* 2011 Jul;4(7):800-2.

Legends to the Figures:**Figure 1:****Numerical modeling of the virtually deployed bioresorbable scaffold in an idealized straight geometry. (post-procedure or stage I)**

CFD simulations visualizing the velocity streamlines and WSS magnitude on the endoluminal and lateral outflow surfaces of the struts following virtual scaffold deployment. Plot of the quantified WSS vs. axial distance on the endoluminal and both strut sides at stage I.

Panels A, B, C: Velocity magnitude, pressure and wall shear stress distribution over the CFD domain

Figure 2:**Numerical modeling of the virtually applied bioresorption in an idealized straight geometry. (follow-up or stage II)**

CFD simulations visualizing the velocity streamlines and WSS magnitude on the endoluminal and lateral outflow surfaces of the struts following virtually applied bioresorption. Plot of the quantified WSS vs. axial distance on the endoluminal and both strut sides at stage II.

Panels A, B, C: Velocity magnitude, pressure and wall shear stress distribution over the CFD domain

Figure 3:**Numerical modeling of the simulated stage I (post-procedure) and stage II (virtually applied bioresorption) at the distal edge in an idealized straight geometry.**

Panels A & A': CFD simulations of the velocity profiles, pressure and WSS. at strut # 19 (distal edge) **Panels B, B':** CFD simulations of the velocity magnitudes visualizing the altered flow patterns over the virtually deployed struts

Figure 4:**Computational Fluid Dynamic Simulations derived from optical coherence tomographic imaging****(reproduced by permission)**

(A, A') Two-dimensional (2-D) angiographic views of the significant proximal left circumflex artery lesion (A) and the scaffolded segment after implantation of a 3.0 18-mm Absorb bioresorbable vascular scaffold (BVS) (B, B') Three-dimensional (3-D) angiographic views before (B) and after (B') scaffold implantation. (C) The Absorb BVS. (D, D') Time-averaged wall shear stress (TAWSS) magnitude distribution from angiographically derived 3-D geometries before (D) and after (D') scaffold deployment. Velocity profiles pre- and post-implantation of the Absorb BVS are superimposed. (E) 2-D OCT cross section with embedded polymeric struts demonstrating in a 3-D pattern the distribution of TAWSS between the polymeric struts. The quantified color coding demonstrates low WSS regions (blue color). The matched OCT cross section is superimposed. (E') Reconstructed streamlines of the velocity field at the systolic peak demonstrating altered flow patterns in the proximity of the arterial wall induced by the polymeric struts. CFD= computational fluid dynamics; GWS= guidewire shadow.

Legends to the Tables:**Table 1:**

WSS quantification over the simulated struts at stages I and II

Table 2:

WSS quantification over the simulated proximal and distal edges in stages I and II

Figure 1

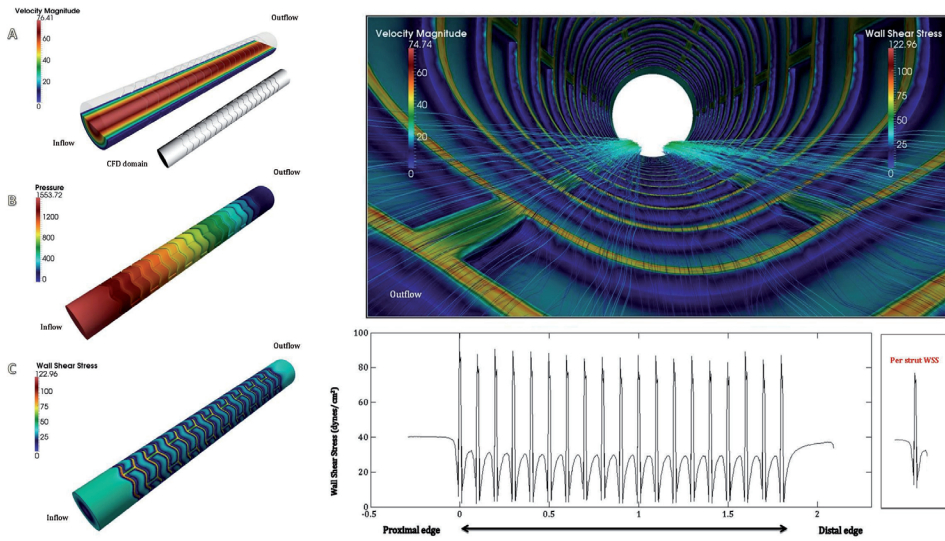


Figure 2

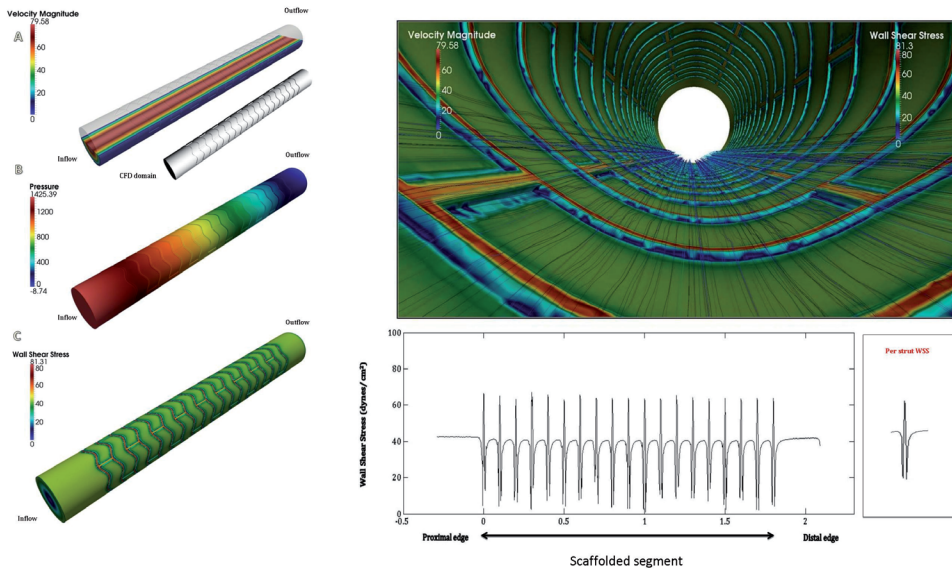


Figure 3

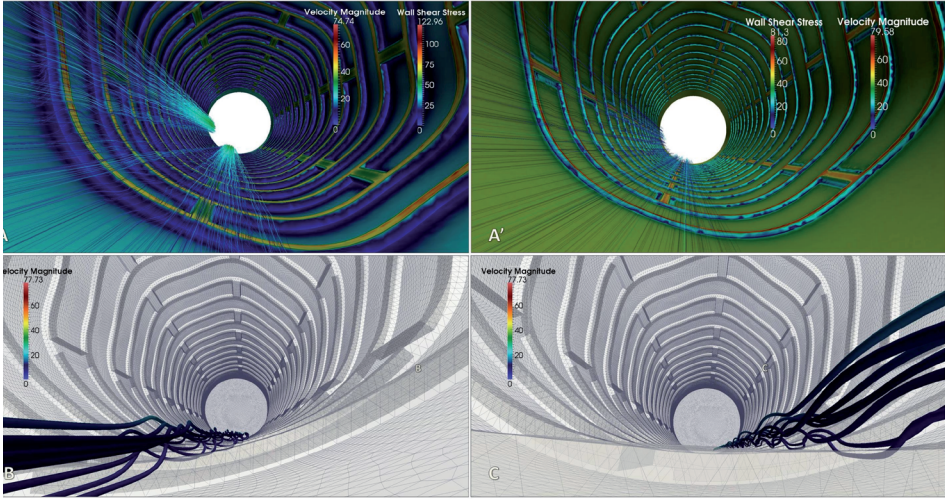
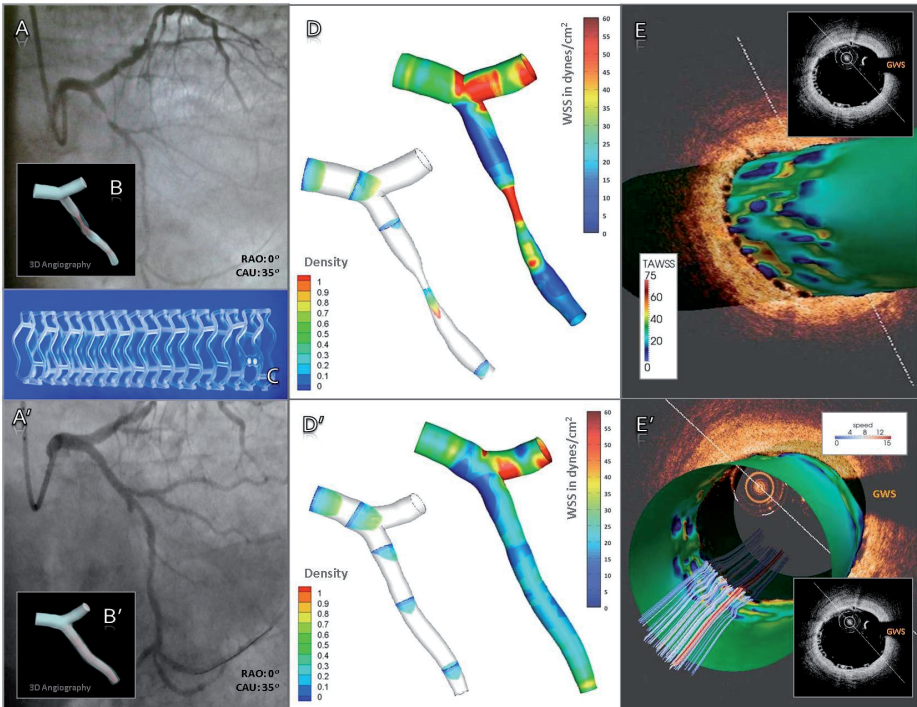


Figure 4



Electronic Supplement

Anatomic model of virtually embedded polymeric struts in idealized straight vessel at stages I and II.

Detailed view of strut geometry and strut surface where WSS quantification was applied:

Stage I:

a: lateral inflow strut surface=0.015 cm (150 μ m) , b: endoluminal strut surface, c: distance from vessel wall=0.0075 cm (half embedded strut), d: distance between struts=0.10cm, d: lateral outflow surface

Stage II:

a'= 0.010 cm (100 μ m), the grey lane presents the generation of neointimal tissue

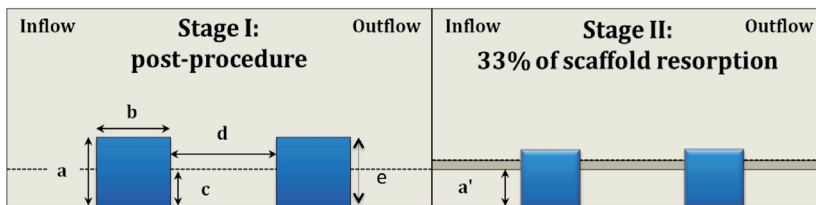


Table 1: WSS quantification over the simulated struts at stages I (post-) and II (follow-up)

Straight Vessel	Average WSS, dynes/cm ²		
	Post-	Follow-up	Relative Change (%)
Inflow	3.2	6.4	100
Endoluminal surface	87.5	64.3	-27
Outflow	3.1	7.5	142

Curved Vessel: Inner	Average WSS, dynes/cm ²		
	Post-	Follow-up	Relative Change (%)
Inflow	4.3	7.0	63
Endoluminal surface	88.6	71.3	-20
Outflow	2.9	4.8	66

Curved Vessel: Outer	Average WSS, (dynes/cm ²)		
	Post-	Follow-up	Relative Change (%)
Inflow	5.8	7.5	29
Endoluminal surface	118.1	84.9	-28
Outflow	3.9	6.1	56

Table 2: WSS quantification over the simulated proximal and distal transition zones in stages I (post-) and II (follow-up)

Straight Vessel, Average WSS (dynes/cm ²)	Proximal edge			Distal edge		
	Post-	Follow-Up	Relative Change (%)	Post-	Follow-Up	Relative Change (%)
Inflow	6.2	4.6	-26	2.7	4.3	59
Endoluminal surface	100.5	66.6	-34	87.2	63.7	-27
Outflow	2.2	12.9	486	2.8	5.0	79

Curved Vessel Average WSS (dynes/cm ²)	Inner Curvature: Proximal edge			Inner Curvature: Distal edge		
	Post-	Follow-Up	Relative Change (%)	Post-	Follow-Up	Relative Change (%)
Inflow	7.7	13.8	79	9.0	3.0	-67
Endoluminal surface	126.1	87	-31	68.5	58	-15
Outflow	5.6	9.3	66	7.9	7.7	-3

Curved Vessel Average WSS (dynes/cm ²)	Outer Curvature: Proximal edge			Outer Curvature: Distal edge		
	Post-	Follow-Up	Relative Change (%)	Post-	Follow-Up	Relative Change (%)
Inflow	6.8	5.2	-24	9.3	3.4	-63
Endoluminal surface	85.8	53.5	-38	170	117.8	-31
Outflow	2.0	3.9	95	2.4	4.9	104

Part 3

***In-Vivo* Assessment of Vascular Responses Utilizing Optical Coherence Tomography**

Chapter 11

Evaluation with In Vivo Optical Coherence Tomography and Histology of the Vascular Effects of the Everolimus-Eluting Bioresorbable Vascular Scaffold at Two Years Following Implantation in a Healthy Porcine Coronary Artery Model: Implications of pilot Results for Future Pre-Clinical Studies.

Bill D. Gogas, Maria Radu, Yoshinobu Onuma, Laura Perkins, Jennifer Powers, Josep Gomez-Lara, Vasim Farooq, Hector M.Garcia-Garcia, Roberto Diletti, Richard Rapoza, Renu Virmani, Patrick W. Serruys

International Journal of Cardiovascular Imaging.2011. Mar; 28(3): 499-511 [IF: 2.53]

Evaluation with in vivo optical coherence tomography and histology of the vascular effects of the everolimus-eluting bioresorbable vascular scaffold at two years following implantation in a healthy porcine coronary artery model: implications of pilot results for future pre-clinical studies

Bill D. Gogas · Maria Radu · Yoshinobu Onuma · Laura Perkins · Jennifer C. Powers · Josep Gomez-Lara · Vasim Farooq · Hector M. Garcia-Garcia · Roberto Diletti · Richard Rapoza · Renu Virmani · Patrick W. Serruys

Received: 16 December 2010 / Accepted: 29 March 2011 / Published online: 19 April 2011
© The Author(s) 2011. This article is published with open access at Springerlink.com

Abstract To quantify with in vivo OCT and histology, the device/vessel interaction after implantation of the bioresorbable vascular scaffold (BVS). We evaluated the area and thickness of the strut voids previously occupied by the polymeric struts, and the neointimal hyperplasia (NIH) area covering the endoluminal surface of the strut voids (NIH_{EV}), as well as the NIH area occupying the space between the strut voids (NIH_{BV}), in healthy porcine coronary arteries at 2, 3 and 4 years after implantation of the device. Twenty-two polymeric BVS were implanted in the coronary arteries of 11 healthy Yucatan minipigs that

underwent OCT at 2, 3 and 4 years after implantation, immediately followed by euthanasia. The areas and thicknesses of 60 corresponding strut voids previously occupied by the polymeric struts and the size of 60 corresponding NIH_{EV} and 49 NIH_{BV} were evaluated with both OCT and histology by 2 independent observers, using a single quantitative analysis software for both techniques. At 3 and 4 years after implantation, the strut voids were no longer detectable by OCT or histology due to complete polymer resorption. However, analysis performed at 2 years still provided clear delineation of these structures, by both techniques. The median [ranges] areas of these strut voids were 0.04 [0.03–0.16] and 0.02 [0.01–0.07] mm² by histology and OCT, respectively. The mean (±SD) thickness by histology and OCT was 220 ± 40 and 120 ± 20 μm, respectively. The median [ranges] NIH_{EV} by histology and OCT was 0.07 [0.04–0.20] and 0.03 [0.01–0.08] mm², while the mean (±SD) NIH_{BV} by histology and OCT was 0.13 ± 0.07 and 0.10 ± 0.06 mm². Our study indicates that in vivo OCT of the BVS provides correlated measurements of the same order of magnitude as histomorphometry, and is reproducible for the evaluation of certain vascular and device-related characteristics. However, histology systematically gives larger values for all the measured structures compared to OCT, at 2 years post implantation.

Bill D. Gogas and Maria Radu contributed equally to this manuscript.

B. D. Gogas · M. Radu · Y. Onuma · J. Gomez-Lara · V. Farooq · H. M. Garcia-Garcia · R. Diletti · P. W. Serruys (✉)
Thoraxcenter, Erasmus University Medical Centre, 's Gravendijkwaal 230, 3015 Rotterdam, The Netherlands
e-mail: p.w.j.c.serruys@erasmusmc.nl

L. Perkins · J. C. Powers · R. Rapoza
Abbott Vascular, Santa Clara, CA, USA

R. Virmani
CVPath, Gaithersburg, MA, USA

Keywords Bioresorbable vascular scaffold · Vascular healing · Optical coherence tomography · Histology

Introduction

Bioresorbable coronary scaffolds are a novel approach to the percutaneous treatment of coronary artery disease. Recently, the everolimus-eluting bioresorbable vascular scaffold (BVS) (Abbott Vascular, Santa Clara, Santa Clara, USA) has been studied in the first-in-man ABSORB cohort A trial, which demonstrated the feasibility and safety of this device, with a rate of major adverse cardiac events of 3.4% up to 3 years [1–3]. The BVS is composed of a backbone of poly-L-lactide (PLLA), covered with the polymer poly-D, L-lactide (PDLLA), containing and controlling the release of the drug, everolimus (Novartis, Basel, Switzerland). PLLA and PDLLA degrade to lactic acid which is metabolized via the Krebs' cycle during the bioresorption process. The radiolucent device is visualized on angiography by radio-opaque platinum markers located at each end [4]. The introduction of these new devices prompts us to refine our methods of evaluation, using state-of-the-art imaging modalities, such as optical coherence tomography (OCT). This imaging technique has a near-histological resolution ($\sim 15 \mu\text{m}$), which makes it ideal for studying the device/vessel interaction in detail [5]. As the polymeric struts are translucent, light-based imaging modalities are particularly suitable for this purpose. Up to now, histological morphometry has been crucial in the evaluation of the performance of new devices [6]. As histology is limited to animal and human post-mortem studies, in vivo assessment using OCT is highly desirable. This porcine study was set up in 2006 with the goal to evaluate the device/vessel interaction after implantation of the BVS at 2, 3 and 4 years, using OCT and histology. The qualitative strut-related characteristics with regards to the process of biodegradation were published recently [7]. In this part of the study, we sought to evaluate whether mimicking the histological morphometric approach using OCT is feasible and reproducible for the evaluation of the vascular healing following implantation with the BVS.

Specifically, we sought to compare a number of quantitative parameters assessed by *ex vivo*/"post

processed" histology and *in vivo*/"non-processed" OCT, in order to assess the agreement between these techniques. These parameters include: the number and size of the structures resembling struts, and quantification of the tissue growth covering the endoluminal surface and the tissue growth between these structures.

Methods

Study sample and OCT imaging

Twenty two polymeric devices, BVS revision 1.0 ($3 \times 12 \text{ mm}$) were implanted in 11 healthy Yucatan minipig coronary arteries, with a balloon: artery ratio of 1.2:1. The BVS revision 1.0 has three main components: the polymeric backbone, the polymeric drug reservoir, and the antiproliferative drug, everolimus. The polymeric scaffold is balloon-expandable, and is composed of a high molecular weight PLLA with serpentine rings interconnected by links. The scaffold body design is coated with a matrix of PDLLA and everolimus in a 1:1 ratio. The device is laser cut from an extruded tube and has two radio-opaque platinum markers at both ends [8]. Since OCT at 3 and 4 years following implantation displayed no signal at the site where struts were expected to have been previously implanted, we evaluated only the devices available at 2 years follow-up. At this time point, the PLLA backbone is almost completely resorbed, as evidenced by gel permeation chromatography, and histology shows accumulations of proteoglycans (stained positively with Alcian blue) at corresponding sites. By OCT, however, these "strut voids" appear as well delineated hyporeflective foci. Since it is known that by OCT, immediately after implantation, BVS polymeric struts appear as black boxes with bright borders [1], these findings indicate that OCT does not distinguish between the BVS strut polymeric material and the provisional matrix that replaces the strut after full bioresorption [7]. Throughout the entire length of this manuscript, we will use the term "strut void" to describe these strut-like structures, previously occupied by the polymeric material.

OCT was performed *in vivo* using the M2 CV imaging system (LightLab Imaging, Westford, MA, USA). In brief, the low-pressure HeliosTM occlusion

balloon catheter was advanced distally to the region of interest over a conventional 0.014 inch angioplasty wire, which was then exchanged with the OCT ImageWire™. After calibration of the image wire by correction of the Z-offset [9], the occlusion balloon catheter was withdrawn proximally to the region of interest, and inflated to 0.5–0.7 atmospheres. During image acquisition, blood clearance was achieved by manual continuous flushing with lactated Ringer's solution. Cross-sectional images were acquired at 15.6 frames/s, with an automatic pullback speed of 1 mm/s. Images were stored digitally for off-line analysis.

Processing for histology and selection of corresponding OCT and histology images

Animal sacrifice was performed immediately after OCT imaging by intravenous sodium pentobarbital infusion. The heart was explanted from the thoracic cavity, the aorta clamped, and the coronary arteries were pressure perfused at 100–120 mm Hg: first with 0.9% saline, followed by 10% neutral buffered formalin for approximately 30 min. Hearts were then immersed in formalin for complete fixation. Following this, arteries were carefully dissected off the heart. The location of the scaffolds was confirmed by high-contrast film-based radiographs (Faxitron X-ray Corp., Lincolnshire, IL, USA) and the specimens were dehydrated in a graded series of ethanol. The scaffold segments were then embedded in methyl methacrylate (MMA) for polymerization [4]. The MMA block was sawed into three 4 mm segments, and three cross-sections were cut using a rotary microtome with a tungsten carbide blade: one at the proximal scaffold segment, 2 mm distal to the proximal metallic marker; one at the middle segment, 6 mm distal to the proximal marker; and one at the distal scaffold segment, 2 mm proximal to the distal marker. Finally, the samples were mounted and stained with hematoxylin and eosin (HE) and/or elastic Van Gieson (EVG).

Corresponding OCT cross-sections were selected by one observer (YO), using the distances from the platinum markers and anatomical landmarks, such as side branches, as references. Two observers (BG, MR) identified the corresponding structures of interest. The quantitative analysis was performed with the observers blinded to each other's results, as well as to

the correspondence between the OCT and histology images. We assumed that the sharp boundary of the strut voids by histology corresponded to the sharply delineated bright borders of the “black boxes” by OCT.

Quantitative analysis of OCT and histology images

OCT and histology images were analyzed with the QCU-CMS software version 4.64 (Laboratory of Clinical and Experimental Image processing, Leiden, The Netherlands), which has previously been shown to provide correlated quantitative measurements as compared to the LightLab software [20]. Once images were uploaded, calibration was performed: for OCT, the diameter (0.36 mm) of the image wire was used, whilst histology images were calibrated using the scale bar provided by the pathologist. After calibration of the images, the following parameters were quantified: (1) the number of strut voids previously occupied by the polymeric struts (2) the lumen area and the area encompassing the abluminal surfaces of these strut voids; (3) the area and thickness of these strut voids and (4) the neointimal hyperplasia (NIH) area covering the endoluminal surface (NIH_{EV}) and the NIH area between the strut voids (NIH_{BV}) (Fig. 1). To be more specific, the measurements were performed in the following way (Figs. 1 and 2): 1. “Scaffold” area: after manual localization of the strut voids by setting a green circle at the mid point of their abluminal surfaces, these points were connected automatically by a trace line placed by the software. In addition, the center of gravity of the scaffold area was determined automatically by the software. 2. Lumen area: the lumen contour was automatically traced by the software; 3. The area of the strut void: this was manually demarcated by following the contour of these structures; 4. NIH_{BV}: in order to demarcate the NIH areas laterally, we used the angle tool of the software, which takes the center of gravity of the scaffold as reference.

The rays of the angle tool were placed as help lines, at the edges of every strut void creating an area between these which was limited axially by the scaffold line and the lumen contour and laterally by the help lines (Fig. 1 and 2); 5. NIH_{EV}: was defined as the area limited by the “help lines” placed at the edges of the strut voids, their endoluminal surfaces,

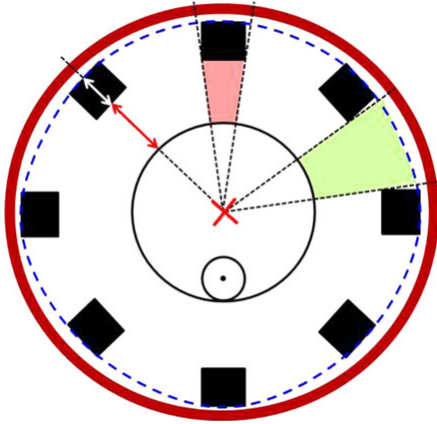


Fig. 1 Schematic representation of the quantitative analysis. Panel a The *thick red line* represents the vessel wall; the *black continuous line*, the lumen contour; *black squares* strut voids previously occupied by the polymeric struts; and the *blue dotted line* the abluminal “scaffold” area. The *red cross* indicates the center of gravity of the remnants of the scaffold, which was provided automatically by the software after manual indication of the mid point of the abluminal surfaces of the strut-like structures. The center of gravity point was used to place “the help lines” (*black dotted lines*) for the measurement of the neointimal hyperplasia area covering the endoluminal surface of these structures (*red area*), and the neointimal hyperplasia area between these structures (*green area*). The neointimal thickness (*red arrow*) was measured from the endoluminal surface of the strut voids to the lumen contour, along a line projected through the center of gravity of the scaffold and the mid point of the abluminal surface of these structures. The strut void thickness (*white arrow*) was measured in a similar way

and the lumen area contour; 6. Neointimal thickness: this was measured from the mid point of the endoluminal surface of the strut voids to the lumen contour, along a line projected through the center of gravity of the scaffold; 7. Strut void thickness: this was assessed by measuring the distance between the mid points of the endoluminal and abluminal surfaces of the strut voids.

Statistical analysis

Statistical analyses were performed with SPSS, version 16 (SPSS Inc., Chicago, IL, USA). Discrete variables are presented as counts and percentages, and continuous variables as mean \pm standard

deviations, or medians and interquartile ranges or ranges (minimum–maximum). The Pearson’s correlation coefficient (r^2) was computed to compare OCT and histological measurements. Bland–Altman plots, displaying the systematic (mean absolute difference) and random (95% limits of agreement) errors, and the interclass correlation coefficient for absolute agreement (ICCa) and consistency (ICCC) were used to assess the agreement between techniques. Interobserver variability was assessed using the correlation coefficient (r^2). A two-sided p-value ≤ 0.05 was considered significant.

Results

A total of six corresponding cross-sections were available for the purpose of this study (Fig. 3). Histology displayed 75 strut voids previously occupied by the polymeric struts whilst OCT showed only 60. Fifteen of these strut voids by histology could not be identified in the OCT images due to non-uniform rotational distortion, marginalization of the image wire into a side branch and a long distance to the image wire, together with a low light incidence angle resulting in a high light attenuation (Fig. 4). Thus, a total of 60 corresponding strut voids were included in the analysis. In only 1 of 6 frames were all corresponding strut remnants visualised by both OCT and histology with the consequence that the lumen and scaffold area was only accurately assessed in this frame (OCT: 2.78 and 5.14 mm²; histology: 1.02 and 4.40 mm², for lumen and scaffold area, respectively). The ratio between the lumen area and stent area for the OCT was 0.54 while for histology was 0.23 and the % area obstruction of the scaffold for OCT was 45% while for histology 76%. Apart from the strut voids that were not adequately visualized, all images were successfully analysed using the histomorphometrical methodology with the dedicated off-line software. Table 1 and Fig. 5 show the descriptive statistics and Bland–Altman plots for the different parameters measured with OCT and histology. The average difference and 95% limits of agreement were: for the strut area: 0.03 [0.07; –0.01], for the strut thickness: 0.10 [0.18; 0.02], for the NIHEV: 0.04 [0.10; –0.02] and for the NIHBV: 0.03 [0.21; 0.15]. In general, histomorphometry provided larger values for all parameters compared

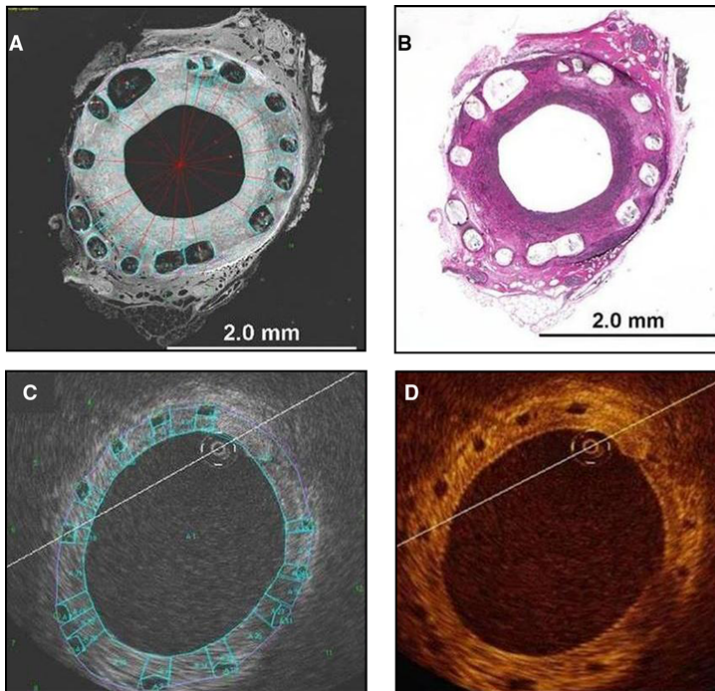


Fig. 2 Demonstration of quantitative measurements by histology and OCT. Panels **A** and **B** show the *inverted grey scale* and color histology images, respectively, with superimposed quantitative measurements (*green lines* in **A**), and panels **C** and **D**, the corresponding grey scale and sepia OCT, with the

respective measurements (only **C**). The *red lines* are provided by the software, and are projected from the center of gravity of the scaffold through the mid points of the abluminal surfaces of the struts

to OCT. Interobserver variability was evaluated for all variables assessed with histology and OCT (Fig. 6). The mean (SD) differences between observers were negligible for the parameters measured in the histological sections (area and thickness of strut voids 0.00 (0.00) mm² and 0 (30) μm, respectively; NIH_{EV} 0.00 (0.00) mm², and NIH_{BV} 0.00 (0.01) mm²), as well as for those assessed in the OCT cross-sections (for area and thickness of strut voids: 0.00 (0.00) mm² and 0 [10] μm, respectively; for NIH_{EV} 0.00 (0.01) mm², and NIH_{BV} -0.03 (0.01) mm²).

The Lin's correlation coefficient interpreted by the ICCs and ICCa for the area of strut voids were: 0.34 [95% confidence interval (CI): 0.10–0.55], $P < 0.004$ and 0.18 [95% CI: -0.08 to 0.43], $P < 0.004$; for the thickness of these structures: 0.08 [95% CI: -0.18 to

0.33], $P = 0.271$ and 0.01 [95% CI: -0.03 to 0.07], $P = 0.271$; for NIH_{EV}: 0.39 [95% CI: 0.15–0.59], $P < 0.001$ and 0.19 [95% CI: -0.09 to 0.46], $P < 0.001$; and for NIH_{BS}: -0.03 [95% CI: -0.29 to 0.29], $P = 0.50$ and -0.03 [95% CI: -0.27 to 0.28], $P = 0.50$.

The Pearson's correlation coefficient (r^2) for the interobserver variability for the histology assessment was: for the thickness and area of the strut voids thickness: $r^2 = 0.89$ and $r^2 = 0.78$, respectively; for NIH_{EV}: $r^2 = 0.87$; and for NIH_{BV}: $r^2 = 0.86$ ($P < 0.001$ for all analyses). Corresponding results for the OCT measurements were: for thickness and area of strut voids: $r^2 = 0.70$ and $r^2 = 0.57$, respectively; for NIH_{EV}: $r^2 = 0.67$; and for NIH_{BV}: $r^2 = 0.66$ ($P < 0.001$ for all analyses).

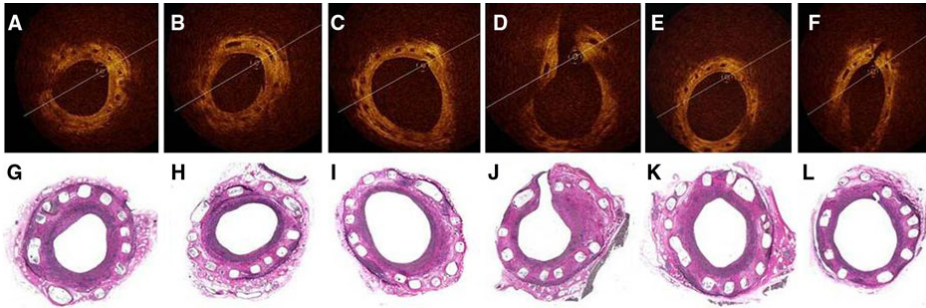


Fig. 3 Cross-sections of corresponding OCT and histology of the left anterior descending artery (*A/G, B/H, C/I*), and the right coronary artery (*D/J, E/K, F/L*). Histology specimens are stained with elastic Van Gieson

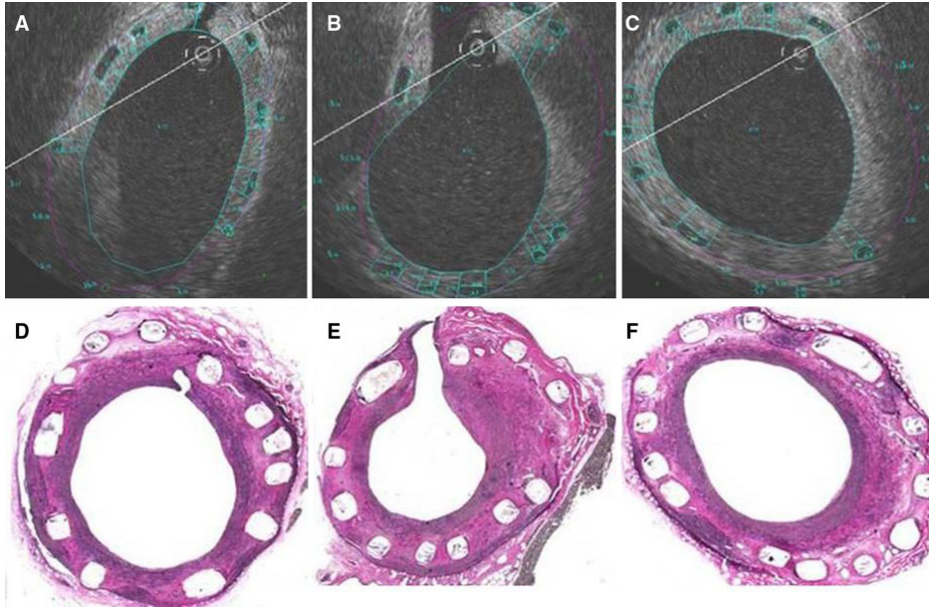


Fig. 4 Factors precluding identification of some of the strut voids in corresponding OCT and histology images. Panels **A–C** demonstrate how non-uniform rotational distortion (**A**), marginalisation of the image wire into a side branch (**B**), and a long distance between the image wire and *black boxes* preclude visualisation of these strut voids by OCT, as compared to corresponding histology (**D–F**). Due to the lack of visualization

of these structures, abluminal scaffold areas could not be accurately assessed. In order to obtain reproducible measurements, it was before the analysis decided to trace the scaffold area only at the sites of *black boxes* that are visualized, with the consequence of an underestimation of the “true” OCT scaffold area

Table 1 Descriptive statistics of all parameters measured by OCT and histology

	OCT	Histology
Area of the strut voids, mm ²	0.02 (0.01–0.07)	0.04 (0.03–0.16)
Thickness of the strut voids	120 (70–180)	220 (120–350)
NIH _{BV} , mm ²	0.03 (0.01–0.08)	0.07 (0.04–0.20)
NIH _{EV} , mm ²	0.09 (0.01–0.27)	0.13 (0.01–0.31)

NIH neointimal hyperplasia, BV between the voids, EV endoluminal surfaces of the voids, values are median (range)

Discussion

In the present study, we performed a quantitative analysis of in vivo OCT images of the remnants of bioresorbable vascular scaffolds at 2 years following implantation, using a methodology similar to the morphometric approach used with histology. The main findings of this pilot study are: 1. Histology appears to systematically give larger values, when compared with OCT; 2. the approach similar to histomorphometry for quantitative analysis of OCT images is feasible and reproducible for the evaluation

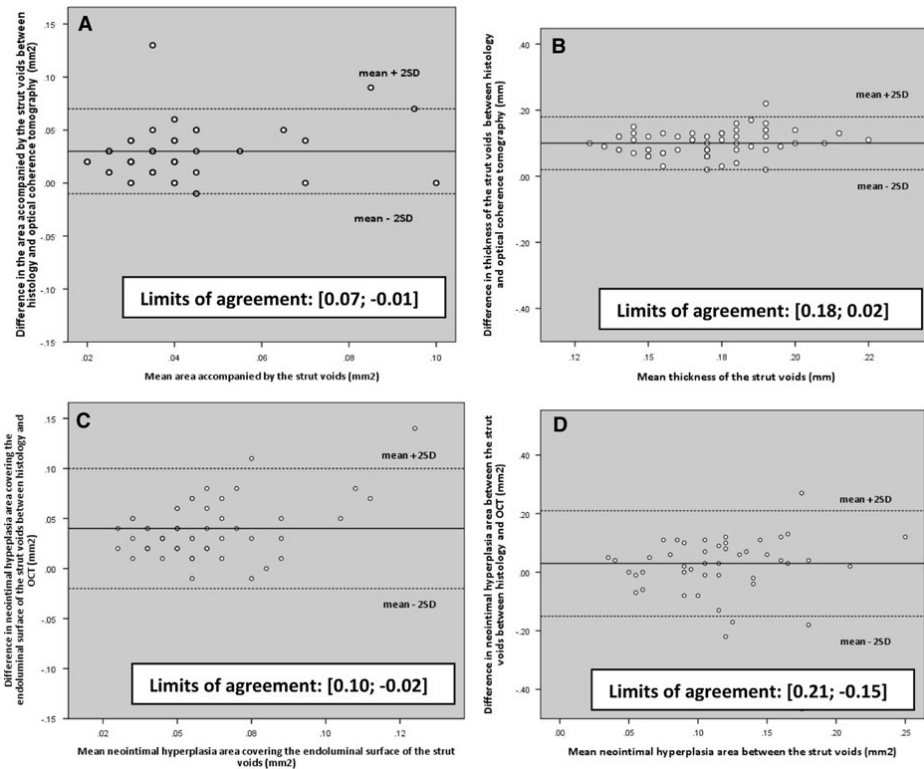


Fig. 5 Bland-Altman plots depicting the agreement between techniques for the evaluation of the area (panel A) and thickness (panel B) of the strut voids previously occupied by the polymeric struts, the neointimal hyperplasia area covering

the endoluminal surface of these voids (panel C), and the neointimal hyperplasia area between the voids (panel D), with histology and OCT

at follow up after implantation of the BVS; and 3. despite the use of anatomical landmarks and intrascaffold radiopaque markers to identify corresponding cross-sections, higher numbers of strut voids were visualized by histology than by OCT.

Differences in quantitative measurements between OCT and histology

The observation that quantitative measurements by histology and OCT may differ is not new, as previous studies have suggested that histological processing may induce a certain degree of artifacts related to formalin fixation and dehydration [10]. Surprisingly however, our study showed that all morphological characteristics analyzed were systematically larger by histology as compared to OCT. More specifically, the strut void area, strut void thickness, NIH_{EV} and NIH_{BV} were 100%, 83%, 130% and 44% larger by histology compared to OCT, respectively. Several factors may have contributed to this difference. The first involves the calibration of the OCT image wire by adjustment of the Z-offset before image acquisition, as well as calibration of the scaling of OCT and histology images before analysis, which are crucial for any quantitative measurement. In the present study, these were all performed according to current standards [9]. Secondly, differences can potentially be related to the application of different analysis softwares for different techniques. We tried to circumvent this by utilizing the same software, as well as by using semi-automatic approaches, for all analyses, which was evidenced in the good interobserver reproducibility seen. Nevertheless, the quantitative results by histology were systematically larger than by OCT, as compared to previous studies, even if these applied different softwares for the different techniques [11, 12]. Other interfering factors are therefore likely to be involved. For the NIH areas, our results resemble those reported by Murata et al. and Templin et al., who found that histology estimated the NIH areas covering metallic stents slightly higher than OCT, at 28 and 90 days, and at 10, 14 and 28 days, respectively [13, 14]. However, in our study, the overestimation by histology was greater. This may be related to the combined differences in: the mechanical constraints imparted on the tissue between the bioresorbable vascular scaffold as

compared to metallic stents; in the tissue composition at time point of examination (2 years), which includes a higher proportion of collagen and smooth muscle cells as compared to time points less than 90 days [15]; and in the composition of the strut voids which, as shown by Onuma et al., are replaced by highly water-containing acid mucopolysaccharides material, which stains positively with Alcian Blue, at this time point [7]. Further, previous studies have indicated that formaldehyde, which we used for tissue fixation, can cause dimensional changes that are dependent on the composition of the tissue (for example causing swelling in liver tissue and shrinkage in muscle tissue), the pH of the tissue, and the temperature and concentration of the fixative [10]. In addition to tissue fixation, dehydration with ethanol, embedding and polymerization in MMA, and subsequent deplastization likely further impacted the tissue dimensions obtained histologically. Considering the contrasting nature of the tissues at late follow-up of the BVS, namely the proteoglycan-rich tissue replacing pre-existing struts compared to the surrounding smooth muscle cell and collagen-dense tissue of the arterial wall, these tissue-specific dimensional changes are especially notable at follow-up after implantation of the BVS. This is supported by the qualitative results regarding the histological appearance of the strut-like structures at 2 and 3 years. At 2 years, the strut voids appear more spherical, having a highly water-containing proteoglycan, while they are contracted and almost completely coalesced into the arterial wall at 3 years (Fig. 6) [7]. Considering this, it is likely that the proteoglycan-based nature of strut foci at 2 years resulted in their swelling as an artifact of histological processing.

The fact that OCT was performed *in vivo*, when the vessel has a tonus and is naturally pressurized, may also explain some of the discrepancies, although efforts were made to pressurize vessels during histology preparation. However, the most plausible explanation involves the attempt to correspond OCT and histology cross-sections, which depends on the orientation of the OCT image wire relative to the vessel curvature and relative to the location in the vessel lumen, which in turn influence how the OCT “biotome” cross-sects the tissue and the scaffold. The difficulty finding completely corresponding cross-sections may be further affected by the

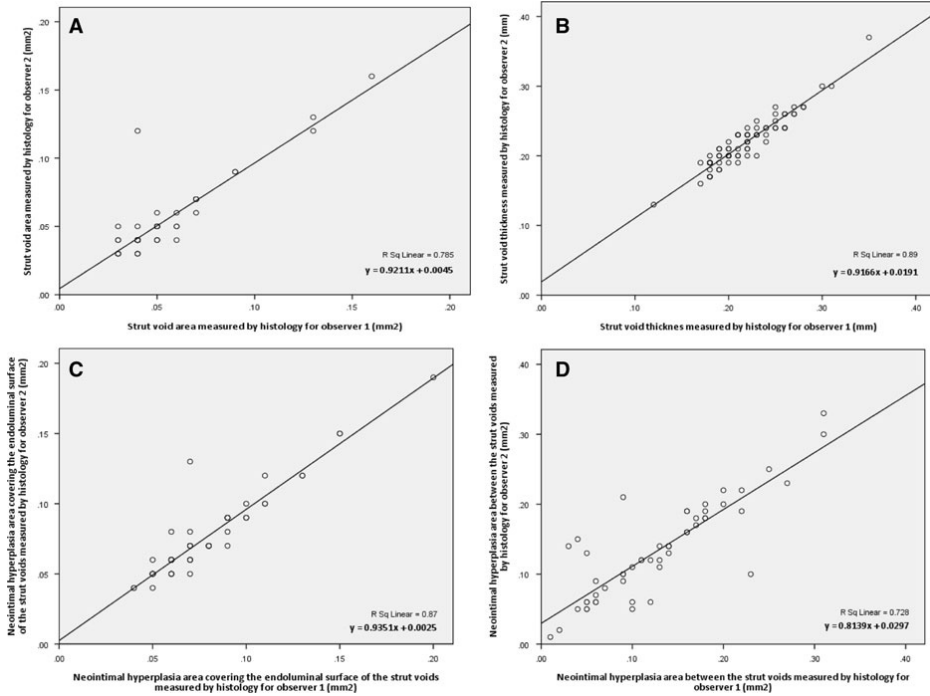


Fig. 6 Linear regression analysis plots depicting the inter-observer variability for the evaluation of the area and thickness of the strut voids, the neo-intimal hyperplasia area covering the

endoluminal surface of these voids, and the neo-intimal hyperplasia area between the voids, with histology (panels A–D) and OCT (panels E–H), respectively

differences in slice thicknesses of the samples provided by the different techniques. For histology, the minimum slice thickness possible to obtain, is in the range of 4–5 μm with a sampling interval of 100 μm [16], and depends on the microtome, while the minimum frame thickness available with the OCT system used in the present study is 60 μm and depends on the longitudinal sampling distance, which is in turn related to the frame rate (15.6 frames/s) and the pullback speed (1 mm/s). Nevertheless, it should be stressed that wherever possible, efforts were made to secure corresponding cross-sections by histology and OCT using the scaffold platinum markers and anatomical structures, as landmarks. Thus, our report highlights some of the difficulties that may be encountered in this type of study, which are important to acknowledge (Fig. 7).

Consideration of technical aspects with OCT imaging

Although efforts were made to obtain matched cross-sections between OCT and histology using landmarks, we found a higher density of strut voids by histology than by OCT. In addition to the factors mentioned above, we noticed that the intrinsic properties of the OCT technology related to the use of light also influenced our analysis. By marginalization of the light source, causing an acute incidence angle of the light on the vessel wall, as well as by the relatively low scan diameter of the employed time domain-OCT system (7 mm) compared to newer generation frequency domain (FD)-OCT systems (10 mm), visualisation of the strut voids along the entire 360 degree vessel circumference was hindered

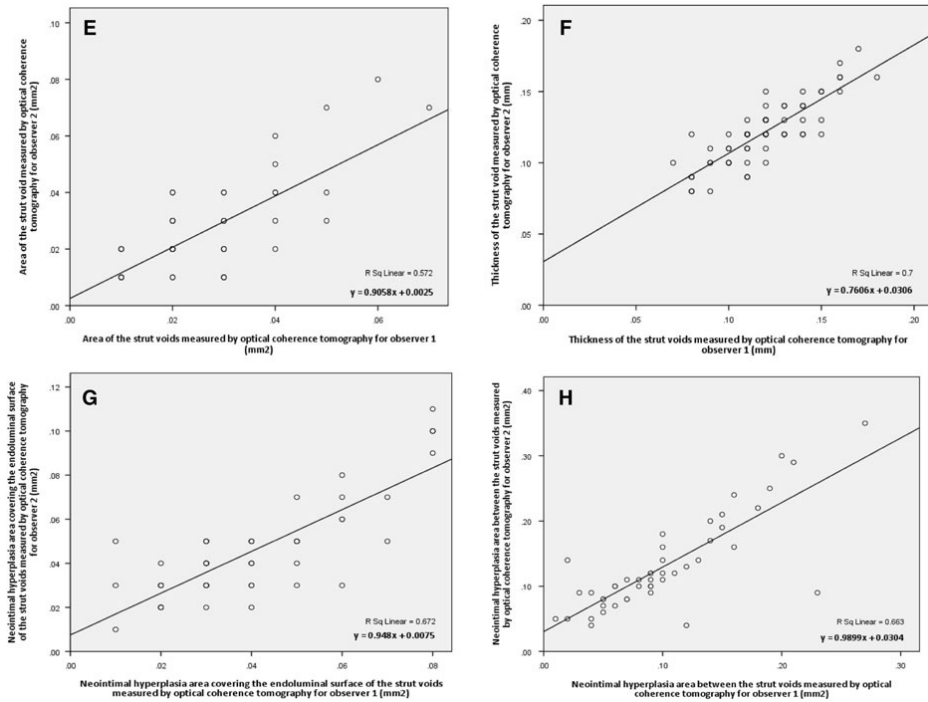


Fig. 6 continued

(Fig. 3B, C), which prevented the identification of these structures and the accurate delineation of the abluminal scaffold area, as well as delineation of the lumen area. Nevertheless, the only available accurate corresponding lumen and scaffold areas by OCT and histomorphometry showed that measurements by OCT were larger than those by histology, which is in line with previous studies [11–13]. Despite the potential advantages of *in vivo* “non-processed” OCT, the presence of non-uniform rotational distortion, which is related to vessel tortuosity, as well as the presence of artefacts due to heart motion in systole and diastole, further complicated the selection of perfectly corresponding frames. The new generation FD-OCT which has a much higher frame rate, allowing a higher pullback-speed without significant loss in longitudinal sampling density [14, 17, 18], promises to overcome some of these issues, together with recent advances allowing retrospective

reconstruction of gated OCT acquisitions [19]. However, these technologies were not available at the time of data acquisition.

Histomorphometry-like analysis with OCT

Onuma et al. recently described a qualitative analysis of OCT images of the polymeric struts of the BVS. As opposed to that analysis, our study focused on the evaluation of the quantitative tissue response around the strut voids previously occupied by the polymeric struts in terms of neointimal hyperplasia between and on the endoluminal surface of these, which we found to be feasible and reproducible, with a good interobserver reproducibility. Despite the mentioned issues regarding comparison between OCT and histology, OCT represents at present the *in vivo* imaging modality with the highest resolution, which enables

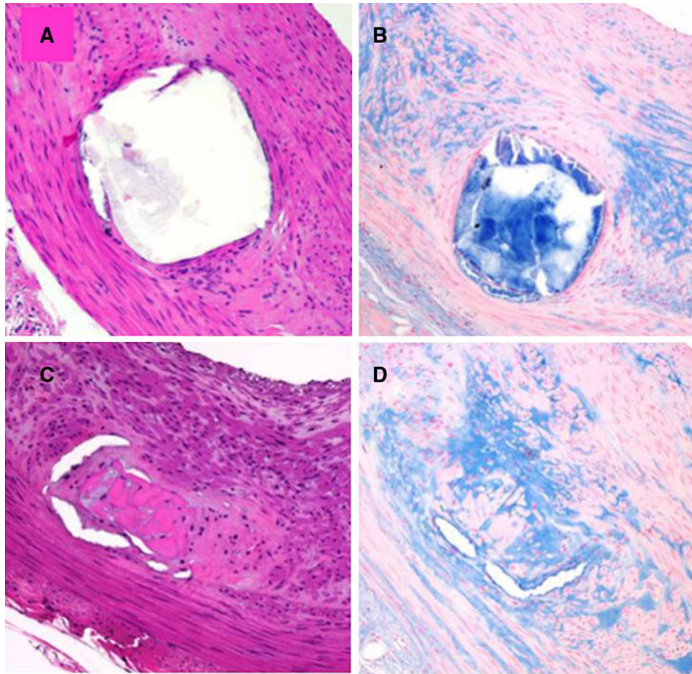


Fig. 7 Histological examples of the appearance of strut voids at 2 and 3 years following implantation of the bioresorbable vascular scaffold. Panels **A–D** show strut voids at 2 and 3 years follow-up, respectively. At 2 years, the proteoglycan-rich matrix appears to collapse in the middle of the void upon histological preparation, giving a spherical appearance, while

the matrix at 3 years is coalesced with the neointima of the vessel wall, giving the impression that the borders of the contents of the void are better held together with the neointima. Panels **A** and **C** are stained with hematoxylin and eosin, while panels **B** and **D** are stained with Alcian blue. Reproduced from Onuma et al. *Circulation* 2010

us to evaluate fine details in the assessment of the device/vessel interaction.

Study limitations

Our initial goal was to assess the morphometric parameters of the remnants of the device implanted with OCT at 2, 3, and 4 years following implantation. As part of the degradation process, the number of bioresorbable struts identified by OCT decreased with time. We now know that the polymeric struts are completely resorbed and replaced by proteoglycans by 2 years. However, this respective time point could not be foreseen at the time of planning of the study. For the comparison of different measurements

by OCT and histology, it was necessary to select a time point where strut-like structures (strut voids) are fully visible with OCT. Consequently, specimens at 3 and 4 years could not be included in this study, wherefore the sample size was relatively small. We cannot dismiss the possibility that the low sample size could, to some extent, explain the relatively large distribution of individual parameters. Nevertheless, we believe that the findings of this pilot study are interesting as they represent our initial quantitative experience with the novel bioresorbable technology, and may serve as a guide to the planning of future trials with corresponding OCT and histomorphometry to evaluate bioresorbable vascular scaffolds.

Conclusion

The present pilot study showed that an approach for quantitative analysis of OCT images akin to histomorphometry is feasible and reproducible for the evaluation of the vascular healing at follow up after implantation of the BVS and that corresponding OCT and histomorphometry provide results of the same order of magnitude. Despite the use of landmarks to identify corresponding cross-sections, histology systematically provided larger measurements for all studied parameters. Whether this is related to factors influencing acquisition and processing of images, or the bioresorbable nature of the device, requires further investigation, for example using the new-generation FD-OCT, and a larger sample analysed with a higher sampling density.

Acknowledgments Bill D. Gogas wishes to acknowledge the continued funding support of the Hellenic Heart Foundation (ELIKAR), Athens, Greece.

Conflicts of interest Laura Perkins, Jennifer Powers, and Richard Rapoza are employees of Abbott Vascular.

Open Access This article is distributed under the terms of the Creative Commons Attribution Noncommercial License which permits any noncommercial use, distribution, and reproduction in any medium, provided the original author(s) and source are credited.

References

- Ormiston JA, Serruys PW, Regar E, Dudek D, Thuesen L, Webster MW, Onuma Y, Garcia-Garcia HM, McGreevy R, Veldhof S (2008) A bioabsorbable everolimus-eluting coronary stent system for patients with single de novo coronary artery lesions (ABSORB): a prospective open-label trial. *Lancet* 371(9616):899–907
- Serruys PW, Ormiston JA, Onuma Y, Regar E, Gonzalo N, Garcia-Garcia HM, Nieman K, Bruining N, Dorange C, Miquel-Hebert K, Veldhof S, Webster M, Thuesen L, Dudek D (2009) A bioabsorbable everolimus-eluting coronary stent system (ABSORB): 2-year outcomes and results from multiple imaging methods. *Lancet* 373(9667):897–910
- Onuma Y, Serruys PW, Ormiston JA, Regar E, Webster M, Thuesen L, Dudek D, Veldhof S, Rapoza R (2010) Three-year results of clinical follow-up after a bioresorbable everolimus-eluting scaffold in patients with de novo coronary artery disease: the ABSORB trial. *Euro Interven* 6(4):447–453
- Ormiston JA, Serruys PW (2009) Bioabsorbable coronary stents. *Circ Cardiovasc Interv* 2(3):255–260
- Regar E, Schaar JA, Mont E, Virmani R, Serruys PW (2003) Optical coherence tomography. *Cardiovasc Radiat Med* 4(4):198–204
- Virmani R, Kolodgie FD, Farb A, Lafont A (2003) Drug eluting stents: are human and animal studies comparable? *Heart* 89(2):133–138
- Onuma Y, Serruys PW, Perkins LE, Okamura T, Gonzalo N, Garcia-Garcia HM, Regar E, Kamberi M, Powers JC, Rapoza R, van Beusekom H, van der Giessen W, Virmani R (2010) Intracoronary optical coherence tomography and histology at 1 month and 2, 3, and 4 years after implantation of everolimus-eluting bioresorbable vascular scaffolds in a porcine coronary artery model. An attempt to decipher the human optical coherence tomography images in the ABSORB trial. *Circulation* 122(22):2288–2300
- Okamura T, Garg S, Gutierrez-Chico JL, Shin ES, Onuma Y, Garcia-Garcia HM, Rapoza RJ, Sudhir K, Regar E, Serruys PW (2010) In vivo evaluation of stent strut distribution patterns in the bioabsorbable everolimus-eluting device: an OCT ad hoc analysis of the revision 1.0 and revision 1.1 stent design in the ABSORB clinical trial. *Euro Interven* 5(8):932–938
- Gonzalo N, Garcia-Garcia HM, Serruys PW, Commissaris KH, Bezerra H, Gobbens P, Costa M, Regar E (2009) Reproducibility of quantitative optical coherence tomography for stent analysis. *EuroIntervention* 5(2):224–232
- Bahr GF, Bloom G, Friberg U (1957) Volume changes of tissues in physiological fluids during fixation in osmium tetroxide or formaldehyde and during subsequent treatment. *Exp Cell Res* 12(2):342–355
- Suzuki Y, Ikeno F, Koizumi T, Tio F, Yeung AC, Yock PG, Fitzgerald PJ, Fearon WF (2008) In vivo comparison between optical coherence tomography and intravascular ultrasound for detecting small degrees of in-stent neointima after stent implantation. *JACC Cardiovasc Interv* 1(2):168–173
- Gonzalo N, Serruys PW, Garcia-Garcia HM, van Soest G, Okamura T, Ligthart J, Knaapen M, Verheye S, Bruining N, Regar E (2009) Quantitative ex vivo and in vivo comparison of lumen dimensions measured by optical coherence tomography and intravascular ultrasound in human coronary arteries. *Rev Esp Cardiol* 62(6):615–624
- Murata A, Wallace-Bradley D, Tellez A, Alviar C, Aboodi M, Sheehy A, Coleman L, Perkins L, Nakazawa G, Mintz G, Kaluza GL, Virmani R, Granada JF (2010) Accuracy of optical coherence tomography in the evaluation of neointimal coverage after stent implantation. *JACC Cardiovasc Imaging* 3(1):76–84
- Templin C, Meyer M, Muller MF, Djonov V, Hlushchuk R, Dimova I, Flueckiger S, Kronen P, Sidler M, Klein K, Nicholls F, Ghadri JR, Weber K, Paunovic D, Corti R, Hoerstrup SP, Luscher TF, Landmesser U (2010) Coronary optical frequency domain imaging (OFDI) for in vivo evaluation of stent healing: comparison with light and electron microscopy. *Eur Heart J* 31(14):1792–1801
- Farb A, Kolodgie FD, Hwang JY, Burke AP, Tefera K, Weber DK, Wight TN, Virmani R (2004) Extracellular matrix changes in stented human coronary arteries. *Circulation* 110(8):940–947
- Bruining N, Knaapen M, de Winter S, Van Langenhove G, Serruys PW, Hamers R, de Feijter PJ, Verheye S (2009) A

- histological “fly-through” of a diseased coronary artery. *Circ Cardiovasc Imaging* 2(2):e8–e9
17. Kawase Y, Suzuki Y, Ikeno F, Yoneyama R, Hoshino K, Ly HQ, Lau GT, Hayase M, Yeung AC, Hajjar RJ, Jang IK (2007) Comparison of nonuniform rotational distortion between mechanical IVUS and OCT using a phantom model. *Ultrasound Med Biol* 33(1):67–73
 18. Okamura T, Onuma Y, Garcia-Garcia H, Bruining N, Serruys P High-speed intracoronary optical frequency domain imaging: implications for three-dimensional reconstruction and quantitative analysis (submitted)
 19. Sihan K, Botha C, Post F, De Winter S, Gonzalo N, Regar E, Serruys P, Hamers R, Bruining N (2010) Retrospective image-based gating of intracoronary optical coherence tomography: implications for quantitative analysis. *EuroIntervention* 6. [Epub ahead of print]
 20. Okamura T, Gonzalo N, Gutierrez-Chico JL, Serruys P, Bruining N, de Winter S, Dijkstra J, Comossaris K, van Geuns RJ, van Soest G, Ligthart J, Regar E (2010) Reproducibility of coronary Fourier domain optical coherence tomography: quantitative analysis of in vivo stented coronary arteries using three different software packages. *EuroIntervention* 6:371–379

Chapter 12

Intracoronary Optical Coherence Tomography and Histology of Overlapping Everolimus-Eluting Bioresorbable Vascular Scaffolds in a Porcine Coronary Artery Model: The Potential Implications for Clinical Practice.

Vasim Farooq, Patrick W Serruys, Jung Ho Heo, **Bill D Gogas**, Laura E Perkins, Yoshinobu Onuma, Roberto Diletti, Maria D. Radu, Lorenz Raber, Christos V Bourantas, Eric van Remortel, Ravindra Pawar, Richard J Rapoza, Jennifer C Powers, Heleen van Beusekom, Hector M. Garcia-Garcia, and Renu Virmani

JACC Cardiovasc Interv. 2013 May; 6(5): 523-32 [IF: 6.83]

Intracoronary Optical Coherence Tomography and Histology of Overlapping Everolimus-Eluting Bioresorbable Vascular Scaffolds in a Porcine Coronary Artery Model

The Potential Implications for Clinical Practice

Vasim Farooq, MB ChB,* Patrick W. Serruys, MD, PhD,* Jung Ho Heo, MD,* Bill D. Gogas, MD,* Yoshinobu Onuma, MD,* Laura E. Perkins, DVM, DACVP,† Roberto Diletti, MD,* Maria D. Radu, MD,* Lorenz Räber, MD,* Christos V. Bourantas, MD, PhD,* Yaojun Zhang, MD,* Eric van Remortel, BSc,‡ Ravindra Pawar, BSc,‡ Richard J. Rapoza, PhD,† Jennifer C. Powers, BS,† Heleen M. M. van Beusekom, PhD,* Hector M. Garcia-Garcia, MD, MSc, PhD,* Renu Virmani, MD, PhD§

Rotterdam, the Netherlands; Santa Clara, California; and Gaithersburg, Maryland

Objectives This study sought to assess the vascular response of overlapping Absorb stents compared with overlapping newer-generation everolimus-eluting metallic platform stents (Xience V [XV]) in a porcine coronary artery model.

Background The everolimus-eluting bioresorbable vascular scaffold (Absorb) is a novel approach to treating coronary lesions. A persistent inflammatory response, fibrin deposition, and delayed endothelialization have been reported with overlapping first-generation drug-eluting stents.

Methods Forty-one overlapping Absorb and overlapping Xience V (XV) devices (3.0 × 12 mm) were implanted in the main coronary arteries of 17 nonatherosclerotic pigs with 10% overstretch. Implanted coronary arteries were evaluated by optical coherence tomography (OCT) at 28 days (Absorb n = 11, XV n = 7) and 90 days (Absorb n = 11, XV n = 8), with immediate histological evaluation following euthanasia at the same time points. One animal from each time point was evaluated with scanning electron microscopy alone. A total of 1,407 cross sections were analyzed by OCT and 148 cross sections analyzed histologically.

Results At 28 days in the overlap, OCT analyses indicated 80.1% of Absorb struts and 99.4% of XV struts to be covered ($p < 0.0001$), corresponding to histological observations of struts with cellular coverage of 75.4% and 99.6%, respectively ($p < 0.001$). Uncovered struts were almost exclusively related to the presence of “stacked” Absorb struts, that is, with a direct overlay configuration. At 90 days, overlapping Absorb and overlapping XV struts demonstrated >99% strut coverage by OCT and histology, with no evidence of a significant inflammatory process, and comparable % volume obstructions.

Conclusions In porcine coronary arteries implanted with overlapping Absorb or overlapping XV struts, strut coverage is delayed at 28 days in overlapping Absorb, dependent on the overlay configuration of the thicker Absorb struts. At 90 days, both overlapping Absorb and overlapping XV have comparable strut coverage. The implications of increased strut thickness may have important clinical and design considerations for bioresorbable platforms. (J Am Coll Cardiol Intv 2013;6:523–32) © 2013 by the American College of Cardiology Foundation

From the *Erasmus University Medical Centre, Rotterdam, the Netherlands; †Abbott Vascular, Santa Clara, California; ‡Cardialysis BV, Rotterdam, the Netherlands; and the §CVPath Institute, Gaithersburg, Maryland. The porcine study was supported by Abbott Vascular (Santa Clara, California). Drs. Perkins, Rapoza, and Powers are employees of Abbott Vascular. Dr. Virmani has received research support from Medtronic AVE, Abbott Vascular, Atrium Medical, OrbusNeich Medical, Terumo

Everolimus-eluting bioresorbable vascular scaffolds (Absorb, Abbott Vascular, Santa Clara, California) are a novel approach to treating coronary lesions, in that they provide transient vessel support and drug delivery to the vessel wall, without the long-term limitations of standard metallic drug-eluting stents (DES), such as metallic caging. Unlike with permanent metallic stenting, the Absorb will potentially allow for future surgical revascularization, expansive remodeling, restoration of reactive vasomotion, and reliable noninvasive imaging of coronary arteries with multislice computed tomography (1–4). Given the temporary presence of the Absorb, the small, but potentially fatal, risk of late or very late stent thrombosis associated with conventional metallic platform DES, may be reduced or even eliminated (5,6).

First-generation DES, namely overlapping sirolimus-eluting and paclitaxel-eluting stents, have previously been demonstrated in pre-clinical models to show evidence of a persistent inflammatory response, fibrin deposition, and delayed endothelialization (7,8). The purpose of this study is to assess the vascular response of overlapping Absorb compared to the overlapping newer generation everolimus-eluting metallic platform stents (Xience V [XV], Abbott Vascular) in a porcine coronary artery model.

Abbreviations and Acronyms

DES = drug-eluting stent(s)

EEL = external elastic lamina

IQR = interquartile range

OCT = optical coherence tomography

SA ratio = scaffold/stent to artery ratio

SEM = scanning electron microscopy

XV = Xience V stent(s)

Methods

Experimental studies received protocol approval from the institutional animal care and use committee and were conducted in accordance with American Heart Association guidelines for

pre-clinical research and the *Guide for the Care and Use of Laboratory Animals* (National Institutes of Health, 2010). Seventeen healthy, nonatherosclerotic Yorkshire-Landrace swine were implanted via femoral access according to standard procedures (9). Each animal was implanted with overlapping 3.0×12.0 -mm Absorb or XV stents in up to 3 of the main coronary vessels according to a pre-determined matrix of randomization. A maximum of 2 overlapping Absorb and 1 overlapping XV were permitted per animal. The Absorb and XV sizes were matched to the vessel size at a target balloon-to-artery ratio of 1.1 to 1.0 (10% overstretch). In total, 17 animals (41 vessels) were

implanted with overlapping Absorb or overlapping XV. Eight and 9 pigs underwent follow-up at 28 days (Absorb $n = 12$, XV $n = 8$), and 90 days (Absorb $n = 12$, XV $n = 9$), respectively (Online Appendix). These time points have been reported to be representative of peak neointimal growth in humans at 6 months (28 days) and 18 months (90 days) (10). Coronary angiography and OCT analyses were performed at baseline and at both time points. One animal from each of the 28 and 90 day time points was excluded from OCT and histological analyses, and implanted arteries evaluated with scanning electron microscopy (SEM) alone. All pigs were humanely euthanized at follow-up immediately after angiography (SEM) or OCT (all others).

OCT analyses. OCT evaluation of the Absorb and XV overlap were performed at a pullback speed of 1.0 mm/s at baseline and at follow-up, utilizing a commercially available time-domain OCT system (M3 System, LightLab Imaging, Westford, Massachusetts). The image wire was passed distal to the treated vessel without the conventional support of the balloon occlusion catheter to minimize the risk of disrupting the endothelial coverage in the treated vessel. Bolus doses of Ringer's lactate were used to clear blood distal to the inflated occlusion balloon in the proximal vessel, and OCT pullbacks were initiated. Quantitative and qualitative analyses were performed with proprietary software for off-line analysis (LightLab Imaging). With adjustment for pullback speed, analyses of continuous cross sections were performed at 1-mm longitudinal intervals consistent with previously validated methodologies (Online Appendix) (1,11,12). OCT analyses were performed by a team of physicians and analysts of an independent core laboratory (Cardialysis BV, the Netherlands). Specifically for the overlapping Absorb, struts were defined by their overlay configuration, namely "stacked inner," "stacked outer," and "other" (i.e., without a clear direct overlay configuration) (Fig. 1) (13). The threshold for coverage of the Absorb strut is $30 \mu\text{m}$, corresponding to the average interobserver measurement (difference in 300 struts analyzed 2 times, $35 \pm 6 \mu\text{m}$) of the endoluminal light backscattering strut boundary (14). To allow full visualization of the spatial distribution of strut coverage struts in the overlapping devices, "spread-out-vessel graphs"—a visual representation of the vessel as if it had been cut along the reference angle (0°) and spread out on a flat surface—were created based upon previously described methodologies (11).

Histological analyses and SEM. Histological analyses are described in the Online Appendix. SEM was performed with a Hitachi Model 3600N scanning electron microscope (Hitachi, Tokyo, Japan). Sections were stained with hematoxylin and eosin and elastic van Gieson or Movat pentachrome.

Statistical analyses. Continuous variables are reported as mean \pm SD, categorical variables as counts (%). Comparisons were made with the Student *t* test/Mann-Whitney *U* test and chi-square/Fisher exact test as appropriate. Tissue

Corporation, Cordis Corporation, and BioSensors International; and is a consultant for Medtronic AVE, Abbott Vascular, W.L. Gore, Atrium Medical, Arsenal Medical, and Lutonix. All other authors have reported that they have no relationships relevant to the contents of this paper to disclose.

Manuscript received November 14, 2012; revised manuscript received December 3, 2012, accepted December 21, 2012.

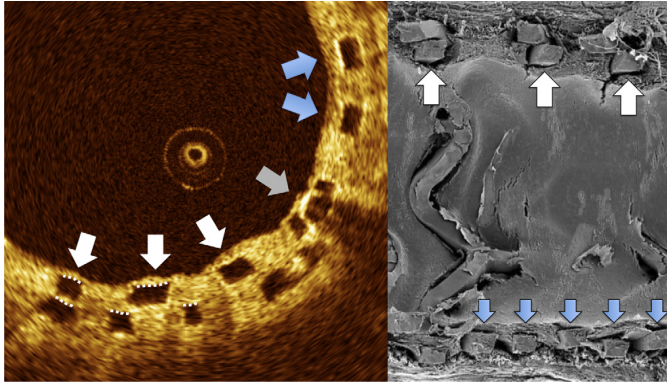


Figure 1. Examples of Absorb Struts According to Their Overlay Configuration in the Overlap

"Stacked inner," "stacked outer," and "other" struts are illustrated on optical coherence tomography (OCT) (left) and scanning electron microscopy (right). **White and gray arrows** indicate "stacked inner" struts with corresponding "stacked outer" struts located abluminally—defined as struts with a direct overlay configuration with each other or lying within 1 strut width of each other. **Blue arrows** indicate "other struts," i.e., struts in the overlap without a clear direct overlay configuration. The **Gray arrow** indicates a strut attached to a platinum marker used to visualize the Absorb during implantation. The **broken white lines** illustrate selected examples of Absorb struts where the neointimal coverage is measured from (mid part of the luminal side of "black core" area of the Absorb strut) to the lumen boundary.

coverage was estimated through the proportion of uncovered struts (dichotomous variable), distribution curves, and areas (continuous variable). Strut-level data were analyzed (dichotomous or continuous variables) using multilevel logistic regression models with random effects at 4 different levels: 1) treatment arm; 2) animal; 3) vessel; and 4) strut. All statistical tests were 2 tailed, and a value of $p < 0.05$ was considered statistically significant. Analyses were conducted

using SAS System Software version 9.2 (SAS Institute, Cary, North Carolina).

Results

All overlapping devices were successfully deployed under angiographic guidance, and all 17 animals remained healthy for the duration of the experiment. The mean overlap length

Table 1. Results of the OCT Analysis at 28 and 90 Days (2 Separate Animal Groups) in the Overlap Porcine Study \pm

	Absorb*			XV†			Overlap p Value‡
	Overlap	Nonoverlap	p Value	Overlap	Nonoverlap	p Value	
28 days							
Coverage, categorical	1,215 (80.1%)	908 (98.2%)	<0.0001	833 (99.4%)	984 (99.8%)	0.33	<0.0001
Neointimal area, mm ²	2.80 \pm 0.51	2.29 \pm 0.49	0.028	2.14 \pm 0.39	1.74 \pm 0.23	0.037	<0.01
Mean lumen area, mm ²	5.44 \pm 0.76	5.11 \pm 0.68	0.31	4.87 \pm 1.01	4.80 \pm 1.08	0.90	0.19
Mean scaffold area, mm ²	8.80 \pm 0.75	7.68 \pm 0.75	0.002	7.01 \pm 0.96	6.54 \pm 1.08	0.27	0.001
% Volume obstruction	31.30 \pm 5.47	29.85 \pm 5.66	0.55	31.01 \pm 7.47	27.62 \pm 4.92	0.34	0.93
90 days							
Coverage, categorical	1,304 (99.5%)	838 (99.8%)	0.26	932 (100.0%)	923 (100.0%)	N/A	N/A
Neointimal area, mm ²	3.84 \pm 0.74	2.43 \pm 1.02	<0.001	2.73 \pm 0.81	2.14 \pm 0.66	0.13	0.005
Mean lumen area, mm ²	4.28 \pm 1.36	4.62 \pm 1.22	0.54	4.52 \pm 1.79	4.66 \pm 1.52	0.87	0.73
Mean scaffold area, mm ²	9.01 \pm 0.56	7.32 \pm 1.96	0.056	7.26 \pm 1.19	6.80 \pm 1.08	0.44	0.006
% Volume obstruction	42.12 \pm 8.02	28.91 \pm 13.09	0.013	39.40 \pm 15.57	33.27 \pm 13.58	0.42	0.64

Values are n (%) or mean \pm SD. Comparisons between overlap and nonoverlap territories for the Absorb and XV individually are shown, with further comparisons between devices. *Absorb threshold for coverage is 30 μ m. †XV threshold for coverage is 0 μ m. ‡p Value comparing overlapping Absorb versus overlapping XV.
N/A = not applicable; XV = Xience V.

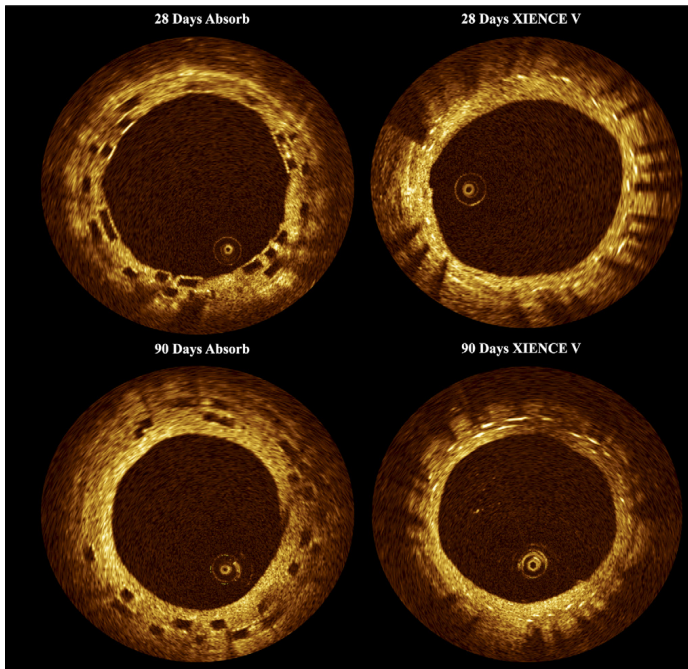


Figure 2. Representative Appearances of Overlapping Absorb and Overlapping XV Devices by OCT at 28 and 90 Days

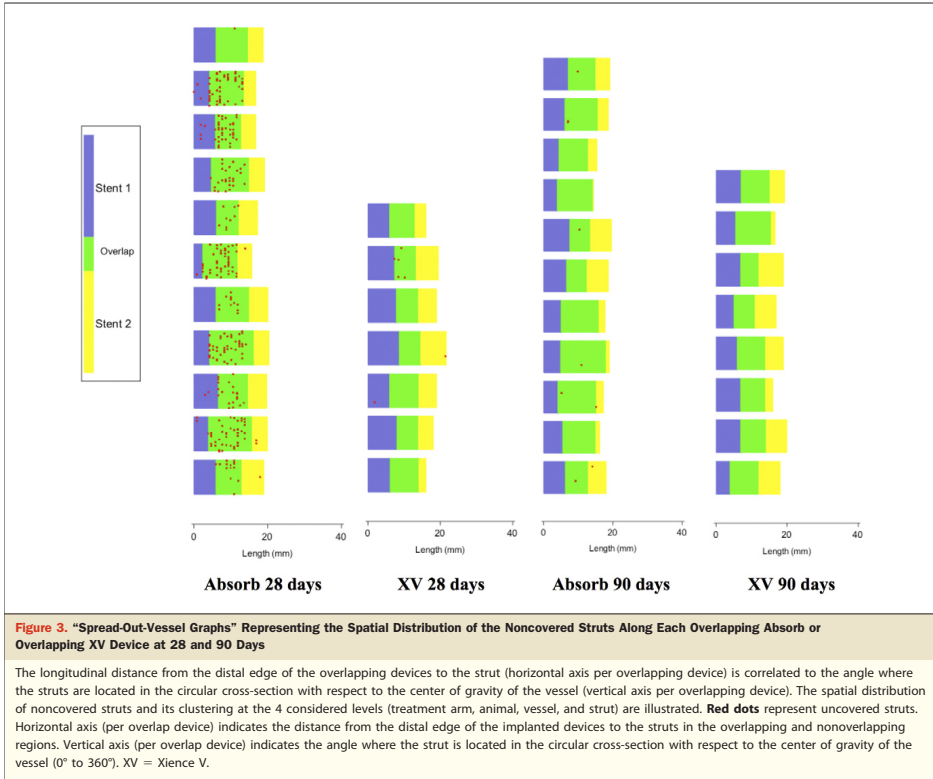
Note the uncovered "stacked inner" struts of the Absorb at 28 days, which was not evident at 90 days. OCT = optical coherence tomography; XV = Xience V.

at 28 days (Absorb 5.16 ± 1.34 mm, XV 5.42 ± 2.44 mm, $p = 0.76$) and 90 days (Absorb 4.82 ± 1.77 mm, XV 5.45 ± 1.73 mm, $p = 0.43$) did not significantly differ between devices. Median scaffold/stent to artery ratio (SA ratio) for the proximal (Absorb SA ratio 1.13 [interquartile range (IQR): 1.06 to 1.18]; XV SA ratio 1.19 [IQR: 1.15 to 1.23], $p = 0.19$) and distal (Absorb SA ratio 1.09 [IQR: 1.02 to 1.13]; XV SA ratio 1.14 [IQR: 1.12 to 1.18], $p = 0.052$) overlapping Absorb or overlapping XV did not significantly differ.

OCT findings. In total, 15,026 struts in 1,407 cross sections were analyzed. All overlapping devices were fully interrogated with OCT and were of adequate image quality. Table 1 indicates the OCT findings. Representative OCT images (Fig. 2) and spread-out-vessel graphs (Fig. 3) are illustrated. At 28 days, strut coverage in the overlapping versus non-overlapping Absorb segments was significantly delayed (80.1% vs. 98.2%, $p < 0.0001$) and to the overlapping XV segment (99.4%, $p < 0.0001$). At 90 days, both overlapping

Absorb and overlapping XV devices demonstrated >99% strut coverage.

Arterial (neointimal) response. Figure 4 illustrates the neointimal distribution curves for the overlapping devices at 28 and 90 days. Table 2 indicates the heterogeneity in the neointimal coverage dependent on the overlay configuration of the Absorb struts. At 28 days, neointimal responses indicated a significantly greater neointimal area in the overlap of both devices compared with the nonoverlap segments (Table 1). This despite the Absorb having reduced binary strut coverage at the overlap. A bimodal neointimal response, secondary to a separate neointimal response for the "stacked inner" and "stacked outer" struts (neointimal coverage: "stacked inner" struts 76 ± 68 μm vs. "stacked outer" struts 240 ± 71 μm , $p < 0.0001$), was evident (Fig. 4), with "stacked inner" Absorb struts primarily responsible for noncovered struts. The mean scaffold area of the overlapping Absorb was significantly greater compared with the nonoverlap-



ping Absorb and to the overlapping XV, which translated into comparable % volume obstructions for vessels implanted with either overlapping device ($p = 0.93$).

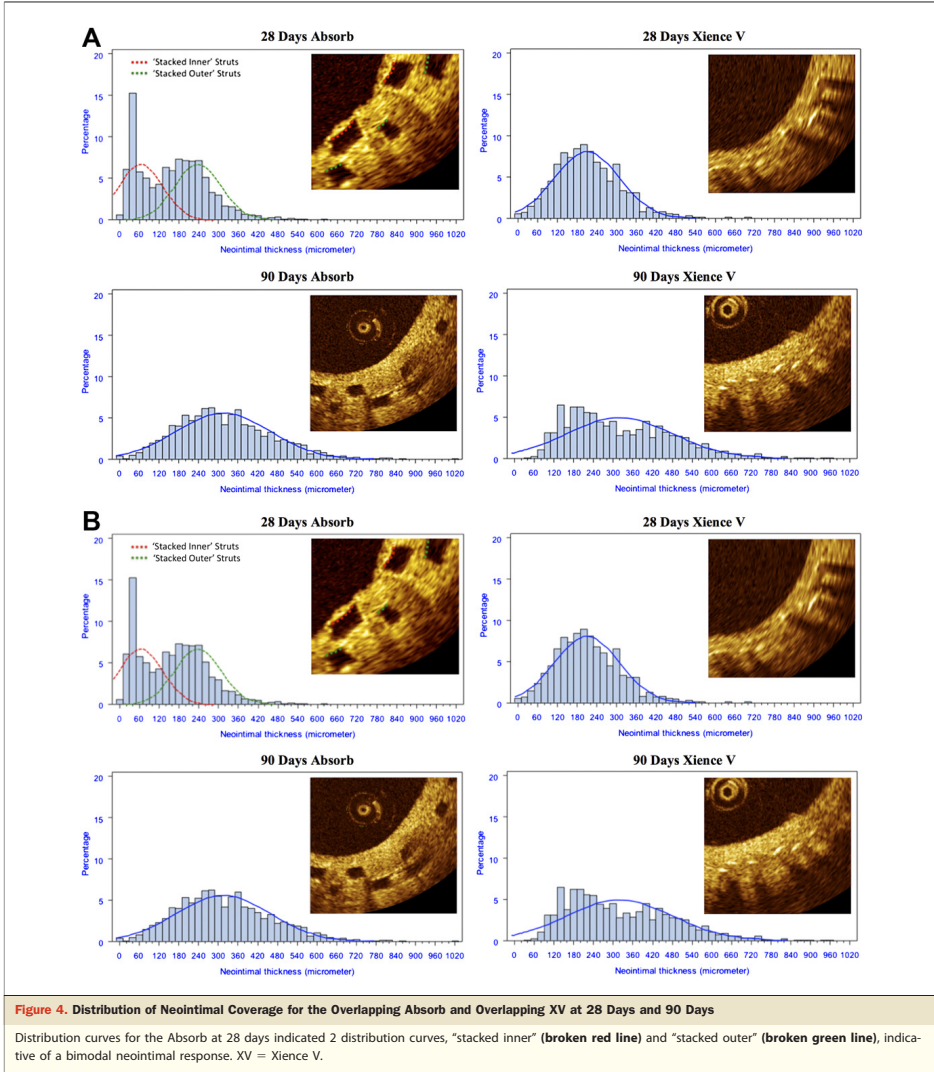
At 90 days, a significantly greater neointimal area ($p < 0.001$) and % volume obstruction ($p = 0.013$) was seen in the Absorb overlap compared with the Absorb nonoverlap (Table 1). As evident at 28 days, the mean scaffold area was greater in the Absorb overlap compared with the nonoverlap, which translated into a comparable % volume obstruction at the overlap between the Absorb or XV ($p = 0.64$).

Histological and SEM findings. In total, 148 histology cross sections were analyzed. Representative histology cross sections (Fig. 5) and SEM (Figs. 6 and 7) at 28 and 90 days for each overlapping device are shown. At all time points, the injury scores were comparable between the overlap and nonoverlap and between devices. The Online Appendix provides the full histomorphometric and qualitative histomorphologic findings in the overlap and nonoverlap.

Histology indicated reduced cellular strut coverage of the Absorb at 28 days ($75.4 \pm 16.4\%$), and broadly corroborated the OCT findings of coverage (80.1%). The internal and external (EEL) elastic lamina areas were significantly greater in the Absorb overlap compared with the Absorb nonoverlap at 28 days (EEL overlap $9.89 \pm 1.02 \text{ mm}^2$ vs. EEL nonoverlap $8.95 \pm 0.77 \text{ mm}^2$, $p = 0.004$) and 90 days (EEL overlap $10.60 \pm 2.01 \text{ mm}^2$ vs. EEL nonoverlap $9.29 \pm 1.48 \text{ mm}^2$, $p = 0.005$). At 90 days, the % volume obstruction did not significantly differ between the overlapping Absorb and overlapping XV ($47.90 \pm 14.37\%$ vs. $37.78 \pm 16.97\%$, $p = 0.18$).

Discussion

The main findings of this study are that: 1) in a porcine coronary artery model, the neointimal coverage of overlapping Absorb struts is delayed at 28 days, and resolves at 90



days; 2) there was a bimodal neointimal response in the overlapping Absorb at 28 days (and not 90 days), with Absorb struts with a direct overlay configuration to each other (i.e., 'stacked' struts), almost exclusively responsible for the reduced cellular coverage; 3) despite the neointimal

response being greater with the Absorb, this did not translate into a significant difference in % volume obstruction for either overlapping device by OCT, at both time points; and 4) the increased strut thickness of the Absorb (156 μm) is likely to be the main mechanism for the

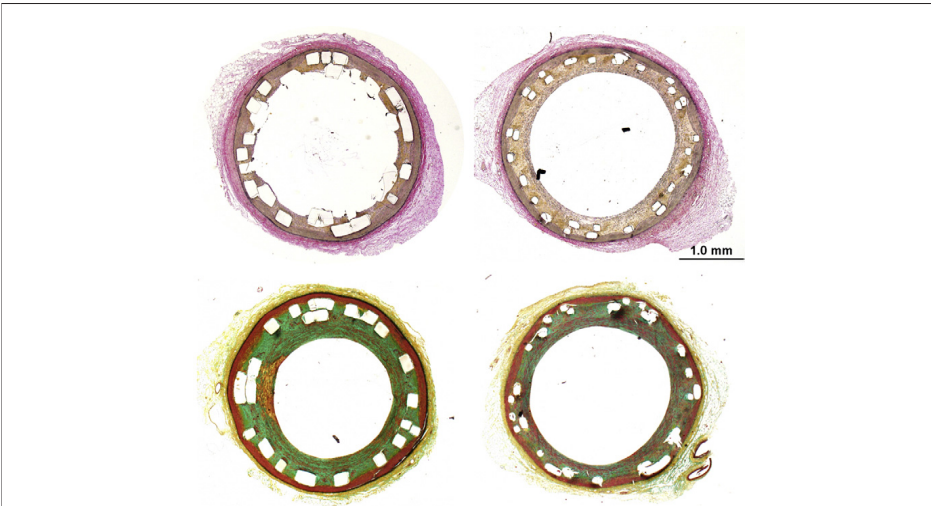
Table 2. Neointimal Strut Coverage (Categorical) by Type of Absorb Strut

	Overlap*	Nonoverlap*	p Value
28 days			
Coverage, categorical			
All vs. all	1,215 (80.1%)	908 (98.2%)	<0.0001
Stacked inner vs. all	286 (54.1%)	—	<0.0001
Stacked outer vs. all	521 (99.4%)	—	0.036
Other vs. all	408 (88.1%)	—	<0.0001
Coverage, μm			
All vs. all	155 \pm 104	150 \pm 73	0.028
Stacked inner vs. all	76 \pm 68	—	<0.0001
Stacked outer vs. all	240 \pm 71	—	<0.0001
Other vs. all	148 \pm 93	—	0.76
90 days			
Coverage, categorical			
All vs. all	1,304 (99.5%)	838 (99.8%)	0.26
Stacked inner vs. all	397 (99.3%)	—	0.15
Stacked outer vs. all	446 (99.6%)	—	0.48
Other vs. all	461 (99.6%)	—	0.61
Coverage, μm			
All vs. all	314 \pm 143	211 \pm 98	<0.0001
Stacked inner vs. all	257 \pm 124	—	<0.0001
Stacked outer vs. all	402 \pm 124	—	<0.0001
Other vs. all	280 \pm 136	—	<0.0001

Values are n (%) or mean \pm SD. *Absorb threshold for coverage is 30 μm .

reduced binary coverage of overlapping Absorb struts at 28 days, compared with the thinner XV struts (88.6 μm).

Strut thickness. Given the similarities between the Absorb and XV, both with biocompatible coatings (bioresorbable or biostable polymers) and low/comparable inflammatory responses, similar vessel injury scores and everolimus release kinetics—essential to the prevention of restenosis after vessel injury (15,16)—it is likely that the increased strut thickness (156 μm) of the Absorb lead to a greater neointimal response compared with the thinner-strut (88.6 μm) XV. This is supported by historical findings of increased strut thickness of bare-metal stents being associated with greater angiographic and clinical restenosis (17,18). Within the DES era, the clinical implications of strut thickness have been more variable, due to the complex relationship between the strut material and characteristics, stent design, polymer type and antiproliferative drug release kinetics (16,19). The findings from SCAAR (the Swedish Coronary Angiography and Angioplasty Registry) (20) (n > 35,000) have provided clarity to this issue, with the thinner-strut (117 μm) Taxus Liberté (Boston Scientific, Natick, Massachusetts) shown to have a mild, but significantly, reduced adjusted risk of restenosis compared with the thicker-strut (154 μm) Taxus Express. Notably, both devices had an identical polymer matrix, the same drug release kinetics, and similar metallic platforms. It is therefore not inconceivable

**Figure 5. Representative Histology Appearances**

Representative appearances of overlapping Absorb and Xience V devices by histology at the time points of 28 (elastic van Gieson stain) and 90 (Movat pentachrome stain) days.

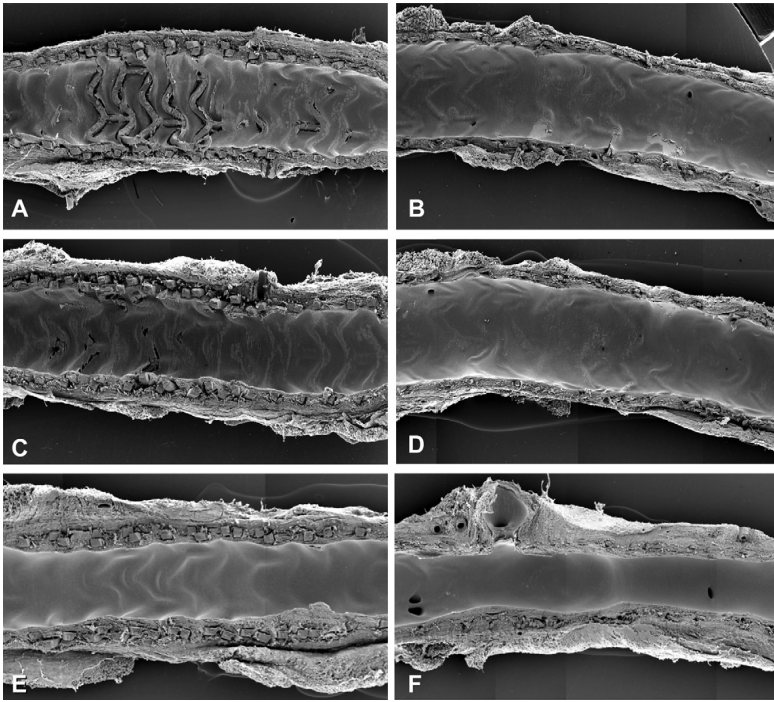


Figure 6. SEM of Overlapping Absorb and Overlapping XV at 28 Days and 90 Days

At 28 days, the Absorb was partially covered by a thin layer of neointima, with many uncovered struts in the overlapping mid-region (**A and C** represent both halves of the vessel); the Xience V (XV) overlap appeared completely covered with a mildly thickened neointima (**B and D** represent both halves of the vessel). At 90 days, based on these single cases of overlapping Absorb (**E**, single half of vessel) and overlapping XV (**F**, single half of vessel), re-endothelialization appeared to be fully complete. SEM = scanning electron microscopy.

that the increased strut thickness of first-generation DES may have contributed to the delayed strut coverage reported in previous animal studies, in addition to the prolonged inflammatory process (7,21).

The mechanism of thicker struts leading to a greater neointimal response, particularly with the “stacked” Absorb struts (approximately 300 μm), is probably related to the role of wall shear stress in modulating the neointimal response. Thicker, rectangular (non-streamlined) struts, characteristic of the Absorb, may theoretically increase the device area exposed to low endothelial oscillatory shear stress areas, leading to the local accumulation of growth factors, mitogenic cytokines, and platelets, which promote neointimal formation until a smooth lumen surface is achieved (22,23). The process of having to fully cover 300 μm of overlapping

Absorb struts is therefore the likely primary reason for the delayed coverage at 28 days, despite the increased neointima associated with the thicker struts. At 90 days, this process is complete. Within the first month, the Absorb elutes 80% of the antiproliferative (everolimus) drug (24) and would substantially suppress the neointimal process. Thereafter, a smaller amount of drug is eluted, leading to a more attenuated effect (compared with the first month) on the synthetic phenotype of neointimal smooth muscle cells (SMC), and thereby its matrix-producing capacity.

Comparison of overlapping Absorb and XV devices. Despite comparable injury scores in vessels treated with either device, the overlapping Absorb exhibited a greater neointimal response in absolute terms compared to the nonoverlapping Absorb segments. This, however, did not trans-

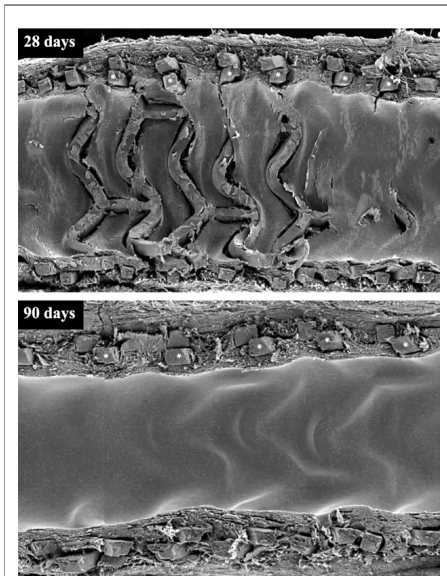


Figure 7. Magnified SEM Views of Overlapping Absorb

Magnified scanning electron microscopy (SEM) view of the overlapping Absorb at 28 days (**upper**), demonstrating multiple uncovered Absorb struts primarily secondary to the direct overlay configuration of the “stacked inner” struts (**white asterisks**) to the corresponding “stacked outer” struts located abuminally. At 90 days (**lower**), all “stacked inner” struts (**white asterisks**) are covered.

late into a significantly greater relative % volume obstruction between either device on OCT analyses, due to a greater vessel/scaffold area associated with the Absorb overlap. The latter allowed for the accommodation of the increased neointima area associated with the overlapping Absorb.

As to why the overlapping Absorb had a greater scaffold/EEL area, it is likely that the addition of overlapping Absorb struts on either side of the deploying device balloon increased the vessel size by 4 layers of Absorb struts (>600 μm thickness), without rupturing the internal elastic lamina and vessel media. In addition, the more conformable, thicker Absorb struts (compared with metal) (25) may have reduced its “cutting effect” when embedded in the vessel media, without any resultant increase in vessel injury. Conversely, previous pre-clinical studies have shown that overstretching of the vessel can induce mechanical injury to neointimal SMCs, leading to changes in synthetic SMC phenotypes, with a resultant increase in constrictive remodeling (26). The

possibility of a greater neointimal response associated with high-grade stenotic lesions treated with overlapping Absorb can therefore not be excluded, as previously reported in 1 clinical study (27).

Implications for current and future bioresorbable devices.

Practical clinical advice for Absorb implantation should therefore include using longer devices to avoid implanting overlapping devices, possible avoidance of overlapping the device at a stenotic lesion as previously discussed, and using design features consisting of radio-opaque markers to allow for fluoroscopic positioning of the devices to minimize or obviate the need to overlap, as reported in previous bench studies (13). Importantly antiplatelet therapy should not be prematurely discontinued, and patients should be monitored closely to ensure compliance.

Study limitations. The nonatherosclerotic porcine model is limited by its ability to replicate conditions in atherosclerotic human coronary arteries, although the porcine model at 28 and 90 days is classically suggested to be representative of 6- and 18-month peak neointimal growth, respectively, in humans (10). Given the 90-day follow-up in the porcine model, the potential late beneficial effects of bioresorption of the Absorb (5) could not be accounted for in the porcine model. In addition, the possibility of an adaptive expansive remodeling process, with the prospect of “late luminal enlargement,” may occur as early as 1 year following partial bioresorption and expected loss of structural integrity of the Absorb device, and may prove to be of additional clinical value (5,28). In view of the delayed cellular coverage of overlapping Absorb struts at 28 days, the duration of antiplatelet therapy required for overlapping Absorb devices cannot be clearly inferred from the present pre-clinical study and requires further clinical investigation.

Conclusions

In porcine coronary arteries implanted with overlapping Absorb or overlapping XV, strut coverage is delayed at 28 days in overlapping Absorb, dependent on the overlay configuration of the thicker Absorb struts. At 90 days, comparable strut coverage and % volume obstruction were evident with either overlapping device. The implications of increased strut thickness and delayed coverage, may have important clinical (e.g., avoiding or minimizing the length of the overlap, duration of antiplatelet therapy), and design considerations (e.g., longer device lengths and the requirement of dedicated bifurcation devices to avoid overlapping the device) for current and future bioresorbable platform devices.

Reprint requests and correspondence: Dr. Patrick W. Serruys, Erasmus MC, 's-Gravendijkwal 230, 3015 CE Rotterdam, the Netherlands. E-mail: p.w.j.c.serruys@erasmusmc.nl

REFERENCES

- Serruys PW, Onuma Y, Ormiston JA, et al. Evaluation of the second generation of a bioresorbable everolimus drug-eluting vascular scaffold for treatment of de novo coronary artery stenosis: six-month clinical and imaging outcomes. *Circulation* 2010;122:2301–12.
- Onuma Y, Serruys PW, Perkins LE, et al. Intracoronary optical coherence tomography and histology at 1 month and 2, 3, and 4 years after implantation of everolimus-eluting bioresorbable vascular scaffolds in a porcine coronary artery model: an attempt to decipher the human optical coherence tomography images in the ABSORB trial. *Circulation* 2010;122:2288–300.
- Serruys PW, Ormiston JA, Onuma Y, et al. A bioabsorbable everolimus-eluting coronary stent system (ABSORB): 2-year outcomes and results from multiple imaging methods. *Lancet* 2009;373:897–910.
- Ormiston JA, Serruys PW, Regar E, et al. A bioabsorbable everolimus-eluting coronary stent system for patients with single de-novo coronary artery lesions (ABSORB): a prospective open-label trial. *Lancet* 2008;371:899–907.
- Serruys PW, Garcia-Garcia HM, Onuma Y. From metallic cages to transient bioresorbable scaffolds: change in paradigm of coronary revascularization in the upcoming decade? *Eur Heart J* 2012;33:16–25b.
- Palmerini T, Biondi-Zoccai G, Della Riva D, et al. Stent thrombosis with drug-eluting and bare-metal stents: evidence from a comprehensive network meta-analysis. *Lancet* 2012;379:1393–402.
- Finn AV, Kolodgie FD, Harnek J, et al. Differential response of delayed healing and persistent inflammation at sites of overlapping sirolimus- or paclitaxel-eluting stents. *Circulation* 2005;112:270–8.
- Wilson GJ, Polovick JE, Huibregtse BA, Poff BC. Overlapping paclitaxel-eluting stents: long-term effects in a porcine coronary artery model. *Cardiovasc Res* 2007;76:361–72.
- Perkins LEL, Boeke-Purkis KH, Wang Q, Stringer SK, Coleman LA. XIENCE Everolimus-eluting coronary stent system: a preclinical assessment. *J Interv Cardiol* 2009;22:S28–40.
- Virmani R, Kolodgie FD, Farb A, Lafont A. Drug eluting stents: are human and animal studies comparable? *Heart* 2003;89:133–8.
- Gutierrez-Chico JL, van Geuns RJ, Regar E, et al. Tissue coverage of a hydrophilic polymer-coated zotarolimus-eluting stent vs. a fluoropolymer-coated everolimus-eluting stent at 13-month follow-up: an optical coherence tomography substudy from the RESOLUTE All Comers trial. *Eur Heart J* 2011;32:2454–63.
- Gutierrez-Chico JL, Regar E, Nuesch E, et al. Delayed coverage in malapposed and side-branch struts with respect to well-apposed struts in drug-eluting stents: in vivo assessment with optical coherence tomography. *Circulation* 2011;124:612–23.
- Farooq V, Onuma Y, Radu M, et al. Optical coherence tomography (OCT) of overlapping bioresorbable scaffolds: from benchmark to clinical application. *EuroIntervention* 2011;7:386–99.
- Serruys PW, Onuma Y, Dudek D, et al. Evaluation of the second generation of a bioresorbable everolimus-eluting vascular scaffold for the treatment of de novo coronary artery stenosis: 12-month clinical and imaging outcomes. *J Am Coll Cardiol* 2011;58:1578–88.
- Serruys PW, Sianos G, Abizaid A, et al. The effect of variable dose and release kinetics on neointimal hyperplasia using a novel paclitaxel-eluting stent platform: the Paclitaxel In-Stent Controlled Elution Study (PISCES). *J Am Coll Cardiol* 2005;46:253–60.
- Farooq V, Gogas BD, Serruys PW. Restenosis: delineating the numerous causes of drug-eluting stent restenosis. *Circ Cardiovasc Interv* 2011;4:195–205.
- Kastrati A, Mehilli J, Dirschinger J, et al. Intracoronary stenting and angiographic results: strut thickness effect on restenosis outcome (ISAR-STEREO) trial. *Circulation* 2001;103:2816–21.
- Pache J, Kastrati A, Mehilli J, et al. Intracoronary stenting and angiographic results: strut thickness effect on restenosis outcome (ISAR-STEREO-2) trial. *J Am Coll Cardiol* 2003;41:1283–8.
- Biondi-Zoccai G, Moretti C, Abbate A, Sheiban I. Percutaneous coronary intervention for small vessel coronary artery disease. *Cardiovasc Revasc Med* 2010;11:189–98.
- Frobert O, Lagerqvist B, Carlsson J, Lindback J, Stenstrand U, James SK. Differences in restenosis rate with different drug-eluting stents in patients with and without diabetes mellitus: a report from the SCAAR (Swedish Angiography and Angioplasty Registry). *J Am Coll Cardiol* 2009;53:1660–7.
- Joner M, Nakazawa G, Finn AV, et al. Endothelial cell recovery between comparator polymer-based drug-eluting stents. *J Am Coll Cardiol* 2008;52:333–42.
- Koskinas KC, Chatzizisis YS, Antoniadis AP, Giannoglou GD. Role of endothelial shear stress in stent restenosis and thrombosis: pathophysiological mechanisms and implications for clinical translation. *J Am Coll Cardiol* 2012;59:1337–49.
- Wentzel JJ, Krams R, Schurbiers JC, et al. Relationship between neointimal thickness and shear stress after Wallstent implantation in human coronary arteries. *Circulation* 2001;103:1740–5.
- Gomez-Lara J, Brugaletta S, Farooq V, et al. Head-to-head comparison of the neointimal response between metallic and bioresorbable everolimus-eluting scaffolds using optical coherence tomography. *J Am Coll Cardiol Intv* 2011;4:1271–80.
- Gomez-Lara J, Brugaletta S, Farooq V, et al. Angiographic geometric changes of the lumen arterial wall after bioresorbable vascular scaffolds and metallic platform stents at 1-year follow-up. *J Am Coll Cardiol Intv* 2011;4:789–99.
- Liu MW, Roubin GS, King SB 3rd. Restenosis after coronary angioplasty. Potential biologic determinants and role of intimal hyperplasia. *Circulation* 1989;79:1374–87.
- Tahara S, Bezerra HG, Sirbu V, et al. Angiographic, IVUS and OCT evaluation of the long-term impact of coronary disease severity at the site of overlapping drug-eluting and bare metal stents: a substudy of the ODESSA trial. *Heart* 2010;96:1574–8.
- Brugaletta S, Heo JH, Garcia-Garcia HM, et al. Endothelial-dependent vasomotion in a coronary segment treated by ABSORB everolimus-eluting bioresorbable vascular scaffold system is related to plaque composition at the time of bioresorption of the polymer: indirect finding of vascular reparative therapy? *Eur Heart J* 2012;33:1325–33.

Key Words: biodegradable polymer ■ drug-eluting stent ■ imaging ■ overlapping stents ■ pathology.

▶ **APPENDIX**

For expanded Methods, Results, and Discussion sections, please see the online version of this paper.

Chapter 13

In Vivo Three Dimensional Optical Coherence Tomography. A Novel Imaging Modality to Visualize the Edge Vascular Response.

Bill D. Gogas, Takashi Muramatsu, Hector M. Garcia-Garcia, Christos V. Bourantas, Niels R. Holm, Leif Thuesen, Yoshinobu Onuma, Patrick W. Serruys
International Journal of Cardiology. 2013 Apr 15; 164(3): e35-7 [IF: 4.12]

Letter to the Editor

In vivo three dimensional optical coherence tomography. A novel imaging modality to visualize the edge vascular response

Bill D. Gogas^{a,c}, Takashi Muramatsu^a, Hector M. Garcia-Garcia^a, Christos V. Bourantas^a, Niels R. Holm^b, Leif Thuesen^b, Vasim Farooq^a, Yoshinobu Onuma^a, Patrick W. Serruys^{a,*}

^a Thoraxcenter, Erasmus University Medical Center, Rotterdam, The Netherlands

^b Skejby Sygehus, Aarhus University Hospital, Skejby, Denmark

^c Andreas Gruentzig Cardiovascular Institute, Emory University Hospital, Atlanta, GA, United States of America

ARTICLE INFO

Article history:

Received 14 September 2012

Accepted 25 September 2012

Available online 15 October 2012

Keywords:

Edge vascular response
Three-dimensional optical frequency domain imaging
Restenosis

The edge vascular response (EVR) has been previously evaluated with sound-based imaging modalities utilizing tissue characterization properties namely intravascular ultrasound (IVUS) and virtual histology IVUS (VH-IVUS) after implantation of metallic devices or bioresorbable drug-eluting platforms [1–3]. The majority of these reports have shown lumen loss (LL) at the proximal edge, although in some studies the vascular response at the edges was diverse with proximal and distal lumen gain.

The advent of light-based modalities such as optical frequency domain imaging (OFDI) appears superior to the previously used intracoronary IVUS based techniques to assess in-vivo the LL and characterize tissue composition at the stent edges [4]. This is mainly due to the ultra-high OFDI spatial resolution of ~15 µm that enables to sharply define the stent edges and characterize plaque components. Additionally the development of intracoronary three-dimensional (3-D) post-processed OFDI reconstructions that visualize the spatial distribution of the EVR enhances our understanding of this effect.

The patient was a 66-year-old female who underwent primary percutaneous coronary intervention to a Type A lesion of the proximal left

anterior descending artery (LAD) (on line Video 1). Pre-dilatation of the lesion was undertaken (15 atm) followed by implantation of a single 3.5 × 14 Nobori metallic stent (TERUMO Europe N.V., Leuven, BG) in the proximal LAD at nominal inflation pressures (14 atm). Post-dilatation with a 4.0 × 10 mm balloon at 16 atm was performed at the distal stent segment to optimize the angiographic result and TIMI III flow was finally obtained (Fig. 1A) (on line Videos 2 and 3). OFDI following post-procedure illustrated a dissection flap at the distal edge and the landing zone of the device in non diseased proximal edge and in fibro-fatty plaque at the distal edge (on line Video 4). The patient presented at 6 months with aggravating episodes of angina and was serially assessed angiographically (on line Video 5) with two-dimensional (2-D) (on line Video 6) and post-processed three-dimensional OFDI (Fig. 1B).

Angiography revealed a 95% mid-LAD in-segment stenosis at the distal edge of the DES (Fig. 1A). OFDI assessment showed distal edge LL from 9.65 mm² to 4.02 mm², causing a significant relative decrease of: Delta LA – 50% [– 74.0; – 0.08], suggestive of distal edge effect.

This report illustrates a case of distal edge effect assessed with 2-D and 3-D post-processed OFDI associated with peri-procedural axial geographical miss (GM) resulting in target lesion revascularization. The dissection flap following post-dilatation of the Nobori device (Fig. 1A and II–IV) may have contributed to the aggressive distal EVR as dissected in the media and was upon a fibro-fatty plaque. Waxman et al. have previously reported the first case of proximal edge stenosis at 15 months following implantation of a sirolimus DES (Cypher, Cordis, Miami, FL) associated with longitudinal GM resulting in restenosis and stent failure [3].

The peri-procedural axial/longitudinal GM are the main iatrogenic factors responsible for the occurrence of the EVR while device related factors depending on the type of device (metal or polymer) and drug-elution (m-TOR or paclitaxel) in association with biologic factors compose the complete spectrum of precipitating factors. The clinical consequences of the EVR are stent failure caused by in-segment restenosis or stent thrombosis.

The 2-D and 3-D post-processed OFDI based edge evaluation are currently the state-of-the-art imaging modalities for the assessment of the EVR. Although a prototype on-line application of 3-D OFDI with gross tissue characterization properties has been developed this imaging technique is not available in the clinical practice yet. Further advances on this direction are expected as will enhance our understanding of the underlying pathology.

Supplementary data to this article can be found online at <http://dx.doi.org/10.1016/j.ijcard.2012.09.161>.

* Corresponding author at: Thoraxcenter, Bd583a, Dr. Molewaterplein 40, 3015-GD, Rotterdam, The Netherlands. Tel.: +31 10 463 5260; fax: +31 10 436 9154.
E-mail address: p.w.j.c.serruys@erasmusmc.nl (P.W. Serruys).

Disclosure

Nothing to disclose.

Acknowledgments

The authors wish to thank Drs Kazuhisa Senshu, Dragica Paunovic and Vladimir Borovicinanin of TERUMO Europe N. V. for their invaluable technical support. Dr Gogas wishes to acknowledge the American College of Cardiology, for the International Society of Translational Research Award 2012.

The authors of this manuscript have certified that they comply with the Principles of Ethical Publishing in the International Journal of Cardiology.

References

- [1] Wakabayashi K, Waksman R, Weissman NJ. Edge effect from drug-eluting stents as assessed with serial intravascular ultrasound: a systematic review. *Circ Cardiovasc Interv* 2012;5:305-11.
- [2] Gogas BD, Serruys PW, Diletti R, et al. Vascular response of the segments adjacent to the proximal and distal edges of the ABSORB everolimus-eluting bioresorbable vascular scaffold: 6-month and 1-year follow-up assessment: a virtual histology intravascular ultrasound study from the first-in-man ABSORB cohort B trial. *JACC Cardiovasc Interv* 2012;5:656-65.
- [3] Kang WC, Park YM, Shin KC, et al. Comparison of edge vascular response after sirolimus- and paclitaxel-eluting stent implantation. *Int J Cardiol* 2011. Sep 6. <http://dx.doi.org/10.1016/j.ijcard.2011.07.108>.
- [4] Gogas BD, Onuma Y, van Geuns RJ, Serruys PW. The edge vascular response following implantation of a fully bioresorbable device: 'a miss always counts'. *Int J Cardiol* 2012;158:455-7.

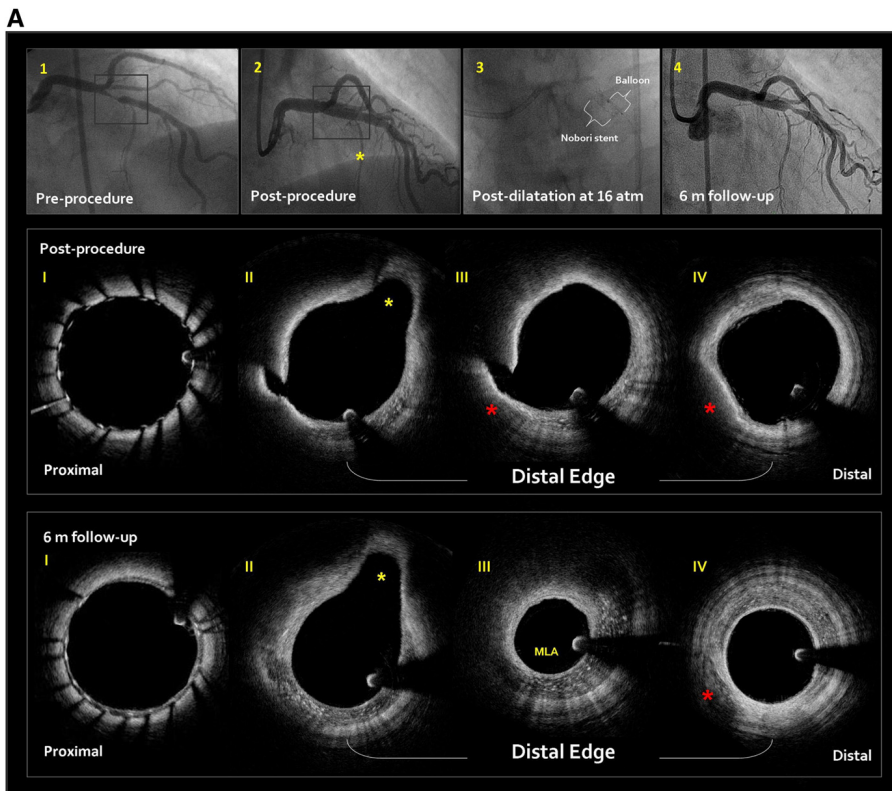


Fig. 1. Two-dimensional and three-dimensional post-processed optical frequency domain (OFDI) imaging for the assessment of the edge vascular response following implantation of the Nobori drug-eluting metallic platform. A: Panels 1–4: Coronary angiographies pre-procedure (1), post-procedure (2), and at 6 month follow-up (4). Panel 3 demonstrates the mechanism of axial geographical miss. Panels I–IV: Two-dimensional (2-D) OFDI serial selected frames demonstrating the most important imaging findings. At post-procedure a disruption of the luminal surface became evident (8 o'clock) (edge dissection) including the media. The trilaminar vascular anatomy is altered due to the pre-existing fibro-fatty plaque (red asterisks). At 6 month follow-up the healed dissection has caused distal edge stenosis (MLA). The yellow asterisks demonstrate the septal branch. B: Panel I–II: 3-D post-processed OFDI post-procedure (1) and at 6 month follow-up (II). The metallic struts appear covered compared to post-procedure. The MLA appears at the 4 mm of the distal edge.

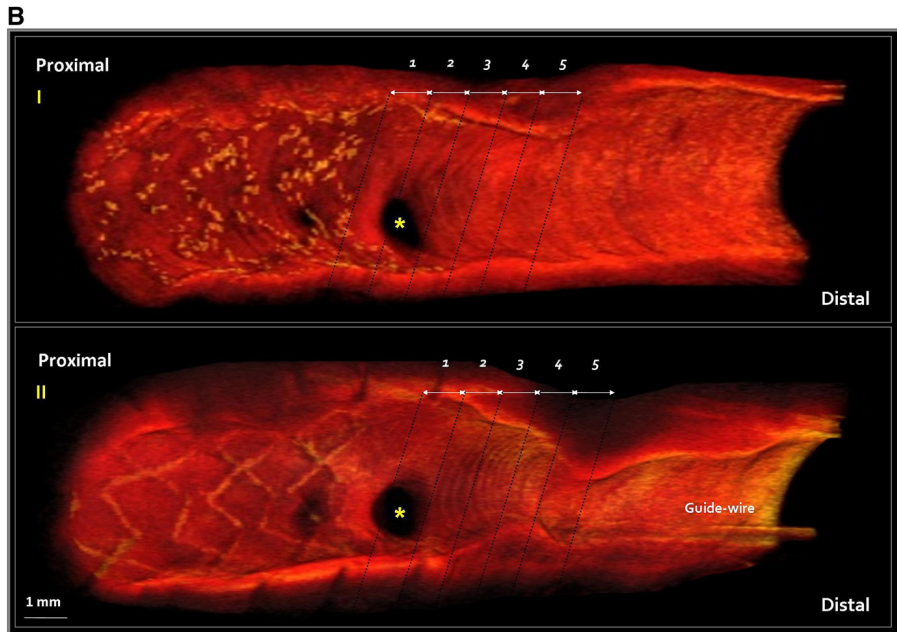


Fig. 1 (continued).

Chapter 14

Natural history of optical coherence tomography-detected edge dissections following drug-eluting stent implantation.

Maria D. Radu, Lorenz Räber, Jung Ho Heo, **Bill D. Gogas**, Erik Jørgensen, Henning Kelbæk, Takashi Muramatsu, Steffen Helqvist, Vasim Farooq, Hector M. Garcia-Garcia, Stephan Windecker, Kari Saunamäki, Patrick W. Serruys

EuroIntervention 2013; 9-online publish-ahead-of-print August 2013 [IF: 3.17]

Natural history of optical coherence tomography-detected non-flow-limiting edge dissections following drug-eluting stent implantation

Maria D. Radu^{1,2}, MD; Lorenz Räber^{2,3}, MD; Jungho Heo², MD; Bill D. Gogas², MD; Erik Jørgensen¹, MD; Henning Kelbæk¹, MD, DMSci; Takashi Muramatsu², MD; Vasim Farooq², MBChB, MRCP; Steffen Helqvist¹, MD, DMSci; Hector M. Garcia-Garcia⁴, MD, PhD; Stephan Windecker², MD; Kari Saunamäki¹, MD, DMSci; Patrick W. Serruys^{2*}, MD, PhD

1. Rigshospitalet, Copenhagen University Hospital, Copenhagen, Denmark; 2. Thoraxcenter, Erasmus University Medical Centre, Rotterdam, The Netherlands; 3. Bern University Hospital, Bern, Switzerland; 4. Cardialysis BV, Rotterdam, The Netherlands

GUEST EDITOR: Michael Joner, MD; Facharzt für Innere Medizin und Kardiologie, Deutsches Herzzentrum München, Technische Universität, Munich, Germany

KEYWORDS

- dissection
- intravascular ultrasound
- optical coherence tomography
- stent implantation

Abstract

Aims: Angiographic evidence of edge dissections has been associated with a risk of early stent thrombosis. Optical coherence tomography (OCT) is a high-resolution technology detecting a greater number of edge dissections – particularly non-flow-limiting – compared to angiography. Their natural history and clinical implications remain unclear. The objectives of the present study were to assess the morphology, healing response, and clinical outcomes of OCT-detected edge dissections using serial OCT imaging at baseline and at one year following drug-eluting stent (DES) implantation.

Methods and results: Edge dissections were defined as disruptions of the luminal surface in the 5 mm segments proximal and distal to the stent, and categorised as flaps, cavities, double-lumen dissections or fissures. Qualitative and quantitative OCT analyses were performed every 0.5 mm at baseline and one year, and clinical outcomes were assessed. Sixty-three lesions (57 patients) were studied with OCT at baseline and one-year follow-up. Twenty-two non-flow-limiting edge dissections in 21 lesions (20 patients) were identified by OCT; only two (9%) were angiographically visible. Flaps were found in 96% of cases. The median longitudinal dissection length was 2.9 mm (interquartile range [IQR] 1.6–4.2 mm), whereas the circumferential and axial extensions amounted to 1.2 mm (IQR: 0.9–1.7 mm) and 0.6 mm (IQR: 0.4–0.7 mm), respectively. Dissections extended into the media and adventitia in seven (33%) and four (20%) cases, respectively. Eighteen (82%) OCT-detected edge dissections were also evaluated with intravascular ultrasound which identified nine (50%) of these OCT-detected dissections. No stent thrombosis or target lesion revascularisation occurred up to one year. At follow-up, 20 (90%) edge dissections were completely healed on OCT. The two cases exhibiting persistent dissection had the longest flaps (2.81 mm and 2.42 mm) at baseline.

Conclusions: OCT-detected edge dissections which are angiographically silent in the majority of cases are not associated with acute stent thrombosis or restenosis up to one-year follow-up.

*Corresponding author: Erasmus MC, Thoraxcenter, Ba583a, 's-Gravendijkwal 230, 3015 CE Rotterdam, The Netherlands. E-mail: p.w.j.c.serruys@erasmusmc.nl

Introduction

Stent implantation is the preferred treatment for coronary artery stenosis. As a consequence of vessel trauma during stent implantation, edge dissections occasionally occur and may lead to abrupt or threatened vessel closure due to obstruction from prolapsing tissue or thrombosis. Previous reports have suggested an association between angiographic as well as intravascular ultrasound (IVUS)-detected edge dissections and early stent thrombosis (ST)¹⁻⁵. At the same time, other studies evaluating the outcomes following stent implantation have shown that only a minority of patients with edge dissections experience clinical adverse events^{6,8}. The impact of these findings and their management has therefore been debated.

Optical coherence tomography (OCT) is a high-resolution technology allowing a detailed assessment of the coronary vessel wall and implanted devices⁹. Consequently, OCT detects a higher number of edge dissections as compared to angiography and IVUS^{9,10}. The often dramatic appearance of these vessel disruptions, even when angiographically silent, may generate concern for further complications and trigger additional stent implantation^{11,12}. The question whether this is justifiable at a time where OCT is increasingly used during interventions has thus resurfaced. At present, the natural history and clinical implications of these findings in the short and long term remain insufficiently described. The objectives of the present study were to assess the morphology, healing response, and clinical outcomes of OCT-detected edge dissections using serial OCT imaging at baseline and at one year following drug-eluting stent (DES) implantation.

Methods

STUDY POPULATION

The study included serial data from the Copenhagen OCT registry and from the OCT substudy of the RESOLUTE all-comers trial¹³. The Copenhagen OCT registry was a single-centre prospective non-randomised evaluation of strut coverage and apposition at 12-month (average) follow-up in relation to apposition at baseline, using the following DES: CYPHER SELECT® Plus (Cordis, Johnson & Johnson, Warren, NJ, USA), TAXUS® Express™ (Boston Scientific, Natick, MA, USA), and Resolute® (Medtronic Inc., Santa Rosa, CA, USA). Patients were included between June 2008 and November 2010, and were eligible if they had ≥ 1 lesion with $>50\%$ diameter stenosis in a native coronary artery, with a reference vessel diameter between 2.25 and 4.0 mm. Exclusion criteria were ST-segment elevation myocardial infarction (MI), left ventricular ejection fraction $<30\%$, renal insufficiency (creatinine >133 $\mu\text{mol/L}$), and lesion location in the left main stem or bypass graft. OCT as well as IVUS were performed after a satisfactory angiographic result, defined as a residual diameter stenosis $<20\%$ and Thrombolysis In Myocardial Infarction (TIMI) flow grade 3. It was prespecified that angiographically visible edge dissections occurring during the procedure would only be treated in case they were obstructive and flow-limiting (defined as dissections at least type C with a residual diameter stenosis $>50\%$ and a TIMI flow ≤ 2). Specifically, treatment of edge dissections visible by OCT was not permitted unless they fulfilled the angiographic criteria. Administration of glycoprotein (GP) IIb/IIIa inhibitors

was left to the discretion of the operator. Whether this was a consequence of the dissection or not was noted. Imaging with both OCT and IVUS was repeated at 12-month (average) follow-up. Of note, six patients (out of a total 49 patients) imaged at baseline in the Copenhagen cohort were excluded due to withdrawal of consent for follow-up.

The RESOLUTE trial was a randomised multicentre all-comers non-inferiority trial comparing the Resolute and XIENCE V® (Abbott Vascular, Santa Rosa, CA, USA) stents¹⁴. Inclusion criteria were broad, including patients with chronic stable angina as well as acute coronary syndromes, having ≥ 1 lesion with $>50\%$ diameter stenosis with a reference vessel diameter between 2.25 and 4.0 mm. Exclusion criteria were known intolerance to any of the stent components, and planned surgery within six months of the index procedure. Administration of GP IIb/IIIa inhibitors was left to the discretion of the operator. The OCT substudy included patients randomly selected for angiographic follow-up at 13 months from centres where OCT was available. The principal endpoint was strut coverage at follow-up¹⁵. A limited number of patients, included between May and November 2008, also had a baseline evaluation. There were no per protocol prespecified instructions regarding the management of edge dissections; however, for the purpose of this study, the occurrence of angiographic edge dissections after stent implantation was noted and, if present, also whether these were treated with additional stent implantation.

From the serial data available, we included lesions exhibiting edge dissections as assessed by OCT after stent implantation. Both studies were approved by the local ethics committees and written informed consent was obtained from all patients prior to enrolment.

OCT AND IVUS ACQUISITIONS

OCT acquisitions were performed with commercially available systems (time-domain M2 and M3 systems; frequency-domain C7 system) from LightLab/St. Jude (Westford, MA, USA). OCT images were acquired at a frame rate of 15.6, 20, and 100 frames/s at a pullback speed of 1, 3 and 10 mm/s with the M2, M3 and C7, respectively. Acquisition with occlusive (M2) and non-occlusive (M3 and C7) techniques has been described previously¹⁵. IVUS images were acquired with the Atlantis SR Pro 40 MHz catheter and iLab system (Boston Scientific, Natick, MA, USA) at a frame rate of 30 frames/s and pullback speed of 0.5 mm/s, according to accepted standards¹⁶.

ANGIOGRAPHIC ANALYSIS

All angiograms were assessed by three independent cardiologists with regard to the presence of edge dissections. In case of disagreement, a consensus diagnosis was obtained. If present, the dissection was graded according to the National Heart, Lung, and Blood Institute classification¹⁷.

OCT IMAGE ANALYSIS

OCT pullbacks were analysed off-line using proprietary software from LightLab/St. Jude. The region of interest included reference vessel segments (RVS) 5 mm proximal and distal to the stent, which were analysed systematically at 0.5 mm intervals. Edge dissections

were defined as disruptions in the luminal vessel surface in the RVS, with or without involvement of the stented segment.

Dissections were classified as flaps, cavities, double-lumen dissections or fissures (**Figure 1A-[Figure 1D](#)**), and their longitudinal extensions along the stented segment were measured. For flaps, the flap root thickness was assessed semi-automatically from the joint point with the vessel wall to the luminal surface along a line projected through the gravitational centre of the lumen. The flap length was measured from the joint point with the vessel wall to the tip of the flap. The flap area was measured as the area bounded by the flap root thickness trace and the luminal contours of the flap. For cavities, the cavity depth was measured along a line projected through the gravitational centre of the lumen, from the deepest point in the cavity to a virtual line extrapolated between the luminal vessel contours on each side of the cavity. The cavity width was quantified at its widest point as parallel to the virtual line as possible, and the cavity area was assessed as the area bounded by the luminal contour of the cavity and the help line extrapolated between the luminal vessel contour on each side of the cavity. Double-lumen dissections were those having a false lumen separated from the true lumen by a cap. The cap thickness was quantified semi-automatically from the joint point with the vessel wall to the luminal vessel contour along a line projected through the gravitational centre of the lumen, and the largest of the two cap thicknesses was used. The cap length was measured as the distance between the two joint points connected by a straight line, while the cap area was defined as the area bounded luminally by the vessel surface to the sides by the cap thickness

traces, and in the depth by the false lumen. Fissures were present when a split was visible delineating a flap-like structure not lifted from the vessel wall, which otherwise displayed an uninterrupted luminal contour. Due to a poor demarcation of the root of the flap-like structure, no measurements were performed on the fissures at the cross-sectional level; however, they were included in the assessment of longitudinal extension as it was hypothesised that they were consistent with injury. The circumferential extension of the dissection was expressed as the number of quadrants involved. The axial injury of the dissection was described as intimal involvement when only the intima was affected and media was still intact, as medial involvement when the dissection extended into the media without disruption of the entire medial layer, and as adventitial involvement when the media was dissected throughout its thickness (**Figure 1E-[Figure 1G](#)**). In case the media was not discernible, the dissection was classified as involving only the intima. The lumen area was assessed in each selected frame of the RVS as the area bounded by the luminal vessel contour. The kappa value for inter-observer reproducibility of the classification of edge dissections at the lesion level was 1.0.

We also assessed the underlying tissue at the site of the dissections (at the lesion level) with respect to plaque type, which was classified as fibrous ($>500 \mu\text{m}$ thick in at least one quadrant), fibrocalcific, or thin-cap (TCFA) fibroatheroma according to the international consensus (the two latter plaque types considered to be present when the calcified or lipid regions extended >1 quadrant)¹⁸. We also noted whether the extension was eccentric or concentric.

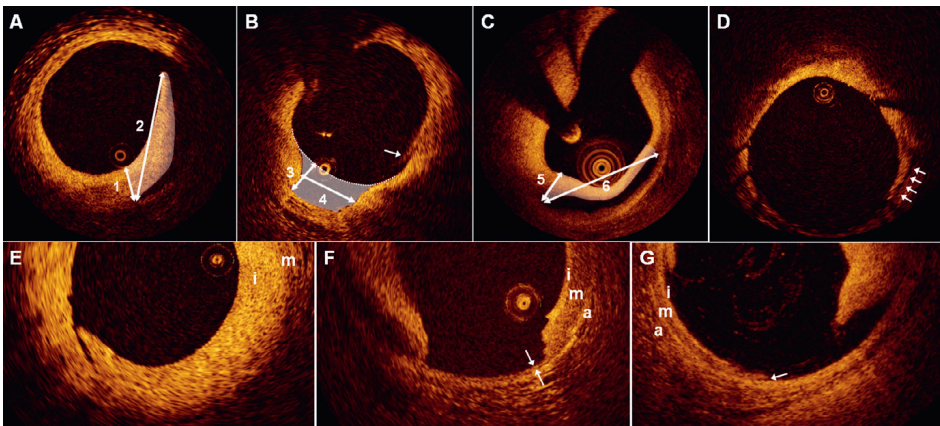


Figure 1. Classification of edge dissections. A) shows a dissection flap with indication of the flap root thickness (1), flap length (2), and flap area (white shading). B) shows a dissection cavity with the cavity depth (3), cavity width (4) and cavity area (white shading) displayed. The white arrow points to an artefact caused by non-uniform rotational distortion, and should not be misinterpreted as a dissection. The diagnosis was made by inspecting adjacent frames (not shown). C) shows a double-lumen dissection with indication of the largest cap thickness (5), cap width (6), and cap area (white shading). D) the arrows point to a fissure. Panels E-G show dissections involving only the intima (i) (E), the media (m) (F), and the adventitia (a) (G). F) the double arrows demarcate the only intact portion of the disrupted media. G) the arrow indicates the point where the media is lifted from the adventitia.

IVUS IMAGE ANALYSIS

IVUS pullbacks were analysed off-line using the QCU-CMS software (Medis, Leiden, The Netherlands) at standard 1 mm intervals in the described region of interest. Dissections were defined as tears in the intima-media with visualisation of blood speckle behind a flap or within a cavity or double lumen. The presence of dissections was assessed at the lesion level. The lumen area was measured in the RVS as the area bounded by the luminal vessel contour, whereas the external elastic membrane (EEM) area encompassed the area bounded by the interface between the intima-media layer and the adventitia. The plaque and media area was calculated as the EEM area minus the lumen area. The kappa value for inter-observer reproducibility of the presence or not of edge dissection by IVUS was 1.0.

CLINICAL OUTCOMES

Clinical outcomes in terms of death, MI, target lesion revascularisation (TLR) and target vessel revascularisation (TVR) were assessed for the Copenhagen OCT registry by two independent observers blinded to the imaging results, and for the RESOLUTE trial by a clinical events adjudication committee. The overall rate of stent thrombosis at one year was assessed according to the Academic Research Consortium definitions¹⁹.

STATISTICAL ANALYSIS

Continuous data were presented as means±standard deviations or median and interquartile ranges (IQR), depending on their distribution, which was assessed using the Kolmogorov-Smirnov test. Categorical data were presented as frequencies and percentages. The morphometric data at baseline and follow-up were compared using a paired t-test, and a two-sided $p < 0.05$ was considered statistically significant.

Results

CLINICAL AND PROCEDURAL CHARACTERISTICS

Out of a total of 57 patients with 63 lesions, 20 patients with 21 lesions and 22 OCT-defined edge dissections were included in the final analysis (Figure 2). Table 1 shows the baseline demographics. The average age was 63 years, 15 (75%) patients were males, and 14 (70%) patients presented with acute coronary syndrome. All lesions had a final TIMI 3 flow. Out of the 22 OCT-defined edge dissections, two (9%) were angiographically visible as type A haziness, and both were located within the same vessel (distal lesion with proximal dissection and proximal lesion with distal dissection), separated by only 2 mm. Of note, none of the 63 lesions was treated with additional stents, whereas five (25%) of 20 patients received treatment with GP IIb/IIIa inhibitors directly as a consequence of the OCT findings.

Results of OCT analysis

Out of the 62 assessable lesions with 58 distal and 30 proximal visible edges, 21 (34%) lesions with 16 (28%) distal and six (30%) proximal edges showed dissections, respectively. One of these lesions had both a proximal and distal dissection. Table 2 shows the characteristics of these dissections at baseline. Six (27%) dissections

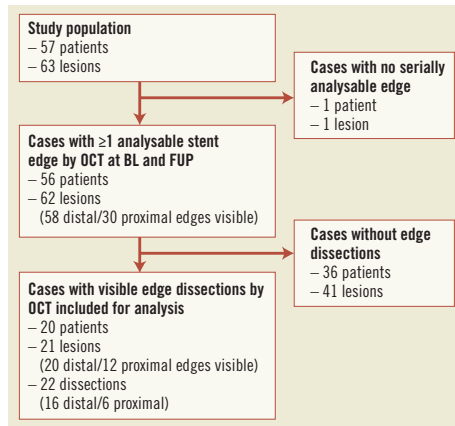


Figure 2. Flow chart.

also involved the stented segments. None of the six patients from the Copenhagen cohort who withdrew consent for follow-up exhibited dissections at baseline examination.

Twenty (90%) out of 22 dissections were completely healed at follow-up (Figure 3). The two dissections that did not heal (Figure 4) exhibited the longest circumferential extension (2.81 and 2.42 mm), and in one case the longest longitudinal extension (6.0 mm) at baseline, and both were combinations of flaps and double-lumen dissections.

The morphometric results are presented in Table 3. Luminal dimensions in the reference vessel segment remained stable at follow-up.

The plaque type at the site of dissection was: an eccentric fibrous plaque in 17 (77.3%) lesions; concentric fibrous plaque in one (4.5%) lesion; eccentric fibrocalcific plaque in four (18.2%) lesions; and an eccentric TCFA in one (4.5%) lesion. In all cases of eccentric plaque, the point of dissection was at the transition site between the normal intima/thinnest point of plaque and the point where the plaque increases in thickness (Figure 2 and Figure 3). The two cases exhibiting signs of incomplete healing at follow-up had both underlying eccentric fibrous plaques.

RESULTS OF IVUS ANALYSIS

IVUS imaging at baseline was available for 18 (82%) lesions, of which nine (50%) exhibited edge dissections. The results of serial morphometric analyses from 17 (77%) lesions are presented in Table 3. The lumen and EEM areas of the RVS increased slightly at follow-up; however, the plaque and media area remained stable.

CLINICAL OUTCOMES

All patients but one received dual antiplatelet therapy with aspirin and clopidogrel during the entire one-year follow-up period. One patient received clopidogrel alone. There were no deaths, MIs,

Table 1. Baseline demographics.

Patient characteristics, N=20		N (%)
Age, years*		63.0 (56.5-67.5)
Male gender		15 (75.0)
Hypertension		11 (55.0)
Hyperlipidaemia		16 (80.0)
Diabetes mellitus		5 (25.0)
Current/previous smoker		4 (20.0)
Family history		14 (82.4)
Previous MI		3 (15.0)
LVEF		60 (55-60)
Clinical presentation	ACS	14 (70.0)
	SAP	6 (30.0)
Multivessel disease		9 (45.9)
Lesion and procedural characteristics, N=21		
Target vessel	LAD	6 (28.6)
	LCX	4 (19.0)
	RCA	11 (52.4)
Target segment	Proximal	9 (42.9)
	Mid	8 (38.1)
	Distal	4 (19.0)
Stent type	CYPHER Select Plus	9 (42.9)
	Resolute	5 (23.8)
	XIENCE V	4 (19.9)
	TAXUS Express	3 (14.3)
Stent diameter, mm*		3.0 (3.0-3.5)
Total stented length, mm*		23 (18-28)
Stents per lesion, n*		1.0 (1.0-2.0)
Overlap		5 (23.8)
TIMI pre	<3	5 (23.8)
	3	16 (76.2)
TIMI post	3	21 (100.0)
Predilatation		15 (71.4)
Post-dilatation		10 (47.6)
Maximum implantation/dilation diameter, mm*		3.0 (3.0-3.5)
Maximum implantation/dilation pressure, atm*		16 (14-20)
GP IIb/IIIa use		5 (25) ^a

*Values are median (interquartile range). ACS: acute coronary syndrome; atm: atmospheres; LAD: left anterior descending artery; LCX: left circumflex artery; LVEF: left ventricular ejection fraction; MI: myocardial infarction; N: number; RCA: right coronary artery; SAP: stable angina pectoris; TIMI: Thrombolysis In Myocardial Infarction. ^adenominator equals n=20 patients.

TLRs or stent thromboses during the entire follow-up for any of the patients. However, at the one-year imaging procedure one patient had a clinically driven TVR. The two patients with lesions exhibiting signs of persistent edge dissections at one-year follow-up were free of any major adverse cardiac events up to three years after the index procedure. None of the six patients from the Copenhagen cohort who had withdrawn consent for a follow-up OCT examination experienced any events at follow-up.

Table 2. Dissection characteristics.

Dissection characteristics, N=22		N (%)
Exhibited features within dissections	Flap	21 (95.5)
	Cavity	8 (36.4)
	Double lumen cap	7 (31.8)
	Fissure	3 (13.6)
Predominant dissection type within dissections	Flap	21 (95.5)
	Cavity	1 (4.5)
	Double lumen cap	0
	Fissure	0
Total longitudinal dissection length, mm*		2.90 (1.60-4.20)
Maximal circumferential extension ^a , mm*		1.20 (0.86-1.67)
Maximal axial extension ^b , mm		0.61 (0.38-0.70)
Maximal dissection area, mm ² *		0.58 (0.27-0.76)
Dissection volume, mm ³ *		0.65 (0.19-1.06)
Maximal circumferential extent	1 quadrant	18 (81.8)
	2 quadrants	4 (18.2)
Maximal vessel injury	Intimal involvement	11 (50.0)
	Medial involvement	7 (33.3)
	Percent frames with medial involvement**	52.8 (33.3-80.0)
	Adventitial involvement	4 (19.5)
	Percent frames with medial involvement**	60.4 (22.2-89.2)

Values are median (interquartile range); N: number; * values are median (interquartile range); ^acircumferential extension refers to the flap length, cavity width and cap length; ^baxial extension refers to flap root thickness, cavity depth and cap thickness; **in the respective lesions

Discussion

Percutaneous coronary interventions are inevitably associated with vascular injury, including intimal tears and medial disruption^{20,21}. Using a systematic classification and quantification of the extent of injury in three dimensions, we studied the natural history of OCT-detected non-flow-limiting edge dissections and found the following: 1) edge dissections were in principle constituted by dissection flaps, although cavity, double lumen and fissure formation were also seen; 2) the majority of OCT-detected edge dissections healed uneventfully without excessive tissue formation; and 3) OCT-detected edge dissections, most of which were angiographically silent, were in this series of patients associated with favourable procedural outcomes and mid-term prognosis.

INCIDENCE OF EDGE DISSECTIONS AND MECHANISM OF HEALING

The incidence of edge dissections following stent implantation ranges from 1.7-6.4%^{1,2} by angiography, increasing to 7.8-19.3% by IVUS^{7,8,22}, and 26.3%¹⁰ up to 34% seen by OCT in the present study. This not only reflects differences in resolution, but also indicates that the use of intracoronary imaging tools more often requires a decision regarding management of apparently "imperfect" results.

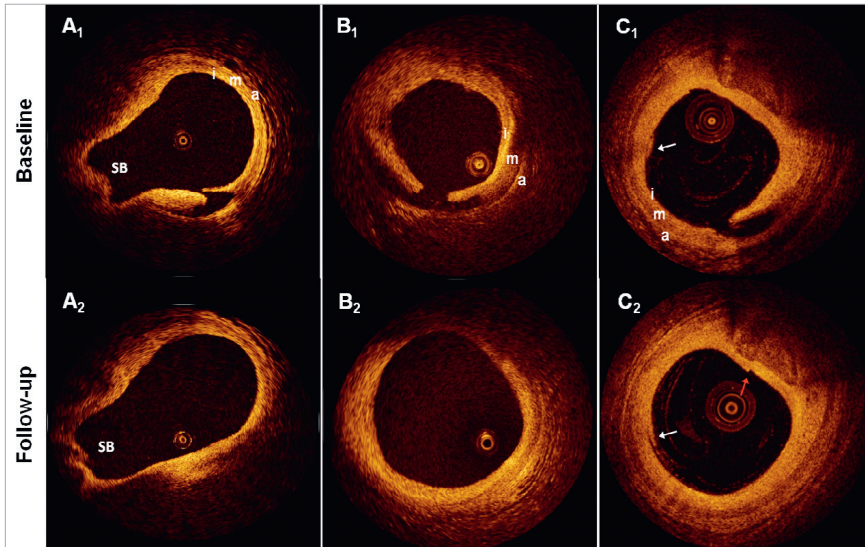


Figure 3. Examples of healed dissections. The figure shows three dissection sites (A-C) at baseline and follow-up. Of note, there were no changes in signal intensity from baseline to follow-up at any of the dissection sites in the study. SB: side branch; i: intima; m: media; a: adventitia; white arrows in C1 and C2 point to residual blood in the vessel lumen, which should not be mistaken for dissections (diagnosis made by inspecting adjacent frames (not shown)); red arrow in C2 points to a seam line artefact, which should not be mistaken for a dissection.

Published evidence, as well as the notable (25%) dissection-triggered use of GP IIb/IIIa inhibitors in the present study, confirm that OCT-detected edge dissections may cause concern for further events^{11,12}, although their sequelae up until now have not been sufficiently explored. Our data show that the majority of edge dissections healed completely during follow-up with only two out of 22 lesions showing residual signs of injury at one year. As indirectly suggested by the absence of an increase in plaque area by IVUS, the mechanism

of healing was previously proposed to be a “layering” or “tacking down” rather than filling in of the gap with plaque material⁷ – something which OCT in our study provided direct evidence for. It may be hypothesised that this is the consequence of the normal physiological response to injury, where fibrin deposition at the disrupted surfaces of exposed tissues contributes to “gluing” the dissected layers together following the approximation of fluttering tissue flaps against the vessel wall by the flowing blood. It therefore

Table 3. Morphometric results by OCT and IVUS.

Parameter	Baseline	Follow-up	Absolute change	Relative change	p-value
Optical coherence tomography, N=22 – Reference vessel segment					
Lumen area, mm ²	5.35±1.73	5.58±1.72	0.21±0.81	6.7±18.4%	0.203
Lumen diameter, mm	2.58±0.42	2.64±0.38	0.06±0.20	3.1±8.8%	0.174
Intravascular ultrasound, N=17 – Reference vessel segment					
Lumen area, mm ²	5.95±2.29	6.84±1.98	0.89±1.51	22.6±34.6%	0.027
Lumen diameter, mm	2.70±0.50	2.92±0.39	0.22±0.35	9.9±15.1%	0.021
EEM area, mm ²	11.20±2.38	12.40±2.58	1.21±1.92	12.9±20.3%	0.020
EEM diameter, mm	3.75±0.40	3.95±0.39	0.20±0.32	5.9±9.4%	0.020
P&M area, mm ²	5.25±1.27	5.56±1.61	0.32±1.09	6.5±20.1%	0.251

Values are mean±standard deviation.

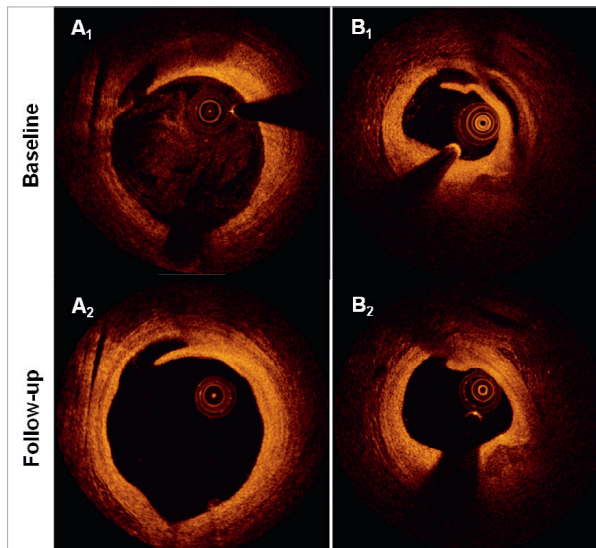


Figure 4. Incompletely healed dissections. The figure shows the serial appearance of the two incompletely healed edge dissections (A-B). Of note is that the flap length in both cases was reduced at follow-up, although the dissection in panel A extended slightly longer longitudinally.

seems reasonable to assume that large flaps, in particular in the circumferential direction, are more mobile than smaller ones, and may not only increase the risk of obstruction and thrombosis, but also predispose to delayed vessel healing if continuously being separated from the vessel wall by blood, somewhat analogous to observations from wound healing²³. In fact, the two edge dissections which healed incompletely at follow-up in the present study exhibited the largest flap length (2.81 and 2.42 mm) at baseline and thus the longest circumferential extension in the entire cohort. Due to the low incidence of incomplete healing, we can only speculate that the maximum flap length may be more important for predicting healing than the extension in the axial and longitudinal direction, since the former is perpendicular to the blood flow. However, the combination with a double-lumen formation, kept open by the blood stream, may also play a role and could possibly have been the cause of the slight progression in longitudinal length in one of these cases at follow-up (from 1.8-2.0 mm). Although the sample size was relatively low, as were the frequencies of TCFA and fibrocalcific plaques at the stent edges, there seemed to be no particular association between the underlying plaque type and propensity of healing.

In terms of healing of edge dissections, our data are in line with a recent report by Kume et al²⁴ who observed, in a total of 36 patients (39 lesions) with 12 edge dissections, that all but one were fully healed at follow-up. However, the following differences should be noted: data in the present study were collected prospectively

(vs. retrospectively); with prespecified instructions on the interventional strategy in 45/63 (71%) lesions (vs. strategy left to the discretion of the operator); with similar follow-up time in all patients (vs. median (range) follow-up of 188 (98-461) days); solely with the use of DES (vs. DES+bare metal stents [BMS]); with a methodology comprising all types of edge dissections including cavities and double-lumen dissections which occurred in 13.6% to 36.4% of cases (vs. flaps alone). Although the number of non-healed dissections at one year was very low, the present study provides details on the characteristics that may have contributed to the lack of complete healing, and which may be regarded as hypothesis-generating for the further understanding of factors of importance for vessel healing.

CLINICAL IMPORTANCE OF EDGE DISSECTIONS

The absence of early events in our study is in line with previous IVUS reports and the OCT report by Kume et al, indicating that there appears to be no increased risk of early stent thrombosis in lesions with residual edge dissections as compared to those without^{6,24-26}. In the present study, this may be attributed to several factors: 1) the small injury defect; 2) an early “tacking down” limiting the risk of obstruction and thrombosis; and 3) a potent antithrombotic and antiplatelet therapy. However, the fact that the vast majority of dissections were angiographically silent and half were unidentified by IVUS indicates that they were relatively smaller in comparison to those previously associated with early stent thrombosis, including angiographic type B-F dissections¹⁻³. Most importantly, however,

these and other studies unanimously showed that, in addition to edge dissections, other “abnormal findings” were concurrently present by angiography and IVUS, most consistently a low final minimal lumen diameter/area and poor stent expansion, but also a reduced final TIMI flow $<3^{4,5,27,28}$, suggesting that stent edge dissections may not *per se* cause acute events.

EDGE DISSECTIONS AND RESTENOSIS

In the long term, our morphometric analysis showed an absence of restenosis at the site of previous dissection despite the presence in several cases of deep vessel injury involving the media and/or adventitia, something otherwise known to be associated with a hyperproliferative response²⁹. Our results confirm previous findings by Sheris et al who similarly observed that the plaque and media area in the RVS by IVUS remained stable over a period of six months, even in the presence of submedial dissections⁷. It could be speculated that the antiproliferative drug from the DES in our study could have had a beneficial effect in preventing restenosis even in the RVS. However, considering that Sheris et al found the same in patients with BMS, together with other data showing that non-occlusive type A-D dissections following balloon angioplasty were associated with a reduced risk of restenosis compared to lesions without dissections⁶, it is likely that the process of “tacking down” by the flowing blood was more important, as it is well known that wounds with separated edges often heal with extensive scar formation, compared with wounds with approximated edges which heal with hairline scars²³.

As it relates to the differences in lumen areas between the various imaging techniques used, it is well known that areas as measured by IVUS tend to be larger than by OCT³⁰⁻³² (with the old as well as the new OCT systems), and our measurements are fully in line with this. The differences have occasionally been shown to be very large (25-72% difference)³¹. This can be caused by the use of an occlusion balloon; however, another possible cause is the relatively greater degree of cardiac motion by IVUS due to a very slow pull-back (0.5 mm/s) as compared to OCT (1-20 mm/s), resulting in a relatively larger “imprecise” matching between baseline and follow-up. In addition, with the resolution of OCT being 10-20 μm , and that of IVUS 100-150 μm , “inaccuracies” within the resolution window are relatively larger by IVUS (± 100 -150 μm) than by OCT (± 10 -20 μm) which may result in significant differences³².

MANAGEMENT OF OCT-DETECTED RESIDUAL EDGE DISSECTIONS

Due to the absence of adverse events in the present cohort, we cannot provide any quantitative directives on which dissections will cause events and which will not. However, longitudinal extensions up to an average of 7.8 mm in previous IVUS studies²⁵, and a circumferential extension up to 2.81 mm by OCT as seen in our study, were both associated with an uneventful mid-term clinical course. The additional mechanical treatment of OCT-detected residual edge dissections being mainly angiographically silent should therefore be carefully evaluated, not least when considering that additional IVUS-guided stent implan-

tation for residual edge dissections has not been shown to entail any benefits in terms of reducing the rate of restenosis and stent thrombosis when compared to an angiographically guided group without treatment of these injuries²⁴, but was rather associated with complications in terms of TLR⁸. Considering that GP IIb/IIIa inhibitors seem to exert a protective effect against early stent thrombosis³³, these may be a reasonable alternative to stent implantation in the presence of large non-flow-limiting OCT-detected edge dissections.

Limitations

The number of patients in this observational study was relatively small, mainly related to the requirement of serial assessment with OCT and IVUS. Furthermore, the inability of OCT to image proximally/ostially located regions, due to the need for blood clearance during acquisition, precluded visualisation of all proximal reference vessel segments. Together with a certain selection of patients, the dissection incidence of 34% may not reflect that in the real world, although it may be assumed that they are fairly representative for OCT-detected edge dissections which are for the most part angiographically silent. The low number of patients further limited our ability to detect rare adverse events and thus to provide recommendations on when a residual dissection imposes an increased risk of, e.g., acute stent thrombosis. Finally, we did not assess the predictors of edge dissections as our focus was on their natural history, and as predictors had previously been evaluated⁸. Furthermore, considering that the majority of these dissections underwent complete healing, this may seem redundant.

Conclusion

OCT-detected edge dissections, which are angiographically silent in the majority of cases, constitute a relatively frequent and benign finding after DES implantation, and are not associated with acute stent thrombosis or restenosis up to one-year follow-up.

Guest Editor

This paper was Guest Edited by Michael Joner, MD; Facharzt für Innere Medizin und Kardiologie, Deutsches Herzzentrum München, Technische Universität, Munich, Germany.

Acknowledgments

M. Radu has received research grants from The Heart Centre Rigshospitalet Research Foundation and Copenhagen University. L. Räber is the recipient of a research fellowship (SPUM) funded by the Swiss National Science Foundation (Grant 33CM30-124112).

Conflict of interest statement

S. Windecker has received consulting and lecture fees from Abbott, Boston Scientific, Biosensors, Cordis, and Medtronic. The other authors have no conflicts of interest to declare. The Guest Editor has no conflict of interest to declare.

References

1. Cutlip DE, Baim DS, Ho KK, Popma JJ, Lansky AJ, Cohen DJ, Carozza JP Jr, Chauhan MS, Rodríguez O, Kuntz RE. Stent throm-

- bosis in the modern era: a pooled analysis of multicenter coronary stent clinical trials. *Circulation*. 2001;103:1967-71.
2. Biondi-Zoccai GG, Agostoni P, Sangiorgi GM, Airoldi F, Cosgrave J, Chieffo A, Barbagallo R, Tamburino C, Vittori G, Falchetti E, Margheri M, Briguori C, Remigi E, Iakovou I, Colombo A. Incidence, predictors, and outcomes of coronary dissections left untreated after drug-eluting stent implantation. *Eur Heart J*. 2006;27:540-6.
 3. van Werkum JW, Heestermans AA, Zomer AC, Kelder JC, Suttrop MJ, Rensing BJ, Koolen JJ, Brueren BR, Dambrink JH, Hautvast RW, Verheugt FW, ten Berg JM. Predictors of coronary stent thrombosis: the Dutch Stent Thrombosis Registry. *J Am Coll Cardiol*. 2009;53:1399-409.
 4. Cheneau E, Leborgne L, Mintz GS, Kotani J, Pichard AD, Satler LF, Canos D, Castagna M, Weissman NJ, Waksman R. Predictors of subacute stent thrombosis: results of a systematic intravascular ultrasound study. *Circulation*. 2003;108:43-7.
 5. Alfonso F, Suarez A, Angiolillo DJ, Sabate M, Escaned J, Moreno R, Hernandez R, Banuelos C, Macaya C. Findings of intravascular ultrasound during acute stent thrombosis. *Heart*. 2004;90:1455-9.
 6. Hermans WR, Rensing BJ, Foley DP, Deckers JW, Rutsch W, Emanuelsson H, Danchin N, Wijns W, Chappuis F, Serruys PW. Therapeutic dissection after successful coronary balloon angioplasty: no influence on restenosis or on clinical outcome in 693 patients. The MERCATOR Study Group (Multicenter European Research Trial with Cilazapril after Angioplasty to prevent Transluminal Coronary Obstruction and Restenosis). *J Am Coll Cardiol*. 1992;20:767-80.
 7. Sheris SJ, Canos MR, Weissman NJ. Natural history of intravascular ultrasound-detected edge dissections from coronary stent deployment. *Am Heart J*. 2000;139:59-63.
 8. Liu X, Tsujita K, Maehara A, Mintz GS, Weisz G, Dangas GD, Lansky AJ, Kreps EM, Rabbani LE, Collins M, Stone GW, Moses JW, Mehran R, Leon MB. Intravascular ultrasound assessment of the incidence and predictors of edge dissections after drug-eluting stent implantation. *JACC Cardiovasc Interv*. 2009;2:997-1004.
 9. Bouma BE, Tearney GJ, Yabushita H, Shishkov M, Kauffman CR, DeJoseph Gauthier D, MacNeill BD, Houser SL, Aretz HT, Halpern EF, Jang IK. Evaluation of intracoronary stenting by intravascular optical coherence tomography. *Heart*. 2003;89:317-20.
 10. Gonzalo N, Serruys PW, Okamura T, Shen ZJ, Garcia-Garcia HM, Onuma Y, van Geuns RJ, Ligthart J, Regar E. Relation between plaque type and dissections at the edges after stent implantation: an optical coherence tomography study. *Int J Cardiol*. 2011;150:151-5.
 11. Imola F, Mallus MT, Ramazzotti V, Manzoli A, Pappalardo A, Di Giorgio A, Albertucci M, Prati F. Safety and feasibility of frequency domain optical coherence tomography to guide decision making in percutaneous coronary intervention. *EuroIntervention*. 2010;6:575-81.
 12. Motreff P, Souteyrand G. Optical coherence tomography to diagnose under-expansion of a drug-eluting stent. *JACC Cardiovasc Imaging*. 2009;2:245-6; author reply 246.
 13. Gutierrez-Chico JL, van Geuns RJ, Regar E, van der Giessen WJ, Kelbaek H, Saunamaki K, Escaned J, Gonzalo N, di Mario C, Borgia F, Nuesch E, Garcia-Garcia HM, Silber S, Windecker S, Serruys PW. Tissue coverage of a hydrophilic polymer-coated zotarolimus-eluting stent vs. a fluoropolymer-coated everolimus-eluting stent at 13-month follow-up: an optical coherence tomography substudy from the RESOLUTE All Comers trial. *Eur Heart J*. 2011;32:2454-63.
 14. Serruys PW, Silber S, Garg S, van Geuns RJ, Richardt G, Buszman PE, Kelbaek H, van Boven AJ, Hofma SH, Linke A, Klauss V, Wijns W, Macaya C, Garot P, DiMario C, Manoharan G, Kornowski R, Ischinger T, Bartorelli A, Ronden J, Bressers M, Gobbens P, Negoita M, van Leeuwen F, Windecker S. Comparison of zotarolimus-eluting and everolimus-eluting coronary stents. *N Engl J Med*. 2010;363:136-46.
 15. Prati F, Regar E, Mintz GS, Arbustini E, Di Mario C, Jang IK, Akasaka T, Costa M, Guagliumi G, Grube E, Ozaki Y, Pinto F, Serruys PW. Expert review document on methodology, terminology, and clinical applications of optical coherence tomography: physical principles, methodology of image acquisition, and clinical application for assessment of coronary arteries and atherosclerosis. *Eur Heart J*. 2009;31:401-15.
 16. Mintz GS, Nissen SE, Anderson WD, Bailey SR, Erbel R, Fitzgerald PJ, Pinto FJ, Rosenfield K, Siegel RJ, Tuzcu EM, Yock PG. American College of Cardiology Clinical Expert Consensus Document on Standards for Acquisition, Measurement and Reporting of Intravascular Ultrasound Studies (IVUS). A report of the American College of Cardiology Task Force on Clinical Expert Consensus Documents. *J Am Coll Cardiol*. 2001;37:1478-92.
 17. Huber MS, Mooney JF, Madison J, Mooney MR. Use of a morphologic classification to predict clinical outcome after dissection from coronary angioplasty. *Am J Cardiol*. 1991;68:467-71.
 18. Tearney GJ, Regar E, Akasaka T, Adriaenssens T, Barlis P, Bezerra HG, Bouma B, Bruining N, Cho JM, Chowdhary S, Costa MA, de Silva R, Dijkstra J, Di Mario C, Dudeck D, Falk E, Feldman MD, Fitzgerald P, Garcia H, Gonzalo N, Granada JF, Guagliumi G, Holm NR, Honda Y, Ikeno F, Kawasaki M, Kochman J, Koltowski L, Kubo T, Kume T, Kyono H, Lam CC, Lamouche G, Lee DP, Leon MB, Maehara A, Manfrini O, Mintz GS, Mizuno K, Morel MA, Nadkarni S, Okura H, Otake H, Pietrasik A, Prati F, Raber L, Radu MD, Rieber J, Riga M, Rollins A, Rosenberg M, Sirbu V, Serruys PW, Shimada K, Shinke T, Shite J, Siegel E, Sonada S, Suter M, Takarada S, Tanaka A, Terashima M, Troels T, Uemura S, Ughi GJ, van Beusekom HM, van der Steen AF, van Es GA, van Soest G, Virmani R, Waxman S, Weissman NJ, Weisz G. Consensus standards for acquisition, measurement, and reporting of intravascular optical coherence tomography studies: a report from the international working group for intravascular optical coherence tomography standardization and validation. *J Am Coll Cardiol*. 2012;59:1058-72.
 19. Cutlip DE, Windecker S, Mehran R, Boam A, Cohen DJ, van Es GA, Steg PG, Morel MA, Mauri L, Vranckx P, McFadden E, Lansky A, Hamon M, Krucoff MW, Serruys PW. Clinical end points in coronary stent trials: a case for standardized definitions. *Circulation*. 2007;115:2344-51.

20. Potkin BN, Roberts WC. Effects of percutaneous transluminal coronary angioplasty on atherosclerotic plaques and relation of plaque composition and arterial size to outcome. *Am J Cardiol*. 1988;62:41-50.
21. Farb A, Virmani R, Atkinson JB, Kolodgie FD. Plaque morphology and pathologic changes in arteries from patients dying after coronary balloon angioplasty. *J Am Coll Cardiol*. 1990;16:1421-9.
22. Hong MK, Park SW, Lee NH, Nah DY, Lee CW, Kang DH, Song JK, Kim JJ, Park SJ. Long-term outcomes of minor dissection at the edge of stents detected with intravascular ultrasound. *Am J Cardiol*. 2000;86:791-5, A799.
23. Harvey C. Wound healing. *Orthop Nurs*. 2005;24:143-57; quiz 158-9.
24. Kume T, Okura H, Miyamoto Y, Yamada R, Saito K, Tamada T, Koyama T, Neishi Y, Hayashida A, Kawamoto T, Yoshida K. Natural history of stent edge dissection, tissue protrusion and incomplete stent apposition detectable only on optical coherence tomography after stent implantation. *Circ J*. 2012;76:698-703.
25. Russo RJ, Silva PD, Teirstein PS, Attubato MJ, Davidson CJ, DeFranco AC, Fitzgerald PJ, Goldberg SL, Hermiller JB, Leon MB, Ling FS, Lucisano JE, Schatz RA, Wong SC, Weissman NJ, Zientek DM. A randomized controlled trial of angiography versus intravascular ultrasound-directed bare-metal coronary stent placement (the AVID Trial). *Circ Cardiovasc Interv*. 2009;2:113-23.
26. Nishida T, Colombo A, Briguori C, Stankovic G, Albiero R, Corvaja N, Finci L, Di Mario C, Tobis JM. Outcome of nonobstructive residual dissections detected by intravascular ultrasound following percutaneous coronary intervention. *Am J Cardiol*. 2002;89:1257-62.
27. Okabe T, Mintz GS, Buch AN, Roy P, Hong YJ, Smith KA, Torguson R, Gevorkian N, Xue Z, Satler LF, Kent KM, Pichard AD, Weissman NJ, Waksman R. Intravascular ultrasound parameters associated with stent thrombosis after drug-eluting stent deployment. *Am J Cardiol*. 2007;100:615-20.
28. Uren NG, Schwarzacher SP, Metz JA, Lee DP, Honda Y, Yeung AC, Fitzgerald PJ, Yock PG. Predictors and outcomes of stent thrombosis: an intravascular ultrasound registry. *Eur Heart J*. 2002;23:124-32.
29. Schwartz RS, Huber KC, Murphy JG, Edwards WD, Camrud AR, Vlietstra RE, Holmes DR. Restenosis and the proportional neointimal response to coronary artery injury: results in a porcine model. *J Am Coll Cardiol*. 1992;19:267-74.
30. Suzuki Y, Ikeno F, Koizumi T, Tio F, Yeung AC, Yock PG, Fitzgerald PJ, Fearon WF. In vivo comparison between optical coherence tomography and intravascular ultrasound for detecting small degrees of in-stent neointima after stent implantation. *JACC Cardiovasc Interv*. 2008;1:168-73.
31. Gonzalo N, Serruys PW, Garcia-Garcia HM, van Soest G, Okamura T, Ligthart J, Knaapen M, Verheye S, Bruining N, Regar E. Quantitative ex vivo and in vivo comparison of lumen dimensions measured by optical coherence tomography and intravascular ultrasound in human coronary arteries. *Rev Esp Cardiol*. 2009;62:615-24.
32. Nakano M, Vorpahl M, Otsuka F, Taniwaki M, Yazdani SK, Finn AV, Ladich ER, Kolodgie FD, Virmani R. Ex vivo assessment of vascular response to coronary stents by optical frequency domain imaging. *JACC Cardiovasc Imaging*. 2012;5:71-82.
33. Dangas G, Aymong ED, Mehran R, Tcheng JE, Grines CL, Cox DA, Garcia E, Griffin JJ, Guagliumi G, Stuckey T, Lansky AJ, Stone GW. Predictors of and outcomes of early thrombosis following balloon angioplasty versus primary stenting in acute myocardial infarction and usefulness of abciximab (the CADILLAC trial). *Am J Cardiol*. 2004;94:983-8.

Chapter 15

Biomechanical Assessment of Fully Bioresorbable Devices.

Bill D. Gogas, Spencer B. King III, Lucas H. Timmins, Tiziano Passerini, Marina Piccinelli, Alessandro Veneziani, Sungho Kim, David S. Molony, Don P. Giddens, Patrick W. Serruys, Habib Samady

JACC Cardiovasc Interv. 2013 July; 6(7): 760-1 [IF: 6.83]

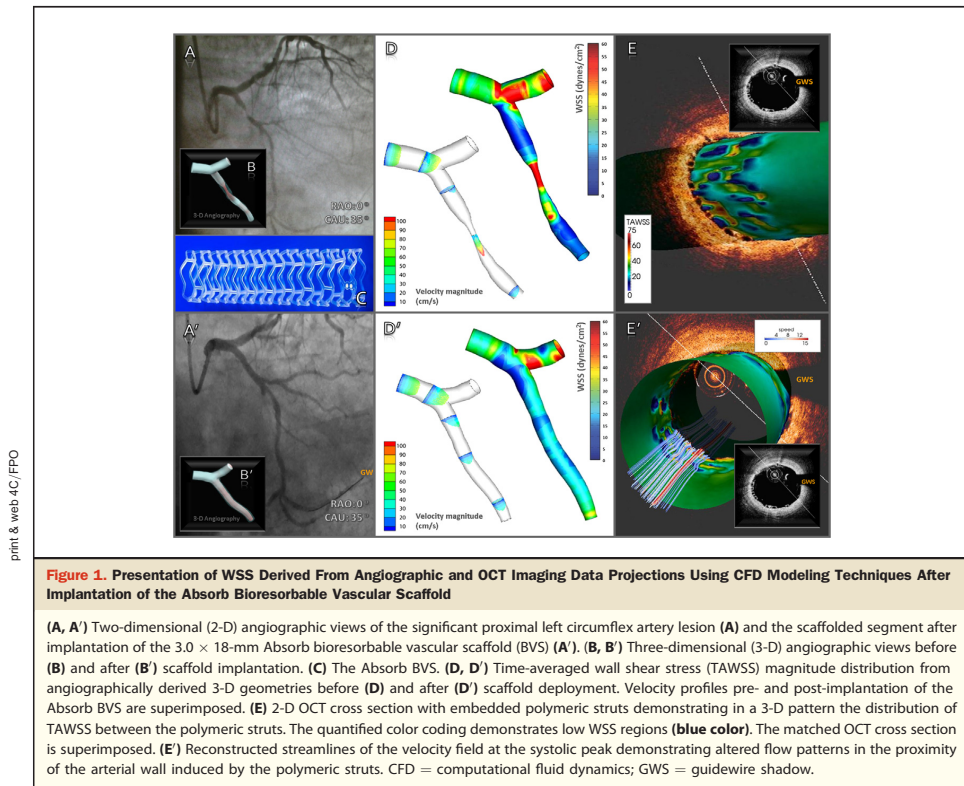
Biomechanical Assessment of Fully Bioresorbable Devices

Bill D. Gogas, MD,* Spencer B. King III, MD,*† Lucas H. Timmins, PhD,‡ Tiziano Passerini, PhD,§ Marina Piccinelli, PhD,|| Alessandro Veneziani, PhD,§ Sungho Kim, PhD,‡ David S. Molony, PhD,‡ Don P. Giddens, PhD,‡ Patrick W. Serruys, MD, PhD,¶ Habib Samady, MD*

Atlanta, Georgia; and Rotterdam, the Netherlands

The use of bioresorbable technologies for the treatment of coronary artery disease is a novel approach with potential advantages over the use of metal stents

(1). Several devices have undergone First-In-Man studies; however, the Absorb bioresorbable vascular scaffold (BVS) (Abbott Vascular, Santa



From the *Andreas Gruentzig Cardiovascular Center, Emory University School of Medicine, Atlanta, Georgia; †Saint Joseph's Heart and Vascular Institute, Atlanta, Georgia; ‡Wallace H. Coulter Department of Biomedical Engineering Georgia Institute of Technology and Emory University, Atlanta, Georgia; §Department of Mathematics and Computer Science, Emory University, Atlanta, Georgia; ||Department of Radiology and Imaging Sciences, Emory University, Atlanta, Georgia; and the ¶Thoraxcenter,

Erasmus University Medical Center, Rotterdam, the Netherlands. Abbott Vascular was the sponsor of ABSORB Extend study. The authors have reported that they have no relationships relevant to the contents of this paper to disclose. Marco Costa, MD, has served as Guest Editor.

Manuscript received January 24, 2013; revised manuscript received March 29, 2013, accepted April 17, 2013.

Clara, California) is the only bioresorbable platform approved for clinical use in Europe (CE mark). The BVS platform is made of poly-L-lactide that is shown to completely resorb over a 2- to 3-year period. Insights from the ABSORB Cohort B trial [NCT00856856] suggest that the scaffold is more conformable than metal stents (Xience everolimus-eluting stent, Abbott Vascular), resulting in less vascular straightening and greater retention of the original angulation and curvature. Although the polymeric struts of the ABSORB BVS are thicker (150 μm) compared with those of second-generation metal stents, the hemodynamic effects change over time as the scaffold resorbs. Therefore, the overall biomechanical footprint of the bioresorbable scaffold compared with metal stents is transient with different effects on local vessel and strut level wall shear stress (WSS). We have proposed that such detailed biomechanical evaluation of the ABSORB BVS will add critical mechanistic insights into its potential beneficial effects, particularly in angulated and curved vessels (2).

Here we illustrate the assessment of biomechanical properties by 2 methods in 2 selected patients who underwent implantation of the ABSORB BVS from the ABSORB Extend study [NCT01023789]. The evaluation used 3-dimensional (3-D) angiographic reconstruction techniques and computational fluid dynamics (CFD) to calculate the WSS pre- and post- BVS deployment (Figs. 1A to 1D) for vessel-level analysis. The second used optical coherence tomography (OCT) imaging data to reconstruct the 3-D geometry and CFD to visualize flow streamlines over the polymeric struts for more detailed strut level analysis. (Figs. 1E and E'). Fusion of angiographic with OCT data has been previously shown to be a feasible approach to calculate WSS by CFD simulations (3), and

biomechanical analyses by these methods may yield important insights into potential advantages of bioresorbable technologies over metal stents.

Acknowledgments

Dr. Gogas acknowledges the American College of Cardiology Foundation for the International Society of Cardiovascular Translational Research Scholarship. Dr. Timmins and Dr. Passerini acknowledge the American Heart Association for their Postdoctoral Fellowships. The authors thank Prof. Didier Carrie from the Hôpital de Rangueil, Toulouse, France, Prof. Stephen Lee, from the Queen Mary Hospital, Hong Kong, and Christos Bourantas from the Thoraxcenter, Erasmus University Medical Center, Rotterdam, for their valuable comments.

Reprint requests and correspondence: Dr. Habib Samady, Emory University School of Medicine, 1364 Clifton Road, Suite F606, Atlanta, Georgia 30322. E-mail: hsamady@emory.edu.

REFERENCES

1. Serruys PW, Garcia-Garcia HM, Onuma Y. From metallic cages to transient bioresorbable scaffolds: change in paradigm of coronary revascularization in the upcoming decade? *Eur Heart J* 2012;33:16–25b.
2. McDaniel MC, Samady H. The sheer stress of straightening the curves: biomechanics of bioabsorbable stents. *J Am Coll Cardiol Intv* 2011;4:800–2.
3. Tu S, Holm NR, Koning G, et al. Fusion of 3D QCA and IVUS/OCT. *Int J Cardiovasc Imaging* 2011;27:197–207.

Key Words: bioresorbable scaffolds ■ optical coherence tomography ■ 3-D wall shear stress.

Part 4

Stent Implantation Assessment Utilizing Three-Dimensional Optical Coherence Tomography

Chapter 16

Three-Dimensional Coronary Topographic Reconstructions Using *In Vivo* Intracoronary Optical Frequency Domain Imaging in the Setting of Acute Myocardial Infarction: The Clinical Perspective.

Bill D. Gogas, Vasim Farooq, Patrick W. Serruys

Hellenic Journal Cardiology. 2012. Mar; 53(2): 148-51 [IF: 1.23]

Three-Dimensional Coronary Tomographic Reconstructions Using *In Vivo* Intracoronary Optical Frequency Domain Imaging in the Setting of Acute Myocardial Infarction: The Clinical Perspective

BILL D. GOGAS, VASIM FAROOQ, PATRICK W. SERRUYS

Thoraxcenter, Erasmus University Medical Center, Rotterdam, The Netherlands

Key words: Three-dimensional optical coherence tomography, acute myocardial infarction.

Manuscript received: August 17, 2011;
Accepted: December 15, 2011.

Address:
Patrick W. Serruys

*Thoraxcenter, Bd583a
Dr. Molewaterplein 40
3015-GD
Rotterdam, Netherlands
e-mail: p.w.j.c.serruys@erasmusmc.nl*

Optical coherence tomography (OCT) is a light-based imaging modality with superior spatial resolution (~15 μm) compared to other intracoronary imaging systems currently used *in vivo*, such as intravascular ultrasonography (~100 μm) and angiography (~150 μm). OCT technology uses a similar algorithm as intravascular ultrasound (IVUS) to reconstruct two-dimensional (2-D) tomographic images, measuring the time delay of the reflected infrared light beam from the biological tissues. The earlier time-domain OCT technology has been replaced by frequency-domain OCT (FD-OCT); more recently, optical frequency domain imaging (OFDI), a variant of FD-OCT, has been introduced. OFDI is an intravascular imaging modality that is capable of obtaining higher frame rates (up to 160/s) and pull-back speeds (up to 40 mm/s). It is these technical components that define the resolution of 3-D tomographic reconstructions from the 2-D post-processed images.

The major contributions of 2D FD-OCT technology in conventional clinical practice are the following: 1) characterization of the initial stages of atherosclerosis (pathological intimal thickening) and

plaque composition (fibrous, fibrofatty, calcific); 2) evaluation of cap thickness (thin cap vs. thick cap fibroatheroma); 3) visualization of plaque complications (erosion, ulceration, rupture); 4) identification of thrombus; and 5) evaluation of stent implantation post intervention (strut apposition, edge dissection, tissue prolapse) and at follow up (strut coverage, late acquired malapposition, in-segment restenosis).

3-D OFDI reconstructions from their respective 2-D images were first described by Tearney et al¹ for the visualization of metallic stents; more recently Okamura et al² demonstrated the potential for this technology in the evaluation of jailed side-branches associated with implantation of a bioresorbable vascular scaffold. Subsequent reports have described the potential use of this technology in the setting of acute coronary syndromes.³ In brief, the major imaging findings that may enhance the decision making process during interventional procedures and confirm the need of a real-time application of this technology are the following: 1) assessment of the flow divider and high resolution visualization of the spatial-distribution of the stent struts covering the side

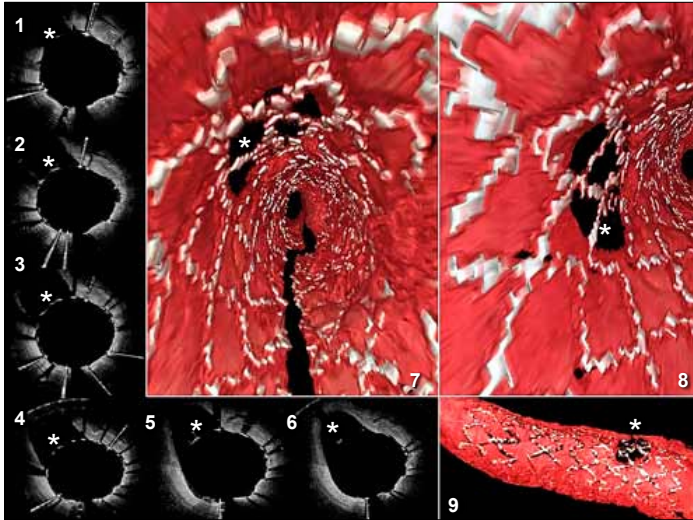


Figure 1. Three-dimensional reconstruction of a jailed side branch.

Three-dimensional post processed reconstruction, demonstrating the jailing of the side branch - a large diagonal branch - after implantation of a Biolimus-A9 cluting stent, in fly-through (Panels 7, 8) and longitudinal views (Panel 9). Two-dimensional optical coherence tomography (OCT) frames (Panels 1, 2, 3, 4, 5, 6) illustrate the region of interest (white asterisks).

The OCT pullback was performed with the TERUMO (Terumo, Corporation, Tokyo, Japan) imaging system. *: Side branch jailing

branch, after main-branch stenting⁴ (Figure 1); 2) assessment of pre/peri-procedural thrombus formation (Figure 2); and 3) evaluation of the stent strut apposition/malapposition (Figure 3).

Bifurcation stenting is a challenging subset of coronary interventions with less satisfactory clinical

outcomes compared to the management of simple lesions.⁵ In the setting of side-branch jailing, recent evidence from benchwork studies suggests the crossing and post-dilatation of the distal cells of the implanted device to clear the struts in the jailed side-branch orifice. Real-time 3-D OCT clinical application appears

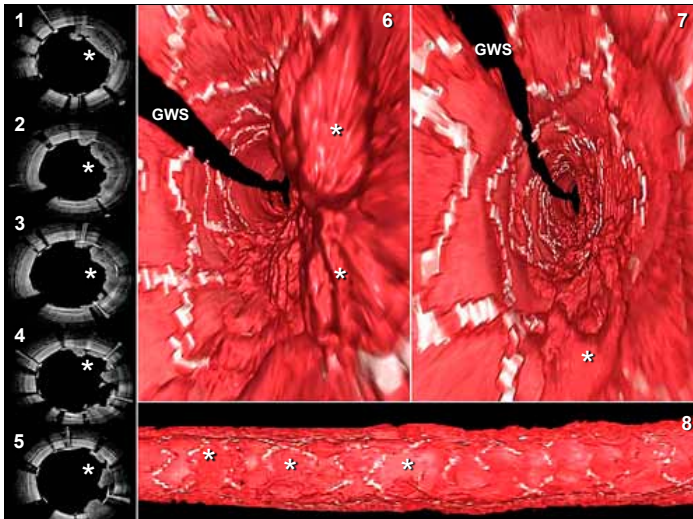


Figure 2. Three-dimensional reconstruction of thrombus.

Three-dimensional post processed reconstruction, demonstrating the thrombus burden covering the metallic struts of an implanted Biolimus-A9 cluting stent, in fly-through (Panels 6, 7) and longitudinal views (Panel 8). The two-dimensional optical coherence tomography (OCT) still frames (Panels 1, 2, 3, 4, 5) illustrate the region of interest (white asterisks).

The OCT pullback was performed with the TERUMO (Terumo, Corporation, Tokyo, Japan) imaging system. GWS – guide wire shadow. *: Thrombus

to have the potential to accurately guide the interventional cardiologist in performing distal cell post-dilatation and restoring the optimal TIMI flow that may influence the patient's clinical outcome.

The evaluation of pre/periprocedural thrombus formation in the setting of acute coronary syndromes is a clinical subset where real-time 3-D OFDI may appear helpful. Real-time 3-D visualization and quantification of thrombus to guide further aspiration thrombectomy may have a future potential role; aspiration thrombectomy has been shown to improve angiographic TIMI flow, myocardial perfusion and subsequent blush score, and has been associated with a possible reduction in the incidence of major adverse cardiac events.^{6,7} Gonzalo et al recently demonstrated the potential of the fusion of tissue characterization with 3-D OFDI technology.⁸ Further improvements are required for precise tissue component quantification, as is currently done using IVUS virtual histology (VH); fusion of 2D FD-OCT with IVUS-VH has also recently been shown to be feasible.⁹ The potential clinical benefit of fusion imaging will be to accurately visualize plaque components during stent implantation in order to allow full coverage of the lesion. This concept, however, remains unproven, though tissue composition has been shown to be directly related to stent healing, thrombosis and tissue protrusion.

Stent malapposition, either post-intervention or

as a late acquired phenomenon, has been incriminated in the pathophysiology of several mechanisms of stent thrombosis. Stent thrombosis has an incidence rate of 0.5-2% and is associated with a high mortality (approximately 45%).

2-D OFDI is currently the imaging modality of choice to visualize incomplete stent apposition. 3-D visualization of the malapposed struts with identification of the underlying mechanism (e.g. underlying thrombus, calcified plaque) may potentially add further to the clinical management of such cases. Conversely, IVUS is unable to visualize thrombus, with the detection of incomplete stent apposition being made on the grounds of an educated guess.

3-D off-line post-processed vascular tomographic reconstructions are for the moment time consuming, as they have to be performed manually. Off-line bitmap sequences are generated from prior 2-D OFDI imaging, each strut is manually detected in each cross section and specific volume rendering software is used for reconstruction with operator-dependent output. Automated strut identification and volume rendering to generate real-time OCT in the catheterization laboratory will potentially allow for immediate 3-D constructions that will guide the operator to the area of interest, where further scrutiny can be undertaken with 2-D imaging.

With the advent of high resolution intravascular

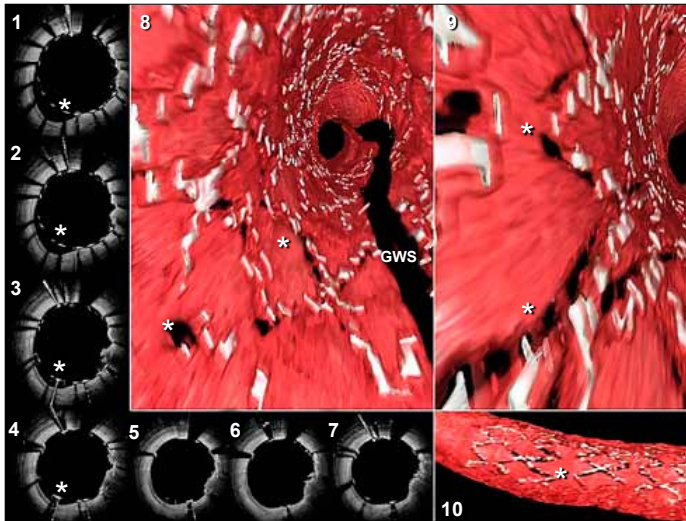


Figure 3. Three-dimensional reconstruction of incomplete stent apposition.

Three-dimensional post processed reconstructions, demonstrating the incomplete apposition (ISA) of the Biolimus-A9 eluting stent in fly-through (Panels 8, 9) and longitudinal views (Panel 10). Malapposed struts are systematically accompanied by a thin wall shadow. The two-dimensional optical coherence tomography (OCT) still frames (Panels 1, 2, 3, 4, 5, 6, 7) illustrate the region of interest (white asterisks).

The OCT pullback was performed with the TERUMO (Terumo, Corporation, Tokyo, Japan) imaging system.

GWS – guide wire shadow.

*: ISA

imaging, the treatment of coronary artery disease has changed, as we understand more about the anatomy, the physiology and the behavior of the treated lesions.

Real time 3-D post-processed OFDI appears to have the potential to guide percutaneous coronary intervention, and the application of this technology in the catheterization laboratory is eagerly expected from the industry. Images with better than the existing resolution (Figures 1, 2, 3) are expected, as the development of 2-D OFDI with faster pullback and frame rates is under intense research. Further development and innovation in this field is required for the patient's clinical benefit.

Acknowledgements

Dr. Bill D. Gogas wishes to thank the Hellenic Cardiological Society (HCS) for the 2011-2012 research grant.

References

1. Tearney GJ, Waxman S, Shishkov M, et al. Three-dimensional coronary artery microscopy by intracoronary optical frequency domain imaging. *JACC Cardiovasc Imaging*. 2008; 1: 752-761.
2. Okamura T, Onuma Y, Garcia-Garcia HM, et al. 3-dimensional optical coherence tomography assessment of jailed side branches by bioresorbable vascular scaffolds: proposal for classification. *JACC Cardiovasc Interv*. 2010; 3: 836-844.
3. Gogas BD, Farooq V, Onuma Y, et al. 3-dimensional optical frequency domain imaging for the evaluation of primary percutaneous coronary intervention in ST-segment elevation myocardial infarction. *Int J Cardiol*. 2011; 151: 103-510.
4. Gogas BD, van Geuns RJ, Farooq V, et al. 3-dimensional reconstruction of the post-dilated second generation everolimus eluting bioresorbable vascular scaffold in a true bifurcation lesion for flow restoration. *JACC Cardiovasc Interv*. 2011; 4: 1149-1150.
5. Koo BK, Waseda K, Kang HJ, et al. Anatomic and functional evaluation of bifurcation lesions undergoing percutaneous coronary intervention. *Circ Cardiovasc Interv*. 2010; 3: 113-119.
6. Vlaar PJ, Svilaas T, van der Horst IC, et al. Cardiac death and reinfarction after 1 year in the thrombus aspiration during percutaneous coronary intervention in acute myocardial infarction study (TAPAS): a 1-year follow-up study. *Lancet*. 2008; 371: 1915-1920.
7. Svilaas T, Vlaar PJ, van der Horst IC, et al. Thrombus aspiration during primary percutaneous coronary intervention. *N Engl J Med*. 2008; 358: 557-567.
8. Gonzalo N, Tearney GJ, van Soest G, et al. Witnessed coronary plaque rupture during cardiac catheterization. *JACC Cardiovasc Imaging*. 2011; 4: 437-438.
9. Waxman S, Freilich MI, Suter MJ, et al. A case of lipid core plaque progression and rupture at the edge of a coronary stent: elucidating the mechanisms of drug-eluting stent failure. *Circ Cardiovasc Interv*. 2010; 3: 193-196.

Chapter 17

New Insights into the Coronary Artery Bifurcation. Hypothesis-Generating Concepts Utilizing 3-Dimensional Optical Frequency Domain Imaging.

Vasim Farooq, Patrick W. Serruys, Jung Ho Heo, **Bill D. Gogas**, Takayuki Okamura, Josep Gomez-Lara, Salvatore Brugaletta, Hector M. Garcia-Garcia, Robert Jan van Geuns

JACC Cardiovascular Interventions. 2011. Aug; 4(8): 921-31 [IF: 6.83]

New Insights Into the Coronary Artery Bifurcation

Hypothesis-Generating Concepts Utilizing 3-Dimensional Optical Frequency Domain Imaging

Vasim Farooq, MBChB, Patrick W. Serruys, MD, PhD, Jung Ho Heo, MD, Bill D. Gogas, MD, Takayuki Okamura, MD, PhD, Josep Gomez-Lara, MD, Salvatore Brugaletta, MD, Hector M. Garcia-Garcia, MD, MSc, PhD, Robert Jan van Geuns MD, PhD

Rotterdam, the Netherlands

Coronary artery bifurcations are a common challenging lesion subset accounting for approximately 10% to 20% of all percutaneous coronary interventions. The provisional T-stenting approach is generally recommended as the first-line management of most lesions. Carina shift is suggested to be the predominant mechanism of side-branch pinching during provisional T-stenting and has been indirectly inferred from bench work and other intravascular imaging modalities. Offline 3-dimensional (3D) reconstructions of patients studied in the first-in-man trial of the high-frequency (160 frames/s) Terumo optical frequency domain imaging system were undertaken using volume-rendering software. Through a series of 3D reconstructions, several novel hypothesis-generating concepts are presented. (*J Am Coll Cardiol Intv* 2011;4:921–31) © 2011 by the American College of Cardiology Foundation

Coronary bifurcations are a challenging lesion subset accounting for approximately 10% to 20% of all percutaneous coronary interventions (PCI). Historically, they have been associated with lower rates of procedural success, higher restenosis rates, in particular at the ostium, and adverse events compared with the treatment of simpler, nonbifurcation lesions (1–3).

The current prevailing opinion in their management is one of a “simpler is better” approach, with provisional T-stenting recommended as the first-line strategy in most lesions (1,2). The traditional concept of plaque shift as the predominant mechanism in the pinching of the side branch (SideB) during this technique has recently been challenged and replaced by carina shift, with the suggestion that up to 30% of bifurcations have involvement of plaque shift, since atheroma is rarely seen at the carina alone

because of it being a high wall shear stress area (2,4). The concept of carina shift has been indirectly inferred from bench work, in vivo longitudinal and cross-sectional intravascular ultrasound intravascular (IVUS) imaging, and computed tomography (CT) imaging modalities (1,4–8).

Both IVUS (image resolution: 100 to 150 μm) and CT (resolution: 300 to 500 μm) lack the imaging resolution to fully appreciate the complex architecture of the bifurcation compared with optical coherence tomography (OCT; image resolution: 10 to 20 μm). Fusion of CT and IVUS in obtaining 3D reconstructions of human coronary bifurcation have previously successfully been undertaken to allow for wall shear stress analyses; this system, however, lacks the resolution obtainable with OCT (9).

Current-generation Fourier-domain OCT (FD-OCT) allows rapid pullback speeds and has allowed visualization of the coronary bifurcation with 2-dimensional (2D) images in great detail (10–12). One of the major limitations of this technology, however, has been the lack of 3-dimensional (3D) images. Trying to mentally reconstruct a

From the ThoraxCenter, Erasmus University Medical Centre, Rotterdam, the Netherlands. All authors have reported that they have no relationships relevant to the contents of this paper to disclose.

Manuscript received March 4, 2011; revised manuscript received May 20, 2011, accepted June 3, 2011.

complex 3D structure from 2D images is difficult; 2D imaging may not allow a full appreciation of the anatomic features of the bifurcation and the effects of PCI.

Three-dimensional, offline FD-OCT reconstructions were first described by Tearney et al. (13) and more recently by Okamura et al. (14) in the assessment of jailed SideB by bioresorbable vascular scaffolds.

Prototypes of current-generation “real-time” (i.e., periprocedural) 3D FD-OCT are experimental, have not yet entered conventional clinical practice, and appear to have a limited resolution compared with the offline 3D optical frequency domain imaging (OFDI) reconstructions; this may be related to the lower frame rate of commercially available systems: the intracoronary Terumo OFDI system (Terumo Corporation, Tokyo, Japan) is currently the only system with a frame rate as high as 160 frames/s (11,14,15).

Through a series of images demonstrating 3D OFDI reconstructions of coronary artery bifurcations, we aim to demonstrate several novel, hypothesis-generating concepts with regard to the anatomic characteristics of this complex structure.

Methodology

Three-dimensional reconstructions of patients who underwent conventional PCI from the original first-in-man study of the intracoronary Terumo OFDI system were undertaken (15). The high-speed Terumo OFDI system is capable of acquiring 160 frames/s during the catheter pullback up to a maximum speed of 40 mm/s; all images were acquired with a pullback speed

of 20 mm/s. The 3D coronary angiography images were constructed from their respective biplane 2D images (CAAS 5.9, Pie Medical Imaging, Maastricht, the Netherlands) (16). All patients studied had stable angina; 3D reconstructions of coronary bifurcations and the consequent effects of provisional T-stenting were performed.

The methodology for the 3D reconstructions has previously been described (14). In brief, offline bitmap sequences (704 × 704 pixels) were generated from prior 2D OFDI imaging. Manual detection of every strut in each 2D cross section were undertaken, and 3D reconstructions of the coronary vessel pre- and post-intervention were performed

using volume-rendering software (INTAGE Realia, KGT, Tokyo, Japan).

Nomenclature for 3D FD-OCT reconstructions. “Fly-through” views indicate a selected still image of an internal view of a vessel looking either downstream (proximal-to-distal vessel) or upstream (distal-to-proximal vessel). An “orientation” figure is located as an inset figure within the 3D reconstruction to best illustrate where the endoluminal point of view is electronically located, and in which direction it is pointing. In 3D reconstructions, the 3D rendering software provides x-, y-, and z-axes within the coronary vessel to allow precise assessment of the location of the endoluminal point of view. Longitudinal and, in some cases, cross-sectional 2D OFDI frames of the vessel and bifurcation, with a blue arrow superimposed on it, are used to orient the reader within the vessel: the base and direction of the blue arrow indicates from and in which direction, respectively, the 3D image is visualized from within the 2D plane(s).

3D Reconstructions

Anatomy of the left main stem, circumflex, left anterior descending, diagonal, and septal branches. Figure 1A demonstrates a fly-through view, looking downstream, from the distal left main stem showing the ostia of the left anterior descending coronary artery (LAD), circumflex, first diagonal (Fig. 1A, D1), and septal branches. Note the appearance of the opening of the diagonal vessel and its relationship to the LAD vessel opening. The main branch (MainB) and SideB appear to diverge parallel to each other at their respective origins, with the carina (labeled) appearing to be “interposed” between both vessel openings at this point of divergence.

Figure 1B demonstrates a close-up fly-through view of the same vessel looking downstream from the proximal LAD and aimed towards the diagonal ostium (upper right image); the left circumflex coronary artery (LCx) orifice appears between 12 and 3 o'clock in relation to the diagonal ostium. For comparison, note the corresponding 2D OFDI frames (lower image). The slit-like, elliptical appearance of the diagonal opening is clearly visible, and when bifurcation is viewed perpendicular to the vessel wall (inset left image—use the orientation figure to allow assessment of the endoluminal point of view), the carina is predominantly visualized, with the proximal course of the diagonal vessel appearing to be hidden behind the rim of the carina so that the diagonal orifice appears, in-depth, as a dead end. This is further suggestive of the proximal parallel course of the diagonal with the LAD at the point of divergence. The yellow arrows in the fly-through and perpendicular views are pointing in identical directions, namely, the direction of the opening of the diagonal vessel.

Figure 1C demonstrates a fly-through view looking further downstream into the same LAD (upper left image).

Abbreviations and Acronyms

2D = 2-dimensional

3D = 3-dimensional

CT = computed tomography

FD-OCT = Fourier-domain optical coherence tomography

IVUS = intravascular ultrasound intravascular

KBPD = kissing balloon post-dilation

LAD = left anterior descending coronary artery

LCx = left circumflex coronary artery

MainB = main branch

OCT = optical coherence tomography

OFDI = optical frequency domain imaging

PCI = percutaneous coronary intervention

RV = right ventricular

SideB = side branch

Observe the large septal branch orifice opening; when viewed perpendicular to the vessel wall (upper right image), and contrary to the observations made with the diagonal branch, the endoluminal opening of the septal branch is entirely visible and does not appear to be concealed behind the carina. This corresponds to the characteristic, almost perpendicular takeoff of the septal branch from the LAD. Corresponding 2D OFDI frames are displayed below the panel.

Anatomy of the proximal, mid, and distal LAD–diagonal branches. Figure 2A demonstrates downstream fly-through views of the LAD, looking distally (Image 1) and aimed towards the proximal diagonal ostium (Image 2). When the bifurcation is visualized perpendicular to the vessel wall (Image 3), the diagonal orifice appears to have a circular appearance with the rim of the carina appearing to be concealing the proximal course of diagonal, so that the diagonal orifice once again appears, in-depth, as a dead end. Yellow arrows (Images 2 and 3) point in identical directions at the opening of the same diagonal vessel. Corresponding 2D OFDI frames are shown below the panel for comparison.

Figure 2B demonstrates fly-through views (looking downstream) of the mid (D2, left image) and distal (D3, right image) LAD–diagonal bifurcations; yellow arrows point at the diagonal vessel openings. The corresponding 2D OFDI frames of each bifurcation are displayed below their respective 3D reconstructions.

All of these images are further suggestive of the proximal parallel course of the diagonal vessels relative to the LAD at their point of divergence.

Anatomy of diagonal branch originating perpendicular to the LAD. Figure 3 demonstrates a coronary angiogram (left image), suggesting the diagonal vessel (asterisk) originates almost perpendicular to the LAD at the point of divergence of both vessel origins. The 3D coronary angiography images (left inset figures) confirmed these findings with a bifurcation angle of 85°. A fly-through view of the LAD looking downstream (upper right image) demonstrates the diagonal vessel opening (asterisk), note the elliptical shape of the vessel opening and the observation that the diagonal vessel opening is fully visible, and not concealed by the carina, when visualized perpendicular to the vessel wall (lower right image). Observe how the stent is able to divide the opening of the diagonal vessel into at least 3 segments. Effectively, the diagonal branch with an almost perpendicular takeoff appears to have similar characteristics to the septal branch as described in Figure 1C.

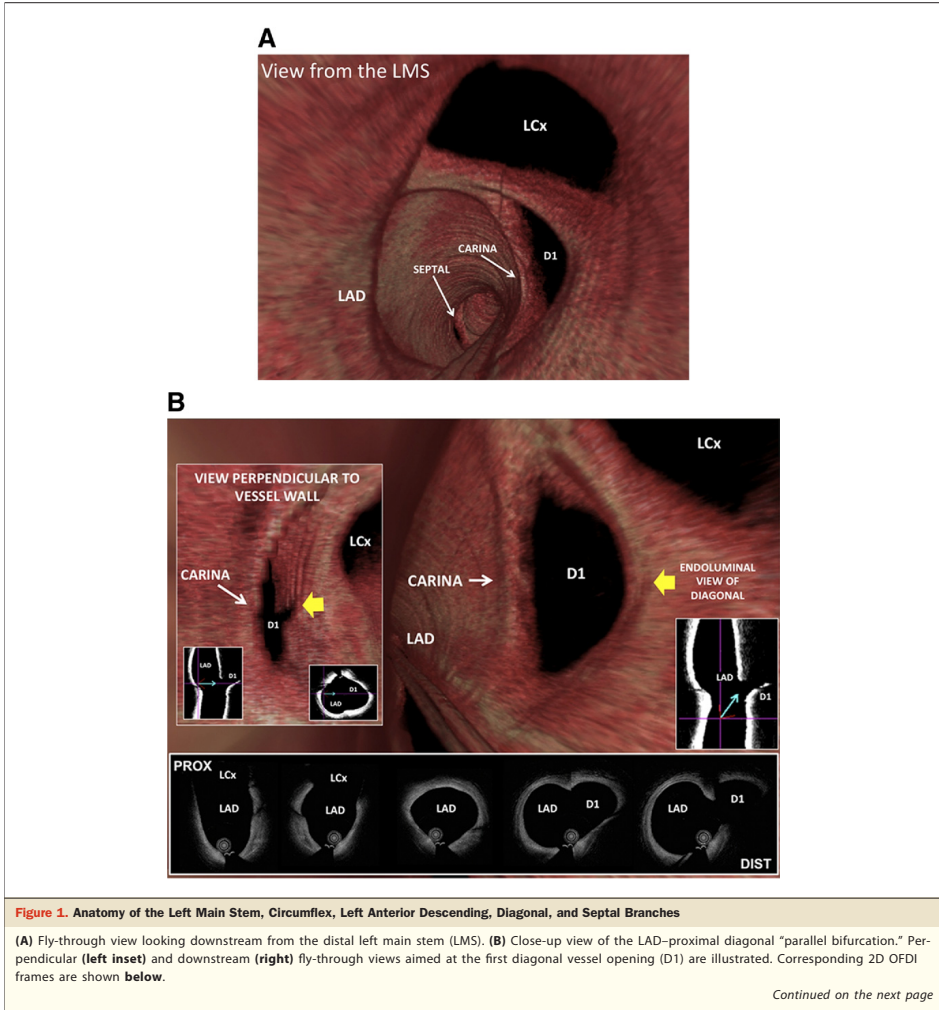
The right ventricular branch of the right coronary artery. Figure 4 demonstrates how the right ventricular (RV) branch of the right coronary artery (RCA) appears to exhibit the phenomenon of a “parallel bifurcation” as described for the diagonal vessel. The downstream fly-through view of the proximal RCA demonstrates the opening of the RV branch (upper left image); note how

the opening of the RV branch (yellow arrows) appears to be concealed behind the proximal rim of the carina in the perpendicular (upper middle image) and retrograde (upper right image) endoluminal point of views. In support of this concept is that the bifurcation angle is 57° on the corresponding 2D and 3D coronary angiograms (lower left images). Corresponding 2D OFDI frames are displayed (lower right images).

Bifurcation treated with provisional-T approach: comparing the diagonal and septal branches on 2D and 3D FD-OCT. Figure 5A demonstrates a long segment of disease in the proximal–mid LAD (upper left image) extending across the bifurcation with a diagonal branch. This was treated with 2 overlapping Xience V stents (Abbott Vascular, Abbott Park, Illinois) that lead to “pinching” of the SideB ostium with Thrombolysis In Myocardial Infarction flow grade 3 (middle left image with corresponding 3D coronary angiogram). Kissing balloon post-dilation (KBPD) was subsequently successfully performed with improvements in the pinched angiographic appearances (lower left image with corresponding 3D coronary angiograms) (Online Video 1). In the fly-through view (looking downstream) of the LAD post-intervention (right image), note the characteristic perpendicular and parallel takeoffs of the septal (asterisk) and diagonal (white arrow) branches at the point of divergence from the LAD lumen, respectively.

Figure 5B demonstrates fly-through views looking downstream at the diagonal and septal branches; note the differences between both branches as a more perpendicular view of the vessel wall is seen. Parallel yellow arrows represent the parallel courses of the diagonal and LAD vessels at their point of divergence. Medina et al. (6) have previously hypothesized the concept of carina shift pinching the SideB by the displacement of the carina so that it appears as an “eye-brow” sign on longitudinal 2D IVUS imaging (17). As shown on the 3D reconstruction, this effect can be more easily appreciated and may be hypothesized to have led to the near closure of the diagonal ostium following post-dilation of the MainB stent; subsequent KBPD may have reopened the SideB ostium by displacing the carina towards the lumen of the MainB. This principle may not be applicable to the septal branch because of the differing appearances of the carina.

Figure 5C demonstrates the corresponding 2D OFDI frames of the septal (asterisks) and diagonal branches (arrows). The almost parallel course of the diagonal vessel (yellow arrow indicates the diagonal vessel in cross-sectional view) in relation to the LAD lumen at the point of divergence appears to determine the 2D FD-OCT characteristics; without careful observation, the diagonal vessel may have been misinterpreted as an area of stent malapposition on the 2D FD-OCT imaging. With the septal branch, this appears to originate perpendicular to the vessel

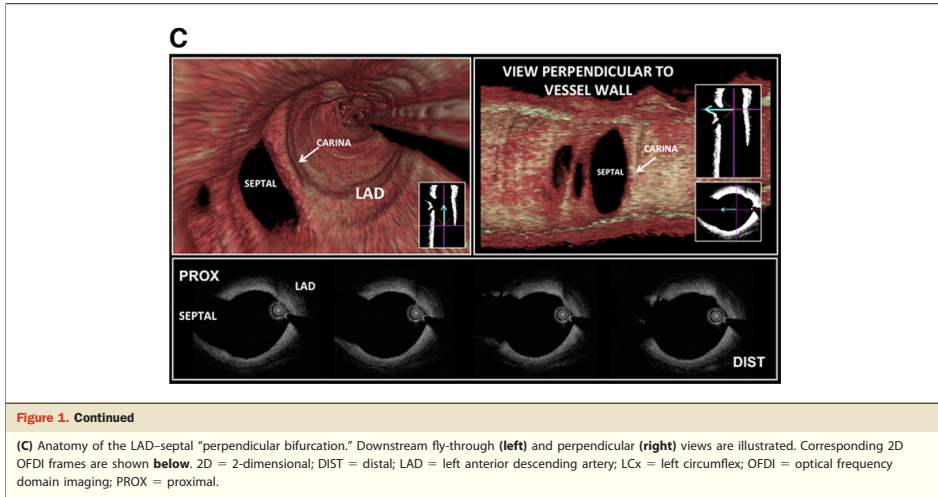


wall giving its characteristic 2D FD-OCT appearances as shown (yellow asterisk).

Bifurcation treated with provisional-T approach: the concept of a parallel bifurcation and carina shift. Figure 6A demonstrates the concept of carina shift with pre- and post-intervention images: the solid line indicates the position of the carina pre-intervention (left image); broken lines demonstrate the position of the carina pre- (left image) and post- (right

image) intervention. Two-dimensional (Online Video 2) and 3D coronary angiograms (inset images) demonstrate disease of the LAD with involvement of the diagonal ostium not evident on subsequent 3D reconstruction.

Implantation of a Xience V stent (Abbott Vascular) in the mid LAD led to angiographic “pinching” of the SideB ostium with Thrombolysis In Myocardial Infarction flow grade 3 maintained in the SideB. Post-dilation of the



MainB alone was performed with the deploying stent balloon; no KBPD was performed. The angiographic appearance of the pinching of SideB ostium improved (Online Video 2).

Figure 6B (upper images) demonstrates the appearance of the SideB opening when viewed perpendicular to the vessel wall (Image 3), illustrating the principle of a “parallel bifurcation” with the concealment of most of the opening of the diagonal vessel by the rim of the carina. It may be speculated that continued post-dilation of the MainB stent alone, especially with larger balloons, may have risked further carina shift and SideB closure.

Note how the MainB struts appear to overhang the carina over the SideB opening, especially evident in the perpendicular view (Image 3), because of the structure of the parallel bifurcation and carina. For comparison, the 2D OFDI frames (lower images) with the stent struts at the SideB ostium are illustrated. Asterisk indicates thrombus and the shadow it casts on the vessel wall, in both the 2D and 3D FD-OCT imaging.

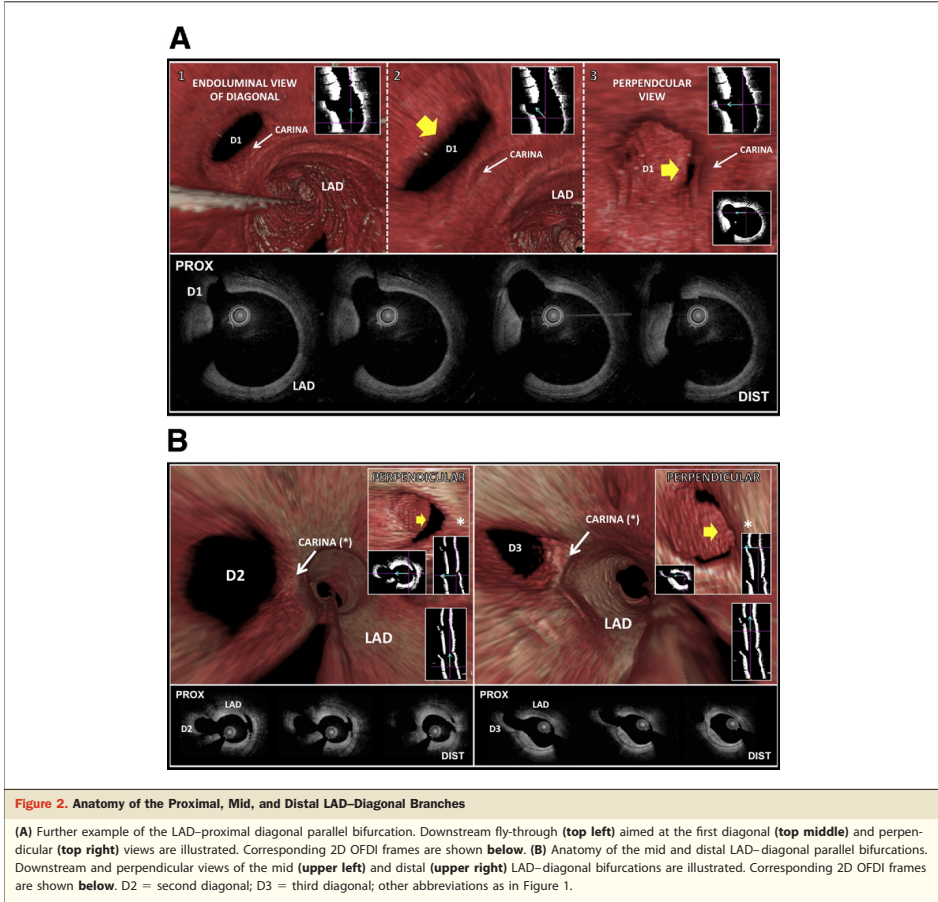
Discussion

On the basis of the offline 3D OFDI reconstructions, we have proposed several hypothesis-generating concepts relating to bifurcation anatomy and the effects of PCI: 1) the concept of the parallel or perpendicular bifurcations and the corresponding 2D and 3D appearances—a reassessment of current interpretations of the 2D FD-OCT imaging of the bifurcation may be warranted; 2) the hypothesis that the angle of divergence between the MainB and SideB at

their respective origins will ultimately determine the anatomic features of the carina and how it potentially interacts with the SideB vessel orifice during MainB stenting; and 3) the potential clinical application of instantaneous 3D FD-OCT in coronary bifurcation treatment.

Based on the appearances of the carina on the 3D reconstructions and the effects of PCI, a more perpendicular takeoff of the SideB from the MainB may be less prone to the effects of carina shift whereas a shallower angle of divergence appears to be more susceptible to the effects of carina shift. This concept is supported by a study suggesting a specific measure of SideB angulation on the coronary angiogram is associated with a higher incidence of SideB compromise (18). Asakura et al. (19) also demonstrated, in a small case series, that a shallower angle, with a cutoff of 80°, between the LCx and LAD was predictive of LCx ostial impairment after stenting within the LAD ostial region—the authors had presumed at the time that the mechanism of SideB (LCx) closure was secondary to plaque shift or coronary dissection. Both of the aforementioned studies are, however, limited by a lack of 3D quantitative coronary angiography to calculate the bifurcation angulation (16). An awareness of the potential increased risk of SideB closure during MainB stenting of coronary bifurcations with a shallower bifurcation angle may be justified—further study into this phenomenon is required.

Angiographic appearances of the SideB ostium after MainB stenting has previously been demonstrated to be unreliable, with only a quarter (27%) of cases with a residual



angiographic narrowing of $\geq 75\%$ in the SideB being found to have a functionally significant narrowing in pressure wire studies (1,8). The main limitation of this technique is the potential risk of dissecting the SideB ostium with a less flexible, less torquable, and less hydrophilic pressure wire and the increase in procedural time in rewiring the SideB through the MainB stent. As the 3D FD-OCT reconstructions can visualize the carina shift and the SideB vessel opening, quantification of the SideB opening as an area may allow the operator to assess whether the SideB ostium is hemodynamically compromised, without the need to perform a pressure wire study. The addition of quantitative measurements to the 3D software as well as the requirement

for instantaneous online 3D FD-OCT availability of a high-enough resolution would, however, be necessary requirements.

Within the parallel bifurcation, the positioning and geometric relationship of the MainB stent over the SideB opening suggested “overhanging” of the struts over the edge of the carina (Fig. 7); this was especially evident in the views perpendicular to the vessel wall (Figs. 5B and 6B) and contrary to the appearances on the corresponding 2D images where a “jailed” appearance of the stent struts covering the SideB opening was suggested; the jailed appearance of the struts covering the SideB ostium was, however, evident with perpendicular bifurcations (Figs. 3 and 5).

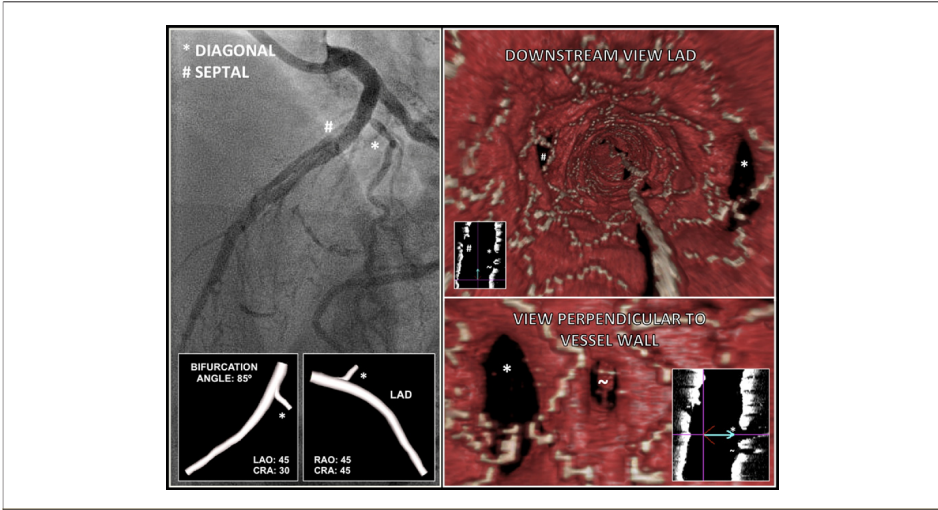


Figure 3. Anatomy of Diagonal Branch Originating Perpendicular to the LAD: Perpendicular Bifurcation

Two-dimensional and 3-dimensional (3D) coronary angiograms (left) and 3D reconstructions (right) are illustrated. An asterisk indicates the endoluminal opening of diagonal branch, a tilde, small diagonal branch, and a hash mark, septal branch. CRA = cranial; LAO = left anterior oblique; RAO = right anterior oblique.

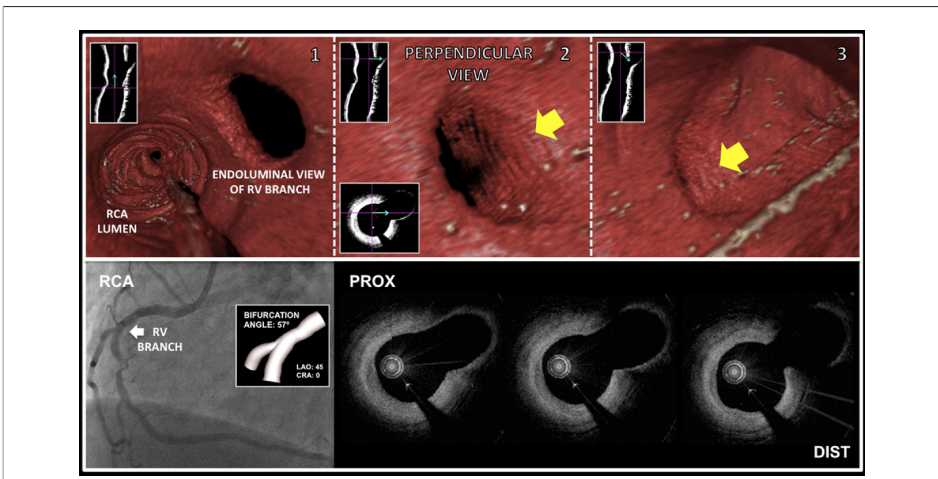
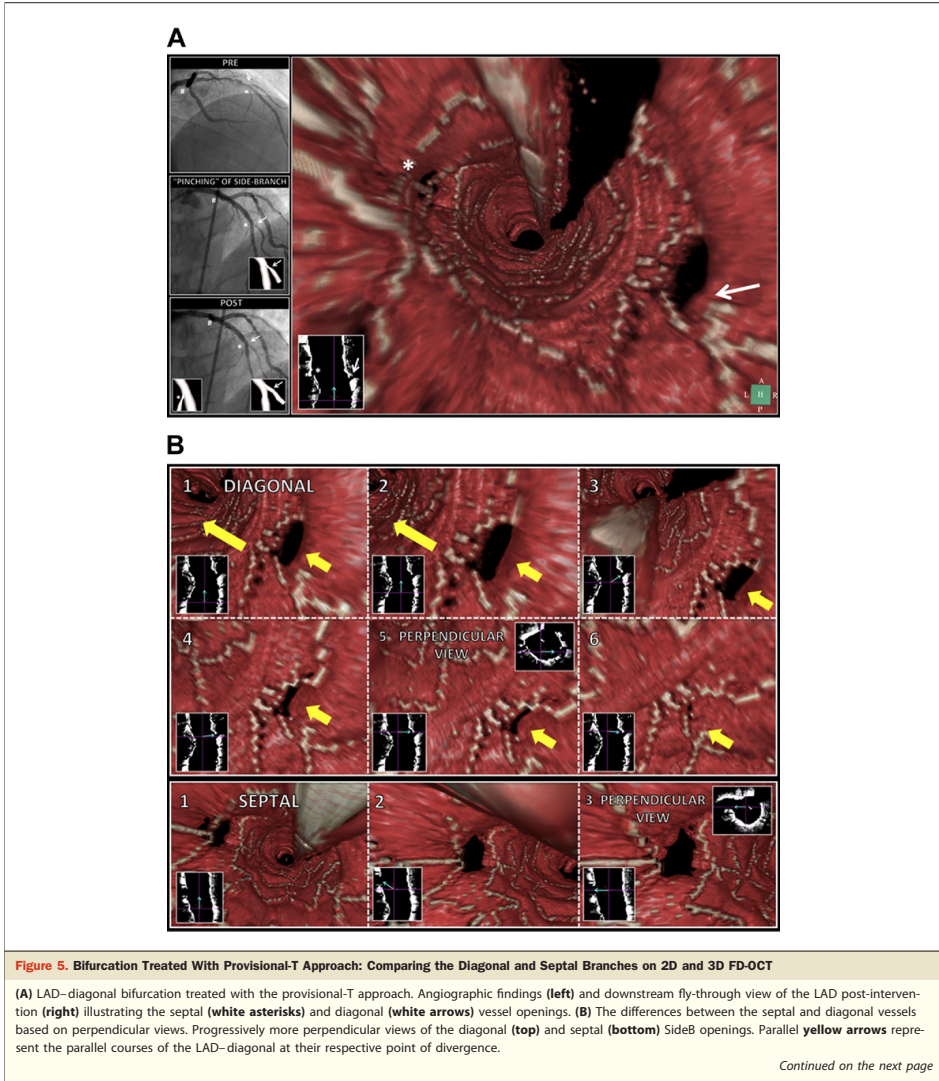


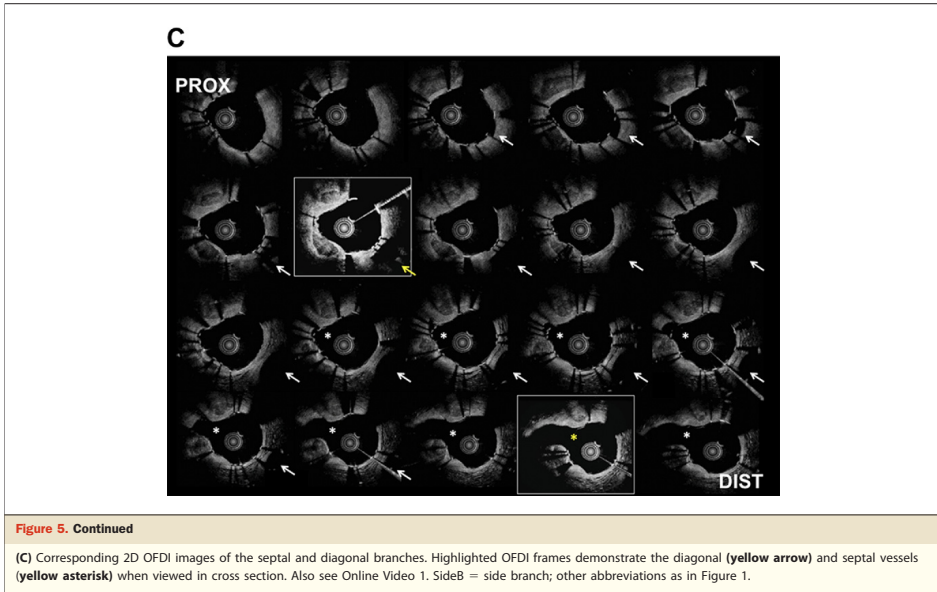
Figure 4. Anatomy of the RCA RV Branch Demonstrating a Parallel Bifurcation

Three-dimensional (3D) reconstructions (top) with the perpendicular view. Two-dimensional (2D) and 3D quantitative coronary angiography (bottom left) and corresponding 2D OFDI frames (bottom right). RCA = right coronary artery; RV = right ventricular; other abbreviations as in Figures 1 and 3.



Current recommendations during provisional T-stenting suggest the recrossing of the coronary wire (after MainB stenting) into the SideB through the most distal cell of the MainB stent covering the SideB opening (11,20,21). If the coronary wire is passed through a proximal cell into the SideB,

this may potentially provide no scaffolding to the SideB ostium and leave many struts unopposed adjacent to the carina. The adoption of this principle to bifurcations with 3D FD-OCT has recently been shown to be potentially feasible in humans (11,22). To help further appreciate this potential appli-



cation, a 3D OFDI reconstruction was performed in a patient separate from this study, utilizing the OFDI system from an ongoing trial (23): the case is of a proximal LCx-obtuse marginal bifurcation in the context of an acute coronary syndrome requiring manual aspiration thrombectomy; malapposition was evident immediately after MainB stent implantation requiring further post-dilation (not illustrated) (Fig. 7).

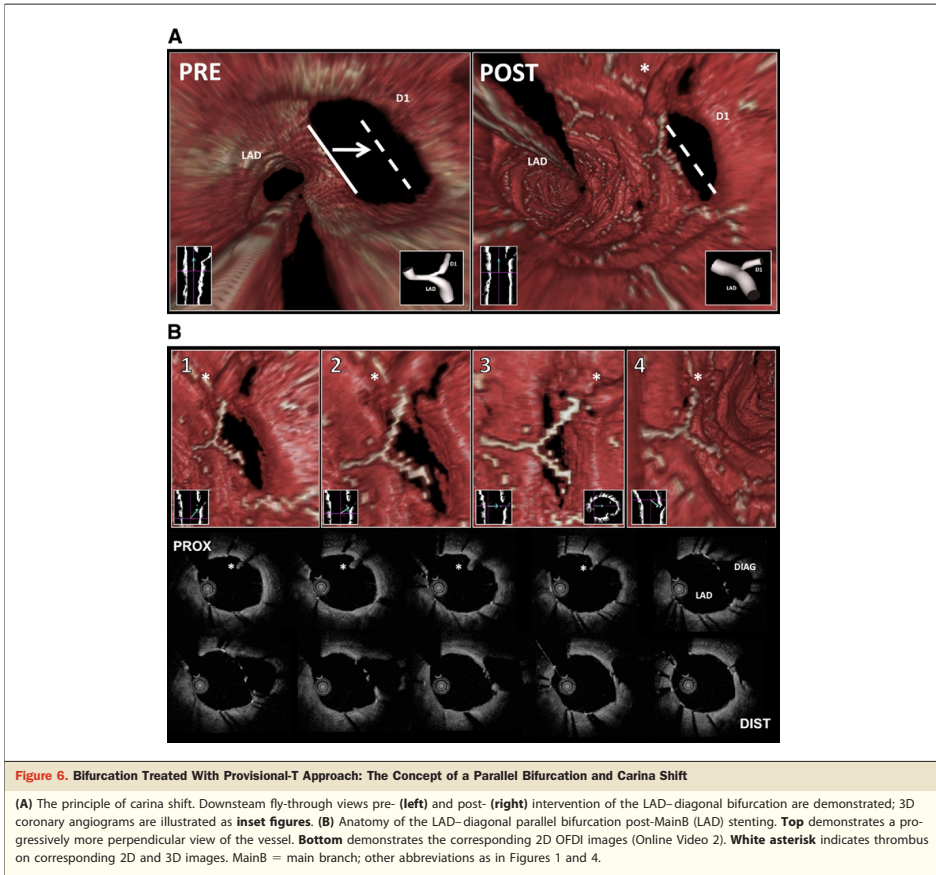
Based on the 3D reconstructions, the malapposed struts located in close vicinity to the proximal ostial rim (i.e., in the “takeoff” position) are overprojected on the true orifice of the SideB, giving the illusion that the SideB orifice is jailed when the orifice is viewed obliquely (Fig. 7A); this, however, appears to be the ideal endoluminal point of view to best select the distal cells of the stent over the parallel bifurcation to pass the coronary wire and perform KBPD (white arrow, Fig. 7A). When moving further downstream along the axis of the MainB, the optical visual perspective of overprojection on the orifice of the SideB is gradually reduced (Fig. 7B) and eliminated when a downstream endoluminal point of view at the level of the carina is selected (Fig. 7C). The struts located in front of the edge of the carina are now seen prominently as a metallic extension of the carina and not covering the SideB opening. The potential to advance a coronary wire beneath the malapposed struts in the proximal vicinity of the ostial rim appears to be very real, and if SideB dilation or stenting were

performed, would result in multiple unapposed struts taking off from the carina.

Other properties of 3D FD-OCT reconstructions that may have a clinical application include the addition of tissue characterization; this has previously been performed offline (13,24,25). Tissue characterization within 3D FD-OCT imaging (25) or fusion imaging of 2D FD-OCT and IVUS virtual histology (26) would have the potential to aid in the identification of clinically useful areas of interest such as fibrocalcific plaque, lipid pools, and vulnerable plaque. A recent study utilizing longitudinal high-resolution intravascular ultrasound has suggested that the effects of carina shift may be limited by the presence of fibro-calcific plaque at the carina, presumably because of resistance to expansion—using 3D FD-OCT, this concept appears easier to appreciate; tissue characterization of intravascular imaging may ultimately aid in identifying these areas (2,17).

Conclusions

The potential for the clinical application of 3D FD-OCT as a complementary tool to 2D imaging is demonstrated. A reassessment of the understanding of 2D FD-OCT imaging may be warranted in light of the 3D findings. Real-time, instantaneous, high-resolution 3D FD-OCT, with the



addition of quantitative and possible tissue characterization properties, are required from industry to validate and apply this technology in conventional PCI practice. This may aid in the further understanding of the complexities of the coronary bifurcation.

Acknowledgments

The first author wishes to thank the Dickinson Trust Travelling Scholarship, Manchester Royal Infirmary, Manchester, England, UK. The authors wish to express their thanks to Evelyn Regar, MD, PhD, Carl Schultz, MD, PhD, Willem J. van der Giessen, MD, PhD, and Jurgen Ligthart, BSc, of the ThoraxCenter, Erasmus University Medical Centre, Rotterdam, the Netherlands, part of the

team who undertook the original first-in-man study of the intracoronary Terumo optical frequency domain imaging (OFDI) system. The authors also thank Dr. Dragica Paunovic and Dr. Vladimir Borovicin of Terumo Corporation and Terumo Europe N.V., and Glenda van Bochove, Ravindra Pawar, and Monique Schuijjer of Cardialysis BV, Rotterdam, the Netherlands, for their invaluable technical support.

Reprint requests and correspondence: Dr. Patrick W. Serruys, Interventional Cardiology Department, ThoraxCenter, Erasmus University Medical Centre, s-Gravendijkwal 230, 3015 CE Rotterdam, the Netherlands. E-mail: p.w.j.c.serruys@erasmusmc.nl

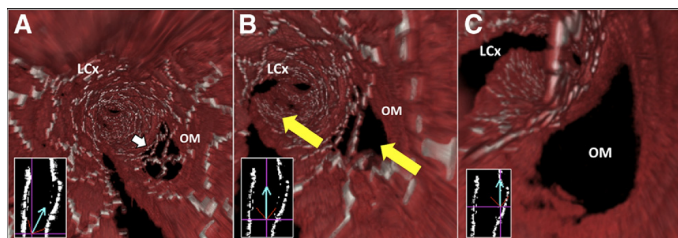


Figure 7. Provisional T-Stenting: The Principle of Recrossing the Coronary Wire (After MainB Stenting) Into the SideB Through the Most Distal Cell

Progressive downstream fly-through views culminating in the endoluminal point of view being located at the carina (A to C). White arrow indicates the most distal cell where the coronary wire would be recommended to be passed; yellow arrows indicates the parallel courses of the left circumflex coronary artery (LCx) and obtuse marginal (OM) vessels at their point of divergence. Abbreviations as in Figures 5 and 6.

REFERENCES

- Colombo A, Al-Lamee R. Bifurcation lesions: an inside view. *Circ Cardiovasc Interv* 2010;3:94–6.
- Hildick-Smith D, Lassen JF, Albiero R, et al. Consensus from the 5th European Bifurcation Club meeting. *EuroIntervention* 2010;6:34–8.
- Hildick-Smith D, de Belder AJ, Cooter N, et al. Randomized trial of simple versus complex drug-eluting stenting for bifurcation lesions: the British Bifurcation Coronary Study: old, new, and evolving strategies. *Circulation* 2010;121:1235–43.
- van der Giessen AG, Wentzel JJ, Meijboom WB, et al. Plaque and shear stress distribution in human coronary bifurcations: a multislice computed tomography study. *EuroIntervention* 2009;4:654–61.
- Vassilev D, Gil R, Kwan T, Nguyen T, Nanjundappa A, Doganov A. Extension distance mismatch—an unrecognized factor for suboptimal side branch ostial coverage in bifurcation lesion stenting. *J Interv Cardiol* 2010;23:305–18.
- Medina A, Martín P, Suárez de Lezo J, et al. Vulnerable carina anatomy and ostial lesions in the left anterior descending coronary artery after floating-stent treatment. *Rev Esp Cardiol* 2009;62:1240–9.
- Koo BK, Waseda K, Kang HJ, et al. Anatomic and functional evaluation of bifurcation lesions undergoing percutaneous coronary intervention. *Circ Cardiovasc Interventions* 2010;3:113–9.
- Koo BK, Kang HJ, Youn TJ, et al. Physiologic assessment of jailed side branch lesions using fractional flow reserve. *J Am Coll Cardiol* 2005;46:633–7.
- van der Giessen AG, Schaap M, Gijzen FJ, et al. 3D fusion of intravascular ultrasound and coronary computed tomography for in-vivo wall shear stress analysis: a feasibility study. *Int J Cardiovasc Imaging* 2010;26:781–96.
- Bezerra HG, Costa MA, Guagliumi G, Rollins AM, Simon DI. Intracoronary optical coherence tomography: a comprehensive review clinical and research applications. *J Am Coll Cardiol Intv* 2009;2:1035–46.
- Di Mario CII, van der Giessen WJ, Foin N, et al. Optical coherence tomography for guidance in bifurcation lesion treatment. *EuroIntervention* 2011;6 Suppl J:99–106.
- Gonzalo N, García-García HM, Regar E, et al. In vivo assessment of high-risk coronary plaques at bifurcations with combined intravascular ultrasound and optical coherence tomography. *J Am Coll Cardiol Img* 2009;2:473–82.
- Tearney GJ, Waxman S, Shishkov M, et al. Three-dimensional coronary artery microscopy by intracoronary optical frequency domain imaging. *J Am Coll Cardiol Img* 2008;1:752–61.
- Okamura T, Onuma Y, García-García HM, et al. 3-Dimensional optical coherence tomography assessment of jailed side branches by bioresorbable vascular scaffolds: a proposal for classification. *J Am Coll Cardiol Intv* 2010;3:836–44.
- Okamura T, Onuma Y, García-García HM, et al. First-in-man evaluation of intravascular optical frequency domain imaging (OFDI) of Terumo: a comparison with intravascular ultrasound and quantitative coronary angiography. *EuroIntervention* 2011;6:1037–45.
- Onuma Y, Girasis C, Aben JP, et al. A novel dedicated 3-dimensional quantitative coronary analysis methodology for bifurcation lesions. *EuroIntervention* 2011 Jan 6 [E-pub ahead of print].
- Medina A, Pan M, Martín P, Suárez de Lezo J. Kissing in simple strategy. I prefer SMS. Paper presented at: 6th European Bifurcation Club; October 22–23, 2010; Budapest, Hungary. Available at: <http://www.bifurc.net>. Accessed March 1, 2011.
- Gil RJ, Vassilev D, Formuszewicz R, Rusicka-Pielkarz T, Doganov A. The carina angle—new geometrical parameter associated with periprocedural side branch compromise and the long-term results in coronary bifurcation lesions with main vessel stenting only. *J Interv Cardiol* 2009;22:E1–10.
- Asakura Y, Takagi S, Ishikawa S, et al. Favorable strategy for the ostial lesion of the left anterior descending coronary artery: influence on narrowing of circumflex coronary artery. *Cathet Cardiovasc Diagn* 1998;43:95–100.
- Stankovic G, Darremont O, Ferenc M, et al. Percutaneous coronary intervention for bifurcation lesions: 2008 consensus document from the fourth meeting of the European Bifurcation Club. *EuroIntervention* 2009;5:39–49.
- Ormiston JA, Webster MW, El Jack S, et al. Drug-eluting stents for coronary bifurcations: bench testing of provisional side-branch strategies. *Catheter Cardiovasc Interv* 2006;67:49–55.
- van Geuns RJ, Gogas BD, Farooq V, Regar E, Serruys PW. 3-Dimensional reconstruction of a bifurcation lesion with double wire after implantation of a second generation everolimus-eluting bioresorbable vascular scaffold. *Int J Cardiol* 2011 Mar 8. [E-pub ahead of print].
- Serruys PW, Marco J. Primary PCI: step-by-step decision process. New optical imaging techniques to guide treatment Presented at: EuroPCR 2011; May 18, 2011; Paris, France.
- Gonzalo N, Tearney GJ, van Soest G, et al. Witnessed coronary plaque rupture during cardiac catheterization. *J Am Coll Cardiol Img* 2011;4:437–8.
- Waxman S, Freilich MI, Suter MJ, et al. A case of lipid core plaque progression and rupture at the edge of a coronary stent elucidating the mechanisms of drug-eluting stent failure. *Circ Cardiovasc Interv* 2010;3:193–6.
- Diletti R, García-García HM, Gomez-Lara J, et al. Assessment of Coronary Atherosclerosis Progression and Regression at Bifurcations Using Combined IVUS and OCT. *J Am Coll Cardiol Img* 2011;4:774–80.

Key Words: 3-dimensional ■ bifurcation ■ carina shift ■ FD-OCT.

APPENDIX

For supplementary videos, please see the online version of this article.

Chapter 18

Three-Dimensional Reconstruction of the Post-Dilated ABSORB Everolimus-Eluting Bioresorbable Vascular Scaffold in a True Bifurcation Lesion for Flow Restoration.

Bill D. Gogas, Robert Jan van Geuns, Vasim Farooq, Evelyn Regar, Jung Ho-Heo, Jurgen Ligthart, Patrick W. Serruys

JACC Cardiovascular Interventions. 2011. Oct; 4(10):1149-50 [IF: 6.83]

Three-Dimensional Reconstruction of the Post-Dilated ABSORB Everolimus-Eluting Bioresorbable Vascular Scaffold in a True Bifurcation Lesion for Flow Restoration

Bill D. Gogas, MD, Robert J. van Geuns, MD, PhD, Vasim Farooq, MBChB, Evelyn Regar, MD, PhD, Jung Ho Heo, MD, Jurgen Ligthart, BSc, Patrick W. Serruys, MD, PhD

Rotterdam, the Netherlands

A 68-year-old male patient presented to our catheterization laboratory with a non-ST-segment elevation myocardial infarction. Coronary angiography suggested a significant true bifurcation lesion in the mid left anterior descending (LAD) artery, appearing to involve the second diagonal side branch (SideB), measuring 1.7 mm in maximal diameter (Medina classification: 1, 1, 1). Both the main branch (MainB) lesion and the SideB were crossed with 0.014-inch Hi-Torque Pilot guide-wires (Abbott Vascular, Santa Clara, California) (Fig. 1A). Pre-dilation of the lesion was undertaken with a Trek-compliant balloon (Abbott Vascular) and implantation of a single 3.0×18 -mm ABSORB bioresorbable vascular scaffold (BVS) (Abbott Vascular) in the LAD across the second diagonal vessel opening was undertaken with nominal inflation pressures. After scaffold implantation, Thrombolysis In Myocardial Infarction (TIMI) flow grade 3 was maintained in the LAD; however, TIMI flow grade 1 immediately became evident at the second diagonal branch with angiographic evidence of pinching of the ostium (Fig. 1C). The patient developed chest pain with mild ST-segment elevation on the chest electrocardiogram. A 1.5×12 mm Trek-compliant balloon was subsequently used to cross the cells of the ABSORB BVS toward the SideB (Fig. 1H) and

post-dilation of the second diagonal branch was undertaken. This led to immediate restoration of TIMI flow grade 3 without significant myocardial damage (Fig. 1E). The following 30-day outcome was uneventful.

Conventional percutaneous coronary intervention for bifurcation lesions, compared with the rest of the lesion types, is associated with greater event rates. Plaque shift (the so-called snow-plough effect) or the carina shift phenomena are the major contributors for the acute events during bifurcation stenting (1). van Geuns et al. (2) recently described the feasibility of crossing the polymeric struts of a fully ABSORB BVS with double wire in a bifurcation lesion.

Offline 3-dimensional reconstructions of the MainB and the SideB constructed using 2-dimensional (2D) frequency domain (FD) optical coherence tomography (OCT) images are a novel approach to visualizing these lesions. The possibility of on-line use of such imaging modalities for bifurcation lesions or other lesion types may help improve our treatment strategies.

Acknowledgment

Dr. Gogas wishes to acknowledge the continued funding support of the Hellenic Heart Foundation and the Hellenic Cardiological Society, Athens, Greece.

From the Thoraxcenter, Erasmus University Medical Centre, Rotterdam, the Netherlands. Jurgen Ligthart has a proctor contract with Boston Scientific; and is a trainer for Volcano Corp. and St. Jude Medical. All other authors have reported that they have no relationships relevant to the contents of this paper to disclose. Drs. Gogas, van Geuns, and Farooq contributed equally to this manuscript.

Manuscript received March 30, 2011; revised manuscript received April 18, 2011, accepted May 3, 2011.

Reprint requests and correspondence: Dr. Robert J. van Geuns, Cardiologist, Erasmus Medical Center, Thoraxcenter, P.O. Box 2040, 3000 CA, Rotterdam, s Gravendijkwal 230, 3015 CE Rotterdam, Room Ba-585. E-mail: r.vangeuns@erasmusmc.nl

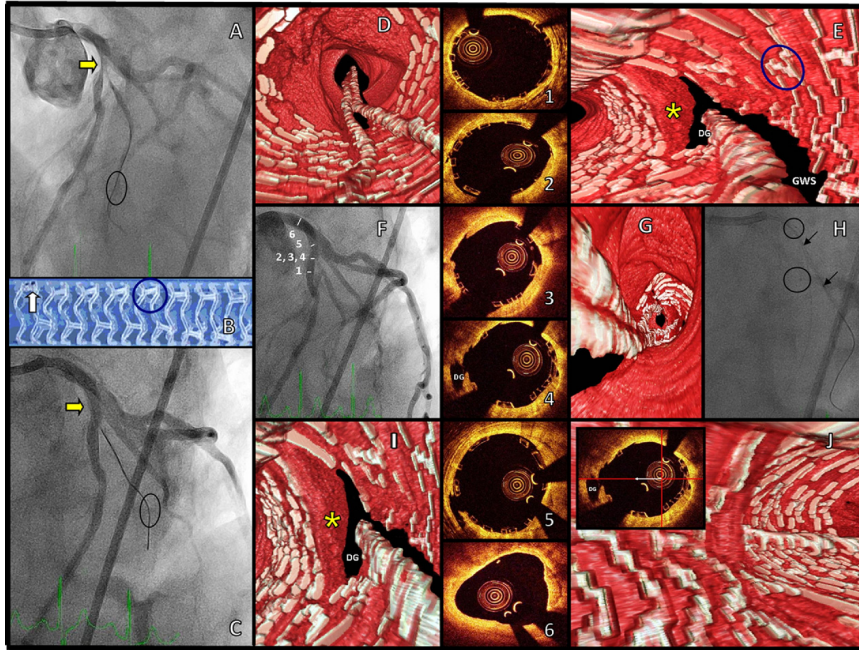


Figure 1. Multimodality Imaging of a True Bifurcation Lesion With 2D Coronary Angiography, 2D FD-OCT, and 3D OCT

(A) Coronary angiogram demonstrating the bifurcation lesion (**yellow arrow**) with guidewires in the main branch (MainB) and the side branch (SideB) (**ellipsoid black circle**). (B) The ABSORB bioresorbable vascular scaffold (BVS) has polymeric struts with a thickness of 160 μm and consists of in-phase zigzag hoops linked by 3 longitudinal bridges (**blue circle**). Two platinum markers are placed at both proximal and distal edges of the device (**white arrow**). (C) Coronary angiogram post-implantation of the ABSORB BVS demonstrating the acute occlusion of the SideB (**ellipsoid black circle**). (D) Virtual fly-through view (distal to proximal). Three-dimensional (3D) reconstruction of the left anterior descending (LAD) artery and the ABSORB BVS with both guidewires; note the well-apposed polymeric struts of the device. (E and I) Reconstructions of the flow divider. The carina of the bifurcation is demonstrated with the **yellow asterisk**, and the ostium of the SideB is demonstrated with diagonal side branch (DG). The **blue circle** demonstrates the longitudinal bridges that link the in-phase zigzag hoops of the implanted device. Note the well-apposed polymeric struts of the BVS at the edges of the carina following balloon dilation. (F) Final angiographic result. The numbered lines correspond to the 2-dimensional (2D) frequency domain optical coherence tomography (FD-OCT) still frames. (G) View from the ostial LAD. Virtual fly-through view (proximal to distal) of the LAD with both guidewires. (H) Coronary angiogram demonstrating: 1) the platinum markers of the BVS (**black circles**); 2) the markers of the balloon used to post-dilate the occluded SideB (**black arrows**). (J) Perpendicular view at the level of the bifurcation after implantation of the device (confirmed by the direction of the **white arrow** as shown with the 2D FD-OCT still frame). Please note the layered appearance of the LAD. (Center panels 1 to 6) The numbers of the cross-sections correspond to the lines shown in F (distal to proximal view). (1) The distal scaffolded segment of the LAD. Note the well-apposed polymeric struts of the ABSORB BVS. (2 and 3) Well-apposed polymeric struts at the edges of the SideB with no evidence of overhanging or malapposed struts. (4) The diagonal vessel opening (DG) is illustrated. (5) The proximal scaffolded segment of the LAD. Note the small dissection covered with the polymeric struts shown at 8 o'clock (2D FD-OCT, cross-section 5). (6) The ostial part of the LAD.

REFERENCES

1. Koo BK, Waseda K, Kang HJ, et al. Anatomic and functional evaluation of bifurcation lesions undergoing percutaneous coronary intervention. *Circ Cardiovasc Interv* 2010;3:113-9.

2. van Geuns RJ, Gogas BD, Farooq V, Regar E, Serruys PW. 3-dimensional reconstruction of a bifurcation lesion with double wire after implantation of a second generation everolimus-eluting bioresorbable vascular scaffold. *Int J Cardiol* 2011 Mar 8 [E-pub ahead of print].

Chapter 19

Three-Dimensional Optical Frequency Domain Imaging in Conventional Percutaneous Coronary Intervention: The Potential for Clinical Application.

Vasim Farooq, **Bill D. Gogas**, Takayuki Okamura, Jung Ho-Heo, Michael Magro, Josep Gomez-Lara, Yoshinobu Onuma, Maria Radu, Salvatore Brugaletta, Glenda van Bochove, RJ vanGeuns, Hector M. García-García, Patrick W. Serruys
European Heart Journal. 2011. [Epub ahead of print] [IF: 14.1]

Three-dimensional optical frequency domain imaging in conventional percutaneous coronary intervention: the potential for clinical application

Vasim Farooq¹, Bill D. Gogas¹, Takayuki Okamura¹, Jung Ho Heo¹, Michael Magro¹, Josep Gomez-Lara¹, Yoshinobu Onuma¹, Maria D. Radu¹, Salvatore Brugaletta¹, Glenda van Bochove², Robert Jan van Geuns¹, Hector M. Garcia-Garcia², and Patrick W. Serruys^{1*}

¹Interventional Cardiology Department, ThoraxCenter, Erasmus University Medical Centre, s-Gravendijkwal 230, 3015 CE Rotterdam, The Netherlands; and ²Cardialysis BV, Rotterdam, The Netherlands

Received 25 June 2011; revised 16 August 2011; accepted 28 September 2011

Introduction

Two-dimensional (2D) frequency domain optical coherence tomography (FD-OCT) has enhanced our understanding of coronary atherosclerotic disease and is increasingly being used in conventional percutaneous coronary intervention (PCI) to elucidate mechanisms of disease and improve our understanding of complex coronary anatomy.

Since the first report of three-dimensional (3D) OCT applied in human coronary vessels,¹ the technology has rapidly progressed.^{2–10} Currently, the main limitation of this technology is the need for off-line creation of 3D reconstructions—prototypes of current generation 'real time' (i.e. available peri-procedurally at the 'push-of-a-button') remain experimental, work in progress, and are limited by relatively poor image quality/resolution.⁴ As of now, the potential clinical application of 3D FD-OCT remains undefined.

Recently, the application of this emerging technology to the coronary bifurcation has allowed visualization and assessment of jailed side branches (SideBs) at a level of detail not previously reported.^{2–7} The assessment of a jailed SideB, after implantation of a bioresorbable scaffold in the main branch (MainB) of a bifurcation, lead to the proposal of a new classification system based on the assessment of the number of compartments the SideB ostium was divided into, with examples of how this may potentially effect the neointimal response and subsequent coverage of the struts.²

More recently, the application of this technology to the coronary bifurcation in patients implanted with conventional metallic stents, utilizing the Terumo optical frequency domain imaging (OFDI) system, was described for the first time.³ Hypotheses related to types of coronary bifurcation ('parallel' and

'perpendicular' bifurcations) based on the bifurcation angle, and how this leads to certain specific characteristics of the carina, which potentially made the SideB more vulnerable to the effects of carina shift and potential SideB closure, were described. Furthermore, the potential practical application of 3D FD-OCT in guiding the rewiring of the distal compartment of the SideB ostium—jailed with stent struts after MainB stenting—to minimize the risk of floating struts was demonstrated, something not easily achievable with conventional 2D FD-OCT systems or other intravascular imaging modalities.^{3,4,6} The potential for jailed stent struts at the SideB ostium, to act as a focus for neointimal 'bridge' formation and focal restenosis warranting further intervention, has also recently been demonstrated with 3D FD-OCT⁷—this was not so apparent on the corresponding 2D images; the practical suggestion from these findings was that final kissing balloon post-dilatation should be performed to clear any jailed struts at the SideB ostium. In addition, the use of 3D FD-OCT in potentially guiding the management of acute myocardial infarction has been reported.¹¹ The identification of thrombus and stent malapposition to guide subsequent further aspiration thrombectomy, post-dilatation, and concomitant use of drugs was proposed.

Three-dimensional reconstructions of other intravascular coronary imaging modalities have previously been described; they have however failed to find a useful clinical role.^{12–18} One of the reasons that potentially makes 3D FD-OCT more clinically applicable is the unrivalled resolution of OCT technology (10–15 μm) compared with other intravascular imaging modalities—coronary angiography: 100–200 μm, computed tomography (CT): 300–500 μm, intravascular ultrasound (IVUS): 100–150 μm, coronary angioscopy: <200 μm¹⁹—and consequent ability to visualize intraluminal structures in unmatched detail. Conversely, with, for

* Corresponding author. Tel: +31 10 7035260, Fax: +31 10 4369154, Email: p.w.j.c.serruys@erasmusmc.nl

Published on behalf of the European Society of Cardiology. All rights reserved. © The Author 2011. For permissions please email: journals.permissions@oup.com

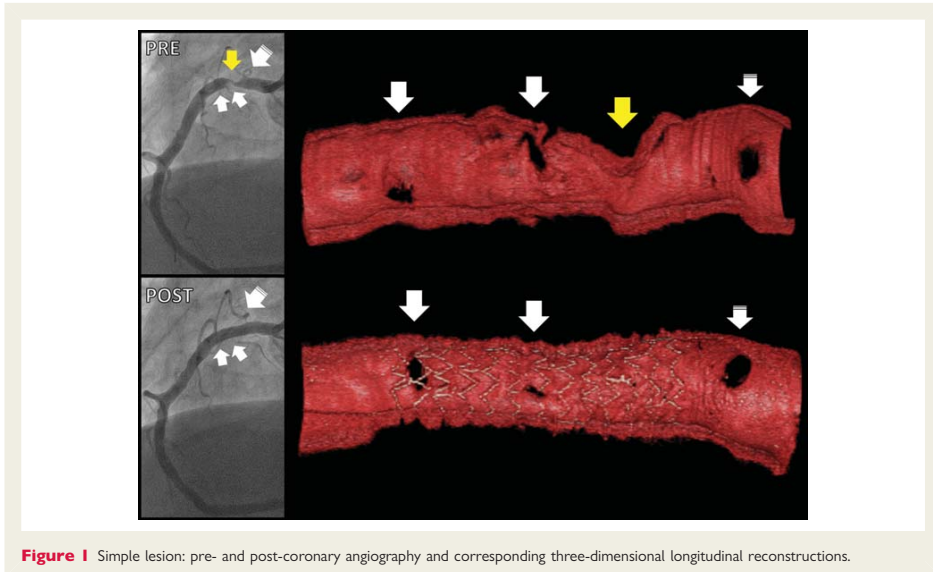


Figure 1 Simple lesion: pre- and post-coronary angiography and corresponding three-dimensional longitudinal reconstructions.

example, IVUS, this cannot reliably visualize intraluminal structures/detail such as thrombus or stent apposition; furthermore, post-processing of 2D IVUS images is required to allow 3D IVUS reconstructions, thus limiting its application in the catheterization laboratory.^{12,13} Despite the appeal of fusion of other intravascular imaging modalities, such as CT and IVUS,^{20,21} these are still limited by the resolution of the images compared with OCT.

Through a series of off-line 3D reconstructions performed with the Terumo OFDI system, in patients undergoing conventional PCI, followed by technical issues performed in a porcine model, the rapid progression of this emerging technology and the potential for clinical application are proposed. Opinion on the future development of 3D FD-OCT is also discussed.

Methodology for undertaking off-line three-dimensional frequency domain optical coherence tomography reconstructions

Three-dimensional frequency domain optical coherence tomography reconstructions of patients who underwent conventional PCI from the original First-In-Man study intracoronary Terumo OFDI system (Terumo Corporation, Tokyo, Japan),²² and of a single patient from a further ongoing study,²³ are presented. All 3D reconstructions were performed at baseline as per the study protocol. The high-speed Terumo OFDI system is capable of

acquiring 160 frames/s during the catheter pull-back, to a maximum speed of 40 mm/s; all images were acquired with a motorized pull-back of 20 mm/s. Comparatively, the current generation LightLab DragonFly C7 system (LightLab Imaging Inc., Westford, MA, USA) is capable of 100 frames/s. The higher frame rate of the Terumo OFDI system appears to be the primary reason why it is capable of producing superior 3D FD-OCT reconstructions compared with the current generation LightLab C7 system.^{3,22}

The methodology for off-line 3D reconstructions has previously been described.² In brief, manual detection of every strut in each cross-section, using bitmap sequences (704 × 704 pixels) generated from prior 2D OFDI frames, was performed and 3D reconstructions were generated utilizing volume-rendering software (INTAGE Realia, KGT, Tokyo, Japan).

Technical issues relating to image quality are also demonstrated in a porcine model.

Nomenclature for three-dimensional frequency domain optical coherence tomography reconstructions

'Fly-through' views indicate a selected still image of an internal view of a vessel looking either downstream (proximal to distal vessel) or upstream (distal to proximal vessel). The fly-through (internal) view of the vessel is akin to the view obtained during endoscopy or angiography showing the internal lumen of the vessel.

Longitudinal views are a cut-away view of the vessel down the longitudinal axis with the internal lumen viewed externally—

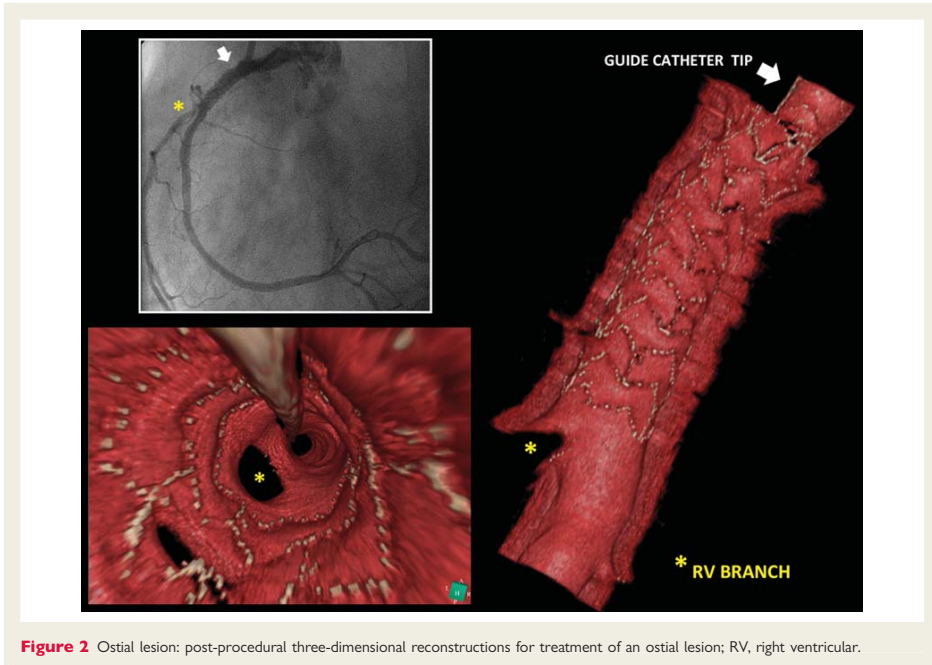


Figure 2 Ostial lesion: post-procedural three-dimensional reconstructions for treatment of an ostial lesion; RV, right ventricular.

wherever possible a view without the guide-wire shadow is shown. External views are taken from outside the vessel with views to show the internal vessel at the region of interest.

Three-dimensional reconstructions

Assessment of simple lesions

Proximal right coronary artery lesion

A severe proximal right coronary artery (RCA) lesion treated with a 3.0×18 mm Xience V drug-eluting stent (Figure 1) is demonstrated on coronary angiography (left images). Three-dimensional longitudinal reconstructions pre- and post-intervention are illustrated. The longitudinal 3D reconstructions represent the horizontal segment of the RCA before the first curvature—the use of the white arrows, identifying the jailed SideBs, will help the reader to co-register the 3D reconstruction with the coronary angiogram. Note the almost identical characteristics of the minimum lumen area on coronary angiography and 3D reconstruction (yellow arrows), indicative of the high resolution of OCT. Also present are one non-jailed SideB (striped white arrow) proximal to the implanted stent, and two jailed SideBs (white arrows) within the implanted stent, in both the coronary angiogram and 3D reconstruction.

Aorto-ostial right coronary artery lesion

A significant RCA aorto-ostial lesion (not illustrated) was directly stented with a 3×15 mm Xience V stent (Figure 2, upper left image). Post-procedural longitudinal (right image) and downstream fly-through (lower left image) 3D reconstructions are demonstrated. Note the jailed SideB in the downstream fly-through view (lower left image), and the guide catheter tip (white arrow), with some of the same render as the vessel, applied by the volume-rendering software. Yellow asterisks highlight the ostium of the right ventricular (RV) branch seen on coronary angiography and longitudinal and fly-through 3D reconstructions. From a technical perspective—one of the difficulties with imaging the aorto-ostial lesions is ensuring that the catheter tip is sufficiently disengaged from the coronary ostium to allow visualization with the OCT imaging wire during the pull-back, but close enough to allow injection of contrast for blood clearance—with inevitable over-spilling of contrast in the aortic cusps—and thus allow appropriate imaging.²⁴

Stent malapposition

Embedded, protruding, and malapposed struts

As the OCT light cannot penetrate metallic struts, OCT can only image the endoluminal strut border. Consequently, a 'shadow' is cast behind the metallic strut, and the adjustment for the thickness of the strut and polymer is therefore required to determine the apposition of the stent strut. Based on this phenomenon, stent

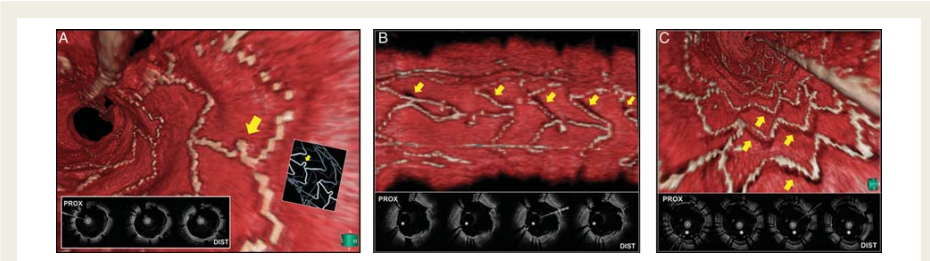


Figure 3 (A) Embedded struts (i.e. strut buried in the intima for more than half its thickness): three-dimensional reconstruction with corresponding two-dimensional optical frequency domain imaging frames—no shadow is visible on the vessel wall. Actual Xience V stent with an interductile hinge is illustrated for comparison (yellow arrows). (B) Protruding struts (i.e. strut in intimal contact): three-dimensional reconstruction—note the shadow on the vessel wall (yellow arrows) can erroneously give the impression of stent malapposition due to the thickness of the metallic strut and polymer, which the optical coherence tomography light cannot penetrate. Corresponding protruding struts on two-dimensional optical frequency domain imaging frames are marked with an asterisk. (C) Malapposed struts: three-dimensional reconstruction with corresponding two-dimensional optical frequency domain imaging frames—true stent malapposition is illustrated (yellow arrows) with corresponding protruding struts on two-dimensional optical frequency domain imaging frames are marked with an asterisk.

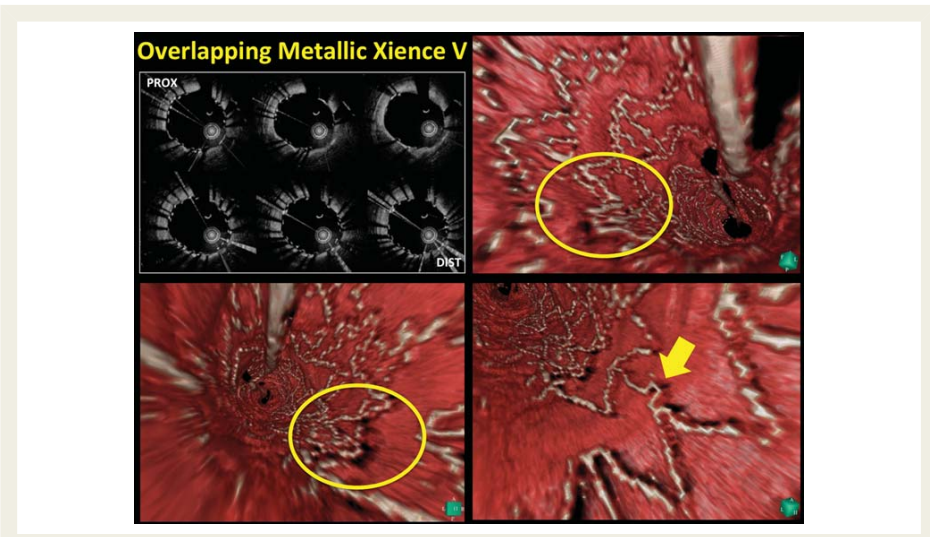


Figure 4 Overlapping Xience V stents: corresponding two-dimensional optical frequency domain imaging frames and downstream fly-through views are illustrated.

strut apposition by post-implantation OCT has been defined as embedded, protruding, or malapposed.²⁵ With an embedded strut, the strut is buried in the intima for more than half its thickness; consequently, the shadow the strut

casts is projected through the vessel wall, with no shadowing visible on the endoluminal vessel surface on post-implantation 2D and 3D FD-OCT imaging (Figure 3A). With a protruding strut, the stent strut is apposed to the intima but not embedded;

consequently, a shadow appears to be 'cast' on the vessel surface and wall (due to the thickness of the metallic strut and polymer which the OCT light cannot penetrate)—this represents a potential limitation of 3D FD-OCT, as the protruding struts erroneously gives the impression of strut malapposition, when it is in actual intimal contact (Figure 3B). With a malapposed strut, there is no intimal contact with the stent strut and vessel wall and appropriately leads to a shadow on the vessel surface and wall (Figure 3C).²⁵

Overlapping drug-eluting stents

Overlapping Xience V stents, used to treat a long segment of disease consisting of severe tandem lesions arising from the proximal first diagonal, are demonstrated (Figure 4). Downstream fly-through 3D reconstructions demonstrate embedded, protruding (yellow circles), and occasional malapposed struts (yellow arrow). Note the malapposed 'interductile hinge' and the shadow it casts on the vessel wall visible in the 3D reconstruction (Figure 4)—for comparison, an interductile hinge in an actual Xience V stent is illustrated in Figure 3A (yellow arrows). Corresponding 2D OFDI frames of the overlap are shown (top left image).

Thrombus and stent malapposition

Primary percutaneous coronary intervention: thrombus and consequent stent malapposition

Three-dimensional reconstructions are illustrated, post-implantation of a 3.0 × 24 Xience V drug-eluting stent with prior aspiration thrombectomy, following an inferior wall ST elevation myocardial infarction with occlusion of the mid-RCA. Downstream fly-through views (Figure 5A), post-stent implantation, demonstrate a large volume of thrombus (white arrows) and consequential stent malapposition at the proximal stent edges (yellow arrows)—note the shadow the malapposed struts cause on the proximal vessel wall (white arrows) and thrombus adhering to the stent strut at the coronary bifurcation. A longitudinal view of the same vessel (Figure 5B) demonstrates the extent of the thrombus (white arrows) and consequential stent malapposition at both stent edges (yellow arrows); also evident are over-hanging struts, with thrombus attached, at the bifurcation (upper white arrow). If the interventional cardiologist saw the 3D reconstruction after stent implantation, this is likely to have been crucial in the subsequent decision-making process in the use of further aspiration thrombectomy, post-dilatation, and concomitant use of drugs such as glycoprotein IIb/IIIa inhibitors. Further aspiration thrombectomy and post-dilatation of the stent were performed with angiographic resolution of the thrombus (not illustrated).

Coronary bifurcation

The promising potential clinical application of coronary bifurcations with 3D FD-OCT has recently been described by our group^{2,3} and is beyond the scope of this paper. Examples of 3D FD-OCT in the coronary bifurcation to demonstrate its potential clinical application are illustrated below.

Right ventricular branch of the right coronary artery

Close-up views of the RV branch of the RCA (Figure 6) from the previous study (Figure 5A and B) demonstrate the thrombus

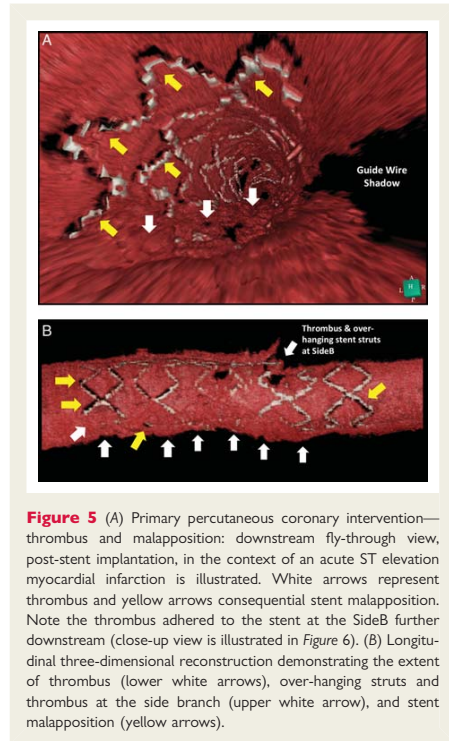


Figure 5 (A) Primary percutaneous coronary intervention—thrombus and malapposition: downstream fly-through view, post-stent implantation, in the context of an acute ST elevation myocardial infarction is illustrated. White arrows represent thrombus and yellow arrows consequential stent malapposition. Note the thrombus adhered to the stent at the SideB further downstream (close-up view is illustrated in Figure 6). (B) Longitudinal three-dimensional reconstruction demonstrating the extent of thrombus (lower white arrows), over-hanging struts and thrombus at the side branch (upper white arrow), and stent malapposition (yellow arrows).

adhering to the over-hanging struts of the SideB. The principle of a 'parallel bifurcation' is demonstrated³—note the corresponding 2D OFDI frames on the left—with the parallel origins of the MainB and SideB at their respective point of take-off. The carina (labelled) appears interposed between the parallel origins of the MainB and SideB at their respective point of take-off; if further MainB post-dilatation was undertaken alone with larger angioplasty balloons, it may be speculated that this would lead to carina shift and potential SideB closure.

Bifurcation stent

A V-shaped bifurcation lesion involving two obtuse marginal (OM) branches of the atrioventricular (AV) circumflex, with severe ostial disease in the first OM branch, was treated with a 2.5 × 18 mm Nile Croco™ bifurcation stent implanted in the diseased branch, with the SideB of the stent deployed into the other branch of the bifurcation; TIMI-3 flow of the AV circumflex, with no angiographic pinching of the ostium, remained throughout. Longitudinal 3D FD-OCT reconstructions of the pre- and post-intervention bifurcation are demonstrated with corresponding 2D coronary angiograms (Figure 7A)—the ostium of the AV circumflex is not

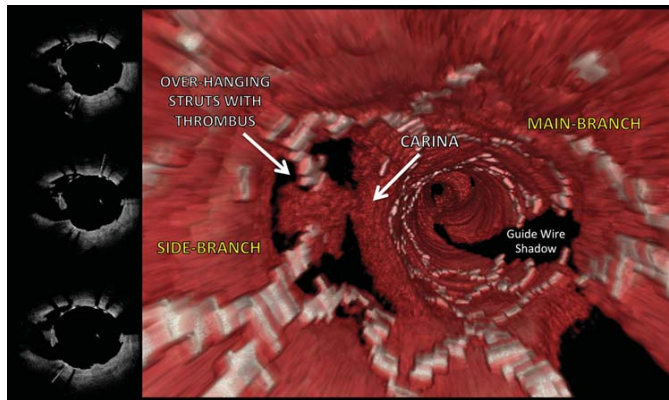


Figure 6 'Principle of a parallel bifurcation'. Close-up view of SideB from Figure 5, with thrombus attached to stent struts at the SideB ostium, in a three-dimensional frequency domain optical coherence tomography downstream fly-through view. Note how the MainB and SideB appear to originate parallel to each other at their respective point of take-off. Corresponding two-dimensional optical frequency domain imaging frames are illustrated on the left.

visualized in the longitudinal 3D reconstructions illustrated, as it exists in a different plane to the ostia of the OM branches. For comparison, a Nile Croco™ bifurcation stent deployed in a phantom model of a bifurcation is illustrated (inset figure of far right image). Note the area of malapposition with the corresponding shadowing on the vessel wall in the proximal stent edge (yellow arrow)—the corresponding 2D OFDI frames are illustrated (Figure 7B). The remainder of the stent appeared to be relatively well apposed; there was however evidence of under-deployment (Figure 7A, white arrow) when compared with the phantom model.

Fly-through downstream views of the treated vessel, pre- and post-intervention, are illustrated (Figure 7C)—within this view, no malapposition or floating struts are evident at the bifurcation. For comparison, corresponding 2D cross-sectional OFDI frames post-implantation are illustrated below.

Miscellaneous

Stent under-deployment and strut malapposition at the ostium

Severe proximal OM coronary disease was directly stented with a 2.5 × 15 mm Xience V stent up to the ostium of the vessel; no post-dilatation was performed (Figure 8A and B).

Figure 8A demonstrates pre- and post-longitudinal 3D reconstructions with corresponding angiograms. White double arrow in the post-implantation longitudinal 3D reconstruction is suggestive of stent under deployment (lower right image), as also seen in the corresponding coronary angiogram lower left image. Note the cardiac motion artefact in the post-implantation longitudinal 3D reconstruction (marked with an electrocardiographic signal), leading to the 'elongation' of the struts (the mechanism is explained in

Figure 10) and the malapposed strut at the ostium, with the shadow it casts on the vessel wall (yellow arrow, lower right image). Changing the endoluminal point of view, for instance with different views in the longitudinal plane (not illustrated) or with fly-through views looking downstream (Figure 8B, upper left image: yellow arrow) or upstream (Figure 8B, upper right image: yellow arrow), can help visualize stent malposition, which subsequently can be confirmed on corresponding cross-sectional 2D OFDI frames if necessary (lower images). The corresponding 2D OFDI frames suggest the presence of several 'floating' malapposed struts at the ostium—yellow arrows indicate the same malapposed strut seen in the 3D reconstructions.

Assessment of the extent of plaque rupture

Diagnostic coronary angiography was performed in a patient with a background of multiple cardiac risk factors and stable angina. Close review of the distal left main stem on coronary angiography suggested possible plaque rupture as evidenced by minor irregularity (Figure 9, inset upper right image: yellow arrow), with no flow-limiting lesion evident. The area of concern was not easily recognizable on 2D FD-OCT imaging—with only a high index of suspicion that an abnormality was present—close review of the individual 2D cross-sectional OFDI individual frames and 2D longitudinal views (in multiple different planes) was undertaken. If 'real-time' 3D FD-OCT was available, this would have potentially immediately highlighted the area of concern and allowed immediate focused assessment with the corresponding 2D imaging. Two-dimensional OFDI frames were subsequently highly suggestive of plaque rupture on 2D axial and longitudinal views (lower images: yellow arrows). Three-dimensional reconstructions demonstrated

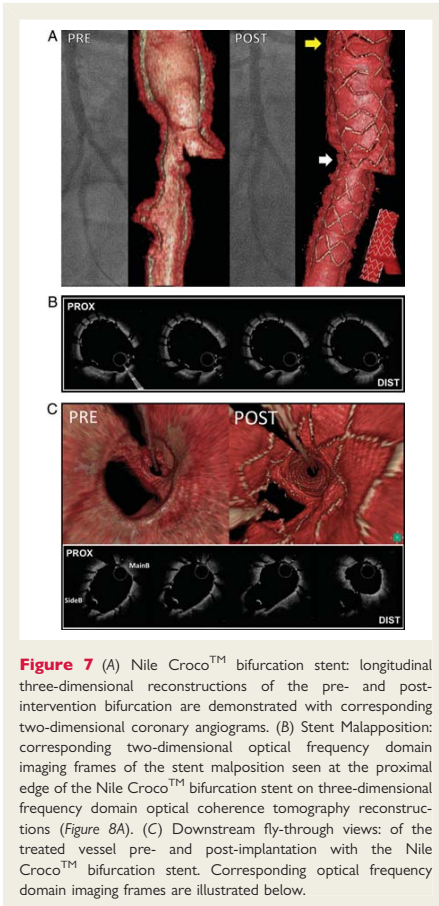


Figure 7 (A) Nile Croco™ bifurcation stent: longitudinal three-dimensional reconstructions of the pre- and post-intervention bifurcation are demonstrated with corresponding two-dimensional coronary angiograms. (B) Stent Malapposition: corresponding two-dimensional optical frequency domain imaging frames of the stent malposition seen at the proximal edge of the Nile Croco™ bifurcation stent on three-dimensional frequency domain optical coherence tomography reconstructions (Figure 8A). (C) Downstream fly-through views: of the treated vessel pre- and post-implantation with the Nile Croco™ bifurcation stent. Corresponding optical frequency domain imaging frames are illustrated below.

the visible plaque rupture in the distal left main stem—yellow arrows in downstream fly-through (upper left image) and longitudinal (upper right image) views. The patient was medically treated.

The principle of three-dimensional reconstructions performed in a non-diseased porcine model

Two-dimensional OFDI were undertaken in a non-diseased porcine model implanted with a Xience V drug-eluting stent, to allow for the assessment of the technical issues relating to undertaking 3D FD-OCT reconstructions. The porcine study has previously been described and was approved by the Institutional Animal Care and Use Committee;²⁶ the study was conducted in

accordance to the American Heart Association guidelines for pre-clinical research and the Guide for the Care and Use of Laboratory Animals (NIH, 1996).

Cardiac motion artefacts

During the early ejection phase, the speed of the cardiac contraction is at the most rapid and faster relative to the pull-back speed of the OFDI probe during image acquisition. This consequently can potentially cause a cardiac motion artefact as illustrated (Figure 10A).

Since the heart contracts with longitudinal (along the longitudinal axis of the vessel) and rotational movements, this can lead to differing types of motion artefacts such as elongation, repetition, or rotational motion artefacts as illustrated in Figure 10B. Solid white arrow indicates an elongated strut; broken white line indicates repetition of same struts due to the forward and backward motion of the vessel over the imaging wire during imaging acquisition in the early ejection phase; white arrowheads indicates rotation due to the twisting motion of the coronary artery over the imaging wire. An example from a human LAD study is shown in the fly-through view (looking upstream in the LAD) of an elongation artefact (Figure 10C).

The trade-off between pull-back speed, cardiac motion artefacts, and image resolution of the three-dimensional reconstructions

Differing pull-back speeds were used to assess image quality and frequency of cardiac motion artefacts in the non-diseased porcine model. Three-dimensional FD-OCT reconstructions were performed from 2D OFDI acquisitions with pull-back speeds of 20, 30, and 40 mm/s (Figure 11). With faster pull-back speeds (40 mm/s), the frequency of the cardiac motion artefacts consequently reduces due to a shorter period of time during imaging acquisition for cardiac motion to occur. This however comes at the expense of a lower longitudinal resolution (due to a thicker slice thickness: 0.25 mm) giving a more 'grainy' appearance. Conversely, with slower pull-back speeds (20 mm/s), the image resolution increases because of a greater longitudinal resolution (due to a 'thinner' slice thickness: 0.125 mm); this is however at the expense of an increased frequency of cardiac motion artefacts due to a longer imaging acquisition time period. A trade-off between image resolution (as determined by the pull-back speeds) and the frequency of cardiac motion artefacts is therefore necessary to ensure the ideal 3D reconstruction.

The recommendation for the Terumo OFDI system, in our experience, is a pull-back speed of 20 mm/s; this will allow optimal imaging while limiting cardiac motion artefacts; cardiac motion artefacts however will still occur as previously illustrated (Figure 9C). For the LightLab C7 system, because of the poorer resolution of the 3D reconstructions, we recommend a pull-back speed of 10 mm/s to improve the resolution;²⁷ this however comes at the expense of substantially increased frequency of cardiac motion artefacts, with the risk of one of these artefacts occurring at the region of interest. Future generations of 3D FD-OCT systems, in our opinion, need to have much higher frame rates (200–300 frames/s +) to allow for even rapid pull-

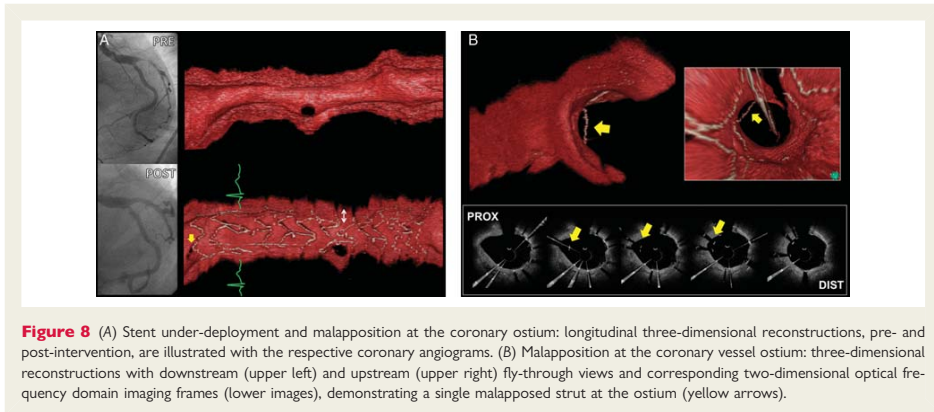


Figure 8 (A) Stent under-deployment and malpositioning at the coronary ostium: longitudinal three-dimensional reconstructions, pre- and post-intervention, are illustrated with the respective coronary angiograms. (B) Malpositioning at the coronary vessel ostium: three-dimensional reconstructions with downstream (upper left) and upstream (upper right) fly-through views and corresponding two-dimensional optical frequency domain imaging frames (lower images), demonstrating a single malpositioned strut at the ostium (yellow arrows).

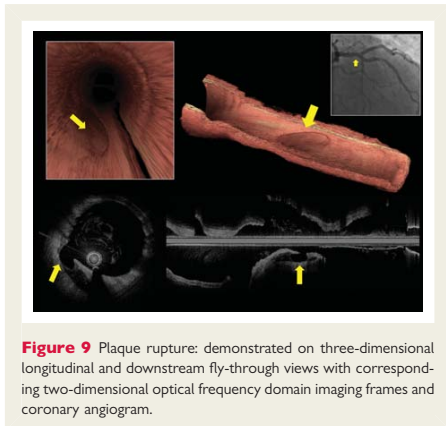


Figure 9 Plaque rupture: demonstrated on three-dimensional longitudinal and downstream fly-through views with corresponding two-dimensional optical frequency domain imaging frames and coronary angiogram.

backs (40 mm/s +)—this will potentially lead to higher resolution 3D reconstructions with limited cardiac motion artefacts.

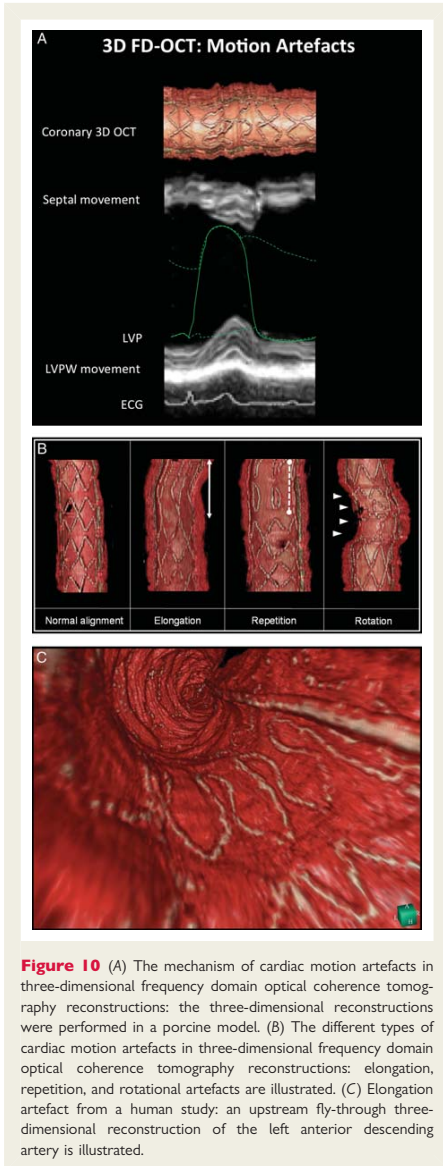
Potential clinical application and opinion for the future development of three-dimensional frequency domain optical coherence tomography technology

Due to the unrivalled resolution of OCT compared with other intravascular imaging modalities, it is the author's opinion that the potential clinical application of this technology, as a

complimentary tool to 2D FD-OCT is real, and if available at the 'push-of-a-button' when 2D intravascular imaging is performed, will provide a global perspective with subsequent targeted assessment with 2D FD-OCT imaging as required. Furthermore, the 3D reconstructions are intuitively easier to understand compared with the 2D images, which further adds to the appeal of this emerging technology.

The current prototypes of online 3D FD-OCT systems have the capacity to automatically detect struts based on their specific optical characteristics, such as the reflective properties of the metallic struts.⁴ The further requirements from industry to potentially make 3D FD-OCT a clinical reality include the improvement in automatic strut detection, higher framer-rate systems with rapid pull-back speeds to improve the resolution of the 3D reconstruction and reduce the likelihood of cardiac motion artefacts, automatic volume rendering of a sufficient calibre to allow for high-resolution imaging, dedicated quantitative software for analyses,²⁸ and a user-friendly interface to allow for full virtual navigation of the vessel. With the latter, as previously illustrated, sometimes several views—such as longitudinal and fly-through views—are required to best visualize the area of interest; with the volume-rendering software utilized in the cases in this paper, practically any view of the vessel was achievable with relative ease. It should also be emphasized that the concept of virtual navigation (fly-through) of the coronary vessel is not new, having previously been implemented for many years in the magnetic navigation catheterization laboratory.^{29,30}

The development of dedicated software, which ultimately is what this technology is reliant upon, is of paramount importance. Dedicated volume-rendering software to achieve consistent and reproducible application of volume rendering—as has been achieved with spiral computed tomography³¹—and dedicated quantitative software²⁸ for the analyses of the 3D constructions are both crucial to allow for comparable, reproducible 3D reconstructions and quantitative data, which can have potential widespread clinical and research applications.



Potential clinical applications of the 3D technology include to allow for the global assessment of areas of possible stent malapposition—by the presence of shadow on the vessel wall as

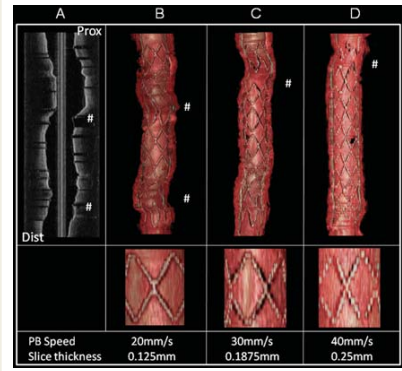


Figure 11 The trade-off between pull-back speed, cardiac motion artefacts, and image resolution of the three-dimensional frequency domain coherence tomography reconstructions: as demonstrated in a porcine model. # represents cardiac motion artefacts; (A) represents 2D (OFDI) longitudinal image; (B–D) represents corresponding 3D reconstructions with progressively increased pullback speeds and consequential fewer cardiac motion artefacts at the expense of a lower resolution. PB, pullback.

seen with protruding and malapposed struts—which may warrant subsequent closer review with 2D imaging to help ascertain areas requiring further post-dilatation; conversely, if malapposition is obvious on the 3D reconstruction, the operator may simply elect to undertake further post-dilatation. To aid with this process, automatic colour coding of apposed, protruding, or malapposed struts may be achievable.

The application of this technology within the coronary bifurcation has previously been described and is a further promising area of the potential for this emerging technology.^{2,3} Trying to visualize the complex anatomy of the bifurcation and the effects of intervention is difficult and not always reliable with 2D imaging.^{2,3} The addition of quantitative measurements, as previously discussed, may have a potential clinical application in the measurement of the SideB ostial area after MainB stenting, to allow assessment as to whether the SideB is haemodynamically obstructed.³ Angiographic assessment of pinched SideB after MainB stenting has previously been shown to be unreliable, with only one-quarter (27%) of SideB with angiographic residual narrowing $\geq 75\%$ being found to be functionally significant on subsequent pressure wire studies.^{3,32}

Other potential clinical applications previously demonstrated include the identification and localization of the extent of thrombus and need for subsequent further aspiration thrombectomy, post-dilatation, and concomitant use of peri-procedural anticoagulants—conversely, thrombus cannot be visualized by the IVUS and if this imaging modality was used, the operator would effectively have to make an educated guess as to whether malapposition is

present or not; a greater understanding of stent conformability, in particular at the coronary ostium; the identification of other intravascular abnormalities such as ruptured plaque (Figure 9) and even stent under-expansion.

Although OCT is not the intravascular imaging modality of choice for the assessment of stent under-expansion due to the limited penetration of OCT in intravascular tissue—whereas IVUS would be more ideal in identifying the media-to-media width for appropriate vessel sizing³³—the 3D reconstructions still identified an area where stent under-expansion was clearly evident (Figure 8) and may have guided the operator to undertake further post-dilation, with or without IVUS guidance. Furthermore, the introduction of quantitative measurements with 3D-OCT may allow defining of these lengths of interest on longitudinal 3D views that may also guide subsequent intervention.

The addition of tissue characterization within 3D FD-OCT reconstructions are further promising areas of research in this technology; these have previously been performed offline and would have the potential to aid in the identification of clinically useful areas of interest, such as lipid pools and vulnerable plaque.^{1,8,34} Fusion imaging of 2D FD-OCT and IVUS virtual histology³⁵ has recently been described; this may subsequently be achievable with 3D FD-OCT. Furthermore, the development of 2D and 3D 'microscopic' OCT—with a resolution of 1–2 μm—has also very recently been shown to provide remarkably clear pictures of cellular and subcellular features, associated with atherogenesis and thrombosis in human cadaveric coronary arteries.³⁶

The realization of the full potential of this emerging technology within interventional cardiology clinical practice—as appears to be currently the case in the field of ophthalmology with, for example, 3D visualization of the retina³⁷—is required from clinicians and industry in order to allow the future development and validation of this innovative technology.

Acknowledgements

All authors wish to express their thanks to Willem J. van der Giessen, MD, PhD, Evelyn Regar, MD, PhD, Carl Schultz, MD, PhD, and Jurgen Ligthart, BSc, of the ThoraxCenter, Erasmus University Medical Centre, Rotterdam, The Netherlands, part of the team who undertook the original First-In-Man study of the intracoronary Terumo OFDI system. We thank Ravindra Pawar and Monique Schuijjer of Cardialysis BV, Rotterdam, The Netherlands, and Dr Dragica Paunovic and Dr Vladimir Borovicaniin of Terumo Corporation and Terumo Europe N.V. for their invaluable technical support.

Funding

V.F. wishes to acknowledge the support of The Dickinson Trust Traveling Scholarship Fund, Manchester Royal Infirmary, Manchester, England, UK. B.D.G. has received grant support from the Hellenic Cardiological Society, Athens, Greece.

Conflict of interest: none declared.

References

1. Tearney GJ, Waxman S, Shishkov M, Vakoc BJ, Suter MJ, Freilich M, Desjardins AE, Oh WY, Bartlett LA, Rosenberg M, Bouma BE. Three-dimensional

- coronary artery microscopy by intracoronary optical frequency domain imaging. *JACC Cardiovasc Imaging* 2008;**1**:752–761.
2. Okamura T, Onuma Y, Garcia-Garcia HM, Regar E, Wykrzykowska JJ, Koolen J, Thuesen L, Windecker S, Whitbourn R, McClean DR, Ormiston JA, Serruys PW. 3-Dimensional optical coherence tomography assessment of jailed side branches by bioresorbable vascular scaffolds: a proposal for classification. *JACC Cardiovasc Interv* 2010;**3**:836–844.
3. Farooq V, Serruys PW, Heo JH, Gogas BD, Okamura T, Gomez-Lara J, Brugaletta S, Garcia-Garcia HM, van Geuns RJ. New insights into the coronary artery bifurcation. Hypothesis-generating concepts utilizing 3-dimensional optical frequency domain imaging. *JACC Cardiovasc Interv* 2011;**4**:921–931.
4. Di Mario CIL, van der Giessen WJ, Foin N, Adrianssens T, Tyczynski P, Ghilencea L, Viceconte N, Lindsay AC. Optical coherence tomography for guidance in bifurcation lesion treatment. *EuroIntervention* 2011;**6**(Suppl. J):J99–J106.
5. Gogas BD, van Geuns RJ, Farooq V, Regar E, Heo JH, Ligthart J, Serruys PW. Three-dimensional reconstruction of the post-dilated ABSORB everolimus-eluting bioresorbable vascular scaffold in a true bifurcation lesion for flow restoration. *JACC Cardiovasc Interv* 2011;**4**:1149–1150.
6. van Geuns RJ, Gogas BD, Farooq V, Regar E, Serruys PW. 3-Dimensional reconstruction of a bifurcation lesion with double wire after implantation of a second generation everolimus-eluting bioresorbable vascular scaffold. *Int J Cardiol* 2011. Published online ahead of print 8 March 2011.
7. Foin N, Viceconte N, Chan PH, Lindsay AC, Krams R, Di Mario C. Jailed side branches: fate of unopposed struts studied with 3D frequency-domain optical coherence tomography. *J Cardiovasc Med* 2011;**12**:581–582.
8. Gonzalo N, Tearney GJ, van Soest G, Serruys P, Garcia-Garcia HM, Bouma BE, Regar E. Witnessed coronary plaque rupture during cardiac catheterization. *JACC Cardiovasc Imaging* 2011;**4**:437–438.
9. Okamura T, Serruys PW, Regar E. Three-dimensional visualization of intracoronary thrombus during stent implantation using the second generation, Fourier domain optical coherence tomography. *Eur Heart J* 2010;**31**:625.
10. Okamura T, Serruys PW, Regar E. Cardiovascular flashlight. The fate of bioresorbable struts located at a side branch ostium: serial three-dimensional optical coherence tomography assessment. *Eur Heart J* 2010;**31**:2179.
11. Gogas BD, Farooq V, Onuma Y, Magro M, Radu MD, van Geuns RJ, Regar E, Serruys PW. 3-Dimensional optical frequency domain imaging for the evaluation of primary percutaneous coronary intervention in ST-segment elevation myocardial infarction. *Int J Cardiol* 2011;**151**:103–105.
12. Reid DB, Douglas M, Diethrich EB. The clinical value of three-dimensional intravascular ultrasound imaging. *J Endovasc Surg* 1995;**2**:356–364.
13. Box LC, Angiolillo DJ, Suzuki N, Box LA, Jiang J, Guzman L, Zenni MA, Bass TA, Costa MA. Heterogeneity of atherosclerotic plaque characteristics in human coronary artery disease: a three-dimensional intravascular ultrasound study. *Catheter Cardiovasc Interv* 2007;**70**:349–356.
14. Krams R, Cheng C, Helderman F, Verheye S, van Damme LC, Mousavi Gouriabi B, Tempel D, Segers D, de Feyter P, Pasterkamp G, De Klein D, de Crom R, van der Steen AF, Serruys PW. Shear stress is associated with markers of plaque vulnerability and MMP-9 activity. *EuroIntervention* 2006;**2**:250–256.
15. Schaar JA, Regar E, Mastik F, McFadden EP, Saia F, Disco C, de Korte CL, de Feyter PJ, van der Steen AF, Serruys PW. Incidence of high-strain patterns in human coronary arteries: assessment with three-dimensional intravascular palpography and correlation with clinical presentation. *Circulation* 2004;**109**:2716–2719.
16. Gijzen FJ, Mastik F, Schaar JA, Schuurbers JC, van der Giessen WJ, de Feyter PJ, Serruys PW, van der Steen AF, Wentzel JJ. High shear stress induces a strain increase in human coronary plaques over a 6-month period. *EuroIntervention* 2011;**7**:121–127.
17. Uchida Y. Recent advances in coronary angiography. *J Cardiol* 2011;**57**:18–30.
18. van Ooijen PM, de Jonge G, Oudkerk M. Coronary fly-through or virtual angiography using dual-source MDCT data. *Eur Radiol* 2007;**17**:2852–2859.
19. Regar E, Schaar JA, Mont E, Virmani R, Serruys PW. Optical coherence tomography. *Cardiovasc Radiat Med* 2003;**4**:198–204.
20. van der Giessen AG, Schaap M, Gijzen FJ, Groen HC, van Walsum T, Mollet NR, Dijkstra J, van de Vosse FN, Niessen WJ, de Feyter PJ, van der Steen AF, Wentzel JJ. 3D fusion of intravascular ultrasound and coronary computed tomography for in-vivo wall shear stress analysis: a feasibility study. *Int J Cardiovasc Imaging* 2010;**26**:781–796.
21. van der Giessen AG, Wentzel JJ, Meijboom WB, Mollet NR, van der Steen AF, van de Vosse FN, de Feyter PJ, Gijzen FJ. Plaque and shear stress distribution in human coronary bifurcations: a multislice computed tomography study. *EuroIntervention* 2009;**4**:654–661.
22. Okamura T, Onuma Y, Garcia-Garcia HM, van Geuns RJ, Wykrzykowska JJ, Schultz C, van der Giessen WJ, Ligthart J, Regar E, Serruys PW. First-in-man evaluation of intravascular optical frequency domain imaging (OFDI) of Terumo: a

- comparison with intravascular ultrasound and quantitative coronary angiography. *EuroIntervention* 2011;**6**:1037–1045.
23. Serruys PW, Thuesen L. *Primary PCI: Step-by-step Decision Process. New Optical Imaging Techniques to Guide Treatment. TROFI Summary and Status of the trial.* Paris: EuroPCR; 2011.
 24. Parodi G, Maehara A, Giuliani G, Kubo T, Mintz GS, Migliorini A, Valenti R, Carrabba N, Antoniucci D. Optical coherence tomography in unprotected left main coronary artery stenting. *EuroIntervention* 2010;**6**:94–99.
 25. Tanigawa J, Barlis P, Di Mario C. Intravascular optical coherence tomography: optimisation of image acquisition and quantitative assessment of stent strut apposition. *EuroIntervention* 2007;**3**:128–136.
 26. Okamura T, Onuma Y, Garcia-Garcia HM, Bruining N, Serruys PW. High-speed intra coronary optical frequency domain imaging: implications for three-dimensional reconstruction and quantitative analysis. *EuroIntervention* (in press).
 27. Farooq V, Onuma Y, Radu M, Okamura T, Gomez-Lara J, Brugaletta S, Gogas BD, van Geuns RJ, Regar E, Schultz C, Windecker S, Lefevre T, Brueren BR, Powers J, Perkins LL, Rapoza RJ, Virmani R, Garcia-Garcia HM, Serruys PW. Optical coherence tomography (OCT) of overlapping bioresorbable scaffolds: from benchwork to clinical application (refers to on-line images available from EuroIntervention website). *EuroIntervention* 2011;**7**:386–399.
 28. Agostoni P, Stella PR. Optical coherence tomography: new (near-infrared) light on stent implantation? *Heart* 2009;**95**:1895–1896.
 29. Patterson MS, Hoeks SE, Rijkenberg S, Ramcharitar S, van Guens RJ, Tanimoto S, van Domburg RT, Serruys PW. Integration of 3D reconstruction in the SElection criteria for Excessive Crossing Times for Magnetically Supported Percutaneous Coronary Intervention. SELECT-MP. *EuroIntervention* 2009;**4**:509–516.
 30. Simsek C, Magro M, Patterson MS, Onuma Y, Ciampichetti I, van Weenen S, van Domburg RT, Serruys PW, Boersma E, van Geuns RJ. Magnetic navigation system assisted stenting of coronary bifurcation lesions. *EuroIntervention* 2011;**6**:970–976.
 31. Calhoun PS, Kuszyk BS, Heath DG, Carley JC, Fishman EK. Three-dimensional volume rendering of spiral CT data: theory and method. *Radiographics* 1999;**19**:745–764.
 32. Koo BK, Kang HJ, Youn TJ, Chae IH, Choi DJ, Kim HS, Sohn DW, Oh BH, Lee MM, Park YB, Choi YS, Tahk SJ. Physiologic assessment of jailed side branch lesions using fractional flow reserve. *J Am Coll Cardiol* 2005;**46**:633–637.
 33. Rogacka R, Latib A, Colombo A. IVUS-guided stent implantation to improve outcome: a promise waiting to be fulfilled. *Curr Cardiol Rev* 2009;**5**:78–86.
 34. Waxman S, Freilich MI, Suter MJ, Shishkov M, Bilazarian S, Virmani R, Bouma BE, Tearney GJ. A case of lipid core plaque progression and rupture at the edge of a coronary stent: elucidating the mechanisms of drug-eluting stent failure. *Circ Cardiovasc Interv* 2010;**3**:193–196.
 35. Diletti R, Garcia-Garcia HM, Gomez-Lara J, Brugaletta S, Wykrzykowska JJ, van Ditzhuijzen N, van Geuns RJ, Regar E, Ambrosio G, Serruys PW. Assessment of coronary atherosclerosis progression and regression at bifurcations using combined IVUS and OCT. *JACC Cardiovasc Imaging* 2011;**4**:774–780.
 36. Liu L, Gardecki JA, Nadkarni SK, Toussaint JD, Yagi Y, Bouma BE, Tearney GJ. Imaging the subcellular structure of human coronary atherosclerosis using micro-optical coherence tomography. *Nat Med* 2011;**17**:1010–1014.
 37. Wojtkowski M, Srinivasan V, Fujimoto JG, Ko T, Schuman JS, Kowalczyk A, Duker JS. Three-dimensional retinal imaging with high-speed ultrahigh-resolution optical coherence tomography. *Ophthalmology* 2005;**112**:1734–1746.

Part 5

***In Vivo* Assessment of the Absorb Bioresorbable Vascular Scaffold Utilizing Intracoronary Ultrasound and Optical Coherence Tomography**

Chapter 20

The ABSORB Bioresorbable Vascular Scaffold: An Evolution or Revolution in Interventional Cardiology?

Bill D. Gogas, Vasim Farooq, Yoshinobu Onuma, Patrick W Serruys

Hellenic Journal Cardiology. 2012. Jul;53(4):301-9 [IF: 1.23]

The ABSORB Bioresorbable Vascular Scaffold: An Evolution or Revolution in Interventional Cardiology?

BILL D. GOGAS, VASIM FAROOQ, YOSHINOBU ONUMA, PATRICK W. SERRUYS

Thoraxcenter, Erasmus University Medical Centre, Rotterdam, the Netherlands

Key words:
Bioresorbable
vascular scaffold,
coronary artery
disease.

Manuscript received:
December 25, 2011;
Accepted:
April 5, 2012.

Address:
Patrick W. Serruys

*Thoraxcenter, Ba-583
's Gravendijkwal 230
3015 CE Rotterdam
Netherlands
e-mail: [p.w.j.c.serruys@
erasmusmc.nl](mailto:p.w.j.c.serruys@erasmusmc.nl)*

The advent of plain-old balloon angioplasty (POBA), first introduced by Andreas Grüntzig in 1977, revolutionised the treatment of coronary artery disease. Significant coronary lesions were shown to be potentially treatable with balloon dilatation, leading to restoration of lumen patency and vascular flow. Although this mode of treatment was undoubtedly a significant technological breakthrough, multiple weaknesses became evident. These either occurred post-procedurally, leading to acute vessel closure necessitating emergency revascularisation as a consequence of acute vessel recoil aggravated by local intimal and media dissections, or longer term, secondary to neointimal proliferation and constrictive remodelling as a consequence of vascular barotrauma.¹

Several of the weaknesses associated with POBA were eliminated with the introduction of bare metal stents (BMS), namely the resolution of the acute and chronic recoil by caging the vessel wall with a permanent metallic prosthesis. The landmark BENESTENT trial^{2,3} first established the feasibility of this therapeutic approach. Although initial studies were promising, a new entity became evident, namely neointimal hyperplasia (NIH), to which restenosis rates of 16-44% were attributed.

Drug-eluting stents (DES) were thus conceived as the next evolutionary step in improving the limitations of BMS. Initial studies were highly promising, with large-scale reductions in restenosis rates that were reported at 0% in highly selective lesions⁴ and up to 16% in a broader range of patients and lesions.^{5,6} A potential complication subsequently became evident with first-generation DES, namely that of subacute and late stent thrombosis as a consequence of delayed healing of the permanent metallic struts. Furthermore, late acquired malapposition of the struts implanted in a thrombotic rich milieu were also demonstrated to be a potential issue.⁷⁻⁹

The prospect of a temporary vascular stent, termed “scaffold” due to its being based on a temporary bioresorbable platform, has been always a goal of the interventional community. Such a device could offer transient radial strength to resist acute vessel recoil, and at a later stage would be fully resorbed, leading to restoration of the vessel’s biological properties.

The purpose of this review is to demonstrate the progress in the development of the ABSORB bioresorbable vascular scaffold (BVS) (Abbott Vascular, Santa Clara CA, USA) from the bench to clinical application. The potential advantages of this emerging technology, recently

termed “vascular reparative therapy”, over the permanent caging of vessels with conventional metallic DES are discussed.

The ABSORB BVS design, material and the bioresorption process

The ABSORB everolimus-eluting scaffolds include the first generation device evaluated in the ABSORB Cohort A clinical trial (ABSORB 1.0)^{10,11} (Figure 1A), the second generation (ABSORB Revision 1.1) (Figure 1B), investigated in the ABSORB Cohort B trial,¹² and the third generation currently under development. The first generation had a crossing profile of 1.4 mm, strut thickness of 150 μm and consisted of out-of-phase zigzag hoops linked together by thin and straight bridges (Figure 1A). This device had to be kept refrigerated at -20°C to prevent physical ageing of the polymer and

ensure device integrity. The second generation (ABSORB Revision 1.1) uses the same polymer as the previous one, with modifications of both the polymer processing and the scaffold design to give the device more prolonged radial support (Figure 1B). Both devices share similar characteristics:

1. A platform made of poly (L-lactide) (PLLA) (PLLA is used in numerous clinical items, such as resorbable sutures, soft tissue implants, orthopaedic implants, and dialysis media). PLLA is a semi crystalline polymer consisting of crystal lamellae interconnected with random polymer chains forming an amorphous segment (Figure 2).
2. A 1:1 mixture of an amorphous matrix of poly-D, L-lactide (PDLLA) and 8.2 $\mu\text{g}/\text{mm}$ of the antiproliferative drug everolimus.
3. A pair of radiopaque platinum markers at the proximal and distal ends of the scaffold to allow

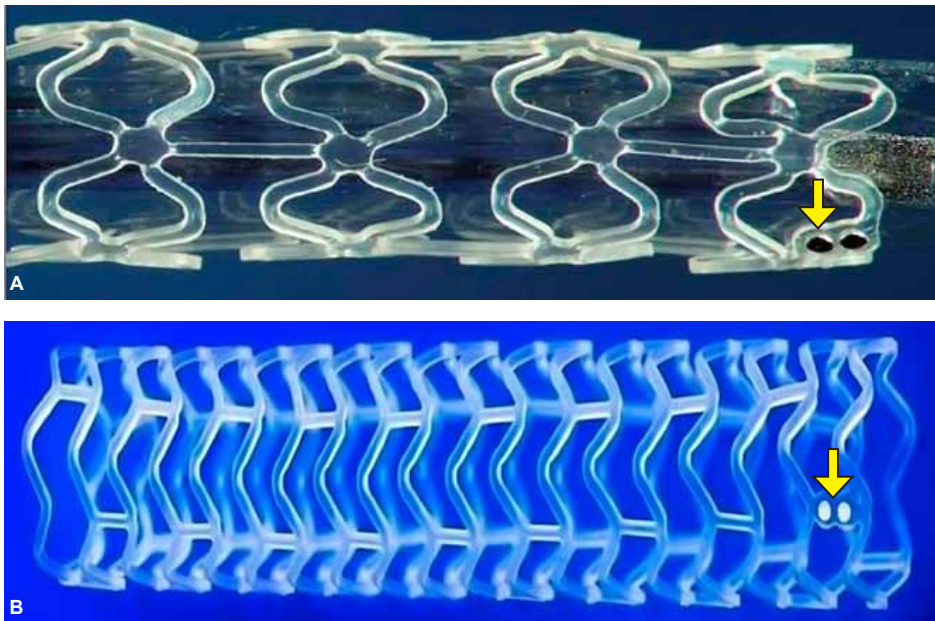


Figure 1. The first and second generations of the ABSORB bioresorbable vascular scaffold (BVS). A: The 1st generation ABSORB BVS had a strut thickness of 150 μm , a crossing profile of 1.4 mm, and consisted of circumferential out-of-phase zigzag hoops linked by thin and straight bridges. The device had one pair of radiopaque platinum markers at each proximal and distal edge (yellow arrow). B: The 2nd generation ABSORB BVS (revision 1.1) has a strut thickness of 150 μm , consisting of in-phase zigzag hoops linked by bridges. The device is radiolucent but has two radiopaque platinum markers at each proximal and distal edge that allow easy visualisation with angiography and other imaging modalities (yellow arrow).

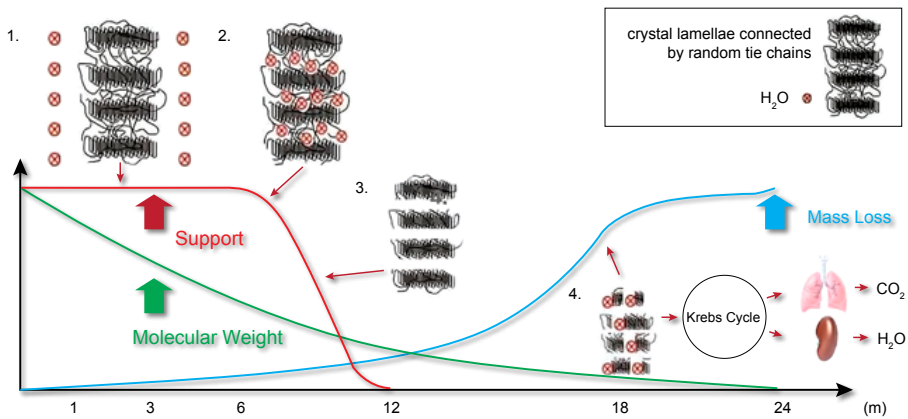


Figure 2. The ABSORB bioresorbable vascular scaffold (BVS) poly-L-lactide bioresorption process up to 24 months, when the polymeric device is expected to be fully resorbed. 1. Polymer hydration (crystalline poly(lactide)) following implantation. Poly(lactides) are hydrophilic, thus water (H_2O) can penetrate the implant. 2. Depolymerisation by hydrolysis, observed as a reduction in molecular weight (green line). 3. Polymer fragmentation into segments of low-weight polymer, resulting in the scission of amorphous tie chains linking the crystalline regions with subsequent gradual loss of the radial strength (red line). 4. Assimilation or dissolution of the monomer. The soluble monomer (e.g. L-lactate) is changed into pyruvate, which eventually enters the Krebs cycle and is further converted into carbon dioxide and water, eliminated by the lungs and kidneys, respectively. From Onuma Y, Serruys PW: Bioresorbable scaffold: the advent of a new era in percutaneous coronary and peripheral revascularization? *Circulation*. 2011; 123: 779-797. Adapted by permission of Wolters Kluwer Health.

visualisation during coronary angiography (Figure 1 A & B).

4. The balloon delivery system.

Bioresorption process

The bioresorption process of the ABSORB BVS PLLA undergoes four stages (Figure 2):

1. Polymer hydration (crystalline poly(lactide)) following implantation. Poly(lactides) are hydrophilic; thus water can penetrate inside the implant.
2. Depolymerisation by hydrolysis, observed as a reduction in molecular weight.
3. Polymer fragmentation into segments of low-weight polymer, resulting in scission of the amorphous tie chains linking the crystalline regions.
4. Assimilation or dissolution of the monomer. Phagocytes can assimilate small particles and lead to soluble monomeric anions. The soluble monomer (e.g. L-lactate) is changed into pyruvate, which eventually enters the Krebs cycle and is further converted into carbon dioxide and water. These final products are eliminated by the lungs and kidneys, respectively.

The assessment of bioresorption was recently evaluated by our group in a porcine coronary artery model at 28-days, 2, 3 and 4 years (Figure 3). Thirty-five ABSORB BVS 3.0×12 mm were implanted in the main coronary arteries of 17 pigs evaluated with optical coherence tomography (OCT) and histology following euthanasia: immediately ($n=2$), at 28 days ($n=2$), 2 years ($n=3$), 3 years ($n=5$) or 4 years ($n=5$). Immediately after implantation, all struts had a preserved box appearance. At 28 days, OCT showed 82% of the struts as preserved box, and 18% as an open box appearance. At 2 years four fifths of the struts showed a preserved box appearance and only a few struts (2.4%) demonstrated open box appearance. Histological analysis at this time point showed the polymeric strut voids to be replaced by proteoglycan-rich matrix, with poly(lactide) residues at low levels, as quantified by chromatography (Figure 3A & B). At 4 years, OCT showed 51.2% of the struts classified as dissolved bright box and 48.8% as dissolved black box. The strut remnants were hardly detectable by histology, appearing as foci of low-cellular-density connective tissue (Figure 3C & D).^{13,14}

Company / Device	Design of the bioresorbable device	Strut thickness, (μ m)	Polymer / Drug	Absorption time	Late loss, (mm)
Kyoto Medical / Igaki-Tamai		170	PLLA	2 years (y)	0.48 (6m)
Biotronik / DREAMS		125	Mg alloy (AMS-4) / sirolimus	4 to 6 months (m)	0.68 (6m)*
Abbott / ABSORB BVS		150	PLLA / everolimus	2y	0.19 (6m)
Reva Medical / ReSolve		200	Tyrosine poly carbonate with iodine / sirolimus ablutinal	2y	1.81 (6m)
- / BTI		200	Salicylic acid into polymer (PLA or adipic acid) / sirolimus	6m	NA
Elixir / DESolve		150	PLLA / novolimus	1 to 2y	NA

Figure 4. The family of bioresorbable devices that have undergone clinical evaluation. The platform design, strut thickness, polymer/drug formulation, absorption time and late lumen loss are illustrated. PLLA – poly-L-Lactide. BVS – bioresorbable vascular scaffold; AMS – absorbable magnesium stent. *Evaluated with the AMS-3 device.

OCT, and an angiographic LL of 0.27 ± 0.32 mm, similar to that reported with the Xience V everolimus eluting stent (LL: 0.23 ± 0.29 mm, as demonstrated in the SPIRIT I trial) at the same time point. Additionally, the hierarchical MACE rate of the 101 patients (Cohort B₁ and B₂ trials) at 1 year (7.1%) was comparable to that observed in the historical series of the Xience V metallic EES.^{16,17}

The ongoing ABSORB EXTEND study, a multicentre single-arm study that aims to recruit approximately 1000 patients from 50 centres worldwide, will further in-

vestigate the ABSORB BVS. Additionally in the pipeline for the near future is the pivotal non-inferiority trial of the ABSORB BVS vs. the metallic EES (Xience Prime) in approximately 500 patients in 2:1 fashion.

The potential benefits of transient bioresorbable vascular scaffolds vs. permanent metallic stents

The advent of the bioresorbable technology in clinical practice has several advantages compared to permanent metallic devices, such as:

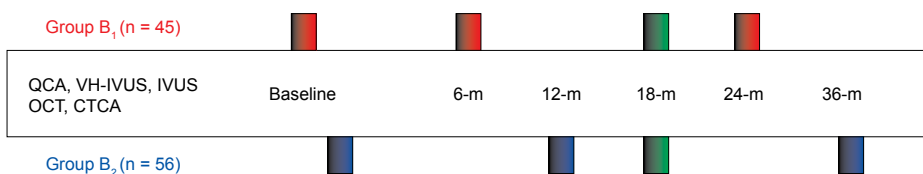


Figure 5. The ABSORB Cohort B study design. The ABSORB Cohort B trial enrolled a total of 101 patients who were split into two groups. Group B₁ underwent invasive imaging post-procedure, at 6 months and 2 years; Group B₂ underwent invasive imaging post-procedure at 1 year and will undergo another imaging follow up at 3 years. At 18 months all patients underwent non-invasive imaging assessment with coronary computed tomography angiography (CCTA).

1. The “liberation” of the treated vessel from its “metallic cage” and the subsequent reactivation of the physiological processes of vasomotion, vascular remodelling and late lumen enlargement.
2. The potential elimination/integration into the vessel wall of the polymeric struts from jailed side-branches after the completion of the bioresorption process.
3. The superior conformability and flexibility compared to conventional metallic stents, thereby leading to a less altered distribution of the tissue biomechanics and preservation of the vessel geometry.
4. The potential long-term beneficial edge vascular response.
5. The elimination of the late acquired or persistent malapposition, which has been implicated in causing thrombotic events with conventional metallic devices.

Vasomotion

In the ABSORB Cohort A trial, either the endothelium-dependent vasoconstrictor methylergonovine maleate (methergin) or the endothelium-dependent vasoactive agent acetylcholine was administered at the 2-year follow up for the study of vasomotion. In the methergin group there was significant vasoconstriction in the scaffolded segment (before methergin: 2.64 ± 0.22 mm; after methergin: 2.44 ± 0.33 mm; $p=0.03$) while in the acetylcholine group five patients exhibited vasodilation in the scaffolded segment.¹¹ The restoration of vasomotion was also recently shown during the 1-year follow up of the ABSORB Cohort B₂, with changes in the mean lumen diameter as assessed by QCA in the target vessel proximal to the scaffold, distal and within the scaffold, following the administration of either acetylcholine or methylergonovine.¹⁷

Arterial remodelling and late lumen enlargement

Arterial remodelling is an adaptive process to compensate for plaque expansion in order to preserve lumen dimensions (Glagov phenomenon), where the threshold for the transition of the expansive (increase of the external elastic membrane, EEM) to constrictive remodelling is highly dependent on the underlying plaque burden being >40%. The implantation of permanent metallic devices interrupts this dynamic process. After the completion of the bioresorption process, in vessels treated with the ABSORB BVS, IVUS based imaging has shown late luminal enlarge-

ment of 10.9%, with a significant plaque media reduction of -12.7%, and no significant change in the vessel area (EEM). This phenomenon of plaque regression requires further investigation, as the interplay among the tissue composition and the artefactual observation of the polymeric struts as dense calcium structures by the VH-IVUS modality have previously been shown to be an issue.¹⁸

Side branch jailing

The jailing of the side branch (SB) is a potential area of concern during bifurcation stenting. Higher incidences of MACE have been reported with bifurcation stenting compared to conventional percutaneous intervention of non-SB lesions. In *post hoc* analyses of the original ABSORB studies, the SB jailing during provisional T-stenting with the ABSORB BVS appeared to have a benign behaviour compared to metallic devices. Okamura et al demonstrated, at 2-year follow up post BVS implantation, that the polymeric struts had cleared at the side branch ostium, with evidence of integration into the underlying tissue and, in some cases, causing a membranous neocarina.¹⁹ Our group recently demonstrated the feasibility of crossing the polymeric struts of the ABSORB BVS using three-dimensional OCT and presented the first report of successful post-dilation of the device's polymeric struts in a jailed SB for flow restoration.^{20,21} Large scale studies to confirm these encouraging preliminary findings are planned.

Conformability

The ABSORB BVS has been shown to be more conformable compared to metallic stents (Multi-link Vision or Xience V EES), altering vessel angulation and curvature to a lesser degree and consequently having a smaller effect on flow dynamics and shear stress distribution in the scaffolded segment and the scaffold edges.²²

Edge vascular response

The edge vascular response (EVR) was firstly described during brachytherapy with the use of radioactive stents²³ and later on with metallic platforms: either first generation DES (SES and PES) up to 6 months, or second generation DES (Xience V EES) up to 2 years. It became evident that the EVR is not the result of a single precipitating factor, but rath-

er the interplay among several confounding factors: 1) device related: platform (metal or polymer) and drug (limus-based elution or paclitaxel); 2) iatrogenic: geographical miss (axial, longitudinal or both); and 3) tissue composition at the edge (necrotic core rich plaque at the landing zone of the device) (Figure 6). The advent of bioresorbable devices with transient scaffolding properties prompted the re-evaluation of the EVR, as any potential initial adverse response might potentially regress in parallel with the bioresorption of the implanted device.

The proximal and distal edges following implantation of the second generation ABSORB BVS were investigated with *in vivo* VH-IVUS, non-serially at 6 months (Cohort B₁) and 1 year (Cohort B₂), and serially at 6 months and 2 years (Cohort B₁).

The non-serial evaluation demonstrated a dynamic biologic behaviour with some degree of proximal edge constrictive remodelling: Δ vessel area -1.80% $[-3.18; 1.30]$ ($p < 0.05$) at 6 months, which tended to regress at 1 year to Δ vessel area -1.53% $[-7.74; 2.48]$ ($p = 0.06$), and distal edge tissue composition changes, mainly with an increase of the fibrofatty (FF) tissue component, Δ FF $+ 43.32\%$ $[-19.90; 244.28]$ ($p < 0.05$).²⁴

The serial evaluation up to 2 years (post-procedure to 2 years) revealed a lumen loss of: Δ -6.68% $[-17.33; 2.08]$, ($p = 0.027$) with a trend toward plaque area increase of: Δ $+7.55\%$ $[-4.68; 27.11]$, ($p = 0.06$) at the proximal edge and distal edge tissue composition changes with a significant increase of the fibrofatty tissue (FF) tissue component (from 6 months to 2 years) from 0.09 mm^2 $[0.04; 0.22]$ to 0.22 mm^2 $[0.14;$

$0.51]$ respectively, translated to a percentage increase of: Δ $+68.37\%$ $[17.82; 171.17]$, ($p = 0.013$).

This dynamic biological behaviour of the vessel wall architecture is seemingly associated with the transient scaffolding properties of the ABSORB BVS, and warrants further observations of the evolving biologic processes manifesting at 3 years when the connective tissue replacing the bioresorbed polymeric strut begins to shrink, as previously shown in preclinical studies.

Incomplete stent apposition

Incomplete stent apposition (ISA) occurring with conventional metallic stents, either immediately post-implantation or as a late acquired phenomenon, has been implicated in late stent thrombosis (LST).²⁵ Additionally, the vascular healing with first generation DES (SES or PES) remains incomplete up to 5 years following implantation and is a potential mechanism of LST with an annual rate of 0.65% .⁹ A potential advantage of the bioresorbable technology over metallic devices is that any visible ISA post-implantation has the potential to resolve after the bioresorption process has been completed; furthermore, the phenomenon of incomplete healing may potentially not be an issue, as the device is expected to have disappeared after the time point of 2 years. Although these are hypothesis-generating concepts, large scale studies to confirm the probable lower incidence of device thrombosis with the use of the bioresorbable devices are eagerly expected and needed.

The challenges faced by the ABSORB BVS

The polymeric material as an implantation medium potentially has numerous advantages compared to metal, as previously discussed. The main challenges faced by the ABSORB BVS are its limited distensibility, and therefore its suitability for implantation in appropriately sized vessels. Consequently, at present QCA guidance is mandatory for implantation of the device.

Although the radial strength of the ABSORB BVS has been reported to be comparable to metallic stents, this is provided the BVS is deployed within the limits of its size. If the BVS is over-stretched beyond its designed limits, it has been shown to lose some of its radial strength and may possibly fracture. Much effort has been invested in improving its supportive properties, with the introduction of a new strut design

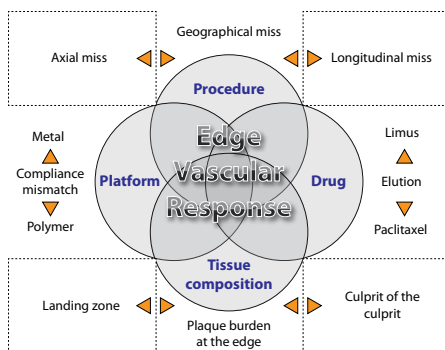


Figure 6. The edge vascular response as a consequence of iatrogenic, device-related and biologic factors.

in order to enhance the distensibility of the device whilst maintaining its radial strength, features which are expected in the next generation BVS.

In an anecdotal case from the ABSORB cohort A, a 3.0 mm scaffold was over expanded with a 3.5 mm balloon, which resulted in strut fracture as documented by OCT,²⁶ additionally, Ormiston et al recently illustrated the strut fracture of a post-dilated ABSORB BVS (24 Atm) with a non-compliant balloon (3.25 mm) to correct underlying malapposition. These clinical examples are proofs that although the technology has immense potential, it needs further improvements.

Conclusion

Bioresorbable technology is an alternative and challenging therapeutic approach for the treatment of coronary artery disease. Although the scenario of a dynamic device that “does the job and disappears”, leading to the restoration of vascular physiology, is here (“vascular reparative therapy”), this innovative and rapidly progressing technology is still in its infancy.

Acknowledgements

Dr. Gogas wishes to thank the Hellenic Cardiological Society, for the 2012-2013 research grant award, and the American College of Cardiology Foundation, for the ISCTR research award.

References

1. Grüntzig A. Transluminal dilatation of coronary-artery stenosis. *Lancet*. 1978; 1: 263.
2. Stefanadis CI. Stents for coronary artery disease: from covered to drug-eluting to bioabsorbable. *Hellenic J Cardiol*. 2012; 53: 89-90.
3. Serruys PW, de Jaegere P, Kiemeneij F, et al. A comparison of balloon-expandable-stent implantation with balloon angioplasty in patients with coronary artery disease. Benestent Study Group. *N Engl J Med*. 1994; 331: 489-495.
4. Morice MC, Serruys PW, Sousa JE, et al. A randomized comparison of a sirolimus-eluting stent with a standard stent for coronary revascularization. *N Engl J Med*. 2002; 346: 1773-1780.
5. Garg S, Serruys PW. Coronary stents: current status. *J Am Coll Cardiol*. 2010; 56: S1-42.
6. Garg S, Serruys PW. Coronary stents: looking forward. *J Am Coll Cardiol*. 2010; 56: S43-78.
7. Byrne RA, Eberle S, Kastrati A, et al. Distribution of angiographic measures of restenosis after drug-eluting stent implantation. *Heart*. 2009; 95: 1572-1578.
8. Sousa JE, Costa MA, Abizaid A, et al. Lack of neointimal proliferation after implantation of sirolimus-coated stents in human coronary arteries: a quantitative coronary angiography and three-dimensional intravascular ultrasound study. *Circulation*. 2001; 103: 192-195.
9. Räber L, Wohlwend L, Wigger M, et al. Five-year clinical and angiographic outcomes of a randomized comparison of sirolimus-eluting and paclitaxel-eluting stents: results of the Sirolimus-Eluting Versus Paclitaxel-Eluting Stents for Coronary Revascularization LATE trial. *Circulation*. 2011; 123: 2819-2828.
10. Ormiston JA, Serruys PW, Regar E, et al. A bioabsorbable everolimus-eluting coronary stent system for patients with single de-novo coronary artery lesions (ABSORB): a prospective open-label trial. *Lancet*. 2008; 371: 899-907.
11. Serruys PW, Ormiston JA, Onuma Y, et al. A bioabsorbable everolimus-eluting coronary stent system (ABSORB): 2-year outcomes and results from multiple imaging methods. *Lancet*. 2009; 373: 897-910.
12. Serruys PW, Onuma Y, Ormiston JA, et al. Evaluation of the second generation of a bioresorbable everolimus drug-eluting vascular scaffold for treatment of de novo coronary artery stenosis: six-month clinical and imaging outcomes. *Circulation*. 2010; 122: 2301-2312.
13. Onuma Y, Serruys PW, Perkins LE, et al. Intracoronary optical coherence tomography and histology at 1 month and 2, 3, and 4 years after implantation of everolimus-eluting bioresorbable vascular scaffolds in a porcine coronary artery model: an attempt to decipher the human optical coherence tomography images in the ABSORB trial. *Circulation*. 2010; 122: 2288-2300.
14. Gogas BD, Radu M, Onuma Y, et al. Evaluation with in vivo optical coherence tomography and histology of the vascular effects of the everolimus-eluting bioresorbable vascular scaffold at two years following implantation in a healthy porcine coronary artery model: implications of pilot results for future pre-clinical studies. *Int J Cardiovasc Imaging*. 2012; 28: 499-511.
15. Dudek D, Onuma Y, Ormiston JA, Thuesen L, Miquel-Hebert K, Serruys PW. Four-year clinical follow-up of the ABSORB everolimus-eluting bioresorbable vascular scaffold in patients with de novo coronary artery disease: the ABSORB trial. *EuroIntervention*. 2012; 7: 1060-1061.
16. Serruys PW, Ong AT, Piek JJ, et al. A randomized comparison of a durable polymer Everolimus-eluting stent with a bare metal coronary stent: The SPIRIT first trial. *EuroIntervention*. 2005; 1: 58-65.
17. Serruys PW, Onuma Y, Dudek D, et al. Evaluation of the second generation of a bioresorbable everolimus-eluting vascular scaffold for the treatment of de novo coronary artery stenosis: 12-month clinical and imaging outcomes. *J Am Coll Cardiol*. 2011; 58: 1578-1588.
18. Sarno G, Onuma Y, Garcia Garcia HM, et al. IVUS radiofrequency analysis in the evaluation of the polymeric struts of the bioabsorbable everolimus-eluting device during the bioabsorption process. *Catheter Cardiovasc Interv*. 2010; 75: 914-918.
19. Okamura T, Serruys PW, Regar E. Cardiovascular flashlight. The fate of bioresorbable struts located at a side branch ostium: serial three-dimensional optical coherence tomography assessment. *Eur Heart J*. 2010; 31: 2179.
20. Gogas BD, van Geuns RJ, Farooq V, et al. Three-dimensional reconstruction of the post-dilated ABSORB everolimus-eluting bioresorbable vascular scaffold in a true bifurcation lesion for flow restoration. *JACC Cardiovasc Interv*. 2011; 4:

- 1149-1150.
21. van Geuns RJ, Gogas BD, Farooq V, Regar E, Serruys PW. 3-Dimensional reconstruction of a bifurcation lesion with double wire after implantation of a second generation everolimus-eluting bioreabsorbable vascular scaffold. *Int J Cardiol.* 2011; 153: e43-45.
 22. Gomez-Lara J, Garcia-Garcia HM, Onuma Y, et al. A comparison of the conformability of everolimus-eluting bioreabsorbable vascular scaffolds to metal platform coronary stents. *JACC Cardiovasc Interv.* 2010; 3: 1190-1198.
 23. Albiero R, Nishida T, Adamian M, et al. Edge restenosis after implantation of high activity (32) P radioactive beta-emitting stents. *Circulation.* 2000; 101: 2454-2457.
 24. Gogas BD, Serruys PW, Diletti R, et al. Vascular response of the segments adjacent to the proximal and distal edges of the ABSORB everolimus eluting bioreabsorbable vascular scaffold: 6 months and 1 year follow-up assessment. *JACC Cardiovasc Interv.* 2012; 5: 656-665.
 25. Ozaki Y, Okumura M, Ismail TF, et al. The fate of incomplete stent apposition with drug-eluting stents: an optical coherence tomography-based natural history study. *Eur Heart J.* 2010; 31: 1470-1476.
 26. Onuma Y, Serruys PW, Ormiston JA, et al. Three-year results of clinical follow-up after a bioreabsorbable everolimus-eluting scaffold in patients with de novo coronary artery disease: the ABSORB trial. *EuroIntervention.* 2010; 6: 447-453.

Chapter 21

Agreement and Reproducibility of Gray-Scale Intravascular Ultrasound and Optical Coherence Tomography for the Analysis of the Bioresorbable Vascular Scaffold.

Josep Gómez-Lara, Salvatore Brugaletta, Roberto Diletti, **Bill D. Gogas**, Vasim Farooq, Yoshinobu Onuma, Pierre Gobbens, Gerrit Anne Van Es, Hector M. García-García, Patrick W. Serruys

Catheter Cardiovascular Interventions. 2012. May 1;79(6):890-902 [IF: 2.51]

Agreement and Reproducibility of Gray-Scale Intravascular Ultrasound and Optical Coherence Tomography for the Analysis of the Bioresorbable Vascular Scaffold

Josep Gómez-Lara,¹ MD, Salvatore Brugaletta,¹ MD, Roberto Diletti,¹ MD, Bill D. Gogas,¹ MD, Vasim Farooq,¹ MBChB, MRCP, Yoshinobu Onuma,¹ MD, Pierre Gobbens,² BSc, Gerrit Anne Van Es,² PhD, Hector M. García-García,^{1,2} MD, PhD, and Patrick W. Serruys,^{1*} MD, PhD

Objective: To report the agreement between gray-scale intravascular ultrasound (GS-IVUS) and optical coherence tomography (OCT) in assessing the bioresorbable vascular scaffolds (BVS) structures and their respective reproducibility. **Background:** BVS are composed of an erodible polymer. Ultrasound and light signals backscattered from polymeric material differs from metallic stents using GS-IVUS and OCT. **Methods:** Forty-five patients included in the ABSORB trial were treated with a 3.0 × 18 mm BVS and imaged with GS-IVUS 20 MHz and OCT post-implantation. Qualitative (ISA, side-branch struts, protrusion, and dissections) and quantitative (number of struts, lumen, and scaffold area) measurements were assessed by two investigators. The agreement and the inter- and intraobserver reproducibility were investigated using the kappa (κ) and the interclass correlation coefficient (ICC). **Results:** GS-IVUS and OCT agreement was predominantly poor at a lesion, frame, and strut level analysis (κ and ICC < 0.4) for qualitative measurements. GS-IVUS demonstrated a reduced ability to detect cross-sections with ISA (4.5% vs. 20.6%), side-branch (SB) struts (6.3% vs. 7.8%), protrusions (3.2% vs. 9.6%), and dissections (0.2% vs. 9.0%) compared with OCT. GS-IVUS reproducibility was poor-moderate (κ and ICC < 0.6) except for ISA and SB-struts (κ and ICC between 0.2 and 0.75). OCT showed an excellent reproducibility (κ and ICC > 0.75) except for the assessment of tissue protrusion (κ and ICC between 0.47 and 0.94). GS-IVUS reproducibility was poor-moderate (ICC \leq 0.5) in assessing the number of struts but excellent with OCT (ICC > 0.85). The reproducibility to assess lumen and scaffold areas was excellent using both techniques (ICC > 0.85). **Conclusions:** GS-IVUS has a poor capacity to detect qualitative findings post-BVS implantation and its reproducibility is low compared with OCT. The use of GS-IVUS should be limited when assessing lumen and scaffold areas. © 2011 Wiley Periodicals, Inc.

Key words: bioresorbable; agreement; reproducibility; intravascular ultrasound; optical coherence tomography

¹Department of Interventional Cardiology, Thoraxcentre, Erasmus Medical Center, Rotterdam, the Netherlands

²Cardialysis B.V., Core-laboratory, Rotterdam, the Netherlands

Conflict of interest: Nothing to report.

Grant sponsor: Biomedical Research Institute of Bellvitge (IDIBELL)

*Correspondence to: Patrick W. Serruys, MD, PhD, Department of Interventional Cardiology, Ba583a, Thoraxcenter, Erasmus MC, 's-Gravendijkwal 230, 3015 CE Rotterdam, The Netherlands. E-mail: p.w.j.c.serruys@erasmusmc.nl

Received 14 January 2011; Revision accepted 7 March 2011

DOI 10.1002/ccd.23108

Published online 30 November 2011 in Wiley Online Library (wileyonlinelibrary.com)

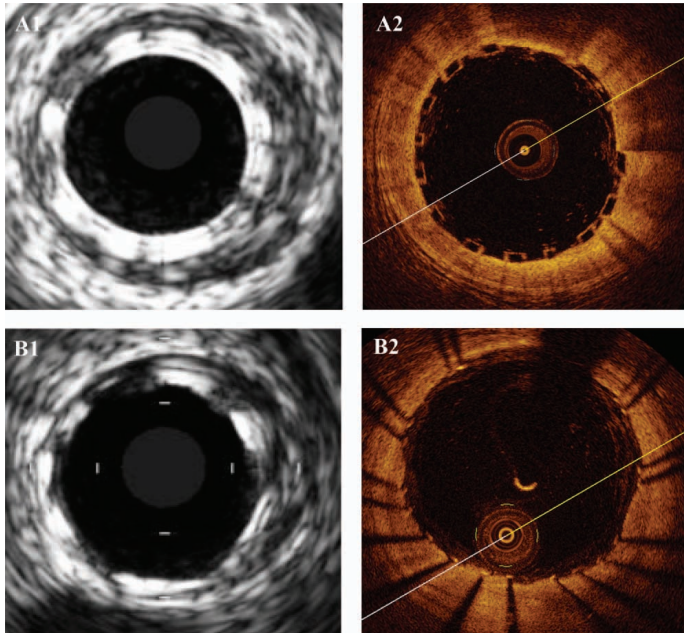


Fig. 1. GS-IVUS and OCT imaging of the bioresorbable scaffolds and metallic stents (A1) GS-IVUS image of a BVS; (A2) OCT image of a BVS; (B1) GS-IVUS image of a metallic stent; (B2) OCT image of a metallic stent. [Color figure can be viewed in the online issue, which is available at wileyonlinelibrary.com.]

INTRODUCTION

Bioresorbable vascular scaffolds (BVS) are a new generation of intravascular devices constructed of polymeric material. The ultrasonic and light wave beams from the gray-scale intravascular ultrasound (GS-IVUS) and optical coherence tomography (OCT) catheters are backscattered in different ways from the polymeric structures as compared with metallic structures. Consequently, GS-IVUS and OCT render the BVS structures differently compared with metallic stents [1,2]. GS-IVUS imaging, with a 20 MHz catheter, renders the polymeric struts as hyper-refractive boxes with an important echogenic blooming effect that confers a double strut appearance. The polymeric struts have an echogenic intensity similar to calcium tissue, but without acoustic shadowing behind the struts (Fig. 1). OCT shows the polymeric struts as a black central core surrounded by a light-scattering frame. The four sides of the polymeric struts are clearly visible without the typical shadowing observed behind metallic structures (Fig. 1).

The GS-IVUS and OCT agreement and their respective inter- and intraobserver reproducibility to assess qualitative and quantitative findings immediately after BVS implantation remain unknown. The aim of our study is to report the agreement of GS-IVUS and OCT in assessing qualitative and quantitative BVS findings post-implantation and to assess their inter- and intraobserver reproducibility.

MATERIALS AND METHODS

Population

The ABSORB Cohort B trial is a non-randomized, multicenter, single arm, efficacy-safety study. The study design has been previously reported [3]. In brief, patients were eligible when aged 18 years or older and were diagnosed with stable, unstable, or silent ischemia. Patients with a stenosis of the left main or ostial right coronary artery, presence of angiographic intracoronary thrombus, heavy calcification, excessive tortuosity, and with lesions involving a side

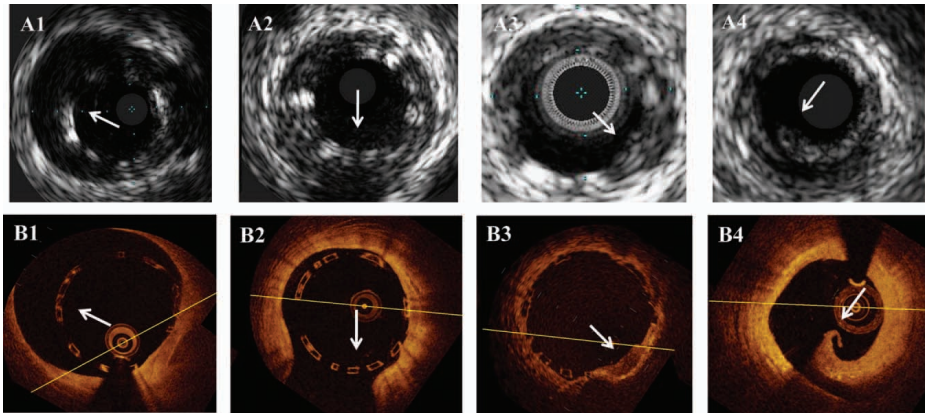


Fig. 2. GS-IVUS and OCT assessment of qualitative findings. Matched images between GS-IVUS (A) and OCT (B) of: (1) incomplete strut/scaffold apposition; (2) side-branch struts; (3) tissue protrusion; and (4) edge dissection. [Color figure can be viewed in the online issue, which is available at wileyonlinelibrary.com.]

branch >2 mm were excluded. All patients were treated with a single size 3.0×18 mm BVS.

At baseline, GS-IVUS 20 MHz imaging was performed in all patients. OCT imaging was performed in selected centers as an optional additional investigation. Both imaging techniques were performed after the last dilatation of the BVS. The present study included only those patients imaged simultaneously with GS-IVUS and OCT immediately after BVS deployment.

Study Device

The BVS balloon expandable device (Abbott Vascular, Santa Clara, CA) consists of a polymer backbone of poly-L lactide coated with a thin layer of a 1:1 mixture of poly-D, L-lactide polymer, and the anti-proliferative drug everolimus. The strut thickness is $150 \mu\text{m}$. The implant is radiolucent, but has two platinum markers at each end that allow easy visualization on angiography and other imaging modalities.

GS-IVUS 20 MHz Acquisition

GS-IVUS acquisition was performed with the Eagle Eye 20 MHz catheter (Volcano Corporation, Rancho Cordova, CA). The acquisition was performed according to standard procedures [4]. After intracoronary nitroglycerin injection, the catheter probe was advanced distally to the lesion. Using an automated pullback device, the transducer was withdrawn at a continuous speed of 0.5 mm/sec. The image data were stored on DVD for offline analysis.

OCT Acquisition

OCT imaging was performed using two different OCT systems (M3 Time-Domain System and C7XR Fourier-Domain System; LightLab Imaging, Westford, MA). The M3 OCT system uses a standard intracoronary guide wire to cross the target lesion. This conventional wire was subsequently exchanged for the Light Lab Image wire using a single or double lumen intracoronary catheter. Pullback was performed during continuous injection of contrast medium ($1\text{--}3$ ml/sec; Iodixanol 370, Visipaque, GE Health Care, Cork, Ireland) through the guide catheter with an injection pump. The automated pullback was performed at 3 mm/sec with a frame rate of 20 images/sec.

The C7XR system uses a conventional wire to cross the segment of interest. The OCT imaging catheter (RX ImageWire II; LightLab Imaging, Westford, MA) was then advanced distally to the treated region. The pullback was performed during a continuous injection of 3 ml/sec of contrast medium (Iodixanol 370, Visipaque, GE Health Care, Cork, Ireland) injected at a maximum pressure of 300 psi through the guiding catheter with an injection pump. In these cases, the automated pullback rate was 20 mm/sec and the frame rate was 100 images/sec.

GS-IVUS and OCT Definitions and Analysis

GS-IVUS and OCT analyses were performed by two experienced analysts. Taking into account the acquisition frame rate and the pullback speed, both GS-IVUS and OCT were analyzed at intervals of 1 mm within the scaffold and 5 mm proximal and distal to the

scaffold edges whenever possible. The first cross-section of the corresponding pullbacks with struts observed in the four quadrants of the lumen perimeter was used as a landmark to establish the scaffold length. Two analysts investigated the same cross-sections and one investigator repeated the same measurements 1 month later. GS-IVUS analysis was performed using the Q-GS-IVUS 2.0 software analysis (Medis, Leiden, the Netherlands). OCT analysis was performed with the proprietary software for offline analysis (LightLab Imaging, Westford, MA). The selected cross-sections were investigated to assess the following.

Number of struts. Using GS-IVUS, the polymeric struts were defined as independent, hyper-echogenic,

TABLE I. Baseline Clinical and Angiographic Characteristics (n = 45 Patients)

	n (%)
Males	32 (71.1)
Age (years)	61.5 ± 10.3
Hypertension	28 (62.2)
Hypercholesterolemia	39 (86.7)
Diabetes mellitus	4 (8.9)
Smokers	11 (24.4)
Previous myocardial infarction	13 (28.9)
Previous coronary revascularization	9 (20.0)
Clinical indication:	
Stable angina	39 (86.7)
Acute coronary syndrome	6 (13.3)
Culprit vessel:	
Left anterior descending	24 (53.3)
Left circumflex	9 (20.0)
Right coronary artery	12 (26.7)
Number of vessels disease:	
One	39 (86.7)
Two	6 (13.3)
Three	0

and double-box shapes without echogenic shadow behind. Using OCT, the polymeric struts were assessed as box-shape light-scattering frames delimiting a black central core (Fig. 1) [1].

Number of malapposed struts. ISA was defined when the abluminal side of the polymeric strut was

TABLE II. Qualitative Agreement Between OCT and IVUS 20 MHz (Lesion Level Analysis) (n = 46 Lesions)

IVUS	OCT				Accuracy of IVUS with respect to OCT (%)
	No	Yes	Total	Kappa	
20 MHz					
Proximal dissection					
No	30	9	39	NA	Se = 0
Yes	0	0	0		Sp = 100
Total	30	9	39		Eff = 77
Distal dissection					
No	28	8	36	0.16	Se = 11
Yes	0	1	1		Sp = 100
Total	28	9	37		Eff = 78
Dissection within BVS					
No	20	25	45	0.03	Se = 4
Yes	0	1	1		Sp = 100
Total	20	26	46		Eff = 46
ISA					
No	6	21	27	0.15	Se = 46
Yes	1	18	19		Sp = 86
Total	7	39	46		Eff = 52
SB struts					
No	10	13	23	0.26	Se = 59
Yes	4	19	23		Sp = 71
Total	14	32	46		Eff = 63
Tissue protrusion					
No	17	22	39	0.00	Se = 15
Yes	3	4	7		Sp = 85
Total	20	26	46		Eff = 46

ISA, incomplete scaffold/strut apposition; SB, side-branch; NA, not applicable; Se, sensitivity; Sp, specificity; Eff, efficiency.

TABLE III. Interobserver Agreement Between OCT and IVUS 20 MHz (Frame and Strut Level Analysis)

	IVUS	OCT	Absolute difference, % (CI 95%)	ICCc (CI 95%)	ICCa (CI 95%)
Frame level					
Frames with ISA, n	37	181	-16.05 (-21.72--10.39)	0.27 (-0.02-0.52)	0.18 (-0.07-0.42)
% Frames with ISA per lesion, mean (SD)	4.5 (7.7)	20.6 (20.9)			
Frames with SB struts, n	57	69	-1.48 (-4.15-1.19)	0.26 (-0.03-0.51)	0.26 (-0.02-0.51)
% Frames with SB struts per lesion, mean (SD)	6.3 (8.3)	7.8 (6.4)			
Frames with tissue protrusion, n	10	69	-6.47 (-9.29--3.66)	0.12 (-0.17-0.39)	0.09 (-0.12-0.31)
% Frames with tissue protrusion per lesion, mean (SD)	1.2 (3.2)	7.7 (9.6)			
Frames with Dissection (within BVS), n	1	79	-8.87 (-12.44--5.29)	0.06 (-0.23-0.34)	0.04 (-0.14-0.25)
% Frames with dissection per lesion, mean (SD)	0.2 (1.1)	9.0 (12.4)			
Strut level					
Struts with ISA, n	74	348	-4.23 (-6.35--2.10)	0.37 (0.09-0.59)	0.31 (0.02-0.54)
% ISA struts per lesion, mean (SD)	1.3 (4.0)	5.5 (8.1)			
Struts at SB, n	84	77	0.12 (-0.49-0.73)	0.18 (-0.11-0.45)	0.19 (-0.11-0.45)
% SB struts per lesion, mean (SD)	1.3 (1.9)	1.2 (1.2)			

ISA, incomplete scaffold/strut apposition; SB, side-branch; ICC, inter-class correlation coefficient; CI, confidence interval.

TABLE IV. Inter and Intra-Observer Reproducibility of IVUS 20 MHz and OCT (Lesion Level)

<i>n</i> = 46 Lesions			Observer A				Observer B (observation 2)				
			No	Yes	Total	Interobserver agreement (Kappa)	No	Yes	Total	Intraobserver agreement (Kappa)	
IVUS 20 MHz	Observer B (observation 1)	Proximal dissection	No	41	2	43	NA	42	1	43	NA
			Yes	0	0	0		0	0	0	
			Total	41	2	43		42	1	43	
		Distal dissection	No	35	3	38	0.37	38	0	38	1.00
			Yes	0	1	1		0	1	1	
			Total	35	4	39		38	1	39	
		Dissection within BVS	No	38	7	45	-0.04	42	3	45	0.38
			Yes	1	0	1		0	1	1	
			Total	39	7	46		42	4	46	
		ISA	No	26	1	27	0.47	20	7	27	0.47
			Yes	10	9	19		5	14	19	
			Total	36	10	46		25	21	46	
		SB struts	No	20	3	23	0.48	20	3	23	0.61
			Yes	9	14	23		6	17	23	
			Total	29	17	46		26	20	46	
		Tissue protrusion	No	29	5	34	0.02	26	2	28	0.23
			Yes	10	2	12		13	5	18	
			Total	39	7	46		38	7	46	
OCT	Observer B (observation 1)	Proximal dissection	No	32	0	32	1.00	32	0	32	1.00
			Yes	0	9	9		0	9	9	
			Total	32	9	41		32	9	41	
		Distal dissection	No	30	1	31	0.94	31	0	31	1.00
			Yes	0	10	10		0	10	10	
			Total	30	11	41		31	10	41	
		Dissection within BVS	No	16	4	20	0.76	19	1	20	0.96
			Yes	1	25	26		0	26	26	
			Total	17	29	46		19	27	46	
		ISA	No	7	0	7	0.85	7	0	7	1.00
			Yes	2	37	39		0	39	39	
			Total	7	37	46		7	39	46	
		SB struts	No	12	2	14	0.89	14	0	14	1.00
			Yes	0	32	32		0	32	32	
			Total	12	34	46		14	32	46	
		Tissue protrusion	No	16	4	20	0.73	18	2	20	0.91
			Yes	2	24	26		0	26	26	
			Total	18	28	46		18	28	46	

ISA, incomplete scaffold/strut apposition; SB, side-branch; NA, not applicable.

clearly separated from the vessel wall in the absence of a side branch [4] (Fig. 2).

Number of side-branch struts. Side-branches were assessed longitudinally and in the immediately proximal and distal 2D cross-sections. Whenever the polymeric struts were not in contact with the vessel wall at the site of the take-off of the side-branch, they were classified as side-branch struts (Fig. 2).

Tissue protrusion. Tissue protrusion was defined as when convex-shaped tissue protruded between the endoluminal sides of adjacent struts and extended within the lumen as a circular arc connecting the adjacent struts [5,6] (Fig. 2).

In-BVS, proximal and distal dissections. Dissections were defined when a disruption of the luminal vessel surface with an overhanging flap within the lumen

was observed within the BVS segment or at 5 mm proximal or distal to the scaffold edges [6] (Fig. 2).

Lumen and scaffold area. Using GS-IVUS, the lumen area was drawn following the endoluminal vessel wall contour. GS-IVUS-derived scaffold area was drawn following the endoluminal side of the polymeric struts. Using OCT, in contrast, the lumen area was defined behind the polymeric struts following the endoluminal vessel contour and the scaffold area was drawn following the abluminal side of the polymeric struts.

Statistical Analysis

Discrete variables are presented as counts and percentages. Continuous variables are presented as means \pm SD. Because of the clustered nature of the GS-IVUS

TABLE V. Interobserver Reproducibility of IVUS 20 MHz and OCT (Frame and Strut Level Analysis)

			Observer A	Observer B	Margin of error of the 95% CI of the absolute difference (%)	ICCc (CI 95%)	ICCa (CI 95%)
IVUS 20 MHz	Frame level (892 cross- sections)	Frames with ISA, <i>n</i>	37	45	7.32	0.21 (-0.08-0.47)	0.22 (-0.08-0.48)
		% Frames with ISA, mean (SD)	4.5 (7.7)	5.2 (1.5)			
		Frames with SB struts, <i>n</i>	57	43	4.68	0.53 (0.28-0.71)	0.52 (0.28-0.70)
		% Frames with SB struts, mean (SD)	6.3 (8.3)	4.9 (7.8)			
		Frames with protrusion, <i>n</i>	10	54	6.28	-0.05 (-0.33-0.25)	-0.05 (-0.33-0.24)
	% Frames with tissue protrusion, mean (SD)	1.2 (3.2)	6.2 (10.9)				
	Frames with dissection (within BVS), <i>n</i>	1	7	1.24	0.15 (-0.14-0.43)	0.13 (-0.12-0.38)	
	% Frames with dissection, mean (SD)	0.2 (1.1)	0.7 (1.7)				
	Strut level (6313 struts)	Struts with ISA, <i>n</i>	74	65	1.50	0.72 (0.54-0.83)	0.84 (0.71-0.91)
		% ISA struts, mean (SD)	1.3 (4.0)	1.0 (2.6)			
Struts at SB, <i>n</i>		84	85	1.28	0.44 (0.18-0.65)	0.45 (0.18-0.65)	
OCT	Frame level (888 cross- sections)	% SB struts, mean (SD)	1.3 (1.9)	1.2 (2.2)			
		Frames with ISA, <i>n</i>	181	175	4.57	0.93 (0.88-0.96)	0.93 (0.88-0.96)
		% Frames with ISA, mean (SD)	20.6 (20.9)	19.8 (20.4)			
		Frames with SB struts, <i>n</i>	69	67	1.96	0.86 (0.76-0.92)	0.86 (0.76-0.92)
		% Frames with SB struts, mean (SD)	7.8 (6.4)	7.6 (6.0)			
	Frames with tissue, <i>n</i>	69	87	6.21	0.48 (0.22-0.67)	0.47 (0.22-0.67)	
	% Frames with tissue protrusion, mean (SD)	7.7 (9.6)	9.8 (10.8)				
	Frames with dissection (within BVS), <i>n</i>	79	109	4.16	0.86 (0.76-0.92)	0.83 (0.67-0.91)	
	% Frames with dissection, mean (SD)	9.0 (12.4)	12.4 (13.9)				
	Strut level (6452 struts)	Struts with ISA, <i>n</i>	348	315	1.15	0.99 (0.97-0.99)	0.98 (0.97-0.99)
% ISA struts, mean (SD)		5.5 (8.1)	5.0 (7.3)				
Struts at SB, <i>n</i>		77	82	0.15	0.78 (0.63-0.87)	0.78 (0.63-0.87)	
% SB struts, mean (SD)	1.2 (1.2)	1.3 (1.1)					

ISA, incomplete scaffold/strut apposition; SB, side-branch; ICC, inter-class correlation coefficient; ICCc, ICC for concordance; ICCa, ICC absolute agreement; CI, confidence interval.

and OCT data at different levels of dependence (strut, cross-sections, lesions, and patients) and the lack of correlation between GS-IVUS and OCT cross-sections, all qualitative measurements have been adjusted at a lesion level dividing the number of observations by the total amount of frames/struts in each lesion. Quantitative measurements to assess the inter- and intraobserver reproducibility are presented at cross-section level analysis.

The GS-IVUS and OCT agreement at lesion level analysis were estimated by the Cohen's κ (kappa) test for concordance [7]. According to previous publications: <0 indicates poor agreement, 0-0.20 indicates slight agreement, 0.21-0.40 indicates fair agreement, 0.41-0.60 indicates moderate agreement, 0.61-0.80 indicates good agreement, and 0.81-1.0 indicates excellent agreement [8]. Because of the higher reproducibility and the higher resolution of OCT when com-

pared with GS-IVUS, we have estimated the sensitivity, specificity, and global efficiency of GS-IVUS 20 MHz with respect to the OCT (as reference). The GS-IVUS and OCT agreement of qualitative measurements at frame and strut level were estimated with the inter-class correlation coefficient (ICC) for concordance (ICCc) and absolute agreement (ICCa). An ICC <0.4 indicates bad agreement, an ICC between 0.4 and 0.75 indicates moderate agreement, and ICC values >0.75 indicates excellent agreement [9].

The inter- and intraobserver reproducibility of qualitative measurements was assessed using the kappa value and the ICC as previously explained. The absolute differences between the percentages of qualitative findings (at lesion level) between observers/observations were estimated for each variable. Bland-Altman plots were drawn for the percentage of malapposed

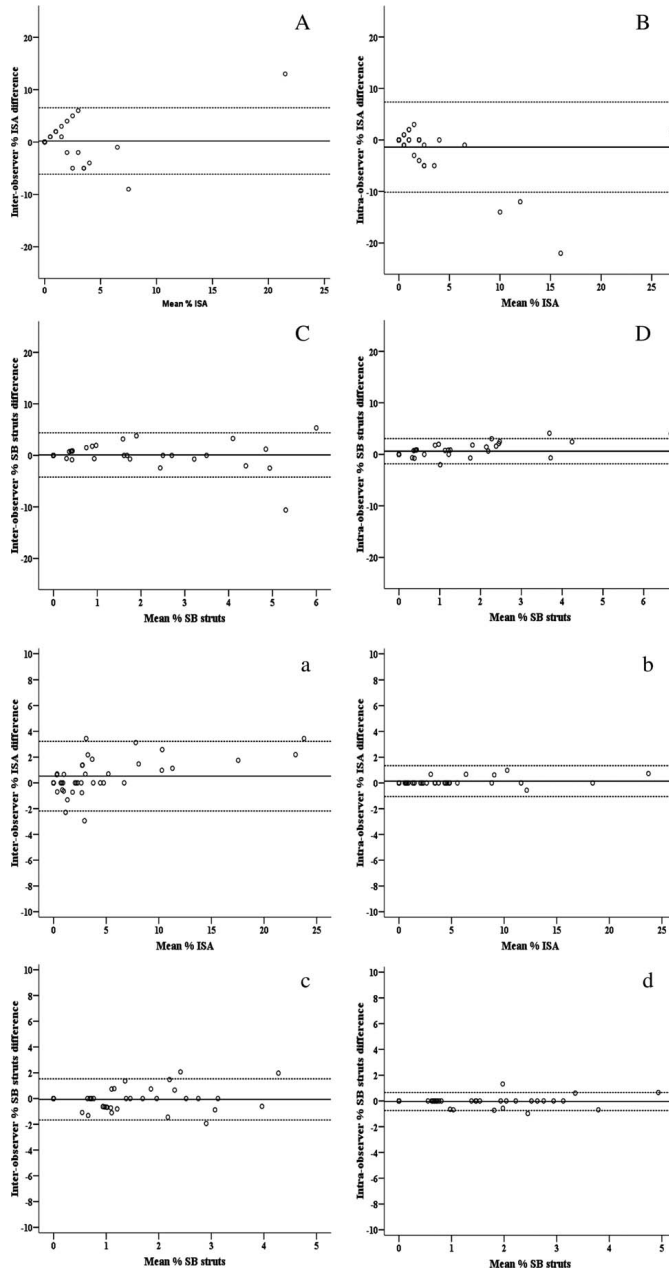


Fig. 3. Inter-observer reproducibility of GS-IVUS (A) and OCT (a) to assess incomplete strut apposition (ISA); Intra-observer reproducibility of GS-IVUS (B) and OCT (b) to assess ISA; Inter-observer reproducibility of GS-IVUS (C) and OCT (c) to assess side-branch (SB) struts; Intra-observer reproducibility of GS-IVUS (D) and OCT (d) to assess SB-struts.

struts and SB-struts at lesion level analysis [10]. Inter- and intraobserver reproducibility of GS-IVUS and OCT to assess quantitative measurements (number of struts, lumen, and scaffold area) were performed in 150 randomly selected cross-sections in 15 patients. Bland-Altman plots were drawn for these quantitative parameters at frame level analysis. Because of the lack of matching images between GS-IVUS and OCT, the agreement of both techniques to assess the number of struts and lumen and scaffold areas were not performed.

RESULTS

Population Characteristics

The ABSORB Cohort B trial included 102 lesions in 101 patients. A total of 48 lesions in 47 patients were imaged with both GS-IVUS 20 MHz and OCT immediately after the BVS implantation. Two cases were excluded due to lack of complete recording of the BVS length by OCT. Therefore, 46 lesions and 45 patients were included in the present study. A total of 892 and 888 cross-sections and 6,313 and 6,452 struts were analyzed with GS-IVUS 20 MHz and OCT, respectively.

The baseline clinical and angiographic characteristics are shown in Table I. In general, patients were predominantly males (71%), had hypercholesterolemia (87%), and were treated due to stable angina (87%).

OCT and GS-IVUS Agreement of Qualitative Measurements

Agreement of qualitative measurements between GS-IVUS and OCT at lesion level analysis are shown in Table II. The agreement between GS-IVUS and OCT to assess scaffolds with at least one cross-section with ISA, tissue protrusion, and dissections were slight. Assessment of at least one cross-section with SB struts showed fair agreement between both techniques. Sensitivity and global efficiency of GS-IVUS analysis were extremely low in all parameters compared with OCT (as reference), but GS-IVUS specificity was moderate to high.

Qualitative agreement of both GS-IVUS and OCT at frame and strut level analysis are shown in Table III. By OCT, a higher number of cross-sections with ISA, SB-struts, tissue protrusions, and dissections were detected compared with GS-IVUS. Moreover, the agreement of both techniques to assess these parameters at a frame level analysis was poor. At a strut level analysis, the agreement of GS-IVUS and OCT was also poor in detecting ISA and SB-struts.

GS-IVUS Reproducibility of Qualitative Measurements

The inter- and intraobserver reproducibility of GS-IVUS 20 MHz to assess qualitative findings at a lesion level analysis is shown in Table IV. Interobserver reproducibility to assess tissue protrusion and dissections within the scaffold length was poor to slight. Distal dissections demonstrated a fair reproducibility and ISA and SB-struts had moderate agreement. Intraobserver reproducibility was fair for tissue protrusion and dissections within the scaffold length. Detection of scaffolds with ISA or SB-struts had moderate and good agreement. Intraobserver reproducibility of distal edge dissections was excellent.

Inter- and intraobserver reproducibility of GS-IVUS 20 MHz at frame and strut level analysis are shown in Tables V and VII. Inter- and intraobserver reproducibility of GS-IVUS 20 MHz to assess cross-sections with tissue protrusion and dissection within the BVS were bad. Inter- and intraobserver reproducibility to assess cross-sections with ISA or SB-struts was poor to moderate. At strut level analysis, the inter- and intraobserver reproducibility of GS-IVUS 20 MHz was moderate to excellent. The Bland-Altman plots of GS-IVUS inter- and intraobserver reproducibility to assess percentage of ISA and SB struts are shown in Fig. 3.

OCT Reproducibility of Qualitative Measurements

The inter- and intraobserver reproducibility of OCT to assess qualitative findings at lesion level analysis is shown in Table IV. Inter- and intraobserver reproducibility to assess scaffolds with at least one cross-section with dissection, ISA, SB-struts, tissue protrusion, and thrombus was excellent except for the interobserver reproducibility of tissue protrusion (moderate).

Inter- and intraobserver reproducibility at a frame and a strut level analysis are shown in Tables V and VI. Inter- and intraobserver reproducibility of OCT was excellent for all parameters except the interobserver reproducibility of frames with tissue protrusion (moderate). The Bland-Altman plots of OCT inter- and intraobserver reproducibility to assess the percentage of ISA and SB struts are shown in Fig. 3.

GS-IVUS and OCT Reproducibility of Quantitative Measurements

GS-IVUS and OCT inter- and intraobserver reproducibility of quantitative measures are shown in Table VII. Assessment of number of struts per cross-section had poor to moderate inter- and intraobserver reproducibility with GS-IVUS-20 MHz and excellent with OCT. Lumen and scaffold areas showed excellent reproducibility with both

TABLE VI. Intraobserver Reproducibility of IVUS 20 MHz and OCT (Frame and Strut Level Analysis)

			Observation 1	Observation 2	Margin of error of the 95% CI of the absolute difference (%)	ICCc (CI 95%)	ICCa (CI 95%)
IVUS 20 MHz	Frame level (892 cross- sections)	Frames with ISA, <i>n</i>	37	61	5.13	0.59 (0.37–0.75)	0.58 (0.35–0.74)
		% Frames with ISA, mean (SD)	4.5 (7.7)	7.1 (11.1)			
		Frames with SB struts, <i>n</i>	57	36	3.17	0.71 (0.53–0.83)	0.68 (0.46–0.82)
		% Frames with SB struts, mean (SD)	6.3 (8.3)	4.0 (5.4)			
		Frames with protrusion, <i>n</i>	10	19	3.19	0.15 (–0.14–0.43)	0.13 (–0.12–0.38)
		% Frames with tissue protrusion, mean (SD)	1.2 (3.2)	2.2 (4.2)			
	Strut level (6313 struts)	Frames with dissection (within BVS), <i>n</i>	1	6	3.17	–0.05 (–0.33–0.24)	–0.05 (–0.33–0.24)
		% Frames with dissection, mean (SD)	0.2 (1.1)	0.66 (2.3)			
		Struts with ISA, <i>n</i>	74	128	1.71	0.79 (0.65–0.88)	0.77 (0.62–0.87)
		% ISA struts, mean (SD)	1.3 (4.0)	2.2 (4.8)			
		Struts at SB, <i>n</i>	84	47	0.72	0.69 (0.50–0.82)	0.65 (0.39–0.80)
		% SB struts, mean (SD)	1.3 (1.9)	0.70 (1.1)			
OCT	Frame level (888 cross- sections)	Frames with ISA, <i>n</i>	181	181	0	1.00 (1.00–1.00)	1.00 (1.00–1.00)
		% Frames with ISA, mean (SD)	20.6 (20.9)	20.6 (20.9)			
		Frames with SB struts, <i>n</i>	69	69	0	1.00 (1.00–1.00)	1.00 (1.00–1.00)
		% Frames with SB struts, mean (SD)	7.80 (6.4)	7.80 (6.4)			
		Frames with protrusion, <i>n</i>	69	73	0.95	0.94 (0.90–0.97)	0.94 (0.90–0.97)
		% Frames with tissue protrusion, mean (SD)	7.7 (9.6)	8.2 (9.1)			
	Strut level (6452 struts)	Frames with dissection (within BVS), <i>n</i>	79	66	3.17	0.88 (0.80–0.93)	0.88 (0.79–0.93)
		% Frames with dissection, mean (SD)	9.0 (12.4)	7.5 (9.7)			
		Struts with ISA, <i>n</i>	348	340	0.36	1.00 (0.99–1.00)	1.00 (0.99–1.00)
		% ISA struts, mean (SD)	5.5 (8.1)	5.4 (7.8)			
		Struts at SB, <i>n</i>	77	79	0.21	0.96 (0.93–0.98)	0.96 (0.93–0.98)
		% SB struts, mean (SD)	1.2 (1.2)	1.2 (1.2)			

Data are expressed in mean (SD).

ICC, inter-class correlation coefficient; ICCc, ICC for concordance; ICc, ICC absolute agreement; CI, confidence interval.

GS-IVUS and OCT. Bland-Altman plots of the inter- and intraobserver reproducibility to assess number of struts, lumen area, and scaffold area are shown in Fig. 4.

DISCUSSION

The main results of our study are follows: (1) The agreement of GS-IVUS and OCT to assess qualitative scaffold parameters immediately after the BVS implantation was predominantly poor at lesion, frame, and strut level analysis; (2) OCT demonstrated a higher ability to detect ISA, SB-struts, tissue protrusion, and dissections compared with GS-IVUS; (3) Inter- and intraobserver reproducibility to assess qualitative findings and number of struts per cross-section was poor to moderate with GS-IVUS and excellent with OCT; (4) Lumen and scaffold areas had an excellent inter- and intraobserver reproducibility with both GS-IVUS and

OCT; but GS-IVUS showed a margin of error (2 SD of the difference between observers/observations) larger than OCT in all measurements.

Intravascular imaging techniques are usually compared according to their spatial resolution. The spatial resolution can be defined as the ability to discriminate small objects in the axial and lateral plans [4]. The axial and lateral resolution of the IVUS 20 MHz systems is 80 and 200–250 μm , respectively [4]. OCT has an axial and lateral resolution of 15–20 and 20–40 μm , respectively [11]. The larger wavelength of the IVUS beam (35–80 μm), compared with the near-infrared light beam of the OCT (1 μm), allows higher tissue penetration and scan diameters but has less spatial resolution [11]. This fact explains the higher accuracy of OCT to detect ISA, tissue protrusion and dissections compared with GS-IVUS in metallic stents [5].

Using polymeric scaffolds, the larger echogenic blooming effect of the polymeric struts compared with the metallic stents challenges even more the assessment of the BVS structures with GS-IVUS 20 MHz; especially when the vessel wall is rich in calcium tissue or the plaque is hyperechogenic. It is uncertain if the visualization of the BVS structures with a high frequency IVUS system (≥ 30 MHz) would improve the assessment and reproducibility of these parameters. High frequency IVUS systems have previously been shown to demonstrate a better image quality when compared with low frequency IVUS (e.g. 20 MHz) [12]. In the ABSORB trial, it was decided to use the IVUS 20 MHz system to add information about compositional changes on top of the geometrical quantification provided by GS-IVUS. As of present, the IVUS 20 MHz Eagle Eye catheter (Volcano Corporation, Rancho Cordova, CA) has been the only system validated for tissue characterization (virtual histology) in native coronary vessels [13]. However, the use of IVUS-virtual histology to assess temporal changes in scaffolded segments has not yet been validated and may suffer from the same problems of saturation/high backscattering and poor resolution as GS-IVUS images.

Although the sensitivity and efficiency of GS-IVUS to assess qualitative findings at a frame or a strut level analysis was low compared with OCT, the specificity of GS-IVUS to assess qualitative findings at a lesion level analysis was high (Table II). The good specificity of GS-IVUS was probably due to the capability to detect the more severe cases of dissections, tissue protrusion, and ISA without false positive observations. On the other hand, the low sensitivity of GS-IVUS was probably due to the omission of the “less severe” cases when the lower resolution of the GS-IVUS did not allow the visualization of these findings (e.g. malapposed struts separated from the vessel wall by less than 200 μm). The assessment of tissue coverage with GS-IVUS presented similar results to our study; GS-IVUS was less able to assess a few degrees of neointimal coverage compared with OCT [14,15]. On the other hand, the assessment of SB struts is a special case in which the take-off of the side branch is usually easily observed by GS-IVUS. In our study, the assessment of SB struts showed better alignment between GS-IVUS and OCT at a lesion and a frame level analysis than the other qualitative findings.

However, the poor to moderate inter- and intraobserver reproducibility of GS-IVUS 20 MHz qualitative measurements represent a clear limitation of the use of this imaging technique. Only the ISA and SB-strut assessment at a strut level analysis showed good reproducibility. However, the comparison of the GS-IVUS

TABLE VII. Inter- and Intraobserver Variability of Quantitative Measurements of IVUS and OCT

IVUS	Cross-sections	$n = 150$	Interobserver variability						Intra-observer variability			
			Observer A	Observer B (1st)	Observer B (2nd)	Absolute difference (95% CI)	ICCc	ICCa	Absolute difference (95% CI)	ICCc	ICCa	
IVUS	No. of struts, n	906	1097	1070								
	struts \times frame, mean (SD)	6.71 (2.05)	8.13 (2.28)	7.93 (2.50)	-1.41 (-1.92--0.91)	0.06 (-0.11--0.23)	0.05 (-0.09--0.20)	0.20 (-0.21--0.61)	0.50 (0.36--0.62)	0.50 (0.36--0.62)		
	Lumen area (mm^2)	6.15 (1.59)	6.24 (1.48)	6.42 (1.53)	-0.09 (-0.17 to 0.00)	0.94 (0.92--0.96)	0.94 (0.92--0.96)	-0.19 (-0.24--0.13)	0.97 (0.96--0.98)	0.97 (0.96--0.98)	0.97 (0.93--0.98)	
OCT	Scaffold area (mm^2)	6.82 (1.77)	6.24 (1.47)	6.33 (1.51)	0.58 (0.49--0.67)	0.94 (0.92--0.96)	0.88 (0.42--0.96)	-0.09 (-0.14--0.04)	0.98 (0.97--0.98)	0.98 (0.96--0.98)	0.98 (0.96--0.98)	
	No. of struts, n	1052	1020	1017	0.11 (-0.10--0.32)	0.87 (0.82--0.90)	0.87 (0.82--0.90)	-0.02 (-0.19--0.14)	0.92 (0.88--0.94)	0.92 (0.88--0.94)		
	struts \times frame, mean (SD)	7.64 (2.44)	7.53 (2.40)	7.56 (2.33)	-0.29 (-0.33--0.26)	0.99 (0.99--0.99)	0.98 (0.63--0.99)	0.17 (0.14--0.21)	0.99 (0.99--0.99)	0.99 (0.95--1.00)	0.99 (0.98--0.99)	
	Scaffold area (mm^2)	6.86 (1.76)	7.15 (1.81)	6.98 (1.77)	0.14 (0.10--0.19)	0.99 (0.98--0.99)	0.98 (0.97--0.99)	-0.03 (-0.07--0.02)	0.99 (0.98--0.99)	0.99 (0.98--0.99)	0.99 (0.98--0.99)	

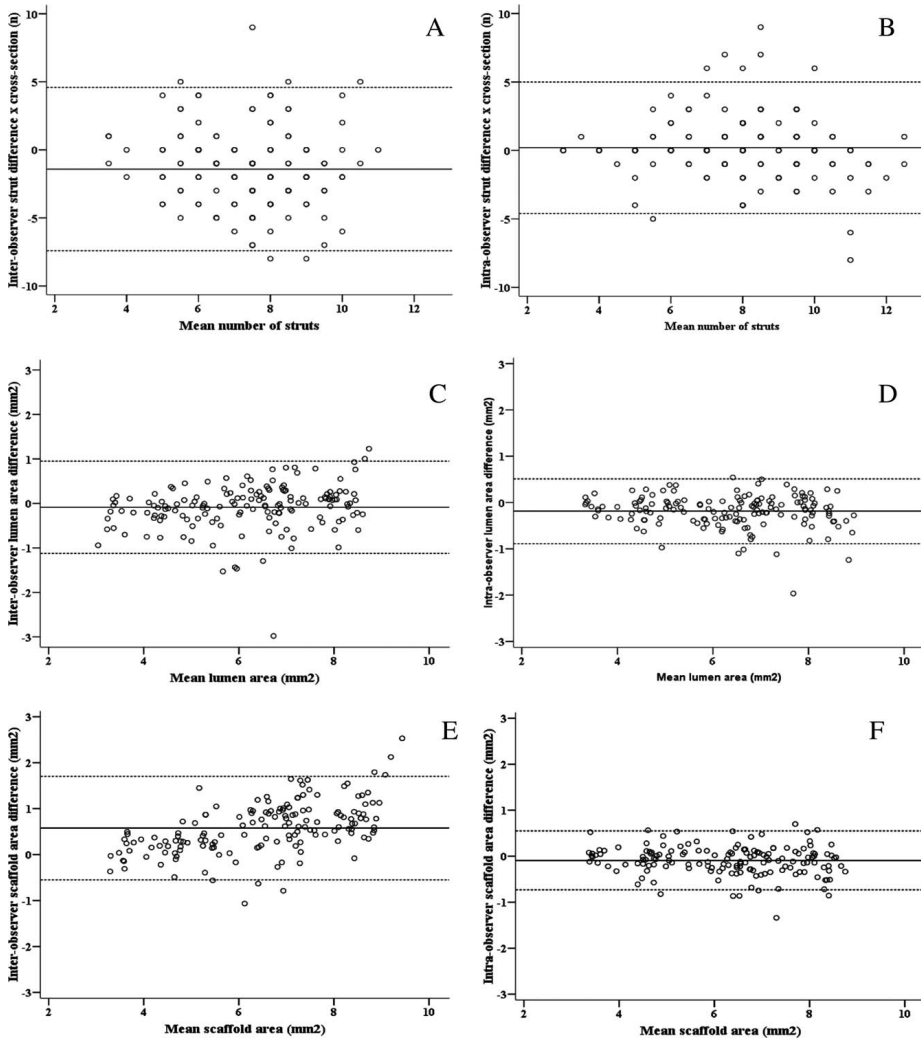


Fig. 4. Bland-Altman graphs of the inter- and intra-observer reproducibility of GS-IVUS and OCT to assess the number of struts, lumen area and scaffold area at cross-frame level. Inter-observer reproducibility of GS-IVUS (A) and OCT (a) to assess number of struts per cross-section; Intra-observer reproducibility of IVUS-GS (B) and OCT (b) to assess number of

struts per cross-section; Inter-observer reproducibility of GS-IVUS (C) and OCT (c) to assess the lumen area; Intra-observer reproducibility of GS-IVUS (D) and OCT (d) to assess the lumen area; Inter-observer reproducibility of GS-IVUS (E) and OCT (e) to assess the scaffold area; Intra-observer-reproducibility of GS-IVUS (F) and OCT (f) to assess the scaffold area.

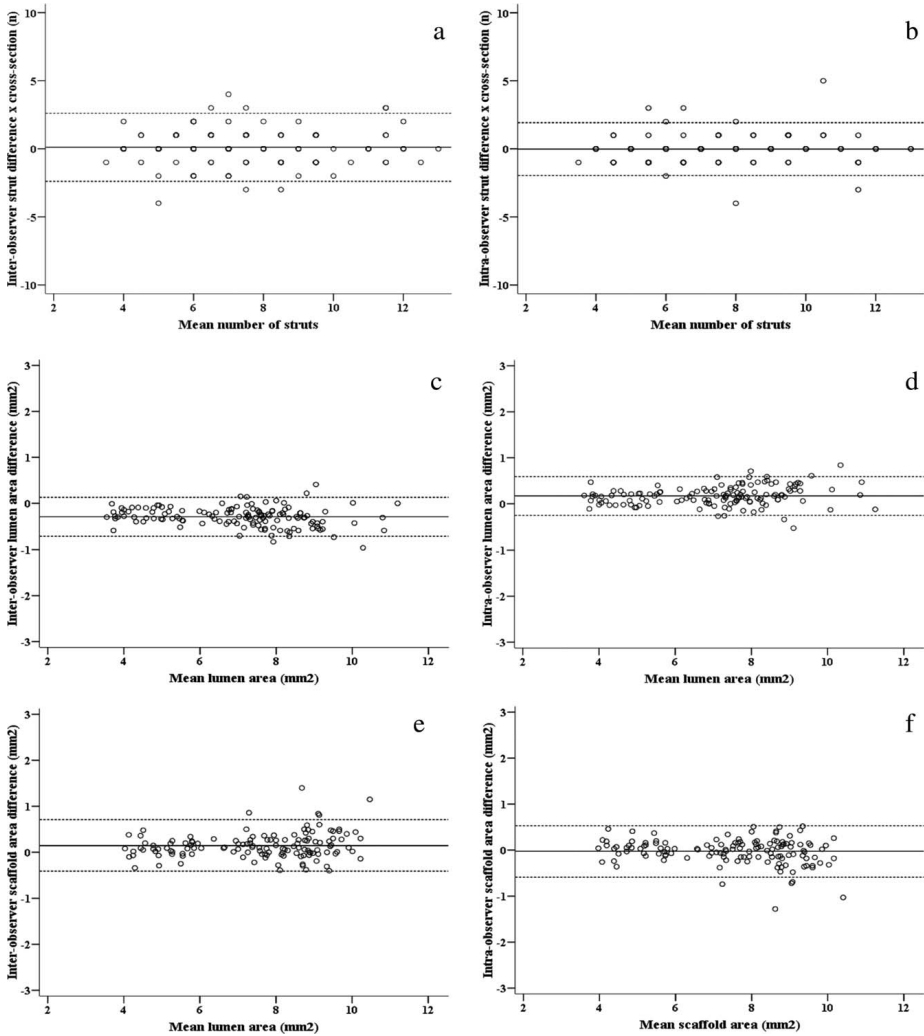


Fig. 4. Continued

20 MHz inter- and intraobserver reproducibility to assess ISA and SB struts using the Bland-Altman graphs at a strut level analysis showed a margin of error 2–3 times larger than with OCT (Figs. 3 and 4). On the other hand, OCT showed excellent reproducibility for qualitative findings and number of struts per

cross-section. These results are similar to those reported by Gonzalo et al. using metallic stents [16]. The inter- and intraobserver reproducibility for lumen and scaffold areas was excellent for both GS-IVUS and OCT. These results are congruent with other studies using GS-IVUS and OCT [16,17]. However, our

study shows that the inter- and intraobserver margin of error of those measurements was larger with GS-IVUS than with OCT (Fig. 4).

Limitations

The main limitation of this study is the lack of matching between GS-IVUS and OCT image cross-sections. Although we tried to assess the same number of cross-sections per lesion measured at each 1 mm with respect to the pullback landmark, the disparity of the scaffold lengths between both techniques did not allow us to ensure the same sequence of cross-sections. Therefore, the percentages of qualitative findings adjusted per lesion may differ and adds variability to the agreement between the two techniques. The second limitation of the study is the use of two different OCT systems. The visualization of the guide-wire and its shadowing in the OCT images obtained with the C7 system did not allow the complete analysis of the lumen/scaffold perimeter. On the other hand, the M3 system and the IVUS 20 MHz catheter allowed the complete visualization of the lumen/scaffold perimeter.

CONCLUSION

Qualitative assessment of BVS structures using GS-IVUS 20 MHz should be avoided due to its poor agreement and reproducibility when compared with OCT. Both GS-IVUS and OCT have good reproducibility to assess lumen and scaffold areas but the margin of error with GS-IVUS is larger than with OCT.

ACKNOWLEDGEMENTS

The authors thank Karine Miquel-Hebert and Susan Veldhof for the critical review of the present manuscript.

REFERENCES

- Ormiston JA, Serruys PW, Regar E, Dudek D, Thuesen L, Webster MW, Onuma Y, Garcia-Garcia HM, McGreevy R, Veldhof S. A bioabsorbable everolimus-eluting coronary stent system for patients with single de-novo coronary artery lesions (ABSORB): A prospective open-label trial. *Lancet* 2008;371:899–907.
- Serruys PW, Ormiston JA, Onuma Y, et al. A bioabsorbable everolimus-eluting coronary stent system (ABSORB): 2-year outcomes and results from multiple imaging methods. *Lancet* 2009;373:897–910.
- Serruys PW, Onuma Y, Ormiston JA, et al. Evaluation of the second generation of a bioresorbable everolimus drug-eluting vascular scaffold for treatment of de novo coronary artery stenosis: Six-month clinical and imaging outcomes. *Circulation* 2010;122:2301–2312.
- Mintz GS, Nissen SE, Anderson WD, et al. American College of Cardiology Clinical Expert Consensus Document on Standards for Acquisition, Measurement and Reporting of Intravascular Ultrasound Studies (GS-IVUS). A report of the American College of Cardiology Task Force on Clinical Expert Consensus Documents. *J Am Coll Cardiol* 2001;37:1478–1492.
- Bouma BE, Tearney GJ, Yabushita H, et al. Evaluation of intracoronary stenting by intravascular optical coherence tomography. *Heart* 2003;89:317–320.
- Gonzalo N, Serruys PW, Okamura T, et al. Optical coherence tomography assessment of the acute effects of stent implantation on the vessel wall: A systematic quantitative approach. *Heart* 2009;95:1913–1919.
- Cohen J. A coefficient of agreement for nominal scales. *Educ Psychol Meas* 1960;20:37–46.
- Fleiss J. *Statistical methods for rates and proportions*. New York: Wiley; 1981.
- Fleiss J. *The design and analysis of clinical experiments*. New York: Wiley; 1986.
- Bland JM, Altman DG. Statistical methods for assessing agreement between two methods of clinical measurement. *Lancet* 1986;1:307–310.
- Prati F, Regar E, Mintz GS, et al. Expert review document on methodology, terminology, and clinical applications of optical coherence tomography: Physical principles, methodology of image acquisition, and clinical application for assessment of coronary arteries and atherosclerosis. *Eur Heart J* 2010;31:401–415.
- Fort S, Freeman NA, Johnston P, Cohen EA, Foster FS. In vitro and in vivo comparison of three different intravascular ultrasound catheter designs. *Catheter Cardiovasc Interv* 2001;52:382–392.
- Nair A, Kuban BD, Tuzcu EM, Schoenhagen P, Nissen SE, Vince DG. Coronary plaque classification with intravascular ultrasound radiofrequency data analysis. *Circulation* 2002;106:2200–2206.
- Suzuki Y, Ikeno F, Koizumi T, Tio F, Yeung AC, Yock PG, Fitzgerald PJ, Fearon WF. In vivo comparison between optical coherence tomography and intravascular ultrasound for detecting small degrees of in-stent neointima after stent implantation. *JACC Cardiovasc Interv* 2008;1:168–173.
- Capodanno D, Prati F, Pawlowsky T, Cera M, La Manna A, Albertucci M, Tamburino C. Comparison of optical coherence tomography and intravascular ultrasound for the assessment of in-stent tissue coverage after stent implantation. *EuroIntervention* 2009;5:538–543.
- Gonzalo N, Garcia-Garcia HM, Serruys PW, Commissaris KH, Bezerra H, Gobbens P, Costa M, Regar E. Reproducibility of quantitative optical coherence tomography for stent analysis. *EuroIntervention* 2009;5:224–232.
- Mintz GS, Griffin J, Chuang YC, Pichard AD, Kent KM, Satler LF, Popma JJ, Leon MB. Reproducibility of the intravascular ultrasound assessment of stent implantation in saphenous vein grafts. *Am J Cardiol* 1995;75:1267–1270.

Chapter 22

Proximal and Distal Maximal Luminal Diameters as a Guide to Appropriate Deployment of the ABSORB Everolimus-Eluting Bioresorbable Vascular Scaffold: A sub-study of the ABSORB Cohort B and the Ongoing ABSORB EXTEND Single Arm Study.

Vasim Farooq, Josep Gomez-Lara, Salvatore Brugaletta, **Bill D. Gogas**, Hector M. García-García, Yoshinobu Onuma, Robert Jan van Geuns, Antonio Bartorelli, Robert Whitbourn, Alexander Abizaid, Patrick W. Serruys

Catheter Cardiovascular Interventions. 2012. May 1; 79(6): 880-8 [IF: 2.51]

Proximal and Distal Maximal Luminal Diameters as a Guide to Appropriate Deployment of the ABSORB Everolimus-Eluting Bioresorbable Vascular Scaffold: A Sub-Study of the ABSORB Cohort B and the On-Going ABSORB EXTEND Single Arm Study

Vasim Farooq,¹ MBChB, MRCP, Josep Gomez-Lara,¹ MD, Salvatore Brugaletta,¹ Bill D. Gogas,¹ MD, Hector M. Garcia-Garcia,¹ MD, MSc, PhD, Yoshinobu Onuma,¹ MD, Robert Jan van Geuns,¹ MD, PhD, Antonio Bartorelli,² MD, Robert Whitbourn,³ MD, Alexandre Abizaid,⁴ MD, PhD, and Patrick W. Serruys,^{1*} MD, PhD

Objectives: Due to the limited distensibility of the everolimus-eluting bioresorbable vascular scaffold (ABSORB) compared to metallic platform stents, quantitative coronary arteriography (QCA) is a mandatory requirement for ABSORB deployment in the on-going ABSORB EXTEND Single-Arm Study. Visual assessment of vessel size in the ABSORB Cohort B study often lead to under and over-sizing of the 3 mm ABSORB in coronary vessels (recommended range of the vessel diameter ≥ 2.5 mm and ≤ 3.3 mm), with an increased risk of spontaneous incomplete scaffold apposition post ABSORB deployment. We report whether mandatory QCA assessment of vessel size pre-implantation, utilizing the maximal luminal diameter (Dmax) and established interpolated reference vessel diameter (RVD) measurements, has improved device/vessel sizing. **Methods:** Pre-implantation *post-hoc* QCA analyses of all 101 patients from ABSORB Cohort B (102 lesions) and first consecutive 101 patients (108 lesions) from ABSORB EXTEND were undertaken by an independent core-laboratory; all patients had a 3 mm ABSORB implanted. Comparative analyses were performed. **Results:** Within ABSORB Cohort B, a greater number of over-sized vessels (>3.3 mm) were identified utilizing the Dmax compared to the interpolated RVD (17 vessels, 16.7% vs. 3 vessels, 2.9%; $P = 0.002$). Comparative analyses demonstrated a greater number of appropriate vessel-size selection (75 vessels, 69.4% vs. 48 vessels, 47.1%; $P = 0.001$), a trend towards a reduction in implantation in small (<2.5 mm) vessels (29 vessels, 26.9% vs. 40 vessels, 39.2%; $P = 0.057$) and a significant decrease in the implantation in large (>3.3 mm) vessels (4 vessels, 3.7% vs. 17 vessels, 16.7%; $P = 0.002$) in ABSORB EXTEND. Bland-Altman plots suggested a good agreement between operator and core-laboratory calculated Dmax measurements. **Conclusions:** The introduction of mandatory Dmax measurements of vessel size prior to ABSORB implantation significantly reduced the under-sizing of the 3.0 mm scaffold in large vessels validating the use of this technique in vessel sizing prior to ABSORB implantation. © 2011 Wiley Periodicals, Inc.

Key words: bioresorbable scaffold; quantitative coronary angiography; maximal luminal diameter; coronary artery disease

¹Thoraxcenter, Erasmus University Medical Centre, Rotterdam, The Netherlands

²Centro Cardiologico Monzino, IRCCS, Department of Cardiovascular Sciences, University of Milan, Milan Italy

³St. Vincent's Hospital, Fitzroy Victoria, Australia

⁴Instituto Dante Pazzanese de Cardiologia, São Paulo, Brazil

Conflict of interest: The authors report no conflicts of interests.

*Correspondence to: Patrick W. Serruys, MD, PhD, FESC, Professor of Medicine, Head of the Interventional Cardiology Department,

Erasmus MC, 's-Gravendijkwal 230, 3015 CE Rotterdam, The Netherlands. E-mail: p.w.j.c.serruys@erasmusmc.nl

Received 17 March 2011; Revision accepted 27 March 2011

DOI 10.1002/ccd.23177

Published online 5 October 2011 in Wiley Online Library (wileyonlinelibrary.com)

INTRODUCTION

Fully bioresorbable drug-eluting vascular scaffolds (BVS) are a novel approach to treating coronary lesions in that they provide transient vessel support and drug delivery to the vessel wall, without the long-term limitations of standard metallic drug-eluting stents (DES) such as metallic caging [1,2]. Unlike with permanent metallic stenting, the BVS will potentially allow future surgical revascularization, expansive remodeling, restoration of reactive vasomotion, and non-invasive imaging of coronary arteries with multislice computed tomography. Given their temporary presence, the potential risk of late or very late stent thrombosis may be reduced or even eliminated [3,4].

Although the short- and long-term clinical results of the first generation ABSORB BVS were favorable, a mild decrease in scaffold area by intravascular ultrasound (IVUS) and optical coherence tomography (OCT) was evident at 6 months (a phenomenon dubbed “late recoil”). Subsequent changes in the platform design and manufacturing processes lead to significant improvements in the mechanical support and prolongation of the mechanical properties of the device, which were incorporated into the second generation ABSORB (Revision 1.1). This was tested in the ABSORB Cohort B trial, which enrolled 101 patients [3,4]. Six-month clinical and angiographic results of the first 45 patients demonstrated that the phenomenon of late recoil appeared to have been almost eliminated, with 6-month MACE rate of 4.4% and an angiographic late loss of 0.19 mm. Full results of the trial are awaited.

Because of the single size availability (3.0 mm in diameter) and limited distensibility of BVS polymeric platforms, the angiographic inclusion criteria of ABSORB Cohort B were appropriately restrictive, in that the target lesion(s) must have been located in a native coronary artery with an estimated vessel diameter of ≥ 2.5 mm and ≤ 3.3 mm. The ABSORB Cohort B study allowed the visual estimation of the vessel diameter to guide ABSORB implantation. *Post-hoc* studies however suggested that the 3.0 mm ABSORB had often been deployed in vessels outside the recommended range of the vessel diameter (≥ 2.5 mm and ≤ 3.3 mm) [5,6].

With the implantation of the 3.0 mm device in small vessels (< 2.5 mm), it was demonstrated that there were potentially no significant differences in late luminal loss, as assessed by angiographic and IVUS criteria, and clinical outcomes when compared to larger vessels (≥ 2.5 mm) [6]. However in larger vessels (> 3.3 mm), a trend towards an increased frequency of scaffold malapposition, as defined by $> 5\%$ incomplete stent apposition (ISA), was observed in an OCT sub-study [5]. Although the clinical events were no differ-

ent in the larger vessels groups (> 3.3 mm), there was potential concern over implanting an ABSORB in an oversized vessel and the consequent long-term risks of the presence of spontaneous ISA immediately after deployment (Fig. 1a and b).

In order to guide angiographic deployment of the ABSORB device further, quantification of lumen dimensions, with either IVUS or QCA-guided ABSORB deployment, were introduced as mandatory requirements in the on-going ABSORB EXTEND Single Arm Study (SAS). This is a large, international, multicenter study, which aims to recruit over 1,000 patients from over 100 centers worldwide. We report as to whether the introduction of mandatory QCA assessment of vessel size prior to BVS implantation, by the use of maximal luminal diameters (D_{max}) and interpolated reference vessel diameters (RVD), have improved the vessel selection criteria prior to implantation with the ABSORB.

METHODS

Study Design and Population

ABSORB Cohort B. The ABSORB Cohort B Trial is a multicenter single-arm, prospective, open-label trial assessing the safety and performance of the ABSORB BVS (Abbott Vascular, Santa Clara, CA). All patients were older than 18 years, and had a diagnosis of stable or unstable angina, or silent ischemia. Major exclusion criteria were patients presenting with an acute myocardial infarction or unstable arrhythmias, left ventricular ejection fraction less than 30%, restenotic lesions, lesions located in the left main coronary artery, lesions involving a side branch more than 2 mm in diameter, and the presence of thrombus or other clinically significant stenoses in the target vessel. The ethics committee at each participating institution approved the protocol and each patient gave written informed consent prior to inclusion.

Protocol treated lesions were a maximum of two, *de-novo* lesions in separate native coronary arteries with a 3.0 mm diameter, a length shorter than 14 mm for the 18 mm scaffold and a percentage diameter stenosis greater than 50% and less than 100%. Pre-dilatation prior to ABSORB implantation was mandatory. Post-dilatation with a balloon shorter than the implanted scaffold was allowed at the operator's discretion. All patients were pre-treated with aspirin and a loading dose of at least 300 mg of clopidogrel, administered according to local hospital practice. Post-procedurally, all patients received aspirin ≥ 75 mg for the study duration (5 years) and clopidogrel 75 mg daily for a minimum of 6 months. Anticoagulation and

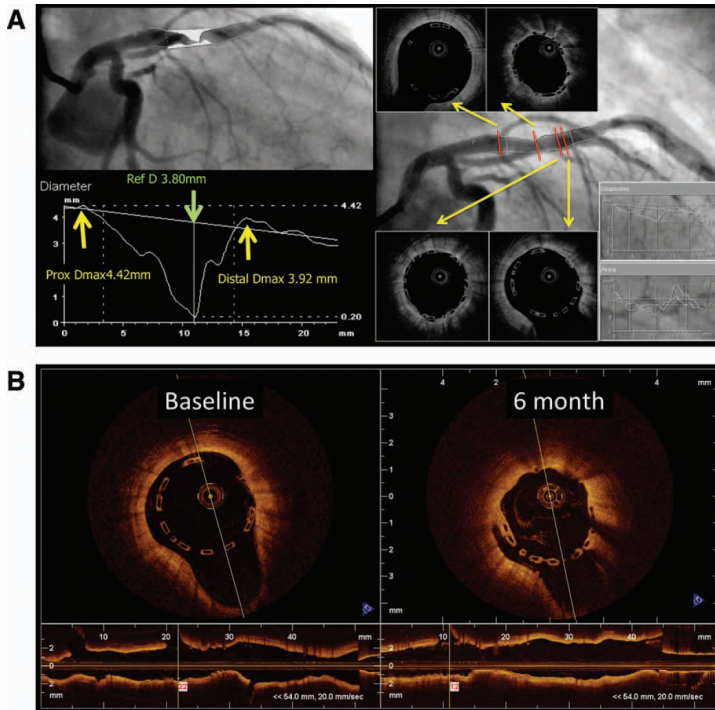


Fig. 1. (a,b) Implantation of a 3 mm BVS in a vessel with an interpolated RVD of 3.80 mm and a proximal and distal Dmax of 4.42 and 3.92 mm, respectively (left image, a) from a patient in ABSORB Cohort B. This leads to under-sizing of the BVS with spontaneous ISA present at both edges of the BVS (right image, a). Six-month follow-up demonstrated incorporation of several struts into the vessel wall and coverage of the struts (b) [5].

glycoprotein IIb/IIIa products were used in accordance with the local hospital standard practice.

ABSORB EXTEND Single Arm Study. The ABSORB EXTEND SAS is an on-going, prospective, single-arm, open-labeled clinical investigation enrolling subjects with target lesion(s) length ≤ 28 mm with a maximum of two *de novo* native coronary artery lesions each located in different epicardial vessels. 3.0 mm \times 18 mm ABSORB devices were available at the start of enrollment. The inclusion and exclusion criteria are almost identical to ABSORB Cohort B except for longer lesions being permitted.

As compared to the ABSORB Cohort B study, the procedural implantation technique differed with respect to the requirement of mandatory proximal and distal Dmax measurements of vessel size prior to device

deployment, with the recommendations of implanting the device only if the vessel diameter was ≥ 2.5 and ≤ 3.3 mm. Post-dilatation of the device was permitted provided the predicted balloon size fell within the range of the 3.0 mm ABSORB size specifications.

QCA analysis. In all patients, *post hoc* analyses of the scaffold and peri-scaffold segments (defined by a length of 5 mm proximal and distal to the ABSORB edges), as well as their combination (in-segment analysis), were undertaken by QCA using the Coronary Angiography Analysis System (Pie Medical Imaging, Maastricht, The Netherlands) by an independent core laboratory (Cardialysis NV, Rotterdam, The Netherlands). The small 37- μ m platinum radiomarkers located at each end of the ABSORB aided in the localization of the non radio-opaque scaffold for QCA analyses.

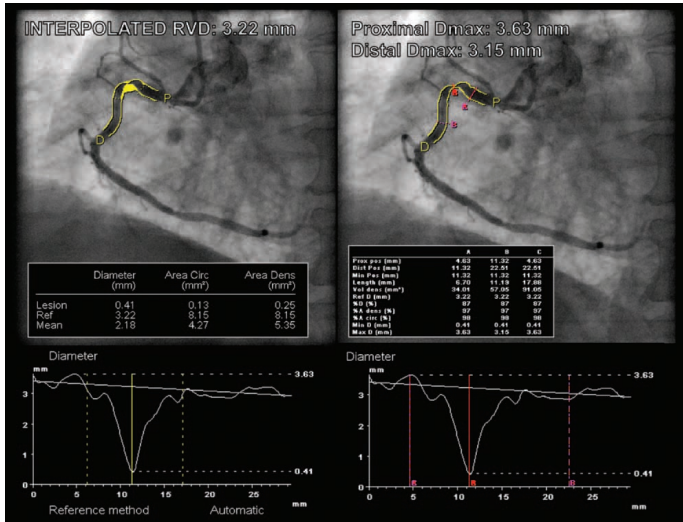


Fig. 2. Comparisons of the interpolated RVD (left) and Dmax (right) measurements in assessing vessel size pre-implantation of a 3 mm BVS. In this example, taken from the ABSORB Cohort B Study, the interpolated reference vessel diameter was calculated to be 3.22 mm. Based on this QCA value, a 3 mm BVS would have been acceptable for implantation

(implantation range ≥ 2.5 mm and ≤ 3.3 mm). However, with the use of Dmax measurements, the proximal Dmax was calculated as 3.63 mm and distal Dmax 3.15 mm. The proximal Dmax measurement would have precluded implantation of the BVS if this assessment had been used.

Within the ABSORB EXTEND SAS, if the device was found to have been implanted in a vessel outside the recommended limits (≥ 2.5 and ≤ 3.3 mm), the study sponsor would subsequently provide appropriate feedback to the operator at the local participating centre and further retraining offered if required.

QCA guidance of device implantation for the 3.0 mm ABSORB device is reliant on the angiographic diameter function of the pre-treatment vessel segment continually containing three non-ambiguous data points; namely the minimal luminal diameter (MLD) and the maximal luminal diameters (Dmax) with respect to the MLD in the proximal (Proximal Dmax) and distal (Distal Dmax) vessel segment of interest. Traditionally, the interpolated RVD (Fig. 2) has been the measurement of choice in guiding stent implantation when QCA analysis is to be performed [7]. An interpolated diameter line is generated from the proximal to the distal healthy segments of the lesion edges (usually located between a proximal and distal side branch). The interpolated line represents a mean average of all the vessel diameters from the proximal to the distal vessel and provides a virtual

reference diameter measurement at the site of the MLD. The theoretical main disadvantage of this technique is that the interpolated RVD can often be below the maximum vessel diameter as it represents a mean value.

Conversely, the proximal and distal Dmax values are measures of the maximal diameter of the vessel in the intended implantation zone (Fig. 2). As the implantation site would include non-diseased vessel segments at the proximal and distal edges, the Dmax measurements would be the maximal vessel diameters located proximal and distal to the MLD, or in rare situations, the maximal diameter of an aneurysmal portion of the vessel. A Dmax outside the reference range of ≥ 2.5 mm and ≤ 3.3 mm for a 3.0 mm ABSORB would therefore imply that the device is too big or small, respectively, for the intended vessel site to be implanted.

Study device. The ABSORB revision 1.1 is a balloon expandable device consisting of a polymer backbone of Poly-L lactide (PLLA) coated with a thin layer of a 1:1 mixture of an amorphous matrix of Poly-D, L lactide (PDLLA) polymer, and $100 \mu\text{g}/\text{cm}^2$ of the anti-proliferative drug everolimus. Two platinum markers located at

TABLE 1. Core Laboratory Assessed Dmax and Interpolated RVD Comparisons for All 101 Patients (102 lesions) in ABSORB Cohort B and the First 101 Patients (108 lesions) in ABSORB EXTEND Single Arm Study

QCA measurement	ABSORB Cohort B (n = 102)	EXTEND SAS (n = 108) ^a (n = 107) ^b	P Value ^c
Pre-implantation Dmax: ≥ 2.5 to ≤ 3.3 mm (%)	48 (47.1%)	75 (69.4%)	0.001
Pre-implantation Dmax: < 2.5 mm (%)	40 (39.2%)	29 (26.9%)	0.057
Pre-implantation Dmax: > 3.3 mm (%)	17 (16.7%)	4 (3.7%)	0.002
Pre-implantation RVD: ≥ 2.5 to ≤ 3.3 mm (%)	58 (56.9%)	61 (57.0%)	0.983
Pre-implantation RVD: < 2.5 mm (%)	41 (40.2%)	44 (41.1%)	0.892
Pre-implantation RVD: > 3.3 mm (%)	3 (2.9%)	2 (1.9%)	0.612

^an = 108 lesions for Dmax assessment.

^bn = 107 lesions for RVD assessment (RVD unavailable in one occluded vessel).

^c2-Sided Pearson Chi-squared analysis.

each ABSORB edge allow for accurate visualization during angiography or other imaging modalities of the radiolucent ABSORB. The PDLLA allows for the controlled release of everolimus, 80% of which is eluted within the first 30-days. Both PLLA and PDLLA are fully bioresorbable. The polymers are degraded via hydrolysis of the ester bonds in the backbone. The resulting lactate and its oligomers eventually leave the polymer matrix and are metabolized through the pyruvate and Krebs energy cycles in the surrounding tissues and blood. Small particles, less than 2 μ m in diameter, are phagocytosed by macrophages. According to preclinical studies, the time for complete bioresorption of the polymer backbone is approximately 2 years [8].

Statistical analysis. Categorical variables are presented as counts and percentages. Continuous variables are presented as means \pm SD. Assumptions for normality distribution of the data were performed with Kolmogorov–Smirnov test and by visual assessment. Comparisons of paired analysis within ABSORB EXTEND were performed with the paired *T*-test. Comparisons of proportions were performed with 2-sided Pearson Chi square analysis. All inference statistics were conducted at a two-tailed α level of 0.05. Bland–Altman plots, displaying the systematic (mean absolute difference) and random (95% limits of agreement) errors were used to assess the agreement between the operator and core laboratory assessed RVD and Dmax measurements. Statistical analyses were performed using SPSS 18.0 (SPSS Inc., Chicago IL).

RESULTS

Pre-implantation interpolated RVD and Dmax measurements were available in 102 lesions in 101 patients from ABSORB Cohort B. In the ABSORB EXTEND SAS, pre-implantation RVD measurements were available in 107 lesions in 101 patients, and Dmax measurements in 108 lesions in 101 patients; one vessel was occluded precluding the calculation of the interpolated RVD. Core lab-

oratory and operator assessed RVD and Dmax measurements followed a Gaussian distribution for both ABSORB Cohort B and ABSORB EXTEND SAS.

Within ABSORB Cohort B, the core laboratory assessed mean interpolated RVD was 2.61 ± 0.37 mm, mean proximal Dmax 2.82 ± 0.46 mm, and mean distal Dmax 2.72 ± 0.42 mm. A greater number of oversized vessels (> 3.3 mm) were identified utilizing the Dmax compared to the interpolated RVD (17 vessels, 16.7% vs. 3 vessels, 2.9%, $P = 0.002$). No differences were however found in identifying small vessels (< 2.5 mm) (40 vessels, 39.2% vs. 41 vessels, 40.2%, $P = 1.000$) and normal size vessels (48 vessels, 47.1% vs. 58 vessels, 56.9%, $P = 0.207$) (Table I).

Within ABSORB EXTEND SAS, the mean core laboratory assessed interpolated RVD was 2.59 ± 0.33 mm; a trend towards a higher operator assessed mean proximal (2.86 ± 0.25 mm vs. 2.81 ± 0.33 mm, $P = 0.072$) and distal (2.73 ± 0.27 mm vs. 2.67 ± 0.33 mm, $P = 0.055$) Dmax measurements, compared to the core laboratory assessed values, were observed; this however did not reach statistical significance.

With the application of mandatory Dmax assessment in the ABSORB EXTEND SAS, this led to a significant increase in appropriately sized vessels for implantation with a 3 mm device when compared to ABSORB Cohort B (75 vessels, 69.4% vs. 48 vessels, 47.1%, $P = 0.001$). A trend towards a reduction in the implantation of the 3 mm BVS device in small vessels (< 2.5 mm) was seen (40 lesions, 39.2% vs. 29 lesions, 26.9%, $P = 0.057$). A significant reduction in the implantation of the 3 mm device in vessels > 3.3 mm was observed (17 lesions, 16.7% vs. 4 lesions, 3.7%). The four cases involving Dmax > 3.3 mm occurred in the first 50 patients in the Extend SAS and involved centers who had performed ABSORB implantation for the first (three cases) or second time (one case). No significant differences were observed in the interpolated RVD to assess vessel size between EXTEND SAS and ABSORB Cohort B (Table I).

Figure 3 demonstrates the comparison of the interpolated RVD and Dmax measurements for assessing

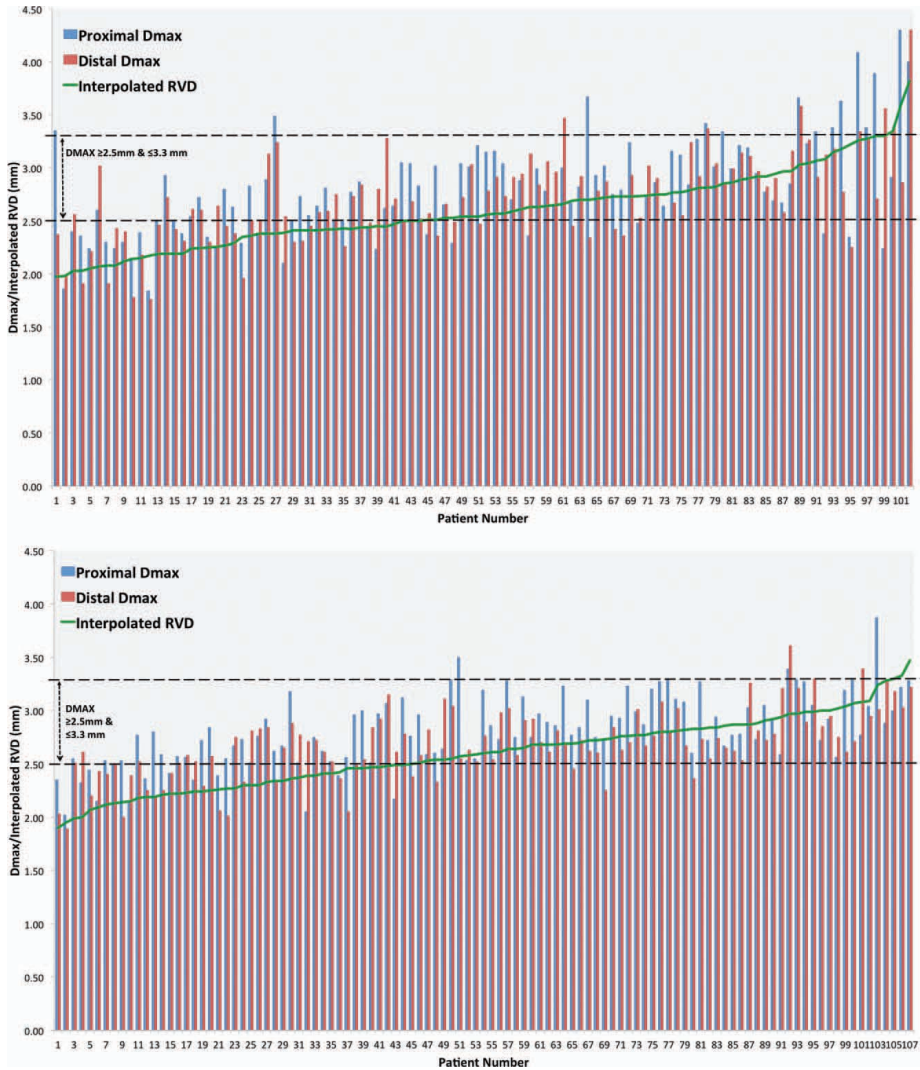


Fig. 3. (a,b) Comparisons of interpolated RVD and Dmax measurements in assessing vessel size pre-implantation from ABSORB Cohort B (a) and ABSORB SAS (b).

vessel sizes for ABSORB Cohort B and EXTEND SAS.

Figure 4a and 4b depict Bland–Altman plots and demonstrate agreement for both the proximal and distal Dmax values between core laboratory and operator cal-

culated Dmax values. The mean delta proximal and distal Dmax values (core laboratory minus operator calculated Dmax) were -0.05 mm [2 S.D. 0.56 to -0.67 mm] and -0.05 mm [2 S.D. 0.53 to -0.63 mm] for proximal and distal Dmax measurements, respectively.

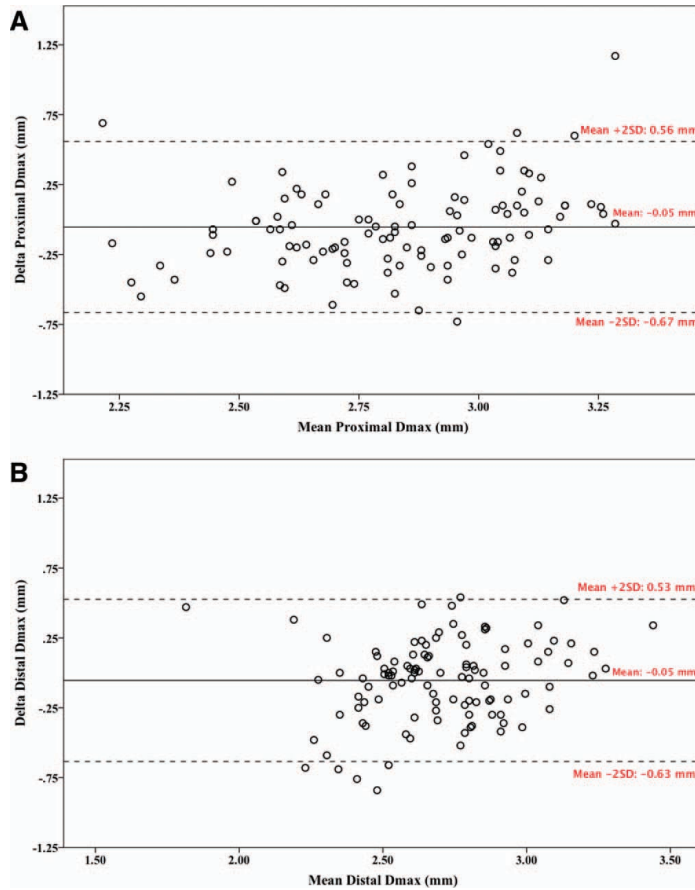


Fig. 4. (a,b) Bland Altman plots depicting the agreement for proximal (a) and distal (b) Dmax measurements between the operator and core laboratory assessed values. Delta Dmax is the core laboratory minus the operator Dmax calculation.

DISCUSSION

The main findings of this study are that (1) the visual assessment of the reference vessel diameter is poor and can lead to under or over-sizing of the ABSORB device as observed in over half the cases in ABSORB Cohort B study; (2) that QCA, utilizing proximal and distal Dmax measurements of the vessel size lead to a statistically significant increase in appropriate vessel size selection for a 3 mm BVS device; (3) that Dmax assessments reduced the under-sizing of the 3 mm

device when compared to the interpolated RVD or visual assessment, this may reduce the risk of post-implantation device malapposition; (4) and that the measurements of proximal and distal Dmax are broadly in agreement between the core laboratory and operator assessed Dmax values.

As shown in Fig. 2, the proximal and distal Dmax values appear to represent a refinement in assessing the vessel size when compared to the interpolated RVD. For example in ABSORB Cohort B, if the interpolated

RVD had been used, only three patients (2.9%) would have been identified as having a vessel diameter >3.3 mm; conversely with the application of the proximal and distal Dmax values, an almost six-fold increase in the number of patients with a vessel size >3.3 mm were identified (17 patients, 16.7%). In keeping with these findings, Gomez-Lara et al demonstrated in an OCT substudy of the first 52 patients in ABSORB Cohort B, a trend towards an increasing frequency of $>5\%$ ISA with a greater Dmax [5].

Conversely, over-sizing of the 3.0 mm device in small vessels (2.5 mm) has recently been shown to be potentially not of concern based on preliminary data from the first 52 patients in ABSORB Cohort B, as assessed by 6-month angiographic, IVUS, and clinical outcomes [6]. In the present study, a trend towards a reduced frequency of the deployment of the ABSORB device in vessels with a Dmax <2.5 mm was observed, although this did not achieve statistical significance (40 cases (39.2%) ABSORB Cohort B vs. 29 cases (26.9%) ABSORB EXTEND SAS, $P = 0.057$).

It is likely that because of the fact that the 2.5 mm ABSORB is actually the same device as the 3.0 mm device but crimped onto a smaller balloon, the deployment of a 3.0 mm ABSORB in small vessels (<2.5 mm) did not compromise safety. The so called “bigger is better paradigm” [9] appears to be the most plausible explanation for the promising results of the implantation of the 3 mm BVS device in small vessels [6]; effectively a larger postimplantation MLD has previously been shown to be associated with a reduced risk of restenosis [9,10].

With metallic platform drug eluting stents (DES), these issues of sizing are equally relevant, perhaps more so given the permanent nature of the platform. Most types of metallic DES consist of two or three (as seen with the Promus Element DES) different stents sizes with differing deploying balloon sizes to reflect the different size vessels they are designed for [11]. High pressure deployment and/or post-dilatation are often undertaken to ensure appropriate deployment. Conversely with the ABSORB, because of the differing properties of the polymeric platform making it potentially less distensible compared to the metallic platform, the operator is required to respect the limits of its maximal diameter. It should however be noted that aggressive post-dilation of a metallic platform DES has been associated with an increased risk of stent fracture *in vivo* [12], and *in-vitro* testing of metallic DES has been associated with polymer cracking and even detachment of polymer fragments when a 3.0 mm DES was post-dilated up to 5 mm [13].

At present, the maximum diameter a 3.0 mm ABSORB can be post-dilated to is no more than

3.5 mm; an awareness therefore of the inflation pressure/diameter compliance charts available for post-dilatation balloons is essential so that post-dilatation is performed within the recommended limits of these devices.

Current conventional PCI practice is reliant on visual vessel size estimation based on operator experience. However, large intra- and inter-observer variability of visual estimation (SD up to 18%) has been a consistent finding since the late 1970s [14–16], whereas QCA has continually been shown to be a more objective and highly reproducible technique for the assessment of vessel size [7]. There are however potential theoretical limitations of using QCA or visual guidance in stenting the proximal coronary vasculature. The proximal vasculature diameter can potentially rapidly taper in size and has been suggested to be associated with stent under-deployment. Evidence however suggests the reason a vessel tapers is predominantly related to the number of bifurcations, with the size of the side-branch being related to the amount of tapering [17]. An awareness of this phenomenon, the selection of multiple angiographic reviews to visualize the proximal vasculature, liberal use of nitrates, lesion pre-dilatation, and QCA measurements may all serve to limit this potential issue.

It should be noted that the evidence in support of IVUS guided DES implantation has to date failed to show any differences in angiographic or clinical outcomes, despite being associated with a higher MLD in one study [18]. OCT guided DES implantation has not been investigated and would not allow the assessment of the media to media distance as a guide to vessel size. Some preliminary evidence has even suggested that IVUS, and to a lesser degree OCT, may potentially over-estimate vessel size; further study is however required to substantiate this evidence further [19].

The issue of vessel size estimation is clearly relevant regardless of what device (metallic or polymeric platform stent) is to be implanted. With the advent of bio-resorbable scaffolds, there is a need to respect the device size limits and with metallic platform DES, aggressive post-dilatation has been shown to be associated with stent fracture or polymer cracking as described [12,13]. QCA assessment is likely to remain a recommendation to allow for a more precise selection of appropriately sized vessels and appropriate deployment of the ABSORB. The results of ABSORB EXTEND SAS are therefore awaited.

LIMITATIONS

The main limitation of this study was the comparison of the Dmax values between the operator and core laboratory assessed measurements. With the operator,

Dmax measurements are calculated at the intended BVS implantation site, whereas the core laboratory calculated the Dmax measurements on the pre-implantation coronary angiogram with a view matched to the postimplantation coronary angiogram. Despite this, Bland–Altman plots suggested good agreement between operator and core laboratory assessed Dmax values with a mean delta Dmax of -0.05 mm for proximal and distal Dmax values, with most delta Dmax values lying within 2 standard deviations (Fig. 4a and 4b). It is however likely that the wider standard deviations observed for the mean delta Dmax are due to this unavoidable limitation.

ACKNOWLEDGEMENTS

The first author thanks the Dickinson Trust Traveling Scholarship, Manchester Royal Infirmary, Manchester, England, United Kingdom. Authors also thank Monique Schuijjer PhD, Lynn Dykema BA and Coby Bouwman of Cardialysis BV, Rotterdam, The Netherlands, and Susan Veldhof, RN, and Wai-Fung Cheong, PhD of Abbott Vascular, Santa Clara, CA, USA, for their invaluable technical expertise.

REFERENCES

1. Tanimoto S, Serruys PW, Thuesen L, Dudek D, de Bruyne B, Chevalier B, Ormiston JA. Comparison of *in vivo* acute stent recoil between the bioabsorbable everolimus-eluting coronary stent and the everolimus-eluting cobalt chromium coronary stent: Insights from the ABSORB and SPIRIT trials. *Catheter Cardiovasc Interv* 2007;70:515–523.
2. Tanimoto S, Bruining N, van Domburg RT, Rotger D, Radeva P, Ligthart JM, Serruys PW. Late stent recoil of the bioabsorbable everolimus-eluting coronary stent and its relationship with plaque morphology. *J Am Coll Cardiol* 2008;52:1616–1620.
3. Serruys PW, Ormiston JA, Onuma Y, Regar E, Gonzalo N, Garcia-Garcia HM, Nieman K, Bruining N, Dorange C, Miquel-Hebert K, et al. A bioabsorbable everolimus-eluting coronary stent system (ABSORB): 2-year outcomes and results from multiple imaging methods. *Lancet* 2009;373:897–910.
4. Onuma Y, Serruys PW. Bioresorbable scaffold: The advent of a new era in percutaneous coronary and peripheral revascularization? *Circulation* 2011;123:779–797.
5. Gomez-Lara J, Diletti R, Brugaletta S, Onuma Y, Farooq V, Thuesen L, McClean D, Koolen J, Ormiston JA, Windecker S, et al. Angiographic maximal luminal diameter and appropriate deployment of the everolimus-eluting bioresorbable vascular scaffold as assessed by optical coherence tomography. *EuroInterv*, in press.
6. Diletti R, Onuma Y, Farooq V, Gomez-Lara J, Brugaletta S, van Geuns RJ, Regar E, de Bruyne B, Dudek D, Thuesen L, et al. Six-month clinical outcome following the implantation of the bioresorbable everolimus eluting vascular scaffold in vessels smaller or larger than 2.5 mm. *J Am Coll Cardiol*, in press.
7. Reiber JH, Serruys PW. *Quantitative Coronary Angiography: Methodologies*. Quantitative Coronary Angiography. Dordrecht, The Netherlands: Kluwer Academic Publishers; 1991. pp 98–102.
8. Onuma Y, Serruys PW, Perkins LE, Okamura T, Gonzalo N, Garcia-Garcia HM, Regar E, Kamberi M, Powers JC, Rapoza R, et al. Intracoronary optical coherence tomography and histology at 1 month and 2, 3, and 4 years after implantation of everolimus-eluting bioresorbable vascular scaffolds in a porcine coronary artery model: An attempt to decipher the human optical coherence tomography images in the ABSORB trial. *Circulation* 2010;122:2288–2300.
9. Honda Y, Fitzgerald PJ. Stent expansion as a mechanical parameter to predict late stent patency: Back to the basics. *JACC Cardiovasc Interv* 2009;2:1276–1278.
10. Biondi-Zoccai G, Moretti C, Abbate A, Sheiban I. Percutaneous coronary intervention for small vessel coronary artery disease. *Cardiovasc Revasc Med* 2010;11:189–198.
11. Garg S, Serruys PW. Coronary stents: Current status. *J Am Coll Cardiol* 2010;56(10 Suppl):S1–S42.
12. Canan T, Lee MS. Drug-eluting stent fracture: Incidence, contributing factors, and clinical implications. *Catheter Cardiovasc Interv* 2010;75:237–245.
13. Basalus MW, van Houwelingen KG, Ankone MJ, Feijen J, von Birgelen C. Micro-computed tomographic assessment following extremely oversized partial postdilatation of drug-eluting stents. *EuroIntervention* 2010;6:141–148.
14. Detre KM, Wright E, Murphy ML, Takaro T. Observer agreement in evaluating coronary angiograms. *Circulation* 1975;52: 979–986.
15. Zir LM, Miller SW, Dinsmore RE, Gilbert JP, Harthorne JW. Interobserver variability in coronary angiography. *Circulation* 1976;53:627–632.
16. DeRouen TA, Murray JA, Owen W. Variability in the analysis of coronary arteriograms. *Circulation* 1977;55:324–328.
17. Girasis C, van Geuns RJ, Onuma YPWS. Essentials of quantitative angiography for bifurcation lesions. *EuroInterv* 2010;6 (Suppl J):J36–J43.
18. Colombo A. AVIO: A Prospective Randomised Trial of Intravascular-Ultrasound Guided Compared to Angiography Guided Stent Implantation in Complex Coronary Lesions. *Transcatheter Cardiovascular Therapeutics*. Washington D.C. 2010.
19. Okamura T, Onuma Y, H.M. G-G, van Geuns RJ, Wykrzykowska J, Schultz C, Van der Giessen AG, Ligthart J, Regar E, Serruys PW. First in man evaluation of intravascular optical frequency domain imaging (OFDI) of Terumo: a comparison with intravascular ultrasound and quantitative coronary angiography. *EuroIntervention*, 2011;6:1037–1045.

Chapter 23

A Comparative Assessment by Optical coherence Tomography of the Performance of the First and Second Generation of the Everolimus-Eluting Bioresorbable Vascular Scaffolds.

Josep Gomez-Lara, Salvatore Brugaletta, Roberto Diletti, Scot Garg , Yoshinobu Onuma, **Bill D. Gogas**, Robert Jan van Geuns, Cecile Dorange, Susan Veldhof, Richard Rapoza, Robert Whitbourn, StephanWindecker, Hector M. Garcia-Garcia, Evelyn Regar, Patrick W. Serruys

European Heart Journal. 2011. Jul; 53(4): 301-9 [IF: 14.1]

A comparative assessment by optical coherence tomography of the performance of the first and second generation of the everolimus-eluting bioresorbable vascular scaffolds

Josep Gomez-Lara^{1†}, Salvatore Brugaletta¹, Roberto Diletti¹, Scot Garg¹, Yoshinobu Onuma¹, Bill D. Gogas¹, Robert Jan van Geuns¹, Cécile Dorange², Susan Veldhof², Richard Rapoza², Robert Whitbourn³, Stephan Windecker⁴, Hector M. Garcia-Garcia¹, Evelyn Regar¹, and Patrick W. Serruys^{1*†}

¹Department of Interventional Cardiology, Ba583a, Thoraxcenter, Erasmus MC, s-Gravendijkwal 230, 3015 CE Rotterdam, The Netherlands; ²Abbott Vascular, Diegem, Belgium; ³St Vincent's Hospital, Melbourne, Australia; and ⁴Swiss Cardiovascular Centre, Bern, Switzerland

Received 8 September 2010; revised 28 October 2010; accepted 18 November 2010; online publish-ahead-of-print 1 December 2010

Aims

The first generation of the everolimus-eluting bioresorbable vascular scaffold (BVS 1.0) showed an angiographic late loss higher than the metallic everolimus-eluting stent Xience V due to scaffold shrinkage. The new generation (BVS 1.1) presents a different design and manufacturing process than the BVS 1.0. This study sought to evaluate the differences in late shrinkage, neointimal response, and bioresorption process between these two scaffold generations using optical coherence tomography (OCT).

Methods and results

A total of 12 lesions treated with the BVS 1.0 and 12 selected lesions treated with the revised BVS 1.1 were imaged at baseline and 6-month follow-up with OCT. Late shrinkage and neointimal area (NIA) were derived from OCT area measurements. Neointimal thickness was measured in each strut. Strut appearance has been classified as previously described. Baseline clinical, angiographic, and OCT characteristics were mainly similar in the two groups. At 6 months, absolute and relative shrinkages were significantly larger for the BVS 1.0 than for the BVS 1.1 (0.98 vs. 0.07 mm² and 13.0 vs. 1.0%, respectively; $P = 0.01$). Neointimal area was significantly higher in the BVS 1.0 than in the BVS 1.1 (in-scaffold area obstruction of 23.6 vs. 12.3%; $P < 0.01$). Neointimal thickness was also larger in the BVS 1.0 than in the BVS 1.1 (166.0 vs. 76.4 μm ; $P < 0.01$). Consequently, OCT, intravascular ultrasound, and angiographic luminal losses were higher with the BVS 1.0 than with the BVS 1.1. At 6 months, strut appearance was preserved in only 2.9% of the BVS 1.0 struts, but remained unchanged with the BVS 1.1 indicating different state of strut microstructure and/or their reflectivity.

Conclusion

The BVS 1.1 has less late shrinkage and less neointimal growth at 6-month follow-up compared with the BVS 1.0. A difference in polymer degradation leading to changes in microstructure and reflectivity is the most plausible explanation for this finding.

Keywords

Bioresorbable vascular scaffold • Shrinkage • Optical coherence tomography • Bioresorption

Background

The first generation of the everolimus-eluting bioresorbable vascular scaffold (BVS 1.0) was tested in 30 patients enrolled in the

ABSORB Cohort A study. At 6-month follow-up, this device showed a late shrinkage of the scaffold area of 11.8% as assessed by intravascular ultrasound (IVUS) and rapid changes in strut appearance, documented by multiple imaging modalities.¹

[†]J.G.-L. and P.W.S. have equally contributed to the writing of the manuscript.

* Corresponding author. Tel: +31 10 7035260, Fax: +31 10 4369154, Email: p.w.j.c.serruys@erasmusmc.nl

Published on behalf of the European Society of Cardiology. All rights reserved. © The Author 2010. For permissions please email: journals.permissions@oup.com.

At variance with metallic stents, which do not exhibit late shrinkage,² the reduction of the BVS 1.0 scaffold area was the main component of late luminal loss at 6 months.

The BVS 1.1 represents a new generation of bioresorbable devices. It utilizes a novel platform design and polymer processing different than the previous BVS 1.0. This new generation is designed to improve the radial force and to slow-down the loss in mechanical integrity, without substantially affecting the bioresorption process.³ It has been investigated in 101 patients enrolled in the ABSORB cohort B trial. Forty-five of these patients were scheduled for a 6-month control with conventional angiography and multiple intravascular imaging techniques.

Optical coherence tomography (OCT) is a high resolution imaging technique capable of an accurate assessment of the polymeric struts, changes in luminal and scaffold dimensions, and the quantification of neointimal hyperplasia.^{4–6}

Our aim is to compare the late shrinkage and neointimal response of the two polymeric devices using OCT imaging and to assess the qualitative changes in strut appearance as a marker of bioresorption at 6-month follow-up.

Materials and methods

Study design and population

The ABSORB trial is a non-randomized, multicentre, single-arm, efficacy–safety study. The first Cohort (A) included 30 patients treated with the BVS 1.0; the trial design and results up to 3-year follow-up have been already published.^{1,4,7} The second Cohort (B) included 101 patients with 102 lesions treated with a single size 3×18 mm of the BVS 1.1 design; the study design is available at clinicaltrials.gov (NCT00856856).

The inclusion criteria were similar in both studies; patients aged 18 years or older diagnosed with stable, unstable, or silent ischaemia, with a *de novo* lesion in a native coronary artery between 50 and 99% of the luminal diameter and a Thrombolysis In Myocardial Infarction (TIMI) flow grade of 1 or more. Exclusions included patients with an evolving myocardial infarction, stenosis of an unprotected left main or ostial right coronary artery (RCA), presence of intracoronary thrombus or heavy calcification. Excessive tortuosity and lesions involving a side branch more than 2 mm in diameter were also exclusion criteria. The ethics committee at each participating institution approved the protocol and each patient gave written informed consent before inclusion.

Four centres (Auckland, Aarhus, Krakow, and Rotterdam) participated in the Absorb Cohort A in 2006 using the BVS 1.0.¹ In this first-in-man study, angiography and IVUS were mandatory investigations at 6 and 24 months of follow-up. Optical coherence tomography was an optional investigation that was only executed and performed in Rotterdam with the available system at that time (M2 Light Lab). Subsequently, the Rotterdam group performed OCT follow-up of their patients at 6 and 24 months. As a result, 13 patients in Cohort A had sequential OCT investigation at baseline and 6 months.⁴ The Cohort B study was started during 2009 using the BVS 1.1. In this study, 7 of the 12 participating centres performed OCT at baseline and follow-up and three of them (Rotterdam = 9, Melbourne = 2, and Bern = 1) used the most advanced system (C7 Light Lab). As a result, 12 patients in Cohort B have been imaged with the OCT C7 system. This limited but almost equal number of patients represents a unique opportunity to analyse, with the high

resolution of OCT, the mechanical behaviour of the first and second generation of everolimus-eluting BVS at baseline and at 6-month follow-up.

Devices

The BVS 1.0 (Abbott Vascular, Santa Clara, CA, USA) is a balloon expandable device built on a backbone of semi-crystalline poly-L-lactide (PLLA) polymer. The polymer consists of crystalline and amorphous domains. The balance between the crystalline and amorphous fractions and the molecular orientation state of these phases depends on their thermal and deformation history. The platform is coated with the poly-D,L-lactide (PDLLA) copolymer that contains and controls the release of the antiproliferative everolimus (Novartis, Switzerland). Both PLLA and PDLLA are fully bioresorbable. The strut thickness is $150 \mu\text{m}$ and the struts are distributed as circumferential out-of-phase zigzag hoops linked together by three longitudinal bridges between each hoop. The BVS 1.0 design is shown in Figure 1.

The manufacturing process the BVS 1.1 (Abbott Vascular, Santa Clara, CA, USA) has been modified to enhance the mechanical strength and mechanical durability of the struts. Moreover, the new design has in-phase zigzag hoops linked by bridges that allow for a more uniform strut distribution, reduce maximum circular unsupported surface area, and provide more uniform vessel wall support and drug transfer.³ The polymer mass, coating content, amount of drug, and the strut thickness remain the same. The BVS 1.1 design is also shown in Figure 1.

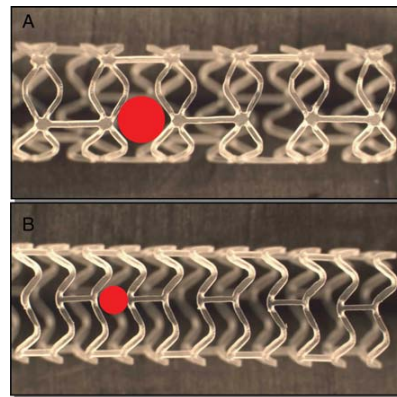


Figure 1 Design of the different bioresorbable vascular scaffold (BVS). (A) BVS 1.0 design. The struts are distributed as circumferential out-of-phase zigzag hoops linked together by three longitudinal bridges between each hoop. The maximal circular unsupported surface area is drawn as a red circle. (B) BVS 1.1 design. The struts are arranged as in-phase zigzag hoops linked together by three longitudinal bridges. The strut distribution is more uniform and allows the maximal circular unsupported surface area (red circle) to be smaller than in the BVS 1.0.

Treatment procedure

All procedures were performed electively. Lesions were treated with routine interventional techniques that included mandatory pre-dilatation. The study protocol forbade the use of pre-dilatation balloons longer than the pre-specified length of the device (18 mm), and recommended using balloons 0.5 mm smaller in diameter than the reference vessel diameter (RVD). The BVS had to be implanted at a pressure not exceeding the rated burst pressure (16 atmospheres). Post-dilation was allowed at the operator's discretion with shorter balloons than the BVS length and inflated at diameters that fit within the boundaries of the scaffold. Bail-out stenting was also allowed at operator's discretion.

Quantitative angiography analysis

The 2D angiograms were stored in DICOM format and analysed offline by the core lab (Cardialysis, Rotterdam, The Netherlands) using the CASS II analysis system (Pie Medical BV, Maastricht, The Netherlands). In each patient, the treated region and the peri-treated regions (defined by a length of 5 mm proximal and distal to the device edge) were analysed. The following quantitative coronary angiography (QCA) analysis parameters were measured: computer-defined minimal luminal diameter (MLD), RVD obtained by an interpolated method, and percentage of diameter stenosis (DS). Late loss was defined as the difference between MLD post-procedure and MLD at follow-up.⁸

Optical coherence tomography acquisition

In the ABSORB Cohort A, baseline and follow-up OCT acquisition was executed with an M2 Time-Domain System (LightLab Imaging, Westford, MA, USA) using the balloon occlusion method. The occlusion balloon Helios (Goodman, Japan) was advanced distal to the treated region over a conventional angioplasty guidewire of 0.014". Then, the conventional guidewire was replaced by the OCT ImageWire (LightLab Imaging, Westford, MA, USA) and the occlusion balloon catheter was positioned proximal to the segment of interest. Pullback of the ImageWire was performed with automated pullback at 1 mm/s and 15.6 frames/s during the occlusion of the artery by the balloon at low pressure (0.5–0.7 atm), and during simultaneous flushing of the vessel distal to the occlusion with lactated Ringer's solution at 37°C (flow rate 0.8 mL/s).

In ABSORB Cohort B, the baseline and follow-up OCT acquisitions were performed with the C7 XR Fourier-Domain System (LightLab Imaging, Westford, MA, USA) without occluding the coronary artery. In these cases, a conventional wire was placed distal to the segment of interest. Then the OCT imaging catheter (RX ImageWire II; LightLab Imaging, Westford, MA, USA) was advanced distally to the treated region. Removal of the conventional wire was left to the operator's discretion. The pullback was performed during a continuous injection of 3 mL/s of contrast medium (Iodixanol 370, Visipaque, GE Health Care, Cork, Ireland) injected at a maximum pressure of 300 psi through the guiding catheter using an injection pump. In this case, the automated pullback rate was 20 mm/s and the frame rate was 100 images/s.

The resolution of both OCT systems is exactly the same (15–20 µm of lateral resolution and 15–20 µm of axial resolution).⁹

Optical coherence tomography analysis

The OCT measurements were performed with proprietary software for offline analysis (LightLab Imaging, Westford, MA, USA). Adjusting for the pullback speed, the analysis of contiguous cross-sections was performed at each 1 mm longitudinal intervals within the treated segment.

The monochromatic peak wavelength of the OCT is differently reflected, refracted, and absorbed by the polymeric or metallic struts. A great deal of the OCT light energy is transmitted through the polymeric struts, such that only part of it is reflected at the endoluminal and abluminal sides of the struts generating a visible optical frame border; the core of the polymeric struts is imaged as a black square at baseline. As a consequence, the vessel wall is easily imaged through the struts without any major signs of shadowing (Figure 2). Thus, OCT analysis of the BVS has several advantages over that of metallic stents. First, at baseline, the vessel wall/lumen and its luminal area can be readily measured behind the polymeric struts. At follow-up, most of the struts are fully covered and embedded in the vessel wall and the luminal area can be drawn with an automated detection algorithm available in the Light Lab proprietary software; manual corrections are performed if necessary. Second, since polymeric struts are accurately imaged at baseline, the device area can be obtained manually by joining the middle point of each consecutive strut around the circumference. In frames with only a few struts, the BVS area was adjusted to follow the lumen area in the regions where its contour was outside the lumen area. At follow-up, the BVS area was also measured by joining the middle point of the struts (Figure 3).

Device shrinkage is defined as the decrease over time of the device area with respect to the area measured immediately after the deployment.^{10,11} Absolute late shrinkage has been measured as the difference between the mean BVS area at baseline minus the mean BVS area at follow-up. Relative late shrinkage has been measured as: [(absolute late shrinkage)/baseline mean BVS area] × 100 (Figure 3).

In case of incomplete scaffold/strut apposition (ISA), the area between the backside of the struts and the vessel wall has been measured as ISA area. The neointimal area (NIA) has been measured at follow-up as: BVS area – (Lumen Area – ISA area). The neointimal thickness (NIT) has been measured at follow-up with the 'thickness ruler' tool from the endoluminal border of the black strut core to the lumen.

Moreover, a qualitative assessment of the appearance of polymeric struts has been obtained at follow-up. Basically, the struts were classified as preserved box, open box, dissolved bright box, and dissolved black box in order of decreasing reflectivity (Figure 4).¹ The kappa index to detect the four types of strut appearance was 0.58.¹² Strut tissue coverage was assessed qualitatively when clear neointimal tissue covered the polymeric strut.

Intra-vascular ultrasound acquisition and analysis

The scaffolded segments were examined with phased array IVUS catheters (EagleEye; Volcano Corporation, Rancho Cordova, CA, USA) with an automated pullback at 0.5 mm/s. Lumen area was measured with a validated computer-based contour detection programme (CURAD BV, Wijk bij Duurstede, The Netherlands) that allows for semi-automatic detection of lumen.¹³

Statistical analysis

Normality distribution of continuous variables was explored with the Kolmogorov–Smirnov test. All continuous variables had normal distribution and have been expressed as means and 1 standard deviation (SD). Categorical variables are presented as counts (%). Paired comparisons of continuous variables within groups between the different time points were done by the Wilcoxon's signed rank test. Comparison of continuous variables between Cohorts A and B has been made using the U-Mann–Whitney test. Comparisons of absolute differences

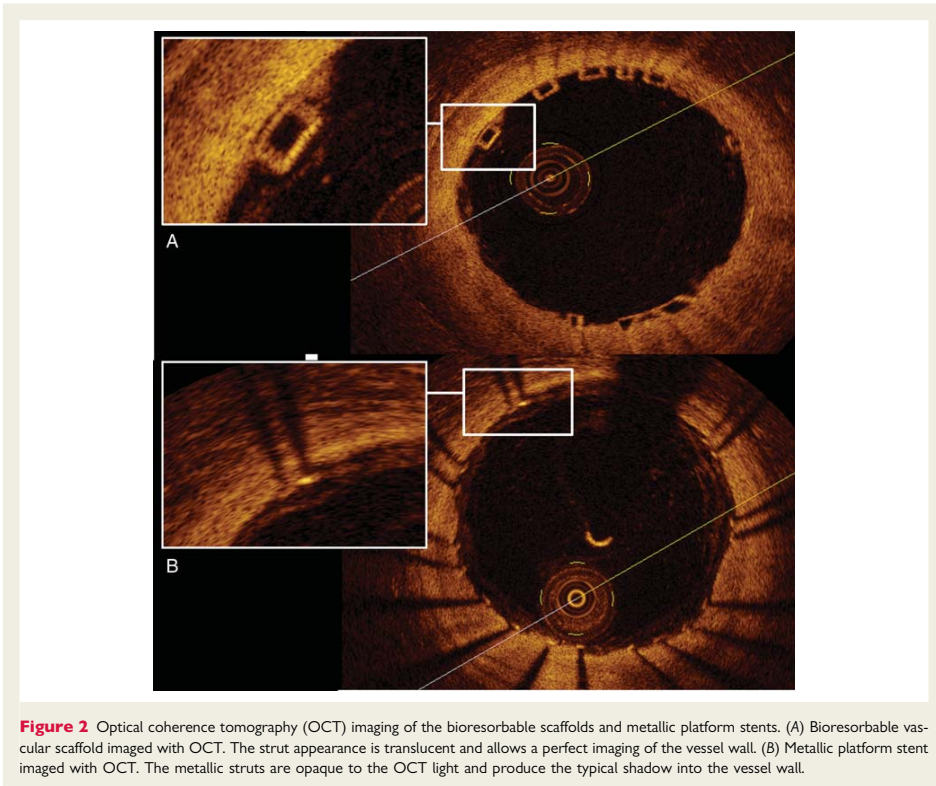


Figure 2 Optical coherence tomography (OCT) imaging of the bioresorbable scaffolds and metallic platform stents. (A) Bioresorbable vascular scaffold imaged with OCT. The strut appearance is translucent and allows a perfect imaging of the vessel wall. (B) Metallic platform stent imaged with OCT. The metallic struts are opaque to the OCT light and produce the typical shadow into the vessel wall.

between baseline and follow-up have also been made with the U-Mann–Whitney test. Comparisons of categorical variables between groups have been made using the Chi-square test or the Fisher test when one of the cells had less than five events. A two-sided P -value ≤ 0.05 was considered statistically significant. All the statistics have been performed with the SPSS 15.0 version for Windows (IL, US).

Results

Study population

A total of 13 lesions in 13 patients had baseline and follow-up OCT imaging in the ABSORB Cohort A study.¹ One of these patients underwent a non-ischæmia driven target lesion revascularization treated with a metallic platform stent at Day 42. The OCT imaging at that time showed strut discontinuation with attached thrombi probably due to overstretching of the BVS during implantation.⁷ This patient has not been included in the present study. In the ABSORB Cohort B study, 28 patients with scheduled imaging control at 6-month follow-up were studied with OCT at baseline.

Two of them were excluded due to the sub-optimal quality of the imaging, and of the remaining 26 patients, 13 were imaged with the M3 OCT system and 13 were imaged with the OCT C7. None of the 13 patients imaged with the M3 system needed an unscheduled angiography and all of them were studied with OCT at 6 months. One patient imaged with the C7 system presented with a symptomatic peri-procedural myocardial infarction at the index procedure secondary to an occlusion of a small diagonal after the implantation of the BVS in the left anterior descending. This patient refused invasive imaging at 6-month follow-up. Finally, 24 patients were included in the present study: 12 were treated with the BVS 1.0 and 12 were treated with the BVS 1.1. None of those patients had BVS fractures at baseline or 6-month follow-up.

The baseline clinical characteristics are shown in Table 1. Both groups were similar in gender and age. There was a trend toward lower percentage of hypercholesterolaemia (72.7 vs. 100.0%; $P = 0.06$) and prior acute myocardial infarction (8.3 vs. 41.7%; $P = 0.06$) in the BVS 1.0 than in the BVS 1.1 group, respectively. There was a significant difference in the smoking status favouring the BVS 1.1 group (33 vs. 0%, respectively; $P = 0.03$).

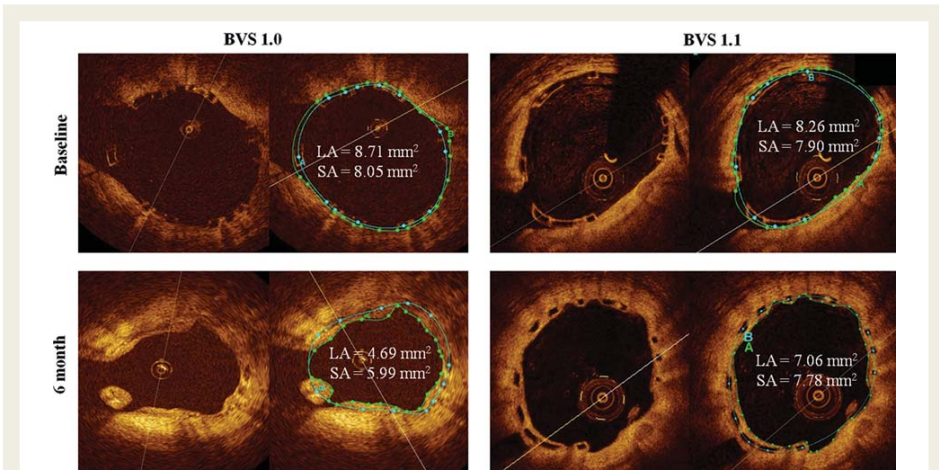


Figure 3 Late shrinkage assessment. Optical coherence tomography (OCT) imaging of the BVS 1.0 and 1.1. At baseline, the scaffold area (SA; blue line) is usually drawn into the luminal area (LA; green line). At follow-up, the neointima covers the polymeric struts and then, the scaffold area usually is drawn outside of the luminal area. The absolute late shrinkage for the BVS 1.0 is 2.06 mm² (relative shrinkage of 25.6%) and for the BVS 1.1 is 0.12 mm² (relative shrinkage of 1.5%).

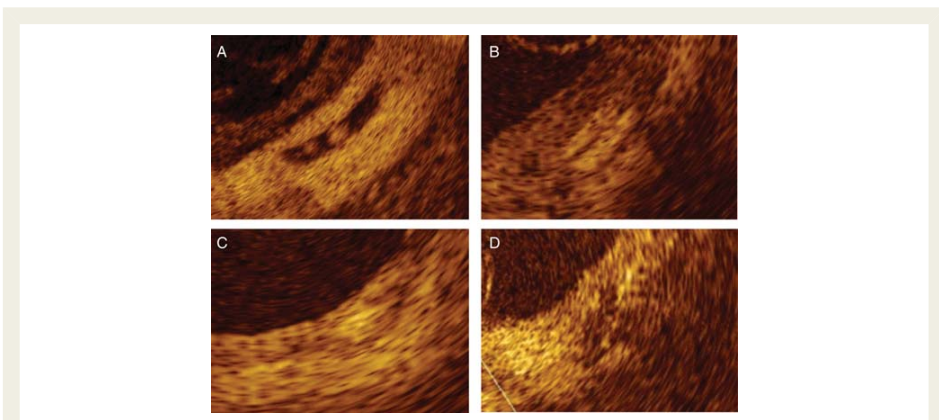


Figure 4 Strut appearance of the bioresorbable vascular scaffold at follow-up. (A) Preserved box appearance: sharp defined, bright reflection borders with preserved box-shaped appearance; strut body shows low reflection; (B) open box: luminal and abluminal long-axis borders thickened bright reflection; short-axis borders not visible; (C) dissolved bright box: partially visible bright spot, contours poorly defined; no box-shaped appearance; (D) dissolved black box: black spot, contours poorly defined, often confluent; no box-shaped appearance.

A total of 11 patients in ABSORB Cohort A were treated with a BVS 1.0 of 3 × 12 mm and 1 was treated with a BVS 1.0 of 3 × 18 mm. All patients of the ABSORB Cohort B were treated with a BVS 1.1 of 3 × 18 mm.

Quantitative coronary angiography results

Baseline and follow-up angiographic parameters are shown in Table 2. Both groups had similar angiographic characteristics at

Table 1 Baseline clinical and angiographic characteristics

	BVS 1.0 (n = 12)	BVS 1.1 (n = 12)	P-value
Male	8 (66.7)	9 (75.0)	0.65
Age (years ± SD)	59.5 ± 8.3	61.2 ± 9.6	0.76
Hypertension	6 (50.0)	7 (58.3)	0.68
Hypercholesterolaemia	8 (72.7)	12 (100.0)	0.06
Diabetes mellitus	1 (8.3)	1 (8.3)	1.00
Smoke	4 (33.3)	0	0.03
Prior MI	1 (8.3)	5 (41.7)	0.06
Prior PCI	2 (16.7)	3 (25.0)	0.62
Clinical indication			0.27
Stable or silent angina	11 (91.7)	9 (75.0)	
Unstable angina	1 (8.3)	3 (25.0)	
Number of vessel disease			0.14
One	12 (100.0)	10 (83.3)	
Two	0	2 (16.7)	
Culprit vessel			0.22
LAD	4 (33.3)	6 (50.0)	
LCX	6 (50.0)	2 (16.7)	
RCA	2 (16.7)	4 (33.3)	
BVS size			<0.01
3 × 12 mm	11 (91.7)	0	
3 × 18 mm	1 (8.3)	12 (100.0)	

Values are expressed as count (%), except for age. MI, myocardial infarction; PCI, percutaneous coronary intervention; LAD, left anterior descending; LCX, left circumflex; RCA, right coronary artery; BVS, bioresorbable vascular scaffold.

pre-implantation. Patients treated with the BVS 1.0 tended to have a larger RVD than patients treated with the BVS 1.1 (2.95 vs. 2.69 mm; $P = 0.14$).

At 6-month follow-up, patients treated with the BVS 1.0 had a significant decrease in MLD (angiographic late loss) of 0.43 mm ($P = 0.01$), whereas a non-significant 0.08 mm decrease was seen in those treated with the BVS 1.1. The difference in late loss between the BVS 1.0 and 1.1, although numerically appreciable, failed to reach statistical significance at 6 months ($P = 0.07$). The serial individual changes in MLD between baseline and follow-up are shown in Figure 5.

Optical coherence tomography results

Baseline and follow-up quantitative OCT and IVUS findings are shown in Table 3. Both groups had similar OCT findings at baseline after the deployment of the BVS. At 6 months, the BVS 1.0 had a significantly higher late shrinkage than the BVS 1.1 (absolute shrinkage of 0.98 vs. 0.07 mm² and relative shrinkage of 13.0 vs. 1.0%, respectively; $P = 0.01$). Neointimal area was significantly higher with the BVS 1.0 when compared with the BVS 1.1 (1.44 vs. 0.87 mm², respectively; $P < 0.01$). NIH was also larger in the

BVS 1.0 than in the BVS 1.1 (166.0 vs. 76.4 μm; $P < 0.01$). These findings at 6 months caused a significantly higher reduction in mean lumen area (relative difference of 35.1 vs. 16.1%; $P < 0.01$) and in minimal luminal area (47.0 vs. 20.7%; $P < 0.01$) with the BVS 1.0 than with the BVS 1.1 as assessed by OCT. Serial individual changes of the BVS area and of the minimal lumen area as assessed by OCT are shown in Figure 5. The ISA area of the BVS 1.0 at 6 months increased significantly with respect to the baseline (0.10 mm²; CI 95%: from -0.02 to 0.21 mm²; $P = 0.04$), while the ISA area of the BVS 1.1 remained unchanged (0.02 mm²; -0.18 to 0.22 mm²; $P = 0.26$).

A total of 662 struts of the BVS 1.0 and 1575 of the BVS 1.1 were detected at baseline. After deployment, all struts appear as preserved box in both BVS devices. At follow-up, 620 struts and 1639 struts were analysed. The strut appearance of the BVS 1.0 showed substantial changes in appearance: at 6 months struts had changed from 100% preserved black box to 29.7% open box, 51.4% dissolved bright box, 16.0% dissolved black box, and only 2.9% were preserved black box. For the BVS 1.1, all struts maintained a preserved black box appearance at 6 months ($P < 0.01$). Uncovered struts were less frequent in the BVS 1.0 (1.1%) than in the BVS 1.1 (5.3%) ($P = 0.01$).

Intravascular-ultrasound results

IVUS results are shown in Table 3. The reduction in mean lumen area was larger with the BVS 1.0 than with the BVS 1.1 (12.71 vs. 6.93%), but this difference was not statistically significant ($P = 0.17$). The reduction in minimal lumen area was significantly larger with the BVS 1.0 than with the BVS 1.1 (22.83 vs. 4.81%; $P < 0.01$).

Reproducibility of optical coherence tomography measurements

The scaffold area reproducibility using our method has been assessed specifically for our study. Two independent analysts measured the scaffold area in 100 images at follow-up. After 1 week, one of the analysts re-analysed the same frames. The inter-observer R^2 for repeated measures was 0.88 and the intraobserver R^2 was 0.98.

Discussion

The main findings of our study are: (i) the BVS 1.1 does not show late shrinkage at 6 months with respect to the baseline scaffold area; (ii) the BVS 1.0 has higher neointimal response and higher in-scaffold area obstruction than the BVS 1.1; (iii) these changes resulted in a higher OCT and IVUS luminal losses and angiographic late loss in the BVS 1.0 than in the BVS 1.1; (iv) the overall strut appearance at 6-month follow-up is dramatically different between the two generations of BVS, which may reflect differences in the polymer's interaction with light, arising from differences in microstructure and its degradation.

A pre-clinical animal study involving histological samples at differing time points divided the evolution process of the BVS into two parts:¹² first, the BVS resorption process, which consists of the disappearance of the polymeric PLA and the subsequent

Table 2 Quantitative coronary angiography findings at baseline and 6-month follow-up

BVS	Pre-deployment	Post-deployment	6-month FU	Difference post-pre (CI 95%)	P-value*	Difference post – 6 m FU (CI 95%)	P-value**	P-value†
QCA								
Lesion length (mm) [§]								
BVS 1.0	9.86 (3.46)	10.34 (1.70)	10.17 (2.20)	-0.48 (-2.90 to 1.94)	0.18	0.18 (-0.26 to 0.61)	0.64	0.93
BVS 1.1	8.99 (2.89)	17.08 (1.12)	16.08 (1.48)	-8.09 (-9.82 to -6.35)	<0.01	1.00 (-0.16 to 2.16)	0.13	
RVD (mm)								
BVS 1.0	2.95 (0.38)	3.03 (0.39)	2.87 (0.41)	0.08 (-0.10 to 0.26)	0.31	0.16 (0.01 to 0.31)	0.04	0.24
BVS 1.1	2.69 (0.35)	2.64 (0.23)	2.53 (0.22)	-0.05 (-0.21 to 0.11)	0.70	0.11 (0.02 to 0.20)	0.03	
MLD (mm)								
BVS 1.0	1.13 (0.30)	2.46 (0.38)	2.03 (0.30)	1.32 (1.03 to 1.62)	<0.01	0.43 (0.13 to 0.73)	0.01	0.07
BVS 1.1	1.23 (0.44)	2.26 (0.28)	2.18 (0.25)	1.03 (0.69 to 1.37)	<0.01	0.08 (-0.14 to 0.30)	0.24	
DS (%)								
BVS 1.0	60.8 (13.4)	18.6 (9.4)	27.8 (16.0)	-42.3 (-50.8 to -33.7)	<0.01	-9.3 (-18.7 to 0.2)	0.07	0.24
BVS 1.1	57.6 (13.1)	14.7 (7.5)	15.7 (9.3)	-42.9 (-50.9 to -35.0)	<0.01	-1.0 (-5.5 to 3.5)	0.66	

Data are expressed as mean (SD).

QCA, quantitative coronary angiography; BVS, bioresorbable vascular scaffold; FU, follow-up; RVD, reference vessel diameter; MLD, minimal lumen diameter; DS, diameter stenosis.

[§]Lesion length at post-procedure and at follow-up has been measured between the platinum markers of the BVS.

*Paired comparison between pre- and post-deployment within each group.

**Paired comparison between post-deployment and follow-up within each group.

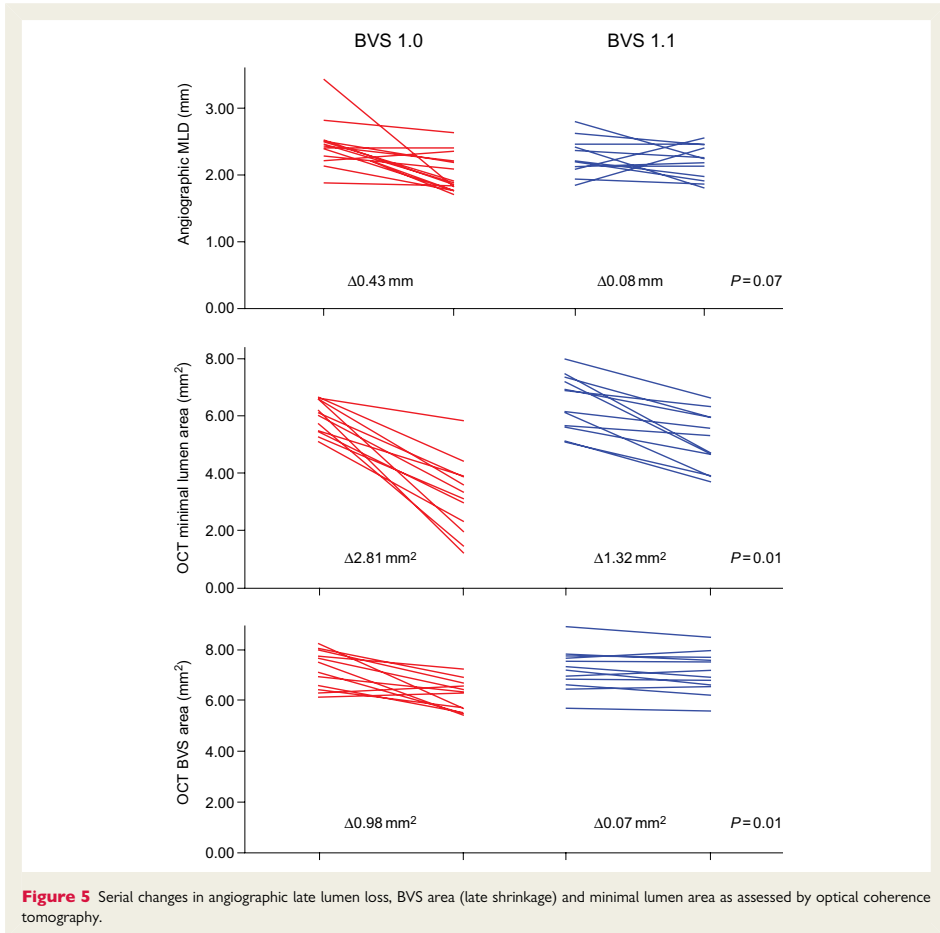
†Comparison of the difference post-deployment—follow-up between the two groups. Comparison between groups at pre-deployment and post-deployment were non-significant ($P > 0.10$).

filling of the strut voids with proteoglycan material; second, the BVS integration process, which consists of the formation of organized tissue with connective cells and connective extracellular matrices replacing the polymeric and the proteoglycan material. In the same study, the strut appearance as assessed by OCT was compared with matched histological sections.¹² At 24 months, all the struts were discernible by OCT and 80.4% of them were classified as having the preserved box appearance (similar to the BVS 1.1 at 6 months). At that point of time, matched histological samples showed that almost all the strut footprints were occupied by proteoglycans and the analysis with gel permeation chromatography did not find traces of the polymeric material. This demonstrated that the polymer was already resorbed at that time, and therefore OCT imaging was not able to assess the resorption process. At 3- and 4-year follow-up, almost all the struts were not discernible and the few observed struts were classified as a dissolved bright or dissolved black box (similar to the BVS 1.0 at 6 months). There was poor correlation of these types of OCT strut appearance with the particular patterns observed on histology. But, the indiscernible struts and the dissolved black box appearance as assessed by OCT were observed as circumscribed regions of dense connective tissue with low cellularity on histology.

Therefore, as assessed by OCT, the most advanced resorption/integration states were characterized as: (i) observation of other types of strut appearance rather than the preserved box; and (ii) the reduction of discernible struts over time jointly with the observation of a dissolved black box strut appearance.¹²

In our study, the number of discernible struts of the BVS 1.1 was slightly lower at baseline than at follow-up (1575 vs. 1639, respectively; $P = 0.06$). At 6 months, the strut appearance was 'preserved' in all the patients. In contrast, the number of discernible struts of the BVS 1.0 was higher at baseline than at follow-up (662 vs. 620, respectively; $P = 0.05$) and at 6 months, only 2.9% of the discernible struts had a preserved box appearance. The correlation of our findings with the animal study shows that the BVS 1.0 had a more advanced resorption/integration state than the BVS 1.1 at 6 months. Our hypothesis is that this faster resorption/integration state is the main cause of the higher late shrinkage and greater neointimal response of the BVS 1.0 compared with the BVS 1.1.

Late shrinkage is a phenomenon resulting from the loss of structural integrity of the polymeric scaffold in conjunction with fatigue and constrictive remodeling of the vessel in the first months following the vessel injury. Loss of structural integrity is an inevitable part of the resorption process of these polymeric devices. The poly-L-lactic acid (PLLA) polymer has a lifecycle which can be divided in five



phases.¹⁴ First, immediately after the deployment, the polymer absorbs water from blood and surrounding tissues. Second, the long chains of PLLA degrade by hydrolysis into smaller chains without affecting the device's structure. Third, the hydrolysis process continues and causes a loss in integrity, with fragmentation of the struts and loss of radial strength. Fourth, soluble monomeric anions dissolve into the intercellular fluid and microparticles of less than 2 μm may be phagocytosed by the macrophages; manifesting in mass loss and bioresorption. Finally, the soluble L-lactate is converted into pyruvate, which enters the Krebs cycle, being eventually converted into carbon dioxide and water. The initial degradation process of the PLLA semi-crystalline polymer depends on the length of the polymers chain (molecular weight), the hydrophilicity, and the degree of crystallinity. In BVS 1.1, initial degradation rate (i.e.

losses in molecular weight leading to structural degradation) has been reduced through changes in the manufacturing process. This slower degradation allows for maintenance of the radial strength over months following the implantation.

The second cause of late shrinkage is the constrictive remodeling of the treated vessel in the first few months after implantation. In the era of balloon angioplasty, more than 70% of the restenotic process was attributed to negative remodeling of the vessel in the treated segment, and less than 30% was done to neointimal growth.¹⁵ In the metallic stent era, late lumen loss within the stent correlated strongly with tissue growth ($r = 0.975$), eliminating negative remodeling as the common cause of restenosis.^{16,17} Thus, the key question for intracoronary bioresorbable scaffolds is for how long radial strength (i.e. scaffolding) must be maintained

Table 3 Quantitative optical coherence tomography and intravascular ultrasound findings at baseline and 6-month follow-up

BVS (n = 12 vs. 12)	Baseline (post-deployment)	6-month FU	Absolute difference between BL and FU (CI 95%)	Relative difference between BL and FU (%)	P-value*	P-value**
OCT						
Mean luminal area (mm ²)						
1.0 BVS	7.63 (0.79)	4.94 (1.10)	2.69 (1.99–3.39)	35.07 (13.31)	<0.01	<0.01
1.1 BVS	7.67 (0.94)	6.44 (0.93)	1.23 (0.89–1.57)	16.09 (6.48)	0.01	
Minimal luminal area (mm ²)						
1.0 BVS	5.99 (0.57)	3.19 (1.28)	2.81 (2.03–3.59)	46.97 (19.67)	<0.01	<0.01
1.1 BVS	6.32 (0.96)	5.01 (0.97)	1.32 (0.83–1.80)	20.65 (10.94)	<0.01	
Mean BVS area (mm ²)						
1.0 BVS	7.18 (0.73)	6.20 (0.64)	0.98 (0.42–1.54)	12.95 (11.70)	0.01	0.01
1.1 BVS	7.21 (0.82)	7.14 (0.84)	0.07 (–0.10 to 0.24)	0.97 (3.73)	0.37	
Minimal BVS area (mm ²)						
1.0 BVS	5.82 (0.60)	4.75 (0.83)	1.07 (0.49–1.66)	17.90 (14.26)	<0.01	0.01
1.1 BVS	6.21 (0.98)	6.00 (0.85)	0.21 (–0.14 to 0.56)	2.81 (8.11)	0.29	
ISA area (mm ²)						
1.0 BVS	0.14 (0.25)	0.22 (0.31)	–0.10 (–0.21 to 0.02)	–36.36 (10.33)	0.04	0.88
1.1 BVS	0.15 (0.30)	0.17 (0.18)	–0.02 (–0.22 to 0.18)	–11.76 (15.35)	0.26	
NIA (mm ²)						
1.0 BVS	NA	1.44 (0.32)	NA	NA	NA	<0.01 ^a
1.1 BVS	NA	0.87 (0.22)	NA	NA	NA	
NIT (mm)						
1.0 BVS	NA	0.17 (0.04)	NA	NA	NA	<0.01 ^a
1.1 BVS	NA	0.08 (0.02)	NA	NA	NA	
In-device area obstruction (%)						
1.0 BVS	NA	23.62 (6.55)	NA	NA	NA	<0.01 ^a
1.1 BVS	NA	12.28 (3.38)	NA	NA	NA	
IVUS						
Mean luminal area (mm ²)						
1.0 BVS	6.84 (0.74)	5.94 (0.67)	0.90 (0.43–1.37)	12.71 (9.89)	<0.01	0.17
1.1 BVS	6.69 (0.81)	6.20 (0.76)	0.47 (0.24–0.69)	6.93 (4.68)	<0.01	
Minimal luminal area (mm ²)						
1.0 BVS	5.75 (0.52)	4.41 (0.70)	1.34 (0.83–1.84)	22.83 (12.73)	<0.01	<0.01
1.1 BVS	5.51 (0.78)	5.15 (0.73)	0.28 (–0.01 to 0.57)	4.81 (7.20)	0.09	

Data are expressed in mean (SD).

OCT, optical coherence tomography; IVUS, intravascular ultrasound; ISA, incomplete scaffold/strut apposition; NIA, neointimal area; NIT, neointimal thickness; NA, not applicable.

Comparison of the OCT and IVUS findings at baseline between groups showed no significant differences.

^aComparison of the neointimal hyperplasia (NIA and NIT) and in-device area obstruction at follow-up between groups.

*P-value between baseline and follow-up within groups.

**P-value comparing the absolute differences between groups.

to avoid constrictive remodelling. In a cohort of patients consecutively re-catheterized at 1, 2, 3, and 4 months, Serruys *et al.*¹⁸ demonstrated that the restenotic process after balloon angioplasty ceases to progress after 4 months. It is possible that after this time, scaffolding is no longer needed, and the structural degradation and bioresorption processes can commence.

It is uncertain whether the constrictive remodelling is more focused in the regions of the vessel with more plaque burden or is equally distributed. This can affect the results of our study due

to the differences in the BVS lengths according to the lesion length. The lesion length prior to the implantation was similar in both groups (around 9–10 mm), but the device length as assessed by QCA at post-deployment was significantly higher in the BVS 1.1 than in the BVS 1.0 (17.08 vs. 10.34 mm; $P < 0.01$). This difference resulted from the fact that all patients treated in the ABSORB Cohort B study received a single size device (3 × 18 mm), while in the ABSORB Cohort A there were two different sizes (3 × 12 and 3 × 18 mm). A sub-analysis of the 12 central millimetre

of the scaffold imaged by OCT (that part of the scaffold is more likely to be located at the nadir of the narrowing) in the patients treated with a 3×18 mm showed that the mean scaffold area at baseline and at 6-month follow-up was 7.18 and 6.19 mm² with the BVS 1.0 (relative shrinkage of 13.09%) and 7.14 and 7.10 mm² with the BVS 1.1 (relative shrinkage of 0.50%); $P = 0.01$.

Until now, four different fully bioresorbable scaffolds have been tested in humans. The polymeric PLLA non-drug-eluting Igaki-Tamai device was the first fully bioresorbable scaffold used in humans. The IVUS analysis did not show bioresorption of the polymeric struts at 6 months and this absence of ultrasonic changes in struts was parallel to the absence of scaffold shrinkage. This device presented a target vessel revascularization of 6.7% at 6 months and a low rate of major cardiac events at 10 years.^{19,20} Conversely, the PROGRESS-AMS magnesium platform non-drug-eluting bioresorbable scaffold had a rapid resorption which was complete at 4-month follow-up. This swift resorption produced an important reduction of the lumen (60% of the late lumen loss) and a high incidence of restenosis (47.5% assessed by QCA).²¹ The REVA device is a poly (iodinated desaminotyrosyl-tyrosine ethyl ester) carbonate non-drug-eluting scaffold. The closed design and the lifecycle of the carbonate provide enough radial strength during the first 3 months following the implantation without appreciable shrinkage. However, focal mechanical failures driven by polymer embrittlement led to a high rate of TLR (66.7% between 4- and 6-month follow-up.²² Finally, the IDEAL™ Poly (Anhydride Ester) Salicylic acid sirolimus-eluting device has been tested in only 11 patients.²³

The shrinkage phenomenon observed in the BVS 1.0 was linked to a significant increase of the ISA area with respect to baseline and with higher neointimal response with respect to the BVS 1.1. The increasing of the ISA area with the BVS 1.0 can be explained by the scaffold shrinkage itself. At baseline, 95% of the struts were apposed or aligned, while in the follow-up only 93% of the struts were apposed to the vessel wall. Moreover, less than 10% of the malapposed struts at baseline were resolved at follow-up.¹ The NIA measured in this population was significantly different between the two generations of BVS (1.44 mm² for the BVS 1.0 vs. 0.87 mm² for the BVS 1.1). In-scaffold area obstruction was also different between BVS 1.0 and 1.1 (23.6 vs. 12.3%, respectively). The significantly lower neointimal response of the BVS 1.1 with respect to the BVS 1.0 has no clear explanation. Both generations of BVS are built with the same polymer mass, strut thickness, drug, and coating elution and the same amount of drug. One hypothesis is that the loss in scaffold area leads to a decreased efficiency in drug transfer to the vessel wall and thus, a reduction in antiproliferative efficacy. Another hypothesis is that the more accelerated resorption/integration process of the BVS 1.0 compared with the BVS 1.1 could generate a larger neointimal response. Unfortunately, this cannot be assessed by OCT due to the lack of correlation between the different types of strut appearance and the histological findings based on animal studies.¹² An exploratory analysis of the patients treated with the BVS 1.0 in our study relating the NIT measured above the preserved box appearance (0.15 ± 0.04 μm) with the NIT measured above the other types of strut appearance (0.18 ± 0.06) failed to be significant ($P = 0.27$). The same patients treated with the BVS 1.0

studied with OCT at 2 years showed few discernible struts with no measurable neointima. Nevertheless, the mean lumen area increased up to 19% from 6-month to 2-year follow-up.⁴ This fact may be a sign of vessel remodelling at the neointimal level but the low number of patients are a clear limitation to this conclusion. This hypothesis will be examined further when the strut appearance of patients treated with the BVS 1.1 changes in future scheduled imaging controls.

The OCT performance of the BVS 1.1 can be compared with some drug-eluting stents (DES). The NIT observed in the BVS 1.1 (0.08 mm) is similar to that seen with the sirolimus-DES (from 0.05 to 0.12 mm) at 6-month follow-up.^{24,25} Paclitaxel-DES and zotarolimus-DES showed an NIT of 0.20 and 0.33 mm, respectively.²⁴ The late shrinkage of metallic DES has not been yet explored with OCT. Using IVUS, the everolimus-DES showed a relative difference in mean stent area of 0.3% at 6-month follow-up.²⁶ This value is similar to the 1.0% found in our study with the BVS 1.1. Based on this information, the BVS 1.1 presents a similar profile as the metallic DES as assessed by OCT.

In summary, our study represents the first comparison of two generations of bioresorbable devices in terms of late shrinkage, neointimal response, and bioresorption state using the most sophisticated intravascular imaging technique (OCT) and the same methodology for both devices. The OCT findings at 6 months show the improvement of the new generation of BVS with respect to the previous generation. The slower bioresorption process of the BVS 1.1, compared with the BVS 1.0, is the most plausible explanation for the near elimination of the late shrinkage and for the higher inhibition of the neointimal response. Further investigations will be required to assess the preservation of these results after 6-month follow-up for the BVS 1.1. A more advanced bioresorption state can contribute to a very late shrinkage of the device or later neointimal responses.

Limitations

The result of the present analysis must be interpreted with caution as a major limitation of our study is the small number of patients who have been enrolled in a non-randomized comparison. Figure 5 shows that there is a homogeneous trend of higher late shrinkage and higher loss in minimal lumen area in the BVS 1.0 than in the BVS 1.1. The histogram distribution of the NIA in the two populations also shows this trend of higher neointimal growth in the BVS 1.0 than in the BVS 1.1 (data not shown). This trend, however, is not observed with the angiographic late lumen loss in which one outlier can be influencing the higher late lumen loss in the BVS 1.0. Moreover, two eligible patients imaged at baseline and scheduled for an invasive follow-up at 6 months did not undergo repeat invasive imaging. It is uncertain how this lack of serial imaging in those patients affects the global results of our study. Although the small number of patients, we have used the maximal number of 'historical' cases performed with the BVS 1.0 and imaged with the best available OCT system M2 at that time and compared with the same number of patients of the BVS 1.1 imaged with the best available system nowadays (OCT C7 system).

These differences in OCT systems are inherent to the fact that the ABSORB Cohort A trial was conducted in 2006, when a

balloon occlusive technique was needed due to the lower frame/rate and acquisition speed of the available systems at that time. One *in vitro* study showed less accuracy in the lumen area measurement with lower frame rate and acquisition speed than with higher frame/rate and speed.²⁷ An *in vivo* study, comparing the non-occlusive and the occlusive technique in the same non-scaffolded native coronary artery, showed systematically smaller mean and minimal lumen areas with the occlusive technique than with the non-occlusive technique (relative differences of 13.2 and 28.2%, respectively).²⁸ These differences were probably produced by the lack of physiological pressurization of the vessel during the occlusive technique imaging and/or the over-pressurization of the vessel during the contrast infusion of the non-occlusive technique.²⁸ These differences represent an important limitation of our study because the two different devices were imaged with different OCT techniques (occlusive for the BVS 1.0 and non-occlusive for the BVS 1.1). However, in our study, the baseline and follow-up acquisition were performed using the same imaging technique in each cohort of patients and also, the analysed region is scaffolded by the BVS. The scaffolded region is probably less susceptible to changes in volumetric parameters according to the intravascular pressure. Unfortunately, there is no current information comparing the changes in lumen areas within the scaffolded regions with the two different OCT techniques.

The method of analysis used in our study is slightly different from the current method of OCT measurement of polymeric scaffold. The strut appearance of the BVS 1.0 at 6 months (and probably the appearance of the BVS 1.1 in later controls) does not permit the delineation of the strut contour at the front or backside of the strut. Using the central part of the strut as landmark for measurement is the most reliable method to assess the scaffold area. However, it must be recognized that the neointima area as such determined is an arbitrary entity resulting from the difference between the luminal area and the scaffold area, and does not depict accurately the neointimal tissue that has grown between, on the top and behind the struts either biologically altered in the case of the BVS 1.0 or almost intact in the case of the BVS 1.1.

Finally, the differences in device lengths in the two groups may be favourable to the BVS 1.1 due to a better anchoring in the healthy part of the vessel that can be subjected to a less constrictive modelling of the vessel.

Conclusion

The two generations of the everolimus-eluting bioresorbable vascular scaffold have different OCT findings at 6-month follow-up. The BVS 1.1 has less late shrinkage and less neointimal growth at 6-month follow-up compared with the BVS 1.0. Consequently, less angiographic late loss and less OCT and IVUS luminal losses were observed with the BVS 1.1. A difference in polymer degradation leading to changes in microstructure and reflectivity is the most plausible explanation for this finding.

Conflict of interest: S.W. is a consultant for Abbott, Biosensors, Boston Scientific, Cordis and Medtronic.

Funding

This work was supported by Abbott.

References

- Ormiston JA, Serruys PW, Regar E, Dudek D, Thuesen L, Webster MW, Onuma Y, Garcia-Garcia HM, McGreevy R, Veldhof S. A bioabsorbable everolimus-eluting coronary stent system for patients with single de-novo coronary artery lesions (ABSORB): a prospective open-label trial. *Lancet* 2008;**371**: 899–907.
- Painter JA, Mintz GS, Wong SC, Popma JJ, Pichard AD, Kent KM, Satler LF, Leon MB. Serial intravascular ultrasound studies fail to show evidence of chronic Palmaz-Schatz stent recoil. *Am J Cardiol* 1995;**75**:398–400.
- Okamura T, Garg S, Gutierrez-Chico JL, Shin ES, Onuma Y, Garcia-Garcia HM, Rapoza R, Sudhir K, Regar E, Serruys PW. In vivo evaluation of stent strut distribution patterns in the bioabsorbable everolimus-eluting device: an OCT ad hoc analysis of the revision 1.0 and revision 1.1 stent design in the ABSORB clinical trial. *EuroIntervention* 2010;**5**:932–938.
- Serruys PW, Ormiston JA, Onuma Y, Regar E, Gonzalo N, Garcia-Garcia HM, Nieman K, Bruining N, Dorange C, Hiquel-Hebert K, Veldhof S, Webster M, Thuesen L, Dudek D. A bioabsorbable everolimus-eluting coronary stent system (ABSORB): 2-year outcomes and results from multiple imaging methods. *Lancet* 2009;**373**:897–910.
- Kawase Y, Hoshino K, Yoneyama R, McGregor J, Hajjar RJ, Jang IK, Hayase M. In vivo volumetric analysis of coronary stent using optical coherence tomography with a novel balloon occlusion-flushing catheter: a comparison with intravascular ultrasound. *Ultrasound Med Biol* 2005;**31**:1343–1349.
- Suzuki Y, Ikeno F, Koizumi T, Tio F, Yeung AC, Yock PG, Fitzgerald PJ, Fearon WF. In vivo comparison between optical coherence tomography and intravascular ultrasound for detecting small degrees of in-stent neointima after stent implantation. *JACC Cardiovasc Interv* 2008;**1**:168–173.
- Onuma Y, Serruys PW, Ormiston JA, Regar E, Webster M, Thuesen L, Dudek D, Veldhof S, Rapoza R. Three-year results of clinical follow-up after a bioresorbable everolimus-eluting scaffold in patients with de novo coronary artery disease: the ABSORB trial. *EuroInterv* 2010;**6**:447–453.
- Reiber JH, Serruys PW, Kooijman CJ, Wijns W, Slager CJ, Gebrands JJ, Schuurbers JC, den Boer A, Hugenholz PG. Assessment of short-, medium-, and long-term variations in arterial dimensions from computer-assisted quantitation of coronary cineangiograms. *Circulation* 1985;**71**:280–288.
- Takarada S, Imanishi T, Liu Y, Ikejima H, Tsuboioka H, Kuroi A, Ishibashi K, Komukai K, Tanimoto T, Ino Y, Kitabata H, Kubo T, Nakamura N, Hirata K, Tanaka A, Mizukoshi M, Akasaka T. Advantage of next-generation frequency-domain optical coherence tomography compared with conventional time-domain system in the assessment of coronary lesion. *Catheter Cardiovasc Interv* 2009;**75**: 202–206.
- Tanimoto S, Serruys PW, Thuesen L, Dudek D, de Bruyne B, Chevalier B, Ormiston JA. Comparison of in vivo acute stent recoil between the bioabsorbable everolimus-eluting coronary stent and the everolimus-eluting cobalt chromium coronary stent: insights from the ABSORB and SPIRIT trials. *Catheter Cardiovasc Interv* 2007;**70**:515–523.
- Tanimoto S, Bruining N, van Domburg RT, Rotger D, Radeva P, Ligthart JM, Serruys PW. Late stent recoil of the bioabsorbable everolimus-eluting coronary stent and its relationship with plaque morphology. *J Am Coll Cardiol* 2008;**52**: 1616–1620.
- Onuma Y, Serruys P, Perkins L, Okamura T, Gonzalo N, Garcia-Garcia HM, Regar E, Kamberi M, Powers JC, Rapoza R, van Beusekom H, van der Giessen W, Virmani R. Intracoronary optical coherence tomography (OCT) and histology at 1 month, at 2, 3 and 4 years after implantation of everolimus-eluting bioresorbable vascular scaffolds in a porcine coronary artery model: An attempt to decipher the human OCT images in the ABSORB trial. *Circulation* 2010; Published online ahead of print 25 October 2010.
- von Birgelen C, de Vrey EA, Mintz GS, Nicosia A, Bruining N, Li W, Slager CJ, Roelandt JR, Serruys PW, de Feyter PJ. ECG-gated three-dimensional intravascular ultrasound: feasibility and reproducibility of the automated analysis of coronary lumen and atherosclerotic plaque dimensions in humans. *Circulation* 1997;**96**: 2944–2952.
- Aalst M, Eenink M, Krufft M, van Tuil R. ABC's of bioabsorption: application of lactide based polymers in fully resorbable cardiovascular stents. *Eurointervention* 2009;**5**(Suppl. F):F23–F27.
- Mintz GS, Popma JJ, Pichard AD, Kent KM, Satler LF, Wong C, Hong MK, Kovach JA, Leon MB. Arterial remodeling after coronary angioplasty: a serial intravascular ultrasound study. *Circulation* 1996;**94**:35–43.
- Hoffmann R, Mintz GS, Dussallant GR, Popma JJ, Pichard AD, Satler LF, Kent KM, Griffin J, Leon MB. Patterns and mechanisms of in-stent restenosis. A serial intravascular ultrasound study. *Circulation* 1996;**94**:1247–1254.

17. Nakamura M, Yock PG, Bonneau HN, Kitamura K, Aizawa T, Tamai H, Fitzgerald PJ, Honda Y. Impact of peri-stent remodeling on restenosis: a volumetric intravascular ultrasound study. *Circulation* 2001;**103**:2130–2132.
18. Serruys PW, Luitjen HE, Beatt KJ, Geuskens R, de Feyter PJ, van den Brand M, Reiber JH, ten Katen HJ, van Es GA, Hugenholtz PG. Incidence of restenosis after successful coronary angioplasty: a time-related phenomenon. A quantitative angiographic study in 342 consecutive patients at 1, 2, 3, and 4 months. *Circulation* 1988;**77**:361–371.
19. Tamai H, Igaki K, Kyo E, Kosuga K, Kawashima A, Matsui S, Komori H, Tsuji T, Motohara S, Uehata H. Initial and 6-month results of biodegradable poly-L-lactic acid coronary stents in humans. *Circulation* 2000;**102**:399–404.
20. Nishio S, Kosuga K, Okada M, Harita T, Ishii M, Kawata Y, Takeda S, Takeuchi Y, Hata T, Ikeguchi S. Long term (>10 years) clinical outcomes of the first-in-man biodegradable poly-L-lactic acid coronary stents. Oral presentation. Paris: EuroPCR; 2010.
21. Erbel R, Di Mario C, Bartunek J, Bonnier J, de Bruyne B, Eberli FR, Erne P, Haude M, Heublein B, Horigan M, Ilseley C, Bose D, Koolen J, Luscher TF, Weissman N, Waksman R. Temporary scaffolding of coronary arteries with bioabsorbable magnesium stents: a prospective, non-randomised multicentre trial. *Lancet* 2007;**369**:1869–1875.
22. Pollman M. Engineering a bioresorbable stent: the REVA programme update. *Euro-Intervention* 2009;**5**(Suppl. F):F54–F57.
23. Jabara R. *Poly-anhydride Basic on Salicylic Acid and Adipic Acid Anhydride*. Barcelona: EuroPCR; 2009.
24. Guagliumi G, Musumeci G, Sirbu V, Bezerra HG, Suzuki N, Fiocca L, Matashvili A, Lortkipanidze N, Trivisonno A, Valsecchi O, Biondi-Zoccai G, Costa MA. Optical coherence tomography assessment of in vivo vascular response after implantation of overlapping bare-metal and drug-eluting stents. *JACC Cardiovasc Interv* 2010;**3**: 531–539.
25. Matsumoto D, Shite J, Shinke T, Otake H, Tanino Y, Ogasawara D, Sawada T, Paredes OL, Hirata K, Yokoyama M. Neointimal coverage of sirolimus-eluting stents at 6-month follow-up: evaluated by optical coherence tomography. *Eur Heart J* 2007;**28**:961–967.
26. Serruys PW, Ong AT, Piek JJ, Neumann FJ, van der Giessen WJ, Wiemer M, Zeiher A, Grube E, Haase J, Thuesen L, Hamm C, Otto-Terlouw PC. A randomized comparison of a durable polymer Everolimus-eluting stent with a bare metal coronary stent: The SPIRIT first trial. *EuroIntervention* 2005;**1**:58–65.
27. Sawada T, Shite J, Negi N, Shinke T, Tanino Y, Ogasawara D, Kawamori H, Kato H, Miyoshi N, Yoshino N, Kozuki A, Koto M, Hirata K. Factors that influence measurements and accurate evaluation of stent apposition by optical coherence tomography. Assessment using a phantom model. *Circ J* 2009;**73**: 1841–1847.
28. Gonzalo N, Serruys PW, Garcia-Garcia HM, van Soest G, Okamura T, Ligthart J, Knaepen M, Verheyde S, Bruining N, Regar E. Quantitative ex vivo and in vivo comparison of lumen dimensions measured by optical coherence tomography and intravascular ultrasound in human coronary arteries. *Rev Esp Cardiol* 2009;**62**: 615–624.

Part 6

Summary and Conclusions

Chapter 24

Summary and Conclusions

SUMMARY AND CONCLUSIONS

Despite the enormous progress made in reducing the incidence of restenosis with first and second generation drug-eluting stents (DES) the incidence of in-stent restenosis requiring target vessel revascularization is estimated 5-10%. The utilization of bioresorbable scaffolds for coronary revascularization has shown comparable in-scaffold restenosis rates with DES; however these devices need to prove their safety, efficacy and performance in larger randomized trials and broader clinical subsets. This thesis provides important data regarding the long-term in-segment vascular responses evaluated with intracoronary imaging modalities and pathology following implantation of either metallic stents or bioresorbable scaffolds.

VASCULAR RESPONSES IN THE ERA OF METALLIC AND BIORESORBABLE DEVICES

Angiographic evaluation of the device/tissue interaction utilizing bare-metal stents (BMS) or drug-eluting metallic stents has shown either focal or diffuse distribution of the restenotic response with multiple subtypes within each group. More specific the pattern of restenosis seen with DES is usually focal and more in particular aggregated at the proximal stent edge. **Chapters 2-3**, describe the underlying mechanisms of DES restenosis which can be broadly divided in 4 main causes, namely implantation, arterial, stent and biological factors. Edge vascular responses (EVR) share similar precipitating factors: 1. Iatrogenic or implantation factors, related to the peri-procedural geographic miss which can be either axial or longitudinal, 2. Device factors, associated with the material properties of the implanted platform (metal or bioresorbable alloy), the device induced edge dissections and the type/release kinetics of the antiproliferative agents and 3. Biologic factors, associated with the remaining plaque burden at the proximal and distal edges. **Chapter 4**, provides evidence of the edge vascular responses (EVR) assessed either angiographically or by IVUS-based imaging modalities up to 2-year following implantation of either metallic stents or bioresorbable scaffolds. The chapter describes a target lesion revascularization rate (TLR) of ~3% up to 2-year following implantation of a fully bioresorbable device attributed mainly to proximal restenosis.

IN VIVO ASSESSMENT OF VASCULAR RESPONSES UTILIZING INTRAVASCULAR ULTRASOUND (IVUS) AND IVUS-BASED IMAGING MODALITIES

Gray-scale IVUS (GS-IVUS) has been the gold standard for *in vivo* imaging of coronary vessel wall and an important invasive diagnostic tool for quantitative assessment of interventional therapies and atherosclerosis progression/regression. Meanwhile gray-scale representation of plaque morphology associated with the limited resolution of current IVUS catheters (~45MHz) makes it challenging, if not impossible, to identify qualitatively (e.g. visually) plaque morphology similar to histopathology, the gold standard for tissue characterization. Meanwhile, this limitation has been partially overcome by novel IVUS-based post-processing modalities such as: virtual histology IVUS (VH-IVUS). The principles of each IVUS-based imaging modality with insights in the process of tissue characterization as fibrous, fibro-fatty, necrotic core and dense calcium are provided in **Chapter 6**.

In the ABSORB Cohort B trial 101 patients (Group B₁=45, Group B₂=56) were treated with the second generation fully resorbable scaffold, ABSORB BVS. The adjacent (5-mm) proximal and distal to the implanted device segments were investigated at either 6-months (Group B₁) or 1-year (Group B₂) with GS-IVUS and VH-IVUS imaging. Twenty-three proximal and 18 distal edge segments were available for analysis at 6-months, while 25 proximal and 30 distal edge segments were available at 1-year. At the 5-mm proximal edge, the only significant change was modest constrictive remodeling at 6-months (Δ vessel cross-sectional area: -1.80% [-3.18; 1.30], $p < 0.05$), with a tendency to regress at 1-year (Δ vessel cross-sectional area: -1.53% [-7.74; 2.48], $p=0.06$). The relative changes of fibrotic and fibro-fatty tissue components at this segment were not significant at either time point. At the 5-mm distal edge, a significant increase in the fibro-fatty tissue of 43.32% [19.90; 244.28], ($p < 0.05$) 1-year post-implantation became evident. (**Chapter 7**) The vascular response up to 1-year after implantation of the ABSORB BVS demonstrated some degree of proximal edge constrictive remodeling and distal edge increase in FF tissue resulting in non-significant plaque progression with adaptive expansive remodeling. This morphological and tissue composition behavior did not significantly differ from the behavior of metallic drug-eluting stents at the same observational time points.

The comparison of the long-term vascular responses at the proximal and distal edges of 2 different everolimus-eluting platforms, the metallic Xience V and the bioresorbable ABSORB BVS were explored for the first time in a longitudinal fashion from the SPIRIT II (n=113) and ABSORB Cohort B₁ (n=45) trials respectively. (**Chapter 8**) The 5-mm proximal and distal segments adjacent to the implanted devices were investigated with GS-IVUS and VH-IVUS post-procedure, at 6-months and 2-year following implantation of the bioresorbable device while similar analysis was performed with GS-IVUS following implantation of the metallic stent.

Twenty-two proximal and 24 distal edge segments were available for analysis in the ABSORB Cohort B1 trial. In the SPIRIT II trial, thirty-three proximal and forty-six distal edge segments were analyzed. At the 5-mm proximal edge, the vessels treated with an Absorb BVS at 2-year demonstrated a lumen loss (LL) of 6.68% (- 17.33; 2.08) (p=0.027) with a trend toward plaque area increase of 7.55% (- 4.68; 27.11) (p=0.06). At the 5-mm distal edge no major changes were evident at either time point. At the 5-mm proximal edge the vessels treated with a XIENCE V EES at 2-years did not show any signs of LL, only plaque area decrease of 6.90% (-17.86; 4.23) (p=0.035). At the distal edge no major changes were evident with regard to either lumen area or vessel remodelling at the same time point. The IVUS-based serial evaluation of the EVR up to 2-year following implantation of a bioresorbable everolimus-eluting scaffold shows a statistically significant proximal edge LL. The upcoming imaging follow-up of the Absorb BVS at 3-year is anticipated to provide further information regarding the vessel wall behavior at the scaffold edges.

In **Chapter 9**, IVUS palpography was used to evaluate changes of vascular compliance in the scaffolded segments and the adjacent proximal and distal edges as the bioresorbable scaffold resorbs over time. IVUS palpography is a technique that allows for the assessment of local mechanical tissue properties. A total of 83 patients from the ABSORB Cohort A and B trials underwent palpography investigations (30 and 53 patients from ABSORB Cohort A and Cohort B, respectively). A significant decrease in compliance in the scaffolded segment post-implantation was evident. At the various follow-up time points, no mismatch in compliance was found either in Cohort A (6-months=proximal edge 0.29 [0.18–0.35] vs. scaffold segment 0.10 [0.06–0.22] vs. distal edge 0.16 [0.05–0.24]; p=0.146; 24-months proximal edge 0.20 [0.09–0.30] vs. scaffold segment 0.24 [0.17–0.29] vs. distal edge 0.11 [0.05–0.24]; p=0.052) or Cohort B (6 months=proximal edge

0.28 [0.16–0.46] vs. scaffold segment 0.23 [0.14–0.29] vs. distal edge 0.11 [0.05–0.17]; $p=0.449$; 12 months=proximal edge 0.18 [0.10–0.36] vs. scaffold segment 0.16 [0.08–0.26] vs. distal edge 0.11 [0.02–0.20]; $p=0.618$). Although the Absorb BVS induced changes in vascular compliance at the site of scaffold implantation, the observed compliance mismatch was transient and normalized over time following scaffold resorption which potentially influences local hemodynamic and rheologic conditions.

In **Chapter 10**, we used finite element methods and advanced computational fluid dynamics (CFD) simulations to visualize the hemodynamic implications following virtual deployment of a bioresorbable scaffold with similar design like Absorb BVS in idealized straight and curved geometries. WSS was calculated at the inflow, endoluminal, and the outflow of each strut surface post-procedure (stage I) and at a time point when 33% of scaffold resorption had been achieved (stage II).

The average WSS at stage I over the inflow and outflow surfaces were 3.2 and 3.1 dynes/cm² respectively and 87.5 dynes/cm² over endoluminal strut surface in the straight vessel. From stage I to stage II, WSS increased by 101% and 145% over the inflow and outflow surfaces, respectively, and decreased by 27% over the endoluminal strut surface. In a curved vessel, WSS change became more evident in the inner curvature with an increase of 60.3% and 63.0% over the inflow and outflow strut surfaces. Similar analysis at the proximal and distal edges demonstrated a dramatic increase of 486.4% at the lateral outflow surface of the proximal scaffold edge. The implementation of CFD simulations over virtually deployed bioresorbable scaffolds demonstrate the transient nature of device/flow interactions as the bioresorption process progresses over time. Such hemodynamic device modeling is expected to guide future bioresorbable scaffold design.

IN VIVO ASSESSMENT OF VASCULAR RESPONSES UTILIZING OPTICAL COHERENCE TOMOGRAPHY

OCT permits high resolution imaging with a near-histologic resolution of ~15 μ m which makes this modality ideal for studying the device/vessel interaction. Histomorphometry has been crucial in the evaluation of the performance of new devices and the subse-

quent vascular responses. As histology is limited to animal and human post-mortem studies *in-vivo* assessment of the vascular responses using OCT is highly desirable.

In **Chapter 11** we assessed morphometric parameters of strut remnants with OCT and histology at 2-year following implantation of 22 polymeric BVS in 11 healthy porcine coronary arteries. We evaluated the area and thickness of strut voids previously occupied by polymeric struts and the neointimal hyperplasia area covering the endoluminal surface of strut voids as well as the neointimal hyperplasia area occupying the space between strut voids. Our study indicated that *in vivo* OCT of the BVS provides correlated measurements of the same order of magnitude as histomorphometry, and is reproducible for the evaluation of certain vascular and device-related characteristics. However, histology systematically gives larger values for all the measured structures compared to OCT, at 2-year post implantation.

In **Chapter 12**, OCT and histology were used to assess and compare the vascular responses following either overlapping Absorb BVS or Xience V (XV) metallic stents at 28- and 90-days in a porcine coronary artery model. At 28-days in the overlap, OCT analyses indicated 80.1% of Absorb struts and 99.4% of XV struts to be covered ($p < 0.0001$), corresponding to histological observations of struts with cellular coverage of 75.4% and 99.6%, respectively ($p < 0.001$).

Uncovered struts were almost exclusively related to the presence of “stacked” Absorb struts, that is, with a direct overlay configuration. At 90 days, overlapping Absorb and overlapping XV struts demonstrated >99% strut coverage by OCT and histology. In porcine coronary arteries implanted with overlapping Absorb or overlapping XV struts, strut coverage is delayed at 28-days in overlapping Absorb scaffolds, while at 90-days both devices have comparable strut coverage which implies the impact of strut thickness in the observed vascular responses.

In **Chapters 13-14**, OCT was used to evaluate the edge vascular responses following edge dissections induced by metallic stents. Although IVUS and IVUS-based modalities with tissue characterization properties were the sole intravascular imaging techniques for the evaluation of the transition zones (edges), OCT with its ultra-high spatial resolution and the faster pull-back speed of 20-40 mm/sec provides more precise identification

of the proximal and distal edges. **Chapter 13**, illustrates for the first time the assessment with two-dimensional and three-dimensional post-processed OCT of distal edge effect (angiographic diameter stenosis $\geq 50\%$) caused by angiographically silent distal edge dissection at 6-months following stenting. OCT-detected edge dissections constitute a relatively frequent finding after DES implantation. In the majority of cases angiographically silent edge dissections are not associated with target lesion revascularization or stent thrombosis at mid-term (1-year), thus mechanical treatment should be carefully evaluated. (**Chapter 14**)

In **Chapter 15**, for the first time OCT cross-sections were used as the backbone upon which three-dimensional reconstructions of strut-level wall shear stresses were applied (local micro-environment) using computation fluid dynamics modelling techniques. Furthermore velocity profiles with reconstructed velocity streamlines were simulated over the polymeric struts pre- and post- Absorb BVS implantation. This study showed that such biomechanical assessment in a three-dimensional pattern is feasible and will potentially provide critical mechanistic insights following implantation of bioresorbable scaffolds.

STENT IMPLANTATION ASSESSMENT UTILIZING POST-PROCESSED THREE-DIMENSIONAL OPTICAL COHERENCE TOMOGRAPHY

Two-dimensional optical coherence tomographic imaging has enhanced our understanding of coronary atherosclerotic disease and is increasingly being used in conventional percutaneous coronary intervention to elucidate mechanisms of disease and improve our understanding of complex anatomy. In **Chapters 16-19** we provide the complementary value of post-processed three-dimensional OCT to two-dimensional OCT imaging in the 1. assessment of flow divider and high resolution visualization of the spatial distribution of the stent struts after main-branch stenting, 2. assessment of pre/peri-procedural thrombus formation in the setting of acute coronary syndromes and 3. evaluation of the stent strut apposition/malapposition following stenting. Real time high resolution three-dimensional optical coherence tomography with the addition of quantitative and possible tissue characterization properties are required from industry to validate and apply this technology in conventional percutaneous coronary

interventional practise. This may aid the decision making process during interventional procedures which will potentially influence future clinical outcomes.

IN VIVO ASSESSEMENT OF THE ABSORB BIORESORBABLE VASCULAR SCAFFOLD UTILIZING INTRACORONARY ULTRASOUND AND OPTICAL COHERENCE TOMOGRAPHY

The Absorb everolimus-eluting scaffolds include the first generation device evaluated in the ABSORB Cohort A clinical trial (ABSORB 1.0) and the second generation (ABSORB Revision 1.1) investigated in the ABSORB Cohort B trial. Insights from multiple imaging modalities showed that: 1. The introduction of mandatory Dmax measurements of vessel size prior to ABSORB implantation significantly reduced the undersizing of the 3.0 mm scaffold in large vessels and 2. The second generation scaffold performed better compared to the first generation with lesser degree of scaffold shrinkage (1% vs. 13% respectively, $p=0.01$) and less in-scaffold neointimal area obstruction (**Chapters 21-23**)

Conclusion

The present thesis has encompassed work undertaken during a very exciting period for Interventional Cardiovascular Medicine as a discipline with the introduction of bioresorbable technologies for percutaneous coronary interventions. The use of a plethora of intravascular imaging modalities either sound- or light-based during the acute phase or at follow-up have facilitated the understanding of vascular responses following stent/scaffold implantation in conventional interventional practise. The “edge effect” firstly introduced during the era of vascular brachytherapy has been replaced by the term “edge vascular response” with the use of newer generation metallic stents or bioresorbable scaffolds. Further improvements in the design of bioresorbable scaffolds are expected to reduce the incidence of proximal edge vascular response which despite is non-flow limiting is still visible at long-term with both sound- and light-based imaging modalities.

Samenvatting en conclusies

SAMENVATTING EN CONCLUSIES

Ondanks de enorme vooruitgang die men heeft geboekt bij het verminderen van het percentage restenose bij gebruik van geneesmiddelfafgevende stents (DES) van de eerste en tweede generatie, wordt het percentage restenose binnen de stent dat revascularisatie van het gestente bloedvat geschat op 5-10%. De toepassing van bioresorbeerbare scaffolds voor coronaire revascularisatie heeft een percentage restenose in de scaffold aangetoond dat vergelijkbaar is met DES; de veiligheid, doeltreffendheid en prestaties van deze hulpmiddelen moeten echter worden aangetoond in grotere gerandomiseerde onderzoeken en bredere klinische subsets. In de onderhavige thesis worden belangrijke gegevens gepresenteerd over de vasculaire respons op de lange termijn in de segmenten; deze respons werd beoordeeld met intrac coronaire beeldvormingsmethoden en histologische analyse na implantatie van metaalhoudende stents of bioresorbeerbare scaffolds.

VASCULAIRE RESPONS IN HET TIJDPERK VAN METAALHOUDENDE EN BIORESORBEERBARE HULPMIDDELEN

Uit angiografische evaluatie van de interactie tussen hulpmiddel en weefsel bij gebruik van niet-gecoate metalen stents (BMS = Bare-Metal Stents) of geneesmiddelfafgevende, metaalhoudende stents bleek hetzij focale hetzij diffuse verdeling van de restenoserespons met meerdere subtypes binnen elke groep. Vooral bij DES is het restenosepatroon gewoonlijk focaal en, meer in het bijzonder, geaggregeerd aan de proximale rand van de stent. Hoofdstuk 2 en 3 beschrijven het onderliggende mechanisme van restenose van de DES dat grofweg kan worden toegeschreven aan 4 hoofdoorzaken, namelijk implantatie-, arteriële, stent- en biologische factoren. De vasculaire respons aan de rand (EVR) is te wijten aan gelijkaardige factoren: 1. iatrogene of implantatiefactoren i.v.m. onjuiste geografische plaatsing tijdens de ingreep (axiaal dan wel longitudinaal), 2. factoren i.v.m. het hulpmiddel, zoals de materiaaleigenschappen van het geïmplanteerde platform (metaal of een bioresorbeerbare legering), de door het hulpmiddel veroorzaakte dissecties aan de rand en het soort en de afgiftekinetica van de antiproliferatieve medicatie en 3. biologische factoren in verband met de resterende hoeveelheid plaque aan de proximale en distale randen. Hoofdstuk 4 legt bewijzen voor over de vasculaire respons aan de rand (EVR) die óf angiografisch óf met op IVUS gebaseerde beeldvormingsmethoden wordt beoordeeld tot 2 jaar na de implantatie van metaalhoudende stents of bioresorbeerbare scaffolds. In dit hoofdstuk wordt een revascularisatiepercen-

tage van de gestente laesie (TLR) beschreven van ~3% tot 2 jaar na implantatie van een volledig bioresorbbaar hulpmiddel wat hoofdzakelijk werd toegeschreven aan proximale restenose.

IN VIVO BEOORDELING VAN DE VASCULAIRE RESPONS MET GEBRUIKMAKING VAN INTRAVASCULAIR ULTRAGELUID (IVUS) EN OP IVUS GEBASEERDE BEELDVORMINGSMETHODEN

Grijsschaal-IVUS (GS-IVUS) is het middel bij uitstek voor de *in vivo* beeldvorming van de coronaire vaatwand en vormt een belangrijk invasief diagnosemiddel voor de kwantitatieve beoordeling van chirurgische behandelingen en de ontwikkeling/regressie van atherosclerose. Desondanks maakt de grijsschaalvoorstelling van de plaque-morfologie het door de beperkte resolutie van de huidige IVUS-katheters (~45MHz) moeilijk, zo niet onmogelijk, om kwalitatief (bijv. visueel) de morfologie van plaque vast te stellen zoals bij histopathologie, wat de methode bij uitstek is voor weefselsanalyse. Deze beperking heeft men echter gedeeltelijk overwonnen met nieuwe, op IVUS gebaseerde nabewerkingsmethoden als virtuele histologie-IVUS (VH-IVUS). De beginselen van de afzonderlijke, op IVUS gebaseerde beeldvormingsmethoden worden beschreven in hoofdstuk 6 en geven inzicht in het proces van weefselsanalyse waarbij wordt bepaald of er sprake is van vezelig weefsel, vetweefsel, of weefsel met een necrotische kern of dichte verkalking.

In het onderzoek ABSORB Cohort B werden 101 patiënten (Group B1=45, Group B2=56) behandeld met de volledig resorbabele scaffold van de tweede generatie, nl. ABSORB BVS. De segmenten die proximaal en distaal aan het geïmplanteerde hulpmiddel waren gelegen (op 5 mm) werden na 6 maanden (Groep B1) of 1 jaar (Groep B2) onderzocht met GS-IVUS en VH-IVUS-beeldvorming. Er waren 23 proximale en 18 distale segmenten aan de distale rand beschikbaar voor analyse na 6 maanden, terwijl er 25 proximale en 30 distale randsegmenten beschikbaar waren na 1 jaar. Aan de proximale rand op 5 mm bestond de enige belangrijke verandering uit geringe constrictieve remodelering na 6 maanden (Δ dwarsdoorsnede bloedvat: -1,80% [-3,18; 1,30], $p < 0,05$), met een neiging tot regressie na 1 jaar (Δ dwarsdoorsnede bloedvat: -1,53% [-7,74; 2,48], $p=0,06$). De relatieve veranderingen van de vezelige en vetweefselcomponenten in dit segment waren op beide tijdstippen niet significant. Bij de distale rand op 5 mm werd 1 jaar na de implantatie een significante toename van het vetweefsel van 43,32% duidelijk [19,90; 244,28], ($p < 0,005$). (Hoofdstuk 7) Tot 1 jaar na implantatie van ABSORB BVS liet de vasculaire respons een zekere mate van constrictieve remodelering zien aan de proximale

rand en een toename van vezelig vetweefsel aan de distale rand dat een niet significante progressie van de plaque met adaptieve expansieve remodellering tot gevolg had. Het morfologische gedrag en de weefselsamenstelling verschilden niet wezenlijk van het gedrag van metaalhoudende medicinale stents op dezelfde waarnemingspunten in de tijd.

De vasculaire respons op de lange termijn aan de proximale en distale randen van 2 verschillende everolimus-afgeevende platformen, nl. de metaalhoudende Xience V en de bioresorbeerbare ABSORB BVS, werd voor het eerst op longitudinale wijze vergeleken aan de hand van het onderzoek SPIRIT II (n=113) en ABSORB Cohort B₁ (n=45). **(Hoofdstuk 8)** De proximale en distale segmenten op 5 mm van de geïmplanteerde hulpmiddelen gelegen werden na de procedure, na 6 maanden en 2 jaar na implantatie van het bioresorbeerbare hulpmiddel onderzocht met GS-IVUS en VH-IVUS, terwijl een soortgelijke analyse met GS-IVUS werd uitgevoerd na implantatie van de metaalhoudende stent.

Bij het ABSORB-onderzoek Cohort B1 waren er 22 proximale en 24 distale randsegmenten beschikbaar voor analyse. Bij het onderzoek SPIRIT II werden drieëndertig proximale en zesenzeventig distale randsegmenten geanalyseerd. Aan de proximale rand op 5 mm vertoonden de met Absorb BVS behandelde bloedvaten na 2 jaar een lumenverlies (LL) van 6,68% (- 17,33; 2,08) (p=0,027) in aanwezigheid van een tendens tot toename van het plaque-oppervlak van 7,55% (- 4,68; 27,11) (p=0,06). Bij de distale rand op 5 mm waren op geen van beide tijdstippen grote veranderingen duidelijk. Aan de proximale rand op 5 mm toonden de met XIENCE V EES behandelde bloedvaten na 2 jaar geen tekenen van LL, doch slechts een afname van het plaque-oppervlak van 6,90% (-17,86; 4,23) (p=0,035). Aan de distale rand was er op hetzelfde tijdstip geen bewijs van belangrijke wijzigingen m.b.t. het lumengebied of vasculaire remodellering. Tot 2 jaar na implantatie van de bioresorbeerbare everolimus-afgeevende scaffold toont de op IVUS gebaseerde seriële evaluatie van de EVR een statistisch significante LL aan de proximale rand. Het komende vervolgonderzoek voor beeldvorming van de Absorb BVS 3 jaar na implantatie zal naar verwachting meer informatie verstrekken over het gedrag van de vaatwand aan de randen van de scaffold.

In **hoofdstuk 9** zijn de veranderingen in vasculaire compliantie in de scaffold-segmenten en de aanliggende proximale en distale randen geëvalueerd met VUS-palpografie, omdat de bioresorbeerbare scaffold na verloop van tijd wordt geresorbeerd. IVUS-palpografie is een techniek waarmee de plaatselijke mechanische weefseleigenschappen kunnen worden bepaald. In totaal zijn 83 patiënten uit Cohort A en B van de ABSORB-studies onderzocht met palpografie (30 en respectievelijk 53 patiënten van ABSORB Cohort A en Cohort B). Een belangrijke afname in compliantie in het scaffold-segment

was duidelijk na de implantatie. Op de verschillende tijdstippen tijdens de follow-up werd er geen verkeerde compliantie gevonden in Cohort A (6 maanden=proximale rand 0,29 [0,18-0,35] t.o.v. scaffold-segment 0,10 [0,06-0,22] t.o.v. distale rand 0,16 [0,05-0,24]; $p=0,146$; proximale rand na 24 maanden 0,20 [0,09-0,30] t.o.v. scaffold-segment 0,24 [0,17-0,29] t.o.v. distale rand 0,11 [0,05-0,24]; $p=0,052$) noch in Cohort B (6 maanden=proximale rand 0,28 [0,16-0,46] t.o.v. scaffold-segment 0,23 [0,14-0,29] t.o.v. distale rand 0,11 [0,05-0,17]; $p=0,449$; 12 maanden=proximale rand 0,18 [0,10-0,36] t.o.v. scaffold-segment 0,16 [0,08-0,26] t.o.v. distale rand 0,11 [0,02-0,20]; $p=0,618$). Hoewel de Absorb BVS veranderingen in vasculaire compliantie veroorzaakte op de plek waar de scaffold was geïmplanteerd, was de waargenomen verkeerde compliantie van voorbijgaande aard en werd na verloop van tijd weer normaal na resorptie van de scaffold, wat mogelijk van invloed is op de plaatselijke hemodynamische en reologische toestand.

In **hoofdstuk 10** hebben we methoden gebruikt met eindige elementen en geavanceerde computersimulatie van stroomdynamica (CFD = Computational Fluid Dynamics) waarmee de hemodynamische gevolgen van de virtuele toepassing van een bioresorbeerbare scaffold met een met de Absorb BVS vergelijkbaar ontwerp kunnen worden gevisualiseerd met rechte en kromme ideale vormen. De WSS (wall shear stress = schuifspanning aan de vaatwand) werd berekend bij de instroom, endoluminaal en bij de uitstroom van elk stutoppervlak na de procedure (stadium I) en op het tijdstip dat 33% van de scaffold geresorbeerd was (stadium II).

De gemiddelde WSS op de in- en uitstroomoppervlakken in stadium I bedroeg 3,2 respectievelijk 3,1 dyne/cm² en 87,5 dyne/cm² op het endoluminale stutoppervlak in het rechte bloedvat. Van stadium I tot stadium II nam de WSS op de in- en uitstroomoppervlakken toe met 101% respectievelijk 145% en daalde met 27% op het endoluminale stutoppervlak. In een krom bloedvat kwam de WSS-verandering meer tot uiting in de binnenkromming met een toename van 60,3% en 63,0% van de WSS op de stutoppervlakken aan de instroom en uitstroom. Een gelijksoortige analyse aan de proximale en distale randen toonde een dramatische toename van 486,4% aan het laterale uitstroomoppervlak van de proximale scaffold-rand. Het uitvoeren van CFD-simulaties over virtueel ingezette bioresorbeerbare scaffolds duidt op de voorbijgaande aard van de interacties tussen hulpmiddel en doorstroming naarmate het bioresorptieproces in de loop van de tijd vordert. Zulke modellering voor een hemodynamisch hulpmiddel zal naar verwachting in de toekomst leiden tot een nieuw ontwerp voor bioresorbeerbare scaffolds.

IN VIVO BEOORDELING VAN DE VASCULAIRE RESPONS MET GEBRUIKMAKING VAN OPTISCHE COHERENTTOMOGRAFIE (OCT)

OCT maakt hoge-resolutiebeeldvorming mogelijk met een nagenoeg histologische resolutie van $\sim 15\mu\text{m}$, waardoor deze methode ideaal is voor het bestuderen van de interactie tussen hulpmiddel en bloedvat. Histomorfometrie is van belang voor het evalueren van de werking van nieuwe hulpmiddelen en de vasculaire respons daarop. Omdat histologische analyse op dieren en mensen beperkt is tot postmortaal onderzoek is *in-vivo* beoordeling van de vasculaire respons met behulp van OCT uiterst welkom.

In **hoofdstuk 11** hebben we 2 jaar na de implantatie van 22 polymere BVS-hulpmiddelen in 11 gezonde kransslagaderen bij varkens de morfometrische parameters van de stentresten beoordeeld met OCT en histologische analyse. Wij hebben het oppervlak en de dikte van de leemten die eerder gevuld waren met polymeerstutten geëvalueerd alsmede het gebied met neointimale hyperplasie dat het endoluminale oppervlak van de stutleemten bedekte en het gebied met neointimale hyperplasie tussen de stutleemten. Ons onderzoek gaf aan dat *in vivo* OCT van de BVS gecorreleerde metingen van dezelfde orde grootte oplevert als histomorfometrie en dat deze methode reproduceerbaar is voor de evaluatie van bepaalde vasculaire en met het hulpmiddel samenhangende eigenschappen. Vergeleken bij OCT levert histologische analyse 2 jaar na de implantatie echter systematisch hogere waarden op voor alle gemeten structuren.

In **hoofdstuk 12** wordt met OCT en histologie de vasculaire respons beoordeeld en vergeleken nadat hetzij overlappende Absorb BVS- hetzij Xience V (XV)-metaalhoudende stents na 28 en respectievelijk 90 dagen in een model van kransslagaderen bij varkens. Na 28 dagen in de overlappende structuur gaf de OCT-analyse aan dat 80,1% van de Absorb-stutten en 99,4% van de XV-stutten bedekt was ($p < 0,0001$), wat overeenkomt met histologische waarnemingen voor met cellen bedekte stutten van 75,4% respectievelijk 99,6% ($p < 0,001$).

Onbedekte stutten werden bijna uitsluitend in verband gebracht met de aanwezigheid van "op elkaar gestapelde" Absorb-stutten, d.w.z. met een directe bedekkingsstructuur. Na 90 dagen bleek uit OCT en histologische analyse dat de overlappende Absorb-stutten en overlappende XV-stutten $>99\%$ bedekt waren. In kransslagaderen van varkens die met overlappende Absorb-stutten of overlappende XV-stutten waren geïmplanteed, was de bedekking van de stutten vertraagd na 28 dagen met overlappende Absorb-scaffolds, terwijl na 90 dagen beide hulpmiddelen vergelijkbare bedek-

king van de stutten vertoonden, wat de invloed van de dikte van de stut aangeeft in de waargenomen vasculaire respons.

In **hoofdstuk 13 en 14** werd de vasculaire respons aan de rand geëvalueerd met OCT na door metaalhoudende stents veroorzaakte randdissecties. Hoewel IVUS en op IVUS gebaseerde methoden met weefselanalyse-eigenschappen de enige intravasculaire beeldvormingstechnieken waren voor de evaluatie van de overgangsgebieden (randen), levert OCT met zijn uiterst hoge ruimtelijke resolutie en grotere terugtreknelheid van 20-40 mm/sec een accuratere identificatie van de proximale en distale randen. In **hoofdstuk 13** wordt voor het eerst de beoordeling met tweedimensionale en driedimensionale nabewerkte OCT van het distale randeffect (angiografische diameter stenose $\geq 50\%$) geïllustreerd zoals veroorzaakt door angiografisch stille dissectie van de distale rand 6 maanden na plaatsing van de stent. Tijdens OCT gedetecteerde randdissecties worden relatief frequent aangetroffen na DES-implantatie. In de meerderheid van de gevallen houden de angiografisch stille randdissecties geen verband met de revascularisatie van de gestente laesie of trombose van de stent op de middellange termijn (1 jaar), zodat de mechanische behandeling zorgvuldig geëvalueerd dient te worden. (**Hoofdstuk 14**)

In **hoofdstuk 15** zijn OCT-dwarsdoorsneden voor het eerst gebruikt als basis waarop driedimensionale reconstructies van de WSS ter hoogte van de stut werden uitgeoefend (plaatselijk micro-milieu) met gebruikmaking van CFD-simulatietechnieken. Verder werden er vóór en na implantatie van de Absorb BVS op de polymeer-stutten snelheidsprofielen met zogenaamde “reconstructed velocity streamlines” gesimuleerd. Uit dit onderzoek bleek dat een dergelijk biomechanische beoordeling in een driedimensionaal patroon mogelijk is en mogelijk kritieke mechanistische inzichten inzake bioresorbabele scaffolds na implantatie kan opleveren.

BEOORDELING IMPLANTATIE STENT MET BEHULP VAN NABEWERKTE DRIEDIMENSIONALE OPTISCHE COHERENTIE TOMOGRAFIE (OCT)

Tweedimensionale beeldvorming met optische coherentie tomografie heeft onze kennis over coronaire atherosclerose uitgebreid en deze methode wordt steeds meer toegepast bij traditionele percutane coronaire ingrepen om de ziektemechanismen te verduidelijken en ons inzicht in complexe anatomische structuren te verbeteren. In **hoofdstuk 16 tot 19** wordt de waarde toegelicht van nabewerkte driedimensionale OCT als aanvulling op tweedimensionale beeldvorming bij de 1. beoordeling van bifurcaties

en hoge-resolutievisualisatie van de ruimtelijke verdeling van de stentstutten na plaatsing van een stent in de hoofdvertakking, 2. beoordeling van trombosevorming vóór en tijdens de ingreep in een omgeving met acute coronaire syndromen en 3. beoordeling van de juiste/verkeerde appositie van de stentstutten na plaatsing van de stent. Aan de fabrikanten van medische hulpmiddelen moet worden gevraagd driedimensionale optische coherentietomografie te produceren met een hoge resolutie in real-time plus kwantitatieve en mogelijke weefselanalyse-eigenschappen, zodat deze technologie in de traditionele praktijk voor percutane coronaire ingrepen kan worden gevalideerd en toegepast.

Dit kan behulpzaam zijn bij het besluitvormingsproces tijdens chirurgische ingrepen en dit kan weer van invloed zijn op toekomstige klinische resultaten.

IN VIVO BEOORDELING VAN DE BIORESORBEERBARE VASCULAIRE SCAFFOLD ABSORB MET BEHULP VAN INTRACORONAIR ULTRAGELUID EN OPTISCHE COHERENTIETOMOGRAFIE

De everolimus-afgeevende ABSORB-scaffolds bestaan uit het hulpmiddel van de eerste generatie dat werd geëvalueerd bij het klinisch onderzoek ABSORB Cohort A (ABSORB 1.0) en het hulpmiddel van de tweede generatie (ABSORB herziening 1.1) dat tijdens het onderzoek ABSORB Cohort B werd bestudeerd. Inzichten uit verschillende beeldvormingsmethoden hebben aangetoond dat 1. de introductie van verplichte Dmax-metingen van de grootte van het bloedvat vóór implantatie van ABSORB het te klein inschatten van de scaffold van 3,0 mm in grote bloedvaten aanzienlijk heeft beperkt en 2. de scaffold van de tweede generatie beter werkte vergeleken bij de hulpmiddelen van de eerste generatie met minder inkrimpen van de scaffolds (1% vergeleken bij 13% respectievelijk, $p=0,01$) en minder obstructie van het neointimaal gebied in de scaffold (**hoofdstuk 21 tot 23**).

Conclusie

De onderhavige thesis is het resultaat van werk dat tijdens een voor het specialisme interventionele cardiovasculaire geneeskunde zeer spannende periode werd verricht omdat dit een vakgebied is waar bioresorbeerbare technologieën voor percutane coronaire ingrepen zijn geïntroduceerd. Het gebruik van een breed gamma aan op ultrageluid of licht gebaseerde intravasculaire beeldvormingsmethoden tijdens de acute fase of bij de follow-upcontrole hebben de interpretatie van de vasculaire respons na

implantatie van een stent of scaffold bij de traditionele chirurgische praktijk vereenvoudigd. Het "randeffect" dat voor het eerst werd geïntroduceerd in de tijd dat vasculaire brachytherapie werd toegepast is vervangen door de term "vasculaire respons aan de rand" sinds er een nieuwe generatie van metaalhoudende stents of bioresorbeerbare scaffolds wordt toegepast. Naar verwachting zal door verdere verbeteringen aan het ontwerp van de bioresorbeerbare scaffolds het percentage vasculaire respons aan de proximale rand dalen; ondanks het feit dat de doorstroming niet wordt belemmerd, blijft deze vasculaire respons zichtbaar op de lange termijn bij zowel op ultrageluid als op licht gebaseerde beeldvormingsmethoden.

Acknowledgements

ACKNOWLEDGEMENTS

The choice to embark on a career in Interventional Cardiology was taken during the last year of medical school straight after the advice of Prof. Ioannis Gkogkas, currently Professor Emeritus of Surgery in Athens University. The years during Cardiology training were fascinating, more in particular the time spent in the catheterization laboratory convinced me that the decision to pursue a career in this field was the right one; furthermore the last 2-years of my clinical training I had the unique privilege to work with the Professor of Cardiothoracic Surgery at Imperial College, Sir. Magdi H. Yacoub who defined later on my career path.

The 2nd Department of Cardiology of the Athens University would start a joined program as part of the Harefield Recovery Protocol Study for Patients with Refractory Heart Failure (HARPS) related to the impact of Left Ventricular Assist Devices (LVAD) in patients with end stage Heart Failure headed by Prof. M. Yacoub. I was further assigned as the cardiology fellow in charge of this program. The collaboration turned out as a unique opportunity by gaining a lot of experience related to the management of such patients and observing a world renowned clinician and scientist in the management of challenging situations. However my passion was Interventional Cardiology. One day following successful LVAD implantation and fast patient recovery we were both sitting in the ICU and Prof. M. Yacoub was asking for my future plans following training completion. I replied: "Professor, my goal now is clinical research in Interventional Cardiology" further requesting for his advice and guidance. He said, I will give you 2 advices that will potentially guide you successfully through your research aspirations: you must be, 1. focused like a laser beam and 2. modest and humble following your endeavors. Additionally, If you want to pursue a career in Interventional Cardiology research the best place in Europe is with Prof. Patrick W. J. C. Serruys in Rotterdam, the Netherlands. I have heard that he has novel projects with bioresorbable stents for treating coronary artery disease."

The following months consisted of numerous emails back and forth, finally setting the date for visiting Rotterdam. I remember that I was at the Thoraxcenter 2-hours in advance of the scheduled meeting with Professor Patrick W. J. C. Serruys, exploring this world-class institution. I finally met with the Professor for the first time at his office, the 5th floor of the Thoraxcenter. His door was wide open and he was reading a Circulation

article. I remember him saying that here we publish about 5-10 of such papers/year in this journal, further asking me how many papers I had already published. I was very proud of showing 4 color printed case reports, 2 of them in a prominent position in my envelope (Prof. Magdi Yacoub was in the authorship); however from his body language I realized that it might be smarter to reply: I have no publications.

The following discussions were in a more relaxed pace with personal questions related to future career plans. Professor's last statement was that at the Thoraxcenter there is huge competition and only a minority of those who travel to Rotterdam for interviews are finally accepted. I left Professor's office with mixed emotions, however soon thereafter realized that it would be a huge opportunity to learn beside this world-renowned Teacher. Three years later, I have to admit: ***"Whatever little I have achieved Professor, is because of you. You took my hand, opened my mind, touched my heart. I will always be grateful to you Sir."*** An enormous thank you must also go out to Dr. Hector M. Garcia-Garcia who has been a strong foundation throughout this thesis as a co-promotor. *"Hector, without your advice and guidance on the how to do..., this thesis would not be possible"*. A big thank you must also go to the committee members for their presence at this thesis: *"It is indeed an honor for me"*.

The course of my fellowship was also enriched by numerous friends who were crucial in the completion of this thesis, all charismatic Interventional Cardiologists with passion for innovation. Maria Radu, Vasim Farooq, Takashi Muramatsu, Salvatore Brugaletta, Josep Gomez-Lara, Yoshinobu Onuma, Jung Ho-Heo, Il-Soo Lee, Roberto Diletti, Christos Bourantas, Yao-Jun Zhang just to name a few. How can I also forget the wonderful Marie-Angele Morell: *"Marie-Angele, hope you remember my digital moments with Queen Maxima of the Netherlands"*. A big thank must go out to Hanny Boutkan who have been so supportive, especially once I left Rotterdam and moved to the United States of America and had additional requests for revised forms from the administration office of the Erasmus University. Finally another thank to the pillars behind EuroIntervention, Paul Cummins and Sylvie Lhoste; without their help the Absorb BVS Compendiums would not be ready on time.

One cannot achieve and develop as an individual without the support and commitment of those close to them. My Parents, Dimitrios and Maria-Angelliki who created a wonderful middle class family worked hard and gave me opportunities that they never

had. On this journey through life, their principles were my compass as well as a map and these fantastic parents were my heroes. Finally my wife Katerina had been always there for me, encouraged me to embark on this challenging path and sacrificed so much of herself for us. She will be carrying our son Dimitrios soon, and I'm sure she will be telling him endless "oranje" stories.

I would like to finish the Acknowledgement section of this Thesis by remembering the two most inspiring pieces which strengthened my 25-min bike ride to Cardialysis every morning in an average winter temperature of -2°C (28°F). The first was a section from the poem of C. P. Cavafy, *Ithaka*: *"Keep Ithaka always in your mind...But do not hurry the journey at all. Better if it lasts for years, so you are old by the time you reach the island, wealthy with all you have gained on the way, not expecting Ithaka to make you rich.*

Ithaka gave you the marvelous journey. Without her you would not have set out. She has nothing left to give you now. And if you find her poor, Ithaka won't have fooled you. Wise as you will have become, so full of experience, you will have understood by then what these Ithakas mean.

The second was one of Prof. Serruys quotes:

"A Dream always comes true, It's just a matter of Time".

Curriculum Vitae List of Publications

CURRICULUM VITAE

Bill D. Gogas, M.D., F.A.C.C.

(a.k.a. Vasileios D. Gkogkas)

Date of Birth: January 17, 1978

Place of Birth/ Nationality: Athens, Greece/ Greek

Professional Address: Andreas Gruentzig Cardiovascular Center of Emory University, Emory University School of Medicine, Department of Medicine, Division of Cardiology, Suite D403A, 1364 Clifton Rd, NE, Atlanta, GA

E-mail: bgogas@gmail.com (primary) & vasileios.gkogkas@emory.edu (secondary)

Education & Appointments

1995-2002: M.D.,

University of Athens Medical School, Athens, Greece

2003-2005: Resident, Internal Medicine,

University of Athens Medical School, University Hospital "ATTIKON", Athens, Greece

2005-2009: Clinical Fellow, Cardiology,

University of Athens Medical School, University Hospital "ATTIKON", Athens, Greece

2007-2009: Interventional Cardiology Fellow,

University of Athens Medical School, University Hospital "ATTIKON", Athens, Greece

2009-2012: Doctoral (Ph.D.) Candidate, Interventional Cardiology,

Erasmus University, Rotterdam, the Netherlands (Supervisor: Prof. Dr. P. W. J. C. Serruys)

2012-2013: Post Doctoral Fellow, Interventional Cardiology,

Andreas Gruentzig Cardiovascular Center of Emory University, Emory University School of Medicine,

Department of Medicine, Division of Cardiology, Atlanta, Georgia (American College of Cardiology

Foundation Scholar)

2013-2015: Senior Post Doctoral Fellow, Interventional Cardiology,

Andreas Gruentzig Cardiovascular Center of Emory University, Emory University School of Medicine,

Department of Medicine, Division of Cardiology, Atlanta, Georgia

Medical Licensure

2009: Medical Practitioner Board of Athens, Greece- Full Registration

2002: General Medical Council (GMC), United Kingdom- Full Registration

Society Memberships

2014: Fellow of the American College of Cardiology Foundation

2012: Member, European Association of Percutaneous Coronary Interventions

2011: Member, Hellenic Cardiology Society

LIST OF PUBLICATIONS

Peer Reviewed Journals

1. Biomechanical Assessment of Fully Bioresorbable Devices

Gogas B.D., King S.B. III, Timmins L.H., et al.
JACC Cardiovasc Interv. 2013, Jul;6(7):760-1

2. Edge Vascular Response after Percutaneous Coronary Intervention: An Intracoronary Ultrasound and Optical Coherence Tomography Appraisal: From Radioactive Platforms to First- and Second- Generation Drug-Eluting Stents and Bioresorbable Scaffolds.

Gogas B.D., Garcia-Garcia H.M., Onuma Y., et al.
JACC Cardiovasc Interv. 2013 Mar; 6(3): 211-21.

3. Does Flow During Rest and Relaxation Suffice?

Samady H., **Gogas B.D.**
J Am Coll Cardiol. 2013 Apr 2; 61(13): 1436-9.

4. Intracoronary Optical Coherence Tomography and Histology of Overlapping Everolimus-Eluting Bioresorbable Vascular Scaffolds in a Porcine Coronary Artery Model: The Potential Implications for Clinical Practice.

Farooq V., Serruys P.W., Heo JH., **Gogas B.D.**, et al.
JACC Cardiovasc Interv. 2013 May; 6(5): 523-32

5. Vascular Response of the Segments Adjacent to the Proximal and Distal Edges of the ABSORB Everolimus-Eluting Bioresorbable Vascular Scaffold: 6-month and 1-year Follow-up Assessment: A Virtual Histology Intravascular Ultrasound Study from the First-In-Man ABSORB Cohort B trial.

Gogas B.D., Serruys P.W., Diletti R., et al.
JACC Cardiovasc Interv. 2012 Jun; 5(6): 656-65

6. In Vivo Three Dimensional Optical Coherence Tomography. A Novel Imaging Modality to Visualize the Edge Vascular Response.

Gogas B.D., Muramatsu T., Garcia-Garcia H.M., et al.

Int J Cardiol. 2013 Apr 15; 164(3): e35-7.

7. The Edge Vascular Response Following Implantation of the Absorb Everolimus-Eluting Bioresorbable Vascular Scaffold and the XIENCE V Metallic Everolimus-Eluting Stent. First Serial Follow-Up Assessment at six months and two years: Insights from the First-In-Man ABSORB Cohort B and SPIRIT II trials.

Gogas B.D., Bourantas C.V., Garcia-Garcia H.M., et al.

EuroIntervention. 2013 Oct 22; 9(6): 709-20. (doi: 10.4244)

8. Natural history of optical coherence tomography-detected non-flow-limiting edge dissections following drug-eluting stent implantation.

Radu MD, Räber L, Heo J, **Gogas B.D.**, et al.

EuroIntervention. 2013 Aug 26. (doi:pii: 20120926-04)

9. Evaluation With In Vivo Optical Coherence Tomography and Histology of the Vascular Effects of the Everolimus-Eluting Bioresorbable Vascular Scaffold at Two Years Following Implantation in a Healthy Porcine Coronary Artery Model: Implications of Pilot Results for Future Pre-Clinical Studies.

Gogas B.D., Radu M., Onuma Y. et al.

Int J Cardiovasc Imaging. 2012 Mar; 28(3): 499-511

10. Three-Dimensional Coronary Tomographic Reconstructions Using In Vivo Intracoronary Optical Frequency Domain Imaging in the Setting of Acute Myocardial Infarction: The Clinical Perspective.

Gogas B.D., Farooq V., Serruys P.W.

Hellenic J Cardiol. 2012 Mar; 53(2): 148-51.

11. Three-Dimensional Reconstruction of the Post-Dilated ABSORB Everolimus-Eluting Bioresorbable Vascular Scaffold in a True Bifurcation Lesion for Flow Restoration.

Gogas B.D., van Geuns R.J., Farooq V., et al.

JACC Cardiovasc Interv. 2011 Oct; 4(10): 1149-50

12. Assessment of Coronary Atherosclerosis by IVUS and IVUS-based Imaging Modalities: Progression and Regression Studies, Tissue Composition and Beyond.

Gogas B.D., Farooq V., Serruys P.W. et al.

Int J Cardiovasc Imaging. 2011 Feb; 27(2): 225-37

13. Acute Coronary Occlusion Following TAVI.

Gogas B.D., Zacharoulis A.A., Antoniadis A.G.

Catheter Cardiovasc Interv. 2011 Feb 15; 77(3): 435-8

14. Severe Anaemia and Subcapital Femur Fracture in a Patient with Left Ventricular Assist

Device Heart Mate II: The Cardiologist's Management of This Rare Patient.

Gogas B.D., Parissis J.T., Filippatos G.S. et al.

Eur J Heart Fail. 2009 Aug; 11(8): 806-8

15. 3-Dimensional Optical Frequency Domain Imaging For the Evaluation of Primary

Percutaneous Coronary Intervention in ST-segment Elevation Myocardial Infarction.

Gogas B.D., Farooq V., Onuma Y. et al.

Int J Cardiol. 2011 Aug 18; 151(1): 103-5.

16. Progress in Treatment by Percutaneous Coronary Intervention: The Stent of the Future.

Muramatsu T, Onuma Y, Zhang YJ, Bourantas CV, et al.

Rev Esp Cardiol. 2013 Jun; 66(6): 483-96

17. Assessment of Plaque Evolution in Coronary Bifurcations Located Beyond Everolimus Eluting Scaffolds: Serial Intravascular Ultrasound Virtual Histology Study.

Lee IS, Bourantas CV, Muramatsu T, **Gogas B.D.**, et al.
Cardiovasc Ultrasound. 2013 Jul 20;11:25

18. Vascular Compliance Changes of the Coronary Vessel Wall after Bioresorbable Vascular Scaffold Implantation in the Treated and Adjacent Segments.

Brugaletta S, **Gogas B.D.**, Garcia-Garcia HM, Farooq V, et al.
Circ J. 2012; 76(7): 1616-23

19. Proximal and Distal Maximal Luminal Diameters as a Guide to Appropriate Deployment of the ABSORB Everolimus-Eluting Bioresorbable Vascular Scaffold: A sub-study of the ABSORB Cohort B and the on-going ABSORB EXTEND Single Arm Study.

Farooq V, Gomez-Lara J, Brugaletta S, **Gogas B.D.**, et al.
Catheter Cardiovasc Interv. 2012 May 1; 79(6): 880-8

20. Optical Coherence Tomography (OCT) of Overlapping Bioresorbable Scaffolds: from benchwork to clinical application.

Farooq V, Onuma Y, Radu M, Okamura T, et al.
EuroIntervention. 2011 Jul; 7(3): 386-99

21. Restenosis: Delineating the Numerous Causes of Drug-Eluting Stent Restenosis.

Farooq V, **Gogas B.D.**, Serruys PW.
Circ Cardiovasc Interv. 2011 Apr 1; 4(2):195-205.

22. 3-Dimensional Reconstruction of a Bifurcation Lesion with Double Wire after Implantation of a second generation everolimus-eluting bioresorbable vascular scaffold.

van Geuns RJ, **Gogas B.D.**, Farooq V, et al.
Int J Cardiol. 2011 Dec 1; 153(2):e43-5

23. A comparative assessment by optical coherence tomography of the performance of the first and second generation of the everolimus-eluting bioresorbable vascular scaffolds.

Gomez-Lara J, Brugaletta S, Diletti R, et al.
Eur Heart J. 2011 Feb; 32(3): 294-304

24. Agreement and Reproducibility of Gray-Scale Intravascular Ultrasound and Optical Coherence Tomography for the Analysis of the Bioresorbable Vascular Scaffold.

Gómez-Lara J, Brugaletta S, Diletti R, **Gogas B.D.**, et al.
Catheter Cardiovasc Interv. 2012 May 1;79(6): 890-902

25. Serial 2- and 3-dimensional visualization of side branch jailing after metallic stent implantation: to kiss or not to kiss...?

Diletti R, Farooq V, Muramatsu T, **Gogas B.D.**, et al.
JACC Cardiovasc Interv. 2012 Oct; 5(10): 1089-90

KEY ABSTRACT PRESENTATIONS

1. The Dynamic Vascular Response at the Proximal and Distal Edges Following Implantation of the ABSORB Everolimus-Eluting Bioresorbable Vascular Scaffold and the Xience V Everolimus-Eluting Stent

Bill D. Gogas, Patrick W. Serruys, Vasim Farooq, et al.

Presented orally at the State-of-the-Art session of the ESC 2012

2. The Dynamic Vascular Response at the Proximal and Distal Edges Following Implantation of the ABSORB Everolimus-Eluting Bioresorbable Vascular Scaffold as Assessed With Virtual Histology Intravascular Ultrasound. A 2-year Follow-up Assesment From the First In Man, ABSORB Cohort B Trial

Bill D. Gogas, Patrick W. Serruys, Vasim Farooq, et al.

Presented orally at the EuroPCR 2012

3. Vascular Responses at the Segments Adjacent to the Proximal and Distal Edges of the ABSORB Second Generation Everolimus Eluting Bioresorbable Vascular Scaffold. 6 Months and 1 Year Follow-up Assessment. A Virtual Histology Intravascular Ultrasound Study from the ABSORB Cohort B Trial

Bill D. Gogas, Patrick W. Serruys, Roberto Diletti, et al.

Presented orally at the ACC 2012

4. Evaluation with In Vivo Optical Coherence Tomography and Histology of the Vascular Effects of the Everolimus-Eluting Bioresorbable Vascular Scaffold at two Years Following Implantation in a Healthy Porcine Coronary Artery Model.

Bill D. Gogas, Maria Radu, Yoshinobu Onuma, et al.

Presented orally at the ACC 2011

5. Intracoronary Optical Coherence Tomography and Histology of Overlapping Everolimus-Eluting Bioresorbable Vascular Scaffolds in a Porcine Coronary Artery Model: The Potential Implications for Clinical Practice

Vasim Farooq, Patrick W. Serruys, Jung Heo, **Bill D. Gogas**, et al.

TCT 2012

6. Comparison of Coronary Artery Endothelial Function after Nobori and Xience V Stent Implantation

Arihiro Sumida, Hiroyuki Nagai, **Bill D. Gogas**, Jinsheng Li, et al.

ACC with TCT 2012

7. Neointimal Tissue Classification Using Optical Coherence Tomography After Paclitaxel-Coating Balloon Treatment in Pig In-Stent Stenosis Model

Arihiro Sumida, Hiroyuki Nagai, **Bill D. Gogas**, Jinsheng Li, et al.

ACC with TCT 2012

